

MASSIVE NEUTRINOS
TESTS OF FUNDAMENTAL SYMMETRIES

XIth Moriond Workshop

Les Arcs, Savoie, France - January 26- February 2, 1991

Massive Neutrinos - Tests of Fundamental Symmetries

Series : Moriond Workshops

ISBN 2-86332-098-X

Copyright 1991 by Editions Frontières

All rights reserved. This book, or parts thereof, may not be reproduced in any form or by any means, electronic or mechanical, including photocopying, recording or any information storage and retrieval system now known or to be invented, without written permission from the Publisher.

EDITIONS FRONTIERES

B. P. 33

91192 Gif-sur-Yvette Cedex - France

Printed in Singapore by Fong and Sons Printers Ltd. Pte.

Proceedings of the XXVIth RENCONTRE DE MORIOND

Series : Moriond Workshops

Les Arcs, Savoie, France

January 26 - February 2, 1991

Moriond Workshop. II.
1991. Les Arcs

MASSIVE NEUTRINOS TESTS OF FUNDAMENTAL SYMMETRIES

edited by

O.²¹ Fackler

G. Fontaine

J. Trần Thanh Vân

C 91/241



~~539.12
MOR~~

EDITIONS
FRONTIERES

XIth Moriond Workshop on : Massive Neutrinos - Tests of Fundamental Symmetries

was organized by

Trần Thanh Vân J. (*Orsay*)

with the active collaboration of :

Aspect A.	(<i>Paris</i>)
Boehm F.	(<i>Caltech</i>)
Chardin G.	(<i>Saclay</i>)
Fackler O.	(<i>Livermore</i>)
Faller J.	(<i>Boulder</i>)
Fischbach E.	(<i>Purdue</i>)
Fontaine G.	(<i>Paris</i>)
Gerbier E.	(<i>Saclay</i>)
Greene G.	(<i>NBS</i>)
Kayser B.	(<i>Washington</i>)
Mugge M.	(<i>Livermore</i>)
Pain R.	(<i>Paris</i>)
Petcov S.	(<i>Sofia/Trieste</i>)
Spiro M.	(<i>Saclay</i>)
Wilkerson J.	(<i>LANL</i>)
Wuthrick J. P.	(<i>Paris</i>)

Sponsored by :

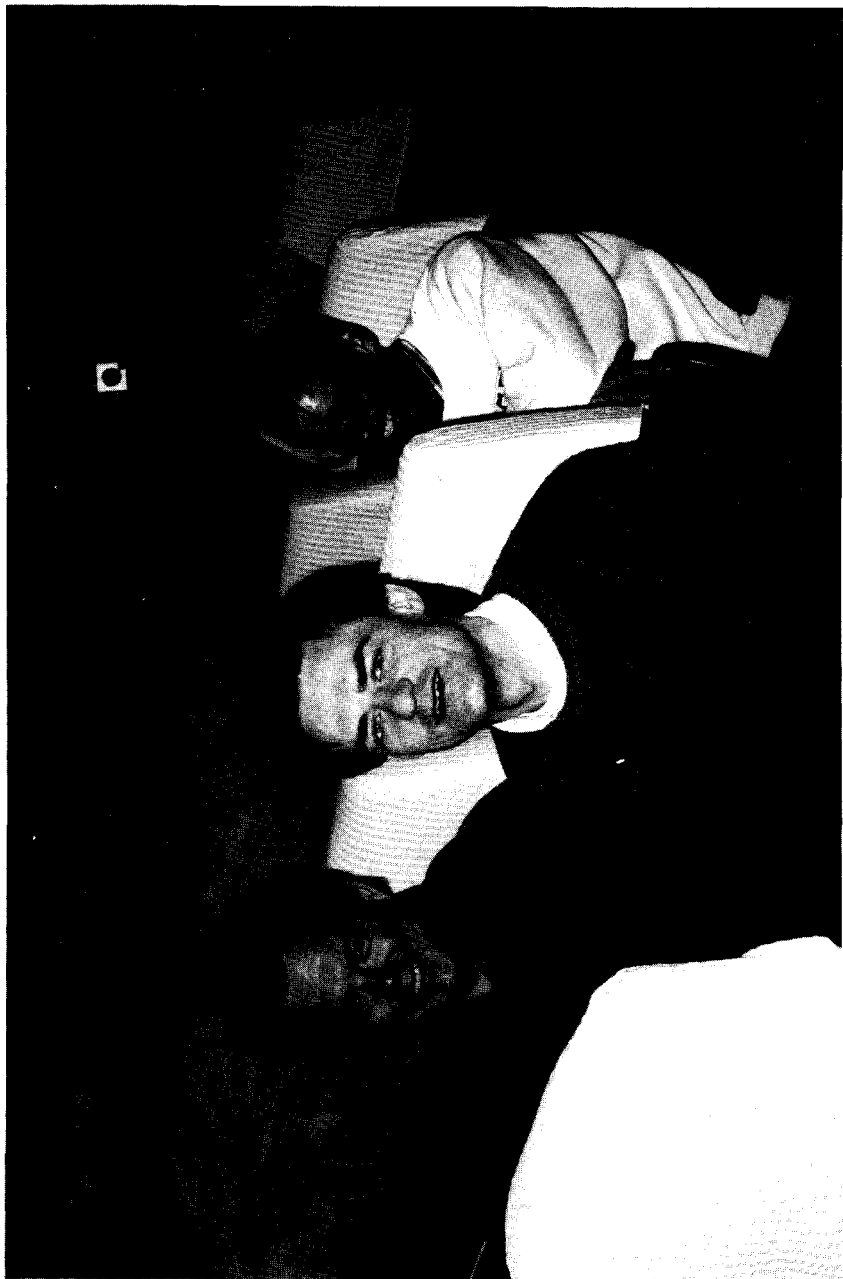
- . Centre National de la Recherche Scientifique (IN2P3, MPB)
- . Commissariat à l'Energie Atomique(DPhPE)
- . National Recherche Foundation

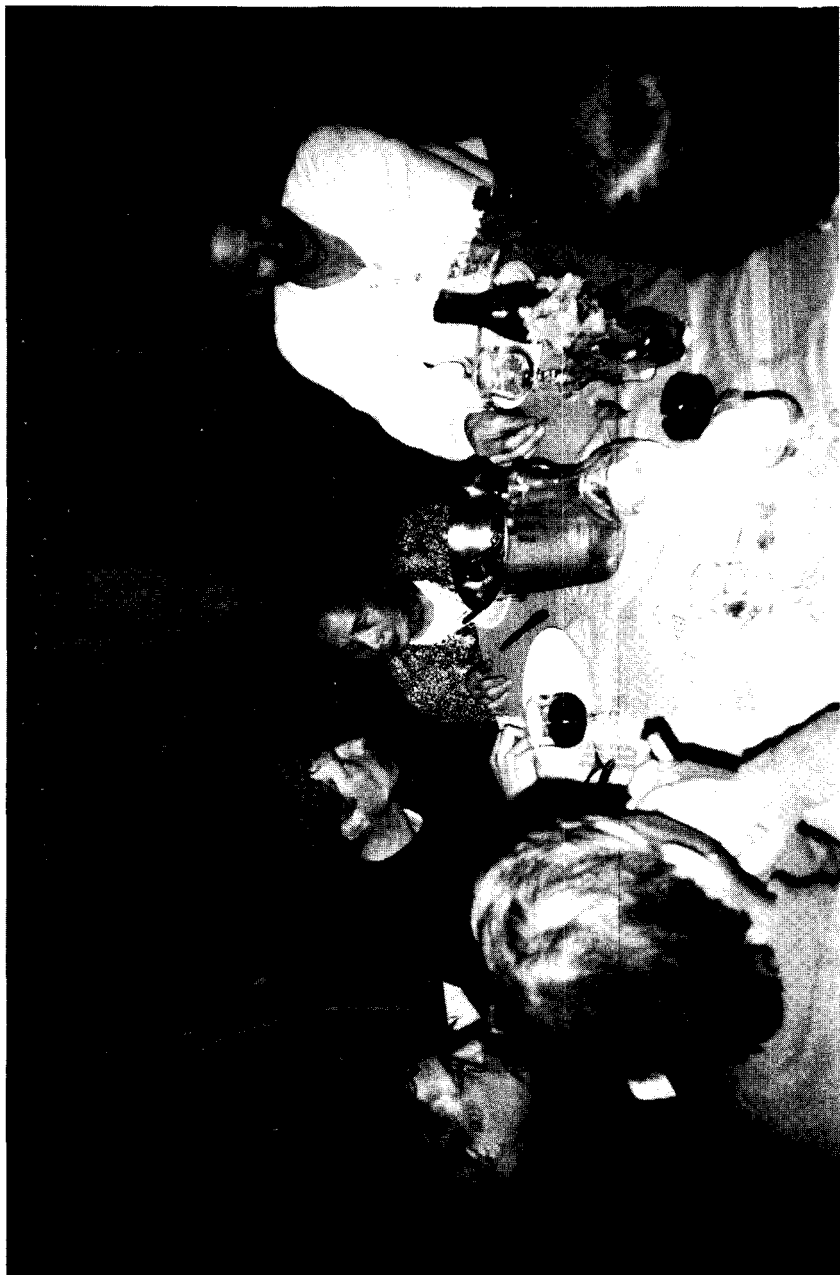
Dedicated to Jean-Pierre Wuthrick















Foreword

The XIth Moriond Workshop of the XXVIth Rencontres de Moriond was held at Les Arcs, Savoie (France) from January 26 to February 2, 1991. It was attended by 123 participants from 14 countries.

The main purpose of the Rencontres de Moriond was to discuss recent developments in contemporary physics and also to promote effective collaboration between experimentalists and theorists in similar fields. By bringing together a relatively small number of participants we hope to develop personal contacts as well as a more thorough and detailed discussion of the scientific contributions in an informal and friendly atmosphere.

The subject of this workshop focused on the tests of fundamental laws in physics and on the search for new and exotic phenomena. Special emphasis was given to the 17 Kev neutrino experiments, to general relativity and gravitational waves and to nonaccelerator physics : solar neutrinos, dark matter and tests of fundamental symmetries. The participation of physicists from various domains : astrophysics, atomic physics, particle physics and solid state physics allowed exchange of knowledge and technology between different fields and conferred to this workshop a frontier physics character.

The success of this workshop was due to the active participation of all participants, to the lively discussions following lectures, and to the efforts of the speakers in providing pedagogical and enlightening lectures.

I would like to thank all participants and programm committee members : A. Aspect, F. Boehm, G. Chardin, O. Fackler, J. Faller, E. Fischbach, G. Fontaine, G. Gerbier, G. Greene, B. Kayser, M. Mugge, R. Pain, S. Petcov, M. Spiro, J. Wilkerson and our regretted friend J. P. Wuthrick for preparing and organizing this workshop.

I am also grateful to MM. D. Touraille, E. Rocca-Serra and Ms N. Rocca-Serra for their hospitality at Les Arcs, and to the conference secretaries : M. Albera, G. Ambonati, A. Cherkaoui, S. Decaux and L. Norry, who have devoted much of their time and energy to the success of this meeting.

The 1991 Moriond workshop was sponsored by the Centre National de la Recherche Scientifique and by the Commissariat à l'Energie Atomique. We are deeply grateful for their financial support.

J. Trần Thanh Vân

Contents

I. SOLAR NEUTRINOS

Vignaud D.	Some facts and some dreams about solar models and solar neutrinos.	3
Smirnov A. Yu.	Berry phase and the solar neutrino problem.	13
Gavrin V. N. et al.	First measurement of the integral neutrino flux by the Soviet-American Gallium experiment (SAGE).	19
Vignaud D.	Report on the Gallex experiment.	29
Meroni E.	The Borexino project to study the solar neutrinos.	37
Lanou R. E.	Prospects for cryogenic detection of solar neutrinos.	41
Neumaier S. et al.	Feasibility studies of the geochemical ^{205}Tl solar neutrino experiment.	49
Akhmedov E. Kh.	Resonant spin-flavor precession and the solar-neutrino problem.	53
Smirnov A. Yu.	Present status of the resonant flavor conversion.	63

II. DOUBLE BETA DECAY AND NEUTRINO OSCILLATIONS

Barabash A. S. et al.	First results from the Soviet-American experiment on double beta decay of ^{100}Mo to the ^{100}Ru excited states.	77
Treichel M. et al.	Latest results on double beta decay and dark matter from the Gotthard Laboratory.	85
Piepkke A. et al.	Status of the Heidelberg-Moscow $\beta\beta$ -experiment using enriched ^{76}Ge .	91
Tabarelli de Fatis T.	A search for double beta decay of ^{136}Xe .	99
Pomansky A.A. et al.	New limit on rate of $2\nu\beta\beta$ decay of ^{136}Xe .	105
Avenier M.	Neutrino oscillations search at the Bugey reactors.	111
Perdereau O.	Final results on the Frejus proton decay experiment on atmospheric neutrinos.	117

Vannucci F.	Detection of the ν_{τ} .	123
Lendermann P. et al.	Scintillating fiber arrays for particle tracking.	129
Zacek G.	Scintillating fiber detectors for neutrino physics.	133
Bonn J. et al.	Performance Report on the Mainz tritium β -decay experiment.	137

III. THE 17 KEV NEUTRINO

Simpson J. J.	The 17-Kev neutrino.	145
Hime A. et al.	17-Kev neutrinos at Oxford.	151
Becker H. W. et al.	Experimental studies of the ^{35}S beta-spectrum anomalies and heavy neutrino admixture ?	159
Zlimen I.	Heavy neutrino emission in EC decay of ^{71}Ge .	165

IV. DARK MATTER, HIGH ENERGY ASTROPHYSICS

Zylberajch S.	Machos, Wimps or Dust : What is dark matter ?	173
Belli P. et al.	Direct detection of dark matter candidates.	185
Gaitskell R. J. et al.	Low temperature superconduction detectors for dark matter and solar neutrino experiments.	191
Tadsen A. et al.	The microwave enhanced bolometer.	195
Kainulainen K.	WIMPs and cosmology, unitarity and experiment.	199
Meyer H.	Origin and nature of cosmic rays and first results from HEGRA.	203
Lorentz E.	A new air Cerenkov array detector for the observation of extended air showers.	211
Ghia P. L. et al.	The EAS-TOP detector at Gran Sasso : recent results.	217
Fontaine G. et al.	Testing the multi-mirror array shower detection technique : status of the THEMISTOCLE experiment.	225
Salomon M. H. et al.	A cosmic background of high energy neutrinos from active galactic nuclei.	233
Moscoso L.	Cosmic neutrino detection with a water Cerenkov.	237

Ignatiev A. Yu.	Millicharged matter.	243
Altherr T.	Axions, plasmons and supernovae.	249

V. GRAVITATION

Schurr J.	A new method for testing Newton's gravitational law.	255
Heckel B. R.	A new test of the equivalence principle an update on the EOT-WASH experiment.	259
Yvert M.	The Virgo project.	265
Cornaz A. et al.	Determination of the gravitational constant G at an effective distance of 125 m.	273
Weber J.	Gravitational and neutrino antennas.	281

VI. PHYSICS AND COMPUTERS

Fredkin E.	A physicist's model of computation.	285
------------	-------------------------------------	-----

VII. TESTS OF FUNDAMENTAL SYMMETRIES

Sromicki J. et al.	Search for time reversal violation in the decay of polarized ^8Li .	303
Severijns N. et al.	Experimental search for extensions of the standard model by relative beta polarization measurements.	311
Toshev S.	Resonant amplification of T-violating effects in matter neutrino oscillations.	317
Iconomidou-Fayard L.	A new measurement of ϵ'/ϵ by the NA31 experiment.	323
Nolte E. et al.	Tests of the Pauli exclusion principle for nucleons and detection of $\beta\beta$ decay products with accelerator mass spectrometry.	331
Mzavia D. et al.	Search for lepton number violation π , μ in and τ decays.	337
Semertzidis Y.	Coherent production of pseudoscalars (axions) inside a dipole magnetic field.	343
He X. G.	Interference between the Aharonov-Bohm and Aharonov-Casher effects.	351

Pendlebury J. M.	Measuring the neutron lifetime using stored neutrons.	359
Last J.	Angular correlations in free neutron decay.	367
Dubbers D.	Search for neutron-antineutron oscillations at ILL.	371
Lamoureaux S. K.	The search for the neutron electric dipole moment : past, present and future.	379
Hinds E. A.	Search for time reversal symmetry violation in Thallium Fluoride using a jet source.	391
Hunter L. R.	Limits on the electron electric dipole moment from atoms.	397
Heckel B. R.	Tests of fundamental symmetries using atomic Hg vapor cells.	403
Gouanère M. et al.	Darmstadt hunting in γ -crystal interaction.	411
Aspect A.	Testing Bell's inequalities.	417
Suzuki Y.	Kamiokande II results on solar neutrinos and the superkamiokande experiment. (<i>this paper arrived too late to be inserted at the right place</i>).	429
VIII. SUMMARY AND CONCLUSIONS		
Ramsey N. F.	Summary talk on discrete symmetries and atomic or neutron systems.	441
Petcov S. T.	Impressions from Moriond '91.	449
<i>List of Participants</i>		455

SOLAR NEUTRINOS

Some facts and some dreams about solar models and solar neutrinos

D. Vignaud
DPhPE/SEPh
CEN Saclay
91191 Gif-sur-Yvette
France

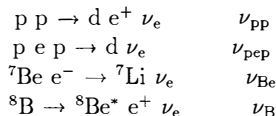
Abstract

A brief account of recent news about solar models and solar neutrino experiments is presented. The predictions of the most recent standard models are compared before emphasizing some difficulties for non standard models. The experimental results are given and some important projects are briefly presented. Finally the possible variation of the neutrino flux with time is discussed.

1. Introduction

Solar neutrino detection is a challenge for astrophysics (test of the standard model of the Sun and of the stars) and for particle physics (the observed deficiency may be due to neutrino oscillations). We do not provide in this short review a full account of solar models and solar neutrino experiments. We just emphasize some recent news which concern the solar models, and present briefly the experimental situation.

The Sun produces pure ν_e , via the four main reactions :



The corresponding ν_e energy spectrum is displayed in Fig. 1. It extends to 0.420 MeV for ν_{pp} and 14 MeV for ν_{B} . The relative amount of these contributions may depend on details of the solar model : central temperature, opacities, cross sections,... [1].

Solar neutrino experiments detect neutrinos via :

- W exchange processes (WEP) : $\nu_x + (A, Z) \rightarrow X^- + (A, Z+1)$. Such experiments are only sensitive to ν_e . The produced electron is almost isotropic and does not give information on the neutrino direction, but the electron energy spectrum reflects directly the neutrino energy spectrum.

- Z exchange processes (ZEP) : $\nu_x + A \rightarrow \nu_x + A^*$. The detection is insensitive to the neutrino flavour.

- elastic scattering on electron : $\nu_x + e^- \rightarrow \nu_x + e^-$. This reaction can occur via both WEP and ZEP for ν_e and only via ZEP for ν_μ and ν_τ . Moreover the cross section for the charged current process is about 6 times larger than for the neutral current process. The scattered electron keeps the direction of the neutrino but the electron energy spectrum does not directly reflect the neutrino energy spectrum.

We first compare the predictions of the most recent standard models before emphasizing some difficulties for non standard models. We then review the solar neutrino experimental results. The solar neutrino problem consists in the discrepancy between the neutrino flux observed by the detectors on earth (chlorine [2], Kamiokande [3] and maybe Sage [4]) and the neutrino flux predicted by standard solar models ([1], [5], [6],...) which is 2-4 times larger. We finally summarize the papers which appeared last year about the possible correlation of the solar neutrinos detected in the chlorine experiment and the solar cycle.

2. Solar models

Since 1964 Bahcall has advocated the construction of a "standard solar model" (SSM) and has, himself, greatly contributed to this project (see [1] for a recent review). He defines a SSM as the "result of the best physics and input parameters that are available". After the surprise of the low flux observed by the chlorine experiment [2] many other astrophysicists also built (standard and non standard) solar models. We just compare here the predictions of some SSM that we can call "reference" models, in the sense that

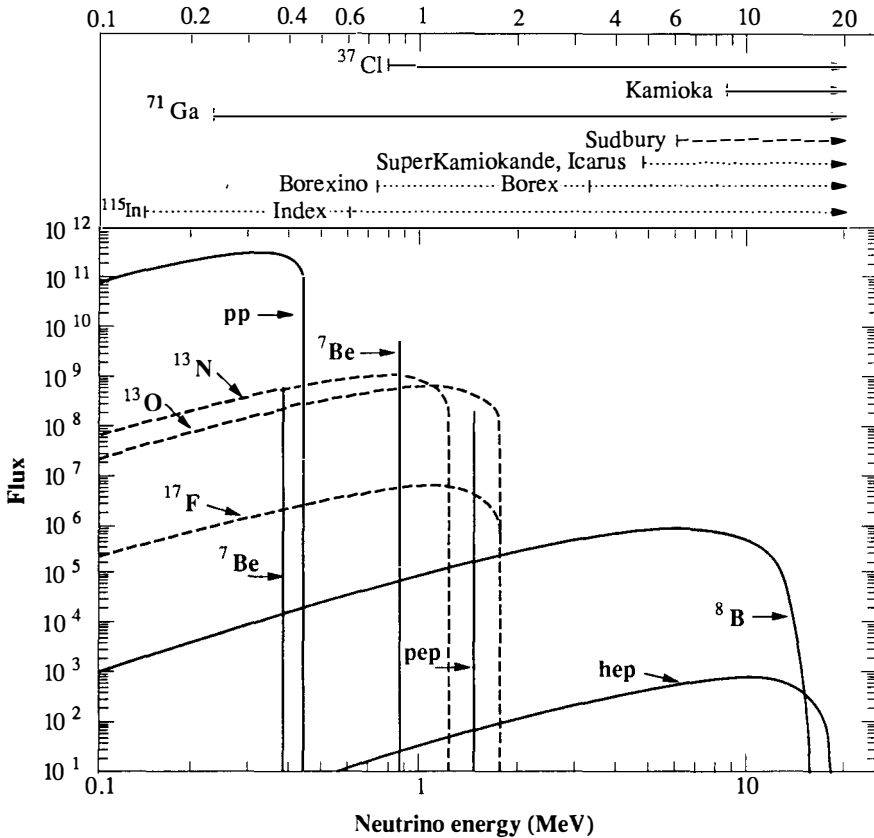


Figure 1 : Solar neutrino energy spectrum (adapted from [1]). Neutrino fluxes from continuum sources are in $\text{cm}^{-2} \text{s}^{-1} \text{MeV}^{-1}$. Line fluxes are in $\text{cm}^{-2} \text{s}^{-1}$. The insert above gives the sensitivity interval of the different detectors above the threshold. Full lines : existing detectors. Dashed lines : detectors under construction. Dotted lines : projects.

they reflect the best situation in the different fields of physics that are used as ingredients of the model. In 1990 a new one due to Sackmann et al. [6] was developed. We compare in the table 1 some relevant outputs for three reference models. Y and Z are respectively the primordial helium and heavy elements fraction in the Sun. The helium abundance Y is a free parameter of the model and Z is determined from surface observations. The number of SNU's for the chlorine and gallium detectors is the product of the neutrino flux and the detection cross section. A SNU corresponds to 10^{-36} capture/atom/second.

	Bahcall-Ulrich [1] (3σ error)	Turck-Chièze et al. [5]	Sackmann et al. [6]
Y (helium)	0.271	0.276 ± 0.012	0.278
Z (heavy elements)	0.0196	0.0197	0.0194
^8B flux ($\text{cm}^{-2}\text{s}^{-1}$)	$(5.8 \pm 1.9) 10^6$	$(3.8 \pm 1.1) 10^6$	$5.8 10^6$
Nb of SNU (^{37}Cl)	7.9 ± 2.6	5.8 ± 1.3	7.7
Nb of SNU (^{71}Ga)	132 ± 17	125 ± 5	125

Table 1 : Predictions from some standard solar models (SSM).

The luminosity of the Sun ($3.86 10^{33}$ erg/s after about 4.6 Gyr) is a common constraint. Other characteristics are very similar in the three models : the central temperature is $15.5 10^6$ K and the central density of about 147 g/cm^3 .

The main discrepancy between the model by Turck-Chièze et al. and the other comes from the cross section of the reaction $p + ^7\text{Be}$ in the core of the Sun and the treatment of opacities near the center [5].

There has been recently a new determination of the cross section for the primordial fusion reaction in the core of the Sun : $p p \rightarrow d e^+ \nu_e$. Gould and Guessoum used more accurate parameters for the deuteron wave function and for the weak-interaction coupling constant which comes from recent measurements of the n lifetime [7]. They found a cross section a little bit larger which induces a reduction of the ^8B flux by a factor 0.92. (This factor is not taken into account in the standard solar models described above).

Another point which is interesting to note is that progress on solar modelling comes largely from helioseismology. Helioseismologists have now developed a method to determine the solar helium abundance. Vorontsov et al., using the frequencies of solar acoustic oscillations sensitive to the behaviour of the speed of sound in the Sun's helium ionization zone found a value $Y = 0.25 \pm 0.01$ [8]. Dziembowski and Gough found 0.234 and 0.268 respectively [9]. The errors are still large but this work in progress is very promising.

About non standard models (i.e. solar models with some non standard or exotic physics) we just quote two recent papers which do not favour them. Elsworth et al. [10] found evidence from solar seismology against non-standard solar-core models (i.e. models with mixing or with WIMPs). Kaplan et al. [11] point out that cosmions are of no help in resolving the discrepancy between the sound speed calculated in standard models and that derived directly from helioseismology measurements.

3. Solar neutrino experiments

Table 2 summarizes the different existing detectors and some projects. The different reaction thresholds are also presented in Fig. 1.

reaction	reaction threshold	exp. technique name of the exp.	results
$\nu_e + {}^{37}\text{Cl} \rightarrow {}^{37}\text{Ar} + e^-$	0.814 MeV	radiochemical	2.19 ± 0.24 SNU
$\nu_e + e^- \rightarrow \nu_e + e^-$	none 7.5 MeV	Cerenkov, H ₂ O Kamiokande	(exp/model) model $0.46 \pm 0.05 \pm 0.06$ [1] $0.70 \pm 0.08 \pm 0.09$ [5]
$\nu_e + {}^{71}\text{Ga} \rightarrow {}^{71}\text{Ge} + e^-$	0.233 MeV	radiochemical Sage Gallex	< 74 SNU (90 % CL) 1991
$\nu_e + {}^{115}\text{In} \rightarrow {}^{115}\text{Sn} + e^-$	0.128 MeV	scintillator junctions,...	"dream" ?
$\nu_e + \text{D} \rightarrow e^- + \text{p} + \text{p}$	1.44 MeV	Cerenkov, D ₂ O Sudbury	1995
$\nu_e + {}^{11}\text{B}$	6 MeV	scintillator (Borex)	199?
$\nu_e + e^-$	none	Borexino	199?

Table 2 : Main solar neutrino detectors.

We describe briefly these detectors and their results, if any. The observed deficit for neutrinos is interpreted in the framework of neutrino oscillations through the MSW effect.

The radiochemical Davis chlorine detector in Homestake (600 tons) [2] counts ${}^{37}\text{Ar}$ atoms every two months. The cumulated result after 20 years of measurement shows a reduction by a factor 2-4 compared to the SSM. The real time Kamiokande experiment (fiducial volume of 680 tons in 2140 tons of water) [3] detects Cerenkov light emitted by electrons with a detection threshold of 7.5 MeV. The reduction factor is only a factor 2 or less, depending on the model. These two experiments, which detect mainly ν_B , have provided results which constitute the solar neutrino problem. We can mention here the difficulty to find an astrophysical explanation which could support both chlorine and Kamiokande results. An upscaled version of the chlorine experiment is planned in USSR (3000 tons of C_2Cl_4 in the Baksan Underground Laboratory) [12]. In Japan, a significant extension of Kamiokande is proposed (SuperKamiokande [13]) : 50000 tons of pure water with thousands of photomultipliers. The threshold for electrons could be lowered to 5 MeV, giving about 20 solar neutrinos per day in a 22000 tons fiducial volume.

There are two radiochemical gallium experiments. Their main purpose is the detection of the neutrinos produced in the primordial pp fusion reaction in the core of the Sun, the ν_{pp} . The first one, Sage, in Baksan, uses 60 tons of metallic Ga [4]. The very surprising preliminary results were presented last summer and have been confirmed here. They quote an upper limit of (74 SNU / A) at 90% CL, where A is the ratio between the recovery efficiencies for ${}^{71}\text{Ge}$ and for natural germanium. Gallex, in the Gran Sasso Underground Laboratory, uses 30 tons of gallium in the form of GaCl_3 [14]. It should present its first results in 1991.

The idea of an indium target is from Raghavan. The threshold is so low (128 keV) that it is very sensitive to ν_{pp} . However the natural radioactivity of ${}^{115}\text{In}$ ($E_{\text{max}}=494$ keV) is a formidable background in the low energy region and none of the many projects could fight against it. Low temperature indium detectors are currently being investigated by various groups, with different approaches (superconducting junctions, super-

conducting granules) [15]. Some recent progresses on low temperature neutrino detectors are reviewed by Lanou [16].

Several real time experiments (Sudbury, Borex,...) aim to measure the ν_B contribution both via WEP and ZEP. They can also detect the elastic interaction on electrons.

The Sudbury experiment (Canada-USA-UK) [17], recently approved, consists in 1000 tons of heavy water D_2O surrounded by 4 m of purified light water H_2O . The Cerenkov light emitted by the electrons is detected by photomultipliers as in the Kamiokande experiment. The detector will be installed in a deep mine near Sudbury in Canada (2070 m underground). The main difficulty of this experiment is to reduce the backgrounds at a very low level. The use of low activity materials and the purity problem of the target is essential for all similar experiments.

The Borex project [18] is a large tank containing 2000 tons of borated liquid scintillator (200 tons of ^{11}B) and immersed in pure water. It could be installed by an USA-Italy collaboration in the Gran Sasso Underground Laboratory. A major difficulty is also to obtain a very pure liquid scintillator. A first step could be the so-called Borexino detector which, with a smaller amount of scintillator could detect the ν_{Be} via the elastic ν_e electron reaction.

Is there any satisfactory interpretation of the low result observed by the chlorine, Kamiokande and maybe Sage experiments? The answer is yes : the MSW effect, i.e. the resonant flavour conversion of ν_e into ν_μ or ν_τ in the matter of the Sun can explain simultaneously the results of the three experiments. If we have to be very sceptical of the "quick" interpretation by Bahcall and Bethe [19] who did not take into account the experimental errors, we can isolate a relatively large area in the oscillation parameters (Δm^2 , $\sin^2 2\theta$) plane which accomodates the chlorine, Kamiokande and Sage experiments (see for example the discussion by Smirnov [20]). This seductive interpretation would save the SSM and would be welcome by particle physicists.

Last year, Spiro and Vignaud, by combining the chlorine, Kamiokande and forthcoming gallium experiments, tried to show how to pinpoint neutrino oscillations almost independently of solar models [21]. They stressed that neutrino oscillations would be unavoidable at the 2σ level if the result of the gallium experiments was outside the range 82-118 SNU. The preliminary result of the Sage experiment would indicate that we are in this situation. Some confirmation by Sage and by Gallex is however needed before being so affirmative.

4. Variation of the neutrino flux with time

Is there any variation of the solar neutrino flux with time? A lot of papers appeared on this topic during the last year. We concentrate here on the variation which could be correlated with the 11-year solar cycle, leaving out seasonal, day-night or others.

Concerning the data themselves, they have been presented by Davis and Lande for the chlorine experiment [2] and correspond to the period between 1970 and 1989, and by the Kamiokande collaboration [3] for the period 1987-1990. To summarize, the chlorine experiment shows a qualitative anticorrelation between the sunspot numbers which represent the solar activity (11-year cycle) and the number of neutrinos detected (see

[2] and Fig. 2). The Kamiokande experiment does not see any day-night or semiannual variations, within statistical errors [22]. (A day-night effect could correspond to a terrestrial regeneration of the neutrinos through the MSW effect).

Several sophisticated statistical analyses were performed by different authors on the chlorine data and are summarized in table 3.

	Bahcall et al. [23]	Filippone et al. [24]	Krauss [25]	Bieber et al. [26]
Years studied	1970-1989	1970-1989	1977-1988	1970-1989
³⁷ Cl	•	•	•	•
Sunspots	•	•	•	•
p modes (helioseismology)			•	
cosmic ray monitor				•
Confidence level	0.987-0.991	0.993	0.97-0.999	0.991
Start of correl.	1979	best fit T = 4.7 yr	1977	1979

Table 3 : Comparison of different statistical analyses of the possible correlation of the chlorine results with sunspots and other. The big dot means that the corresponding observation has been studied.

The statistical significance of all the analyses seems very high, with confidence levels around 0.99 or even higher. Bahcall and Press establish a correlation which was rejected in a previous analysis with a different technique three years earlier [27]. The particularity of the work by Krauss [25] is to correlate the modulation of the neutrino signal not only with the sunspots number but also with the solar cycle variation in p-mode acoustic spectra. Bieber et al. [26] explain that the strength of the correlation rises when a semiannual variation is included. They exclude a correlation with a cosmic-ray monitor. Fiorentini and Mezzorani [28], who are not quoted in table 3, tried a parametrization of the argon rate production which is proportional to $\cos^2(f\sqrt{N_{ss}})$ (N_{ss} is the number of sunspots) instead of a linear parametrization and find also a correlation.

There are however some strange things. First the correlation between the sunspots and the argon production starts suddenly in 1979 as shown by Bieber et al. [26] and indirectly by Bahcall and Press [23] who separate the data in two periods. Second, if the period of the oscillation for the chlorine data is left free, Filippone and Vogel fit a value $T = 4.7$ year, which does not correspond to the 11-year period of the sunspots. I would like to add that the correlation looks more or less clear if there is a line to guide the eye, but the errors for each run are so large that the full plot is not so evident. One could assume that some underestimation of the errors could lead to correlations that are not real. If the community is not yet convinced, it is nevertheless necessary to investigate this point which would constitute a real surprise.

What would be the interpretation of such a variation of the solar neutrino flux with the 11-year solar cycle? The most natural one would be that the neutrino has a magnetic moment which precesses in the solar magnetic field (a left-handed ν_e would be transformed into a right-handed sterile one). The reader is referred to Akhmedov [29] who develops also the possibility of a resonant spin-flavor precession of neutrinos, or to

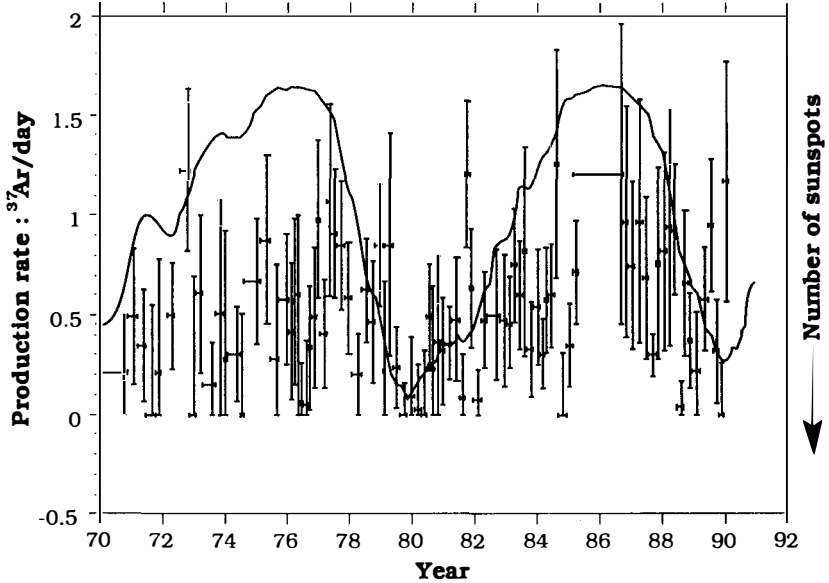


Figure 2 : Neutrino detection rate (^{37}Ar production) versus year in the chlorine experiment [2]. The full line corresponds to the number of sunspots (this number is inverted, i.e. the small number are at the top, and the scale is arbitrary).

the recent paper by Minakata et al. [30]. All these interpretations necessitate a magnetic moment of the neutrino of about 10^{-10} Bohr magneton μ_B and a solar magnetic field of several kG. Note that such a magnetic moment appears to be excluded by SN1987A.

I could conclude that further investigation is needed, which one needs mainly is more statistics. Three forthcoming experiments are well placed to do this : Sudbury, the chlorine experiment in Baksan and SuperKamiokande. The answer to this question will not be immediate : several years of data taking will be necessary to confirm or infirm the correlation.

5. Conclusion

The solar neutrino problem is the observed deficit of ν_E and/or ν_{Be} in the chlorine and Kamiokande experiments. The preliminary result of the Sage experiment seems to indicate that there is also a deficit of the ν_{pp} which are produced in the primordial fusion reaction in the core of the Sun. A confirmation or infirmation by Sage and Gallex is expected this year. The measurement of the neutrino spectrum and the observation of neutrinos via Z exchange processes will be done in the future by the Sudbury and possibly Borex. The correlation of the solar neutrino flux with the 11-year solar cycle has been widely studied last year. There is some statistical evidence for such a

correlation, but a confirmation by a large statistics experiment (chlorine in USSR or SuperKamiokande) would be welcome.

A new standard model by Sackmann et al. gives predictions similar to that of Bahcall and Ulrich or Turck-Chièze et al.. The helioseismology will constrain more severely the center of the Sun in the near future and makes more and more difficult several classes of non standard models, like cosmions.

It is difficult to find an astrophysical explanation which would support both the chlorine and Kamiokande experiments. The most simple explanation of the observed deficit is today the MSW effect, i.e. a transformation of ν_e into ν_μ or ν_τ in the matter of the Sun. Particle physicists would be very happy with such an interpretation.

Acknowledgements : It is a pleasure to thank M. Cribier, T. Kirsten, J. Rich, M. Spiro and S. Turck-Chièze for discussions and comments.

References

- [1] J. N. Bahcall and R. K. Ulrich, Rev. of Mod. Phys. 60 (1988) 297
J. N. Bahcall, Neutrino Astrophysics, Cambridge University Press, 1989
- [2] R. Davis et al., Proc. of the 21st ICRC, Adelaide, 6-19 January 1990, ed. by R.J. Protheroe, vol. 12, p. 143
K. Landé, talk at ν' 90 Conference, Geneva, June 1990
- [3] K. S. Hirata et al., Phys. Rev. Lett. 65 (1990) 1297
Y. Suzuki, these proceedings
- [4] V. N. Gavrin, ν' 90 Conference, Nucl. Phys. B Proc., to appear
V. N. Gavrin, these proceedings
- [5] S. Turck-Chièze, S. Cahen, M. Cassé and C. Doom, Ap. J. 335 (1988) 415
S. Turck-Chièze, Proc. of the 121st IAU Colloquium, "Inside the Sun", Versailles (1989), ed. by G. Berthomieu and M. Cribier, Kluwer Academic Pub., p. 125
S. Turck-Chièze, in "New and Exotic Phenomena", Les Arcs, January 1990, ed. by O. Fackler and J. Tran Thanh Van, p. 571
- [6] I. J. Sackmann, A. I. Boothroyd and W. A. Fowler, Ap. J. 360 (1990) 727
- [7] R. J. Gould and N. Guessoum, Ap. J. 359 (1990) L67
- [8] S. V. Vorontsov, V. A. Baturin and A. A. Pamyatnykh, Nature 349 (1991) 49
- [9] W. Dziembowski, preprint (1991), D. O. Gough, preprint (1991)
I thank G. Berthomieu for providing me these results
- [10] Y. Elsworth, R. Howe, G. R. Isaak, C. P. McLeod and R. New, Nature 347 (1990) 536
- [11] J. Kaplan, F. Martin, C. Tao and S. Turck-Chièze, "A critical look at cosmions", to appear in Ap. J.
- [12] A. Pomansky, these proceedings

- [13] Y. Suzuki, these proceedings
- [14] T. Kirsten, ν' 90 Conference, Nucl. Phys. B Proc., to appear
M. Cribier, Proc. of the 25th Int. Conf. on High Energy Physics, Singapore, 1990, to appear,
D. Vignaud, these proceedings
- [15] N. E. Booth, in Superconducting and Low-Temperature Particle detectors, G. Waysand and
G. Chardin ed., Elsevier Science Pub. (1989) p. 69
- [16] R. Lanou, these proceedings
- [17] G. T. Ewan et al., Sudbury Neutrino Observatory Proposal, SNO 87-12, October, 1987 ,
G. Aardsma et al., Phys. Lett. B194 (1987) 321
J. J. Simpson, these proceedings
- [18] R. S. Raghavan and S. Pakvasa, Phys. Rev. D37 (1988) 849
R. S. Raghavan et al., Design concept for Borex, AT&T Bell Labs report 88-01, March 31,
1988 , E. Meroni, these proceedings
- [19] J. N. Bahcall and H. A. Bethe, Phys. Rev. Lett. 65 (1990) 2233
- [20] A. Yu. Smirnov, these proceedings
S. P. Mikheyev and A. Yu. Smirnov, Nuovo Cimento 9C (1986) 17
L. Wolfenstein, Phys. Rev. D17 (1978) 2369
- [21] M. Spiro and D. Vignaud, Phys. Lett. B242 (1990) 279
- [22] K. S. Hirata et al., Phys. Rev. Lett. 66 (1991) 9
- [23] J. N. Bahcall and W. H. Press, submitted to Ap. J.
- [24] B. W. Filippone and P. Vogel, Phys. Lett. B246 (1990) 546
- [25] L. M. Krauss, Nature 348 (1990) 403
- [26] J. W. Bieber, D. Seckel, T. Stanev and G. Steigman, Nature 348 (1990) 407
- [27] J. N. Bahcall, G. B. Field and W. H. Press, Ap. J. 320 (1987) L69
- [28] G. Fiorentini and G. Mezzorani, Phys. Lett. B253 (1991) 181
- [29] E. Kh. Akhmedov, "On time variations of the solar neutrino flux", Report IAE-5017/1
(January 1990) , E. Kh. Akhmedov, Phys. Lett. B257 (1991) 163
E. Kh. Akhmedov, these proceedings
- [30] H. Minakata and H. Nunokawa, Phys. Rev. D43 (1991) 297

BERRY PHASE AND THE SOLAR NEUTRINO PROBLEM

A.Yu.Smirnov

Institute for Nuclear Research, Academy of Sciences
of the USSR. 117312 Moscow, USSR

ABSTRACT

The influence of geometrical phase on neutrino spin-precession in the magnetic field is considered. At large geometrical phase velocity the depth of precession and therefore the probability of $\nu_L \rightarrow \nu_R$ transition are strongly suppressed in contradiction with J.Vidal and J.Wudka result. We propose the effect of resonant spin conversion induced by the geometrical phase, and consider its application to solar neutrinos.

Appearance of the Berry (geometrical) phase¹⁾ in the neutrino spin-precession is related to the rotation of the magnetic field, \vec{B} , in the transverse (with respect to neutrino trajectory) plane²⁻⁴⁾. More precisely, the geometrical phase is determined by the angle of B - rotation, ϕ , and adds to the usual dynamic phase. It may influence on the solar ν_{eL} -flux²⁻⁴⁾. And moreover, according to J.Vidal and J.Wudka paper⁴⁾ the geometrical phase, being much larger than the dynamic one, may solve the solar neutrino problem even at small field strength: $B \leq 10^3 \text{G}$ and small magnetic moment: $\mu_\nu \leq 10^{-13} \mu_B$ (μ_B is the Bohr magneton); compare with usual VVO - scenario⁵⁾.

In this paper we show that the result by J.Vidal and J.Wudka is incorrect. New effect - the resonant spin conversion, induced by the geometrical phase, is proposed.

Consider the system of the left, ν_L , and the right, ν_R , neutrinos, $\vec{\nu}_S = (\nu_L, \nu_R)$, with magnetic moment, evolving in matter and in the transverse magnetic field. Let the field rotates on the neutrino way in the transverse plane: $\vec{B} = B_x + iB_y = B e^{i\phi}$, $\phi = \phi(t)$. Then the evolution equation for $\vec{\nu}_S$ can be written as

$$i \frac{d\vec{\nu}_S}{dt} = \hat{H} \vec{\nu}_S, \quad \hat{H} = \begin{pmatrix} V/2 & \mu_\nu B e^{-i\phi} \\ \mu_\nu B e^{i\phi} & -V/2 \end{pmatrix} \quad (1)$$

where $V(t)$ is the ν_L - and ν_R - levels splitting due to interactions with matter and due to possible mass difference:

$$V = \sqrt{2} G_F n^{\text{eff}} - \frac{\Delta m^2}{2E} \quad (2)$$

here G_F is the Fermi constant, $\Delta m^2 = m^2(\nu_L) - m^2(\nu_R)$, E is the neutrino energy and n^{eff} is the effective concentration of particles interacting with neutrinos: $n^{\text{eff}} = n_e - n_n$ for $\nu_{eL} - \bar{\nu}_{\mu R}$ and $n_e - n_n/2$ for $\nu_{eL} - \nu_{eR}$, n_e and n_n are the concentrations of electrons and neutrons correspondently. The imaginary part of \hat{H}

can be eliminated by the transformation $\vec{\nu}_S = \hat{U}\vec{\nu}'_S$, where $\hat{U} = \text{diag}[e^{-i\phi/2}, e^{i\phi/2}]$ and the evolution equation for $\vec{\nu}'_S$ is:

$$i\frac{d\vec{\nu}'_S}{dt} = \left[\begin{pmatrix} V/2 & \mu_\nu B \\ \mu_\nu B & -V/2 \end{pmatrix} + \frac{\dot{\phi}}{2} \begin{pmatrix} -1 & 0 \\ 0 & 1 \end{pmatrix} \right] \vec{\nu}'_S \quad (3)$$

$\dot{\phi} = d\phi/dt$ is the geometrical phase velocity. The mixing angle of $\vec{\nu}'_S$, θ_m , depends now on $\dot{\phi}$: $\tan 2\theta_m = 2\mu_\nu B / (V - \dot{\phi})$. Since \hat{U} is diagonal, the transition probabilities for $\vec{\nu}_S$ and $\vec{\nu}'_S$ are the same.

For constant parameters n^{eff} , B , $\dot{\phi}$ (B rotates steady) the equation (3) has the analytic solution. The survival probability (the probability of $\nu_L \rightarrow \nu_L$ transition) can be written as $P = \bar{P} + (A_P/2)\cos(2\pi t/l_P)$ where the depth, A_P , and the length, l_P , of precession are

$$A_P = \sin^2 2\theta_m = \frac{(2\mu_\nu B)^2}{(V - \dot{\phi})^2 + (2\mu_\nu B)^2} \quad (4)$$

$$2\pi l_P^{-1} = \Delta E = [(V - \dot{\phi})^2 + (2\mu_\nu B)^2]^{1/2} \quad (5)$$

and the average probability equals $\bar{P} = 1 - A_P/2$. Eqs. (4,5) generalize the results obtained in³⁾ for precession in matter.

If the matter effect and mass splitting are small, $V \ll \dot{\phi}$, then the depth (4) can be rewritten as $A_P = \dot{\phi}_{\text{dyn}} / (\dot{\phi}^2 + \dot{\phi}_{\text{dyn}}^2)$, where $\dot{\phi}_{\text{dyn}} = 2\mu_\nu B$ is the dynamic phase velocity. At $\dot{\phi} \gg \dot{\phi}_{\text{dyn}}$ (the case considered in³⁾) the depth of precession turns out to be very small: $A_P \approx (\dot{\phi}_{\text{dyn}}/\dot{\phi})^2 \ll 1$, i.e. large geometrical phase velocity suppresses the depth of precession and consequently the $\nu_L \rightarrow \nu_R$ transition in spite of large total phase. In the opposite case $\dot{\phi} \leq \dot{\phi}_{\text{dyn}}$ the depth is not suppressed but the geometrical phase does not exceed the dynamic one. In paper³⁾ the dependence of the precession depth on $\dot{\phi}$ is missed, so the depth turns out to be unsuppressed even at large $\dot{\phi}$. (The error comes from omission of

the proportional to $\dot{\phi}$ nondiagonal terms in equation for the eigenstates of the Hamiltonian \hat{H} (1)).

Geometrical phase may induce the resonant conversion. At $V = \dot{\phi}$ or

$$\sqrt{2}G_F n^{\text{eff}} - \frac{\Delta m^2}{2E} = \dot{\phi} \quad (6)$$

the mixing θ_m becomes maximal, so the equality (6) is nothing but the resonance condition⁶⁾. According to (6) the geometrical phase velocity shifts the resonance of spin-flavor precession⁷⁾ in E or n^{eff} scales. Essentially new situation realizes for Dirac or Zeldovich-Konopinski-Mahmoud (ZKM) neutrinos. In this case the ν_L - ν_R mass splitting is zero ($\Delta m^2 = 0$), and at $\dot{\phi} = 0$ there is no level crossing inside the Sun at all: $n^{\text{eff}} > 0$. Nonzero geometrical phase velocity can compensate the matter effect and

the resonance condition turns out to be fulfilled: $\sqrt{2}G_F n^{\text{eff}}(t) = \dot{\phi}(t)$. This condition does not depend on the neutrino energy, and moreover it can be satisfied only at definite direction of \vec{B} -field rotation, namely at $\dot{\phi} > 0$, when $n^{\text{eff}} > 0$. Such an asymmetry is related to the difference in interactions of the left (helicity $-1/2$) and the right (helicity $+1/2$) components of neutrinos.

The level crossing⁷⁾ at monotonous density change (n^{eff}) and at slowly enough change of $\dot{\phi}$ results in the resonant spin conversion: $\nu_L \rightarrow \nu_R$. Its efficiency depends on the adiabaticity⁶⁾. The adiabaticity condition ($\Delta E \gg \dot{\theta}_m$ ⁶⁾) in resonance ($V = \dot{\phi}$) is

$$\frac{2(2\mu_\nu B)^2}{\sqrt{2}G_F n^{\text{eff}} - \dot{\phi}} \gg 1 \quad (7)$$

At $\dot{\phi}$ the geometrical phase disappears from (7). At $n^{\text{eff}} < 0$ the negative $\dot{\phi}$ improves the adiabaticity.

Consider the application to the Sun. The rotation of \vec{B} on the way of neutrino may be stipulated by that the magnetic force lines

of the toroidal field form the helixes, which wind around torii³⁾. Let us evaluate the angle of rotation, $\Delta\phi$, needed for resonant conversion. Suppose the resonance takes place in the layer at $R = 0.8 R_{\odot}$ (or $R = 0.9 R_{\odot}$), where the density is 0.06 g/cm^3 (0.015 g/cm^3), R_{\odot} is the Sun radius. Then it follows from (6) (at $\Delta m^2 = 0$), that $\dot{\phi} = 2.2 \cdot 10^{-10} \text{ cm}^{-1}$ ($0.55 \cdot 10^{-10} \text{ cm}^{-1}$). Consequently for the distance $\Delta R = 0.1 R_{\odot}$ and for steady rotation one finds $\Delta\phi = \dot{\phi} \Delta R = \pi/2$ ($\pi/8$).

If $\dot{\phi}$ is constant, the effect of conversion induced by the geometrical phase coincides with that, calculated for the spin-flavor conversion⁸⁾ at $\Delta m^2/2E = \dot{\phi}$. So for the corresponding survival probabilities, P_{geom} and $P_{\text{s-f}}$, one has $P_{\text{geom}}(\dot{\phi}) = P_{\text{s-f}}(E/\Delta m^2 = 1/(2\dot{\phi}))$, and P_{geom} does not depend on E .

If the magnetic field twists in different directions in southern and in northern hemispheres, then the resonant conversion takes place only in the first or in the second half-year and the annual variations are expected. If the directions are the same, then one expects the semiannual variations. Also the anticorrelations of ν -signals with solar activity can be reproduced⁵⁾.

In conclusion, in presence of rotating field the depth of precession depends on the geometrical phase velocity, so that at large $\dot{\phi}$ the depth is strongly suppressed: $A_p \propto 1/\dot{\phi}^2$ and the transformation $\nu_L \rightarrow \nu_R$ is very small in contrast with result of⁴⁾. No essential gain in $\mu_{\nu} B$ is achieved with $\dot{\phi}$. Geometrical phase may induce the resonant spin conversion of Dirac or ZKM neutrinos inside the Sun.

Acknowledgement.

The author is grateful to Professor Ya.A.Smorodinski, who in

1986 for the first time pointed out on the possibility of Berry phase effect in mixed neutrino system.

References

- [1] M.Berry, Proc.Roy.Soc. A362 (1984) 45.
- [2] J.Wudka and J.Vidal, Univ. of California preprint UCD-88-40 (November 1988).
- [3] C.Aneziris and J.Schechter, Syracuse Univ. preprint SU-4228-449 (August 1990).
- [4] J.Vidal and J.Wudka, Phys.Lett. B249 (1990) 473.
- [5] M.B.Voloshin and M.I.Vysotsky, Sov.J.Nucl.Phys. 44 (1986) 544; L.B.Okun, M.B.Voloshin and M.I.Vysotsky, Sov.Phys.JETP 64 (1986) 446.
- [6] S.P.Mikheyev and A.Yu.Smirnov, Sov.J.Nucl.Phys. 42 (1985) 913; A.Yu.Smirnov, Proc. of the Int.Conf. "Neutrino-88", Boston, June 1988, Eds. J.Schneps, T.Kafka, W.A.Mann, Pran Nath, p.123.
- [7] C.-S.Lim and W.J.Marciano, Phys.Rev. D37 (1988) 1368; E.Kh.Akhmedov, Phys.Lett. B213 (1988) 64.
- [8] E.Kh.Akhmedov and O.V.Bychuk, ZhETF 95 (1989) 442
P.I.Krastev and A.Yu.Smirnov, Z.Phys. C (1991) to be published.

FIRST MEASUREMENT OF THE INTEGRAL SOLAR NEUTRINO FLUX BY THE
SOVIET-AMERICAN GALLIUM EXPERIMENT (SAGE)

V.N.Gavrin

*Institute for Nuclear Research of the Academy of Sciences of
the USSR, Moscow 117312, USSR*

SAGE Collaboration:

A.I.Abazov, O.L.Anosov, E.L.Faizov, V.N.Gavrin, A.V.Kalikhov,
T.V.Knodel, I.I.Knyshenko, V.N.Kornoukhov, S.A.Mezentseva,
I.N.Mirmov, A.V.Ostrinsky, A.M.Pshukhov, N.E.Revzin,
A.A.Shikhin, P.V.Timofeyev, E.P.Veretenkin, V.M.Vermul, and
G.T.Zatsepin; *Institute for Nuclear Research, Academy of
Sciences, USSR, Moscow 117312, USSR.*

T.J.Bowles, B.T.Cleveland, S.R.Elliott, H.A.O'Brien, D.L.Wark,
and J.F.Wilkerson; *Los Alamos National Laboratory, Los Alamos,
NM 87545 USA.*

R.Davis, Jr. and K.Lande; *University of Pennsylvania,
Philadelphia, PA 19104 USA.*

M.L.Cherry; *Louisiana State University, Baton Rouge, LA 70803
USA.*

R.T.Kouzes; *Princeton University, Princeton, NJ 08544 USA*

ABSTRACT

A radiochemical ^{71}Ga - ^{71}Ge experiment to determine the integral flux of neutrinos from the Sun has been constructed at the Baksan Neutrino Observatory INR AS USSR. Five measurements with 30 tons of Gallium made during first half of 1990 indicate that the total flux is less than 50 SNU (68% CL), 74 SNU (95% CL).

INTRODUCTION

Forty years ago the inverse beta-decay of ^{37}Cl was proposed to measure the solar neutrino flux $^{1,2)}$. Such a measurement was initiated in the 1960's in the Homestake gold mine in the USA. The measured value in the Chlorine experiment averaged over 1970-1988 was $2.2 \pm 0.3 (1\sigma)$ SNU $^3)$ (1 SNU = 10^{-36} captures per target atom per second). Recent calculated values of the flux are $7.9 \pm 2.6 (3\sigma)$ SNU in the Bahcall and Ulrich standard solar model (SSM) $^4)$. This deficit has now been corroborated by the Kamiokande II Water Cherenkov experiment $^5)$ in Japan which observed only $0.46 \pm 0.05 \pm 0.06$ of the flux predicted by the Bahcall-Ulrich SSM. in fare agreement with the Chlorine result of last years.

The low energy neutrinos produced in the proton-proton fusion in the Sun. which account for more than 90% of solar neutrinos, are far below the threshold of the Chlorine and Kamiokande experiments, which are primarily sensitive to the high energy ^8B solar neutrinos whose production rate depends critically on the core temperature of the Sun. The p-p neutrinos production rate in the Sun is fundamentally linked to the observed solar luminosity. and is insensitive to alteration in the Solar Models.

A radiochemical experiment using ^{71}Ga $^6)$ as the capture material provides a feasible means to measure the p-p neutrino flux. The SSM predicts $^4)$ that the total expected capture rate in ^{71}Ga is 132^{+20}_{-17} SNU, with the dominant contribution (71 SNU) from the p-p neutrinos. Observation of significantly less than this would be difficult to explain without invoking new

neutrino physics. This paper will present the results of initial measurements with a detection system based on neutrino capture by ^{71}Ga .

THE BAKSAN GALLIUM EXPERIMENT

The Soviet-American Gallium Solar Neutrino Experiment (SAGE) is situated in an underground laboratory specially built in the Baksan Valley of the Northern Caucasus, USSR. The laboratory is 60m long, 10m wide, and 12m high. It is located 3.5km from the entrance of a horizontal adit driven into the side of Mount Andvrchi, and has an overhead shielding of about 4700 mwe.

Chemistry

The experiment exploits a radiochemical procedure. The Ga metal about 30 tons, kept molten ($\sim 30^\circ\text{C}$) in four chemical reactors, each with internal volume 2m^3 and lined with teflon. The process of extraction of ^{71}Ge has been described in detail elsewhere⁷⁾ and will only briefly be described here. At the beginning of each run, approximately 120 microgrammes of natural Ge carrier is added to each reactor in the form of solid Ga-Ge alloy. After a suitable exposure interval (typically 3-4 weeks), the Ge carrier and any ^{71}Ge atoms that have been produced by neutrino capture are chemically extracted from the gallium. The extraction procedure concentrates the carrier and ^{71}Ge atoms from the Ga metal to 100 ml of final solution. From

this final solution. the counting gas GeH_4 (Germane) is synthesized. The efficiency of extraction of Ge from the reactors is measured in two stages of the extraction procedure by atomic absorption analysis. A final determination of the quantity of Ge is made by measuring the volume of the synthesized GeH_4 . The overall extraction efficiency is typically 80%. The uncertainty in the extraction efficiency is typically $\pm 6\%$.

The GeH_4 is mixed with measured quantity of Xe, and is inserted into a low-background proportional counter with an internal volume of about 0.75cm^3 .

Counting

The proportional counter is placed in the well of a NaI detector inside a large passive shield and counted for 2-3 months. The counting of the ^{71}Ge decays has been described in detail elsewhere⁷⁾. The number of ^{71}Ge atoms is determined by detecting the Auger electrons and/or X rays in the K- and L-peaks of Ge (at 10.4 and 1.2 KeV respectively) that are produced by ^{71}Ge decay. Due to considerably higher background in the L-peak, only the K-peak can be used in the analysis presented here.

Pulse shape discrimination based on risetime measurements is used to separate the ^{71}Ge decays from the background. In contrast to the localized ionization produced by Auger electrons or X rays from ^{71}Ge decay the background radioactivity primarily produced fast electrons in the counter which produced extended ionization. Pulses from the counter are

differentiated with a time constant of 10 ns. The amplitude of the differentiated pulse (ADP) is proportional to the product of the amplitude and the inverse of the rise-time of the pulse. For every event in the counter, the energy, the amplitude of the differentiated pulse, the time, and any associated NaI signal are recorded. The total background rate of selected counters from 0.7/13.0 KeV is approximately 1.5 cds/day. The counter is calibrated at one month intervals using an external ^{55}Fe source, which illuminates the central part of the counter through a thin side window. The ^{55}Fe calibration is used to generate an acceptance window in a two-dimensional plot of ADP/energy versus energy. The acceptance cuts in energy and in ADP/energy are both 95%. The measured total counting efficiency is about 40%. This efficiency includes geometrical effects inside the counter. The position of the acceptance window for the ^{71}Ge K-peak is calculated by extrapolating from the ^{55}Fe -peak. The extrapolation procedure was checked by filling a counter with $^{71}\text{GeH}_4$ together with the standard counter gas. This data clearly shows that the extrapolation method used correctly includes the ^{71}Ge events in the window.

The analysis searches for events which are within the ^{71}Ge K-peak acceptance window and which have no NaI activity in coincidence. A maximum likelihood analysis⁸⁾ is then carried out on these events by fitting the time distribution to an 11.4 days halflife exponential decay plus a constant ray background.

The SSM predicts a production rate of $1.2 \text{ }^{71}\text{Ge}$ atoms/day in 30 tons of Ga. The mean number of detected ^{71}Ge atoms expected in each run is 4.0.

Background

The main source of ^{71}Ge in the reactors other than from solar neutrinos is from protons arising as secondary particles produced by external neutrons, internal radioactivity, and cosmic-ray muons. The measurements and calculation of these background channels indicate that the total background production rate of ^{71}Ge is less than 2.5% of the SSM predicted rate.

The main task at the beginning of the experiment was the need to remove from the Ga long-lived ^{68}Ge (half-life 287 days) produced by cosmic rays while the Ga was on the surface. The ^{68}Ge activity in the first extraction from 30 tons of Ga was 7700 cps/day in the Ge K-peak. ^{68}Ge decays by electron capture, so its decays can not be differentiated from those of ^{71}Ge .

The experiment began operating in May of 1988, when the removal of the ^{68}Ge from 30 tons of Ga commenced. Data from extractions made during 1988-1989 is not included in the analysis here due to the high background in earlier extractions from ^{68}Ge and then from Rn.

Additional purification procedures were implemented beginning with the January 1990 extraction which resulted in

the reduction of radioactive backgrounds of the samples from the extractions.

RESULTS

Extractions from 30 tons of Ga were carried out in January, February, March, April, and July of 1990.

The results of the maximum likelihood analysis are shown in

Table 1.

Table 1. Statistical Analysis

Run	Counting time	Number of events	68%CL	95% CL
	days		SNU	SNU
Jan.	57.6	8	57	112
Feb.	57.4	1	80	137
Mar.	46.8	7	162	256
Apr.	89.5	7	98	182
July	59.3	11	144	266
Sum		34	35 SNU	58SNU

Systematic effects

Systematic effects fall into three categories: uncertainties in efficiencies, a possible variation in time of the detector background causing an incorrect background subtraction, and uncertainties in the extrapolation of the ^{71}Ge K-peak acceptance window from the ^{55}Fe calibration.

The overall uncertainty in the detection efficiency due to the systematic uncertainties in the chemical extraction and the counting efficiency produced a change in the ^{71}Ge rate not more than 6 SNU (68% CL) and 15 SNU (95% CL).

The uncertainty in the background subtraction under ^{71}Ge decay curves due to possible time variations of the counter background produced a maximum change in the ^{71}Ge rate of 35 SNU (68% CL) and 40 SNU (95% CL)

The uncertainty in the position of the ^{71}Ge acceptance window did not produce any change in the best fit value of 0 SNU, but increased the upper limit by 7 SNU (68 % CL) and 19 SNU (95% CL).

The overall upper limit was determined by adding the statistical uncertainties in quadrature with the systematic uncertainties. The results of the analysis of the 5 runs are 50 SNU (68% CL) and 74 SNU (95% CL).

As an initial test of the extraction process, we doped one of the reactors holding 7 tons of Ga with a known number of ^{71}Ge atoms, along with the natural Ge carrier. Three extractions were carried out and the number of ^{71}Ge atoms was counted.

Table 2 shows the results of this measurement and indicates that the extraction efficiency of the natural carrier and ^{71}Ge track very closely.

Table 2. Extraction efficiency of the Ge carrier and ^{71}Ge

Run	Carrier ug	^{71}Ge atoms	Carrier efficiency %	^{71}Ge efficiency %
1	410± 10	4900±500	77±2	81± 8
2	97± 2	980±220	80±2	84±19
3	21± 1	130± 45	84±4	72±25
Sum	528±10	6010±550		
Amount added	525±26	6050±600		

CONCLUSIONS

The results of the analysis of the first five measurements of the Baksan Solar Gallium Neutrino Experiment is consistent with no solar neutrino induced events being observed. The initial data indicates that the flux may be less than that expected from p-p neutrinos alone, thus indicating that the solar neutrino problem also applies to the low energy p-p neutrinos.

Final conclusions can be made after a test of the efficiency of the overall procedure of the experiment using a ^{51}Cr neutrino source⁷⁾.

FUTURE PLANS

Monthly extraction from 30 tons of Ga will continue. At the same time, the detector will be extended to the 60 tons of Ga. The additional 30 tons is now stored underground and will be installed into reactors shortly. A final calibration of the detector is planned using the ^{51}Cr neutrino source⁷⁾.

ACKNOWLEDGEMENTS

The SAGE collaboration wishes to thank A.E.Chudakov, G.T.Garvey, M.A.Markov, V.A.Matveev, J.M.Moss, V.A.Rubakov, and A.N.Tavkhelidze for their continued interest in our work and for stimulating discussions. We are also grateful to J.N.Bahcall and A.Yu.Smirnov for useful discussions. We wish to acknowledge the support of the Academy of Sciences of the

USSR. the Institute for Nuclear Research AS USSR, the High Energy Physics Council of the State Committee for Science and Technology of the USSR, the Division of Nuclear Physics of the U.S. Department of Energy , the National Science Foundation, and Los Alamos National Laboratory. V.N.Gavrin, A.M.Pshukov, and I.I.Knyshenko would like to thank the the organizers of the Xith Moriond Workshop in particular Prof.Tran Thanh Van, for their hospitality.

REFERENCES

1. B.Pontecorvo. 'Inverse Beta Decay'. Chalk River report PD-205 (1946); Usp.Fiz.Nauk. 141 (1983) 675 [Sov.Phys.Usp.26 1087].
2. L.W.Alvarez, 'A Proposed Experimental Test of the Neutrino Theory', Univ.of California Radiation Laboratory Report UCRL-328, Berkeley, California (1949).
3. R.Davis et.al., Proc. of Neutrino'88 Intern.Conf.(1988) 518.
4. J.N.Bahcall and R.K.Ulrich, Rev.Mod.Phys.60(1988) 297.
5. Y.Totsuka et.al. Proc.of the XXV Intern.Conf.on High Energy Physics, Singapore(1990).
6. A.Kuzmin, Lebedev Physical Institute Preprint A-62(1964); Sov.Phys.JETP 49 (1965) 1532.
7. V.N.Gavrin et.al.(SAGE), Proc.'Inside the Sun' Conf., Versailles, ed. by G.Berthomieu and M.Cribier, Kluwer Acad. Publ.(1989) 201.
8. B.T.Cleveland, Nuclear Instruments and Methods 214(1983) 451.

Report on the Gallex experiment

D. Vignaud
DPhPE/SEPh
CEN Saclay
91191 Gif-sur-Yvette
France

Abstract

The Gallex collaboration [1] is now starting an experiment for the detection of low energy solar neutrinos via the reaction $\nu_e + {}^{71}\text{Ga} \rightarrow {}^{71}\text{Ge} + e^-$. The target consists of 30 tons of gallium in the form of a GaCl_3 solution and is installed in the Gran Sasso Underground Laboratory. All the different steps of the experimental process (germanium extraction, germane synthesis, radioactive germanium counting) are now working with a very good and well-controlled efficiency. The removal of long-lived radioactive germanium isotope ${}^{68}\text{Ge}$ which was produced by cosmic-rays outside the underground laboratory and simulates ${}^{71}\text{Ge}$ decay (except for the lifetime) is in progress.

1. Introduction

A summary of the experimental and theoretical situation concerning solar neutrinos has been presented previously [2]. The main purpose of the gallium solar neutrino experiments is the detection of the ν_{pp} which are produced in the primordial proton proton fusion reactions in the core of the Sun. Two radiochemical experiments using gallium are now working : Sage [3], which has presented some preliminary results and Gallex, which is starting. We present here a status report of Gallex. More details can be found elsewhere [4].

The solar ν_e interact with the ^{71}Ga isotope of a gallium target, producing the radioactive ^{71}Ge isotope, whose lifetime is $T_{1/2} = 11.43$ d. The reaction threshold is 233 keV, well below the maximum energy of the ν_{pp} (420 keV). The production rate of ^{71}Ge given by standard solar models is around 125-132 SNU's (solar neutrino unit) (see [2]) of which about 55% are expected to come from ν_{pp} . The experimental procedure consists in extracting the radioactive ^{71}Ge atoms which are produced after an exposure time of several weeks and to observe their decays.

The experimental setup includes mainly the target, a germanium extraction system and a radioactive ^{71}Ge counting system. It is installed in the Gran Sasso Underground Laboratory (Italy), 125 km east of Rome. The target consists of 100 tons of a liquid GaCl_3 solution containing 30 tons of gallium, all of which has been inside the laboratory since June 1990. We present in the following the performances of the extraction system and of the counting system, and the problem of the removal of long-lived radioactive germanium isotope ^{68}Ge which was produced by cosmic-rays outside the underground laboratory. This isotope decays with a lifetime $T_{1/2} = 288$ d.

The experiment will be calibrated with an artificial neutrino source (37 PBq of ^{51}Cr) after two years of measurement [5]. This source will be made by irradiating 40 kg of chromium enriched in ^{50}Cr in the reactor Silo  at Grenoble, France.

2. Status of the extraction

Two tanks (70 m³ each) are available in the Gallex main building : a process tank which is equipped with a large tube in order to hold the ^{51}Cr neutrino source and a second tank, needed for safety reasons and equipped with a smaller sweeping system, mainly for the final outgassing of the solution. The target solution (53 m³ of 8.135 M GaCl_3 + 1.94 M HCl) is in the second tank and will be transferred soon to the process tank. Solar neutrinos should produce 1.19 ^{71}Ge atom a day for a standard solar model prediction of 132 SNU's. Before each run a given amount (normally 1 mg) of non radioactive germanium isotopes (^{72}Ge , ^{74}Ge ,... or natural germanium) is put in the tank and dissolved in the solution. This carrier has two purposes : to check the germanium extraction efficiency and to be used as counting gas once transformed into germane.

Germanium atoms are incorporated into GeCl_4 molecules, which are volatile in presence of HCl, but dissolve immediately in pure water. They are extracted from the gallium solution by circulating several thousand m³ of N_2 gas through the tank containing the solution (see Fig. 1). The germanium is then absorbed in the pure water of large absorption columns (about 30 l of water). A series of smaller columns serves to con-

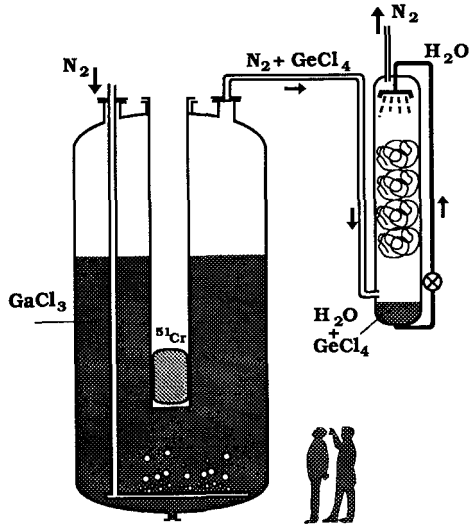


Figure 1 : Scheme of the gallium tank and of the Ge extraction system

concentrate the germanium in a smaller volume of about 0.5l of water. The germanium extraction efficiency is measured for the germanium carrier by an atomic absorption method with a precision of about 1 %.

More than 20 runs have been performed since June 1990, in order to desorb the residual ^{68}Ge atoms (see section 4 below). Values between 95 % and 99 % have been measured for the extraction efficiency, depending on the total amount of circulated nitrogen and on the temperature of the solution.

The GeCl_4 is transformed chemically into germane (GeH_4) which is purified from remaining impurities (air, radon,...) by gas chromatography before filling the counters. The efficiency of the germane synthesis and counter filling is measured and is typically 95 %. The counters are filled with a mixture of 30 % GeH_4 and 70 % Xe to optimize the counting efficiency.

3. Status of the counting

A Gallex run consists of a 3 weeks exposure time after which there are 14 ^{71}Ge atoms in the tank if the standard solar model is correct. Taking into account extraction, synthesis and filling efficiencies (about 90 %) there will be less than one decay the first day of counting, this number decreasing the next days, following the ^{71}Ge lifetime. The measurement of such low decay rates is an extreme low-level counting task and can only be achieved with miniaturized proportional counters (volume $\approx 1 \text{ cm}^3$) constructed from ultrapure materials [6]. ^{71}Ge decays by electron capture and the resulting spectrum of Auger electrons and absorbed X-rays in the counter has two peaks at 1.2keV and 10.4keV, corresponding respectively to L and K-capture. In order to reach sufficiently low background rates, pulse shape analysis of the proportional counter pulses is done to

discriminate between fast pulses originating from point-like ^{71}Ge decays and background from Compton scattering with a spatially extended track. The Camac-based counting system is thus equipped with a fast transient digitizer (sampling every 0.5 ns) to record the shape of each preamplifier output pulse.

The counters are placed into a copper box which is inserted into a passive copper shielding or into the well of a NaI(Tl) detector (active shielding). The NaI detector is used either as an anticoincidence detector device or in coincidence mode to distinguish ^{71}Ge decays from ^{69}Ge decays. This setup is installed inside a steel vessel filled with low activity lead and closed by an air-tight box to prevent radon from entering, the radon produced inside being trapped. The complete system, including the associated electronics, is inside a Faraday cage connected with a "microvax" through an optical link.

Very good performances have been obtained recently for several counters, the passive shielding giving better results than the active one by a factor greater than 2. As an example Fig. 2 presents the results of a counter filled with with non radioactive germane using the synthesis and filling line, i.e. in the same conditions as a normal run, and put in the passive shielding for 128 days. The risetime is plotted as a function of the energy. The two windows corresponding to the L and K-peak have been defined from the calibration of the counter with a cerium source [7]. The width in energy corresponds to the resolution of the counter. The counting efficiency for the L and K-peaks, i.e. the number of decays in the corresponding windows for ^{71}Ge decay, is respectively 35 and 30 %. The background rate (0.06 cpd in the L-peak and < 0.02 cpd in the K-peak) is obtained in the passive shielding. (This can be compared to an expected value of 0.5 cpd for ^{71}Ge the first days of the counting). Similar values or even better are obtained for several other counters.

Such counters will allow the experiment to measure a solar neutrino production rate of 90 SNU (as an example) with a 1σ statistical uncertainty of 8 % after 4 years of data taking.

4. Cosmogenic radioisotopes and the ^{68}Ge problem

Natural gallium is formed by 39.9 % of ^{71}Ga and 60.1 % of ^{69}Ga . Solar neutrinos interact only with ^{71}Ga to produce ^{71}Ge (lifetime $T_{1/2} = 11.43$ d). [The production of ^{69}Ge ($T_{1/2} = 1.63$ d) from ^{69}Ga by solar neutrinos is negligible due to a high threshold (2.225 MeV) and a small capture cross section. ^{69}Ge decays by positron emission (36 %) and electron capture (64 %)]. Any other physical process which produces ^{71}Ge constitutes a background for the experiment. The main source of such a background is the production of ^{71}Ge via the (p,n) reaction : $p + ^{71}\text{Ga} \rightarrow ^{71}\text{Ge} + n$. These (p,n) reactions can also produce ^{69}Ge ($p + ^{69}\text{Ga} \rightarrow ^{69}\text{Ge} + n$) while (p,xn) reactions produce ^{68}Ge ($T_{1/2} = 288$ d) : $p + ^{69}\text{Ga} \rightarrow ^{68}\text{Ge} + 2n$ and $p + ^{71}\text{Ga} \rightarrow ^{68}\text{Ge} + 4n$. The cross section for such (p,n) reactions peaks at low energy (few tens of MeV) and the protons come mainly from cosmic ray interactions in the tank or surrounding material. The problem with ^{68}Ge is that, like ^{71}Ge , it decays to ^{68}Ga by electron capture (^{68}Ga , whose lifetime is 68 mn, decays mainly by positron emission). The ^{68}Ge decay is thus identical to ^{71}Ge decay, except for the difference in lifetimes and for the radioactive

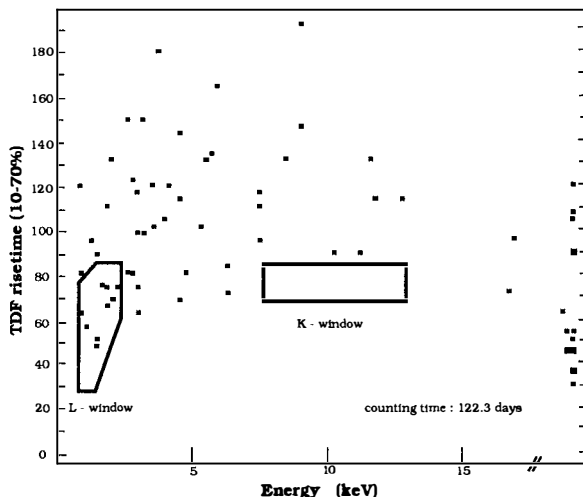


Figure 2 : Counting results (risetime versus energy) for a typical counter filled with a germane-xenon mixture. The two windows define the L and K-regions where are expected the ^{71}Ge decays.

daughter.

Once the ^{68}Ge atoms produced by cosmic rays at the Earth's surface are extracted there will be no problem. A calculation of the ^{71}Ge and ^{68}Ge production by cosmic rays underground, based on measurements in muon beams, has been performed [9]. ^{71}Ge production has been shown to represent about 3 % of the signal expected from the standard solar models. ^{68}Ge production is 3 times larger but its much longer lifetime makes its contribution to the counting completely negligible.

The gallium target has been exposed to cosmic rays at the ground level (about 900 m above sea level) for several months. The total amount of ^{68}Ge in the GaCl_3 solution before the transportation inside has been evaluated to about 20 million atoms. It has been shown in the previous section that the germanium extraction efficiency can reach 99 %. This is why a first sweeping of the solution was performed just before the transportation from outside to the underground site. We could expect at this level having reduced the number of ^{68}Ge atoms to few hundreds of thousands. Three or four sweepings inside would in principle have reduced the number to few tens and the experiment could have started. However impurities in the solution (organic or silicated colloids) could have trapped a small fraction ($\sim 10^{-3}$) of the germanium atoms. The 99 % extraction efficiency is measured for what is called the volatile component of the GeCl_4 . Any non volatile component has a desorption characteristic time much larger and its chemistry is not well known.

More than 20 desorptions have been performed since July 1990, showing the presence of a ^{68}Ge component more important than had been expected at the beginning. Fortunately this component has now decreased and the ^{68}Ge desorption level is around 100 atoms a day, corresponding to few counts per day in the counter for a three-week

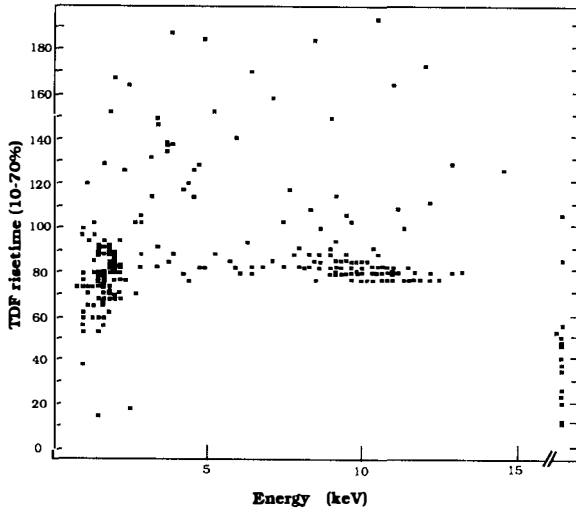


Figure 3 : Counting results (risetime versus energy) for a ^{68}Ge desorption run. The accumulation in the L and K region is due to ^{68}Ge decay (about 50 days of counting).

accumulation time, and continuously decreasing. One way to accelerate the desorption process of the non volatile component is to heat the target solution. This has been done since November 1990. The temperature is now about 40°C , which increases by a factor about 5 the ^{68}Ge desorption. We are aiming to achieve soon an acceptable level (less than 0.1 cpd). Fig. 3 presents an example of the counting results (risetime versus energy) for a recent run. The signal of the radioactive germanium decay is clearly observed in the accumulation in the L and K region. ^{68}Ge is identified by the time distribution (not shown).

Once the ^{68}Ge problem has been solved, we can expect some production of ^{71}Ge through (p,n) or equivalent reactions. The two main sources of slow protons are secondaries from cosmic ray muon interactions and fast neutrons. They have been evaluated recently [9]. ^{71}Ge production induced by cosmic ray muons could represent about 3% of the expected solar neutrino signal, as stated previously. An estimation of the ^{71}Ge production induced by fast neutrons has been done from the results of a radiochemical experiment based on the reaction $n + ^{40}\text{Ca} \rightarrow ^{37}\text{Ar} + \alpha$. The value obtained (0.5 SNU) indicates that this source of background is negligible.

5. Conclusion

The Gallex experiment is fully installed in the Gran Sasso Underground Laboratory since June 1990. The germanium extraction system works with an efficiency of 99%. The synthesis and counter filling line has been tested and operated several tens of times with a measured efficiency of 95%. The low level counting station is fully satisfactory, with rates below 0.1 cpd for several counters. The residual ^{68}Ge present in the tank and which still dominates the solar neutrino signal should disappear in the forthcoming

months. We hope to have our first real runs this year, going quickly from "Gallex News" to "Gallex SNU's".

Acknowledgements : It is a pleasure to thank M. Cribier, T. Kirsten, J. Rich and M. Spiro for their fruitful comments, and J. K. Rowley for an invaluable remark.

References

- [1] **Gallex collaboration - Gran Sasso** : E. Bellotti, C. Cattadori, H. Lalla, **MPI Heidelberg** : P. Anselmann, M. Breitenbach, W. Hampel, G. Heusser, J. Kiko, T. Kirsten, E. Pernicka, R. Plaga, B. Povh, C. Schlosser, H. Völk, R. Wink, M. Wojcik, **KfK Karlsruhe** : R. von Ammon, M. Balata, K. Ebert, T. Fritsch, K. Hellriegel, E. Henrich, L. Stieglitz, F. Weyrich, **Milano** : O. Cremonesi, E. Fiorini, S. Ragazzi, L. Zanotti, **T.U. München** : F. von Feilitzsch, R. L. Mössbauer, U. Schanda, **Nice** : G. Berthomieu, E. Schatzman, **Saclay** : M. Cribier, G. Dupont, B. Pichard, J. Rich, M. Spiro, T. Stolarczyk, C. Tao, D. Vignaud, **Rehovot** : I. Carmi, I. Dostrovsky, **Roma** : S. d'Angelo, C. Bacci, P. Belli, R. Bernabei, L. Paoluzi, **Brookhaven** : R. L. Hahn, F. X. Hartmann, J. K. Rowley, R. W. Stoenner, J. Weneser
- [2] D. Vignaud, these proceedings
- [3] V. N. Gavrin, ν' 90 Conference, Nucl. Phys. B Proc., to appear
V. N. Gavrin, these proceedings
- [4] T. Kirsten, Proc. of the 121st IAU Colloquium, "Inside the Sun", Versailles (1989), ed. by G. Berthomieu and M. Cribier, Kluwer Academic Pub., p. 187
W. Hampel, in "TAUP 89", ed. by A. Bottino and P. Monacelli, Editions Frontières, p. 189
M. Cribier, Proc. of the 25th Int. Conf. on High Energy Physics, Singapore, 1990, to appear
- [5] M. Cribier et al., Nucl. Instr. and Methods A265 (1988) 574
- [6] R. Wink, Ph. D. Thesis, Heidelberg, 1988
- [7] A. Urban, Ph. D. Thesis, München, 1989
- [8] V. N. Gavrin and A. Yu. Zakharov, Moscow preprint (in russian), 1987
- [9] T. Stolarczyk, Thèse de Doctorat, Université de Paris-Sud, 1990



THE BOREXINO PROJECT TO STUDY THE SOLAR NEUTRINOS*

E.Meroni

Dipartimento di Scienze Biomediche e Biotecnologie,
via Valsabbina 19, 25123 Brescia Italy
and I.N.F.N Milano

ABSTRACT:

Borexino, developed to operate in the GranSasso Underground Laboratory, aims to clarify the nature of the solar neutrino problem looking at the ${}^7\text{Be}$ and ${}^8\text{B}$ neutrinos. The detector is based on a high light yield boron loaded liquid scintillator.

*The Borexino Collaboration:

C.Arpesella⁴, G.Bellini⁷, S.Bonetti⁷, M.Campanella⁷, G.Cecchet⁸, M.Deutsch⁶, A.De Bari⁸, A.Donati⁴, S.J.Freedman², P.Inzani⁷, D.Krakauer², I.Manno⁷, E.Meroni, J.Mitchell¹, S.Pakvasa⁵, A.Perotti⁸, P.Raghavan¹, R.S.Raghavan¹, G.Ranucci⁷, F.Ragusa⁷, R.I.Steinberg³, P.Ullucci⁷, O.Zaimidoroga⁹

¹AT&T Bell Laboratories, Murray Hill NJ, ²Argonne National Laboratory, ³Dept. of Physics, Drexel University, Philadelphia, ⁴Laboratori Nazionali del GranSasso, ⁵Dept. of Physics, University of Hawaii at Manoa, Honolulu, ⁶Lab.for Nuclear Science, Massachusetts Inst. of Technology, ⁷Milano University and I.N.F.N, ⁸Pavia University and I.N.F.N, ⁹Joint Institute for Nuclear Research, Dubna.

Introduction.

The solar neutrino data at our disposal come from Homestake ^{37}Cl detector¹⁾, from Kamioka-II detector¹⁾ and most recently from the Soviet-American Gallium experiment (SAGE)¹⁾. The first two experiments measured values of the solar neutrino flux about 40% of that predicted by the Standard Solar Model. The data from SAGE tend towards a low signal rate. These results encourage the possibility of new neutrino physics based on a non-zero value of neutrino mass/mixing angle and/or magnetic moment, because the astrophysics alone cannot explain the fluxes from present experiments and the possible correlation of the Homestake flux with solar activity. Borexino, developed to operate at the GranSasso Underground Laboratory, aims to clarify the solar neutrino problem measuring both the low energy (≈ 0.86 MeV) high-flux ^7Be monoenergetic neutrinos with a signal rate of few tens of events/day and the high energy (up to 14.5 MeV) ^8B neutrinos. The detector is a boron loaded liquid scintillator with a high luminosity, 100 keV of released energy corresponds to ≈ 28 detected photons in P.M.'s. The detection energy threshold is constrained by the intrinsic background from the radioactive traces of ^{238}U , ^{232}Th , ^{40}K , ^{14}C in the active volume of the detector. If the contamination of ^{238}U , ^{232}Th is limited to 10^{-16} g/g, K_{nat} to 10^{-13} g/g and ^{14}C to 10^{-18} g/g, the event threshold could be 200 keV. Radiopurity of the scintillator material is thus the central issue.

Neutrino physics with Borexino.

The neutrino reactions available in the detector are: I) ν - e scattering. II) Inverse β -decay in ^{11}B in the scintillator; this reaction is sensitive only to ^8B ν_e 's and can be tagged by mean of a delayed coincidence. III) Inverse β -decay in protons in the scintillator; this reaction is induced by $\bar{\nu}_e$'s and can be tagged by a fast coincidence with the γ from the neutron capture by ^{10}B . (I) is the main reaction and allows the detection of ^7Be neutrinos.

Borexino can investigate many aspects of neutrino physics:²⁾

A) Assuming the Standard Solar Model predictions, for a target of 104 t of scintillator, a signal rate of ≈ 65 ev/d can be observed in the spectral region 200 – 800 keV and a ^8B signal rate of ≈ 0.8 ev/d in the spectral region ranging between 3.5 – 14.5 MeV. The total rate becomes ≈ 14 ev/d in the hypothesis of MSW effect in the sun with nearly complete ν_e conversion to $\nu_{\mu(\tau)}$. The signal is due to $\nu_{\mu(\tau)}$ scattering via neutral current only. A strong signal enhancement may occur in the hypothesis of a ν added magnetic moment due to magnetic scattering. If we attribute to neutrinos the lowest laboratory limit on μ_ν ³⁾

($\simeq 1.5 \cdot 10^{-10} \mu_B$) the result is a rate of ≈ 100 ev/d changing to ≈ 350 ev/d for a value of μ_ν ($\simeq 4 \cdot 10^{-10} \mu_B$) necessary to explain the constancy of Kamioka-II signal⁴).

B) Time variation: the energy, the monoenergetic nature and the high signal rate of the ${}^7\text{Be}$ neutrinos allows to study with Borexino detector the time variation of the signal to demonstrate neutrino flavour conversion phenomena. The measurement of the day-night effect is a signature for MSW conversion⁵). The MSW effect requires that the ν_e 's produced in the sun are firstly converted into $\nu_{\mu(\tau)}$ in the dense solar matter, then some of them can be reconverted to ν_e by a reverse MSW effect as they pass through the earth resulting in a day-night effect. Using the $(\Delta m^2, \sin^2 2\theta)$ allowed region overlapping Kamioka-II and Homestake results, a day-night effect should be observable in Borexino for $10^{-6} < \Delta m^2 < 5 \cdot 10^{-8} \text{ eV}^2$ and $\sin^2 2\theta > 5 \cdot 10^{-2}$. The minimum detectable effect will be a day/night rate excess $\Delta \approx 1$ ev/d and a minimum detector exposure of 30 to 41 weeks with a signal rate of 14 – 29 ev/d is implied for 3σ C.L.; the rate of 14 or 29 ev/d corresponds to a complete conversion into $\nu_{\mu(\tau)}$ in the sun or to a 70% conversion respectively.

C) Borexino can observe the seasonal variation of the solar neutrino flux due to vacuum oscillations. This effect is predicted for $\Delta m^2 \approx 10^{-10} \text{ eV}^2$ and for near maximum mixing.

D) The detection of $\bar{\nu}_e$ interaction allows to study the possibility of spin-flavour conversion via a neutrino transition moment.

Apparatus and experimental features.

The detector design aims to suppress the radioactive background external to the fiducial volume due to the rock and to the materials surrounding the scintillator. Borexino may be sketched as 3 concentric spheres separated by thin walls of acrylic. The innermost one of 4m radius, contains the liquid scintillator (85% of TMB ($\text{B}(\text{OCH}_3)_3$), 15% of Pseudocumene), surrounded by a buffer of a very pure liquid (10^{-15} g/g of ${}^{238}\text{U}$, ${}^{232}\text{Th}$). The external one is filled by water. The support structure is a 2 cm thick steel sphere with circular windows for the P.M.'s. The most external shield is made by polyethylene. The cover of the P.M.'s plus the light guides is 50%. This configuration allows a good energy resolution ($\Delta E/E = 20\%$) and a spatial error (1σ) of 13 cm at 0.5 MeV. This multilayer configuration reduces the external background to a negligible level in the fiducial mass (104 t) confined in a volume of 3 m radius. The background in the fiducial volume is dominated by the radioactivity in the liquid scintillator itself. On the base of the expected SSM signal rate the maximum allowed limits for the radiopurity of scintillator is a concentration of 10^{-16} g/g for ${}^{238}\text{U}$, ${}^{232}\text{Th}$, 10^{-13} g/g

for K_{nat} . Decisive progress has been made on radiopurity; levels demonstrated so far are lower than 10^{-15} g/g for ^{238}U , ^{232}Th . New analysis are presently planned to further lower these limits. The energy distributions for simulated events and background are shown in fig.1. These distributions are obtained by reconstructing the MonteCarlo events assuming the SSM flux and the desired contamination for U and Th. Under these assumptions the expected background in the ^7Be neutrino region is ≈ 30 ev/d and .02 ev/d in ^8B region. The events with a β -decay (such as $^{121,214}\text{Bi}$) that are time correlated with α 's as well as α - α correlated events are subtracted in these background spectra while the α particles can be tagged by time-distribution tails of the scintillator light. Using these tagged background events as normalization, it is possible to reduce to 1/3 the background shown in fig.1. The only other source of unshieldable background is radioisotopes produced in scintillator by cosmic muons, mainly ^7Be and ^{10}Be , before the storage in the GranSasso laboratory; the measurement of the concentration of these long lived radioisotopes is now planned.

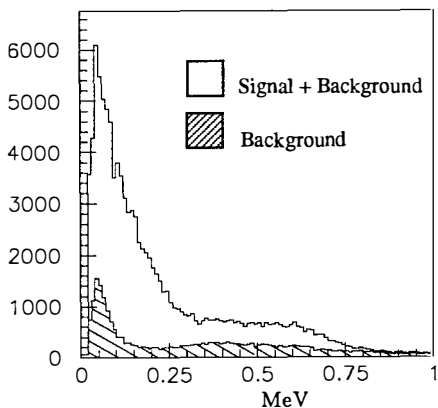


Fig.1a: Energy of solar ν events + background from 0 to 1 MeV

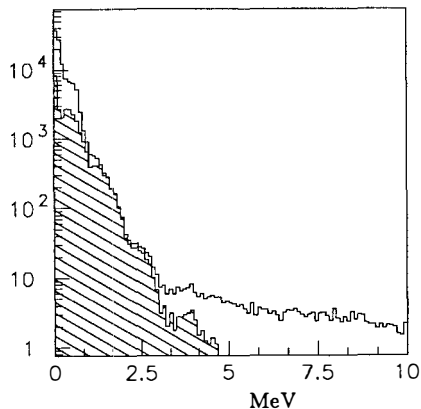


Fig.1b: Energy of solar ν events + background from 0 to 10 MeV

REFERENCES

- 1) See talks presented on this conference
- 2) R.S.Raghavan, 25 Int. Conference High Energy Physics, Singapore, 1990.
R.S.Raghavan et al., AT&T Bell Labs Tech.Memor. 11121-910204-16(1991), to be published.
- 3) A.V.Kjuldiev, Nucl.Phys. B243(1984) 387.
P.Vogel and J.Engel, Phys. Rev. D39 (1989) 3378.
- 4) A.Suzuki et al., KEK Preprint 90-51 (1990)
- 5) M.Cribier et al., Phys.Lett. B182 (1986) 89.

PROSPECTS FOR CRYOGENIC DETECTION OF SOLAR NEUTRINOS

*Robert E. Lanou, Jr.**
Department of Physics
BROWN UNIVERSITY
Providence, Rhode Island 02912 USA



ABSTRACT

Several projects are underway aimed at developing techniques to detect low energy ($E_\nu < 1\text{keV}$) neutrinos. They are based on cryogenic methods. The reasons why the study of solar neutrinos requires such techniques, the principles on which they are based and their present status are discussed.

* This work supported in part by U.S. Department of Energy

Introduction – For particle, nuclear and astrophysics, a measurement of the entire neutrino energy spectrum from the sun has emerged as a goal of first importance.

As the progress and exciting results reported at this workshop show, impressive strides are being made toward this goal. At the high end of the spectrum we have the complementary techniques based on inverse β -decay^{1]} (${}^{37}\text{Cl}$) and $\nu - e$ scattering^{2]} (H_2O Cherenkov) – the latter introducing real time detection for the first time as well as some sensitivity to neutrinos other than ν_e . These capabilities will soon be significantly extended by the D_2O Cherenkov method^{3]}. At the lowest end of the spectrum, where the neutrinos from the $p - p$ branch dominate, we are seeing the remarkable, early results^{4]} from the inverse β -decay (${}^{71}\text{Ga}$) experiments. However, to date we have no analogue to the Cherenkov technique which would permit measurements in real time, with energy resolution and some sensitivity to all neutrino species originating in the fundamental solar action $p + p \rightarrow d + e^+ + \nu_e$. The reason for this lack is not far to seek. It is because the experimental requirements imposed for achieving low threshold, low noise and adequate signal/noise discrimination are formidable.

Experimental Requirements – Fluxes at the low end of the spectrum are expected to be $\phi(p - p) = 6.1 \times 10^{10} \text{cm}^{-2} \text{s}^{-1}$ and $\phi({}^7\text{Be}) = 0.4 \times 10^{10} \text{cm}^{-2} \text{s}^{-1}$ in standard solar models^{5]}. It would be desirable in a single detector to be able to measure interactions from both. The end point neutrino energy for the $p - p$ reaction is 420 keV and the dominant line from the ${}^7\text{Be}$ reaction is at 860 keV. The reactions favored^{6]} for detecting these neutrinos are elastic scattering from atomic electrons or coherent neutral current scattering from nuclei of the detector medium. The recoiling electron or nucleus is measured. Inverse β -decay does not seem a likely avenue due to the high reaction thresholds for the elements whose other properties suggest themselves as feasible target media from which to extract the deposited energy. The cross section for electron scattering has some valuable features. Although it rises as E_ν for all neutrino species, it is about six times larger for ν_e than for ν_μ and ν_τ . Cross sections for these reactions have been extensively measured and are well given by the standard model of electroweak interactions. Coherent neutral current cross sections from nuclei have not been measured but are also expected to be as predicted by the standard model given approximately as follows $\sigma_{\nu-N} \simeq G_F^2 N^2 E_\nu^2$ where G_F is the Fermi constant and N is the number of neutrons. The quadratic dependence on both energy and neutron number (the value of $\sin^2\theta_w$ suppresses the proton contribution) enhances any detector's chances of sampling the lower ${}^7\text{Be}$ flux. The recoil energy, E_{rec} , for

these reactions is given by $E_{rec} = 2Mc^2 E_\nu^2 \cos^2 \theta [E_\nu^2 \sin^2 \theta + 2Mc^2 E_\nu + (Mc^2)^2]$ where M is the target mass and θ is the scattered electron angle with respect to the incident neutrino. To set the scale, consider typical E_{rec} values for the electron and for a silicon or a helium nucleus recoil.

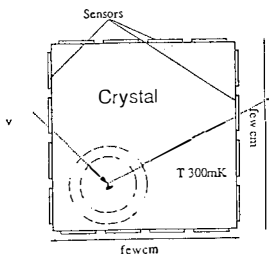
Target	$E(p-p)_{rec}^{max}$	$E(^7\text{Be})_{rec}^{max}$	$E(^8\text{B})_{rec}^{max}$
e^-	261keV	663keV	13.8MeV
Silicon	13eV	56eV	15keV
Helium	94eV	393eV	103keV

These are very low energies to detect by conventional means especially if the volume in which the events occur is large. For example, if the entire flux appeared as ν_e and if at least 20 events/day were taken as a goal then 10 tons of target material is needed. Small by comparison to present day detectors but large from the point of view of signal extraction. When a recoiling particle deposits its energy into a medium, it is desirable in order to achieve low thresholds and good energy resolution, to have that energy transferred to the largest number of secondary carriers as possible. Although energy deposition mechanisms vary in detail among media (e.g., crystals versus liquids) they all share in an initial division of deposited energy between direct ionization and direct excitation of the bulk (i.e., phonons/heat). Eventually, at least 90% ends up in the latter form. Additionally, since ion pairs require several eV whereas phonons are in the milli-eV range it is very suggestive that detection of phonons either in or out of equilibrium with the medium might be a powerful approach to pursue. In order to detect a phonon pulse above an equilibrium background that equilibrium background must be reduced to a level appropriate to the sensitivity required, consequently, cryogenic methods are required.

Cryogenic Approaches – There is a very active and successful community which has done pioneering work in cryogenic detection of radiation for gamma ray astronomy, double beta decay, dark matter searches and possibly reactor experiments⁷¹. However, all of these are in solids and, by solar neutrino standards, are exceedingly small ranging from a few micrograms to 280 grams. Nonetheless, depending upon the degree of segmentation, extent of instrumentation and radioactive purity (see below) it is not inconceivable that one or more of these crystalline solids might become a feasible solar neutrino medium. At the very low energy thresholds ($E_\nu < 1\text{keV}$) needed for

accessing the $p - p$ reaction and at low event rates, it is absolutely essential to have as little internal radioactivity as possible. This internal activity can arise primarily from three sources: heavy elements such as U or Th, active isotopes of the primary medium or long lived transmutation activity induced in the medium by fast, cosmic ray neutrons while the medium was on the surface of the earth. For example, even silicon, which because of the very high purity achievable on a large industrial scale would appear to be the logical crystal, has prohibitive activity^{8]}. Specifically, the activity in silicon from the beta emitters ${}^3\text{H}$, ${}^{22}\text{Na}$ and ${}^7\text{Be}$ would be 3.5, 0.3, and 0.02 counts- $\text{kg}^{-1} - \text{day}^{-1}$ even after one year underground. Consequently, it is clear that exceptional methods of mining, refining and fabrication underground would be necessary.

A completely different approach to low energy solar neutrino detection is underway at Brown University^{9]}. It is based upon the use of ${}^4\text{He}$ in its superfluid state. This cryogenic liquid recommends itself for several reasons. At the temperatures involved it is the purest known material; all other atomic species freeze out and even ${}^3\text{He}$ can be reduced to $< 10^{-13}$. It possesses a variety of quantum phenomena which permit detection of energy deposition. Finally, it is inexpensive and readily available commercial equipment exist for handling it on a large scale. In the remaining, I would like to sketch the generic differences and similarities of the two cryogenic approaches: liquid helium and crystals. And to briefly indicate what has been achieved so far.



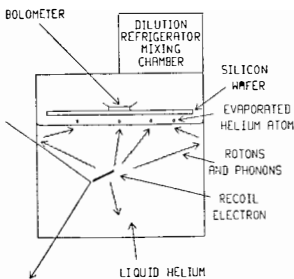
a) The Crystal Technique: The cartoon at the left illustrates the technique in general terms.^{10]} The device is divided by function: the target crystal and the phonon sensor.

The recoil particle stops and deposits its energy in a tiny volume ($\sim 0.01\mu^3$) if it is a nucleus and a somewhat larger volume if it is an electron ($\sim 5 \times 10^3\mu^3$).

Phonons emerging from that region are generated directly by the recoil but also by the ionization products either directly or upon recombination. The exact spectrum of the emerging phonons is not well known; however, their subsequent behavior is. Phonons can undergo decay and they can scatter from impurities, other phonons (equilibrium) and isotopes. The impurities can be controlled to an acceptable level by refining while the equilibrium density of phonons is reduced by going to low temper-

ature ($\sim 100mK$). The isotope scattering rate goes as E_{ph}^4 while the decay rate goes as E_{ph}^5 . As the highest energy ones decay and scatter the mean free path of the resulting phonon population increases very quickly. The phonons propagate through the crystal at the appropriate velocity of sound. One can then speak of two components to the population: those with long mean free paths (ballistic) and those with many scatters (quasi-diffuse). While it is usually the ballistic (out-of-equilibrium) phonons which are of primary interest in most applications; the quasi-diffuse contribution to the general temperature rise of the crystal can sometimes be utilized. In all cases the effects are detected by sensors on the surface. The investigation and development of these sensors is a field in itself in which many different approaches are being taken and much progress is being made; among them: semiconductor thermistors, transition edge superconducting films, and tunnel junctions.

b) The Superfluid Helium Technique: Again with reference to the cartoon at the left, a separated function of target and sensor is employed.



The target medium is isotopically pure 4He ($< 10^{13}He - 3$) achieved by filling via a heat flush/superleak system and by keeping the liquid in the main vessel at $\sim 100mK$.

(Solubility of H_2 in $^4He \propto \exp(-\frac{80^\circ K}{T})$) so it has been removed by absorption to walls.) A recoiling electron of about 300keV deposits its energy in a distance of $\sim 8mm$ while a 5MeV helium nucleus deposits in $\sim 0.2mm$. These regions are then the dense energy sources of the bulk excitations of the medium as they are in crystals;

however in 4He there are some important differences as determined by the dispersion curve for these excitations. The curve divides naturally into two regions: phonons, in the linear region at low momentum and rotons in the very non-linear region at the higher momentum. The rotons, due to the non-linear nature of the dispersion curve, are stable against decay and consequently if there are few scattering sites (achieved by the low temperature equilibrium density of phonons and the isotopic purity) have long mean free paths. That is, they propagate ballistically and carry energies greater than the binding energy of helium liquid at its free surface. Since their typical energy is $8.9K(.7meV)$ there are about 10^7 rotons for a 200 keV electron. Upon reaching a free surface they are known to induce quantum evaporation 10-30% of the time -

i.e., a single roton ejects a single helium atom which, in our method of sensor, are physisorbed onto a thin silicon crystal wafer (at 30° mK) where they release their surface binding energy (100°K) as phonons which then come to quasi-equilibrium and this temperature rise $\Delta T = \Delta E/C (C \propto [\frac{T}{635}]^3)$ is detected. C is the heat capacity. As discussed earlier there are many possibilities for devices to measure this temperature rise. We have used thermistors in our early tests. Obviously, it is important to keep C as small as possible and the presence of superfluid helium requires extra precaution otherwise the superfluid film will cover the sensor and add enormously to the heat capacity.

Examples of Present Status – a) Crystals. Here I make a subjective selection of two examples. My two criteria are that as cryogenic techniques they illustrate contrasting approaches (equilibrium versus non-equilibrium phonon detection) and some stated objectives by the authors to have a goal of neutrino detection. Space does not permit the reproduction here of the relevant figures but I refer the reader to some of the original papers;^{11,12]} I will summarize the interesting results here.

A very important result has been achieved by W. Seidel et al^{11]} at the Technical University - Munich. They have achieved, using quasi-equilibrium phonons, a temperature sensitivity of 54 nanokelvin on a 280 gram sample of sapphire. (These are very significant improvements in sample size ($\times 100$) and sensitivity ($\times 10$) over previous work). This was done using a superconducting thin film sensor of iridium ($T_c = 135mK$) operated well within the steepest portion of the transition edge. The particles detected were alphas of 5.15, 5.48 and 5.8 MeV with $\Delta E/E = 1.2\%$ and a 0.03% non-linearity. The typical temperature rise was 4 micro-K with a 70 micro-sec rise time. The decay time exhibited a fast component (~ 2 milli-sec) and a slower one (~ 200 milli-sec) containing most of the energy. This latter effect is attributed to impurities and new experiments are underway with purer crystals.

By way of contrast, B. Cabrera et al^{12]} at Stanford University are also working with superconducting thin film sensors but in a mode optimized for ballistic phonons. The detecting medium is silicon and the samples much smaller (~ 2 grams); however, in an interesting series of experiments involving coincidences between two sensors they have detected 5 MeV alphas and 25 keV gammas and utilized them to analyze phonon processes. The initial film was titanium ($T_c = 340mK$). In their application whole regions of the film are driven fully normal ($\sim 3eV/(\mu m)^2$) by the ballistic phonons. In this mode the sensor is a threshold device and to this end the group

is testing other films such as tungsten ($T_c = 14\text{mK}$) in an effort to achieve very low thresholds. An important feature of the use of ballistic phonons in crystals is the possibility of taking advantage of the phonon focusing in the lattice to increase higher surface energy density and utilization of the focusing pattern for background discrimination.

Both groups are forging ahead with further ideas and foresee configurations suitable for dark matter searches and reactor tests in the very near future.

b) Liquid Helium. In order to test the basic ideas of the superfluid helium technique the Brown group of S. Bandler et al^{9]} have constructed a 2 liter prototype. We have just completed our first series of tests and now have preliminary results. The goals of the first tests were five fold: to set the scale of the sensitivity problem, to generate rotons by radioactive particles, to see quantum evaporation at a free surface by rotons, establish that the rotons are indeed ballistic and to measure^{13]} a temperature rise of the silicon wafer by physisorption of the helium. In these tests we utilized several sources: 5MeV alphas, 364 keV electrons and a tungsten heater. The silicon wafer was operated at several temperatures in the vicinity of 30 mK while the helium in the cell was at 100 mK. The noise level was seen to be equivalent to 20 keV – very gratifying for a first attempt. Alpha particles were detected by the full chain of processes ending in the detection of a temperature rise on the silicon wafer above the liquid. By use of the heat flush and superleak, the helium was isotopically pure ^4He ; since ^3He – a fermion – does not participate in the superfluid state, ballistic propagation can be destroyed by injecting ^3He atoms which serve as scattering centers. This was done (5 parts in 10^8) and severe degradation of the pulse (1/50) and appropriate signal delays (from the pulsed source) were observed thus establishing the change from ballistic to diffuse propagation.

Thus we feel that the fundamental processes for the technique have been shown and we are now beginning further tests designed to evaluate feasibility for solar neutrino detection as well as for dark matter and earth-based experiments to test other properties of neutrinos.

Conclusion – In a talk such as this one to so general a physics audience one can only hope to give a superficial sampling of an area of detector development which is actually extremely diverse in both the physics brought to bear on techniques and the physics to which they are being applied. I hope I have given you a flavor of this

active and growing field and shown some of its promise for opening new approaches to neutrino physics.

References

- 1] R. Davis, Jr., in *Proceedings of Seventh Workshop on Grand Unification*, ICOBAN'86, edited by J. Arafune (World Scientific, Singapore), 237 (1987).
- 2] See talk by Y. Suzuki, this workshop.
- 3] Sudbury Solar Neutrino Observatory Report #SN0-87-12 (1987); H. H. Chen, *Phys. Rev. Lett.* **55**, 1534 (1985).
- 4] See talk by V. Gavrin, this workshop.
- 5] See, for example, J. N. Bahcall and R. K Ulrich, *Rev. Mod. Phys.* **60**, 297 (1988); D. Sackmann et al, *Ap. J.* **360**, 727 (1990); C. Turck-Chieze et al, *Ap. J.* **335**, 415 (1988).
- 6] B. Cabrera, L. Krauss and F. Wilczek, *Phys. Rev. Lett.* **55**, 25 (1985).
- 7] An excellent reference for all of these techniques is "Low Temperature Detectors for Neutrinos and Dark Matter III", edited by L. Brogiato et al, Edition Frontieres, Gif-Sur-Yvette (1990).
- 8] C. Martoff, *Science*, **237**, 507 (1987).
- 9] R. E. Lanou, H. J. Maris and G. M. Seidel, *Phys. Rev. Lett.* **58**, 2498 (1987); S. Bandler et al in Brown University Progress Report to U.S. D.O.E. #DOE/ER/40452-5 (Dec. 1990).
- 10] H. Maris et al, *Proc. of PHONON89 (Heidelberg)* (World Scientific, Singapore, 1989) p. 175. H. Maris in *Phonon Scattering in Condensed Matter V*, Ed: A. Anderson and J. Wolfe (Springer- Verlag Berlin, 1986) p. 404.
- 11] W. Seidel, W. Christen, F. V. Feilitzsch, G. Forster, H. Gobel, E. Kellner, F. Probst and R. Mossbauer in Ref. 7 p. 137; *Phys. Lett.* **B236**. 483 (1990).
- 12] B. Young, A. Lee, B. Cabrera in Ref. 7 above, p. 183.
- 13] E. E. Haller provided the NTD Germanium thermistor; E. E.Haller, *Infrared Phys.* **25**, 257 (1985).

**FEASIBILITY STUDIES OF THE GEOCHEMICAL
 ^{205}Tl SOLAR NEUTRINO EXPERIMENT**

S. Neumaier, B. Dockhorn, E. Nolte, H. Morinaga
Faculty of Physics, Technical University of Munich,
8046 Garching, FRG

Presented by S. Neumaier



ABSTRACT

New investigations on the signal to background ratio of the geochemical $^{205}\text{Tl}(\nu_e, e^-)^{205}\text{Pb}$ solar neutrino experiment are presented. The neutrino capture rate of ^{205}Tl and a possible reduction of the neutrino signal due to neutrino oscillations in matter are discussed. The contributions of natural radioactivity, stopped negative muons and fast muons to the background of ^{205}Pb are estimated. The production of radioisotopes in the lead region induced by cosmic ray muons was studied at the high energy muon beam (M2) of CERN with 120, 200 and 280 GeV muons. The background contribution of cosmic ray muons is found to be significantly higher than expected by former estimations and restricts the feasibility of the ^{205}Tl solar neutrino experiment.

1. Introduction

The feasibility of the geochemical ^{205}Tl solar neutrino experiment using thallium minerals from Allchar (Yugoslavia) depends on the ratio of neutrino induced reactions to background reactions. First estimates of the signal to background ratio were given by M.S. Freedman in 1979 [1]. During the last years, new investigations were presented [2, 3] which indicate that some of the main assumptions of [1] are not in agreement with present data. Therefore, a reexamination of the signal to background ratio has been performed [4]. The main results of these investigations are presented.

2. Neutrino capture and neutrino oscillations

The ^{205}Tl solar neutrino experiment is distinguished by a very low effective threshold for neutrino absorption of $E_{\text{thr}} = (53.6 \pm 0.6)$ keV [5] for the most probable transition to the first excited state of ^{205}Pb at $E_{\text{exc}} = 2.3$ keV. Therefore, a ^{205}Tl detector is sensitive to pp neutrinos.

The neutrino capture rate of ^{205}Tl was estimated, using a $\log ft_{1/2}$ -value of 5.7 for transitions to the first excited state of ^{205}Pb as suggested by Braun and Talmi [6] and preliminary Gamow-Teller strengths given by Krofcheck et al. [7] for transitions to higher excited states. It is found that higher excited states contribute considerably to the capture rate, as predicted by Morinaga [2]. The total capture rate was found to be 260 SNU in full agreement with Bahcall and Ulrich [8]. A detailed description of the calculations is given in [4]. With suppression factors for electron neutrinos due to neutrino oscillations in matter and in vacuum calculated by A. Urban [9] the reduction of the capture rate was evaluated taking into account transitions to the first excited state of ^{205}Pb as done by Mikheyev and Smirnov [3] as well as transitions to higher excited states. If the strong reduction of the neutrino capture rate of ^{71}Ga as indicated by first results of the SAGE collaboration [10] is due to the MSW effect, a similar reduction of the neutrino signal is expected for the ^{205}Tl experiment, as shown in Fig. 1.

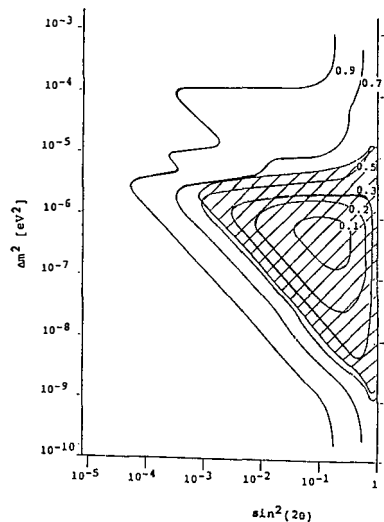


Fig. 1.: Lines of constant suppression for the neutrino capture rate of ^{205}Tl . The dashed region corresponds to a ^{71}Ga capture rate of less than 70 SNU as indicated by first preliminary results of the SAGE collaboration [10].

3. Background reactions

The main sources of background producing ^{205}Pb ($T_{1/2} = 1.5 \cdot 10^7\text{y}$) are natural radioactivity, stopped negative muons and penetrating fast muons produced by cosmic radiation.

Natural contaminations of Uranium and Thorium contained as trace elements in the

lorandite mineral and the surrounding ores produce neutrons by spontaneous fission and (α, n) -reactions as well as protons by (α, p) -reactions on light nuclei. The contributions of these background reactions are estimated, using the chemical composition of lorandite and the surrounding ores [3]. The deduced production rate of ^{205}Pb by natural radioactivity is less than 15 SNU [4].

The rate of stopped negative muons as a function of depth decreases more rapidly than the fast muon component. Therefore the contribution of stopped negative muons to the background via the production of secondary particles and the $^{209}\text{Bi}(\mu^-, \nu_{\mu}4n)^{205}\text{Pb}$ reaction becomes important only at shallow depths and is expected to be negligible at the present depth of the lorandite deposit (120 m). The main contribution to the background is due to interactions of high energy muons produced by cosmic radiation. In interactions with the surrounding ore body, nuclear and electromagnetic cascades are induced producing nucleons, pions and photons. Subsequent nuclear reactions like $^{205}\text{Tl}(p, n)^{205}\text{Pb}$, $^{205}\text{Tl}(\pi^+, \pi^0)^{205}\text{Pb}$ and $^{205}\text{Tl}(\gamma, \pi^-)^{205}\text{Pb}$ transform ^{205}Tl nuclei into ^{205}Pb . Experimental investigations of the production rate of ^{205}Pb initiated by cosmic ray muons and their secondary particles were performed with high energy muons at the CERN Super Proton Synchrotron (SPS).

4. Experiments with high energy muons at CERN

To study the production of radioisotopes by cosmic ray muons, we exposed various materials of the lead region to the high energy muon beam (M2) of CERN, which provides muon energies of 90 GeV up to 280 GeV. With targets of 8 cm in diameter a time averaged muon flux of about $2 \cdot 10^4 \text{cm}^{-2}\text{sec}^{-1}$ can be achieved. During the whole age of the Allchar deposit the lorandite minerals and the surrounding ores were irradiated with a muon fluence of less than $8 \cdot 10^9 \text{cm}^{-2}$. The same fluence of muons can be achieved by an exposure time of about 5 days at CERN. Targets were irradiated for several days with 120, 200 and 280 GeV muons, respectively. In the irradiated samples, about 30 radioisotopes in the lead region were identified off beam by γ -ray spectroscopy. The production rate of ^{205}Pb by cosmic ray muons was calculated using muon spectra underground and measured cross sections of similar transitions in the vicinity of ^{205}Pb .

5. Measurements and results

The production of secondary particles was investigated with heavy concrete absorbers ($5 \times 1 \times 2 \text{ m}^3$). It is found that an absorber thickness of about 3 m in beam direction is sufficient to reach equilibrium of the secondary particle fluxes responsible for the production of ^{205}Pb . The energy dependence measured at 120 and 280 GeV is in full agreement with "Wolfendale's rule" [4]. The method of accelerator mass spectrometry (AMS) [11], most sensitive to determine the extremely small concentrations of ^{205}Pb ($T_{1/2} = 1.5 \cdot 10^7 \text{y}$) of the irradiated samples is still in development and could not be used for these investigations. With a high purity germanium detector (44 %, 1.95 keV) and a passive shielding of 15 cm of lead, cross sections for the production of ^{203}Pb ($T_{1/2} = 52 \text{h}$) by high energy muons and their secondary particles were measured with targets of natural and highly enriched thallium. Assuming that ^{203}Pb and ^{205}Pb are mainly produced by low energy

protons via $^{203,205}\text{Tl}(p, xn)^{203,205}\text{Pb}$ reactions, the production rate of ^{205}Pb in thallium induced by cosmic ray muons is derived from the production rates of ^{203}Pb in natural thallium and in ^{203}Tl (enriched to 96%) measured at CERN and from the shape of the secondary proton spectrum suggested by [1].

6. Signal to background ratio

The signal to background ratio was calculated as a function of depth, assuming a neutrino capture rate of 260 SNU (SSM) and the depth dependent background discussed in [4]. At the present depth of the Allchar deposit (120m), the background is by a factor of 2 higher than the neutrino signal. From geological investigations however, it is assumed that the location of the deposit at the time of the mineralization was about 200-300m beneath the surface (see S. Jankovic in [3]). The effective shielding of the lorandite mineral therefore depends on the history of erosion during the last millions of years. For a first approach, the background was calculated as a function of a constant (time independent) erosion rate. Assuming an age of the mineral of $5 \cdot 10^6$ y the mean erosion rate was only $40\text{m}/10^6\text{y}$. Under these conditions the background of ^{205}Pb due to cosmic ray muons is estimated to be 200 SNU.

7. Conclusions

The background induced by cosmic ray muons seems to be significantly, by a factor of 3, higher than expected by former estimations [1, 4]. For the most probable case of a medium erosion rate of about $40\text{m}/10^6$ y, the background is not negligible and has to be measured with a sufficiently high accuracy. The determination of background therefore restricts the feasibility of the ^{205}Tl solar neutrino experiment. Further investigations are necessary to study the erosion rate problem especially during the last million of years, and to proof that a reliable determination of background can be achieved.

Acknowledgements

This research was supported by the New Muon Collaboration (CERN), D. Vignaud (Gallex) and the BMFT. We are grateful to M. Meier, C. Seidl and M. Boulouednine who helped us preparing the experiments and analysing the data.

References

- [1] M.S. Freedman, Proc. Informal Conf. on Status and future of solar neutrino research, ed. G. Friedlander, vol. 1, BNL Report 50879 (1979), p. 313.
- [2] Proc. Workshop on the feasibility of the Solar Neutrino Detection with ^{205}Pb , Munich 1985, ed. E. Nolte, Report GSI-86-9.
- [3] Proc. of the Intern. Conf. on Solar Neutrino Detection with ^{205}Tl , Dubrovnik 1986, ed. E. Nolte and M.K. Pavicevic, Nucl. Instr. and Meth. A271 (1988) 237.
- [4] S. Neumaier, PhD thesis, Technical University of Munich (Germany) 1990.
- [5] H. Lindner et al., Nucl. Instr. and Meth. A297 (1990) 217.
- [6] E. Braun and I. Talmi in Proc. Intern. Symposium Weak and Electromagnetic Interactions in Nuclei, Heidelberg 1986, ed. H.V. Klapdor, Springer Berlin 1986, p. 47.
- [7] D. Krofcheck, private communication 1989.
- [8] J.N. Bahcall and R.K. Ulrich, Rev. Mod. Phys. 60 (1988) 297.
- [9] A. Urban, private communication 1989.
- [10] M. Mitchell Waldrop, Science 248 (1990) 1607.
- [11] H. Ernst et al., Nucl. Instr. and Meth. B5 (1984) 426.

RESONANT SPIN-FLAVOR PRECESSION
AND THE SOLAR-NEUTRINO PROBLEM

E.Kh. Akhmedov

Kurchatov Institute of Atomic Energy, Moscow 123182, USSR



ABSTRACT

Main features of resonant spin-flavor precession of neutrinos due to the interaction of their flavor-off-diagonal magnetic dipole moments with transverse magnetic fields in the presence of matter are reviewed. Implications of this phenomenon for the solar-neutrino problem are discussed.

1. Introduction

If lepton flavor is not conserved, neutrinos can possess flavor-off-diagonal (transition) magnetic dipole moments. Under transverse magnetic fields such transition moments will cause the rotation of left-handed neutrinos of a given flavor into right-handed neutrinos (or antineutrinos) of another flavor. In vacuum this spin-flavor precession (SFP) of neutrinos is suppressed (as compared to the flavor-conserving precession) due to the energy splitting of the neutrinos of different flavors: $\Delta E \approx (m_2^2 - m_1^2)/2E \approx \Delta m^2/2E$ for relativistic neutrinos. However, in matter this kinetic energy difference can be canceled by the difference of their potential energies, resulting in the resonant enhancement of the precession¹⁻⁴). The resonant spin-flavor precession (RSFP) is analogous to the resonant flavor oscillations (RFO) of neutrinos⁵⁻⁷), although there are some important differences between these two phenomena^{1,3,4}). In this report we review the main features of the RSFP and its implications for the solar-neutrino problem.

2. General formalism

Interaction of neutrinos with external magnetic fields due to their magnetic moments is described by the following effective lagrangians:

$$\mathcal{L}_{\text{int}}^{\text{D}} = \sum_{i,k} \frac{1}{2} \mu_{ik}^{\text{D}} [\bar{\nu}_{kR} \sigma_{\alpha\beta} \nu_{iL}] \cdot F^{\alpha\beta} + \text{h.c.} \quad (1)$$

for Dirac neutrinos and

$$\mathcal{L}_{\text{int}}^{\text{M}} = \sum_{i,k} \frac{1}{2} \mu_{ik}^{\text{M}} [\bar{\nu}_{kR}^{\text{C}} \sigma_{\alpha\beta} \nu_{iL}] \cdot F^{\alpha\beta} + \text{h.c.} \quad (2)$$

for Majorana neutrinos. For the latter, the matrix of magnetic moments μ_{ik}^{M} is antisymmetric, so that $\mu_{ii}^{\text{M}} = 0$. In the case of Dirac neutrinos, SFP transforms left-handed ν_{eL} 's into right handed sterile ν_{jR} 's ($j = \mu, \tau$), whereas for Majorana neutrinos it transforms ν_{eL} 's into right-handed antineutrinos ν_{jR}^{C} . Although the

latter are not sterile, they cannot be detected in charged-current (CC) experiments, such as ^{37}Cl or ^{71}Ga ones.

Consider evolution of the neutrino system in matter and magnetic field in the two-flavor approximation. Let us first suppose that the vacuum mixing angle of neutrinos θ_0 is small enough, so that the flavor eigenstates approximately coincide with mass eigenstates: $\nu_e \approx \nu_1$ and $\nu_j \approx \nu_2$, and one can neglect the neutrino oscillations. Then the evolution of the neutrino system is described by the equation 1-4)

$$i \frac{\partial}{\partial t} \begin{pmatrix} \nu_{eL} \\ \nu_{jR}^{(c)} \end{pmatrix} = \begin{pmatrix} m_1^2/2E + C_L(t) & \mu_{ej} B_\perp(t) \\ \mu_{ej} B_\perp(t) & m_2^2/2E + C_R(t) \end{pmatrix} \begin{pmatrix} \nu_{eR} \\ \nu_{jR}^{(c)} \end{pmatrix} \quad (3)$$

In eq. (3) B_\perp is the transverse magnetic field strength, $C_L = 2^{1/2} G_F \times [N_e(t) - N_n(t)/2]$, $C_R = 0$ for Dirac neutrinos and $2^{1/2} G_F N_n(t)/2$ for Majorana neutrinos; G_F , N_e and N_n are the Fermi constant and electron and neutron number densities, respectively.

For uniform magnetic field and matter density, eq. (3) can be easily solved yielding the $\nu_{eL} \rightarrow \nu_{jR}^{(c)}$ transition probability

$$P(\nu_{eL} \rightarrow \nu_{jR}^{(c)}; t) = \sin^2 2\theta \cdot \sin^2(\pi t/l), \quad (4)$$

where

$$\sin^2 2\theta = (2\mu_{ej} B_\perp)^2 / \{ (2\mu_{ej} B_\perp)^2 + [\Delta m^2/2E - (C_L - C_R)]^2 \} \quad (5)$$

$$l = 2\pi / \{ (2\mu_{ej} B_\perp)^2 + [\Delta m^2/2E - (C_L - C_R)]^2 \}^{1/2} \quad (6)$$

The resonance condition is $\Delta m^2/2E = C_L - C_R$; it can be seen from eqs. (4)-(6) that at the resonance $\sin^2 2\theta = 1$, $l = l_R = \pi / \mu_{ej} B_\perp$, and the SFP proceeds with the maximal amplitude.

In general case of non-uniform matter density and magnetic field, eq. (3) must be solved numerically. For monotonously varying matter density the avoided level-crossing phenomenon

occurs at the resonance, which is analogous to that in the case of RFO⁵⁻⁷). If the adiabaticity condition is satisfied, i.e. the resonance width at half height Δr is greater than the precession length at the resonance, the resonant conversion will take place, transforming practically all the ν_{eL} 's into $\nu_{jR}^{(c)}$ 's¹⁻⁴). The adiabaticity condition can be written as

$$\lambda \equiv \pi \frac{\Delta r}{l_r} \approx 8 \frac{E}{\Delta m^2} [(\mu_{ej} B_{lr})^2 L_\rho] > 1 \quad (7)$$

where B_{lr} is the magnetic field strength at the resonance and L_ρ is the characteristic length over which matter density varies significantly. Note that the adiabaticity parameter λ depends on B_{lr} quadratically. There is a significant difference between the RFO and RSFP: the adiabaticity parameter of the RFO $\lambda_{MSW} = (\sin^2 2\theta_o / \cos 2\theta_o) (\Delta m^2 / 2E) L_\rho$ is inversely proportional to neutrino energy, whereas the parameter λ of eq (7) is directly proportional to it. For non-uniform magnetic field, however, the E dependence of λ is more complicated since with varying E the coordinate of the resonance point changes and so does B_{lr} . Therefore the B_{lr}^2 factor in λ brings in an additional E dependence.

3. RSFP and the solar-neutrino problem

The RSFP can account¹⁻⁴) for both the solar-neutrino deficiency and the 11-yr variations of the solar-neutrino flux in anticorrelation with solar activity, for which there is some evidence in the ³⁷Cl experiment of Davis and his collaborators⁸). The latter follows from the fact that the magnetic field in the convective zone of the sun ($0.7R_\odot < r < R_\odot$, $\rho < 0.16$) is correlated with solar activity. Expressing $E/\Delta m^2$ through the resonant density ρ_r , to which it is inversely proportional, we can rewrite the adiabaticity condition (7) in the following form:

$$\beta_r > 100 \sqrt{\rho_r} \quad (8)$$

Here $\beta_{\text{r}} \equiv (\mu_{\text{ej}}/10^{-11}\mu_{\text{B}})B_{\perp\text{r}}/\text{KG}$, μ_{B} being the Bohr magneton, and ρ_{r} is in g/cm^3 . Thus for the resonance occurring near the center of the sun ($\rho_{\text{r}} \approx 150$) and $B_{\perp} (r \approx 0) \sim 10^7$ G the transition moment as small as $10^{-12}\mu_{\text{B}}$ is sufficient to explain the observed solar neutrino deficiency. However, the inner magnetic field of the sun is expected to be frozen; it is only the toroidal magnetic field in the convective zone of the sun that exhibits the 11-yr variations. Therefore the RSFP can account for the apparent time variation of the ^{37}Cl detection rate only if a significant fraction of ^8B neutrinos undergo the resonant conversion in the convective zone. For $\mu_{\text{ej}} \sim 10^{-11}\mu_{\text{B}}$, eq.(8) requires $B_{\perp} > 40$ KG for the resonance occurring at the bottom of the convective zone to be adiabatic. Note that in the case of non-resonant neutrino spin precession one needs $\beta > 500\rho$ to overcome matter-suppression effects^{9,10}); thus one has a factor of two gain in β for the RSFP as compared to the non-resonant precession at the bottom of the convective zone.

The RSFP predicts also the semiannual variations of the ν_{eL} flux at the periods of high solar activity. The reason for these variations is exactly the same as that for the semiannual variations of the ν_{eL} flux in the non-resonant neutrino spin precession scenario^{9,10}): they should occur due to peculiarities of the magnetic field configuration in the convective zone of the sun and non-zero angle between the orbit of the earth and the solar equator plane.

Numerical calculations with "plausible" magnetic field configurations^{4,11,12}) yield the $E/\Delta m^2$ dependence of the ν_{eL} survival probability P_1 which is somewhat similar to that in the case of the RFO. However, there are important differences, too. For the RFO, the ν_{eL} survival probability inside the "suppression pit" generally increases with increasing $E/\Delta m^2$ since the

adiabaticity of the conversion decreases. For the RSFP, the $E/\Delta m^2$ dependence of the adiabaticity parameter is defined by an interplay of two values, L_ρ and L_B , where L_B is the characteristic size over which $B_1(r)$ changes significantly. If L_B is $>2L_\rho$, the RSFP becomes more adiabatic (and the survival probability decreases) with increasing $E/\Delta m^2$, and vice versa^{1,3,4,12}).

In ref.¹²⁾ detailed calculations were carried out of the ν_{eL} survival probabilities and ^{37}Cl detection rates Q_{Cl} for a number of magnetic field configurations. It was shown that for the magnetic field in the convective zone calculated in ref.¹³⁾ it is difficult to reproduce the observed time variations of the Q_{Cl} unless there is a strong inner magnetic field in the sun and the equatorial gap in the toroidal magnetic field is less than usually taken value of 5° . Obviously, more calculations with various possible magnetic field configurations are needed to draw any definitive conclusion. Unfortunately, there are very few calculations of the solar magnetic fields.

The inner magnetic field of the sun may play a significant role, suppressing the low-energy neutrino flux and bringing the theoretical predictions into better agreement with the experiment^{4,12,14-16}). The magnetic field near the top of the radiation zone can also increase the adiabaticity of the RSFP occurring in the convective zone by enlarging the resonance width^{3,4,14,15}).

It is not difficult to estimate the expected effect of the RSFP for various solar-neutrino experiments¹⁵⁾. The detection rate in the ^{71}Ga experiments Q_{Ga} , to which the low-energy pp-neutrinos give the major contribution, should not exhibit any significant time variations provided that the inner magnetic field is relatively weak and the low-energy neutrino flux is not

suppressed, since the ^8B neutrinos contribute $\leq 10\%$ in this case. However, if the flux of the low-energy neutrinos is suppressed, time variations of the ^8B -neutrino flux will result in the sizable time variations of Q_{Ga} . One should expect a strong suppression of the average Q_{Ga} value as compared to the standard solar model (SSM) prediction in that case.

In the CC reactions in SNO and Borex detectors only the ^8B neutrinos can contribute; therefore there one can expect strong suppression and sizable time variations of the ν_e signals.

For the neutral-current (NC) neutrino detection reactions such as the neutrino-deuteron disintegration $\nu d \rightarrow np\nu$, neutrino-nucleus excitation $\nu A \rightarrow \nu A^*$ or ν -e scattering (to which both the CC and NC contribute), the results depend on whether the neutrinos are Dirac or Majorana particles. For Dirac neutrinos the suppression factors of $Q_{\nu d(\text{NC})}$, $Q_{\nu A(\text{NC})}$ and $Q_{\nu e}$ coincide with that for $Q_{\nu d(\text{CC})}$. For Majorana neutrinos the $\nu d(\text{NC})$ and $\nu A(\text{NC})$ detection rates should be constant and equal to the corresponding SSM prediction, whereas for the ν -e scattering experiments one can expect moderate neutrino flux suppression and time variation¹⁵⁾.

Let us now make some remarks on recent experimental results on solar neutrinos. It was claimed by the Kamiokande II collaboration that the ratio of the average detection rate of the solar neutrinos over the three years of observation to the SSM prediction is $0.46 \pm 0.05(\text{sta.}) \pm 0.06(\text{sys.})$, and the time variations, if any, do not exceed 30% ¹⁷⁾. This seems to be at variance with the results of the ^{37}Cl experiment of Davis et al., in which much stronger time variations are observed. However, one can readily make sure that these two results can be reconciled in the RSFP scenario provided that the low-energy ν contributions to the ^{37}Cl experiment are strongly suppressed. This is because in that case

weaker suppression of the ${}^8\text{B}$ ν 's is needed, i.e. their flux may be higher. Since the ν_μ^c and ν_τ^c do contribute to the νe reaction which is employed in the Kamiokande II experiment (though with 6-7 times smaller cross sections), a 30% time variations in the Kamiokande II detection rate may be compatible with a factor 2-3 variation in the ${}^{37}\text{Cl}$ experiment^{15,16}). One can expect strong suppression of the ${}^{71}\text{Ga}$ counting rate in this case, which is consistent with the first results of the SAGE collaboration¹⁸). A drastic suppression of low-energy ν_{eL} 's we need in this scenario may be either due to the strong inner magnetic field or due to the RFO when the RSFP and RNO operate jointly¹⁶).

4. Combined effect of oscillations and spin-flavor precession

RSFP can occur only if the neutrino flavor is not conserved; this implies that the neutrino oscillations must also take place. Thus in general the RSFP should be considered jointly with the RFO. A combined effect of neutrino oscillations and SFP in the sun was studied in a number of papers both analytically¹¹) and numerically^{2,11,19,20}). We shall discuss the case of Majorana neutrinos following ref. 11). If

$$\left[|\tan 2\theta_0| + |2\mu_{ej} B_{IR} / (\Delta m^2 / 2E)| \right] / [1 + |\tan 2\theta_0|] < N_n / N_e, \quad (9)$$

the resonances of the oscillations and SFP do not overlap, so that these two phenomena can be considered separately. The resonant density for the RSFP is greater than that for the RFO^{2,11}); therefore if the ν_{eL} 's are born in a high-density region, they first encounter the resonance of SFP. If the adiabaticity condition (7) is satisfied, the ν_{eL} 's will be converted into the ν_{jR}^c 's and then never reach the resonance of RFO. Therefore in this case the RFO will be inoperative in the sun, no matter how good the adiabaticity of the oscillations is¹¹). If, however, the

adiabaticity condition (7) is badly violated, practically all the ν_{eL} 's will pass through the SFP resonance without being converted into ν_{jR}^c 's. Then they encounter the RFO resonance in which the $\nu_{eL} \rightarrow \nu_{jL}$ conversion may occur. This conversion will be almost complete provided the adiabaticity condition for the RFO is fulfilled.

When the condition (9) is not satisfied, i.e. the resonances of oscillations and SFP overlap, these two effects can either suppress or enhance each other, depending on the degree of the adiabaticity of both the conversions. The overlap of the RFO and RSFP resonances improves their adiabaticity, since (i) the widths of both the resonances become larger, and (ii) the oscillation and precession lengths become smaller¹¹⁾. This implies that the RFO and RSFP enhance each other in the non-adiabatic regime. At the same time, if both the resonant conversions are adiabatic, the RFO and RSFP suppress each other.

Combined effect of the RFO and RSFP may have important consequences for solar neutrinos. Although the neutrino oscillations cannot give rise to the apparent time variations of the solar neutrino flux in the ^{37}Cl experiment, they can efficiently assist the RSFP to do so. As a result, smaller values of the neutrino transition magnetic moments are required, which are compatible¹⁶⁾ with the recently derived astrophysical upper bound $\mu \leq 3 \cdot 10^{-12} \mu_B$ ²¹⁾.

In the case of Majorana neutrinos the combined effect of RFO and RSFP must result in a flux of electron antineutrinos ν_{eR}^c from the sun^{2,22)}. The most striking consequence of the oscillations +SFP scenario is that the ν_{eR}^c flux must exhibit time variations in *direct* correlation with solar activity. This distinguishes this mechanism clearly from the other ν_{eR}^c -producing mechanisms since

none of them is capable of inducing such time variations. This should also be compared with the spin precession^{9,10)} and RSFP¹⁻⁴⁾ scenarios which predict time variations of the ν_{eL} flux, but in anticorrelation with solar activity. There should also exist semiannual variations of the ν_{eR}^c flux which are different from those of the $\nu's^{22)}$.

5. Conclusion

The neutrino conversion mechanism due to the RSFP can account for both the solar-neutrino deficiency and apparent time variations of the solar-neutrino flux in the ³⁷Cl experiment. It has specific consequences for various solar-neutrino experiments and therefore is distinguishable from the other possible solutions of the solar-neutrino problem.

References

1. E.Kh. Akhmedov, preprint IAE-4568/1, January 1988.
2. C.-S. Lim and W.J. Marciano, Phys. Rev. D37 (1988) 1368.
3. E.Kh. Akhmedov, Phys. Lett. B213 (1988) 64.
4. E.Kh. Akhmedov and O.V. Bychuk, Sov. Phys. JETP 68 (1989) 250.
5. L. Wolfenstein, Phys. Rev. D17 (1978) 2369.
6. S.P. Mikheyev and A.Yu. Smirnov, Sov. J. Nucl. Phys. 42 (1985) 913
7. S.P. Mikheyev and A.Yu. Smirnov, Sov. Phys. Usp. 30 (1987) 759.
8. R. Davis, Jr. Talk given at the XXIst Int. Conf. on Cosmic-Ray Physics, Adelaide, Australia, 1990.
9. M.B. Voloshin and M.I. Vysotsky, Sov. J. Nucl. Phys. 44 (1986) 544.
10. M.B. Voloshin, M.I. Vysotsky, and L.B. Okun, Sov. Phys. JETP 64 (1986) 446.
11. E.Kh. Akhmedov, Sov. Phys. JETP 68 (1989) 690.
12. P.I. Krastev and A.Yu. Smirnov, Z. Phys. C, to be published.
13. H. Yoshimura, Astrophys. J. Suppl. 29 (1975) 467.
14. H. Minakata and H. Nunokawa, Phys. Lett. B245 (1990) 197.
15. E.Kh. Akhmedov, preprint IAE-5017/1, January 1990 (to be published).
16. E.Kh. Akhmedov, preprint IAE-5194/1, August 1990; Phys. Lett. B, in press.
17. Y. Totsuka, Talk given at the 14th Int. Conf. on Neutrino Physics and Astrophysics "Neutrino 90", CERN, Geneva, June 10-15, 1990.
18. V.N. Gavrin, ref. 17.
19. H. Minakata and H. Nunokawa, Phys. Rev. Lett. 63 (1989) 121.
20. A.B. Balantekin, P.J. Hatchell and F. Lorati, Phys. Rev D41 (1990) 3583.
21. G.G. Raffelt, Phys. Rev. Lett. 64 (1990) 2856.
22. E.Kh. Akhmedov, Phys. Lett. B255 (1991) 84.

PRESENT STATUS OF THE RESONANT FLAVOR CONVERSION.

A.Yu.Smirnov

Institute for Nuclear Research,
Academy of sciences of the USSR, 117312 Moscow, USSR**ABSTRACT**

The latest experimental data on solar neutrinos are considered and the status of the resonant flavor conversion (MSW-effect) is formulated. We discuss (1) the restrictions on the neutrino parameters from the existing ^3Ar -solar data; (2) the possibilities to explain time variations of ^3Ar -production rate; (3) the progress in the identification of the true solution of the ν_{\odot} -problem.

I. INTRODUCTION.

At present the status of the resonant flavor conversion (MSW-effect)¹⁾ is determined by

- data from three solar neutrino experiments: Cl - Ar at Homestake²⁾, Kamiokande-II³⁾, and SAGE at Baksan⁴⁾;
- physics of the Sun itself, and here further confirmation of the standard solar model (SSM)⁵⁾, especially by helioseismology, is very important;
- particle physics data.

In this review we concentrate on the first item, and begin with some features of the solar neutrino data.

2. COMMENTS ON THE SOLAR NEUTRINO DATA.

Considering the experimental results since 1987, when both Cl - Ar and Kamiokande-II were taking data (fig.1) one finds

- 1). The Ar-production rate, Q_{Ar} , averaged over period 1987 - 1990,3 is appreciably larger, than the average over all time of observations. The corresponding suppression factors $R_{Ar} = Q_{Ar}/Q_{Ar}^{SSM}$ (Q_{Ar}^{SSM} is the prediction in the SSM) are

$$\bar{R}_{Ar}(>1987) = 0.38 \pm 0.07 \quad (1)$$

$$\bar{R}_{Ar}(>1970) = 0.28 \pm 0.03 \quad (2)$$

It is important that since 1987 the solar activity changes from minimum to maximum, and one expects the equality of (1) and (2).

- 2). The suppression (1) is not much stronger than that in Kamiokande-II³⁾:

$$\bar{R}_{\nu e} = 0.46 \pm 0.06 \pm 0.05 \quad (3)$$

and moreover apart from one time bin (1987.5 - 1989.0) R_{Ar} and $R_{\nu e}$ coincide within the errors bars.

- 3). Time variations of Q_{Ar} since 1987 are less profound than in previous solar cycle. In particular the average over the year of minimal signal (1988.5 - 1989.5) is $Q_{Ar}^{\min} = 1.6 \pm 0.6$ SNU, which agrees with average value (2) and appreciably larger than in 1979: (0.4 ± 0.2) SNU. Moreover, the year of minimal signal is shifted with respect to the period of maximal activity by $\Delta t = 0.5 - 1.0$ year in contrast with previous cycle.

- 4). There are strong indications on the anticorrelations of Ar-production rate with solar activity - sunspots number, N_{sp} (see review⁶⁾). The probability to reproduce the observed time sequence of experimental points as a fluke at constant

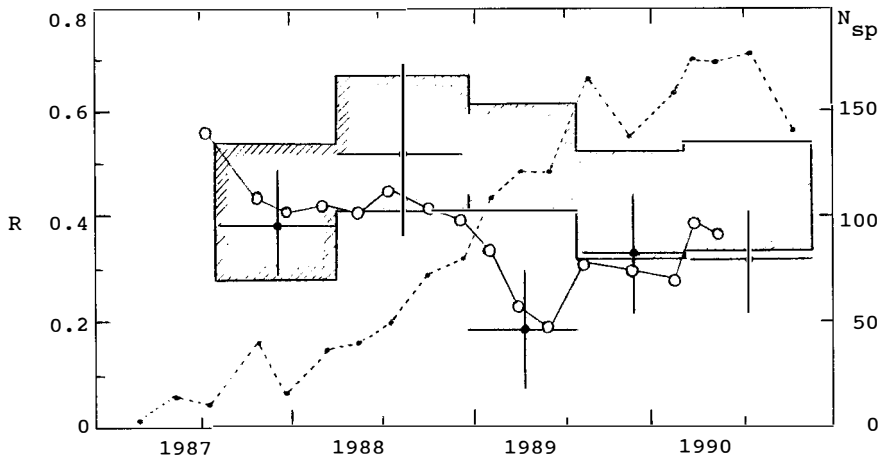


Fig.1. The suppressions of signals in Cl - Ar and Kamiokande-II (rectangles) experiments. For Cl - Ar the data averaged over the same bins as in Kamiokande-II (crosses) and (5 points) running means (hollow circles) are presented. Dotted line shows the time dependence of sunspots number.

ν_e -flux is $P_{\text{const}} = 0.005 - 0.02$. Are these results decisive? Is the probability P_{const} small enough to conclude that time variations of ν_e -flux exist? In this connection several remarks are in order.

- Runs 106 - 110 are not yet included in the analyses but they definitely diminish the probability of anticorrelations.

- The probability of temporal dependence, $Q_{\text{Ar}}(t)$, to be a fluke at constant ν_e -flux is small, but Davis's data contain others even more rare statistical features. In particular, an amazing coincidence run by run of the data Q_{Ar} from previous (21) and present (22) solar cycles during about 2 years have been found, when overlaped with a 9.5 years delay. The distribution of $\Delta Q_{\text{Ar}} = Q_{\text{Ar}}^{(22)} - Q_{\text{Ar}}^{(21)}$ has a half-width ~ 0.08 , whereas the average error in the individual run equals 0.32.

- The distribution of N_{Ar} (production rate in atoms/day) since 1987 differs appreciably from the Poisson one: second narrow peak exists at $N_{\text{Ar}} = 0.9$ at/day.

- There is no direct contradiction between possible time dependencies of Q_{Ar} and $R_{\nu e}$ but $R_{\nu e}$ is constant within 30%.

5). Cl - Ar -data show some seasonal variations during the period of the active Sun both in previous and in present cycles (fig.2a). But as follows from fig.2b maximum of Q_{Ar} is not in runs nearest to June 5 and December 5, which may indicate, that seasonal

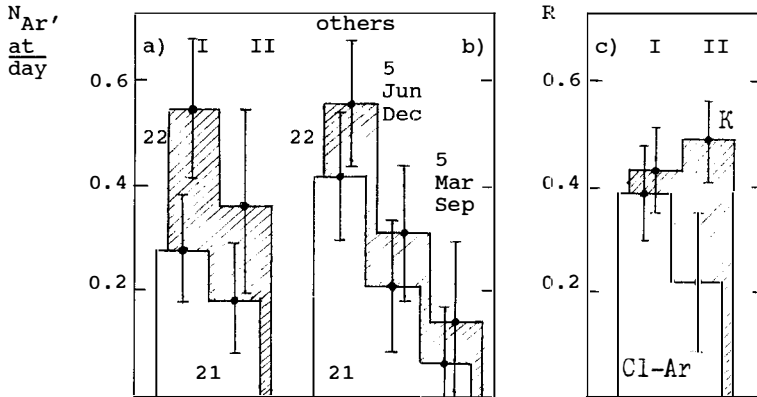


Fig.2. Search for semiannual variations of ν -signals in years of active Sun (cycles 21 and 22). a). Comparison of Ar-production rates averaged over period I (Apr.22-Jul.21 and Oct.21-Jan.20) and period II (Jan.21-Apr.21 and Jul.21-Oct.20); b). Comparison of Ar-production rates averaged over runs nearest to June 5 and December 5, nearest to March 5 and September 5, and over others. c). Comparison of signals suppressions in Cl - Ar and Kamiokande-II experiments averaged over periods I and II (cycle 22).

variations, if any, differ from those predicted in VVO-scenario⁷⁾. And again the Kamiokande-II does not show semiannual variations (fig.2c).

Confronting these facts we conclude that at present it is difficult to exclude any of the following possibilities: (1) Q_{Ar} -variations exist and are stipulated by time variations of ν_{\odot} -flux; (2) variations of Q_{Ar} exist, but they do not related to ν_{\odot} ; (3) the observed time sequence of experimental points on is a fluke.

3. GAMES ON THE $(\Delta m^2 - \sin^2 2\theta)$ - PLOT.

Suppose ν_{\odot} -flux is constant, and the suppression of experimental signals (2,3) is due to resonant flavor conversion. What are the appropriate values of neutrino parameters? To find a complete solution -- contours of definite confidence level on $\Delta m^2 - \sin^2 2\theta$ plot -- one needs the distributions of experimental values of signals in different experiments: $P(Q_{Ar})$, $P(R_{\nu e})$, $P(Q_{Ge})$ etc as well as the distributions of parameters describing the solar neutrino spectrum. Also one should take into account the correlations of results from different experiments, in particular from Kamiokande-II and Cl - Ar. Such a programm has been realized partly in a number of papers⁸⁻¹³⁾. Here the results¹²⁾ are

presented based on the following approach. For fixed values of solar parameters (and thus predictions for signals) we obtained the $\Delta m^2 - \sin^2 2\theta$ regions allowed by data of individual experiments with 1σ - or 2σ - errors. The intersection of these allowed regions was found. We will refer to it as to the intersection region with 1σ or 2σ errors. Then we have studied the modifications of the intersection region when changing the solar parameters, or including third neutrino etc. In such a way the effect of astrophysical uncertainties are found explicitly and moreover the correlations of different experimental results are taken into account. But it is impossible to prescribe a definite confidence level for the intersection region.

In fig.3 and 4a the 1σ and 2σ intersection regions are shown for central values of the SSM-predictions⁵⁾. They agree with the results of another analyses (fig.4b). The nonadiabatic solution region, parameterized as

$$\Delta m^2 = (3.6 \pm 1.0) 10^{-8} \text{eV}^2 / \sin^2 2\theta, \quad \sin^2 2\theta \geq 4 \cdot 10^{-3} \quad (4)$$

is in favor. Consider some implications of these results. Suppose, (which is quite natural) that mixing of leptons coincides with mixing of quarks. Then

$$\sin^2 2\theta_{12} = 0.16 - 0.23, \quad \sin^2 2\theta_{13} \leq 2 \cdot 10^{-3} \quad (5)$$

and it follows from fig.3 that 1-3-mixing is outside the MSW-triangle, whereas the 1-2 mixing - the stripe for $\sin^2 2\theta_{12}$ overlaps the intersection region. In the overlap one has

$$\Delta m^2 \sim m_2^2 = (1.3 - 2.0) 10^{-7} \text{eV}^2 \quad (6)$$

or $m_2 = (3.6 - 4.5) 10^{-4} \text{eV}$, and the prediction for Ga-Ge

$$Q_{\text{Ge}} = (14 - 22) \text{SNU} \quad (7)$$

Moreover the overlap is in the region of the Earth's matter effect (seasonal, day-night variations) for ${}^7\text{Be}$ -neutrinos. So, one expects appreciable (of the order of (7)) variations of Q_{Ge} . Supposing the neutrino mass hierarchy $m_\nu \sim m^\alpha$, where m is the mass of an upper quark or charged lepton and $\alpha = 1$ or 2 , we obtain

$$m_3 = (0.7 - 4.5) 10^{-2} \text{eV} \quad (\alpha = 1, \text{ linear hierarchy})$$

$$m_3 = (0.15 - 4.5) \text{eV} \quad (\alpha = 2, \text{ quadratic hierarchy})$$

In "see-saw" mechanism the mass of the right-handed neutrino equals according to (6): $m_N = 2.5 \cdot 10^{10} - 2.5 \cdot 10^{13} \text{GeV}$.

The intersection region is modified when Q_{Ar} averaged since

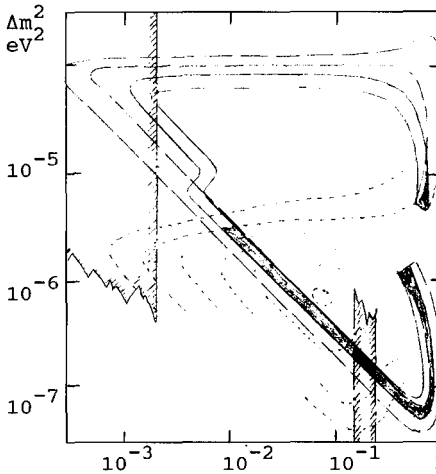


Fig.3. The $\Delta m^2 - \sin^2 2\theta$ regions allowed by data with 1σ errors from Cl-Ar (solid lines), Kamiokande-II (dashed curves) and Ga-Ge (dashed-dotted curves) experiments. Dotted curves are ISOSNU lines for Ga-Ge experiment (figures at the curves correspond to Ge-production rates in SNU's).

Central values for predictions in the SSM⁵⁾ are used. The vertical bands show lepton mixing, expected according to quark-lepton symmetry.

1987 is used (fig.4b). In particular, large values of Δm^2 (corresponding to the mixed and partly the adiabatic solutions) are unexcluded now.

Also the intersection region becomes larger when a third neutrino is included (fig.4c) (now ν -system is described by two points on $\Delta m^2 - \sin^2 2\theta$ plot, see^{12,14)} for more details). Two possibilities, interesting from phenomenological point of view, are shown in fig.5: a) The inequality $R_{Ar} < R_{\nu e}$ as well as the distortion of the 8B -neutrino spectrum in the adiabatic or mixed solutions can be reconciled with strong suppression of signal in Ga - Ge experiment. b) one of $(\Delta m^2 - \sin^2 2\theta)$ points is in the MSW-triangle, whereas another one in the region of nonaveraged vacuum oscillations ($\Delta m^2 \sim 10^{-10} \text{eV}^2$, $\sin^2 2\theta_{12} \sim 0.7 - 1.0$ ¹⁷⁾). Now the beryllium line may fall in the fast oscillating part of the survival probability and thus undergoes the seasonal variations related to the ellipticity of the Earth's orbit. In this case one predicts $Q_{Ge} = (57 \pm 17) \text{SNU}$.

Consider the dependence of the intersection region on solar parameters. Even within the SSM-predictions this region may be changed drastically and disappear (fig.4e). The observed values of ν -signals result from the interplay of astrophysics (deviations from SSM) and the neutrino properties. So, the change of central temperature of the Sun by $\pm 1.5\%$ shifts the intersection region by factor of ~ 5 in Δm^2 scale (fig.4f).

4. TIME VARIATIONS OF ν -SIGNALS AND RESONANT FLAVOR CONVERSION.

Suppose that Q_{Ar} -variations are induced by time variations of

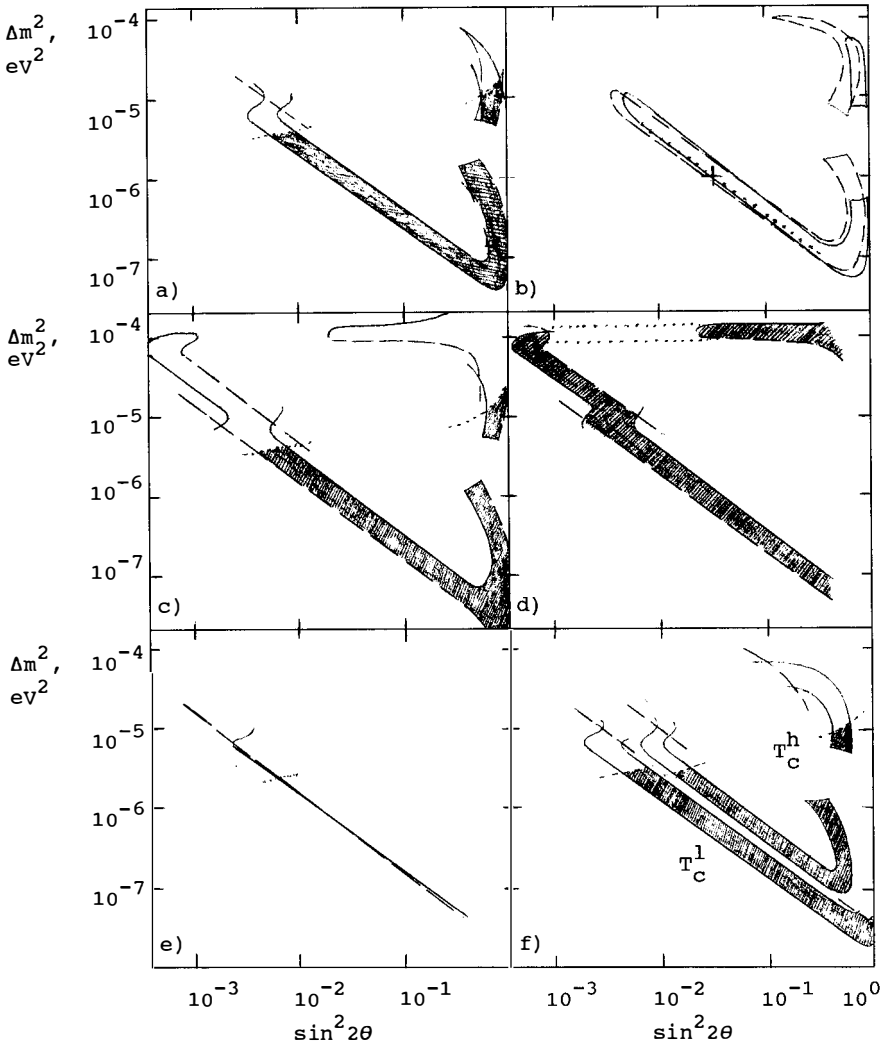


Fig.4. The modifications of the allowed and the intersections ($\Delta m^2 - \sin^2 2\theta$) regions in different suggestions (compare with fig.3): a) the data with 2σ -errors are used; b) the intersection regions according to another analysis: solid curves - 13 , dashed curves - 11 , dotted line - 10 , cross corresponds to the best fit in 11 ; c) Cl-Ar data since 1987 are used only; d) 3ν -mixing case - ISOSNU band for $R_{Ar} = 0.25$ is used, dotted curve restricts the region excluded by the analysis of recoil-electron spectrum in the Kamiokande-II; e) the predictions for ν -signal in the SSM by Turck-Chiese et al 16 (1σ); f) intersection regions T_C^h and T_C^l for non-standard solar models with $T_C = 0.985 T_C^{SSM}$ and $T_C = 1.015 T_C^{SSM}$ (2σ -errors).

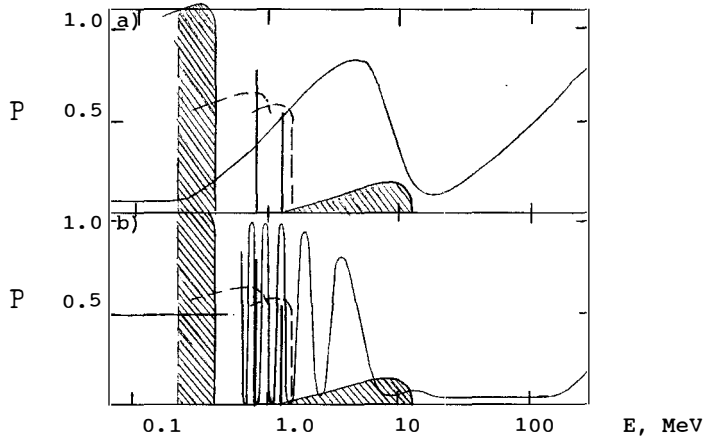


Fig.5. The suppression factors for 3ν -case and the solar neutrino spectrum (shadowed) a). $m_3/m_3=10^2$, $\sin^2 2\theta_{12}=0.16$, $\sin^2 2\theta_{13}=0.0025$ b). $\Delta m_2^2=0.8 \cdot 10^{-10} \text{eV}^2$, $m_3^2=3 \cdot 10^{-5} \text{eV}^2$, $\sin^2 2\theta_{12}=1$, $\sin^2 2\theta_{13}=0.1$.

ν_e -flux. There is no contradiction between Q_{Ar} -change and weak (or absent) variations of $R_{\nu e}$. Indeed

- there are no strong variations of Q_{Ar} since 1987 and within the errors bars possible time dependencies of Cl- and νe -signals can be reconciled;

- the transition of ν_e to ν_μ and ν_τ results in smoothing of $R_{\nu e}$ - variations in comparison with $Q_{Ar}(t)$: ν_μ and ν_τ , being sterile for Cl - Ar, give an appreciable contribution to νe -scattering through the neutral currents;

- if the ^7Be -neutrinos flux changes with time, whereas ^8B -neutrino flux is constant, at least for $E_\nu > 7 \text{ MeV}$, then Q_{Ar} varies at constant $R_{\nu e}$. In terms of resonant conversion such a possibility can be achieved by local (in space) change of solar density profile, and consequently by time variations of suppression factor, $P(E)$, in a thin energy region¹²⁾.

So the problem is to reproduce large changes of Q_{Ar} . The dynamics of resonant flavor conversion is determined by the effective density profile $\rho^{\text{eff}}(r)$ ¹⁾:

$$\rho^{\text{eff}} = \rho \frac{\Delta f^\alpha(0) Y^\alpha}{\sqrt{2} G_F k} \quad (8)$$

where ρ is the total density, $\Delta f^\alpha(0) = f_e^\alpha(0) - f_x^\alpha(0)$, $f_x^\alpha(0)$ is the amplitude of forward ν_x -scattering on α - component of matter, Y^α is the number of α - particles per nucleon ($\alpha = e, p, n$). Existing

solar data exclude strong (> few per cents) variations of density profile and ¹⁷⁾. Therefore the most promising possibility is a local (in space) $\rho^{\text{eff}}(r)$ -perturbations, which destroy (or change the degree of) the adiabaticity of ν -propagation¹⁸⁾. Here "local" means a thin layer of the Sun in radial direction ($\leq 10^{-3}R_{\odot}$), which may be spherical or even stripe-like with angular size $\leq 7^{\circ}$ about the equator.

According to (8) the variations of ρ^{eff} may be induced by - change of total density $\rho(r)$, or change of chemical composition, Y^{α} , or matter moving¹⁸⁾ - it changes the concentration, or polarization of medium, which influence $f(0)$, or destruction of coherence of the forward scattering.

The response of the neutrino system (converting in matter) on different perturbations of ρ^{eff} are summarized in fig.6. General consideration allows to put the lower limit on value of density perturbation, needed to obtain $\Delta Q_{\text{Ar}} = (1 - 2)$ SNU:

$$\Delta\rho^{\text{eff}}/\rho^{\text{eff}} \geq 0.05 \quad (9)$$

Moreover the perturbations with minimal size are situated in the inner part of the Sun¹⁹⁾. The mixing angle should be as small as possible ($\sin^2 2\theta \sim 10^{-3}$), but it may become larger, if there are several perturbations N_{per} : $\sin 2\theta \leq (\Delta\rho/\rho)N_{\text{per}}$. Some analytical solutions have been obtained for this case¹⁸⁾.

Any proposed mechanisms reproducing (9) are faced with difficulties, and we give some comments.

1). *Local ρ -perturbations.* In principle they can be stipulated by differential rotation, by oscillations of the Sun (g-modes), by the magnetic field, by some instabilities of nuclear energy release etc. Also local 5% ρ -perturbations can not be excluded immediately, they seem to be too large, especially for the central region of the Sun.

2). *Chemical composition.* The transitions $\nu_e \rightarrow \nu_{\mu}, \nu_{\tau}$ are sensitive to the electron concentration, Y_e , which in turns depends on the respective concentrations of hydrogen (X), helium and heavy elements. For central region of the Sun and at unchanged ρ one has $\Delta\rho^{\text{eff}}/\rho^{\text{eff}} = \Delta Y_e/Y_e \sim \Delta X/1.4$, therefore (9) implies very large ΔX : ≥ 0.07 .

3). *Matter moving.* If electrons move with velocity v , at the angle β with respect to neutrinos, then the effective density modifies as²⁴⁾

$$\rho_{\text{O}} \rightarrow \rho = \rho_{\text{O}}(1 - v \cos\beta) \quad (10)$$

Such a moving may be related to the existence of eddies inside the

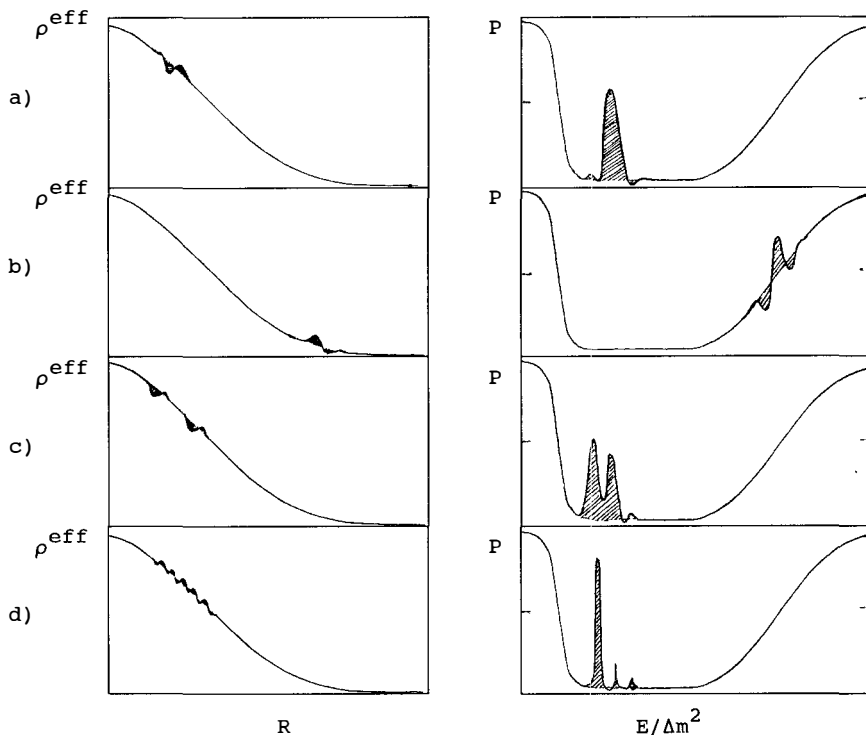


Fig.6. The influence of different effective density perturbations (left) on the resonant flavor conversion. The corresponding changes of suppression factors (shadowed) are shown to the right. a). ρ -perturbation in the adiabatic region; b) ρ -perturbation in the non-adiabatic region; c). effect of two (several) perturbations; d) periodic modulation of ρ -profile.

Sun¹⁸⁾. For several (many) addis on the neutrino trap the periodic change of velocity v may appear: $v(x) = v_0 \sin \pi r / r_{\text{edd}}$, where r_{edd} is the radius of individual eddy. According to (10) this change results in periodic density modulation and at $2r_{\text{edd}} \sim l_m$ (l_m is the oscillation length) the parametric enhancement of flavor transition may take place¹⁸⁾. But this scenario faces many difficulties: (1) the considered v_0 ($v_0 > 0.005$) is 1.5 -2 orders of magnitude larger than any expected velocities in the Sun, and even this value is insufficient to explain Q_{Ar} -variations ($v_0 \geq 0.02$ is needed); (2) fine tuning of parameters (parametric resonance) and large number of eddies ($N > 70$) are needed; (3) the eddies should be situated deep in the Sun; (4) it is practically impossible to satisfy the geometry conditions.

5).Polarization. The electrons polarization gives through the

change of scattering amplitude²¹⁾:

$$\rho^{\text{eff}} = \rho_0^{\text{eff}} \left(1 + \frac{\kappa}{2} \cos \delta\right)$$

where κ is the degree of polarization and δ is the angle between vector of polarization and the neutrino moment. The polarization may be induced by the magnetic field, but to have an appreciable effect in the Sun the enormously large strength of the field is needed. From the condition $2\mu_B B > 3kT$ (μ_B is the Bohr magneton) at $T \sim 10^6$ ° one has $B \geq 10^{11}$ G.

5. IDENTIFICATION OF SOLUTION.

What is the "rating" of the MSW-effect among the other possible solutions of the ν_\odot -problem? Let us comment on the discrimination of solutions. Following facts are the most crucial: 1). The $(Ar/\nu e)$ -signals ratio is smaller than 1: $R_{Ar}(>1970)/R_{\nu e} = 0.61 \pm 0.09$. This excludes the astrophysical solutions (low T_c) as well as MSW-adiabatic solution, for which $(Ar/\nu e) > 1$. It also disfavors the averaged vacuum oscillations and ν -spin precession. But one should keep in mind that according to data since 1987 the ratio is closer to 1: $R_{Ar}(>1987)/R_{\nu e} = 0.83 \pm 0.11$.

2). The SAGE - result, $Q_{Ar} < 50$ SNU, being supported excludes any astrophysical solutions (if the Sun is in thermal equilibrium).

3). No distortion of energy spectrum is observed in Kamiokande-II. This excludes partly the region of the MSW-adiabatic solution^{3,9)} (Also the day-night effect is not found).

4). Following solutions survive if the above mentioned facts are accepted: (1) non-adiabatic MSW, mixed MSW (in the case of 3ν), non-averaged vacuum solution, non-adiabatic spin-flavor resonant precession. The average vacuum oscillations as well as neutrino spin-precession can not be excluded too.

5). Time dependence of ν -signals will give strong discrimination of solutions but at present the situation is unclear.

6. CONCLUSIONS.

1). At present the experimental situation is not clear. The average value of Q_{Ar} since 1987 is larger than the average over all the time of observations. The status, the character and the origin of Q_{Ar} -time variations are questionable.

2). Resonant flavor conversion can explain quite naturally the average results of all three experiments taking data. There are the regions of $\Delta m^2 - \sin^2 2\theta$ parameters, where the agreement is found between the experimental data and the original neutrino flux

- predicted by the SSM. The non-adiabatic solution, parameterized by (4) is the most preferable. Moreover if the mixing in the lepton sector coincides with that in the quark sector, then one predicts: $\sin^2 2\theta = 0.14 - 0.18$, $m_2 = (3 - 5) 10^{-4} \text{ eV}$, $Q_{\text{Ge}} = 10 - 25 \text{ SNU}$.
- 3) The intersection $(\Delta m^2 - \sin^2 2\theta)$ -region is very sensitive to inclusion of third neutrino, and to change of solar parameters (even in the regions allowed by SSM).
- 4). It is difficult to explain large variations of Q_{Ar} in terms of resonant flavor conversion. Although such an explanation is not excluded, some contrived suggestions are needed for all proposed mechanisms. Local perturbation of the effective density profile in the inner part of the Sun are preferable.
- 5). The existing data do not allow to perform strong discrimination of solutions of the ν_{\odot} -problem. But they indicate against the astrophysical explanations.

REFERENCES

1. S.P.Mikheyev and A.Yu.Smirnov, Sov.J.Nucl.Phys., 42 (1985) 913, and Prog. in Part. and Nucl. Phys., 23 (1989) 41; L.Wolfenstein, Phys.Rev., D17 (1978) 2369.
2. R.Davis and K.Lande Proc. of the XXV Int. Conf. on High Energy Physics, Singapore, August 1990.
3. K.S.Hirata et al., Phys.Rev.Lett., 65 (1990) 1297; ICRR-Report-222-90-15.
4. V.N.Gavrin et al., these Proceedings
5. J.N.Bahcall and R.K.Ulrich, Rev.Mod.Phys., 60 (1988) 297.
6. D.Vignaud, these Proceedings.
7. M.B.Voloshin, M.I.Vysotsky, L.B.Okun', Sov.Phys.JETP, 64 (1986) 446.
8. J.N.Bahcall and W.Haxton, Phys.Rev., D40 (1989) 931.
9. K.S.Hirata et al., Phys.Rev.Lett., 65 (1990) 1301.
10. S.P.Rosen and J.H.Gelb, Phys.Rev., d39 (1989) 3190.
11. H.A.Bethe, Phys.Rev.Lett., 63 (1989) 837; J.N.Bahcall and H.A.Bethe, Phys.Rev.Lett., 65 (1990) 2233.
12. P.I.Krastev, S.P.Mikheyev and A.Yu.Smirnov, INR-preprint P-0695 (1991).
13. T.K.Kuo, J.Pantaleone, Phys.Rev D41 (1990) 279 and Preprint UCR-HEP-T-60, August 1990.
14. S.P.Mikheyev and A.Yu.Smirnov, Phys.Lett., 200B (1988) 560.
15. J.Pantaleone, Preprint UCR-HEP-T-64, October 1990.
16. S.Turck-Chieze et al., Ap.J., 335 (1988) 415.
17. A.J.Baltz and J.Weneser, Nucl.Phys., A505 (1989) 67.
18. W.C.Haxton and W.-M.Zhang, "Solar weak currents, neutrino oscillations and time variations", University of Washington report Seattle 1991
19. P.I.Krastev and A.Yu.Smirnov., Proc. of the Xth Moriond Workshop, Ed. by O.Fackler and J.Tran Thanh Van (1990) 521.
20. A.Yu.Smirnov, Proc. of the VIIth Moriond Workshop, ed. by O.Fackler and J.Tran Thanh Van (1987) 275.
21. P.I.Krastev (unpublished), M.A.Stefanov, Yad.Fiz., (Sov.J.Nucl.Phys) 49 (1990) 908.

DOUBLE BETA DECAY
AND NEUTRINO OSCILLATIONS



FIRST RESULTS FROM THE SOVIET-AMERICAN EXPERIMENT ON
DOUBLE-BETA DECAY OF ^{100}Mo TO THE EXCITED STATES OF ^{100}Ru

A.S. Barabash
Institute of Theoretical and Experimental Physics
B. Chermushkinskaya 25, 117159 Moscow, USSR

F.T. Avignone III and C.K. Guerard
Department of Physics and Astronomy
University of South Carolina, Columbia, SC 29208, USA

R.L. Brodzinski, H.S. Miley, and J.H. Reeves
Pacific Northwest Laboratory
Richland, WA 99352, USA

V.I. Umatov
Branch of Kurchatov Institute of Atomic Energy
Troitsk, 142092 Moscow region, USSR

ABSTRACT

The half-life for the double-beta decay of ^{100}Mo to the 1130 keV-level of ^{100}Ru has been measured to be $(1.78^{+1.85}_{-0.60}) \cdot 10^{21}$ y by observing the 590.76- and 539.53-keV gamma rays emitted in the $0^+_1+2^+_1+0^+_0$ de-excitation cascade.

1. Introduction.

Double-beta decay ($\beta\beta$ -decay) is at the intersection of nuclear and elementary particle physics due to the constraints that neutrinoless modes place on gauge field theories beyond the standard model. Double-beta decay modes to excited states of the daughter nuclide also offer significant insight into fundamental aspects of weak currents. Neutrinoless $\beta\beta$ -decay to the 2^+ level of the daughter nuclei is interesting, because it can only proceed through right-handed currents. Detection of $\beta\beta$ -decay to excited 0^+ states in the daughter nuclei provides information equivalent to the measurement of the decay to the 0^+ ground state. Since decay to the 0^+ excited states of the daughter nuclei is predominantly followed by prompt de-excitation of the daughter nuclei to the ground state via $0^++2^++0^+$ gamma-ray cascades, the measurement of double-beta decay to these excited states may be more experimentally favorable than measurement directly to the ground state by taking advantage of detection of these gamma rays through high-resolution or coincidence experiments. Three candidate nuclides having large available transition energies to the first excited 0^+ state in the

daughters are ^{98}Zr , ^{100}Mo , and ^{150}Nd . This paper deals with our experiments to measure this transition following the decay of ^{100}Mo .

Since the first direct observation of 2ν $\beta\beta$ -decay of ^{82}Se by Moe et al. /1/, there have been several additional direct measurements of ground state 2ν $\beta\beta$ -decay in ^{76}Ge /2-4/ and ^{100}Mo /5-8/. The relevant portions of the ^{100}Mo decay scheme are shown in fig. 1. The measured half-life of the $0^+ \rightarrow 0^+$ transition in ^{100}Mo is $1.16 \cdot 10^{19}$ y /7,8/, and the calculated half-life for the $0^+ \rightarrow 0^+$ transition is $(5-8) \cdot 10^{20}$ y /9/.

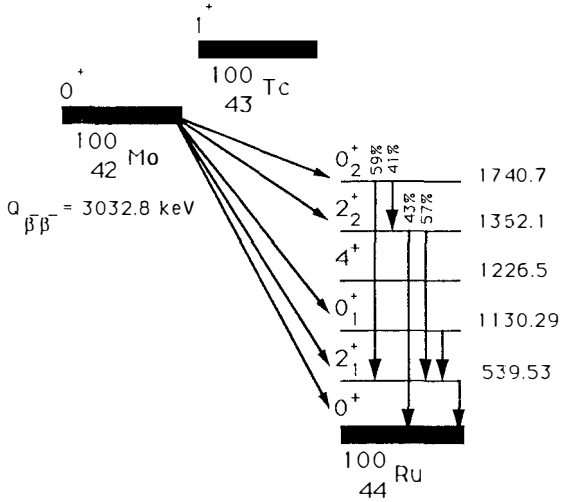


Fig.1. Partial decay scheme of pertinent mass 100 isotopes.

2. Experimental.

The counting facility used in this experiment is located in the Soudan II mine in Minnesota at a depth of 2090 m.w.e. The system consists of a 122-cm³ intrinsic germanium detector with an energy resolution of 2.5-keV FWHM at 1332 keV assembled in low-background copper components, housed in a large bulk shield of ordinary lead that has an inner liner of 5-cm-thick, ~150-year-old lead recovered from a German ship that sank in the North Sea. The old lead liner is used to shield the detector from the radiations of ^{210}Pb and its progeny present in the contemporary lead. The bulk shield is atmospherically sealed and

slightly pressurized with the nitrogen boil-off gas from the detector dewar to eliminate radon and its progeny from the shield.

The sample consists of 956 g of powdered molybdenum metal enriched to 92.8% ^{100}Mo contained in a plexiglass Marinelli beaker. The sample counting arrangement is shown in fig. 2. The sample nearly surrounds the detector, and this configuration is well suited for detecting single gamma-ray events. The photopeaks of interest are the 590.76- and 539.53-keV lines corresponding to the de-excitation gamma-ray cascade through the $0_1^+2_1^+0_2^+$ levels.

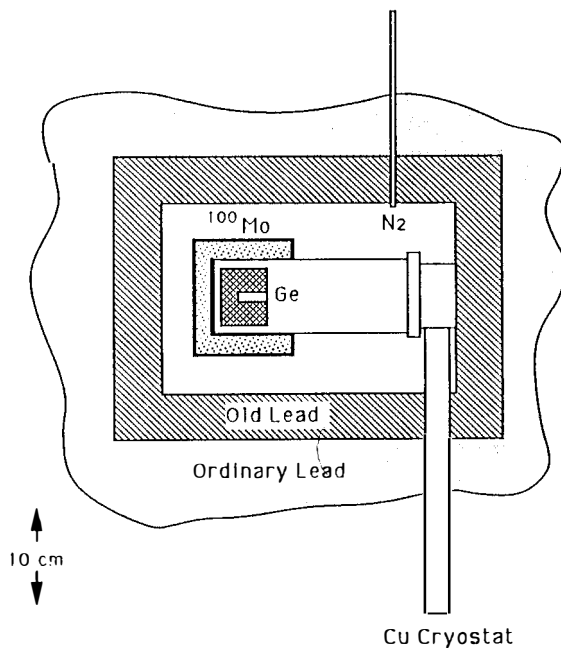


Fig.2. Sample counting arrangement.

3. Results.

The energy spectrum obtained in 195 days of counting is shown in the region of interest at 1 keV per channel in fig. 3. Radioactive impurities identified in the sample include primordial potassium, thorium, uranium, and radium as well as traces of ^{134}Cs and ^{137}Cs . The 511-keV line from positron annihilation, the

583.14-keV line from ^{208}Tl (^{228}Th), the 604.66-keV line from ^{134}Cs , and the 609.32-keV line from ^{214}Bi (^{226}Ra) are shown in the figure and provide an internal check on the resolution and energy calibration of the system. A straight baseline assumption was used to determine the number of net events in each photopeak of interest. The results are 10.5 ± 12.5 net counts at 590.76 keV and 26.5 ± 14.2 net counts at 539.53 keV where the uncertainties represent one standard deviation (1σ). Monte Carlo calculations were used to obtain efficiency factors of 0.0160 and 0.0173, respectively, for these gamma rays. In the final analysis, it will be necessary to measure these efficiencies using known radioactive standards. The half-life for this decay mode can be calculated according to the formula

$$t_{\frac{1}{2}} = (\ln 2)Nt/dN$$

where N = the number of ^{100}Mo atoms, $5.343 \cdot 10^{24}$; t = the length of the count, 0.5331 y; and dN = the number of decays. Therefore, at the 68% confidence limit, the half-life based on the 590.76-keV photopeak is

$$t_{\frac{1}{2}} = (3.0_{-1.6}^{+2.0}) \cdot 10^{21} \text{ y}$$

and based on the 539.53-keV photopeak is

$$t_{\frac{1}{2}} = (1.29_{-0.46}^{+1.48}) \cdot 10^{21} \text{ y}.$$

Since the de-excitation cascade produces almost identical numbers of the 590.76- and 539.53-keV gamma rays in this decay, the area of the two photopeaks can be added together to improve the statistical accuracy. This results in 37.0 ± 18.9 counts, and assuming an average efficiency of 0.0166 yields

$$t_{\frac{1}{2}} = (1.78_{-0.68}^{+1.85}) \cdot 10^{21} \text{ y}.$$

If the net peak areas that lead to the above half-life were to prove fortuitous, the lower limit on the half-life obtainable from these data is

$$t_{\frac{1}{2}} \geq 1.1 \cdot 10^{21} \text{ y}$$

at the 90% confidence limit.

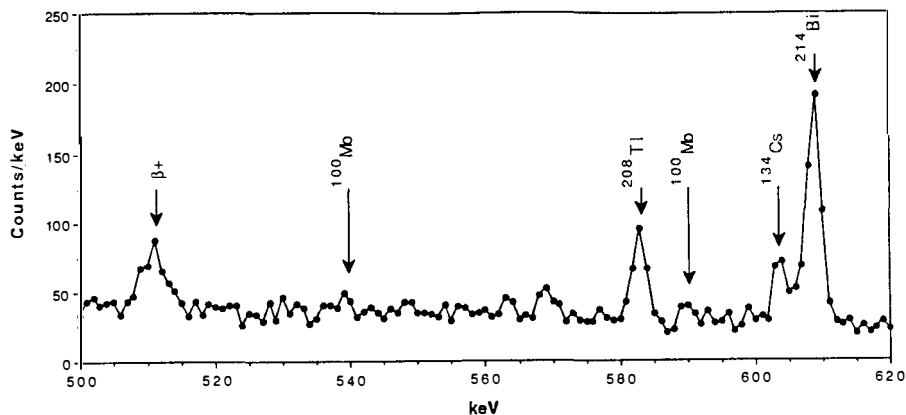


Fig.3. Energy spectrum in the region of interest.

Double-beta decay of ^{100}Mo is energetically possible to a host of excited states in ^{100}Ru , and half-lives or limits can also be obtained from the data for each of those possible transitions. The measured half-lives or limits for decay to the first four $J=0,2$ levels in ^{100}Ru are given in Table 1 without regard to the decay modes which could populate that state. Results from this work are given at both the 68% and 95% confidence limits (CL) and are compared to literature values at 68% CL for the same transitions.

Table 1. Half-lives and limits for $\beta\beta$ -decay of ^{100}Mo to selected excited levels in ^{100}Ru .

^{100}Ru levels (J^{π}_n , keV)	$t_{1/2}$ (y) $\cdot 10^{-21}$			
	This work		Ref. 10	Ref. 11*
	68% CL	95% CL		
2^+_1 , 539.53	>2.1	>1.2	>0.14	>0.4
0^+_1 , 1130.29	1.78	1.78	>0.042	
2^+_2 , 1362.1	>1.9	>0.96	>0.058	
0^+_2 , 1740.7	>1.8	>1.0	>0.035	

*for the neutrinoless decay mode only

4. Conclusions.

This experiment is continuing, and data will be acquired until the statistical significance is beyond question. If the above positive values remain justified, perhaps additional data accumulation will also lead to measurement of double-beta decay to other excited states in ^{100}Ru . Similar experiments are being contemplated for measuring the double-beta decay of ^{96}Zr and ^{118}Cd to the excited states of their daughters.

This measured double-beta decay rate of ^{100}Mo to the first excited 0^- level in ^{100}Ru can now be used in conjunction with the previously measured ground state double-beta decay rate to calculate the relevant nuclear matrix elements.

5. Acknowledgments.

The portions of this work conducted in the United States were supported by the U.S. Department of Energy (DOE) under Contract DE-AC06-76RLO 1830 and the National Science Foundation under grant PHY-8805401. Pacific Northwest Laboratory is operated for the DOE by Battelle Memorial Institute.

6. References.

1. S.R. Elliot, A.A. Hahn, and M.K. Moe, Phys. Rev. Lett. 59, (1987) 2020.
2. A.A. Vasenko, I.V. Kirpichnikov, V.A. Kuznetsov, A.S. Starostin, A.G. Djanyan, V.S. Pogosov, S.P. Shachysisyan, and A.G. Tamanyan, Mod. Phys. Lett. A5, (1990) 1299.
3. H.S. Miley, F.T. Avignone III, R.L. Brodzinski, J.I. Collar, and J.H. Reeves, Phys. Rev. Lett. 65, (1990) 3092.
4. F.T. Avignone III, R.L. Brodzinski, C.K. Guerard, I.V. Kirpichnikov, H.S. Miley, V.S. Pogosov, J.H. Reeves, A.S. Starostin, and A.G. Tamanyan, Phys. Lett. B00, (1991) 0000.
5. H. Ejiri, K. Okada, H. Sano, T. Shima, J. Tanaka, and Y. Yamamoto, Proc. WEIN-89, Montreal, (1989) 695.
6. S.I. Vasiliev, A.A. Klimenko, S.B. Osetrov, A.A. Pomansky, and A.A. Smolnikov, Pis'ma Zh. Eksp. Teor. Fiz. 51, (1990) 550.
7. T. Watanabe, H. Ejiri, K. Okada, H. Sano, T. Shima, J. Tanaka, K. Fushimi, H. Kinoshita, Y. Nagai, T. Shibata, and N. Kamikubota, Proc. 14th Europhysics Conference on Nuclear Physics, Bratislava, (1990) to be published in J. Phys. G.

8. S.R. Elliott, M.K. Moe, M.A. Nelson, and M.A. Vient, Proc. 14th Europhysics Conference on Nuclear Physics, Bratislava, (1990) to be published in J. Phys. 6.
9. A.S. Barabash, Proc. Int. School on Low-Energy Weak Interactions, Dubna, (1990) 0000.
10. A.S. Barabash, A.V. Kopylov, and V.I. Cherekhovsky, ITEP Report No. 184-89 (1989).
11. M. Alston-Garnjost, B.L. Dougherty, R.W. Kenney, R.D. Tripp, J.M. Krivicich, H.W. Nicholson, C.S. Sutton, B.D. Dieterle, S.D. Foltz, J. Kang, C.P. Leavitt, R.A. Reeder, J.D. Baker, and A.J. Caffrey, Phys. Rev. Lett. 63, (1989) 1671.

Latest Results on Double Beta Decay and Dark Matter from the Gotthard Laboratory

F. Boehm^a, C. Brogini^b, P. Fisher^a, L. Fluri^b, K. Gabathuler^c, H. Henrikson^a, D. Imel^a,
M.Z. Iqbal^a, V. Jörgens^b, L.W. Mitchell^b, C. Nussbaum^b, B.M. O'Callaghan-Hay^a,
D. Reusser^b, J. Thomas^a, M. Treichel^b, J.-C. Vuilleumier^b, J.-L. Vuilleumier^b, H. Wong^a

a) California Institute for Technology, Pasadena, CA 91125, USA

b) Institut de Physique, Université de Neuchâtel, CH-2000 Neuchâtel, Switzerland

c) Paul Scherrer Institute, CH-5232 Villigen PSI, Switzerland

presented by Michael Treichel

ABSTRACT: An array of eight high purity germanium crystals has been operated for several years in the Gotthard road tunnel in Switzerland to look for double beta decay of ^{76}Ge . Three of these crystals have also been used to search for weakly interacting dark matter. Limits on $\beta\beta$ decay life times and a cross section versus mass exclusion plot for dark matter particles are presented. Recently, a TPC filled with enriched ^{136}Xe has started taking data in the same laboratory. Its performance as well as first results are discussed.

1. Introduction

Neutrinoless double beta decay ($0\nu\beta\beta$) is a lepton number violating process requiring a nonzero Majorana mass of the neutrino¹). The experimental signature is a peak in the sum spectrum of the two electrons at the endpoint energy. The decay rate is proportional to the square of the effective neutrino mass, to nuclear transition matrix elements and a phase space factor which grows very rapidly with rising endpoint energy. Together with practical aspects, the last two factors determine the choice of nuclides to be studied experimentally. A popular candidate is ^{76}Ge , because high resolution detectors of reasonable size can be made of Germanium monocrystals. The low detection threshold can also be exploited to search for galactic dark matter. Another good choice is ^{136}Xe , which can be used in a tracking chamber with good energy resolution. Both nuclides are presently studied in an underground laboratory, situated in the Gotthard road tunnel and covered by about 1000 m of rock (3000 m.w.e.).

2. Search for Double Beta Decay

The Germanium experiment²⁾ employs eight high-purity crystals of 140-145 cm³ each. The active volume is 1095 cm³, the active mass is 5.83 kg of ^{nat}Ge . The detectors are shielded against ambient radioactivity by layers of 15 cm of copper and 18 cm of lead, contained in an aluminium radon shield, which is constantly flushed with nitrogen.

Figure 1 shows a fraction of the sum spectrum of the eight crystals after 13192 hours of running time, corresponding to 8.78 kg years. In this energy domain, close to the $\beta\beta$ endpoint (2040.71 keV), the background is dominated by the Compton continuum of the 2614 keV transition in ^{208}Tl and by β^+ activity from ^{68}Ga . Thus, $0\nu\beta\beta$ decay would show as a Gaussian peak with a width of 3.2 keV FWHM (the experimental resolution) on top of a flat background. A fit minimizing a χ^2 derived from the likelihood function for Poisson statistics³⁾ yields a background of 2.4 counts per keV, kg and year, and a peak content of -5.0 ± 9.9 counts. Assuming only positive values to be allowed, one obtains 90% and 68% C.L. upper limits of 13.5 and 7.6 counts, respectively. The 90% C.L. upper limit is represented by the smooth curve in Figure 1. The corresponding half-life limits are:

$$T_{1/2}^{0\nu}(0^+ \rightarrow 0^+) > 2.9(5.2) \cdot 10^{23} \text{ years at } 90\%(68)\% \text{ C.L.} \quad (1)$$

For comparison, the present best limits are $T_{1/2}^{0\nu} > 1.2(2.2) \cdot 10^{24}$ years at 90%(68)% C.L.⁴⁾. The half-life limits (1) can be translated into upper limits on the effective Majorana neutrino mass. Using the matrix elements calculated by Engel et al.⁵⁾, in the parameter range that reproduces measured $2\nu\beta\beta$ half-lives, one obtains $\langle m_\nu \rangle < (5.4 - 7.6)$ eV at 68% C.L. The matrix elements of Muto et al.⁶⁾ yield $\langle m_\nu \rangle < 2.5$ eV at 68% C.L. In the same way, the sum spectrum around 1481.6 keV was used to get a limit on the $0^+ \rightarrow 2^+$ half-life. From the fitted signal, -11.4 ± 15.3 counts, and taking into account the 35% escape probability for the 560 keV γ ray, one obtains:

$$T_{1/2}^{0\nu}(0^+ \rightarrow 2^+) > 0.7(1.3) \cdot 10^{23} \text{ years at } 90\%(68)\% \text{ C.L.}$$

in clear disagreement with the positive result of ref. 7).

Recently, data taking with a Xenon TPC⁸⁾ started in the same laboratory. The chamber gas is 62.5% enriched ^{136}Xe with a 3.6% admixture of CH_4 . The active volume is 207 liters, and the chamber is operated at 5 atm. The active mass is 5.75 kg of ^{136}Xe . Electrons from the active volume drift in a homogeneous electric field of 1 kV/cm to an anode system which consists of alternating 20 μm sense wires and 100 μm field wires, 2.5 mm apart. The amplified charge is registered in a 8 MHz transient recorder and provides the energy signal with a resolution

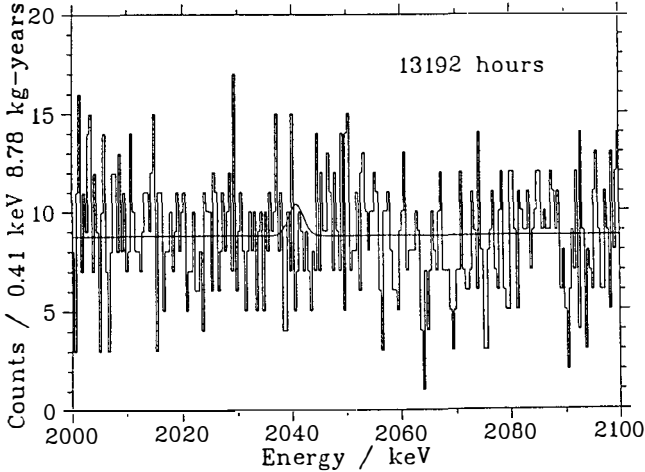


Figure 1: The spectrum of the eight Germanium crystals around the $\beta\beta$ endpoint.

of 10% at 2480 keV. The anode is sandwiched between a grid, separating it from the drift region, and a pad structure, that defines 2×168 strips in orthogonal directions, with 3.5 mm pitch. Tracks are reconstructed from the induced charge on the strips, read out at a rate of 2 MHz via two level discriminators, in order to distinguish charge blobs, due to increased energy loss at the end of the range, from the minimum ionizing track. This information is used to select two-electron events which give continuous tracks with charge blobs at both ends. The efficiency for complete energy deposit in the active volume is determined by a Monte-Carlo simulation to be 25% for two-electron events at 2500 keV.

A data sample of 88.4 kg-days was analysed so far. The offline analysis is done in two steps: first, a computer analysis removes about 85% of the raw data, then the remaining events are scanned visually. The overall efficiency of this procedure is conservatively estimated to be 80%. A typical two-electron event is shown in Figure 2. The charge blobs at both ends, correlated with increased ionization in the anode signal, are clearly visible. Figure 3 shows the two-electron spectrum above 1500 keV. The energy calibration of this sample was done once a week with ^{22}Na and ^{137}Cs sources. The 68% and 90% C.L. upper limits for a peak at the endpoint (2480 keV) are 2.9 and 5.1 counts, respectively. The corresponding limits on the half-life for $0\nu\beta\beta$ decay are:

$$T_{1/2}^{0\nu}(0^+ \rightarrow 0^+) > 2.9(5.1) \cdot 10^{22} \text{ years at } 90\%(68)\% \text{ C.L.}, \quad (2)$$

to be compared with the best limit available so far, $2 \cdot 10^{22}$ years at 90% C.L.⁹⁾. The 68% C.L. limit on the effective neutrino mass, derived from (2), is $\langle m_\nu \rangle < (9.3 - 11.1) \text{ eV}$ or $\langle m_\nu \rangle < 6.6 \text{ eV}$ with the matrix elements of ref. 5) or 6), respectively.

3. Search for Weakly Interacting Dark Matter

It has been suggested that galaxies contain a stationary halo of cold dark matter (CDM), made from heavy non relativistic weakly interacting particles, about 3 to 10 times more than luminous matter¹⁰⁾. Stars would move relative to the halo. With a small probability, certain CDM particles scatter coherently from a nucleus and transfer energy to it. The small recoil

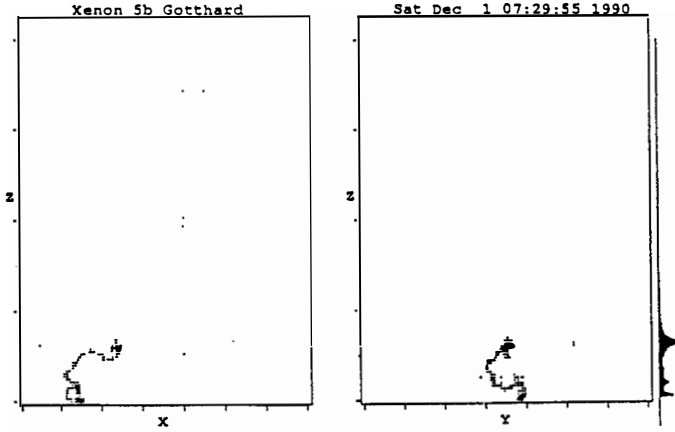


Figure 2: A typical two-electron event in the Xenon TPC. The width of the active volume is about 59 cm, the height about 64 cm. The anode signal is on the right.

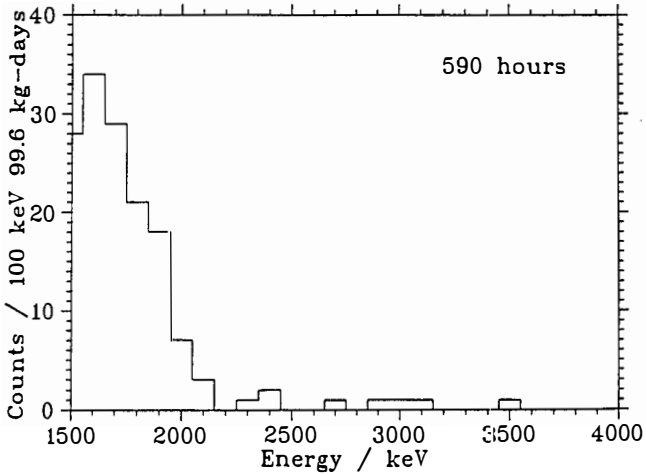


Figure 3: The two-electron spectrum in the Xenon TPC above 1500 keV.

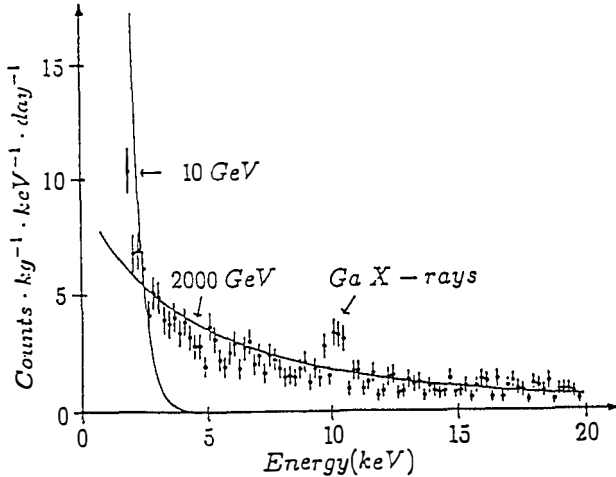


Figure 4: The low energy spectrum of the best crystal.

energy can be measured if the nucleus belongs to the active part of a detector. Germanium detectors in an underground laboratory, with their large masses, low energy threshold and low background, are ideally suited for CDM searches^{11,12}.

The experimental set-up was modified to perform a CDM search at the same time as the double beta program. A separate electronic circuit is used for the three crystals with the lowest electronic noise. Noise from microphonics was greatly reduced by cutting time bins with high count rate. The energy calibration was performed by means of radioactive sources and a precision pulser. Details of the analysis are described in ref. 13). The spectrum of the best crystal, corresponding to a life time of 1662 hours (51.6 kg days), is shown in Figure 4, together with the expected recoil spectra for Dirac neutrinos of mass 10 and 2000 GeV. The peak at 10.37 keV is due to Gallium X-rays emitted after electron capture in ^{68}Ge . This X-ray line provides a cross-check of the energy calibration.

In the analysis it is assumed, as described in ref. 10), that the dark matter has a local density of $0.3 \text{ GeV}/\text{cm}^3$, a Maxwellian velocity distribution with $\langle v^2 \rangle^{1/2} = 261 \text{ km/s}$ truncated at the escape velocity $v_e = 640 \text{ km/s}$, and that the relative Earth to halo velocity is 230 km/s . In the calculation of the expected recoil spectrum, an isotropic differential cross-section is assumed, including a form factor to account for the loss of coherence at high momentum transfers, and the 30% ionization efficiency of Germanium nuclei as compared to electrons is corrected for. Again, details may be found in ref. 13). The calculated spectrum is then folded with the response function, the energy resolution being 800 eV FWHM at low energy. The area in the σ (interaction cross section) vs. m (mass of the CDM particle) plane one can rule out this way is shown in Figure 5. Also shown is the predicted cross-section in function of mass for heavy Dirac neutrinos (ν_D) with standard coupling. One sees that ν_D with masses between 10 and 2400 GeV are ruled out. The limits obtained from this analysis are more reliable and more restrictive by a factor of 2 to 4 than those of ref. 12).

From the absence of Germanium K X rays at 11.10 keV , a limit on the half-life of the electron decay into weakly interacting particles, for example $e^- \rightarrow \nu_e \nu_e \bar{\nu}_e^{(4)}$, can be deduced.

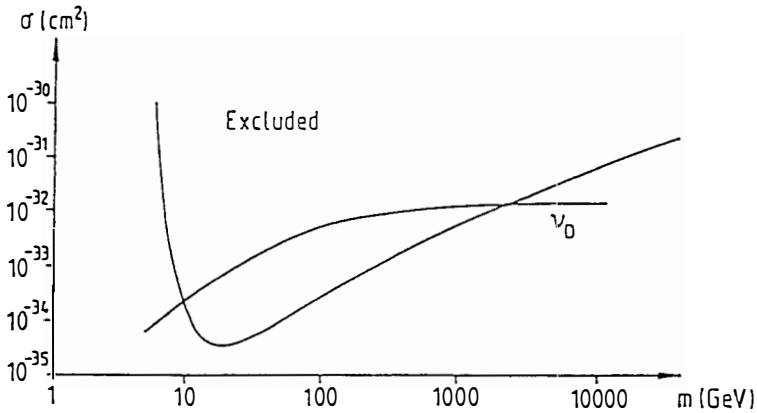


Figure 5: Exclusion plot for CDM

From a fit to the sum spectrum of three crystals with two Gaussian peaks and a parabolic background one gets a lower limit on the half life of the electron of $1.9(1.2) \cdot 10^{23}$ years at the 68(90)% confidence level, almost an order of magnitude better than the previous one¹⁵.

Acknowledgements

This work was supported by the Fonds National Suisse pour la Recherche Scientifique and by the US Department of Energy.

References

- 1) See, for example, J.-L.Vuilleumier, Rep. Prog. Phys. **49** (1986) 1293 and F.Boehm and P.Vogel, Physics of Massive Neutrinos, Cambridge University Press, 1987
- 2) P.Fisher et al., Phys. Lett. **B218** (1989) 257
- 3) S.Baker and R.D.Cousins, Nucl. Instr. Meth. **221** (1984) 437
- 4) D.O.Caldwell et al., contribution to the EPS Nuclear Physics Conference, Bratislava, Oct., 22-26, 1990 (unpublished)
- 5) J.Engel, P.Vogel and M.R.Zirnbauer, Phys. Rev. **C37** (1988) 731
- 6) K.Muto, E.Bender and H.V.Klapdor, Z. Phys. **A334** (1989) 187
- 7) J.Busto et al., Nucl. Phys. **A513** (1990) 291
- 8) M.Z.Iqbal et al., Nucl. Instr. Meth. **A259** (1987) 459
- 9) L.Zanotti et al., contribution to the EPS Nuclear Physics Conference, Bratislava, Oct., 22-26, 1990 (unpublished) and T.Tabarelli de Fatis, these proceedings
- 10) J.Primack, D.Seckel and B.Sadoulet, Ann. Rev. Nucl. Part. Sci. **38** (1988) 751
- 11) S.P.Ahlen et al., Phys. Lett. **B195** (1987) 603
- 12) D.O.Caldwell et al., Phys. Rev. Lett. **61** (1988) 510
- 13) D.Reusser et al., Phys. Lett. **B255** (1991) 143
- 14) L.B.Okun and Y.B.Zeldovich, Phys. Lett. **B78** (1978) 597
- 15) E.Bellotti et al., Phys. Lett. **B124** (1983) 435

Status of the Heidelberg – Moscow $\beta\beta$ – Experiment using enriched $^{76}\text{Ge}^{+}$, *)

*M. Beck, J. Echternach, J. Gebhard, G. Heusser, H.V. Klapdor-Kleingrothaus,**)
M. Krause, A. Piepke, U. Schmidt-Rohr, H. Strecker and K. Zuber
Max-Planck-Institut für Kernphysik, 6900 Heidelberg, Germany*

*A. Balish, S.T. Belyaev**), A. Demehin, A. Gurov, I. Kondratenko and V.I. Lebedev
Kurchatov Institute of Atomic Energy, Moscow, USSR*

*A. Müller
Istituto Nazionale di Fisica Nucleare, 67010 Assergi, Italy*

The search for the $\beta\beta 0\nu$ -decay is at present the most powerful tool for investigating a Majorana mass of the neutrino. The Heidelberg-Moscow group has now 16.9 kg of 86% enriched ^{76}Ge at its disposal. End of July 1990 the first phase of the experiment has been started in the Gran Sasso underground laboratory. The results after 135.1 days of data taking with a 980 g detector are: background around 2 MeV $B=0.5$ counts/keV \cdot y \cdot kg, half life limit for the $\beta\beta 0\nu$ -decay to the ground state of ^{76}Se $T_{1/2} > 3.8 \cdot 10^{23}$ y (90% c.l.). A possible $\beta\beta 0\nu$ -decay to the first excited state can be excluded with $T_{1/2} > 1.8 \cdot 10^{23}$ y (90% c.l.). The statistical significance of these results is 3.9 mol.y.

**) Presented by A. Piepke*

**) Supported by: - Bundesministerium für Forschung und Technologie der Bundesrepublik Deutschland
- State Committee of Atomic Energy of the USSR*

****) Speakers of the collaboration*

1. Introduction

The successful test of the standard model at LEP raises the question whether this model is the ultimate description of nature or whether there is new physics beyond. One key for our understanding of nature could be the physics of the neutrino, from which only very little is known up to now. It is still an open question whether the neutrino is a Dirac or a Majorana particle and whether it carries a finite rest mass.

Many models of grand unification (GUT's, SUSY's...) are predicting a non-vanishing Majorana mass of the neutrino, which has to be zero in the standard model since no right-handed neutrinos are available. Unfortunately these predictions are strongly divergent ranging from 10^{-11} eV to values of the order of 1 eV ¹⁾.

In a recent paper S. Glashow showed that also the possible existence of 17 keV neutrinos does not necessarily imply that neutrinos are Dirac particles.²⁾

The investigation of the neutrinoless nuclear $\beta\beta$ -decay is up to now the most sensitive probe of a possible Majorana mass of the neutrino. At present this mass is tested to be smaller than ~ 1.7 eV.

Double beta decay which is one of the rarest processes in nature is expected to proceed mainly via two decay modes:

$$(\beta\beta 2\nu) \quad A(Z) \rightarrow A(Z+2) + 2e + 2\bar{\nu}_e \quad (1)$$

$$(\beta\beta 0\nu) \quad A(Z) \rightarrow A(Z+2) + 2e \quad (2)$$

It should become observable in those nuclei where ordinary alpha or beta decay is forbidden (for example in the case of ^{76}Ge). The measurement of the decay rate of process (1), which is allowed in the standard model and has been already observed, is important to check theoretically calculated nuclear matrix elements and consequently the understanding of nuclear structure. The electrons emitted in this process have a continuous energy spectrum.

The so far unobserved $\beta\beta 0\nu$ -decay would require massive Majorana neutrinos and consequently imply physics beyond the standard model. Through a measured half life (or limit) the effective Majorana mass $\langle m_\nu \rangle$ of the neutrino (or a limit for it) can be deduced using theoretically calculated nuclear matrix elements for example from ref. ³⁾. A discussion of $\langle m_\nu \rangle$ and its dependence on the mixture of the different mass eigenstates can be found in ref. ⁴⁾. Since process (2) is a two body decay the summed energy of the electrons should be a discrete line at the Q-value of the decay ($E=2040.71$ keV).

A new generation of $\beta\beta$ -experiments can test the neutrino mass down to ~ 0.1 eV through the use of large amounts of isotopically enriched source materials and test a class of left right symmetric GUT models (for the latter see¹⁾).

The collaboration between the MPI in Heidelberg and the KIAE in Moscow has 16.9 kg of Ge metal enriched to 86% in ^{76}Ge at its disposal. The natural abundance of this isotope is only 7.8%.

In this experiment semiconductor detectors made from the isotopically enriched Ge are used simultaneously as source and detector for electrons emitted in the $\beta\beta$ -decay of ^{76}Ge . The strong enrichment helps to increase the source strength

without simultaneously raising the sensitivity towards background radiation as would be the case if simply a larger amount of natural Ge would be used. This fact is reflected in the figure of merit of this experiment given in units of the half life limit $T_{1/2}$ [y] deduced if no peak can be found at the correct energy after measuring time t [y].

$$T_{1/2} > (4.18 \cdot 10^{24} \text{ kg}^{-1}) \cdot \frac{a}{f} \cdot \sqrt{\frac{M \cdot t}{B \cdot \Delta E}} \quad (3)$$

a : isotopical abundance of ^{76}Ge

M : active mass of the detector [kg]

B : average background at the energy of the peak [counts/keV·y·kg]

ΔE : energy resolution (FWHM) [keV]

The factor f connects the limit to a confidence level (c.l.). $f=1.35$; 3.62 ; 8.74 corresponds to 68%, 90% and 99.9% c.l. respectively. This conservative choice of f is derived from the concept of minimal detectable activity described for example in ref. ⁵⁾. In this approach the risk of rejecting the peak hypothesis if it is true and accepting the nopeak hypothesis if it is wrong (this is not the same) is included in the limit.

In a less conservative approach which measures only the first risk, f is equal to 0.48; 1.28; 3.09 for 68%, 90% and 99.9% c.l. respectively. In the literature f is often used in an undefined way.

The isotopical abundance is obviously the most effective parameter to increase the sensitivity. Since the hypothetical peak lies in the energy range of the natural radioactivity and the expected count rate is extremely small (for $T_{1/2} > 8 \cdot 10^{23}$ y lower than 6 counts/kg·y) the background reduction is the biggest experimental challenge. The experiment claiming at present still the most stringent half life limit for the $\beta\beta 0\nu$ -decay has an average background around 2 MeV of $B=1.2$ counts/keV·y·kg ⁶⁾. The lowest background reported in the literature is $B=0.3$ counts/keV·y·kg ⁷⁾.

2. Experimental set up

In the first phase of our experiment a 980 g p-type enriched HP Ge detector with an active mass of about 927 g is used to study the $\beta\beta$ -decay. Approximately 10.5 mol ^{76}Ge are contained in this first detector. As far as the source strength is concerned even this first detector is one of the biggest ^{76}Ge $\beta\beta$ -experiments in operation. The HP crystal was grown at ORTEC (USA). At 2 MeV this detector has an energy resolution of $\Delta E=3.0$ keV. It is the first HP detector from enriched Ge ever operated.

All detector parts have been carefully selected for lowest activity with existing low-level Ge spectrometers ⁸⁾.

The cryostat of the detector is made from electrolytic copper. To avoid activation through the cosmic radiation the copper was obtained directly from the producer and than quickly stored underground. No soldering was done near the

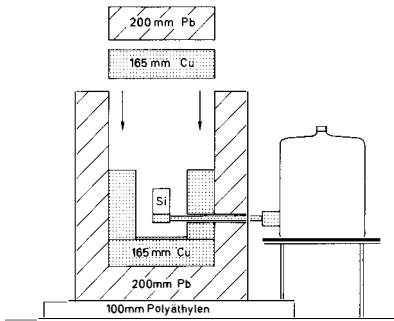


Fig. 1 Cross section of the set up. The inner cavity is now filled with LC2 grade Pb.

The detector is surrounded by a passive shielding composed of 20 cm low-activity lead, 16.5 cm electrolytic copper and 10 cm radio pure so-called LC2 grade lead.

Special care was taken to remove the air containing Rn from the inner cavities of the shielding. The whole set up is surrounded by an airtight steel container. The shielding is always flushed with nitrogen gas giving a constant excess pressure to the steel box.

The experiment is located in the Gran Sasso underground laboratory of the INFN (Istituto Nazionale di Fisica Nucleare) in Italy with a shielding thickness of about 3500 m w.e. The muon-flux is reduced by six orders of magnitude. The INFN has constructed a special low-level building for this experiment to allow clean, stable and quiet working conditions.

To control the systematic errors during the long measuring time data taking is done in an event-by-event mode. Together with the detector signal several control signals are recorded like: high voltage applied to the crystal, temperatures of the electronic components, status of the electrical network and absolute time of the event. Through these additional parameters the data can be checked for correlations with external parameters. The time distribution of the events offers the possibility to identify artificial signals. The temperatures can be used for a software stabilisation of the calibration drifts. Weekly calibration measurements with ^{60}Co and ^{228}Th sources are performed to check the performance and stability of the experiment.

3. Experimental Results

The results of 135.1 days of data taking will be discussed. This measuring time corresponds to a statistical significance of 3.9 mol.y. In Fig. 2 the background spectrum from 100 to 2700 keV is shown. The integral countrate in this inter-

crystal. The detector endcap is made from a zone refined Si crystal. To avoid surface contaminations all detector parts were etched or electropolished before assembling. The cryostat system was mounted under cleanroom conditions. The FET is located at a remote position. Charcoal made from coconuts selected for their low Ra content serves as a molecular sieve. The development of the low-level cryostat was done in cooperation with CANBERRA (Belgium).

Fig. 1 depicts a cross section of the set up.

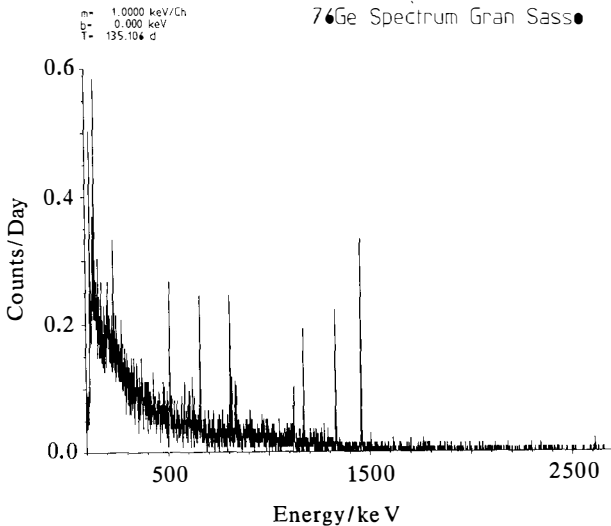


Fig. 2 Background spectrum of the enriched detector.

respectively. In this way the $^{57,58}\text{Co}$, ^{54}Mn and ^{65}Zn activities can be located. This is very important for a reliable Monte Carlo simulation of the detector.

From man-made radioactivity only ^{137}Cs is present. Above the $E=1461$ keV γ -line of the ^{40}K decay no strong lines are visible after 135 days.

The background around 2 MeV is mainly formed by

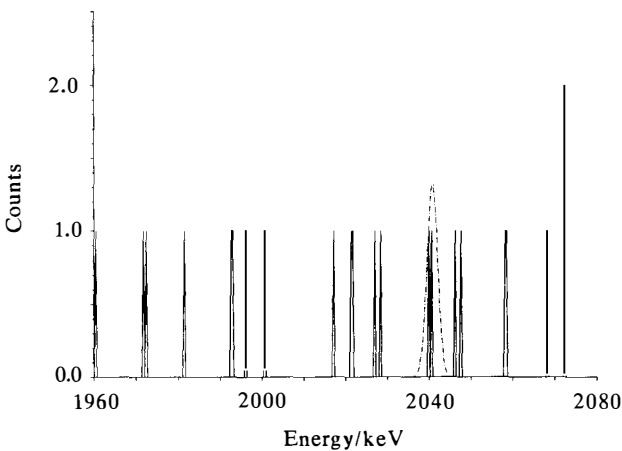


Fig. 3 Background around 2 MeV. The dotted curve represents the excluded $\beta\beta\nu$ -signal of 4.2 counts.

val is 0.05 counts/min·kg.

A major part of the background is composed from the cosmogenic isotopes $^{57,58,60}\text{Co}$, ^{54}Mn and ^{65}Zn . They were formed via the interaction of the cosmic radiation with the Cu (mainly absorption of neutrons) and the Ge (mainly spallation) while being exposed above ground. Radioisotopes decaying by EC can be distinguished to originate from Ge or Cu by giving either the total decay energy (inclusive follow up x -rays) or the x -ray escape peak re-

spectively. In this way the $^{57,58}\text{Co}$, ^{54}Mn and ^{65}Zn activities can be located. This is very important for a reliable Monte Carlo simulation of the detector. From man-made radioactivity only ^{137}Cs is present. Above the $E=1461$ keV γ -line of the ^{40}K decay no strong lines are visible after 135 days. The background around 2 MeV is mainly formed by Compton scattered γ -quanta emitted from isotopes of the natural ^{232}Th and ^{238}U decay chains. At present only members of the Th chain are visible. The absence of lines of the U chain shows that the Rn system works quite efficiently. ^{68}Ge is in contrast to experiments working with natural Ge no problem here because its target isotope ^{70}Ge in the cosmic ray reaction $^{70}\text{Ge}(n,3n)^{68}\text{Ge}$ is reduced by about 3 or-

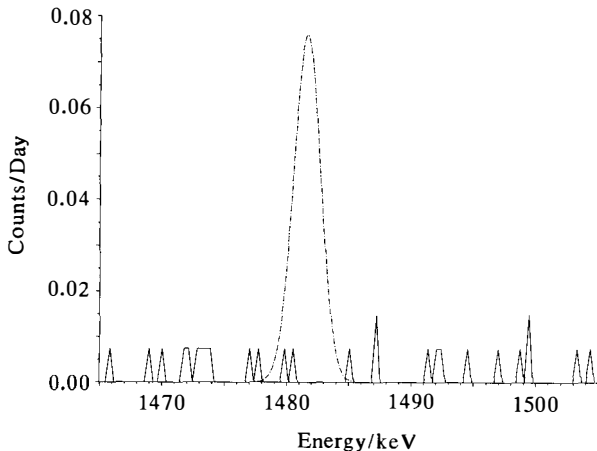


Fig. 4 Background around 1.48 MeV. The dotted curve shows the signal which should be there if the signal of ref. ¹⁰⁾ would be $\beta\beta 0\nu$ -decay.

This corresponds to a limit of 2.4 eV for the Majorana mass of the neutrino. The data were also checked for a possible $\beta\beta 0\nu$ -decay of ^{76}Ge to the first excited ($J=2^+$) state of ^{76}Se . Observation of such a decay would require right handed admixtures to the weak interaction because of conservation of angular momentum. Such a decay should result in a line at the decay energy lowered by the energy of the excited state. The probability for the total escape of deexcitation γ -quanta with an energy of $E=559$ keV has been calculated with a Monte Carlo program (based on the CERN code GEANT 3) to be 43% for our detector. In a recent publication a French group reported a coincidence signal which could be identified with the discussed $\beta\beta 0\nu$ -decay to the first excited state. Their published half is $T_{1/2}=1 \cdot 10^{22} \text{y} \pm 50\%$ ¹⁰⁾. Even if a half life at the upper end of the 3σ -error bar of ref. ¹⁰⁾ is assumed ($T_{1/2}=2.5 \cdot 10^{22} \text{y}$) we should find according to the exponential decay law 28 events. Fig. 4 shows the spectrum around the energy of the peak at $E=1482$ keV. The dotted curve corresponds to the peak which should be there if the coincidence signal of ref. ¹⁰⁾ would be $\beta\beta 0\nu$ -decay. We find only 3 events in the energy interval of the peak. The average background in this energy range is in our experiment $B=1.8$ counts/keV \cdot y \cdot kg. Therefore $\beta\beta 0\nu$ -decay of ^{76}Ge to the first excited state can be excluded to have a half life as large as reported in ref. ¹⁰⁾. Since the background is very low, a statistical fluctuation can not explain the discrepancy. From our spectrum we deduce a half life limit of $T_{1/2} > 1.8 \cdot 10^{23} \text{y}$ (90% c.l.).

With the data available at this moment we can give a half life limit for the $\beta\beta 2\nu$ -decay of $T_{1/2} > 7.5 \cdot 10^{20} \text{y}$ (90% c.l.).

ders of magnitude in the enrichment process. In Fig. 3 the energy range around 2 MeV is displayed. The average background there is $B=0.5$ counts/keV \cdot y \cdot kg. Since the number of counts contained in this interval is still extremely small the method recommended by the particle data group ⁹⁾ for a Poisson process with background was applied to calculate the half life limit for the $\beta\beta 0\nu$ -decay to the ground state of ^{76}Se . The result after 135.1 days is $T_{1/2} > 3.8 \cdot 10^{23} \text{y}$ (90% c.l.).

4. Future Perspectives of the Heidelberg-Moscow experiment

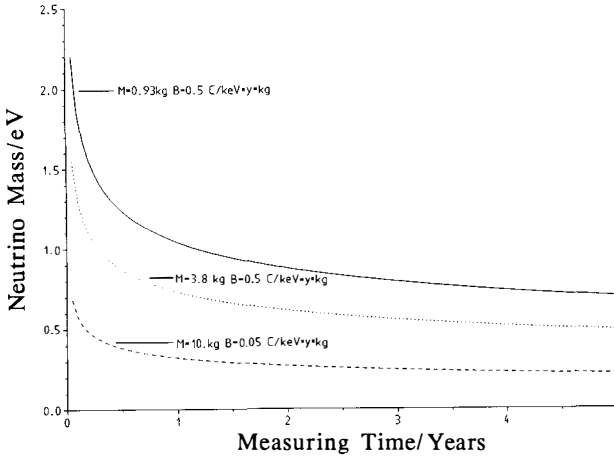


Fig. 5 Neutrino mass limit for different experimental parameters.

To estimate the perspectives of the described experiment the neutrino mass limits (90% c.l.) deduced via the discussed $T_{1/2}$ -formula (conservative f) and the matrix elements from ref ³⁾ are plotted as a function of the measuring time in Fig. 5. The solid curve represents the sensitivity of the discussed detector. Even with this first detector it will be possible to reach the results of the leading experiment ⁶⁾ within one year.

Currently a second enriched detector with a mass of 2.9 kg is under construction. In a test cryostat this detector has an energy resolution of 2.0 keV.

The pointed curve shows the sensitivity of the experiment if this new detector will have the same background as the previous one. With this source strength neutrino masses below 1 eV can be probed. A third detector grade enriched crystal with a mass of 3.3 kg has been recently grown at ORTEC.

To test new ideas for a further background reduction a detector made from natural Ge was equipped with a crystal holder and cap made from zone refined Si. Test measurements with this detector are performed in the Gran Sasso lab. In a second step it is planned to replace the LC2 grade Pb shielding bricks by Ge bricks. For this purpose ~ 400 kg of semiconductor purity Ge is available.

In the dashed curve the potential of the full-scale experiment is estimated. If ~ 10 kg detector mass and a factor ~ 10 background reduction are assumed mass limits around 0.2 eV can be reached.

Through the use of highly enriched source materials $\beta\beta$ -experiments can probe the Majorana neutrino mass beyond today's possibilities. The first phase of the Heidelberg-Moscow experiment is in operation in the Gran Sasso underground lab. since July 1990. The background characteristic and the source strength makes

this first enriched HP Ge detector to one of the most sensitive systems searching for the $\beta\beta$ -decay of ^{76}Ge . Further enriched detectors are in preparation. The time scale of the full experiment is approximately 5 years.

The authors greatly acknowledge the generous support of the experiment by the INFN. They also want to thank Mr. D. Röttges from Norddeutsche Affinerie AG (Hamburg) for his help to obtain the electrolytic copper.

References

- ¹⁾ P. Langacker in "Neutrinos", edited by H.V. Klapdor, Springer Verlag Berlin, Heidelberg, New York (1988) 71
- ²⁾ S.L. Glashow, Phys. Lett. B 256 (1991) 255
- ³⁾ A. Staudt, K. Muto and H.V. Klapdor-Kleingrothaus, Europhys. Lett. 13 (1990) 31
- ⁴⁾ K. Grotz and H.V. Klapdor in "The Weak Interaction in Nuclear, Particle and Astrophysics", Adam Hilger Bristol, Philadelphia and New York (1990)
- ⁵⁾ I. Bucina and I. Malátová, Proc. of "The Third Int. Conf. Low Radioactivities '85", Bratislava 1985, edited by P. Povinec, VEDA (1987) 49
- ⁶⁾ D.O. Caldwell, R.M. Eisberg, F.S. Goulding, B. Magnusson, A.R. Smith and M.S. Witherell, Nucl. Phys. B (Proc. Suppl.) 13 (1990) 547
- ⁷⁾ H.S. Miley, F.T. Avignone III, R.L. Brodzinski, J.I. Collar and J.H. Reeves, Phys. Rev. Lett. 65 (1990) 3092
- ⁸⁾ G. Heusser, Nucl. Inst. Meth. B 17 (1986) 418
- ⁹⁾ G.P. Yost et al., Phys. Lett. B 204 (1988) 81
- ¹⁰⁾ J. Busto, D. Dassié, O. Helene, Ph. Hubert, P. Larrieu, F. Leccia, P. Mennrath, M.M. Aléonard and J. Chevallier, Nucl. Phys. A 513 (1990) 291

A SEARCH FOR DOUBLE BETA DECAY OF ^{136}Xe

E. Bellotti, O. Cremonesi, E. Fiorini, G. Gervasio, S. Ragazzi, L. Rossi,
P.P. Sverzellati, J. Szarka, T. Tabarelli de Fatis, L. Zanotti

Presented by:

Tommaso Tabarelli de Fatis

Dipartimento di Fisica dell'Università di Milano
INFN, Sezione di Milano
Via Celoria 16
20133 Milano, Italy

ABSTRACT

An experiment on double beta decay of ^{136}Xe has been performed at the Gran Sasso Underground Laboratory (L.N.G.S.). From 6210 h of run with xenon enriched to 64% in ^{136}Xe we derive a 90% C.L. lower limit for neutrinoless double beta decay of 2.0×10^{22} y and 6.5×10^{21} y, for the $0^+ \rightarrow 0^+$ and $0^+ \rightarrow 2^+$ transitions respectively. From a comparison between enriched xenon and cleaned xenon a lower limit for the two neutrinos double beta decay of 1.4×10^{20} y at 90% C.L. is also obtained.

1. Experimental setup and running conditions.

The experiment was performed with a multiclement proportional chamber consisting of 61 exagonal cells arranged in a honeycomb structure, with an active volume of 79.4 litres. The wire cage was enclosed in a Ti vessel with steel flanges. The detector was shielded with copper and lead. Oxygen-like impurities in the pure xenon were kept below 50 ppb by a gas purification system. Pulses from each channel were encoded by FADC's. The risetime information was used to reject electrical discharges and alpha particles. More details on the apparatus are reported in ref.(1,2,3,4,5).

Data were collected at a pressure of 9.5 bar - corresponding to an active mass of 32.3 moles - with three different gas mixtures: i) natural xenon (8.9% ^{136}Xe), ii) xenon enriched to 64% in ^{136}Xe by ultracentrifugation (E-xenon) and iii) 'cleaned' xenon (C-xenon). The third gas sample, with a ^{136}Xe isotopic abundance of 10%, is the result of an ultracentrifugation of the natural sample with a mass cut-off just below the lightest xenon isotope. This procedure allowed to clean out the contamination of ^{85}Kr shown by the natural xenon^{2,3,5}.

2. Neutrinoless double beta decay.

The 0ν -DBD of ^{136}Xe could occur both by direct $0^+ \rightarrow 0^+$ transition to the ground state of ^{136}Ba ($\Delta m = 2479 \pm 8$ KeV) and by $0^+ \rightarrow 2^+$ transition to the excited state at 818 KeV of the ^{136}Ba ($\Delta m = 1161$ KeV), followed by gamma emission.

To extract a limit on these two processes we have considered the spectrum for the enriched sample only (6210 hours), since a comparison between E-xenon and C-xenon is limited both by statistics and systematic effects (see below).

In the $0^+ \rightarrow 0^+$ analysis only events with 3 to 8 contiguous fired cells (single cluster) have been selected to optimize the signal to background ratio. The composition of the background observed in the region of $0^+ \rightarrow 0^+$ transition is discussed elsewhere^{2,3}). The spectrum obtained with the selection criteria mentioned above has been fitted in the region of interest with a quadratic background plus a gaussian peak centered at 2479 KeV. The energy resolution was conservatively assumed to be of 5% FWHM as discussed in ref. 4). From a Monte Carlo calculation efficiencies of 36.8% and 31.6% have been evaluated for 0ν -DBD due to neutrino mass and RHC mechanism respectively. The corresponding limits, determined with a maximum likelihood analysis, are:

$$\begin{aligned} \tau_{1/2}(0^+ \rightarrow 0^+; \text{RHC} = 0) &> 2.0 \times 10^{22} \text{ y} && 90\% \text{ C.L.} \\ \tau_{1/2}(0^+ \rightarrow 0^+; \langle m_{\nu} \rangle = 0) &> 1.7 \times 10^{22} \text{ y} && 90\% \text{ C.L.} \end{aligned}$$

The transition to the first excited state of ^{136}Ba was studied by looking for a peak at 1661 KeV, selecting only single cluster events with 2 to 4 fired cells. A procedure similar to the one described for the $0^+ \rightarrow 0^+$ transition gives a limit:

$$\tau_{1/2}(0^+ \rightarrow 2^+) > 6.5 \times 10^{21} \text{ y} \quad 90\% \text{ C.L.}$$

Table 1. The four subsets of data.

ref.- gas sample	hours	609 KeV (h^{-1})	running conditions
A - E-xenon	1112.7	3.00 ± 0.14	=
B - E-xenon	2016.1	2.32 ± 0.12	plastic bag
C - C-xenon	800.1	2.09 ± 0.17	plastic bag
D - C-xenon	1293.1	1.78 ± 0.15	plastic bag + N ₂

3. Two neutrinos double beta decay.

The sum of the energies of the two electrons emitted in the 2ν -DBD gives a spectrum with a continuum peaked at about 1/3 of the transition energy. This process could then be searched for by comparing samples with the same number of atoms, but different abundance of the DBD-active isotope. Several groups have already made use of such a method either to claim evidence⁶⁾ or to set a lower limit⁷⁾ for 2ν -DBD.

Here our results are reported about a comparison between 1205.3 h of E-xenon and 800.1 h of C-xenon. A selection of single cluster events with 2 to 4 fired cells and an energy in the range 800-2000 KeV optimizes the signal to background ratio, giving a detection efficiency of 38% and a background of about 315 h^{-1} . A 10^{20} y half-life would then result in an excess of about 1% in the count rate of E-xenon with respect to C-xenon. In order to perform a significant comparison one has to take care of all possible sources of systematic effects and of the fact that a difference in the background could mask or fake the effect. Therefore in our analysis we didn't make use of the full statistics. As a first selection we conservatively excluded all the runs with a high rate of electrical discharges^{*)}. In addition, as shown in table 1, data had to be divided in at least 4 subsets, corresponding to different running conditions. In the first subset the shielding was not radon tight; therefore the data of the samples B and C were collected with a plastic bag enclosing the shielding to prevent possible radon contaminations. Finally, to further reduce the radon, N₂ was flown into the plastic bag. The presence of a different radon background is revealed by the decrease of the count rate of ^{214}Bi γ -line at 609 KeV, visible in the spectra as well as the 661 KeV peak of ^{137}Cs , which on the contrary turned out to be stable within statistical errors.

A deeper analysis revealed a residual radon contamination in the first 810.8 h of the sample B. In fact splitting B into the subsets B1 (810.8 h) and B2 (1205.3 h), we found at the ^{214}Bi peak 2.86 ± 0.17 and 1.93 ± 0.15 conts/h respectively. Therefore the comparison was restricted to the samples B2 and C.

*) In fact this is an extremely conservative selection, because from a deeper study of the instability in the count rate reported in our previous papers^{4,5)}, we learned that it's neither due to errors in dead time correction, nor to bad rejection of electrical discharges, but to differences in radon contamination.

Since statistical errors on the peak count rate are about 7%, this method is not sensitive enough to rule out further radon variations inside the two selected samples. Nevertheless the count rate on the continuum in subsets of about 400 h is stable within statistical errors at a level of 10^{-3} both in B2 and C samples.

A $26 \pm 7\%$ contribution of the γ activity associated to the ^{214}Bi to the continuum in the range 800-2000 KeV can be estimated from the scaling of the count rate on the continuum with the count rate at the 609 KeV in the four subsets. Other contributions to the background come from the measured β activity of the Ti vessel surface and Cu-Be wires^{2,3}), and are evaluated with a Monte Carlo to be $7 \pm 2\%$ and $41 \pm 13\%$ respectively. The remaining part of the background can be attributed to the γ activity of the ^{232}Th chain in and outside the Ti vessel.

The difference between the E-xenon and the C-xenon spectra, obtained with the above described cuts, is shown in fig.1a. The substantial disagreement between the background in the two samples ($-6.05 \pm 0.81 \text{ h}^{-1}$ in the 800-2000 KeV region) is almost completely removed ($-0.84 \pm 0.55 \text{ h}^{-1}$) selecting events in anticoincidence with the outer ring of counters of the detector (fig.1b). An excess of about 30% of the α activity in the 6 cells at the vertices of the hexagon, the nearest to the chamber walls, was also observed in the C-xenon with respect to the E-xenon. Both these results are clear indications of an increase of the activity of the Ti vessel surface. The α activity was measured during several dedicated runs just before (E-xenon) and after (C-xenon) the gas was changed. Since a great care was taken in order not to move parts of the detector and of the gas system when the gas was changed, the contamination must have been introduced by C-xenon.

In our previous papers^{4,5}) the hypothesis of a gas contamination was ruled out by comparing the α activity measured at 9.5 and 4 bar with E-xenon and C-xenon. In fact, once the data are corrected in order not to be affected by the Ti vessel α activity, the α rates turn out to be independent on the gas pressure both in E-xenon and in C-xenon. There is anyway an excess of $(0.81 \pm 0.26) \times 10^{-2} \alpha/\text{s}$ in C-xenon both at 4 and 9.5 bar with respect to E-xenon, which can again be attributed to contaminations introduced by C-xenon.

In order to get rid of most of the discrepancy between E-xenon and C-xenon spectra we decided to compute a limit for 2v-DBD using only spectra taken with the veto on the outer ring of the detector; such a selection reduces the efficiency for the 2v-DBD to 19% and the background in the 800-2000 KeV region to about 150 counts/h. A 10^{20} y half-life would then again result in an excess of about 1% in the count rate of E-xenon with respect to C-xenon. If we assume that the contamination introduced is completely due to isotopes of natural radioactive chains, the measured excess of $(0.81 \pm 0.26) \times 10^{-2} \alpha/\text{s}$ in C-xenon gives, via a Monte Carlo simulation, an excess of $0.5 \pm 0.2 \beta/\text{h}$ in the 800-2000 KeV region, corresponding to about 0.3% of the background. As a consequence we can correct the difference between the two spectra of fig.1b according to the Monte Carlo finding a difference of $-0.34 \pm 0.59 \text{ h}^{-1}$, where the error includes statistical uncertainty both on the spectra difference and on the α activity measurement; to such error only the contribution due to energy calibration must still be added, since, according to ref. (4), this is the most relevant. The final count rate

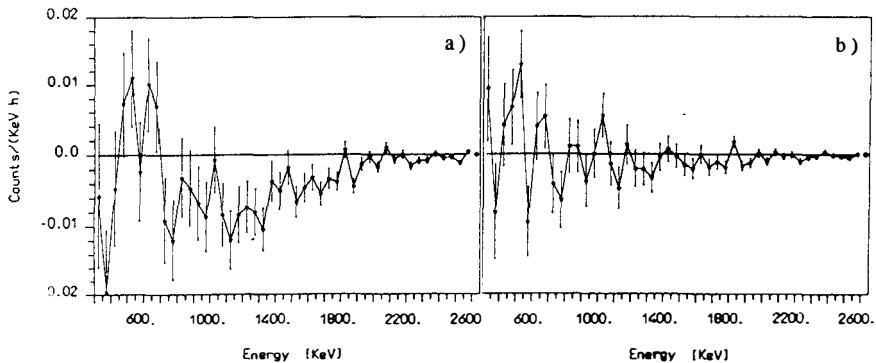


Fig. 1 - a) difference in count rate between enriched Xe and cleaned Xe. Single cluster events with 2 to 4 fired cells have been selected. b) Same difference vetoing outer ring of counters.

turns out to be $-0.34 \pm 0.68 \text{ h}^{-1}$, corresponding to a lower limit on the half-life time of $1.4 \times 10^{20} \text{ y}$ at 90% C.L.

The above outlined analysis shows clearly all the difficulties connected with the technique of comparing samples of different isotopic composition. Great care has therefore to be devoted to the understanding of all possible sources of background to obtain a significant result.

References

- 1) A. Alessandrello et al., Nucl. Inst. Meth. A252 (1986) 227
- 2) E. Bellotti et al., Phys. Lett. B221 (1989) 209
- 3) E. Bellotti et al., Proceedings of the XXIVth Rencontre de Moriond: "Tests of Fundamental Laws in Physics", ed. O. Fackler and J. Tran Than Van, Editions Frontières 1989, 355.
- 4) E. Bellotti et al., Proceedings of the XXVth Rencontre de Moriond: "Tests of Fundamental Laws in Physics", ed. O. Fackler and J. Tran Than Van, Editions Frontières 1990, 23.
- 5) E. Bellotti et al., "The Milano experiment on double beta decay of ^{136}Xe ", Proceedings of the XIV EPS Conference on nuclear Physics. Bratislava, Tchechoslovakia, 22-26 October 1990.
- 6) A.A. Vasenko et al., preprint ITEP 178-89 (1989)
- 7) A.S. Barabash et al. Phys. Lett. B223 (1989) 273

NEW LIMIT ON RATE OF 2ν $\beta\beta$ DECAY OF ^{136}Xe

V.V.Kuzminov, V.M.Lobashev, V.M.Novikov,
B.M.Ovchinnikov, A.A.Pomansky, and B.V.Pritychenko

Institute for Nuclear Research of the USSR Academy of
Sciences, Moscow, USSR

Abstract

A significant background suppression was achieved in a new step of measurements in the Baksan ^{136}Xe $\beta\beta$ experiment. Half-life limit of $2.7 \cdot 10^{20}$ yrs is obtained for 2ν $\beta\beta$ mode of ^{136}Xe .

Many experiments in last few years aimed to examine ^{136}Xe as a potential $\beta\beta$ source were done or prepared ¹⁻⁴). In particular case of $2\nu\beta\beta$ a half-life limit of $3.4 \cdot 10^{19}$ yrs (68 % c.l.) was obtained in our work ¹⁾ while theoretical predictions are $2.3 \cdot 10^{19}$ ⁵⁾, $3.3 \cdot 10^{19}$ and $6.0 \cdot 10^{19}$ ⁶⁾, $(1.5-15) \cdot 10^{20}$ ⁷⁾, $2.0 \cdot 10^{20}$ and $8.2 \cdot 10^{20}$ yrs ⁸⁾. New limit on the rate of $2\nu\beta\beta$ of ^{136}Xe is presented in this paper.

1. Experimental details.

The high pressure gridded ionization chamber used in the experiment was described elsewhere ^{9,10)}. The experiment was performed in the underground laboratory (850 m w.e.) of the Baksan neutrino observatory, INR. In order to reduce outer γ -ray background, the chamber was placed inside the passive shielding consisting of 15 cm of lead and of 10 cm of copper. Two samples of xenon were used: the first one is xenon (^{136}Xe) enriched up to 93 % in ^{136}Xe while the second one is natural xenon depleted significantly with krypton (Xe^{dpl}). The energy resolution for 0.662 keV γ -rays (^{137}Cs source) was about of 15 % (FWHM) in the chamber filled up to the pressure of 20 bars of xenon at the operating high voltage of 6 kV.

2. Background conditions.

In previous measurements ¹⁾ high counting rate in the chamber was attributed mainly to inner radiation: (a) ^{222}Rn emanated from different parts of the chamber, (b) β - and γ -rays from ^{40}K contained in glass-made resistors used for shaping of

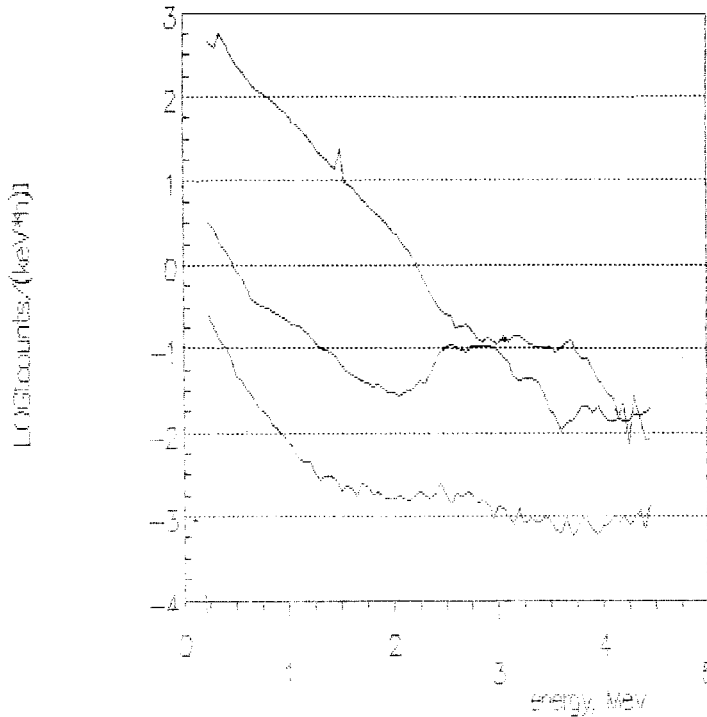


Fig. 1. Background spectra obtained in the ionization chamber in underground laboratory (850 m w.e.) at Baksan in previous 1) (middle line) and recent measurements (upper and lower lines): without passive shielding (upper) and in passive shielding of 15 cm of lead and 10 cm of copper (middle and lower). Pressure of xenon is 25 bar (upper and middle lines) and 20 bar (lower line).

homogeneous electric field, (c) α 's and β 's from the surface of grid's wires made of berillium bronze. Many changes in construction of the chamber were performed, some of them are follows: quartz tube (used to prevent sparks between shaping rings and grounded frame) was took off; 50 μ m tungsten wire was used instead of 100 μ m berillium bronze wire; mylar film

with high resistant material deposited on its surface is used as a resistor. As a result, significant background suppression is achieved compare to previous measurements ¹⁾. Fig.1 shows background spectra of the ionization chamber obtained in last measurements both inside and outside of passive shielding as well as that of inside the passive shielding in measurements ¹⁾. Compare to ¹⁾, overall background suppression in the region of interest (0.7 - 2.0 MeV) is improved by a factor of about 20.

3. Processing and measurements.

A simple one-channel electronic circuit is used: signals from the ionization chamber are accumulated in MCA followed by charge sensitive preamplifier and spectrometry amplifier (18 μ s shaping time). We have conducted measurements in several short (~100-150 h) runs. The total live time is 800 h for ¹³⁶Xe and 400 h for Xe^{dpl}. Two γ -ray sources, ¹³⁷Cs and ²³²Th, were used in two-step calibration procedure. ¹³⁷Cs source gives rough energy calibration while ²³²Th provides much more accurate one. A ²³²Th calibration is performed only in a time of changing a gas by comparing of counting rates for ¹³⁶Xe and Xe^{dpl} in different energy intervals. Thus, it provides amount of gas and precise calibration to be controlled in the same time.

4. Results.

Fig.2 shows spectra obtained for ¹³⁶Xe and Xe^{dpl}. In spite

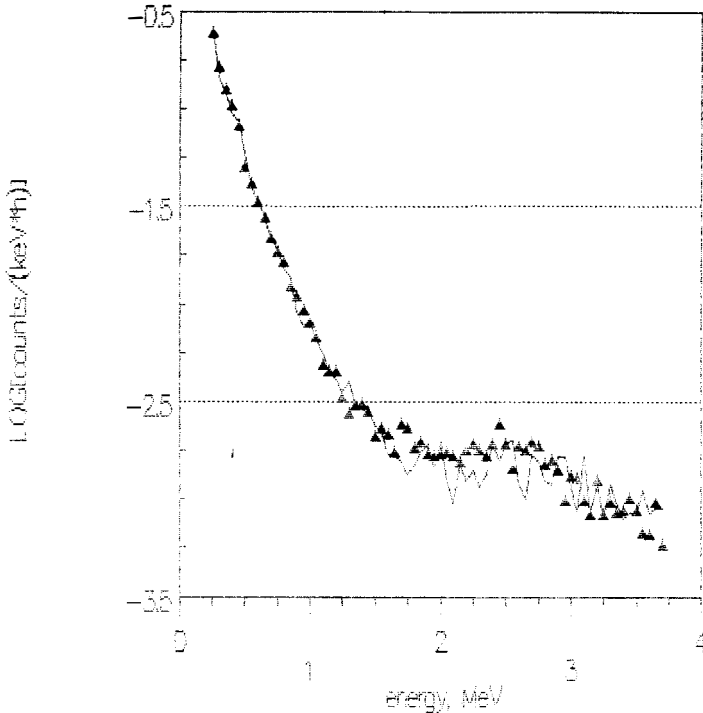


Fig. 2. Background spectra obtained in the ionization chamber filled with ^{136}Xe (triangles) and Xe^{dpl} (line).

of the fact that both these spectra are very similar, higher counting rate was found in the case of ^{136}Xe at low energies (≤ 0.6 MeV). We explain this activity by ^{85}Kr originated in ^{136}Xe due to contamination of ^{136}Xe sample with natural xenon during previous measurements ¹⁾; the corresponding amount of natural xenon in ^{136}Xe is of about 100 cm^3 . Counting rates for ^{136}Xe and Xe^{dpl} could be compared only in energy interval of 0.7–2.0 MeV in order to derive some result for $2\nu \beta\beta$ of ^{136}Xe . They are 7.64 oph for ^{136}Xe and 7.48 oph for Xe^{dpl} , and counting rate difference is $0.16 \text{ oph} \pm 0.18 \text{ oph (stat)} \pm 0.09 \text{ oph (syst)}$. Taking into account detection efficiency for $2\nu \beta\beta$

of ^{136}Xe in ionization chamber (0.5), number of atoms ($2.3 \cdot 10^{24}$) and isotope abundance of ^{136}Xe in both samples (0.930 for ^{136}Xe and 0.092 for Xe^{dpl}) one can extract half-life limit for $2\nu \beta\beta$ of ^{136}Xe :

$$T_{1/2} \geq 2.7 \cdot 10^{20} \text{ yrs} \quad (68 \% \text{ c.l.})$$

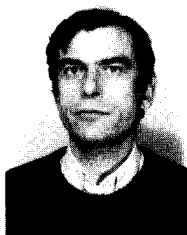
Other recent results both on 2ν and $0\nu \beta\beta$ of ^{136}Xe are reported in these Proceedings ^{11,12}).

References

1. A.S.Barabash, V.V.Kuzminov, V.M.Lobashev, V.M.Novikov, B.M. Ovohinnikov and A.A.Pomansky. Phys. Lett., **223** (1989) 273.
2. F.Boehm and M.Z.Iqbal, in *FestiVal - Festschrift for Val Telegdi*, ed. K.Winter, Amsterdam, North Holland (1988); M.Treichel, these proceedings.
3. E.Bellotti, O.Cremonesi, E.Fiorini et al., Phys.Lett., **221**(1989)209.
4. M.S.Ainutdinov, V.A.Artemiev, E.V.Brakhman et al. Pribori i Tekhnika Eksperimenta, **6** (1989) 60 (in Russian).
5. P.Vogel and P.Fisher, Phys. Rev., **C32** (1985) 1362.
6. K.Grotz and H.Klapdor, Nucl. Phys., **A460** (1986) 395.
7. P.Vogel and M.R.Zirnbauer, Phys.Rev.Lett., **57** (1986) 3148.
8. J.Engel, P.Vogel and M.Zirnbauer, Phys.Rev., **C37** (1988) 731.
9. A.S.Barabash, V.M.Novikov and B.M.Ovohinnikov, Pribori i Tekhnika Eksperimenta, **6** (1989) 68 (in Russian).
10. A.S.Barabash, A.A.Golubev, O.V.Kazachenko et al., Nucl.Instr Meth., **B17** (1986) 450.
11. M.Treichel, these Proceedings.
12. T.Tabareli, these Proceedings.

NEUTRINO OSCILLATIONS SEARCH AT THE BUGEY REACTORS

AVENIER Michel
INSTITUT DES SCIENCES NUCLEAIRES (IN2P3)
53 AVENUE DES MARTYRES
38026 GRENOBLE CEDEX FRANCE



Abstract:

In the Bugey III experiment three detection modules of reactor anti-neutrinos are now installed at two distances from the core, one at 16m and the two others at 40m. Both positions are runned simultaneously. Detection make use of liquid scintillator loaded with highly purified Lithium. We plan to take data for one year after the present shut-down of the reactor. It could be possible detect oscillations at distance of 120m.

As is well known, the existence of a possible violation of the specific family lepton number could be revealed through neutrino flavour oscillations caused by a possible non identity between mass eigenstates and flavour (i.e. weak) eigenstates. Differences in the time evolution of the flavour state components lead to interference effects and an oscillating behaviour of the lepton flavour.

Nuclear reactors are powerful sources of $\bar{\nu}_e$'s with energies up to 10 MeV, a mean energy of 2 MeV and a very low ν_e contamination ($\nu_e/\bar{\nu}_e \sim 10^{-4}$). The anti-neutrinos come from beta decays of fission products with a source strength of $1.9 \cdot 10^{17}$ $\bar{\nu}_e$ /s. MWth. The shape of the spectrum depends on the core arrangement and to the fuel composition (burn-up). Nuclear power reactors are thus well suited to study oscillations in the disappearance channel ($\bar{\nu}_e \rightarrow \nu_x$). In the scheme of the two-neutrino state mixing, the probability to retrieve the initial state at the distance L from the source is.

$$P(L, E, \Delta m^2, \Theta) = 1 - \sin^2 2\Theta \sin^2(1.27 \Delta m^2 L/E)$$

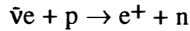
with $\Delta m^2 = |m_1^2 - m_2^2|$ and Θ being the only two parameters of the model (m_1^2 and m_2^2 are the eigenmasses and Θ the mixing angle).

The Bugey III experiment, conducted by a Paris, Saclay, Annecy, Grenoble, Marseille collaboration, is located at the Bugey 5 reactor. The Bugey plant consists of five aligned reactors among which the four last are 2800 MWth Pressurized Water Reactors. The fifth reactor is 87 m away from the fourth and 252 m from the third.

We chose to develop a modular system consisting of three identical detection modules. One of them is installed at a distance of 16m from the core in an experimental room located underneath the reactor. The two others are at ground level, 40m from the core, grouped together in a common shielding inside a concrete bunker. When running simultaneously the comparison of recorded events is to first order independent upon the emitted spectrum of the reactor. This reduces

the systematic uncertainties coming from our limited knowledge of the source. Each module will be sequentially positioned, in a permutation operation, at the nearest position from the core to establish their relative behaviour under some reference conditions.

The detection proceeds through the use of the reaction :



a time coincidence between both the positron and the neutron is required as the signature of an anti-neutrino event. The neutrino energy is determined from the measured positron kinetic energy E_e (the neutron has only a few tens of keV) using the relation :

$$E \sim E_e + 1.8 \text{ MeV}$$

One detector consists of a 600 liter tank of liquid scintillator, optically segmented into 98 elementary cells ($8.6 \times 8.6 \times 87 \text{ cm}^3$) as described earlier ¹⁾. The scintillator - NE320 - ²⁾ loaded with ${}^6\text{Li}$ (0.15 % in weight) serves as proton target, positron detector, neutron moderator and thermal neutron detector. The neutron signature is the detection of an alpha-triton pair from the breakup of ${}^6\text{Li}$ nuclei by thermal neutrons with a monoenergetic deposit of 4.8 MeV but producing only a light yield equivalent to that of a 530 keV electron. Discrimination between thermal neutron captures and electrons is achieved through the good Pulse Shape Discrimination properties of this scintillator. Neutrino events are strongly confined due to the very short range of the capture products ($\sim 100 \mu\text{m}$) combined with the quite low thermalization and migration path ($\sim 6 \text{ cm}$) of neutrons. The neutron will then be searched for within the cells surrounding that one revealing the positron candidate. A trigger condition is therefore a delayed coincidence between a positron candidate and a following neutron candidate, fulfilling proximity conditions both in space and time.

Beside the transverse localization given by the pattern of struck cells, a longitudinal localization based on time and amplitude at each side of cells is used in the analysis allowing restriction on the relevant volume of detection.

The relative amount of light at each phototube is affected by light attenuation in the medium and by solid angle effects so that the light output is sensitive to the longitudinal localization. To avoid too much loss of energy resolution it must be corrected for in off-line analysis. A calibration of the longitudinal response has been performed using the backscattering technique. The width of the neutron peak, corresponding to neutrino events over the whole detector, shows that this effect is well corrected.

To closely follow the evolution of our detectors we calibrate each cell monthly or weekly with a source and daily with a monitoring system. For long term calibrations, an AmBe source is used : fast neutrons give access to the neutron capture peak and the 4.4 MeV gamma rays permits monitoring of the positron response and the balance of phototubes. Short term monitoring of detector stability uses a spark gap as a light generator associated with filters and optical fibers to illuminate both side of each cell. This spark system allows monitoring of each phototube gain and is used to interpolate the response between successive calibrations using the source.

Another way to obtain information on stability is to look in the collected data for ^{214}Bi events (from ^{238}U decay chain and from Radon emanations) which exhibit a beta-alpha sequence mimicking neutrino events. These events are discriminated through the energies of the heavy particle and the associated electron. Cosmic ray induced fast neutrons can also simulate neutrino events as

recoil protons associated with thermalized neutrons. In this case the PSD of the positron candidate helps us to reject these events. Furthermore as these event rates are constant in time, they are removed in the ON-OFF subtraction.

Bismuth and cosmic ray induced events represent the correlated part of the background as 5 % and 25 % respectively. The remaining 70 % is concerned with accidental events and is composed of 7 % due to two gamma rays where the second survive to PSD selection and 63 % of the gamma-alpha type where the alpha particle is associated with ^{238}U decay. To study these accidental events the trigger condition is reversed looking for a "positron" following a heavy particle. Normal and reversed triggers are operated simultaneously.

The Uranium comes from the LiOH compound used to make the scintillator. A new LiOH has been purchased with higher purity giving a decrease of at least a factor 7 in Uranium content down to a contamination level of about 10^{-10}g of Uranium/g of scintillator, the Bismuth rate being kept at a factor 2 lower. The signal over noise ratio will then be about 25 and 5 for the two positions.

The fifth reactor is stopped for four months up to June 1991 (decennial shut-down). This period will be used to pursue background studies. At the same time we collect neutrinos from the fourth reactor giving access to oscillations at 120 m in case the fourth reactor will also shutdown for some time. In this situation the signal over noise ratio will be around unity.

- 1) J. Collot, Proc. 23rd Moriond Workshops (Editions Frontières, 1988) p. 153
- 2) S. Aït-Boubker et al, Nucl. phys. and Meth. A277 461 (1989)

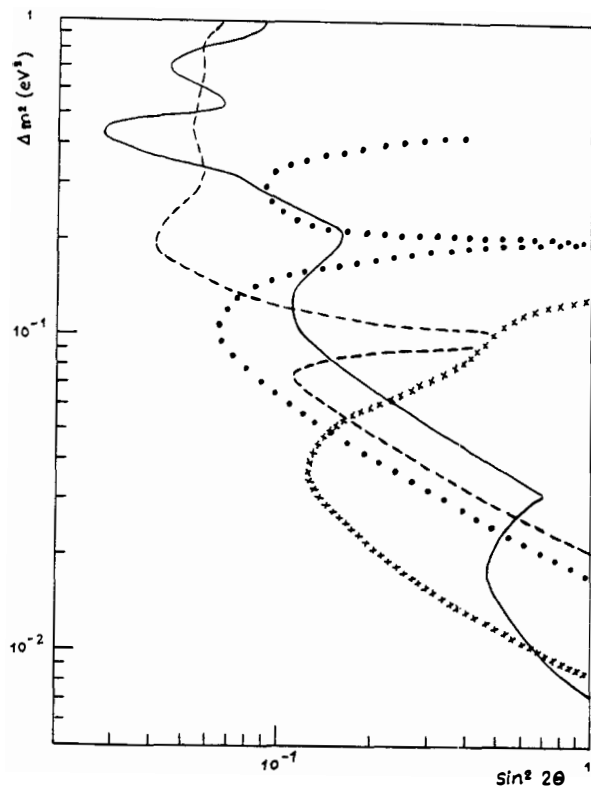


Figure 1 Sensitivity expectations for
the new Bugey experiment.

————— zone already excluded
 One year data taking at 16 and 40 meters:
 - - - - - relative shapes
 •••••••• relative rates
 Six months at 16 and 120 meters:
 + + + + + relative rates.

FINAL RESULTS OF THE FREJUS PROTON DECAY EXPERIMENT ON ATMOSPHERIC NEUTRINOS

The FREJUS Collaboration :

*I. Physikalisches Institut der RWTH Aachen, L.A.L. Orsay, LPNHE Ecole Polytechnique,
DPhPE Saclay, Universität-Gesamthochschule Wuppertal*

Presented by :

Olivier Perdereau

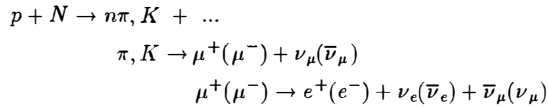
*Laboratoire de l'Accélérateur Linéaire, IN2P3 - CNRS
et Université de Paris-Sud, F-91405 ORSAY Cedex, FRANCE*

Abstract :

The Fréjus nucleon decay detector has been operated between 19-02-84 and 13-09-88. In this paper I will summarize the results of the analysis of atmospheric neutrino interactions recorded in this experiment. The flavor composition of the atmospheric neutrino flux is inclusively determined, and compared with the expectations of Monte Carlo simulations. A good agreement is found, which is translated into new limits on the neutrino oscillations parameters (Δm^2 , $\sin^2 2\theta$).

Introduction :

Atmospheric neutrinos are generated in the high energy cosmic-ray showers in the atmosphere, mainly through the decay chain :



They have been observed for the first time 30 years ago^[1]. However they have only recently being precisely studied, primarily as the main source of background for the nucleon decay searches in the 80's.

The main proton decay experiments, I. M. B.^[2], Kamiokande^[3], NUSEX^[4] and the Fréjus^[6] have published or reported atmospheric neutrino analyses. The most striking result is the report by the Kamiokande-II collaboration of an apparent muon-like event deficit which could be interpreted as an evidence of neutrino oscillations. Other topics, such as search for neutrinos generated by dark matter particles annihilations in the sun, or cosmic flux of exotic particles, have also been covered within these studies.

Neutrino oscillations have been searched in various experiments^[9]. They arise under the hypothesis of massive and non diagonal mass eigenstates in the flavor basis^[8]. In the two flavor hypothesis this mixing is described by a 2×2 rotation matrix, parametrized using a mixing angle, θ . Considering a relativistic neutrino of flavor l and energy E , the transition probability to the other flavor, l' , after a flight distance D in vacuum is given by

$$P(\nu_l \rightarrow \nu_{l'}) = \sin^2 2\theta \sin^2(\pi D/L_o)$$

The "oscillation length" L_o is given by :

$$L_o = 4\pi E/\Delta m^2 \ (\approx 2.5 \text{ (km)} E \text{ (GeV)} / \Delta m^2 \text{ (eV}^2))$$

This length is a crucial parameter for the possibility for observing oscillations : the distance between the neutrino source and the detector has to be greater or equal than L_o .

This picture is modified by the presence of matter in the flight path of the neutrino. Electron (anti-) neutrino have, due to weak interactions with atomic electrons, have a different index of refraction than (anti-) neutrinos from other flavors. As shown by Wolfenstein^[11], and Mikheyev and Smirnov^[12], this can result in resonant amplification or suppression of neutrino oscillations in matter.

The final sample of neutrino interactions (188 events), corresponding to a 1.56 Kt-y sensitivity, is analysed. It is compared with the results of a detailed simulation of the atmospheric neutrino flux. From this comparison neutrino oscillations are investigated.

The apparatus was located in the Fréjus underground laboratory, located in the Fréjus highway tunnel connecting France and Italy. Its geographical coordinates are 45.2° N and 6.7° E. The averaged rock cover amounts to about 1780 m. The Fréjus proton decay detector

has been described in details elsewhere^[5]. It was a fine grain calorimeter measuring $12.3 \times 6 \times 6 \text{ m}^3$, consisted by a sandwich of iron plates, flash chambers and Geiger tubes planes. The trigger was provided by the Geiger tubes, requiring a coincidence of at least 5 hits in 5 adjacent planes, with a maximal multiplicity per plane of 3 hits. The trigger rate was of about 45 per hour, 20 due to cosmic-ray muons and 25 to local radioactivity. This detector provided 2 orthogonal views of each event.

1. Data and Monte Carlo samples

Atmospheric neutrino interactions were selected on line by the shift physicist. Events have been afterwards rescanned by a pattern recognition program. The combined efficiency of these methods to select neutrino interactions has been estimated to about 98%.

To suppress the possible backgrounds, events fulfilling one of the following criteria were rejected : events with a vertex outside a fiducial volume (50 cm from any detector's edges), events associated with a muon track crossing the detector and events with only an outgoing track, possibly confused with muons stopping in the apparatus. The latter case is a consequence of the ambiguity in the track direction determination in our apparatus.

The remaining events have been measured using different methods, from a purely visual one (done by a physicist on a graphic terminal) to an mostly automatic one (done by a program)^[7]. Both methods were based on the event topology. This enabled us to investigate systematics induced by the measurement and identification procedure. All events, including contained and non-contained ones, are analysed.

Events are classified according to the nature of the lepton in the final state, if any, in one of the following categories : $CC\mu$ (muon-like), CCe (electron-like) and NC . The topological criteria used to identify muons and electrons are explained in reference 6.

Atmospheric neutrino interactions in our detector have been simulated in detail. We used a flux computation described in reference 10, based on a Monte Carlo simulation of cosmic-ray showers in the atmosphere. This calculation takes into account the muon polarisation in the pion and kaon decay chains which had been previously neglected. The neutrino interaction simulation program is described in details in reference 6. Experimental data and weak interaction phenomenology are both used. Nuclear effects are simulated using a cascade model originally developed for the Gargamelle neutrino experiment at CERN. Both hadrons, electromagnetic showers and muons are simulated in the detector. The program was calibrated using test beam data from prototype experiments at CERN, Bonn and DESY.

Simulated events have been analysed using the same methods and classified using the same criteria as data. The simulated measured statistics corresponds to a 10 Kt-y statistics in the manual case, and to 30 Kt-y in the automatic one. Trigger efficiencies of the apparatus were estimated using the simulation and are given on Figure 1 for Charged Current (CC) interaction. Neutral Current (NC) have a much lower trigger efficiency, due to the energy carried out by the neutrino. The efficiency of the identification procedure has also been checked : the probability for a muon (respectively electron) neutrino (or anti-) CC interaction to be classified as $CC\mu$ (resp. CCe) is 95% (res. 86%).

2. Comparison of the two samples

From the Monte Carlo 212 events are expected for the experimental sensitivity, which is in good agreement with the observed number of events (185) recalling the large uncertainty usually quoted (about 20%) on the flux global normalisation.

The results obtained using any of the analysis methods agree with each other, for the data and Monte Carlo samples. The number of events observed and expected in each categories are given in Table I.

Sample	$CC\mu$	CCe	NC	ϵ/μ Ratios
Data	108 (66)	57 (56)	23 (20)	0.53 ± 0.09 (0.85 ± 0.16)
Monte Carlo	125.8 (90.0)	70.6 (66.8)	16 (15.3)	0.56 ± 0.08 (0.74 ± 0.09)

Table I : Composition of the Data and Monte Carlo samples for all events (resp. for contained events). ϵ/μ ratios are given with total errors ; for details on the error calculation, see reference 7.

The flux composition can be accurately investigated by using the ratio of the number of CCe and $CC\mu$ events, the ϵ/μ ratio, since some of the systematics cancel or are largely reduced. For example, the uncertainty on this ratio from the flux calculation is estimated to be 0.03 . Table I also displays the values of this ratio, computed from the experimental data and expected from the Monte-Carlo, that are in nice agreement with each other.

From this agreement one concludes that our data do not show evidence for processes that could modify the atmospheric neutrino flux composition, such as neutrino oscillations. In the following we derive limits on the parameters of this process.

3. Neutrino oscillations analyses

The first stage is to obtain a prediction for the ϵ/μ ratio in each oscillation hypothesis. This was done using our simulated sample in the following way. A flux taking into account the oscillations is computed for any value of $\sin^2 2\theta$ and Δm^2 . Neutrino are assumed to be generated at a constant altitude in the atmosphere ; the effect of a more detailed model for this generation was checked to be negligible. For neutrino propagation through the Earth, matter effects are taken into account, using a detailed model for the electronic density in the Earth. This however introduced only minor corrections to the results. Simulated events were weighted, according to the incoming neutrino flavor, energy and direction, by the ratio of the flux with and without oscillations. This weighted sample is used to compute a prediction for the ϵ/μ ratio.

To exclude a parameter region in the $(\Delta m^2, \sin^2 2\theta)$ plane we use the following procedure. In this plane, each value of the ϵ/μ ratio defines a curve. For each channel, this ratio can have only values in a certain range (e.g. in the $\nu_e(\bar{\nu}_e) \leftrightarrow \nu_\mu(\bar{\nu}_\mu)$ channel it can lie between about 0.5 and about 1.). We combine in quadrature the statistical and systematic errors and compute the probability that the ratio could have fallen. This is renormalized to the total probability contained in the allowed region, given by the Monte Carlo, according to the procedure recommended by the Particle Data Group.

We obtain bounds on e/μ at 90% and 95% confidence level (CL) that are used to define the limits in the $(\Delta m^2, \sin^2 2\theta)$ plane. Figure 2 and 3 show the limits (90% and 95% CL) in the $\nu_e(\bar{\nu}_e) \leftrightarrow \nu_\mu(\bar{\nu}_\mu)$ and $\nu_\mu(\bar{\nu}_\mu) \leftrightarrow \nu_\tau(\bar{\nu}_\tau)$. In the third channel, $\nu_e(\bar{\nu}_e) \leftrightarrow \nu_\tau(\bar{\nu}_\tau)$, the low CCe statistics and the systematic uncertainties make it impossible to set any limit at 90% CL.

Conclusions

We presented the final results from the oscillations analysis of the atmospheric neutrino events (1.56 Kt-y sensitivity) recorded in the Fréjus experiment. No evidence for oscillations are found by comparing a detailed Monte Carlo simulation and the data. This is translated into new limits on the two flavor neutrino oscillations parameters in the $\nu_e(\bar{\nu}_e) \leftrightarrow \nu_\mu(\bar{\nu}_\mu)$ (resp. $\nu_\mu(\bar{\nu}_\mu) \leftrightarrow \nu_\tau(\bar{\nu}_\tau)$) channel which improves by about one order of magnitude (resp. a factor of 30) existing limits on the squared mass difference. These results are, due to the limited statistics, limited to large mixing angles.

A muon type atmospheric neutrino events deficit was reported by the Kamiokande-II collaboration, using a large water Čerenkov detector. The IMB collaboration, after having improved the light collection of the apparatus, reported recently a large improvement in the electron identification which enable them to measure the flux composition. Their latest results tend to confirm the Kamiokande deficit, with a statistical significance of about 2 sigmas. There is no evidence for such a signal in our data. The other large underground calorimeter, NUSEX, with a lower sensitivity (0.72 Kt-y), observes a flux compatible with expectations. It could be worthwhile to notice that the water Čerenkov experiments do a kind of inclusive measurement, selecting “one ring” events, which differs from our exclusive measurement of the flux composition, less sensitive to details in the atmospheric neutrino interactions simulation.

Acknowledgements

The author would like to dedicate this work to the memory of J.P. Wuthrick.

References.

1. M.F. Crouch et al., *Phys. Rev.* **D18** (1978), 2369
2. R.M. Bionta et al., *Phys. Rev.* **D38** (1988), 768
D. Casper et al., BU preprint **90-23** (1990), submitted to *Phys. Rev. Lett.*
3. H. Hirata et al., *Phys. Lett.* **205B** (1988), 416
M. Nakahata et al., proc. of the “New and exotic phenomena” workshop,
XXVth Rencontres de Moriond, ed. Frontieres (1990), 449
4. M.A. Aglietta et al., *Europhys. Lett.* **8** (1989), 611
5. Ch. Berger et al., *Nucl. Inst. and Methods* **261** (1987), 540
6. Ch. Berger et al., *Phys. Lett.* **227B** (1989), 489
7. Ch. Berger et al., *Phys. Lett.* **245B** (1990), 305
8. S.M. Bilenky and S.T. Petcov, *Rev. of Mod. Phys.* **59** (1987), 671
9. M. Talby, Proc. XXIVth Conf. on High energy physics
(Münich, 1988), eds. R. Kotthaus and S.H. Kühn (Springer, Berlin, 1989) p. 1072.
G. Bernardi, Proc. XXIVth Conf. on High energy physics
(Münich, 1988), eds. R. Kotthaus and S.H. Kühn (Springer, Berlin, 1989) p. 1076
10. G. Barr, T.K. Gaisser and T. Stanev, *Phys. Rev.* **D39** (1989), 3532
E.V. Bugaev and V.A. Naumov, *Phys. Lett.* **232B** (1989), 391
11. L. Wolfenstein, *Phys. Rev.* **D17** (1978), 2369
12. S.P. Mikheyev and A.Yu. Smirnov, *Sov. J. of Nucl. Phys.* **42** (1985), 913

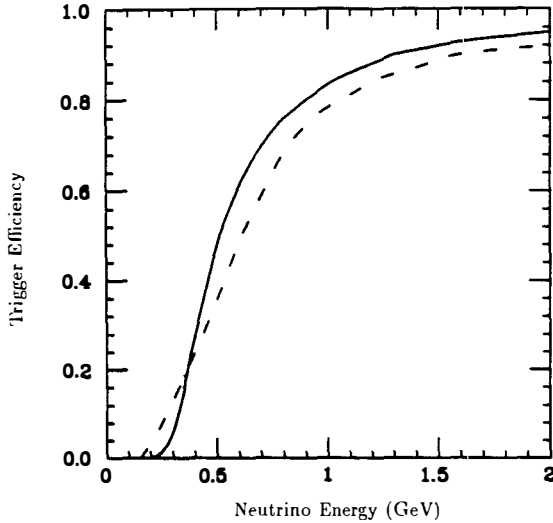


Fig. 1 : Trigger efficiencies for Charged Current interactions of $\nu_\mu(\bar{\nu}_\mu)$ (solid line) and $\nu_e(\bar{\nu}_e)$ (dashed line) as a function of the neutrino energy.

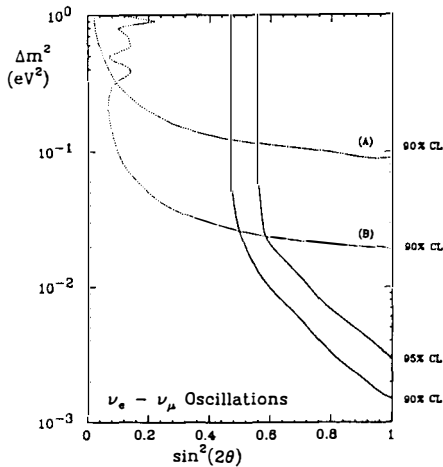


Fig. 3 : $(\Delta m^2, \sin^2 2\theta)$ diagram for $\nu_e(\bar{\nu}_e) \leftrightarrow \nu_\mu(\bar{\nu}_\mu)$ oscillations. The two plain line curves correspond respectively to 90% and 95% CL limits on ϵ/μ . (A) is the region excluded by accelerator appearance experiments (90% CL).

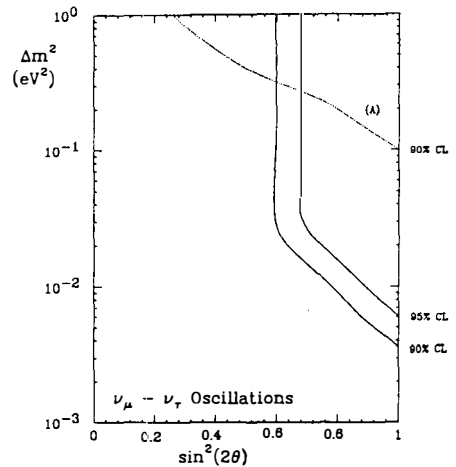


Fig. 2 : $(\Delta m^2, \sin^2 2\theta)$ diagram for $\nu_e(\bar{\nu}_e) \leftrightarrow \nu_\mu(\bar{\nu}_\mu)$ oscillations. The two plain line curves correspond respectively to 90% and 95% CL limits on ϵ/μ . (A) is the region excluded by accelerator appearance experiments (90% CL) ; (B) is the region excluded by reactor disappearance experiments (90% CL).

DETECTION OF THE ν_e *François VANNUCCI**LPNHE PARIS VI ET VII*

After an overview of the physics associated with the ν_e , its detection is discussed with an emphasis on a method only using kinematical criteria. The simulation of a new experiment proposed to look for the oscillation $\nu_\mu \rightarrow \nu_e$ is presented.

MOTIVATIONS

The ν_e remains a "theoretical" particle. It has never been seen through its interactions with matter. The charged current process is supposed to give :

$$\nu_e + N \rightarrow \tau^- + X$$

Because of the large τ mass this is only possible above a threshold energy of order 5 GeV. The CERN SPS beam is adapted for such a search, but the content of ν_e in the ν_μ beam is extremely small $\sim 10^{-6}$.

In a beam dump type of experiment the conditions are different : the ν_e component can reach a few % of the total flux, but rates are too small at present energies, and the direct search has to wait for machines such as UNK or better LHC/SSC where one expects some 100 ν_e events /ton/year.

A ν_e detector could nevertheless look for the oscillations $\nu_\mu \rightarrow \nu_e$. This is especially interesting if one interprets the missing mass of the Universe as composed of ν_e (1). The mass of this neutrino would be a few 10 eV and could mix with ν_μ at a level of 10^{-3} . These parameters are accessible in an appearance search at SPS type of energies in a detector collecting 10^5 ν_μ events. This is obtained in a 1 ton target.

Furthermore recent results (2) claim the existence of a 17 KeV neutrino state mixing with the ν_e . If this state were the third mass eigenstate, one could expect an oscillation $\nu_e \rightarrow \nu_e$ at a level $\sin^2 2\theta \sim 4\%$ testable experimentally.

CHARACTERISTICS OF ν_e EVENTS

The ν_e interacts via the charged current process giving :

$$\nu_e + N \rightarrow \tau^- + X$$

The lifetime of the τ corresponds to a track length of order 1mm at SPS energies. To see a ν_e interaction through the short track left by the τ , it is necessary to have a very high

spatial resolution detector. This is a difficult task over a large volume. Emulsions offer this possibility. They give the best experimental limit on the $\nu_\mu \nu_e$ mixing at 5.10^{-3} (3). Proposals exist to continue with this technique (4). Other techniques being considered are scintillating fibers and liquid argon TPC.

Apart from a secondary vertex $\text{CC } \nu_e$ interactions differ from $\text{CC } \nu_\mu$ or ν_e interactions by the large missing p_T due to escaping neutrinos in $\bar{\nu}$ decays. The discrimination is particularly clear when considering the angle between the missing p_T and the transverse momentum of the hadronic jet, and the angle between the lepton and the hadrons in the transverse projection. The figure shows the scattered plots of these two angles for the cases of ν_e and ν_μ separately. It is possible to define a cut which efficiently selects ν_e interactions.

THE PROPOSED EXPERIMENT (5)

It is advantageous to select $\bar{\nu}$ decaying with an electron. This is due to the low ν_e contamination in the ν_μ beam (1%).

Thus the experiment measures as best as possible the full event kinematics, and identifies electrons. This is achieved by filling the inside volume of the UA1 magnet ($7 \times 3.5 \times 3.5 \text{ m}^3$) with polypropylène foils which act as target and as transition radiation medium. Drift chambers are interspersed within the target which is followed by an electromagnetic calorimeter.

It is possible to have more than one ton of target, and the full expected statistics is 800 000 $\text{CC } \nu_\mu$ interactions. The main background to the searched-for signal comes from ν_e interactions and neutral current events with $\bar{\nu} \rightarrow e^+ e^-$ giving a Dalitz pair. A careful simulation shows that it is possible to reach a level of a few 10^{-4} for the maximum amount of ν_e present in the ν_μ beam.

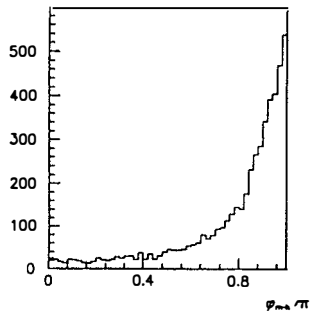
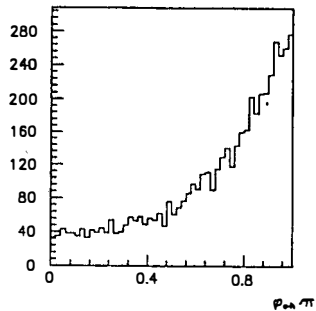
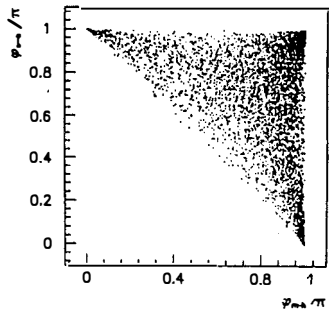
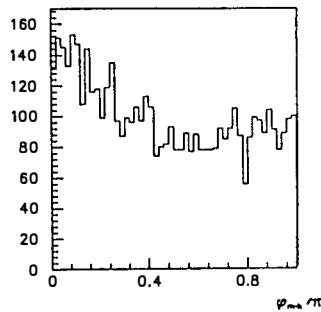
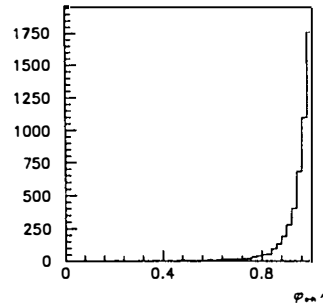
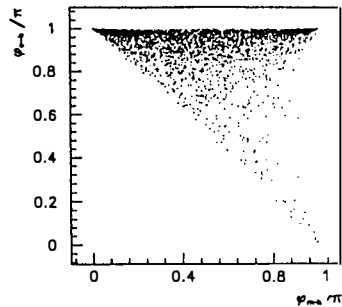
Apart from the search for the oscillation $\nu_\mu \rightarrow \nu_e$, the detector is well suited to study final states showing electrons and photons.

REFERENCES

- 1) H. HARARI, *Phys. Lett. B* 216, 413 (1989)
- 2) J.J.SIMPSON and A.HIME *Phys.Rev D* 39,1825 (1989)
- 3) N. USHIDA et al. *Phys. Rev. Lett* 57, 2897 (1986)
- 4) Proposal CHARM2 CERN-SPSC/ 90-42 and Draft proposal Fermilab P803.
- 5) P.ASTIER et al CERN-SPSC/ P 261.

FIGURE CAPTION

Scattered plots showing in the plane transverse to the neutrino direction the angle between the electron and the hadronic jet, versus the angle between the missing p_T and the hadrons, for the cases of ν_c and ν_e separately.

ν_τ  φ_{e-h} versus φ_{m-h} ν_e  φ_{e-h} versus φ_{m-h}

SCINTILLATING FIBER ARRAYS FOR PARTICLE TRACKING

J. Bähr^{*1}, E. Birckner², W. Flegel³, B. Friend³, M. Gruwé^{/4}, K. Hiller¹,
 P. Lendermann⁵, C. Mommaert^{&4}, R. Nahnauer¹, E. Pesen⁶, G. Stefanini³,
 G. Wilquet⁵⁴, K. Winter³ and V. Zacek³

presented by Peter Lendermann

Abstract

Scintillating fiber arrays offer interesting possibilities for massive active target detectors in high and low energy neutrino physics. A very promising technique in this context is the use of coherent glass capillary arrays filled with liquid scintillator of high refractive index, since suitable scintillators have been developed and reflection losses at the capillary walls are very small. For 120 μm - capillary bundles an attenuation length $\lambda_{\text{att}} = 110$ cm has been obtained, essentially limited by self absorption of the scintillating core. The possibility of surrounding each fiber with an extramural absorber allows sufficient reduction of crosstalk.

¹ Institut für Hochenergiephysik, Berlin - Zeuthen, Germany

² Friedrich Schiller Universität, Jena, Germany

³ CERN, Geneva, Switzerland

⁴ Inter-University Institute for High Energies (ULB - VUB), Brussels, Belgium

⁵ Sektion Physik der Universität München, Munich, Germany

⁶ Middle East Technical University, Ankara, Turkey

* presently Research Associate at CERN

[/] Institut de Recherche Scientifique pour l'Industrie et l'Agriculture, Belgium

[&] Inter - University Institute for Nuclear Sciences, Belgium

⁵ National Fund for Scientific Research, Belgium

1. Introduction

In this report we describe recent progress in the development of a high resolution active target detector based on coherent scintillating fiber arrays, and especially the application of liquid scintillator filled capillaries. These results have been obtained in a Research & Development - Project in the frame of the CHARM II - Collaboration at CERN. Originally this work was initiated by the search for new techniques for efficient ν_τ - detection [1].

2. Scintillating fiber detectors for neutrino physics

Several important requirements have to be fulfilled by future neutrino detectors. Because of very small cross sections in ν -induced reactions and therefore low event rates, a detector mass of at least 10^2 kg is necessary, as well as a sufficiently good time resolution ($10 \text{ ns} \leq \Delta t \leq 1 \text{ ms}$) for background suppression. Since particles with short decay times (e.g. τ - lepton, D - meson) have to be detected, a spatial resolution better than $100 \mu\text{m}$ is needed. Taking into account these requirements, detectors built of coherent arrays of scintillating fibers can in many respects be superior to other common tracking techniques.

Applications of scintillating fiber detectors in neutrino physics are explained in detail in [2]. Possible detector designs especially in view of the search for $\nu_\mu - \nu_\tau$ - oscillations are discussed in [3] and [4].

3. Tracking with scintillating fibers

In a coherent fiber detector each fiber consists of a high refractive scintillating core ($n_{\text{core}} \approx 1.6$) surrounded by a cladding of lower refractive index ($n_{\text{clad}} \approx 1.5$). In this case total reflection inside the fiber occurs for a certain fraction ($\epsilon_{\text{trap}} \approx 5\%$) of scintillation light, which will be trapped and travel towards the fiber endface [5]. As a result the projected track image in an array can be recorded (fig.1). In order to preserve a good spatial resolution, a fiber array must have a coherency better than a single fiber diameter. For reduction of crosstalk it is important to surround each fiber with an extramural absorber (EMA).

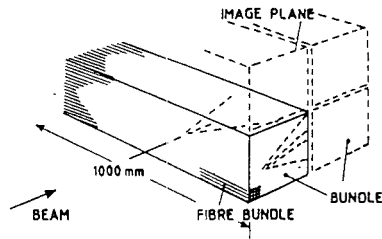


fig. 1. Tracking with scintillating fibers.

In comparison with plastic and glass fibers, liquid scintillator filled capillaries offer several advantages: Binary liquid scintillator systems exist with short fluorescence decay times ($\tau \approx 5 \text{ ns}$), high refractive indices up to $n \approx 1.66$, good light transmittance and high light yields ($10 \gamma/\text{keV}$, i. e. comparable with the common plastic scintillator NE 102 A). Reflection losses are by 1-2 orders of magnitude smaller than for plastic microfibers.

Furthermore, a technique has been developed, which allows the production of capillary bundles with lengths up to 2 m, a sensitive volume of $\sim 60\%$ and excellent coherency (fig. 2) [*]. The capillary walls consist of a multicomponent borosilicate glass ($n = 1.487$),

which is transparent above 380 nm. Pore diameters from 1000 μm down to 5 μm are possible. Details concerning their fabrication - especially in view of the performance of EMA - can be found in [6].

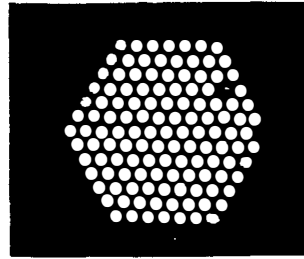


fig. 2. Coherent capillary bundle (fiber- $\Phi = 120\mu\text{m}$), 60 cm long, illuminated from the opposite end.

4. Recent progress in development of new liquid scintillators

The feasibility of capillary targets is essentially dependent on a suitable scintillator, as well as on careful preparation, cleaning and filling of micro-capillaries [6]. Among the available solvents Isopropylbiphenyl and 1-Methylnaphthalene can best meet the demands for high refractive index ($n_{\text{IBP}} = 1.582$, $n_{1\text{MN}} = 1.617$) and good transmittance. Concerning promising dyes, 1-phenyl-3-mesityl-pyrazoline (PMP, $\lambda_{\text{max}} = 430 \text{ nm}$) and 3-Hydroxyflavone (3 HF, $\lambda_{\text{max}} = 540 \text{ nm}$) have not only a satisfying quantum fluorescence efficiency [7], but also a large Stokes' shift, which makes the light attenuation properties being limited rather by the solvent transmittance itself.

Light yield and attenuation length have been measured for various liquid scintillators by exposure of 1m long single capillaries ($\Phi = 2 \text{ mm}$) in a 5 GeV- π -beam (fig.3). The light output was measured with a standard bi-alkaline photocathode (exception: S20 photocathode for the green emitting dye 3 HF). For comparison the results of a standard plastic fiber (Polystyrene/Butyl-PBD/POPOP, UA2 type, $\Phi = 1 \text{ mm}$) are added. The best result was found for 1MN+PMP (0.01 mole/l): 4.2 detectable photoelectrons per mm of traversed scintillator were recorded after 1 m light pathlength in the capillary.

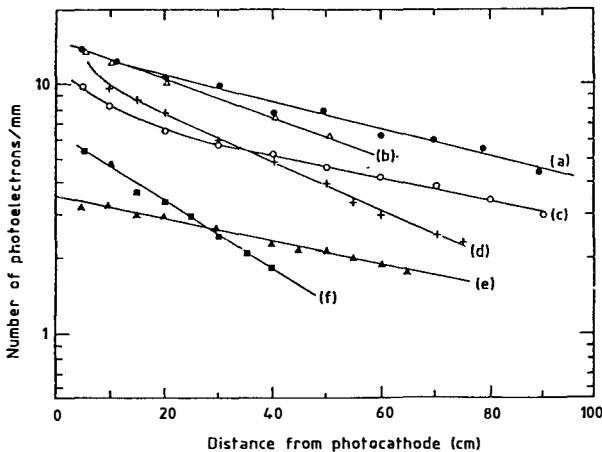


fig. 3. Light output of liquid scintillators in single capillaries:

- (a) 1MN+PMP, 0.01 mole/l
- (b) IBP + PMP, 0.015 mole/l
- (c) UA2 plastic fiber (for comparison, see text)
- (d) 1MN+PMP, 0.1 mole/l
- (e) IBP + 3HF, 0.06 mole/l
- (f) IBP+BBQ, 0.08 mole/l

Capillary bundles of various diameters have also been tested in beam exposures. Fig. 4 shows the attenuation curve for IBP + 3 HF (0.008 mole/l) in a 120 μm -capillary bundle. For comparison data obtained with a single capillary are also displayed. The weak

dependence of the attenuation length on the fiber diameter proves that reflection losses at the core/cladding - interface are very small (1 part in 10^5).

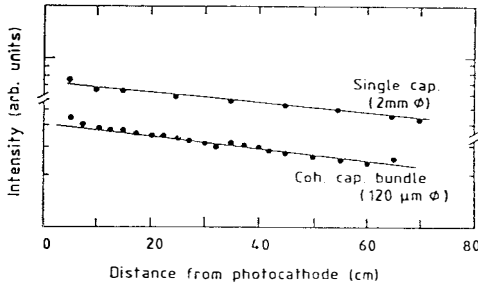


fig. 4. Comparison of light attenuation (IBP+3HF, 0.008 mole/l) in a 2 mm diameter single capillary to that in a bundle of 120 μm diameter capillaries. The attenuation lengths are 130 cm and 110 cm, respectively.

The dye concentration was optimized for PMP with a Monte-Carlo calculation, requiring maximum light yield after 1 m light pathlength [6]. An optimum concentration of 0.01 mole/l was found for 1MN as well as for IBP. For lower concentrations the decrease in light output is due to a lower primary light yield, for higher concentrations it is due to light yield saturation and increasing dye absorption (fig. 5)

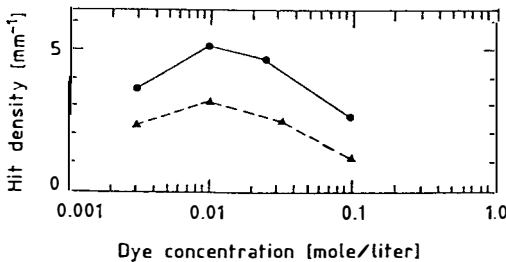


fig. 5. Light yield for 1MN+PMP/IBP+PMP as a function of dye concentration, expected after 1 m light pathlength in a single capillary with 2 mm diameter (based on a Monte-Carlo calculation).

5. Track Imaging with optoelectronic readout chains

In a recent test run, track images produced by 5 GeV - pions in 20 μm - bundles filled with 1MN+PMP/IBP+PMP, could be viewed for the first time with an optoelectronic readout chain. Details can be found in [8]. Very remarkable are an excellent track resolution ($\sigma_{tr} \approx 15 \mu\text{m}$) and a strong suppression of crosstalk due to the presence of EMA in the capillary target.

6. References

- [1] CHARM II - Collaboration et al., Letter of Intent, CERN SPSC/89 - 46 (1989)
- [2] G. Zacek, these proceedings and CERN PPE/91 - 06 (1991)
- [3] R. Nahnhauser and V. Zacek, CERN PPE/90 - 138 (1990)
- [4] CHORUS - Collaboration, Proposal, CERN SPSC/90 - 42 (1990)
- [5] A. Artamonov et al., Nucl. Instr. and Meth. A 300 (1991) 53
- [6] J. Bähr et al., Liquid Scintillator Filled Capillary Arrays for Particle Tracking, CERN PPE/91, submitted to Nucl. Instr. and Meth., Feb. 1991
- [7] E. Birckner, Proc. on Applications of Scintillating Fibers in Particle Physics, September 1990
- [8] M. Adinolfi et al., A High Resolution Tracking Detector Based on Capillaries Filled with Liquid Scintillator, CERN PPE/91, submitted to Nucl. Instr. and Meth., March 1991
- [*] SCHOTT Fiber Optics Inc., 122 Charlton Street, USA - 01550 Southbridge

Scintillating Fiber Detectors for Neutrino Physics

Gabriele Zacek

CERN



Abstract

A new detector technique based on scintillating optical fibers with $100\mu\text{m}$ to $200\mu\text{m}$ diameter is proposed for the use in neutrino physics. These detectors can be realized with large fiducial masses and have an excellent spatial resolution, good energy and time resolving capabilities. The application of this detector concept for the search of $\beta\beta$ -decay, the measurement of the magnetic moment of the neutrino and for an improved search for $\nu_\mu \rightarrow \nu_\tau$ oscillations is discussed.

Introduction

Neutrino physics still belongs to a field of elementary particle physics where many interesting results are still to be expected. To initiate the next round of neutrino experiments a new generation of neutrino detectors seems to be necessary. The following contribution introduces a new detector technique based on scintillating optical lightguides. Large active fiducial target masses, mandatory for neutrino physics, can be realized with this new detection concept. In addition a good energy and an excellent spatial resolution allows a high efficient identification of valid candidate events. At the same time powerful background suppression is possible. The proposed detector concept can find promising application in low and high energy neutrino physics, such as the search for neutrinoless double beta decay, the detection of a magnetic neutrino moment and the investigation of $\nu_\mu \rightarrow \nu_\tau$ oscillations [1], [2].

General Features of a Scintillating Fiber Detector

For the applications discussed here we are concerned with fibers in the range of $100\mu\text{m}$ to $200\mu\text{m}$ diameter, coherently arranged in ribbons or bundles. To avoid crosstalk each single lightguide is surrounded by an extramural absorber, i.e. a thin layer of light absorbing material. Following particle interaction, the scintillator light is transported along a fiber by reflection at the core-cladding interface. Typical trapping efficiencies are of the order of 3% to 5%.

The active detector volume of a scintillating fiber detector is completely made out of coherent bundles of scintillating optical lightguides. In case of $100\mu\text{m}$ fibers a detector submodule consists of a square rod of $5 \times 5\text{cm}^2$ surface area and 1m length comprising 500×500 fibers. This submodule is coupled at one of its endfaces to a high resolution electrooptical image intensifier chain which provides a two dimensional image of the event and an analog energy information. The opposite endface is viewed by a system of photomultipliers giving the global event trigger and calorimetric energy information. To reduce the number of electrooptical readout channels the output of several modules can be fanned together for large detector volumes (optical multiplexing).

There are three possibilities for scintillating optical lightguides: scintillating glass or plastic fibers and glass capillaries filled with liquid scintillators. Most promising at the moment is the last option since new liquid scintillators with high light yields (partly superior even to plastic scintillators), have been developed and it was shown in recent test beam exposures at CERN that reflection loss limited attenuation lengths are better than 3m for $100\mu\text{m}$ diameter capillary bundles [3].

Scintillating Fibers for $\beta\beta$ -decay Experiments

Improvement on present limits on the halflife of neutrinoless $\beta\beta$ -decay can be achieved by reducing the background rate due to cosmic rays, natural radioactivity and single Compton electrons beyond presently obtained levels. A scintillating fiber detector has the advantage of using topological criteria for event selection and background suppression. In addition since events will be contained within a few cm compact detector geometries are possible and large quantities of materials can be examined. The application of a magnetic field ($B \approx 20\text{ kG}$) in direction of the fibers is favorable for event selection and should therefore be envisaged.

A thin target foil ($\approx 200\mu\text{m}$) containing the $\beta\beta$ -active source material will be inserted between two 1cm wide fiber tracking regions. Signature for a $\beta\beta$ -decay event is the presence of two electrons originating at the same location of the $\beta\beta$ -active source foil. Since the position of the foil is known, the background events occurring in the source free detector volume can be rejected. In addition it is required that the $\beta\beta$ -decay event is isolated and fully contained in the

fiducial detector volume. Increasing energy loss along the path of the two electrons manifests itself as 'blobs' and as an increase of curvature at the end of both tracks. Furthermore since the two electrons share the available energy, there should be an equivalent energy deposition along both tracks. Fig.1 shows several $\beta\beta$ -decay events, simulated for the case of $100\mu\text{m}$ fibers with and without the application of a magnetic field.

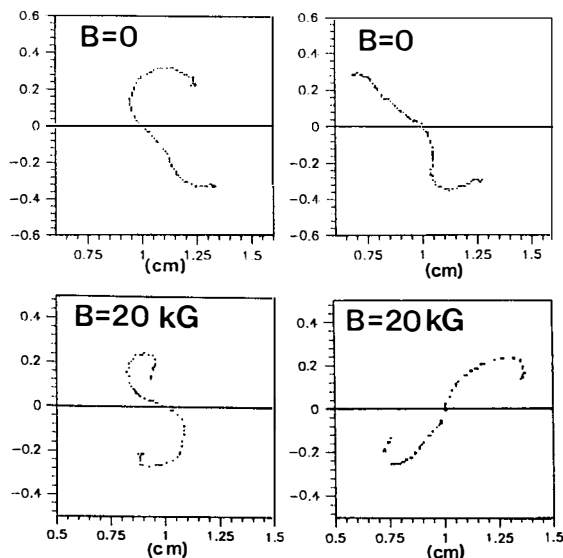


Figure 1: Simulation of $\beta\beta$ -events for $100\mu\text{m}$ fibers. The Q -value of the simulated events is 3MeV . A hit density of 8hits/mm is used. The solid line indicates the position of the source and the scale on both axes is in cm.

Events due to single Compton scattered electrons of the same energy as the $\beta\beta$ -reaction Q -value, can easily be distinguished according to different track topologies.

A preliminary analysis based on Monte Carlo studies showed that the selection criteria outlined above promise a background suppression by more than a factor of 100 in addition to the reduction obtained by today's well known standard shielding methods. For one target foil of e.g. ^{48}Ca corresponding to a mass of 15.3gr , an improvement of three orders of magnitude over presently quoted limits can be achieved.

Scintillating Fibers for the Neutrino Magnetic Moment

In the laboratory the possibility to measure the magnetic moment of the neutrino is given in neutrino electron scattering experiments. Since the standard electroweak cross section rises proportionally to the neutrino energy and the contribution of an interaction via the magnetic moment drops essentially like $1/E_\nu$, an increased sensitivity to the magnetic moment is obtained in the domain of low neutrino energies. In this region fission processes in a nuclear reactor provide a strong source of electron antineutrinos with energies up to 10MeV .

Two different approaches for a detector layout can be envisaged. One concept is based on the use of plastic fibers or liquid scintillator filled capillaries. Due to the presence of free protons care has to be taken to identify events from the inverse β -decay reaction which on the one hand constitute a reactor correlated background, but on the other hand could be exploited for a ν -flux normalization. The second concept is based on glass fibers. In this case no background from the inverse β -decay reaction is present and the larger density of glass would allow more compact detector geometries.

Limits on the magnetic moment are derived from a comparison of the observed neutrino flux and the one expected from weak interactions only. In case the expected neutrino flux is known with a precision of 10% a limit of $3 \times 10^{-11} \mu_B$ is in reach with a detector mass of 1 ton running for 1 year at a distance of 35 m from the core of a 2800 MW power reactor.

Scintillating Fibers for the Search of $\nu_\mu \rightarrow \nu_\tau$ Oscillations

Presently a scintillating fiber detector is discussed at CERN for an appearance search of τ -neutrinos in the SPS neutrino beam. At SPS energies ($\langle E_\nu \rangle \approx 25 \text{ GeV}$) a τ -lepton, produced in a charged current ν_τ interaction decays with an average longitudinal decay length of about 1 mm, an impact parameter of $80 \mu\text{m}$ and a branching ratio of 17.8% into a muon and two neutrinos. The high spatial resolution of a scintillating fiber detector allows a detection of the impact parameter by precisely tracking the decay muon. Using a 1 ton detector estimates give a limit on the neutrino mixing parameter of 8×10^{-4} (90% c.l.) for a measuring time of 200 days in case no event is observed. This constitutes a factor 5 improvement over present results [4]. Expected background rates are in the order of 0.4 events. The detection of other decay modes (e.g. $\tau \rightarrow \pi + X_0$) are under investigation and an extension of the measuring time can be envisaged.

Acknowledgement

I would like to thank the members of the CHARM II-Zeuthen group involved in the scintillating fiber development for many stimulating discussions.

References

- [1] G.Zacek, CERN-PPE/91-06, "Low Energy Neutrino Physics with Scintillating Fibers", January 1991
- [2] R.Nahnhauser and V.Zacek, CERN-PPE/90-138, "Search for $\nu_\mu \rightarrow \nu_\tau$ Oscillations with a Massive Active Target Detector Based on Scintillating Fibers", September 1990
- [3] P.Lendermann, these proceedings; J.Bähr et al., to be published in NIM "Liquid Scintillator Filled Capillary Arrays for Particle Tracking"
- [4] N.Ushida et al., Phys.Rev.Lett. 57 (1986) 2897, "Limits to $\nu_\mu \nu_e \rightarrow \nu_\tau$ Oscillations and $\nu_\mu \nu_e \rightarrow \tau^-$ Direct Coupling

Performance Report on the Mainz Tritium β -Decay Experiment

H. Backe, H. Barth, J. Bonn, R. Haid, A. Hermann, A. Molz, E. W. Otten, A. Picard, M. Przyrembel, M. Schrader, M. Steininger, C. Weinheimer (Institut für Physik, Univ. Mainz, FRG)

R. B. Moore (Foster Radiation Laboratory, McGill Univ., Montreal, Canada)

P. Leiderer (Fakultät für Physik, Univ. Konstanz, FRG)

A. Osipowicz (Fachhochschule Fulda, FRG)



Presented by J. Bonn

Abstract:

At Mainz University a solenoid-retarding-spectrometer (SRS) for the investigation of the tritium β -spectrum close to the endpoint has been constructed. The performance of the apparatus has been tested with conversion electrons of ^{83m}Kr . The measurements show that it reaches its design parameters of a resolution of $E/E_0 = 5000$ at an accepted solid angle of 40% of 4π . First tests with a tritium source showed an excellent signal to background ratio. The improvement of the present m_ν limit should be possible in near future.

We have built a solenoid-retarding-spectrometer (SRS) combining high resolution with large luminosity. It is designed for the measurement of the endpoint region of the tritium β -spectrum, in order to improve substantially the current limit on the neutrino rest mass /1/. The instrument consist essentially of two superconducting solenoids that are separated by a system of ring electrodes 4m in length which provides the energy analyzing electrostatic potential /2./3/.

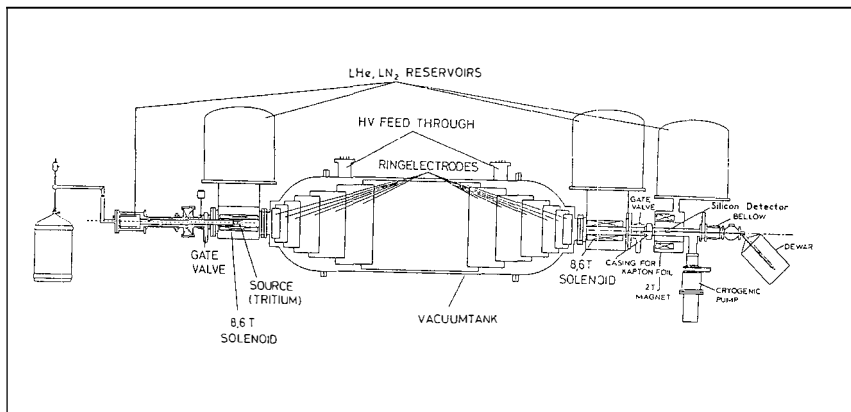


Fig.1: The experimental setup

The source is placed close to the maximum field in the left spectrometer solenoid, the silicon detector is placed in a third solenoid behind the right spectrometer solenoid. It is operated at about $B_0/4$ to limit the angle at which electrons impinge onto the detector to about 25° to minimize backscattering. The maximum of the analyzing potential is reached in the symmetry plane between the two solenoids, where the magnetic field has a minimum of about 10^{-3} T. Decay electrons spiraling adiabatically into the low field region, transform their transverse cyclotron energy into longitudinal energy, in proportion to the decrease of the magnetic field. Simultaneously, their longitudinal motion is decelerated by the electric field, which shaping designed in a way to be parallel to the magnetic field lines. Electrons with energy above the potential barrier are transmitted into the second half of the spectrometer, where they are re-accelerated by the electric field, and where they are re-focused onto PIN-photodiode detector by the magnetic field of the solenoid. The electronic resolution of the PIN-diode is 1keV, with about 1.6keV FWHM at 20keV. The transmission function of the SRS was investigated with conversion electrons from a frozen ^{83m}Kr -source. Fig. 2 shows a scan around the N32.147 keV transition.

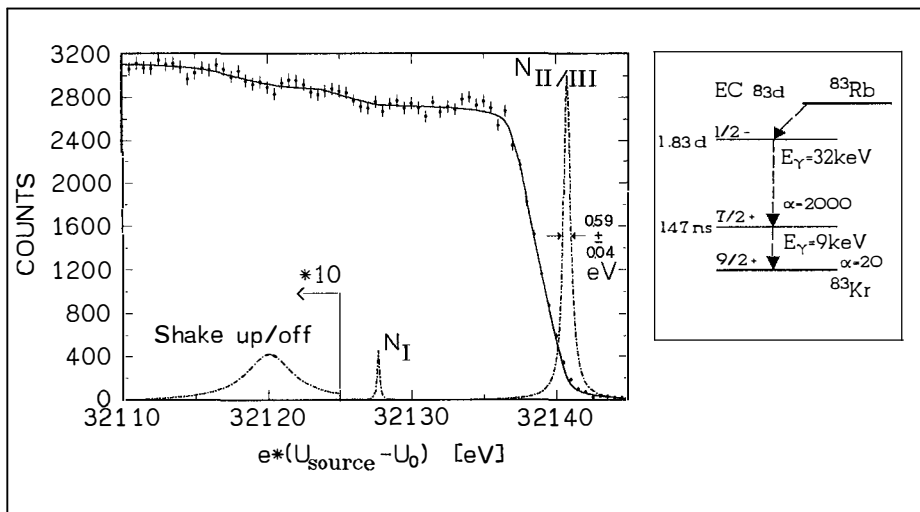


Fig.2: Test measurements with electrons for ^{83m}Kr .

The sharp rise in the count rate originates from $N_{II/III}$ conversion electrons, followed by the weaker N_I component and a small tail of electrons, having lost energy by shakeup/off and backscattering (dash-dotted lines). The full curve is a fit of the conversion lines and energy loss spectrum convoluted with the analytically known transmission function of the spectrometer, to the data. The spectrometer was operated at $\approx 18\text{keV}$ and the Krypton source was put at 14kV . The resolution of the spectrometer is $20\text{keV}/3.9\text{eV} \approx 10^4$ (10%-90% value). The accepted solid angle is reduced to 16.3% of 4π due to the bias of the source. In the course of the test measurements with ^{83m}Kr all conversion electron lines have been examined. The energy of the γ -transition was determined to $32.151(3)\text{keV}$, in good agreement with the value given by Robertson et al. /4/.

First test measurement with a $^3\text{H}_2$ source frozen on an aluminium backing.

The source, combining maximum specific activity and acceptable stability, consists of $^3\text{H}_2$ -molecules frozen on a backing of low Z to minimize backscattering. In off line tests we have found that these $^3\text{H}_2$ -films are sufficiently stable at the temperature of liquid Helium /6/. $^3\text{H}_2$ forms a van der Waals crystal with a binding energy of $\approx 15\text{meV}$. It is evident that the recoiling decay products with an energy $E_R < 3\text{eV}$ and the decay electrons will sputter off the source material. The $^3\text{H}_2$ released from the source itself is to a very large fraction 99% condensed on a 10 cm tube placed as a thermal shield in front of the source. The tube does not touch the imaged flux tube, so decay electrons starting from this shield are not accepted by the detector. The small fraction of $^3\text{H}_2$ released into the spectrometer will also be adsorbed on surfaces which are not imaged into the detector.

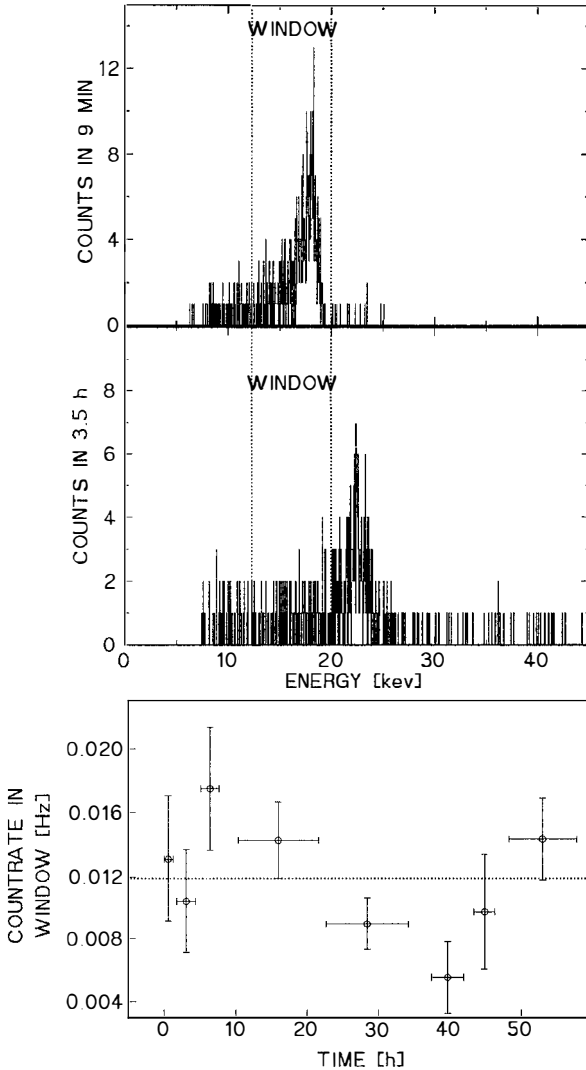


Fig.3: Spectrum of electrons from $^3\text{H}_2$ taken $\sim 200\text{V}$ below the endpoint. In comparison with the background spectrum the excellent signal to background ratio close to the endpoint is clearly shown.

The temporale development of the background shows no hint of an increase due to $^3\text{H}_2$ contamination.

In the first test measurement with $^3\text{H}_2$ the evaluation of the background count value as shown in Fig. 3 gives indeed no evidence for a visible $^3\text{H}_2$ contamination of the spectrometer. The background level was constant at $\sim 12\text{mHz}$ in the true event window. The dominant part of the background electrons is shifted to energies higher than the energy window of interest. Their energy is given by the sum of their kinetic energy with which they are created plus the potential of the emitting surface. With the field configuration used, only electrons with high energies can be imaged onto the detector. Low energy electrons have no overlay with the imaged flux tube.

The quality of the ${}^3\text{H}_2$ data is rather limited as the fraction shown here contains about one day of effective measuring time with a $100\mu\text{Ci}$ source. A 1mCi source and a measuring time of several weeks are planned. A first preliminary analysis gives a statistical 1σ error of $\Delta m_\nu = 200\text{eV}^2$ with a value for m_ν^2 compatible with zero. This value, however, should not be taken as a final result, because backscatter and energy loss have to be investigated to more details.

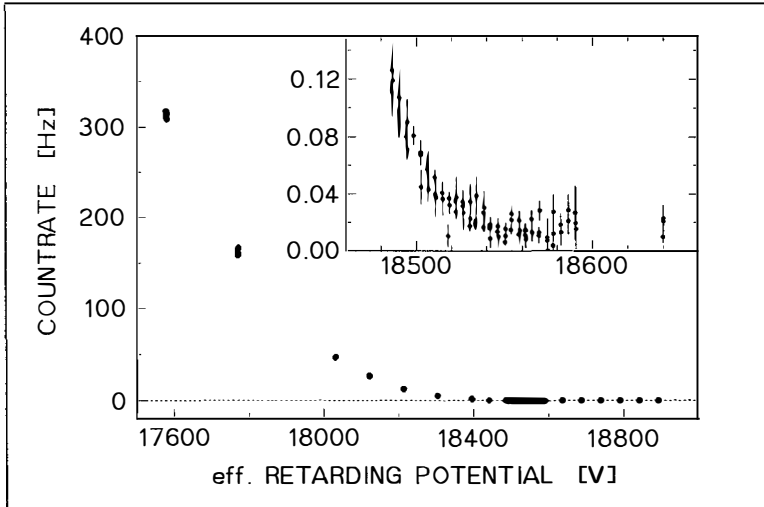


Fig.4: First ${}^3\text{H}_2$ spectrum taken with the Mainz SRS-spectrometer. The data represent about one day of effective measurement time.

In summary we claim to have shown that we can achieve a high statistical accuracy due to the high resolution and transmission of our spectrometer. The background did not increase during our measuring time. Systematic uncertainties have to be investigated. We therefore hope to be able to improve the present limit on m_ν by taking more data with a stronger source.

References

- /1/ A. Picard, doctoral thesis, Mainz 1989
- /2/ A solenoid retarding spektrometer with high resolution and transmission for the determination of the neutrino restmass from ${}^3\text{H}_2$ - β -decay. Picard et al., to be published
- /3/ R. E. Schrock, Phys. Lett. B239 (1990) ch. IV.2
- /4/ Robertson et al., Los Alamos, Phys. Rev. C (1989) v. 39 (4) p. 1503-1510
- /5/ A. Picard, H. Backe, H. Barth, J. Bonn, B. Degen, R. Haid, A. Hermanni, P. Leiderer, A. Osipowicz, E. W. Otten, M. Przyrembel M. Schrader, M. Steininger, to be published
- /6/ M. Przyrembel, H. Fischer, A. Hermanni, E. W. Otten, P. Leiderer, Phys. Letters A147 (1990) 517

THE 17 KEV NEUTRINO

THE 17-KEV NEUTRINO

J.J. Simpson
Guelph-Waterloo Program for Graduate Work in Physics
and
Department of Physics
University of Guelph
Guelph, Ontario N1G 2W1, Canada



Abstract

The experimental evidence of a distortion in the β -spectra of ^3H , ^{35}S and ^{14}C is reviewed. The distortions seen in the three nuclei are consistent with their interpretation as the signal of the emission of a heavy neutrino of 17-keV mass and mixing angle of about 0.1.

One of the outstanding questions in particle physics is whether neutrinos have non-zero masses, and how large they are. In this talk I described the evidence that there is a very heavy neutrino, with a mass of 17 keV, coupled weakly to the electron. Since it is all in readily accessible publications, I shall only summarize my talk.

The first evidence was found in the β -decay of ${}^3\text{H}$ measured in a Si(Li) detector where a kink 17.1 ± 0.2 keV below the end-point could be interpreted as due to the emission of a heavy neutrino¹⁾. If the electron neutrino ν_e is described as a linear combination of two mass eigenstates ν_1 and ν_2 ,

$$\nu_e = \nu_1 \cos\theta + \nu_2 \sin\theta \quad (1)$$

where ν_1 is the very light mass eigenstate (< 11 eV), then the data suggested that the mixing angle is between 0.14 to 0.2. Subsequently it was realized that the electronic screening of the nucleus would be modified because the ${}^3\text{H}$ is bound in the silicon lattice. The results were reanalyzed using information about the electronic screening obtained from muonium in silicon to give a mixing angle of 0.09 to 0.12 for the 17-keV neutrino²⁾.

A second experiment, this time with ${}^3\text{H}$ in a hyperpure germanium detector was also carried out. The use of germanium permitted the complete annealing of radiation damage and linearity checks over the energy range of the whole β spectrum above 1.3 keV. The result was in agreement with the previous one, giving a mass of 16.9 ± 0.1 keV and a mixing angle between

0.09 and 0.12, and is reported by Hime and Simpson³⁾.

Although the shape of the distortion seen in the β -decay of ^3H is consistent with the phase-space expected for the emission of a heavy neutrino, and is inconsistent with other possibilities such as a β -branch to an excited state or a four-body phase space, for example, certainty that it arises from the emission of a heavy neutrino is obtained if it is seen in other β -decays. The first experiment⁴⁾ giving unmistakable evidence of the heavy neutrino was a measurement of the β -spectrum of ^{35}S which yielded a distortion consistent with the emission of a neutrino of 16.9 ± 0.4 keV mass and a mixing angle of 0.085 ± 0.007 . In this experiment the result is a significant 7-sigma effect having the unique phase-space shape of a heavy neutrino. Recently B. Sur et al⁵⁾ found a feature in the β spectrum of ^{14}C which can be explained by the emission of a heavy neutrino of mass 17 ± 2 keV and mixing angle of 0.12 ± 0.02 . In this experiment the spectrum was obtained from ^{14}C which had been incorporated in the Ge detector when the Ge crystal was grown, thus helping to reduce many systematic sources of error. A summary of the results presented in this talk are shown in the table.

Experimental Evidence for a 17-keV Neutrino

Isotope	ν Mass (keV)	Mixing Angle θ
^3H in Si(Li)	17.1 ± 0.2	0.105 ± 0.015
^3H in Ge	16.9 ± 0.1	0.105 ± 0.015
^{35}S	16.9 ± 0.4	0.085 ± 0.007
^{14}C in Ge	17 ± 2	0.12 ± 0.02

The nature of this neutrino is probably an open question; however if we restrict the possibilities to the three known neutrinos which couple to the Z^0 , then the absence of $\nu_e \leftrightarrow \nu_\mu$ oscillations⁶⁾ at an appropriately high level would suggest that the 17-keV neutrino is the dominant component of ν_τ . In addition the non-observation of neutrinoless double β -decay suggests that this 17-keV component is of Dirac character. However, cosmological constraints require that a 17-keV neutrino be unstable and decay with a lifetime of $< 10^{14}$ sec⁷⁾. Such a short lifetime does not seem to be possible within the constraints of the standard model, which suggests that there exists new particle physics beyond the standard model, unless there is something inherently lacking in our understanding of the early universe.

References

- 1) J.J. Simpson, Phys. Rev. Lett. 54, 1891 (1985).
- 2) A. Hime and J.J. Simpson, Phys. Rev. D39, 1837 (1989), appendix C.
- 3) A. Hime and J.J. Simpson, Phys. Rev. D39, 1837 (1989).
- 4) J.J. Simpson and A. Hime, Phys. Rev. D39, 1825 (1989).
- 5) B. Sur et al., submitted to Phys. Rev. Lett., Dec. 1990.
- 6) L.A. Ahrens et al., Phys. Rev. D31, 2732 (1985).
- 7) E.W. Kolb and M.S. Turner, The Early Universe (Addison-Wesley (1990) Redwood City, (A) p. 140.



17-keV Neutrinos at Oxford

A. Hime and N.A. Jelley

Nuclear Physics Laboratory, Keble Road, Oxford OX1 3RH, England



Abstract

We report on two high statistics measurements of the beta spectrum of ^{35}S . Particular emphasis is given to the sensitivity of results on details of the electron response function. In both measurements we find an 8 standard deviation from the single component neutrino spectrum 17-keV below the endpoint. The data are in strong support of earlier claims that the neutrino emitted in beta decay contains a 17 keV mass component with a mixing probability given by $\sin^2 \theta = 0.0084 \pm 0.0006 \pm 0.0005$.

1. Experiment

The spectrometer constructed at Oxford makes use of a cooled, thin window, Si(Li) detector with a 200 mm² active area and is 5 mm thick. The detector operates with a cold FET package and feed-back circuit in order to optimize resolution. A cross-section of the main features of the spectrometer is shown in fig.1 where a radiation source is positioned in parallel with the silicon detector. The key improvement in this experiment over that performed at Guelph (see J.J. Simpson in these proceedings) lies in the implementation of source/detector collimation as depicted in the figure. Both the detector and source apertures are chamfered with an angle of 10° and an aluminium baffle is situated between the source and detector in order to prevent electrons from scattering from the walls of the vacuum chamber into the detector. This provides a well defined geometry in which electrons are essentially normally incident on the detector. Mono-layer sources of ³⁵S were prepared using the technique of chemical adsorption by depositing solutions of high specific activity on mylar substrates that are 2.8 micron thick. A thin layer of gold (100Å) covers the mylar film so as to provide an electrical ground to the source during the course of a measurement.

Calibration of the spectrometer and determination of the detector energy resolution function were accomplished using X-ray and gamma ray lines from ⁵⁷Co and ¹⁰⁹Cd sources prepared in the same manner as the ³⁵S sources. The response of the detector to monoenergetic electrons deviates from the gaussian function for photons on two accounts. In the first place there is a finite probability that electrons loose energy through ionization when passing through the contact on the front of the detector (about 200Å of Au). Secondly, electrons undergo multiple scattering in the sensitive volume of the detector and can back-scatter or back-diffuse out of the detector thus depositing only a fraction of their incident energy in the system. These phenomena give rise to a low energy tail to an otherwise symmetric response function. K-shell internal conversion(IC) electrons from the decay of ⁵⁷Co and ¹⁰⁹Cd serve as a measure of the electron response function. A measurement of the response function is shown in fig.2a where the peak of the IC line is shifted down by 1.5 keV owing to the bias on the detector. In fig.2b the fraction of electrons in the low energy tail is plotted as a function of the fraction ($X = E/E_0$) of the total incident electron energy (E_0). The total fraction of electrons in the back-scatter tail is normalized to 0.135 using a bin width of 0.04 in units of E/E_0 . For comparison the low energy tail for a diffuse geometry (as employed in ³⁵S work at Guelph) is drawn to scale along with the distribution for normally incident electrons. In that case the distribution is essentially flat, extending to zero energy and containing about 30% of the incident electrons. Hence, it becomes quite clear that a normal incidence geometry provides a significant change not only in the amplitude of the backscatter signal but also in the shape of that signal.

In the first case a ^{35}S spectrum was acquired (Run #1) with the source positioned at a distance of 67.0 mm from the detector using a Cu source aperture 8mm in diameter. In this configuration the live count rate was about 4100 counts/second. With a pile-up rejection system active the unrejected pile-up signal consists only of double pulses that enter the counter essentially simultaneously. The pile-up signal is manifest as a smooth background underlying the β spectrum and extends up to an energy that is twice the endpoint energy of the raw spectrum. This background can then be removed from the raw signal after normalizing the generated pile-up signal to data above the endpoint. This normalization procedure indicates that the pile-up background represents $0.15 \pm 0.01\%$ of the total signal. There is also a weak ambient background signal present that arises predominantly from cosmics passing through the sensitive volume of the detector. This spectrum is essentially flat and was measured after removing sources from the spectrometer. After removing the background signal from the raw data a DC energy shift was invoked to the spectrum to account for the negative bias on the detector.

After analysing the data taken from this first experiment it was necessary to invoke a small correction to the data due to additional energy loss of electrons penetrating the edges of the detector aperture. In order to circumvent this problem a second experiment was performed (Run #2) after changing the 8 mm source aperture to 5 mm and moving the source to a distance of 56.5 mm. In this way the normal incidence geometry was maintained as in Run #1 while reducing the fraction of electrons striking the edges of the detector aperture. The reduced source size and activity in this experiment meant a reduction in counting rate (3000 counts/second) and thus the unrejected pile-up rate also dropped to $0.09 \pm 0.01\%$ of the total signal.

2. Data Analysis and Results

For purposes of analysis we consider the case where the electron neutrino is a linear combination of two mass eigenstates with masses $M_1 = 0$ and M_2 respectively. In that case the beta spectrum becomes a sum of two beta spectra with different endpoints

$$\frac{dN(E)}{dE} = \cos^2 \theta \frac{dN(E, M_1)}{dE} + \sin^2 \theta \frac{dN(E, M_2)}{dE} \quad (1)$$

where $\sin^2 \theta$ denotes the probability for the emission of a heavy neutrino with mass M_2 and $dN(E, M_i)/dE$ is the usual beta energy spectrum involving the emission of a single neutrino with mass M_i :

$$\frac{dN(E, M_i)}{dE} \propto pEF(E, Z)(W - E)[(W - E)^2 - (M_i c^2)^2]^{1/2} \quad (2)$$

In equation (2) p and E are respectively the momentum and total energy of the beta particle and W represents the total energy available to the lepton field. A fully relativistic Fermi function $F(E, Z)$ was employed while invoking a screening potential of 1.73 keV.

The data were analysed by comparing the experimental spectra to the theoretical spectrum described above after convoluting the theoretical spectrum with the experimental response function. Free parameters in the fitting routine are the heavy neutrino mass M_2 , the heavy neutrino mixing probability $\sin^2 \theta$, along with the end-point energy $Q = W - m_e c^2$. While an overall normalization constant is also simultaneously varied along with Q and $\sin^2 \theta$ its value is tightly constrained due to the large number of decay events in the fitting interval (120 — 167 keV). In particular there are 110×10^6 and 87×10^6 events in this energy interval for runs #1 and #2 respectively.

Table 1 lists the results of fitting the two ^{35}S spectra above 120 keV for both the case when no mixing is allowed and after optimizing $\sin^2 \theta$ for the emission of a 17-keV neutrino. While the minimum chi-square achieved in the case of run #1 is reasonable a slightly deeper minimum occurs when correcting for a possible 1% increase in the amplitude of the energy loss tail, indicating that a small fraction of electrons might have penetrated the detector aperture. The value deduced for $\sin^2 \theta$ in this case is not, however, sensitive to this small correction. Furthermore, the data of run #2, taken with a smaller source aperture, did not require this correction. Combining the results from both data sets yields $M_2 = 17.0 \pm 0.4$ keV with $\sin^2 \theta = 0.0084 \pm 0.0006 \pm 0.0005$ and an endpoint energy $Q = 167.067 \pm 0.004 \pm 0.065$ keV, where the first uncertainty is statistical and the last uncertainty reflects the estimated systematic uncertainty in the low energy component of the electron response function.

Table 1

	Response		M_2 (keV)	$(\sin^2 \theta) \times 100$	Q (keV)	χ^2/ν
	Function					
Run #1	§(1)	—	—	0.0*	167.013	144.4/75
	§(1)	17*	17*	0.80 ± 0.10	167.061	85.6/75
	§(1)	16.7 ± 0.5	16.7 ± 0.5	0.79 ± 0.10	167.069	85.1/74
	1% corrected	17*	17*	0.75 ± 0.11	167.070	79.5/75
Run #2	§(1)	—	—	0.0*	167.016	132.3/75
	§(1)	17*	17*	0.88 ± 0.11	167.068	66.4/75
	§(1)	17.2 ± 0.5	17.2 ± 0.5	0.90 ± 0.11	167.065	66.2/74

* parameter held fixed in fit.

The deviation of the data from a single component, massless neutrino spectrum is shown in fig.3. In the first place shape factors are shown for the data of runs #1 and #2 in figs.3a and 3b respectively, where a ratio is plotted of the experimental data to the best fit theoretical β spectrum when no heavy neutrino mixing is allowed. In this comparison the theoretical spectrum has been convoluted with the experimental response function and normalized over the entire interval from 120 to 167 keV. In fig.3c we show the shape factor resulting from an analysis of the combined data from run #1 and run #2 after fitting the data to a single component spectrum above 150 keV. Apart from small effects due to finite resolution it is straight forward to show that the shape factor resulting in this case is given by,

$$S = 1 + \tan^2 \theta \left[1 - \frac{(M_2 c^2)^2}{(Q - T)^2} \right]^{1/2} \quad (3)$$

The smooth curve in fig.3c is obtained from eq. 3 with $M_2 = 17$ keV and $\sin^2 \theta = 0.009$ after accounting for resolution effects at the heavy neutrino endpoint. The agreement of the experimental shape with that expected for the emission of a 17-keV neutrino is now quite clear. The shape factor is flat down to a visible threshold at $Q-17$ keV, and asymptotically approaches the value $1 + \tan^2 \theta$ well below $Q-17$ keV as predicted above.

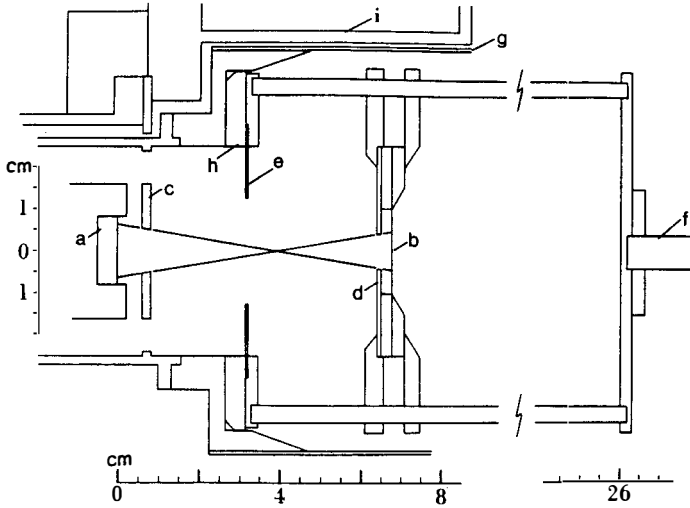


Fig. 1 Cross-section of source/detector geometry (see section 2) (a) Si(Li) detector (b) source substrate (c) Al detector aperture (d) Cu source aperture (e) Al anti-scatter baffle (f) linear motion feed-through (g) liquid nitrogen cryo-panel (h) teflon centering ring (i) vacuum chamber

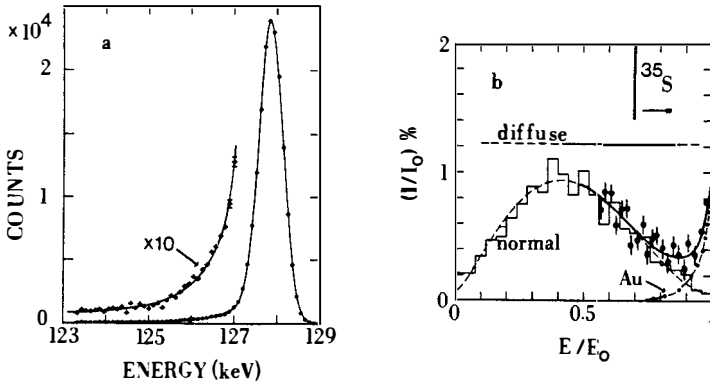


Fig. 2 (a) 129.36 keV Internal Conversion line from ^{57}Co . Points are experimental and the smooth curve models the electron distribution after accounting for ionization losses and the finite resolution of the detector. (b) Distribution of electrons contained in low energy tail of the electron response function. The histogram and dashed curve represent the component due to back-scattering of electrons normally incident on Si. The dash-dot curve is the energy loss component due to ionization in the Au contact on the front of the detector. The solid curve combines the two components and experimental points are shown.

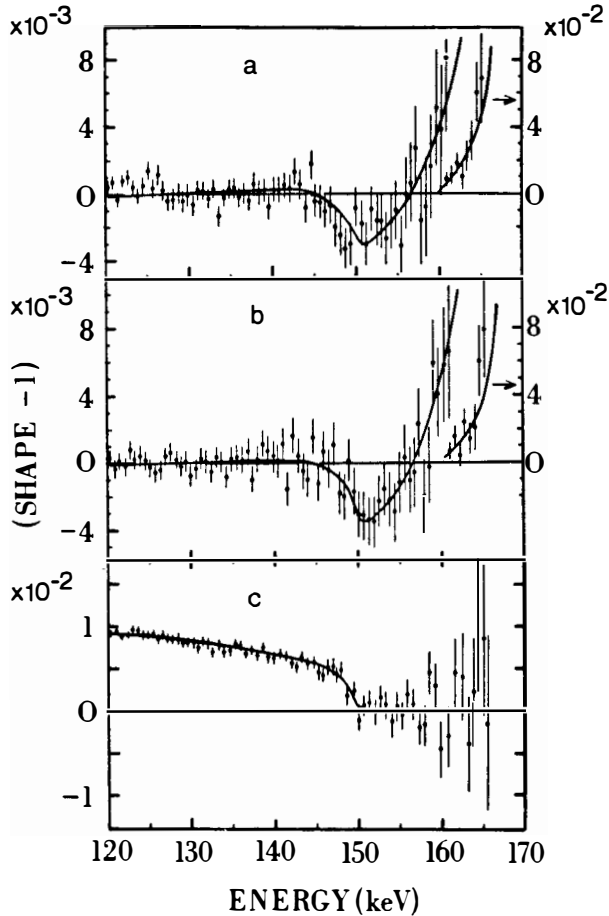


Fig. 3 Shape factors for (a) run #1 and (b) run #2 obtained by dividing the experimental spectra by the best least squares fit to the region 120-167 keV when no heavy neutrino mixing is allowed. The data plotted in (a) and (b) above 161 keV go off the scale set by the left ordinate and should be read using the scale indicated by the right ordinate. (c) Shape factor for combined data of runs #1 and #2 when normalizing a single component spectrum to the data over the region above 150 keV. The smooth curves in each case indicate the expected deviation for the emission of a 17-keV neutrino with $\sin^2 \theta = 0.009$.

EXPERIMENTAL STUDIES OF THE ^{35}S BETA-SPECTRUM
ANOMALIES AND HEAVY NEUTRINO ADMIXTURE ?

H.W. Becker¹, D. Imel, H. Hendrikson, V.M. Novikow²
California Institute of Technology, Pasadena



ABSTRACT:

We have examined the beta-spectrum of ^{35}S using the π 2 iron-free double focussing beta spectrometer at Caltech. No evidence is found in the spectrum for the admixture of a massive neutrino in the beta decay. Specifically, our data allow to rule out the hypothesis of a 0.8% admixture of a 17 keV neutrino at a 99% confidence limit.

- 1) present address: Institut für Kernphysik, Universität Münster,
Germany
- 2) present address: Institute for Nuclear Research,
USSR Acad.Sc., Moskow, USSR

INTRODUCTION:

In 1985, Simpson reported a distortion in the spectrum of ^3T , which could be explained by an heavy neutrino of mass 17 keV with an admixture of 3% to the predominant light or massless electron neutrino. A refined analysis of this experiment and studies of the spectrum of ^{35}S resulted 1989 in the suggestion of a 17 keV neutrino, admixed with an amplitude of 0.7%.

Stimulated by this results five experimental studies of the ^{35}S or ^{63}Ni beta spectra were published in 1985, all of which could not confirm a 3% admixture of a heavy neutrino. Quoting partly substantial lower limits for such an effect they also exclude it at the 0.7% level.

In the ongoing discussion about this discrepancy several problems of such experiments and their analysis have been addressed, which could decrease the accuracy quoted. In this sense all of those studies have been criticized and their upper limits called to optimistic.

As discussed already elsewhere, the main problems in the experiments and their analysis and deduced confidence limits arise with corrections to the shape factor, necessary due to uncertainties in the Q-value of the decays and experimental influences such as the response function of the spectrometer used, scattering of electrons, effects of sources, pile up and background. All this effects have to be small and smooth with energy to detect a threshold effect caused by a heavy neutrino emission.

APPARATUS:

The experiment has been performed with the CALTECH ironfree, double focussing beta spectrometer, modified to minimize internal

scattering. The vacuum system was improved, including the addition of a LN₂ cryoplate, so that the pressure inside the spectrometer was better than 10⁻⁶ torr.

A 20 μ Ci ⁵⁷Co conversion electron source and a 3 mCi ³⁵S source were prepared by evaporating CoCl₂ or (NH₄)₂SO₄ in vacuum through an mask onto the backing in a strip of (2 x 20)mm. Backings were produced by stretching a 140 μ g/cm² Mylar foil over an aluminum ring. The foils were aluminized with a layer of less than 20 μ g/cm². With this technique very uniform and thin layers can be produced, the energy loss and spread can be estimated from the specific activity of the start material to be less than 5 eV and thus negligible for this experiment.

A surface barrier detector with a thickness of 300 μ m and an active area of (4 x 25) mm, collimated by the resolving slits to (2 x 20)mm is utilized at the focal plane of the spectrometer to count the electrons. Cooled to about 5°C a resolution of 4.7 keV was achieved.

The usual backscattered intensity in the spectra amounts for the ⁵⁷Co source to \approx 17% of the total intensity in quite good agreement with literature and increases for the ³⁵S measurements near the endpoint to maximal some 20%. From this we conclude that scattering in the spectrometer is small and negligible if the region of the full energy peak is analyzed only.

We used the ⁵⁷Co K-conversion lines to determine the calibration of the spectrometer and its response function. The response function could be described by a Gaussian with a small exponential tail, revealing a resolution of the spectrometer of 0.27% FWHM in momentum. The resulting response function drops outside the energy range of the conversion lines by several

orders of magnitude showing that the scattering of electrons in the spectrometer to either higher or lower energies is negligible.

Great care was taken to ensure the stability of the magnetic spectrometer. By selecting the high-momentum edge of the K-conversion line of Co-57 at 115 keV, small changes in the magnetic field producing large changes in the count rate could be monitored. In this way, we could observe variations in the magnetic field of 10^{-5} . At this level neither hysteresis effects nor effects of the room temperature, which was stabilized, were observed. The only source of changes in the magnetic field was the current, which was kept stable during the data taking to 10^{-5} .

DATA TAKING AND ANALYSIS:

The data, taken over a month, consisted of three separate data runs. Run A was a low-statistics overview run, run B is the main data run, and run C is an auxiliary set of low-energy data points which served to check for possible systematic errors with high statistics. Here we only refer to Run B.

Data have been taken with no consecutive order with respect to the energy, thus all long term instabilities of the experimental set up can be seen as scattering of the data points beyond those expected from statistics.

In a preliminary analysis the surface barrier detector spectra have been analyzed by integrating the spectrum above the centroid of the full energy peak only. Though this method utilizes less than half of the intensity of the full spectrum it rules out influences of any change in the backscattertail. The data were corrected for the acquire time, the decay of the source, the changing momentum window of the spectrometer and the

varying backscatterfraction and then compared to the theoretical spectrum. This was calculated by the Fermi theory including effects for Coulomb screening and finite nuclear size effects (Petr Vogel, private communication). In fitting the data all experimental influences on the shape factor such as mentioned in the beginning have been taken into account by including a term $a_1(p_{\max} - p) + a_2(p_{\max} - p)^2$, where p is the momentum of the electrons and p_{\max} the momentum corresponding to the endpoint energy. The coefficients a_1 and a_2 are allowed to vary as free parameters in addition to the amplitude and Q-value.

RESULTS AND DISCUSSION:

A fit of all the data from 100 to 165 keV to a spectrum with 0% admixture gives a total chi-squared of 53 for 35 degrees of freedom (39 data points), and, for an admixture of 0.8% of a 17 keV neutrino gives a total chi-squared of 83. Clearly, this result strongly favors the 0% admixture solution, although the reduced chi-squared appears to be excessive (1.5). The excess is attributed to the high statistics data points in the low-energy region (away from the threshold region). The apparent nonstatistical variation of these high data rates demonstrates the limit from systematic errors for run B presented here.

If we restrict ourselves to the "narrow scan" suggested by Simpson and Hime, fitting only the data between 132 and 163 keV, we obtain a chi-squared of 13.8 for 20 degrees of freedom (24 data points) for 0 admixture, and a chi-squared of 23.1 for 0.8% admixture of a 17 keV neutrino. In addition, we find that the best chi-squared fit to the data of the admixture for masses between 10 and 30 keV is obtained for mixings of less than 0.1%. Thus, we conclude that the data are incompatible with the hypo-

thesis of a massive subdominant neutrino admixture with masses between 10 and 30 keV, and specifically, we rule out the possibility of a 17 keV neutrino, 0.8% admixed, at a confidence level of greater than 99%.

The values of the endpoint energy parameter is 167.2 keV. We have verified that the shape factors (linear and quadratic terms) do not mask the threshold effect.

The results reported here are incompatible with those reported by Simpson and Hime and more recently by Hime and Jelly as well as results of a group at Berkely, studying the spectrum of ^{14}C and work done by Zlimen et al. with the bremsstrahlung from a ^{55}Fe source. It is interesting to note that all experiments which disclaim evidence for the heavy neutrino were carried out with magnetic spectrometers which provide high resolution energy binning. Those which claim evidence have been carried out with semiconductor detectors. They rely to a much larger extend on the deconvolution of the response.

In comparison to previous experiments we note that in the present work the sum of all corrections is rather small and included in the fit to the data by the parameters a_1 and a_2 , no a priori knowledge of any effects is assumed. In particular, the statistical significance of the threshold effect, doubtlessly seen in the works of Simpson and Hime, may be considerably reduced by allowing a shape correction.

ACKNOWLEDGEMENTS:

This work was performed with the support by DOE under grant DE-FG03-88ER40397. We thank F. Böhm and P. Vogel for stimulating and supporting this experiment.

HEAVY NEUTRINO EMISSION IN EC DECAY OF ^{71}Ge

IGOR ŽLIMEN

Ruđer Bošković Institute, P.O.Box 1016, 41000 Zagreb,

Croatia, Yugoslavia

The possibility of neutrinos having masses in the range of 12–40 keV was investigated by studying internal bremsstrahlung emitted by a ^{71}Ge source. We find a 17.2 keV neutrino with a mixing probability of 1.6%.

In 1985 Simpson found evidence that 2→4% of neutrinos emitted in tritium β -decay have a mass of 17 keV¹⁾; an alternative explanation of Simpson's results has been given²⁻⁴⁾. Other β -decay investigations⁵⁻⁹⁾ and searches for heavy neutrinos which analyzed internal bremsstrahlung in electron capture (IBEC)¹⁰⁻¹³⁾ gave negative results. Recently Simpson and Hime^{14,15)} found new evidence for a 17 keV neutrino. We have also found evidence for a 17 keV neutrino in an IBEC measurement with ⁷¹Ge; a preliminary results has been reported¹⁶⁾.

For two types of neutrinos, the IBEC spectrum has is given by

$$\frac{dW(k)}{dk} = \frac{dW(k, m_L)}{dk} \cdot \cos^2\vartheta + \frac{dW(k, m_H)}{dk} \cdot \sin^2\vartheta \quad (1)$$

where k is the neutrino energy, m_L and m_H are the masses of the light and heavy neutrino, respectively, and R , the fraction of heavy neutrinos, is given by $R = \sin^2\vartheta$. We searched for m_H values in the 10→40 keV mass range and take m_L as zero.

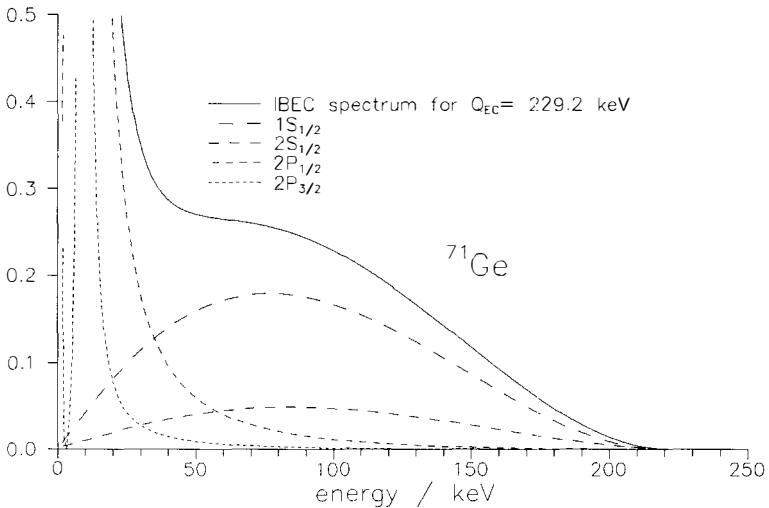


Fig 1. IBEC spectrum of ⁷¹Ge

Theoretical distributions for ^{71}Ge , assuming a zero-mass neutrino, are shown in Fig.1. A heavy neutrino will produce a kink, or distortion, in the IBEC spectrum.

The ^{71}Ge decay is an allowed transition 100% to the ground state of ^{71}Ga . There is excellent agreement between experiment and theory for allowed transitions^{10,17}). In our technique it is only necessary that the theory is sufficiently well-known that we can be confident there are no kinks in the IBEC spectrum, other than those due to heavy neutrino emission. Although kinks can be associated with each initial state, the capture from the 1S state is dominant in the region of interest, and we searched for kinks at an energy of $(Q-B(1S)-m_{\text{H}}c^2)$, where Q is the transition energy and $B(1S)$ is the binding energy of the 1S state.

A 10 mCi ^{71}Ge source ($T_{1/2} \approx 11$ d) was made by the (n,γ) reaction on natural germanium and radiochemical techniques were used to reduce radioactive impurities to $<10^{-7}$ of the ^{71}Ge activity. Gamma-rays from the thick GeO_2 source were detected in a HPGe detector; the source and detector were shielded with 6 cm of lead. Data were accumulated for about 8 days in a MCA with an energy dispersion of 0.157 keV/channel with the same time being allocated to a background measurement. Energy drifts were $<\pm 2$ channels.

The response of the detector was carefully determined with variety of sources and the mathematical description of the lineshape agreed with other results^{18,19}). The efficiency for carrier-free point sources was shown to be accurately represented by $k^{-A} \cdot \exp(B \cdot k^{-D})$, where A , B and D are constants. To allow for the effect of the source thickness the efficiency for carrier-free point sources was multiplied by a polynomial $(a+b \cdot k+c \cdot k^2)$, where a , b and c are constants. The polynomial term is a smooth function of energy.

The theoretical IBEC spectra (N_{IBEC}), which included contributions from S- and P- initial states, for different m_H and R values were multiplied by the carrier-free point source efficiency (ϵ_{PS}) and convoluted with the response function of the detector (f_{RESP}). The experimental spectrum was prepared for the fitting procedure by subtracting room background, pile-up, and contributions from radioactive impurities. The resulting corrected spectrum (N_{EXP}) is shown in Fig.2: the analysis involved energy regions on the downward slope between 155 keV and the endpoint.

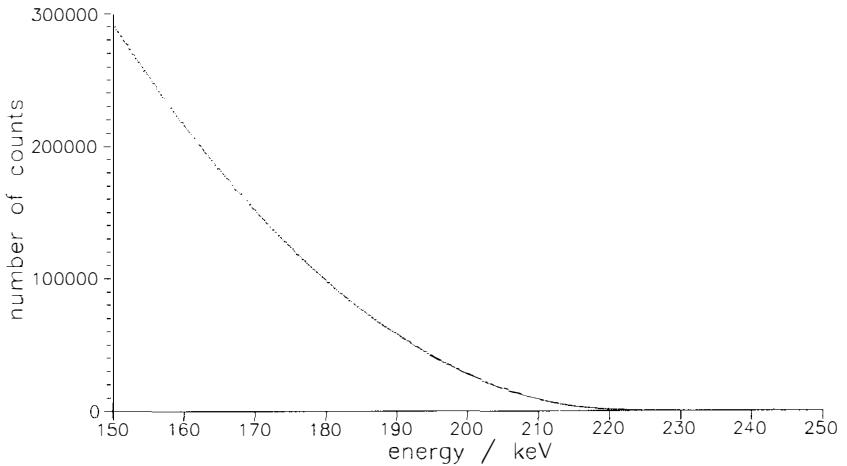


Fig. 2. Experimental spectrum of ^{71}Ge after subtraction of background, impurities and pile-up

The analysis technique has been described¹¹⁻¹³⁾. The corrected experimental spectrum was divided with the theoretical spectrum, modified to include the point-source efficiency and response function, in the energy region above a possible kink position. A, B and D were fixed and the coefficients a, b and c were adjusted to give the best fit to the ratio $N_{EXP}/(N_{IBEC} \cdot \epsilon_{PS} \cdot f_{RESP})$. In that way, an accurate estimate of the

coefficients a, b and c was made. This efficiency polynomial term was then extrapolated below the kink position and a χ^2 comparison was made between it and the ratio $N_{\text{EXP}}/(N_{\text{IBEC}} \cdot \epsilon_{\text{PS}} \cdot f_{\text{RESP}})$ for different R, which was the only parameter varied in the fit. For each m_{H} value the R was varied from -1% to +2%. For each m_{H} five different number of channels were used and the final result for R was the average of the values which corresponded to minima in χ^2 . An accurate Q value is needed in the analysis and we determined Q using a method similar to that used in the estimate of R; a value of $229.2 \pm_{0.9}^{1.1}$ keV (95% CL) was obtained.

The R values for possible m_{H} values are shown in Fig.3. There is clear evidence for a non-zero R value value in the mass region near 17 keV. We obtain $m_{\text{H}} = 17.2 \pm_{1.1}^{1.3}$ keV (95% CL) and a R value of $(1.6 \pm 0.7)\%$ (95% CL).

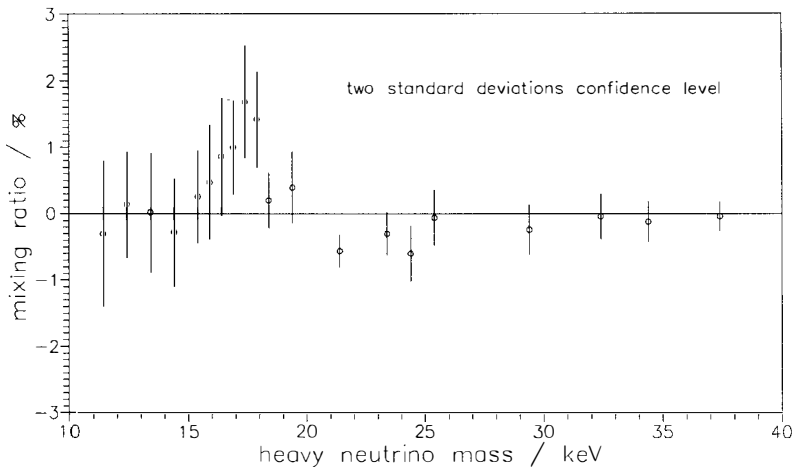


Fig. 3. The mixing ratio R obtained for possible heavy neutrino masses m_{H} between 10 and 40 keV

Our result, based on a completely different physical process and involving a different technique, confirms the existence of the massive neutrino and is in general agreement with some other recent results^{14,15,20}.

REFERENCES

- 1) J.J. Simpson, Phys. Rev. Lett. 54 (1985) 1891.
- 2) B. Eman and D. Tadić, Phys. Rev. C33 (1986) 2128.
- 3) E.G. Drukarev and M.I. Strikman, Zh. Eksp. Teor. Fiz. 91 (1986) 1160.
- 4) J. Lindhard and P.G. Hansen, Phys. Rev. Lett. 57 (1986) 965
- 5) T. Altizoglou et al., Phys. Rev. Lett. 55 (1985) 799.
- 6) T. Ohi et al., Phys. Lett. 160B (1985) 322.
- 7) A.M. Apalikov et al., Zh. Exp. Theor. Fiz. (Pisma) 42 (1985) 233.
- 8) J. Markey and F. Bhoem, Phys. Rev. C32 (1985) 2215.
- 9) D.W. Hetherington et al., Phys. Rev. 36C (1987) 1505.
- 10) M.J.G. Borge et al., Phys. Scripta 34 (1986) 591.
- 11) I. Žlimen et al., Phys. Scripta 38 (1988) 539.
- 12) I. Žlimen et al., Fizika 22 (1990) 423.
- 13) B.A. Logan, Nucl. Instr. and Meth. A280 (1989) 167.
- 14) J.J. Simpson and A. Hime, Phys. Rev. 39D (1989) 1825.
- 15) A. Hime and J.J. Simpson, Phys. Rev. 39D (1989) 1837.
- 16) I. Žlimen et al., in: Thallium Neutrino detection 1990, International Symposium on Solar Neutrino Detection with ^{205}Tl , Dubrovnik, Croatia, Yugoslavia, to be published.
- 17) D. Berényi et al., Phys. Lett. B18 91965) 293.
- 18) R.P. Gardner et al., Nucl. Instr. Meth. A242 (1986) 399.
- 19) Y. Jin et al., Nucl. Instr. Meth. A242 (1986) 416.
- 20) E.B. Norman et al., in: 14th Europhysics Conference on Nuclear Physics, Rare Nuclear Decays and Fundamental Processes, Bratislava, Czecho-Slovakia, 1990, to be published.

DARK MATTER, HIGH ENERGY ASTROPHYSICS

MACHOS, WIMPS or DUST : WHAT IS DARK MATTER ?

S.Zylberajch

DPhPE - CEN Saclay
F 91191 Gif sur Yvette Cedex



ABSTRACT :

A review of the Dark Matter status is given. After a short presentation of the Dark Matter problem, the experimental aspects of its detection is presented, with the known results and the experiments under way.

INTRODUCTION

Dark Matter (DM) exists [1]. We know it is there because we can measure its gravitational effects. At the periphery of the galaxies, the kinematics of the stars does not seem to obey Newton's law if we suppose that the mass distribution inside the galaxy is the same as the brightness distribution (fig 1a) : one clearly see a flat rotation curve (fig 1b) where newtonian motion would give a curve decreasing like the inverse square root of the distance to the center of the galaxy.

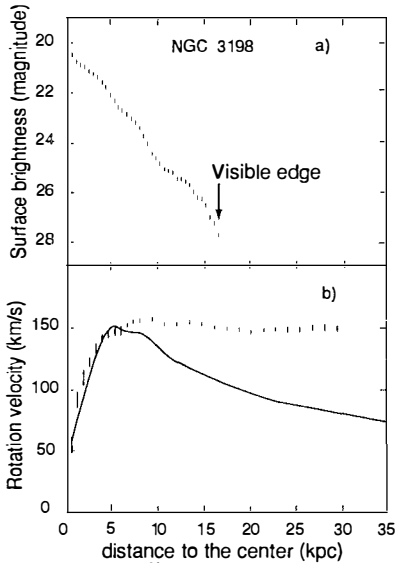


figure 1

Looking farther, at the H_I (21 cm) and H_{II} lines[2] one still finds the same flat curves. This flatness seems to be due to the presence of an invisible halo, roughly spherical, the Dark Matter Halo, whose radius can be ten time larger than the galaxy's radius. When looking at a much larger scale (fig 2), it is found that the mass to luminosity ratio increases with the distance : When one looks farther and farther, one needs more and more Dark Matter to account for the cinematic of the galaxies inside clusters, in the frame of standard newtonian dynamics. At very large scale, M / L seems to be consistent with the $\Omega = 1$ limit, where Ω is the ratio of the matter density to the critical density which closes the universe. Table I shows the relation between the structure scale and Ω ; One important result is that the

Table I

Structure scale	$\langle M / L \rangle$	Ω
Visible stars and clusters	1	0.001
Visible parts of galaxies	10	0.01
Binary galaxies and groups	10 - 100	0.01 - 0.1
Rich clusters and super clusters	100 - 300	0.2 \pm 0.1
Largest scale coherent structures	700 \pm 150 ?	0.5 - 1.0
Inflationary scenario	1000 h	1.0

luminous matter cannot account for more than 2 % of the total mass of the universe.

There is also some theoretical needs for Dark Matter. For instance the inflation scenario requires Ω to be identically equal to 1. The 3° K fossil radiation is a clear signature of an homogeneous universe at very large scale, but to explain the galaxy formation, one needs some gravitational seeds; one favourite model is the Bottom-Up scenario [3] which needs the presence of Cold Dark Matter. The success of the primordial

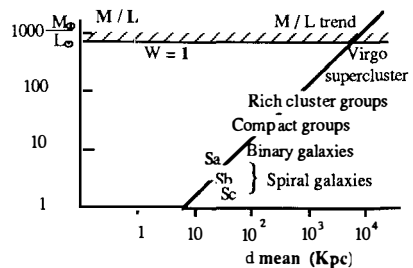


figure 2

nucleosynthesis imposes a limit $\Omega_{\text{bar}} \leq 0.2$ to the baryonic matter. As $\Omega_{\text{luminous}} \sim 0.02$, the general conclusion is :

- 1- We need Dark Matter, which may represents more than 90% and may be up to 99% of the total mass of the universe.
- 2- There is still room for the baryonic DM.
- 3- If $\Omega = 1$, the main component seems to be constituted of non baryonic DM.

Until now we do not understand the DM composition (fig 3). It could be formed either by microscopic non baryonic elementary particles - the **WIMPS** (for Weakly Inteaacting Massive Particles) like massive neutrino, the Lightest Super Symmetric particle - or by still more exotic particles like the **CHAMPS** (for Charged HALo Massive Particles). It could also be formed by macroscopic **dust** particles or by the **MACHOS** (for MAssive Compact Halo Objects).

It is believed that these materials have to be cosmologically stable and have non dissipative interactions in order to preserve the halo structures. Near the Sun, the observation of the rotation velocity of the Galaxy gives an average velocity of about 300 km / s and a mean density of about 0.3 Gev / cm³ for the DM candidates.

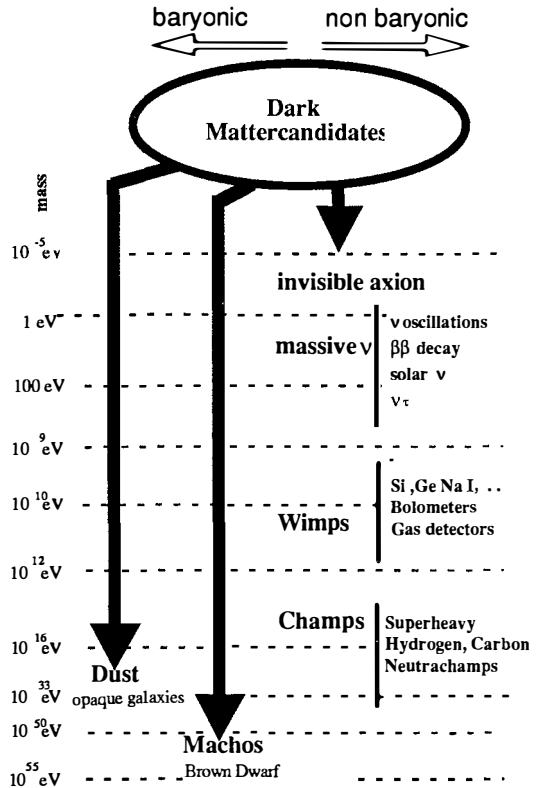


figure 3

IS DUST THE LOCAL DARK MATTER ?

Last summer Valentijn sent a letter to Nature [4] in which he claimed that the late spiral galaxies were opaque. The Sun belongs to such a type of galaxy. According to Valentijn, we could see only 15% of the stars by the light emitted in the outer regions of the galaxies. The opacity came from dust clouds lying inside the galactic disk, and these clouds could explain the velocity rotation curves, so that they were no more needs of any DM halo around the galaxies.

To support his argument Valentijn used the ESO Uppsala [5] catalogue data to look at the dependence of the galaxy surface brightness on the galaxy inclination : as seen from the earth a galaxy looks like an ellipse; its brightness decreases roughly exponentially from the center and is quantified by a serie of isophotes of increasing magnitude per square arc second toward its edge. The cosine of the inclination angle is estimated by the minor to major axis ratio. Valentijn's argument went in 3 steps :

- first he looked at the central brightness the galaxy and found it independent of the inclination. The opacity dependence on the inclination angle θ was parametrized as :

$$\mu = \mu_0 \frac{1}{(\cos\theta)^C}$$

where μ_0 is the face-on brightness and C is the absorption coefficient. He concluded that the center of the galaxies was opaque .

- second he looked at the brightness in the half total radius region, which defines the central region from which half of the total light output is emitted. He found this region opaque too - But due to the exponential decrease of the luminosity and the presence of a bulge in the central region, this radius is still near from the center of the galaxy.

- third he looked at the ratio of the 26th isophote radius to the half total light radius and found it independent of the inclination of the galaxy. From that he concluded that the galaxies were opaque till their outer regions. - This conclusion is not correct as it can be shown that this ratio is insensitive to whether the galaxies are opaque or transparent (both radii increase with the inclination in the same way).

A group at Saclay [6] decided to use the same catalogue to look more carefully at the galaxy's outer regions.

The basic idea is to select a clean sample of spiral galaxies and to look at the distribution of the cosine of their inclination angle θ . As the galaxies are randomly distributed, one must get a flat distribution. The sample was defined by imposing the angular diameter of the 26th magnitude isophote to be bigger than 80 arc second. In the opaque hypothesis, as the brightness does not depend on $\cos\theta$, the cut can be applied directly on the data in the catalogue. But in the transparent hypothesis, we must apply the cut on the diameter the 26th magnitude isophote would have if the galaxy was seen face-on because the brightness varies as the inverse of $\cos\theta$. This diameter can be easily computed according to the following formula :

$$D_{\text{face on}} = D_{26} - 2.5 (D_{25} - D_{26}) \log(\cos\theta)$$

where the only hypothesis is that the brightness decrease is locally exponential.

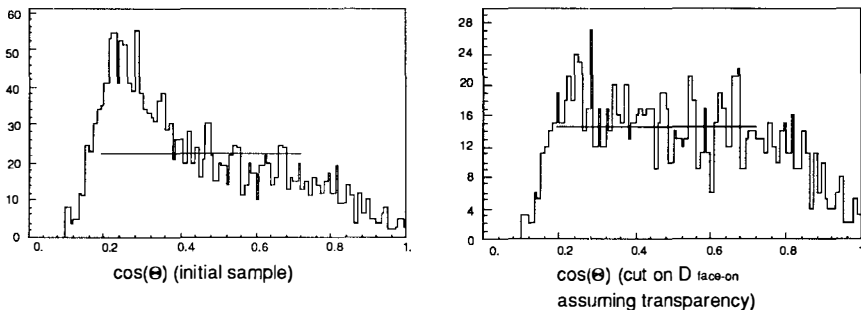


figure 4

On figure 4 it is clearly seen that the observations agree with a model transparent near the 26th magnitude isophote, with a χ^2 / degree of freedom equal to 1.2 for 40 channels.

The observed excess of data in the low $\cos\theta$ bins, on the initial sample, comes from the fact that for very tilted galaxies, the diameter D_{26} increases if the galaxies are transparent and some galaxies that pass the angular cut $D_{26} > 80''$ would have not, if they have been more face-on oriented. The opacity coefficient was fitted for magnitude 23 to 27 and the result is seen on figure 5 where the opacities giving a probability bigger than 10% are plotted.

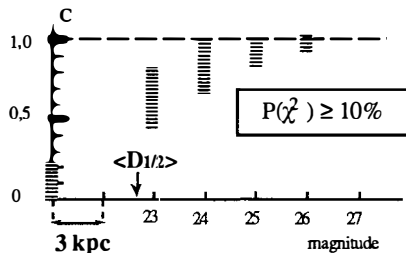


figure 5

This correspond to a semi-opaque scheme and the main conclusion, as far as the Dark Matter is concerned, is that the problem of finding direct evidence of the DM Halo is still open.

MACROSCOPIC OBJECTS

These candidates are called Machos for massive compact halo objects (for instance brown dwarfs or black holes). B.Paczynski^[7] proposed to use gravitational microlensing to detect MACHO's : when a spatially-small massive object D (fig. 6) passes near the line of sight of a star S observed from the earth , light passing

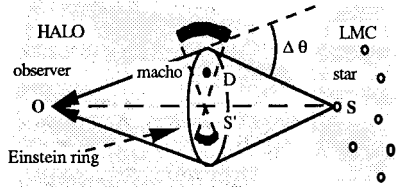


figure 6

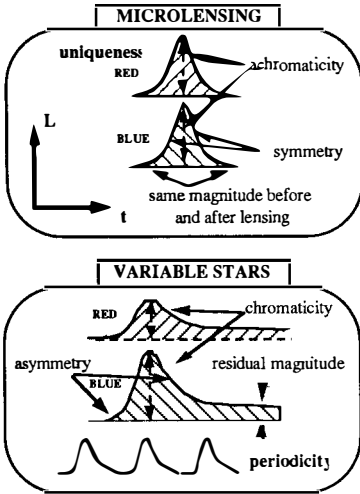


figure7

both sides of D is bent back to the observer O. If the star, the Macho and the observer were perfectly aligned, the observer should see a luminous ring at the Einstein radius given by :

$$R_0^2 = \frac{4 G M d}{c^2}$$

where G is the Newton constant, M the deflector mass and d a distance such that

$$\frac{1}{d} = \frac{1}{d_{OD}} + \frac{1}{d_{DS}}$$

R_0 defines roughly the region inside which the microlensing phenomenon is effective. For not perfectly aligned system, the observer should see 2 images, but the angular separation is so small ($< 10^{-3}$ arc second) that the net result is a luminosity increase of about 30 %.

The proposed procedure to detect Machos^[8] is to monitor the luminosity of several millions of stars in the Large Magellanic Cloud (LMC) for one or two years. When a Macho passes near the line of sight of a star a peak should appear in the star luminosity. The microlensing signature is quite characteristic (fig 7) :

- the light curve must be symmetric with the same magnitude before and after lensing.
- it must be achromatic, that is identical in blue and red light.
- it must appear only once.

Table II

Deflector Mass (M _☉)	Mean R ₀ (km)	Mean μlensing time	Nb of μlensing events / 4 months
> 10	3 10 ⁹	> 1 year	0.5
1	10 ⁹	3 mths	1.0
10 ⁻²	10 ⁸	9 days	5
10 ⁻⁴	10 ⁷	1 day	50
10 ⁻⁶	10 ⁶	2 hrs	500
10 ⁻⁸	10 ⁵	12 mins	5000

These characteristics are very different of those of variable stars, whose light curves generally do not satisfy at least one of the above criteria. The characteristic time of the microlensing phenomenon varies with the mass of the deflector from a few minutes to more than one year (table II). The status of the French microlensing search is given in these proceedings by A.Milsztajn^[9].

ELEMENTARY PARTICLES

A lot of new particles, beyond the Standard Model, have been proposed as non baryonic DM candidates . They have a life time greater than or of order of the age of the universe.

Axions

It is the lightest candidate. It was invented by Weinberg and Wilczek^[10] to solve the problem of CP conservation in the strong interactions. This axion had a mass higher than 150 keV^[11] and was not seen, but it reappeared soon as the "invisible" axion^[12]. Cosmology and stellar evolution constrain this axion to have very low mass window : An axion lighter than 10^{-5} eV would have a density overclosing the universe, and with axions heavier than 10^{-2} eV the red giant stars and the white dwarf stars would have burnt too fast^[13]. Direct detection is a hard task. Several experiment^[14] try to detect axions by converting them into light through interactions with magnetic fields (fig.8 a) or by modifying the polarisation of a laser beam through interactions with magnetic fields (fig.8 b).

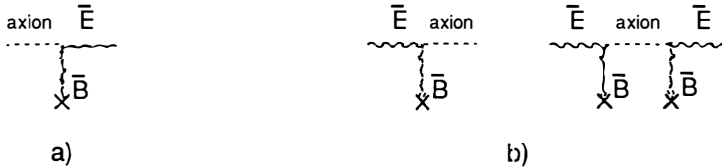


figure 8

Wimps

They are massive particles and in order to close the universe their annihilation cross section has to be of the order of that of the weak interactions. Wimps could be either massive Dirac or Majorana neutrinos, or the lightest super symmetric particle (photino or neutralino ...) which is stable by Supersymmetric R conservation or still more exotic particles like the cosmion, an ad hoc particle^[15] devised to solve both the dark matter and the solar neutrino problems.

Indirect searches :

We have already some information^[16] on the mass spectra thanks to neutrino physics, collider experiments (LEP and Tevatron), astrophysics and cosmological constraints (for example see fig 9 for Dirac neutrino constraints) :

- for the light photinos and neutrinos, the mass window is between 10 and 100 eV due to cosmological limits .
- for more massive particles, unseen in the present e^+e^- and $p\bar{p}$ experiments(fig 10), the lower limit is of the order of 10 to 50 GeV depending on the SUSY models used to interpret the absence of signal.

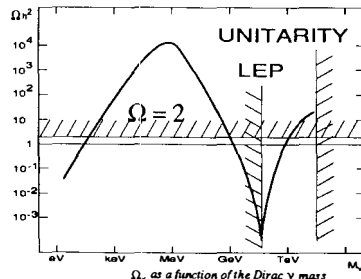


figure 9

- massive underground detectors^[17], looking at neutrinos produced by DM particles annihilations in the sun, exclude masses between 4 GeV and 90 GeV.

- unitarity and the observed limit : $\Omega \leq 2$ constraint the DM particles to be lighter than 340 TeV^[18]. For SUSY particles, this limit could be of the order of 3 TeV^[19]. All those values are model dependent and must be regarded as indications rather than definitive limits.

Direct searches :

The only way to get model independent limits is to look at direct evidence of Wimps through elastic scattering with nucleus^[20]. Due to the low Wimp's velocity, the expected recoils are very weak from O(10 eV) to O(100 keV) depending on the Wimp and target masses. The expected cross sections depend on the coupling type :

- For vector coupling like dirac neutrino, there is a coherent effect, as the Wimp associated compton wave length is of the order of the nucleus radius. The cross sections are roughly proportional to the square of the atomic number.
- For axial coupling like majorana neutrino, there is no such a coherent effect. Moreover we have to use targets with non zero spin. This rules out the most abundant silicon and germanium isotopes.

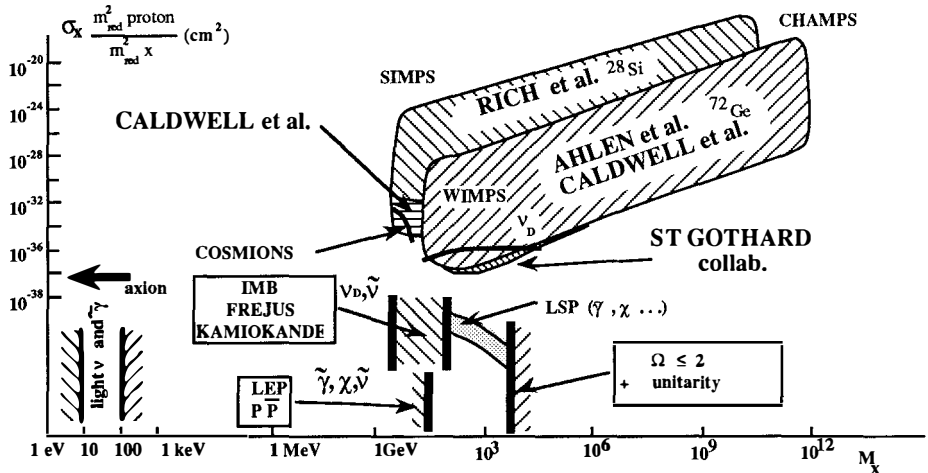


figure 10

All other things being equal, the event rates for axial coupling are 3 to 4 orders of magnitude less than for vector coupling. The expected rate must be less than the actual experimental limit which is of the order of 10 events kilo⁻¹ day⁻¹.

Galactic dark matter distribution can be approximated near the Sun by a gas distribution with a density of 0.3 MeV cm⁻³ and a maxwellian velocity distribution with an average velocity of about 300 km s⁻¹. If we guess the mass and the cross section of the DM candidate, we deduce the flux, the recoil and the event rate.

DM signature :

A clear DM signature will be provided by the recoil energy on different target nuclei as the recoil energy and event rate depend on the target mass and elastic cross section. A more precise signature will be found in annual modulation of the event rate of the order of 10%, due to the relative Earth to Sun velocity. But the best evidence will be a clear correlation between the recoil nucleus direction and the Earth trajectory in the Galaxy.

Background :

The main background is due to cosmic rays - DM searches have to be done in deep underground laboratories - and the natural radioactivity of the detectors - detectors must be made out of very low radioactive materials and have a good electron rejection to eliminate Compton scattering of γ . Detectors must be as massive as possible and have a very low energy threshold, to take into account the expected low event rates and small recoil energies.

Results :

The first measurements were made in double β experiment using germanium or with silicon semiconductor detectors. To interpret the signal we must know the calibration of the diode which is given by the ratio of the charge deposited by the interaction of a neutral massive particle to the charge deposited by an electron of the same energy. The response of such a diode has been modeled by Lindhard et al.[21] and confirmed by direct measurement[22]. Figure 10 shows the results of 4 experiments :

The first ones done by Ahlen et al. and Caldwell et al.[23] used germanium diodes. The left side of the exclusion contour is due to the electronic noise. The lower side is due to natural radioactivity : for low cross section the Wimp's signal disappears in the background. The right limit is due to the fact that as the Wimp's density is constant, when the mass increases, the corresponding flux vanishes and we can't get any signal. The upper limit is due to the fact that particles with stronger cross section (SIMPS) cannot hit the detector as they are stopped in the material above the detector. To bypass this difficulty, data recorded in the upper atmosphere from a silicon detector placed in a balloon were reanalysed[24]. This gives the upper contour of figure 10. A germanium result from the St Gothard collaboration[25] was presented in this session and gives a new rejection limit toward the low cross sections.

A dedicated experiment[26] using silicon crystal was done to search the cosmions. Cosmion must be lighter than 8 GeV - to produce efficient cooling of the sun's core - and heavier than 2 GeV to avoid fast evaporation. On figure 11 the corresponding enhanced region of the contour plot is shown. Results of calculations made by Kaplan et al.[27] show that the vector cosmion is practically excluded. On the same figure it is seen that the Dirac neutrino is excluded but we still need an increase of 2 to 3 orders of magnitude in sensibility to reach the region of axial coupling.

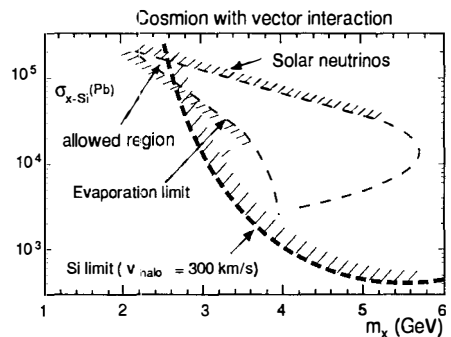


figure 11

Next generation experiments :

To improve the exclusion regions, news technologies will be used :

- bolometers and gas detectors toward lower masses
- bolometers and sodium iodide scintillators toward lower cross sections.
- sodium iodide scintillators used in delayed coincidence could also be used for the higher mass and cross section regions.

A Saclay group is looking at the feasibility of an hydrogen low pressure TPC experiment. Using hydrogen as target and detector will give access to axial coupling and determine the direction of the incident Wimp and the Earth's motion. Good electron rejection (10^{-3} to 10^{-4}) could be achieved with a moderate magnetic field and there is no need of target modelling as the hydrogen nucleus is a simple one .

Several communications were given in this session on the prospect of bolometer^[28] and sodium iodide^[29] experiments. Sodium iodide is easy to use, it can be used in massive detectors with contact vetoes, and provides a possible electron rejection. The bolometer could be the most promising way : phonon detection can be used to get a very low threshold energy, the simultaneous ionisation measurement could give a good electron rejection and a large choice of crystals could provide a good mass identification and access to axial coupling.

Champs

In a paper sent to Nuclear Physics last year, Glashow, De Rujula and Sarid^[30] claimed that very massive charged particles could be good DM candidates, provided there exists one neutral bound state to form the DM halo. Positive Champs would behave like nuclei, negative one's would be bound to ordinary nuclei to give heavy exotic isotopes and the lightest one composed of a negative Champ bound to a proton, the neutrachamp is the neutral component needed to form the DM halo. Champ's mass should be found between 1 TeV and 1 to 10 PeV, depending on their annihilation cross section, but to prevent positive champs setting to fast in the galactic disk the lower limit must be raised up to 20 TeV.

Indirect evidence of the existence of such Champs could be found in astronomic spectroscopy in the same way as helium was found, but direct detection trough elastic collisions is hopeless because of the short range of such particles which will be stopped very quickly in the atmosphere. The only way to find Champs on earth is to search for super heavy isotopes, and principally to look at super heavy hydrogen - an electron surrounding a positive Champ - and super heavy carbon - a negative Champ bound to a nitrogen nuclei (like an hyperfragment).

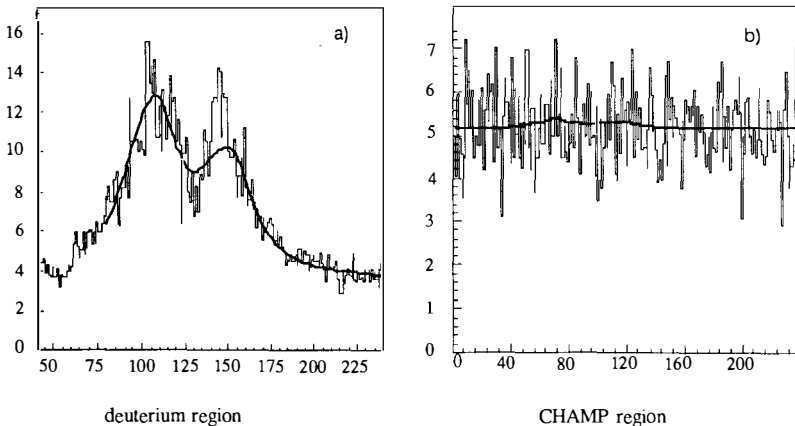


figure 12

Smith and al.^[31] using enriched heavy water and mass spectroscopy found an abundance of Champ relative to nucleon smaller than 10^{-28} for Champs lighter than 1 TeV. Turkevitch et al.^[32] using irradiated graphite and radio chemistry found an abundance smaller than $2 \cdot 10^{-15}$ for Champs lighter than 100 TeV. There is presently a french collaboration between Ecole Normale Supérieure, Institut Pasteur and Saclay which look at Champs lighter than 10 PeV in oceanic waters. Starting from the known DM density it is easy to find the flux of falling Champs in the ocean :

$$\frac{[C^-]}{[H]} = 2.1 \cdot 10^{-18} \frac{\text{tyear}}{M_{\text{TeV}} \text{ hkm}}$$

The accumulation of Champs with a mass of 10^4 TeV in an average thickness of 3000 meters of water during 10^6 years would yield an abundance of the order of $2 \cdot 10^{-16}$ which is well within the reach of today possibilities. Oceanic water is first centrifugated, which gives an enrichment factor of $4 \cdot 10^4$. The reduced hydrogen is then analysed by two-photons transition in laser spectroscopy^[33]. With the present statistics the preliminary analysis gives an upper limit of $4 \cdot 10^{-15}$ for the negative Champs abundance. Figure 12-a shows the excitation curve in the deuterium region. The fitted curve determines the width and position of the hyperfine structure, allowing for the calibration of the detector. On figure 12-b is shown the excitation curve in the expected Champ's region.

CONCLUSION

Dark Matter problem is one of the most fascinating problems of today's physics. Located at the frontier between particle physics, astrophysics and cosmology, its solution could open new windows - in particles physics, beyond the standard model - in astrophysics to explain stellar evolution and in cosmology to explain the galaxy formation. Until now the only clear evidence of its existence is negative : there is something which gravitationally determines the movement of astronomical structures, but which still remains unseen in all electromagnetic modes. There is still a lot of work to do in order to improve the sensitivity to detect the axial Wimp. However, positive evidence of its existence and nature may be provided in the next few years thanks to present searches either in neutrino physics^[34] or machos survey^[8].

I wish to thank Drs. R. Barloutaud, G. Gerbier and J. Rich for comments and criticisms.

Références :

- 1- for a recent review see V.Trimble, Ann. Rev. Astron. Astrophys. 25 (1987) 425
A.Bouquet; Gif 1989
- 2- A.Bosma, Ap. J. 86(1981) 1825
V.C.Rubin et al., Ap.J. 238 (1980) 471
- 3- J.R. Primack SLAC-PUB-3387 (1984), Invited talk at the 2nd ESO/CERN
Symposium on Cosmology, Astronomy and fundamental Physics SCIPP86/65
(1986)
- 4- E.A.Valentijn, Nature 346 (1990) 153
- 5- A. Lauberts and E.A.Valentijn, the Space Catalogue of the ESO Uppsala galaxies,
Munich (1989)
- 6- C.Cesarsky et al. DPhPE 90-22 (1990)
- 7- K.Griest CfPA-TH-90-007 (1990)
B. Paczynski, Ap. J. 304(1986) 1
- 8- A. Milsztajn , DPhPE 90-06, 10th Moriond Workshop on New and Exotic
Phenomena Les Arcs (1990)
- 9- A. Milsztajn , this session
- 10- F.Wilczek, Phys. Rev. Lett. 40 (1978) 279
S. Weinberg, Phys. Rev. Lett. 40 (1978) 223
- 11- R.D.Peccei and H.R.Quinn Phys. Rev. Lett. 38 (1977) 1440; Phys.Rev. D 16
(1977) 1791
- 12- for a recent review see M.Srednicki, Nucl. Phys. B260(1985) 689,
M.Davies XXII Rencontre de Moriond 8-15 March 1987
J.E. Kim, Phys. Rep. 150 (1987) 1
- 13- G.G Raffelt MPI-PAE/TPh 67/85 Axion constraints from White Dwarf cooling
times and ref.4 to 6

- 14- P.Sikivie, Phys.Rev. Lett. 51 (1983) 1415 ; Phys. Rev. D 32 (1985) 2988
Y.Semertzidis et al. Phys. Rev. Lett. 64 (1990) 2988
- 15- D.N.Spergel and W.H.Press, Ap. J. 294 (1985) 663
W.H.Press and D.N.Spergel, Ap. J. 296 (1985) 679
R.L.Gilliland et al., Ap. J. 306 (1986) 703
- 16- K. Enquist et al.,Nucl. Phys. B 317 (1989) 647; T.K. Gaisser et al., Phys. Rev. D 34 (1986) 2206
- 17- KEK preprint 90-166 (1990); H.J.Daum, Thesis Wuppertal (1990)
- 18- K.Griest et al.,Phys. Rev. Lett. 64 (1990) 615
- 19- K.Griest et al.,Phys. Rev. D (1990) 3565
- 20- M.W.Goodman and E.Witten Phys. Rev. D 31 (1985) 3059
- 21- J.Lindhard et al. Mat.-Fys. Medd. 33 (1963) 14
- 22- G.Gerbier et al., Phys. Rev. D 42 (1990) 3211
- 23- P.O.Caldwell et al., Phys. Rev. Lett. 61 (1988) 510
S.P.Ahlen et al., Phys. Lett. B 195 (1987) 603
- 24- J.Rich et al. Phys. Lett. B 194 (1987) 173
- 25- Treichel report on the CALTECH-Neuchâtel-PSI collaboration in this session;
D.Reusser et al. Phys. Lett. B 255 (1991) 143
- 26- P.O.Caldwell et al., Phys. Rev. Lett. 65 (1990) 1305
- 27- J. Kaplan et al. DPhPE 90-15 (1990); PAR-LPTHE 90-38
- 28- R.Gaitskel, report on cryogenic detectors in this session
A.Taden, report on cryogenic detectors in this session
R.E. Lannou, report on cryogenic detectors in this session
- 29- P.Belli report on Roma-Saclay collaboration in this session
- 30- A.De Rulula et al. Nucl. Phys. B333 (1990) 173
- 31- P.F. Smith et al., Nucl. Phys. B206 (1982) 333
- 32- A. Turkevitch et al. Phys. Rev. D 30 (1984) 1876
- 33- P. Verkerk et al., Opt. Com. 72 (1989) 202
- 34- M. Cribier, 25th Int. Conf. on High Energy Physics - Singapore 1990
V. Gavrin, 25th Int. Conf. on High Energy Physics - Singapore 1990

Direct detection of dark matter candidates +)

C. Bacci⁽¹⁾, P. Belli⁽²⁾, R. Bernabei⁽²⁾, G. Gerbier⁽³⁾, A. Incicchitti⁽¹⁾, R. Marcovaldi⁽¹⁾, L. Mosca⁽³⁾, D. Prospero⁽¹⁾, C. Tao⁽³⁾.

⁽¹⁾*Dipartimento di Fisica, Università di Roma and Istituto Nazionale di Fisica Nucleare, Sez. di Roma, Roma -Italia.*

⁽²⁾*Dipartimento di Fisica, II Università di Roma and Istituto Nazionale di Fisica Nucleare, Sez. di Roma II, Roma -Italia.*

⁽³⁾*DPhPE, Saclay, France.*

Abstract

We present here preliminary studies on the feasibility of a dark matter experiment using low activity scintillators. Encouraging performances of low activity NaI(Tl) crystals have been measured at the Laboratori Nazionali del Gran Sasso and at the Fréjus tunnel.

1. Introduction

There is some evidence by the observations of galaxy dynamical behaviour that a large amount of the mass of the Universe is composed by "dark matter"⁽¹⁾. Nucleosynthesis considerations suggest that this "dark matter" has almost a non-barionic component; furthermore the theory of galaxy formation indicates that the reliable candidates are the non relativistic ("cold") Weakly Interacting Massive Particles (WIMPs) with masses greater than few GeV. This particles would be trapped in the gravitational field of our Galaxy and would make up the halo in which our planetary system is embedded.

Several efforts are in progress to search for WIMPs using direct detection methods⁽²⁾. WIMPs would interact by elastic scattering on various target nuclei, transferring them a small amount of energy. So they could be detected by measuring this recoil energy of the nucleus. The interaction could be either via weak coherent ν -like vector coupling or via axial vector coupling⁽³⁾. Obviously, even-even nuclei do not allow detection of spin-dependent interacting candidates.

The cross sections for supersymmetric candidates — quoted in the literature⁽³⁾ — are very small, leading to a rate of the order of 1 event/day/100 kg.

The existing results on dark matter candidates have been obtained with semiconductor detectors: silicon with 1.2 keV of energy threshold and germanium with 3 keV energy threshold. They have allowed the exclusion of vector coupling

+) Presented by P. Belli

cosmions⁽⁵⁾ (solar neutrino solving WIMPs), Dirac neutrino with masses between 10 and 2400 GeV⁽⁶⁾ and the whole shadow region of the cross section vs dark matter particle mass plot (see fig. 1). The lowest background rate obtained in germanium experiments is ≈ 3 events/kg/keV/day at the threshold energy⁽⁶⁾. The best limits which can be presently set on pure axial coupling WIMPs come also from germanium experiments, through the non zero spin isotope, ⁷³Ge (7.67% natural abundance).

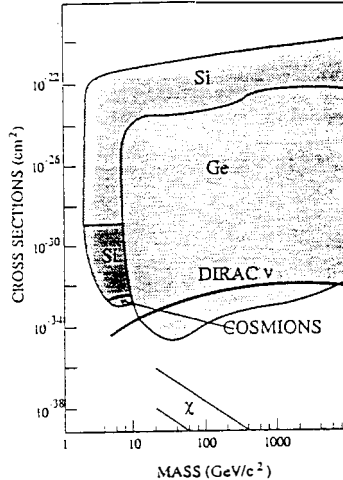


Fig. 1 - Exclusion plot for dark matter particles⁽⁴⁾.

A dark matter signal can be evidenced by: 1) the energy spectrum shape, that gives an estimate of the mass of the dark matter particle; 2) the annual modulation of the counting rate and of the energy spectrum (may vs november periods); 3) crossing checks using a set of different target-nuclei and so different interaction cross sections. Furthermore, a strong signature would be the detection of the recoil nucleus track, which is correlated with the direction of dark matter particle; but the present detectors cannot see them (a low pressure TPC has been proposed for this purpose⁽⁷⁾). Therefore, we need to explore the dark matter particle scenario using new target-materials and detectors possibly as large as needed to observe the annual modulation of the counting rate. Low activity scintillators could be used to achieve these purposes.

2. NaI(Tl) as "dark matter" detector

In the following we point out that very low activity NaI(Tl) is an interesting material for direct detection of dark matter particles by elastic scattering^(8,9). In fact NaI(Tl) is a "new" target-nucleus, which allows to explore also the axial coupling (²³Na has spin 3/2), its energy threshold can be as low as a few keV because of the high light response, it is easier to handle and to build in larger size than the germanium and silicon ones and finally its cost/mass ratio is interestingly low. Its light yield response to nuclear recoils has been measured⁽⁸⁾ and has been found to be 25% of that of electrons of the same kinetic energy. A possible pulse shape discrimination between nucleus recoils and electron induced pulses has been investigated⁽⁸⁾.

In order to reach with a NaI(Tl) detector the same sensitivity to the pure axial vector coupling dark matter particles than germanium experiments the rates measured in NaI(Tl) crystals should be lower than 5 events/kg/keV/day at 5 keV if we assume similar spin corrections and nuclear form factors. Actually, the theoretical estimates for axial couplings would yield larger cross sections for ^{23}Na than for $^{73}\text{Ge}^{(10)}$, but the absolute values are too model dependent to be reliable, so we think that it is important to perform experiments using different target nuclei.

3. Is an NaI(Tl) experiment possible?

In order to perform an experiment to detect dark matter candidates by using NaI(Tl) scintillators we have to consider all the possible sources of background and how to remove them. At low energy (below 7 keV), the background is mainly due to the noise of the photomultiplier. Adequate choice of the photomultipliers, its voltage dividers and the electronic chains, the use of 2 or more photomultipliers in coincidence on the same crystal, and/or analysis of the pulse shape should allow us to reach an energy threshold of 2 to 3 keV. The radioactive background below an energy of 50 keV has to be controlled by identifying the various sources (crystal itself, reflector, housing and photomultiplier radioactivity, content of radon in the air, cosmic rays and environmental radioactivity) and by reducing each one (choice of materials, passive shielding, active veto). Dedicated tests for this problem have been already started and will be continued before designing the final experimental set-up.

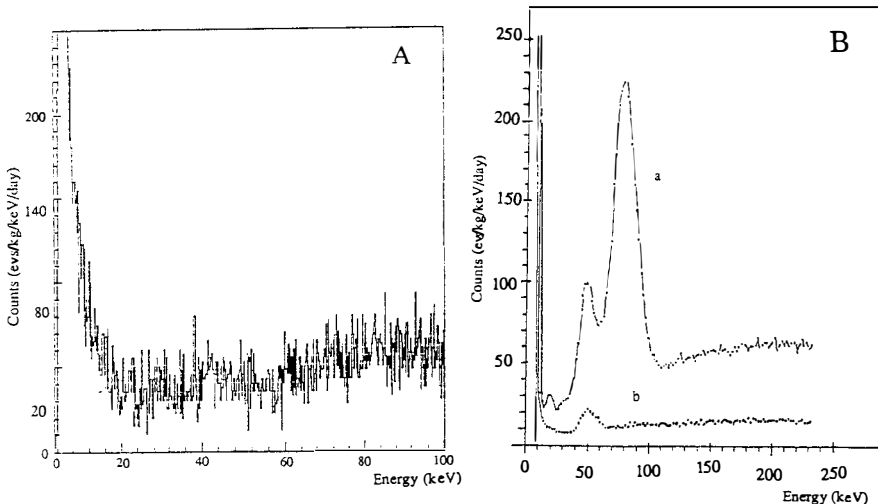


Fig. 2 - Some preliminary energy spectra obtained A) at LNGS using a prototype of about 400 g of "low activity" NaI(Tl) crystal inside 15 cm boliden lead external and 3.5 cm LC2 lead; and B) at Fréjus Laboratories with a 11 kg NaI(Tl) crystal inside: a) 25 cm lead and b) 15 cm lead external and 4 cm copper. It is clear that a high photopeak efficiency is relevant.

Tests have been performed both in the Gran Sasso (LNGS) and Fréjus Laboratories using NaI(Tl) crystals and photomultipliers of various companies and shieldings mainly made with low activity copper and lead. For the moment, all these tests have been performed using only one photomultiplier per NaI(Tl) crystal. In fig. 2 we report some preliminary results; as shown in this figure a large counting reduction

has been obtained selecting the quality of NaI(Tl) detectors and of the shieldings. Efforts are in progress to decrease the energy threshold and to reject the noise; energy threshold of about 4 keV has been already reached. These encouraging results obtained with preliminary set-ups suggest that a significant improvement of the present-day knowledge on dark matter may be achieved by NaI(Tl) detectors.

Our future goals are to obtain a lower threshold and a decreasing of the residual radioactive background. A reasonable goal to reach is to gain a factor 10 in sensitivity. This is an essential step towards the sensitivity required for the detection of SUSY particles.

A good signature for dark matter is the annual modulation of the counting rate. We expect a difference of counting rate between May and November which can reach 10%. In order to observe a statistically significant modulation, a large mass is necessary, inversely proportional to the observed rate, R , namely $M > 50\text{kg}/R$ (in events/kg/keV/day). This large amount is certainly not possible to consider for other types of detectors (semiconductors, TPC, bolometers) in the near future.

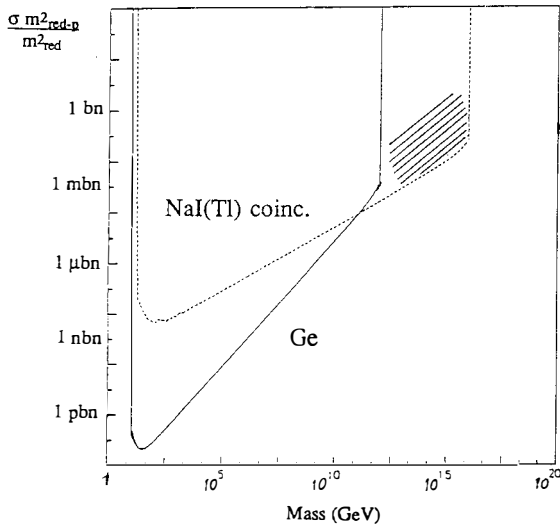


Fig. 3 - Cross section-mass region that could be explored by an NaI(Tl) coincidence experiment with 1000 cm^2 surface, a $\Delta\Omega=0.4$ and 0.1 evs/d . The region excluded by germanium experiments is also shown. The shaded region corresponds to the SIMPs region

There m_{red-p}^2 is the reduced mass between dark matter particle and proton, while m_{red}^2 is the reduced mass between dark matter particle and target nucleus.

Another region of interest which is not excluded by any direct detection experiment so far, is the high mass (around 10^{15} GeV) and high cross section (around 1 barn) region. Strongly interacting particles (SIMPs)⁽³⁾ would have a typical interaction length in the ordinary matter of the order of few tens of centimeters and in each interaction the deflection of the flight direction would be of the order of the nucleus—particle mass ratio ($M_{nuc}/M_S \approx 10^{-14}$); of the same order of magnitude would be the relative kinetic energy loss. Thus, the direction and kinetic energy of these strongly interacting particles would not change appreciably. As a consequence SIMPs could be

detected by their interactions in different nearby crystals by studying delayed coincidences. Typical time delays are of about $1\mu\text{s}/30\text{cm}$. In fig. 3 it is shown the cross section-mass region that an NaI(Tl) coincidence experiment could explore compared with the region excluded by germanium experiments. A suitable geometrical setup should allow in principle to identify the incoming direction of dark matter particle and to reject spurious coincidences.

4. Liquid xenon detector

Some of us (Italian group) are also studying the possibility to use liquid xenon scintillator as a dark matter detector. As already pointed out^(9,11) liquid xenon should be an interesting material to detect dark matter induced Xe-recoil by means of the collection of its scintillation light. The properties of such a detector are reported in the literature⁽¹²⁾ and have been studied by the Italian group using a prototype of 118 cc; an energy threshold of about 15-20 keV and an energy resolution comparable to NaI(Tl) up to 122 keV was obtained. Obviously, it's necessary to know the light response to a recoil Xe-nucleus of few keV; so, a measurement of the relative scintillation efficiency using a neutron beam is foreseen. Up to now, we can only quote an estimation of about 20% at energies above 7 keV using the Lindhard theory⁽¹³⁾.

5. Conclusions

Relevant problems are still open about dark matter. Nucleosynthesis, cosmological inflation and galaxy formation support the existence of non-barionic dark matter particles as one of the most likely solutions for this missing mass problem. We are studying the possibility to use low activity scintillators as target-detectors in the search for WIMPs. They could allow to explore different new regions in the cross section vs mass plot.

Acknowledgements

The Italian group wish to thank Proff. Silio d'Angelo and Gerd Heusser for helpful discussions on related topics.

References

- 1 - Zwicky F., *Helv. Phys. Acta*, 6 (1933) 110;
 - Oort J.H., *Bull. Astr. Instr. Neth.*, 6 (1932) 249;
 - Rubin V.C. et al., *Ap. J.* 238 (1980) 471;
 - Trimble V., *Contemp. Phys.*, 19 (1988), 373;
 - Belli P. et al., *int. rep. INFN/AE-90/01* (1990).
- 2 - Smith P.F. and Lewin J.D., *Phys. Rep.* 187 (1990), 203;
 - Ellis J., "Experimental constraints on dark matter", Nobel Symposium on Early Cosmology, Graftavallen, Sweden, June 1990. Preprint CERN-TH 5822/90;
 - Spiro M., talk given to Neutrino Telescope Conference, Venice mar. 1991.

- 3 - Goodman M.W. and Witten E., Phys. Rev., D31 (1985) 3059.
- 4 - Spiro M., "Detection of dark matter", 25th Int. Conf. on High Energy Physics, Singapore, 1990. Saclay preprint 90-10.
- 5 - Caldwell D.O. et al., Phys. Rev. Lett., 65 (1990) 1305.
- 6 - Reusser D. et al., Phys. Lett., B255 (1991) 143;
- Caldwell D.O. et al., Phys. Rev. Lett., 61 (1988) 510;
- Ahlen S.P. et al., Phys. Lett. B195 (1987) 603.
- 7 - Tao C., pre-print DPhPE 89-02 (1989).
- 8 - Gerbier G., Proc. Rencontres de Moriond, Les Arcs jan. 1990.
- 9 - Belli P. et al., Rencontres de Moriond, Les Arcs mar. 1990.
- 10 - Kaplan J. et al., "A critical look at Cosmions", PAR-LPTHE 90-38/DPHPE 90-15, Sept. 1990.
- 11 - Belli P. et al., Nuovo Cim. 103A (1990) 767;
- Bacci C. et al., Proc. Vulcano Workshop, may 1990, to be published on Nuovo Cim.
- 12 - Barabanov I.R. et al., Nucl. Instr. and Meth. A254 (1987) 355;
- Incicchitti A. et al., Nucl. Instr. and Meth. A289 (1990) 236;
- Belli P. et al., Nucl. Instr. and Meth. A299 (1990) 191;
- Belli P. et al., to be published on Nucl. Instr. and Meth.
- 13 - Lindhard J. et al., Mat. Fys. Medd. Dan. Vid. Selsk., 33 n°10 (1963).

LOW TEMPERATURE SUPERCONDUCTING DETECTORS FOR DARK MATTER AND SOLAR NEUTRINO EXPERIMENTS

R J Gaitskell, D J Goldie, N E Booth and G L Salmon

Department of Physics, University of Oxford
Nuclear Physics Laboratory, Keble Road, Oxford OX1 3RH, United Kingdom



We are developing Low Temperature Superconducting Detectors with the goal of improving on the energy thresholds and energy resolutions obtainable at present with existing detectors. Such detectors have important applications in particle physics experiments including dark matter searches and solar neutrino experiments. We have shown that series arrays of superconducting tunnel junctions (SASTJs) are superior to other low temperature detectors in their sensitivity to non-equilibrium signals arising from particle interactions within bulk absorbers. The performance of the SASTJs has been studied in conjunction with bulk particle absorbers of single crystal Si, InSb and a number of superconductors (including In, Nb and Pb).

Results indicate that a new generation of bulk particle detectors based on cryogenic techniques will make possible the construction of an indium based solar neutrino observatory capable of obtaining real time neutrino spectra at energies not accessible to current experiments, and will also allow dark matter searches at recoil thresholds some two orders of magnitude lower than existing experiments.

Introduction

Cryogenic detectors allow in principle the tailoring of absorber materials to match the particle physics goals. For superconducting absorbers the energy required to break a Cooper pair and create two excess quasiparticles is only ~ 1 meV compared with ~ 1 eV energy gap in semiconductors. The excess quasiparticles can be detected with tunnel junctions directly, or by detection of the phonons emitted in the quasiparticle trapping process. For semiconductor absorbers one can detect the phonons produced copiously in the initial interaction provided the temperature is sufficiently low that the quiescent phonon population is small. A good detector of these phonons is a superconducting film where Cooper pairs are broken by the phonons. In Oxford we are exploring a variety of materials as large mass cryogenic particle detectors for the following experiments:

- | | | |
|-------|---|--------------------|
| (i) | solar neutrino detection based on Indium ¹⁾ | (In, InSb), |
| (ii) | dark matter searches ²⁾ | (Nb, Si, Al, LiF), |
| (iii) | neutrinoless $\beta\beta$ -decay search ³⁾ | (Mo, CdTe), |
| (iv) | 17 keV neutrino observation in β -decay ⁴⁾ | (Si). |

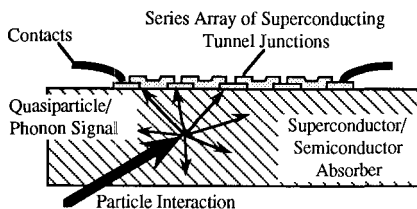
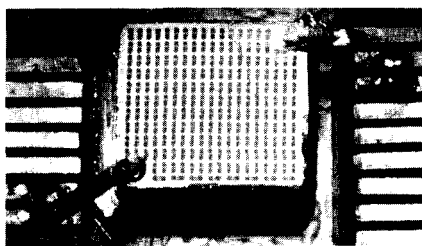


Fig.1. Photograph of SASTJ on single crystal absorber and schematic showing signal propagation from interaction

The pair breaking process by phonons can be detected with high sensitivity with a series-connected array of superconducting tunnel junctions (SASTJs) fabricated on the surface of the absorbers (Fig.1). These devices have outstanding low temperature performance and permit the simultaneous measurement of the time (< 100 ns) at which a particle interaction is detected and also a determination of the total energy deposited.

Absorber	Mass	Radiation Energy (E)	Resolution FWHM (ΔE)
Si ⁵⁾	0.2 g	x-ray 25 keV	700 eV
Nb	3.0 g	alpha 6 MeV	250 keV (phonon signal only)
InSb	2.0 g	x-ray 60 keV	2.5 keV

The table above summarizes the performance of a number of recently constructed detectors. In all cases the signals from the gamma or alpha interactions demonstrated position dependence. However, the quoted energy resolutions represent realistic values for interactions throughout the bulk of the absorber. Importantly these results were achieved at 360 mK well above the optimum and widely used temperatures for such large mass cryogenic detectors.

Single Crystal Silicon Absorbers (Mass: 0.2g - 1.0g)

Figure 2 shows typical voltage pulses from a SASTJ on the surface of a Si crystal irradiated by 60 keV gamma rays giving interactions distributed throughout the crystal. The signal is due to phonons propagating within the Si and has two distinct parts. The leading edge of the pulse carries detailed position and timing information about the interaction. By using two arrays we have established that this leading edge propagates quasidiffusively. Its amplitude is larger in higher purity crystals. This early signal is followed by a longer lived reverberation signal which contains some 95% of the total energy observed. The later signal is position independent and corresponds to long-lived phonons rebounding around the crystal (with a characteristic lifetime of 600 μ s). Time integration of this signal gives a signal proportional to the energy deposited by the particle. A spectrum obtained for 25 keV x-rays is shown in Fig.3. The 700 eV FWHM was limited by electronic noise and temperature drift in the cryostat.

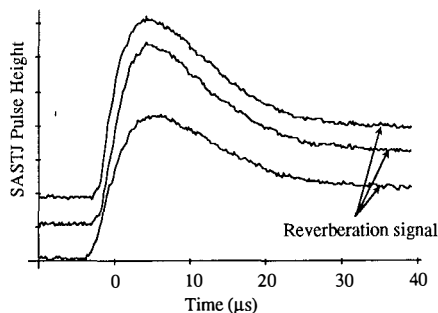


Fig.2. Pulses from the SASTJ due to 60 keV gamma ray interactions in a 0.2 g Si absorber.

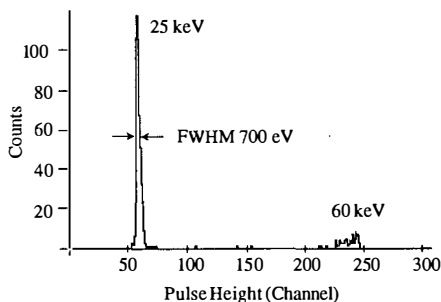


Fig.3. Spectrum obtained from the SASTJ for 25 keV x-rays (and a few 60 keV γ -rays) in a 0.2 g Si absorber

Single Crystal Superconducting Niobium Absorber (Mass: 3g)

The interaction of a particle within Nb generates both phonons and quasiparticles.^{6,7)} The phonons propagate diffusively with a characteristic diffusion length of the order of 100 μm . The phonon signal in a SASTJ on the surface of the crystal is strongly position dependent. The quasiparticle signal within the Nb is very long ($\sim 100\text{ms}$) due to the low quasiparticle recombination rate below 1K (Fig.4a) and contains some 90% of the observed energy from the interaction. The quasiparticle signal collection time can be significantly reduced through the mechanism of quasiparticle trapping as suggested by Booth.⁸⁾ An Al trap on the surface of a Nb crystal reduces this time to 70 μs in the example shown in Fig.4b. In contrast to the phonon signal, the trapped quasiparticle signal is position independent and yields a calorimetric measurement of the energy deposited by the original interaction. The fabrication of SASTJs, both above and away from a trap, on the surface of a larger Nb absorber would provide simultaneous position and energy information on an interaction. Figure 5 shows a comparison of the phonon signal amplitudes arriving in two separate arrays due to alpha particles interacting on the far side of the crystal in three localised regions. Crude triangulation of the phonon signal alone gives a detector energy resolution of 250 keV for 6 MeV alpha particles. In the same circumstances, but with a quasiparticle trap under the SASTJs, the signals would be position independent and an order of magnitude larger in amplitude, as indicated by the single point in Fig.5. The question of whether nuclear and electron recoils in the absorber yield different ratios of quasiparticles and phonons is being investigated.

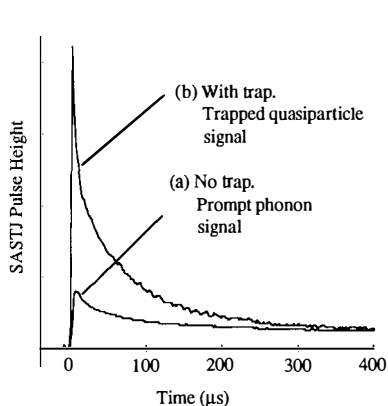


Fig.4. Signals from a SASTJ due to particle interactions in 3 g Nb single crystal.

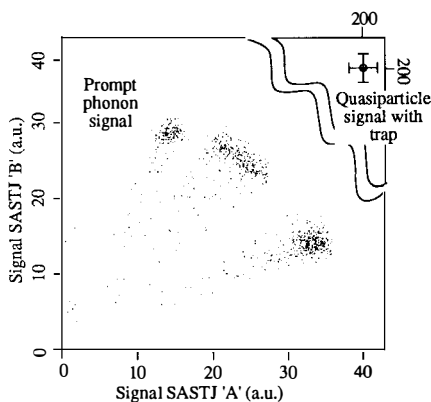


Fig.5. Signals from two SASTJs due to 6 MeV alpha particles incident at three regions of 3 g Nb single crystal.

Indium Absorbers (Mass: In 2g , InSb 2g)

The low energy electron neutrino flux from the Sun could be observed by its charged current weak interaction with the ^{115}In nucleus. This inverse β -decay has a very characteristic signature since the product Sn nucleus undergoes a delayed de-excitation ($\tau = 3.3\mu\text{s}$) emitting two gamma rays of energies 116 keV and 497 keV. The observation of this coincident signal along with that from the earlier emitted electron identifies a neutrino interaction and gives the neutrino energy for each event. A detector of a total mass of a few tonnes would provide a spectrum of solar neutrinos down to a threshold of 120 keV representing a significant advance on existing experiments. Our investigations of superconducting In have been motivated by the desire to realise such a detector. During this work it became apparent that, although diffuse laser excitation of the surface of an In single crystal absorber generates quasiparticles, the higher energy densities created by an alpha particle or gamma ray in the In apparently suppress the numbers of quasiparticles generated. The "Big Bang" model of particle interactions within superconductors developed by the authors sets out to explain the apparent differences between this result and that observed in Nb. This model makes a number of predictions about the suitability of other superconducting absorbers.⁷⁾

As an alternative we are investigating the semiconductor InSb as a bulk absorber, detecting the phonons generated from the particle interaction. Results show that this material works even better than the Si absorber. In high purity material the phonons propagate ballistically, accompanied by a longer reverberation signal which is partly due to the recombination of electron-hole pairs created in the initial interaction. Current devices already demonstrate an energy resolution of 2.5 keV for 60 keV gamma rays with a threshold of 10 keV and a linear response up to 0.5 MeV.

The Way Ahead

We have been successful in demonstrating good position and energy resolution in a number of absorbers of masses of a few grams. We have obtained a detailed understanding of non-equilibrium signal propagation and believe that our current results on detector performance are not limited by the underlying properties of the materials. We have established that the electronic signals available from SASTJs scale with the number of junctions. Improved signal-to-noise ratios will be obtained with increased numbers of junctions (currently only 200-400 junctions in series). Also the signal improvement expected by cooling from our current base temperature of 360 mK to 100 mK is up to 6 orders of magnitude. One short run at a lower temperature has already established that at least a 1000-fold improvement can be achieved. This should permit scaling from the 1 g regime to single absorbers of 1 kg. It is our belief that the potential detector performance we have outlined will make a new generation of particle physics experiments possible.

References

- 1) N E Booth, *Sci. Prog. Oxf.* **71** (1987) 563
- 2) J R Primack, B Sadoulet and D Seckel, *Ann. Rev. Nucl. Part. Sci.* **38** (1988) 751
- 3) A Barabash, *these proceedings*
- 4) J J Simpson, A Hime, *these proceedings*
- 5) D J Goldie, *International Workshop on Superconducting Tunnel Junctions for X-Ray Detection, Naples, Italy, 12-14 December 1990*, "Energy Resolved γ -Ray Detection using Tunnel Junction Arrays on Single Crystal Silicon"
- 6) R J Gaitskell, D J Goldie, N E Booth, C Patel and G L Salmon, *Physica B167* (1990), *Proceedings of the 19th International Conference on Low Temperature Physics, Brighton, Sussex 16-22 August 1990*
- 7) N E Booth, R J Gaitskell, D J Goldie, G L Salmon, *International Workshop on Superconducting Tunnel Junctions for X-Ray Detection, Naples, Italy, 12-14 December 1990*, "Single Crystal Superconductors as X-Ray Detectors"
- 8) D J Goldie, N E Booth, C Patel, G L Salmon, *Phys. Rev. Lett* **64** (1990) 954

THE MICROWAVE ENHANCED BOLOMETER

A.Tadsen, A.Haldemann, A.Paic,
D.Twerenbold, J.-L.Vuilleumier
Institut de Physique, Université de Neuchâtel
Rue A.-L. Breguet 1, 2000 Neuchâtel
Switzerland



Abstract

A new cryogenic detector is presented which consists of a bolometer crystal covered with a superconducting film exposed to a microwave flux. In this way the energy deposited by a particle in the crystal could be amplified linearly. Gains up to 10^4 may be obtained, making it possible to build a large volume detector with an excellent energy resolution.

Introduction

In recent years various developments have been pursued to build cryogenic detectors with high energy resolution and high energy sensitivity. For all these detectors optimal properties are achieved at low temperatures and small volumes while for physics applications like dark matter search or double beta decay, masses in the kg range are necessary.

One detector type is the bolometer, a crystal which is heated up by the incident particle. The temperature rise ΔT is proportional to the energy deposited E

$$\Delta T \sim \frac{E \Theta_D^3}{V T^3}$$

where Θ_D is the Debye temperature, V the volume and T the temperature of the crystal. The intrinsic energy resolution is given by the phonon fluctuations between the detector and the heat sink. An energy resolution of 17 eV for 6 keV X-rays has been achieved¹⁾ at a temperature of 80 mK but for a volume of only $4 \cdot 10^{-4} \text{mm}^3$. A group in Munich²⁾ reached a resolution of 1.2 % for a 6 MeV α -source with a bolometer of 280 g at 140 mK.

We propose³⁾ a large energy amplification scheme which could lead to excellent energy resolution at even higher masses.

The signal enhancement

In a bolometer, particles interacting with the crystal produce mainly nonthermal phonons. These phonons thermalize and lead to a measurable temperature rise. The microwave enhanced bolometer is again a crystal, but covered with a superconducting film. This film is irradiated with microwaves. The process of particle detection is then as follows: As in the case of a normal bolometer the incident radiation produces nonthermal phonons. These energetic phonons propagate into the superconducting film, break up Cooper pairs and produce excess quasiparticles, a highly efficient process which has been observed with superconducting tunneling junctions⁴⁾. The quasiparticles absorb microwaves and deexcite again, emitting thermal phonons leading to a temperature rise which can be measured as for any bolometer. The lifetime of the quasiparticles is of the order of $100 \mu\text{s}$ ⁵⁾ whereas the microwave absorption phonon emission is a nanosecond process, thus every quasiparticle can absorb many microwave photons, assuming its lifetime is not affected by this.

The energy needed to produce one quasiparticle is orders of magnitude lower than the microwave energy converted into thermal phonons by this single quasiparticle. The number of quasiparticles produced, and therefore the final temperature pulse, is proportional to the energy deposited in the crystal by the incident particle. The mechanism is similar to the principle of a transistor; a large energy flow from the microwaves to the crystal being controlled by a small number of quasiparticles. Without radiation the 'barrier' is closed because there are almost no quasiparticles; if a particle arrives excess quasiparticles are created, the 'barrier' opens and the energy can flow. For a given detector volume and temperature the energy deposited by the incident particle is amplified while the noise due to thermal fluctuations and electronic noise is unchanged, leading to a much better signal to noise ratio.

Calculations

The different processes leading to the amplification and the final temperature rise are all understood and can be calculated. This leads to a heat balance equation³⁾

$$\frac{dT}{dt} = \frac{1}{c_V V_b} [P_Q(t) + P_{bias} + P_{eq}] - \frac{T(t)^4 - T_0^4}{4 \tau_c T(t)^3}$$

where the first term describes the heating and the second the cooling of the bolometer. The cooling is approximated by the thermal coupling to the heat sink with temperature T_0 and time constant τ_c . The temperature rise is inversely proportional to the volume V_b and the specific heat c_V of the bolometer. $P_Q(t)$ is the microwave power absorbed by the excess quasiparticles and P_{bias} the heat dissipated by the thermistor. P_{eq} , the microwave power absorbed without incident particle is proportional to the microwave flux ϕ and depends on the residual resistance of the superconducting film R_{res} and the thermal quasiparticle density n_{qp}

$$P_{eq} \sim \phi \cdot [R_{res} + n_{qp}(T)]$$

In order not to absorb too many microwaves without particles the residual resistance has to be very low.

The signal S one obtains is proportional to the microwave flux, the quasiparticle lifetime τ_{qp} which is assumed to be unaffected by the absorption emission process and the number of quasiparticles created Q_0 which depends linearly on the energy deposited

$$S \sim \frac{\phi Q_0 \tau_{qp}}{c_V}$$

Contributing to the noise of the system are phonon fluctuations and electronic noise—both present without microwaves—which limit the energy sensitivity. In the limit of large amplification the FWHM energy resolution ΔE is limited by fluctuations in the number of quasiparticles created which lead to fluctuations in the gain;

$$\Delta E \sim \Delta \text{gain} \sim \Delta Q_0 = 2.35 \sqrt{f E \Delta}$$

where f is the Fano factor ($f \leq 1$) and Δ the superconducting gap (of the order of 1 meV). For 6 keV energy deposition one gets a resolution of about 6 eV (assuming $f = 1$).

As superconductors reflect nearly 100 % of incident microwaves a high microwave flux of the order of 10^5 W/cm^2 is needed to get enough photons absorbed by the quasiparticles. This can only be obtained by making the detector part of a resonant cavity with a high Q-value. The Q-value is the ratio of the energy stored in the cavity to the power loss per cycle and is limited by the surface resistance of the cavity. Values larger than 10^{12} have been obtained⁶⁾ for niobium cavities at 1.4 K. A technical problem will be to produce superconducting films with sufficiently low residual resistance not to decrease these values.

A possible detector and its performance

Fig. 1 shows what a detector scheme may look like; a germanium crystal of 1000 cm^3 is surrounded by four microwave cavities. Two different superconducting films are used to improve performance, the outer thinner one exposed to the microwaves has a lower energy gap than the inner thicker one. In this way the quasiparticles produced end up in the outer

film by quasiparticle trapping⁷⁾. As this film is thin the microwaves can penetrate into it and 'reach' all quasiparticles to excite them while the thicker inner film prevents transmission of microwaves directly into the crystal.

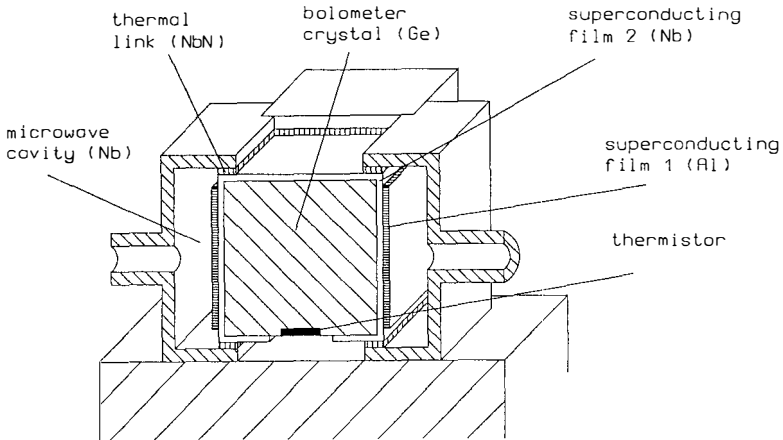


Figure I: A possible detector scheme

The calculated energy sensitivity of this detector operated at 100 mK is less than 10 eV for a Q value of 10^{12} . The energy resolution for 1 MeV deposited energy is 31 eV, limited by gain fluctuation.

Conclusions

With the presented energy amplification mechanism a new bolometer type can be built with the same intrinsic high energy resolution as other cryogenic detectors but for larger volumes and operating at higher temperatures. The relatively free choice of materials would make it possible to use this device for dark matter search or double beta decay where in the latter case the candidate material itself may form the crystal. Applications for coherent neutrino nucleon scattering or X-ray astrophysics are also possible.

A small prototype is now being built and tested at the University of Neuchâtel with the aim to prove the amplification process and the feasibility of this detector type.

References

1. D.McCammon et al., Jpn. J. Appl. Phys. 26, (1987) suppl. 26-3
2. W.Seidel et al., Phys. Lett. B236, (1990) 483
3. D.Twerenbold, Physica C 168, (1990) 381
4. Y.de Coulon, D.Twerenbold and J.-L.Vuilleumier, NIM A294, (1990) 259
5. D.Twerenbold, Phys. Rev. B34, (1986) 7748
6. N.Klein et al., IEEE Trans. Mag., MAG-25, (1989) 1362
7. H.Kraus et al., Phys. Lett. B231, (1989) 195

WIMPs AND COSMOLOGY, UNITARITY AND EXPERIMENT

Kimmo Kainulainen

Nordita, Blegdamsvej 17, DK-2100 Copenhagen Ø, Denmark

Abstract

I study the limits which cosmology, unitarity considerations and experiments impose on heavy WIMPs with an effective neutral current coupling constant g' or with a new $U(1)'$ -interaction. It is shown that their masses are restricted from the above as well as from the below. There are also absolute lower limits of $4 \times 10^{-5}g$ and $6 \times 10^{-5}g$ on the couplings of Dirac and Majorana neutrinos, respectively. In the experimentally interesting region $m_N \simeq \mathcal{O}(100)$ GeV I find a stringent bound $g' \gtrsim 0.1g$. In $U(1)'$ models cosmology implies an upper limit of about 1 TeV on the Z' and on the WIMP masses, but only in the absence of Z - Z' mixing.

Any massive particle species N , with no appreciable initial asymmetry and with a lifetime that exceeds the age of the Universe, contributes to the present energy density of the Universe a fraction which is inversely proportional to the temperature averaged annihilation cross section for $N\bar{N} \rightarrow X$ 1,2)

$$(\Omega h_0^2)_N \sim \frac{1}{\langle v_{\text{rel}} \sigma \rangle_f}. \quad (1)$$

Here the subscript f refers to the fact that $\langle v_{\text{rel}} \sigma \rangle_f$ is calculated at the 'freeze-out' temperature, where the N -distribution drops from the chemical equilibrium; typically $T_f/m_N \simeq 1/20$. Observations restrict the total energy density of the Universe to $\Omega h_0^2 \lesssim 1$ 3) which then sets an lower bound on $\langle v_{\text{rel}} \sigma \rangle_f$, or on the allowed range of the interaction strength of the species N . The precise value of the bound on $\langle v_{\text{rel}} \sigma \rangle_f$ depends slightly on the details of the model at hand, and e.g. in the case of a Dirac neutrino annihilating dominantly in the s-wave it is $\langle v_{\text{rel}} \sigma \rangle_f \gtrsim 3 \times 10^{-4} \text{ TeV}^{-2}$.

At the freeze-out temperature WIMP:s annihilate practically at rest and hence the cross section is dominated by the lowest allowed partial wave. It is then possible to impose an upper bound on $\langle v_{\text{rel}} \sigma \rangle_f$ using the partial wave unitarity argument. That is, a particle species with a mass m_N must obey 4)

$$\langle v_{\text{rel}} \sigma \rangle_f < (v_{\text{rel}} \sigma_J)_{\text{max}} = \frac{4\pi(2J+1)}{m_N^2 v_{\text{rel}}^2}. \quad (2)$$

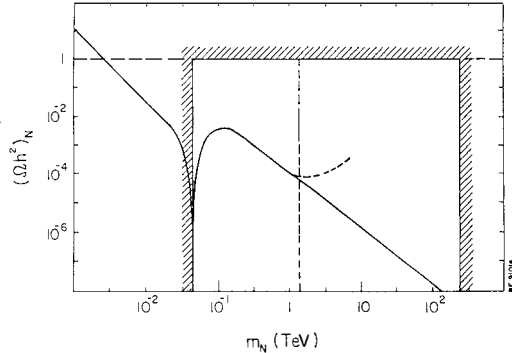
It is crucial that $(v_{\text{rel}} \sigma_J)_{\text{max}}$ for a given J depends only on m_N^{-2} , whence Eq. (2), when combined with the lower limit on $\langle v_{\text{rel}} \sigma \rangle_f$ imposed by cosmology, leads to an almost model independent upper limit on the mass of a generic WIMP-species N . Indeed, it was found in ref. 4 that a Dirac neutrino annihilating in the s-wave must obey $m_N \lesssim 240 \text{ TeV}$. Note however that if $\langle v_{\text{rel}} \sigma \rangle_f$ is dominantly in J th wave with $J \neq 0$, the limit becomes weaker by a factor $\sqrt{2J+1}$ 2). It should also be stressed that these considerations neither assume nor tell anything about the internal consistency of the theory.

Of course the violation of unitarity alone is not sufficient to exclude a given particle species as a dark matter candidate, but it casts doubt to the existence of such WIMPs as elementary particles. Unitarity is also a useful tool when one considers some effective theory giving a candidate for dark matter, as one can use it to check the range of validity of the (perturbative) cross sections and hence of the calculated relic density.

I will now apply these general ideas to some particular models. As an example I will first discuss the case of a standard model 4:th family heavy Dirac neutrino. The $(\Omega h_0^2)_N(m_N)$ -plot shown in Fig. 1 displays a distinctive drop at $m_N \simeq M_Z/2$ due to strong annihilation at the Z-peak and a monotonous decrease above the W^+W^- -threshold, which is due to annihilation into longitudinal W-bosons 5). At first sight there seems to be no cosmological upper bound on the mass of such a neutrino. However, the relevant cross section into the W^+W^- -final state increases

like $\sim m_N^2$ and as such is bound to violate the unitarity at some mass scale; one can show 2) that in the Dirac case this happens if $m_N \gtrsim 1.5$ TeV (3.2 TeV in the Majorana-case). As explained above, we cannot trust the calculated relic density above that limit but neither can we discard the species as a dark matter candidate on the basis of cosmological considerations except when the mass m_N exceeds the general unitarity limit of 240 TeV (400 TeV in the Majorana case 2)).

Figure 1. Relic abundance $(\Omega h_0^2)_N$ in the case of a standard model 4th family Dirac neutrino. Shown is the excluded region due to LEP-experiment, constraint $\Omega h_0^2 \lesssim 1$ and the general unitarity bound $m_N \lesssim 240$ TeV. Also shown is the limit above which cross section violates unitarity (dashed line).



Next I will study a standard model singlet WIMP, which however has a superweak coupling $g' < g$ to the standard model and no other low energy interactions. Such a coupling can arise because of mixing between gauge bosons or because of mixing between WIMPs themselves, and actually it suffices to assume that the WIMP has an effective coupling to the Z-boson only. I will again restrict myself to the Dirac case, the Majorana case is studied in ref. 2. The annihilation cross section of such a WIMP is simply given by $\langle v_{\text{rel}} \sigma \rangle \simeq (g'/g)^2 \langle v_{\text{rel}} \sigma \rangle_{\text{f,SM}}$ and especially above the W^+W^- -threshold one has 2)

$$\langle v_{\text{rel}} \sigma \rangle_{\text{D}} \simeq \left(\frac{g'}{g}\right)^2 \frac{G_{\text{F}}^2 m_N^2}{8\pi}. \quad (3)$$

Also the unitarity limit scales as a function of the coupling:

$$m_N \lesssim 1.5 \left(\frac{g}{g'}\right)^{\frac{1}{2}} \text{ TeV}. \quad (4)$$

I have plotted the cosmologically excluded $(\Omega h_0^2)_N \gtrsim 1$ region in $(g'/g, m_N)$ -plane in Fig. (2a). I have also plotted the unitarity limit, above which the tree level cross sections become unreliable and I also display for comparison the germanium detector data 6) and LEP-data 7) which shows the experimentally excluded region. One should note that there is an absolute lower limit for the coupling $g'/g \gtrsim 4 \times 10^{-5}$ (6×10^{-5} in the Majorana case) and that around $m_N \simeq \mathcal{O}(100)$ GeV there is a suprisingly stringent bound of $g'/g \gtrsim 0.1$, which might be in the reach of the future dark matter experiments.

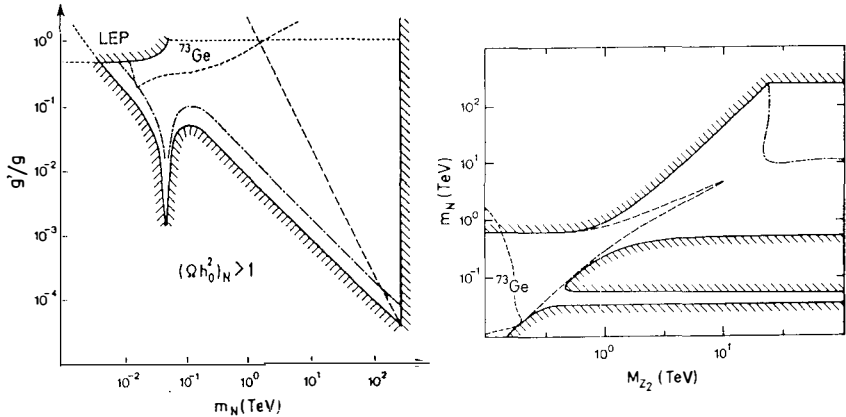


Figure 2. (a) Allowed region in the $(m_N, g'/g)$ -space. Shown is also the closure density-curve (dash-dotted curve) and the unitarity limit (dashed line). (b) Allowed region in the $(m_N, M_{Z'})$ -space. Here $\theta_{\text{mix}} \equiv 0.02$ in accordance with the latest LEP-limit 9). Dashed line corresponds to $\theta_{\text{mix}} = 0$. Also shown is the unitarity limit (dash-dotted curve).

Finally I will consider E_6 -based $U(1)$ -models 8); more specifically the "model A", where E_6 is directly broken to a rank five subgroup. The qualitative features remain the same in all different E_6 -models. Here the coupling-strength is fixed to $\bar{g} = g\sqrt{5/3} \tan \theta_W \sim 0.46$ but we have a new low energy interaction. The details of the calculations are given in ref. 2. It turns out, as is shown in Fig. 2b, that even a small mixing between the ordinary Z and the new Z' leads to significant change in predictions because the allowed parameter-space (see Fig. 2b) in the $(m_N, M_{Z'})$ -plane opens up in contradistinction to the $\theta_{\text{mix}} = 0$ -case, where the allowed region is closed and one actually would obtain an upper bound on the Z' -mass.

References

- 1) G. Steigman, *Ann. Rev. Nucl. Part. Sci.* **29** (1979) 313; K. Griest and D. Seckel, *Nucl. Phys.* **B283** (1987) 681; K. Enqvist, K. Kainulainen and J. Maalampi, *Nucl. Phys.* **B316** (1989) 456.
- 2) K. Enqvist and K. Kainulainen, preprint NORDITA-90/79 P.
- 3) A. Sandage and G.A. Tamman in *Inner Space/Outer Space*, eds. E. Kolb et al., (University of Chicago Press) 1986, p. 41.
- 4) K. Griest and M. Kamionkowski, *Phys. Rev. Lett.* **64** (1990) 615.
- 5) K. Enqvist, K. Kainulainen and J. Maalampi, *Nucl. Phys.* **B317** (1988) 647.
- 6) D.O. Caldwell et al., *Phys. Rev. Lett.* **61** (1988) 510; D.O. Caldwell, priv. comm.
- 7) J. Ellis and D.N. Schramm, CERN preprint TH-5705/90 (1990).
- 8) For a review, see. J. Hewett and T. Rizzo, *Phys. Rep.* **183** (1989) 193.
- 9) A. Chiappinelli, LAPP preprint LAPP-TH-327/91 (1991).

ORIGIN AND NATURE OF COSMIC RAYS
AND FIRST RESULTS FROM HEGRA

Hinrich Meyer
University of Wuppertal
Germany

Abstract: In part 1 a brief review of basic facts on the origin and the nature of cosmic rays is given for the energy range from 1 GeV to 10^{11} GeV. It is argued that our knowledge on the most interesting questions on cosmic rays is very limited. Recently new experimental attempts are made to detect the photon component of the cosmic rays and to measure the chemical composition of the charged nucleonic part of cosmic rays. One such experiment is described in part 2 of this paper where the status of HEGRA is reviewed an air shower array at La Palma Canary Islands that aims for the detection of photons, protons and heavier nuclei in the energy range from 10^3 GeV to 10^7 GeV. First results on the performance of HEGRA and the searches for photons from point sources are given. The array will be upgraded in the near future as discussed at the end of this report.

Introductory remark.

The organizers of this meeting have asked me to give a short introduction to the field of cosmic ray experiments at very high energy. It was planned that this talk would be given by Jordan Goodman, Maryland who was however unable to come due to concerns with the safety of airtravel these days. I tried to do it on short notice. The material presented can be found in part I of this paper. Secondly, in part II the status and future development of the airshower experiment HEGRA is given and some of the preliminary results on searches for point sources of cosmic rays.

I. 1 Energy spectrum and particle composition of primary cosmic rays.

The energy spectrum of cosmic ray particles considered here extends from the GeV region where the earth magnetic field and the local environment of the solar system have strong influence up to about 10^{11} GeV an energy high enough that the structure of our galaxy loses influence and the interaction of protons with the cosmological photon background is an important consideration.

The all particle energy spectrum follows a power law $dN/dE \propto E^{-\alpha}$, with $\alpha=2.7$ up to $\sim 10^6$ GeV and $\alpha=3.1$ at higher energies. At the very end of the spectrum uncertainties are rather large due to small statistics and unknown systematics ¹⁾. At the lower end of the energy range considered here the relative abundance of nuclei in cosmic rays is rather well determined and is found to follow, at least up to Fe, the so called solar system abundance with notable exceptions for Li, Be, B and F, Sc, Ti, V, Cr, Mn that are more abundant in cosmic rays by several orders of magnitude, about 10^5 and 10^2 respectively ²⁾. This is readily explained as due to spallation of heavier nuclei in interactions with the interstellar medium, mostly protons during the effective lifetime of charged cosmic ray particles within our galaxy ³⁾. At higher energies $> 10^4$ GeV/nucleus, the relative abundance of nuclei heavier than carbon seems to become more important the data however from the JACEE experiment ⁴⁾ has still rather small statistics. Above an energy of 10^6 GeV where the spectral index changes to a value $\alpha=3.1$ nothing is known about the charge of the primary cosmic ray particles.

Electrons (and positrons) as primary particles in cosmic rays have been detected up to 3 10^3 GeV, ⁵⁾, and their spectrum falls off rather more steeply with $\alpha=3.2$ and a flux lower by a factor of 100 than the all particle flux at 10 GeV.

Primary photons have been detected by the satellite experiments SAS 2 ⁶⁾ and COSB ⁷⁾ up to energies of 5 GeV. The diffuse galactic flux seems to have a rather flat spectral shape with index $\alpha=2$ in the outer galaxy and $\alpha=2.4$ in the inner galaxy ⁸⁾ at a flux level of 10^{-4} below the flux of charged particles at 1 GeV. In case this trend would continue to higher energies, photons would become more abundant than electrons at $E > 10^{3-4}$ GeV.

Cosmic ray photons are most important for two of the basic questions of cosmic ray physics

- 1.) sites of C.R. acceleration
- 2.) distribution of C.R. in the galaxy

It would be of great interest to observe also primary neutrinos of cosmic rays however due to the very small reaction crosssection of neutrinos with matter this is not feasible with present experimental techniques. Only very strong point like sources of neutrinos can be detected the most spectacular example (and so far the only one) has been the recent observation of supernova SN1987A, but for about 10 sec only at a neutrino energy of about 10 MeV.

I. 2. Galactic Sources of photons

Photons can be produced in electromagnetic interactions, including Bremsstrahlung of electrons on electrons and nuclei, inverse Compton scattering of high energy electrons on photons, where most of the electron energy is transferred to the target photon and synchrotron radiation of electrons in the ambient magnetic fields. All these processes require electrons to be accelerated to very high energies. Hadronic interactions are also a possible source of high energy photons, the dominant process is neutral pion production and decay to two photons, other possible processes like production of other unstable particles that decay to photons are known (from the systematics of hadronic interactions studied in great detail at accelerators) to be of much less importance. Alongside with neutral pions charged pions are produced that decay to neutrinos and muons which in turn decay to neutrinos and electrons thus creating a muon (anti) neutrino and electron (anti) neutrino flux in the ratio of 2:1 and of intensity similar to photons from neutral pion decay.

At any given environment matter is neutral overall and therefore, if ionised, both electrons and protons (nuclei) will be accelerated by whatever mechanism is at work. In general electrons will finally have much less energy however, since electromagnetic energy loss processes are rather efficient in reducing electron energies, at very high energy then proton acceleration with neutral pion production is expected to be the dominant source of photons. The protons hit the matter in the region nearby the acceleration site, or further out the protons of interstellar matter. Atomic hydrogen can be quantitatively traced through 21 cm line mapping of the galaxy while the density of molecular hydrogen can be determined using the assumption of proportionality to carbonmonoxid (CO). This rather general picture is quantitatively succesfull as applied to the COSB data on the diffuse galactic photon flux under the assumption of a cosmic ray particle flux everywhere in the galaxy similar to the flux observed near earth ⁹).

Both SAS 2 and COSB resolved a few (about 10) galactic sources compatible with pointlike origin and only two associated with known astronomical objects (Vela and Crab ¹⁰). At higher energies only the Crab nebula has been observed ¹¹), other reports of observations,

like from X-ray binaries (HerX1 or CygX3) lack sufficient significance to be accepted as photon detections.

I. 3. Extragalactic photons

Reports on the detection of extragalactic photons are very sparse, SAS 2 may have seen a diffuse flux at energies of 10^{-1} GeV, a claim that could not be substantiated by COSB due to higher background at a more unfavorable orbit. COSB concentrated on observations alongside the galactic disk but may have seen the quasar 3C273 at an observation at higher galactic latitudes¹²⁾. On this matter new information is expected soon, since the gamma ray observatory GRO has just been successfully launched.

The prospects of observing extragalactic photons at very high energies, much above the range accessible to GRO is however restricted to energies less than 10^5 GeV. Above this energy the absorption length of photons due to electron positron pair production on the ubiquitous 3^0 K background photons is about 7 kpc¹³⁾ comparable to galactic scales and much shorter than distances to extragalactic objects. On the other hand observing this cutoff on - say photons from M31 provides both a new method to determine astronomical distances and a proof that photons have been detected.

This same mechanism may be responsible for a cosmological photon flux at energies below 10^5 GeV originating from the proton cutoff due to photopionproduction at 10^{11} GeV. Assume protons have been accelerated to energies beyond 10^{11} GeV since galaxy formation in the early universe as a universal phenomenon. The energy lost to pions at $E > 10^{11}$ GeV is converted to photons and electrons that cascade down in energy through collisions with the 3^0 K background until below 10^5 GeV, where the universe becomes transparent to photons. This photon flux has been estimated recently and may reach the level of $5 \cdot 10^{-5}$ of the all particle flux¹⁴⁾. There is the possibility that this flux is virtually impossible to detect since it may be covered by the electron flux⁵⁾ that is also isotropic and photons and electrons detected as airshowers can not be distinguished at these energies. In any case only a rather narrow energy range from 10^4 - 10^5 GeV seems to be open for detection of this most interesting source of photons. The same mechanism may also enhance the photon flux from the direction of clusters of galaxies, like Virgo¹⁵⁾.

II. HEGRA

An overview of the status and some preliminary results from the HEGRA experiment will be presented in this second part of my talk. HEGRA is an airshower array still under construction by a collaboration from Hamburg, Kiel, Madrid, Munich, Nottingham, Wuppertal and Yerevan at the Canarian island La Palma. Nevertheless, parts of the installation takes data continuously and results on the performance of the array and limits of photon fluxes from some of the prominent sources can be given.

II. 1. Goals of HEGRA

The array is designed to

- a) find a photon signal from the well-established source of the Crab nebula
- b) detect the diffuse flux of photons from the galactic disk
- c) determine the mas distribution of charged primary cosmic rays

in the energy range from $\sim 10^4$ GeV to 10^7 GeV. Beyond those well defined aims the experiment should be capable to find more point like sources then just the Crab. In particular sources identified at energies of ~ 1 GeV by COSB (and future new sources to be detected by GRO) are an obvious target for HEGRA. As a more spectacular goal I would consider the discovery of a source visible only at energies $> 10^4$ GeV!

II. 2. Site and Experiment

The experiment is located at the astronomical site of the *observatorio del Roque de los Muchachos* at the Canarian island La Palma, at an elevation of 2200 m a.s.l. and usually well above the passat clouds that stay below 1800 m. The geographical coordinates are $18,1^\circ$ west and 28.8° north. At present ~ 190 counter stations are installed on a regular 15 meter grid with in an area of 180×195 m². Each station consist of a scintillator 3 - 5 cm thick and ~ 1 m², viewed from below by two PMT's to determine time and amplitude of particle signals from airshowers. All stations are covered with lead sheets of 1 r.l. thickness. This simple procedure considerably improves ($\sim 40\%$) the precision of the directional reconstruction of the airshowers on the basis of the arrival times at the counters. It is mainly due to photons converted to e^+e^- pairs, since photons form a more precise time front of the airshowers.

The array was started in summer 1988 with 37 counters from the Kiel group¹⁶⁾ and later extended by the groups from Munich and Madrid to the present size. The array is triggered on a very simple multiplicity requirement, e.g. 7 or more stations fired in the whole array at a rate of a few Hz. All information on showers is logged via a MAC SE to a worm optical disk. Offline analysis is presently performed in Munich. About 80 Million triggers have been recorded. Well over 99% are due to airshowers with an energy threshold at about $5 \cdot 10^4$ GeV. The acceptance for airshowers in terms of celestial coordinates is almost uniform in RA (the plane of the array is slightly inclined with horizontal) and a gaussian in declination centered a 29° and with a FWHM of 53° . The shower front for most of the data is found to be of conical shape with a slope of ~ 14 nsec/100 m. The angular resolution is $< 1^\circ$ for most of the showers and improves with shower energy (number of stations) to about 0.3° at the higer energy end.

The absolut pointing of the array as well as the angular resolution was checked by searches for the shadow of moon and sun that both should completely absorb particles incident from their direction. We find as a preliminary result a reduction in flux due to moon and sun an absorption of about 20% at a significance level $> 3.5 \sigma$. This is well consistant with our Monte

Carlo estimates of the angular resolution and constitutes a proof of a much improved performance of HEGRA over previous arrays.

II. 3. Results

The results reported here are preliminary in nature to the extent that our full data set in conjunction with a more refined analysis will certainly result in considerable improvements. A search was made for an excess flux of airshowers from preselected locations in the sky. The procedure is simply to compare the number of showers in a bin size of $3^{\circ} \times 3^{\circ}$ centered at the possible source with the predicted number of showers from the bins shifted in RA but at the same declination. No excess has been observed. The data cover the range from 5.8.89 till 13.8.90; $2.2 \cdot 10^7$ event are used, for an effective lifetime of 218 days. Limits for fluxes are given at 90% c.l. at an estimated energy threshold of $7 \cdot 10^4$ GeV and for an effective detection area of 13000 m^2 (table 1).

Table 1: Flux limits of a steady excess of airshowers from some possible sources that were claimed to show excess fluxes in some earlier reports.

Object	Flux Limit ($\text{cm}^{-2} \text{ sec}^{-1}$)
Cygnus X3	$3.8 \cdot 10^{-13}$
Cygnus X1	$3.6 \cdot 10^{-13}$
Her X1	$5.0 \cdot 10^{-13}$
Crab	$4.3 \cdot 10^{-13}$
PSR 1937+21	$5.3 \cdot 10^{-13}$
PSR 1953+29	$5.4 \cdot 10^{-13}$
M31	$4.3 \cdot 10^{-13}$
Geminga	$5.8 \cdot 10^{-13}$

For the much discussed source Cyg X3 the present flux limits are more than an order of magnitude below earlier observations, either Cyg X3 has been dormant in 1989 - 1990 or the reported fluxes were just fluctuations whose significance was overinterpreted. For the Crab the present sensitivity is not good enough to reach the flux levels at $E > 10^4$ GeV predicted on the basis of extrapolations from the Whipple results at 10^3 GeV. No attempt was yet made to see an excess of flux from the galactic disk, the statistics of our data however is not sufficient by at least an order of magnitude to have a real chance to see a photon flux at the level of 10^{-3} of the cosmic ray flux.

II. 4. Extensions of the HEGRA

We plan to install more detectors inside the limits of the present array ($\sim 200 \times 200 \text{ m}^2$) in the very near future. The aim is an identification of the nature of the primary particle, in particular photons and heavier nuclei on the basis of muon detection..

II. 5 Lower threshold

We consider it of great importance to lower the trigger threshold of HEGRA at least for part of the area. Therefore 50 stations will be added to the array in the central part covering about 10^4 m^2 effective area. This primarily improves the angular resolution of lower energy showers. The trigger threshold could have been lowered already now by requiring ≥ 4 stations, however the determination of shower directions would be too poor. A lower threshold will also increase the trigger rate and therefore the statistics of our data samples by about an order of magnitude. This can no longer be handled with the present online system. A new setup will therefore consist of Fastbus modules with an online computer based on a microprocessor. We hope to finish this part of the HEGRA extension this year.

II. 6. Muon counting

Muons will be identified in a 6 layer sandwich type structure based on lead sheets as absorbers and 6 meter long Geigertubes to track muons. The Geigercounters are taken from the FREJUS proton decay experiment that finished running Sep. '88. A total area of about 600 m^2 will be covered this way and the muon energy threshold is at about 0.5 GeV .

II. 7. Cerenkov light detection

We are going to build two rather different sets of detectors to record the Cerenkov light emitted by (mostly) the electrons in the airshowers. Firstly an array of $7 \times 7 = 49$ PMT's with 30 m grid spacing will be installed inside the HEGRA area. Each station will have one PM hemispherical in shape with 20 cm in diameter to collect the night sky light through a conical mirror with a half angle acceptance of 35° . The PM's have only seven stages followed by a fast amplifier to register the extremely fast (few nsec) Cerenkov light pulse from airshowers on top of a rather high, but very uniform star light background. Tests carried out recently with specially designed PM's are very promising. We expect an ontime of the Cerenkov array of $\sim 17\%$ of total time due to the excellent viewing conditions at the observatorio del Roque de los Muchachos.

The primary aim with this array is twofold, an improved time resolution of the shower front as compared to the e.g. detection with the normal stations of the array resulting in a better angular resolution by a factor of 3 - 5. Secondly, the light distribution of the array can be used to discriminate photon induced showers from hadron induced ones.

Furthermore five imaging telescopes of about 3 meter diameter and with 19 60 cm diameter mirrors will be constructed. At the focal point a camera with 37 pixels of PM's will be installed. The 5 telescopes will be separated by 60 meters each inside the HEGRA array. Both imaging of showers and angular resolution based on timing will be used to identify photon sources. The first of the five telescopes will be installed by late summer this year.

The improvement program sketched here will give HEGRA unique capabilities to do very interesting physics in the regime of high energy astrophysics and possibly in the longer term future on particle physics as well.

Acknowledgements

It is a great pleasure to thank the organizers of MORIOND '91 for a most enjoyable meeting. Discussions with H. Daum, G. Fontaine and E. Lorenz have been most helpful on the matter presented here.

This work has been supported by the BMFT under 055WT82B.

References

1. For an excellent review see A.A. Watson, in Proc. of the 12th European Cosmic Ray Symposium Nottingham, July '90.
2. P. Meyer, *Naturwissenschaften* 77, 353 (1990).
3. S.P. Swordy et al. *Ap.J.* 349, 625 (1990).
4. Th.H. Burnett et al. *Ap. J.* 349, L25 (1990) see also S.P. Swardy et al. *Ap. J.* 349, 625 (1990) and J.M. Grunsfeld et al. *Ap. J.* 327, L31 (1988).
5. D. Müller and K. Tang, *Ap. J.* 312, 183 (1987) and Ref. therein.
6. C.E. Fichtel et al., *Ap. J.* 198, 163 (1975).
7. H. Bloemen, *Ann. Rev. Astron. Astrophys.* 27, 469 (1989).
8. H. Bloemen, *Ap. J.* 317, L15 (1987).
9. A.W. Strong et al. *Astron. Astrophys.* 207, 1 (1988) and Ref. 7.
10. H.A. Mayer-Haßelwander and G. Simpson MPE Preprint 136, December 1988 and also A.M.T. Pollock et al. to be published in *Astron. Astrophys.*
11. T.C. Weeks et al. *Ap. J.* 342, 379 (1989).
12. G.F. Bignami et al. *Astron. Astrophys.* 93, 71 (1981).
13. For an extended discussion see R.J. Protheroe, *Mon. Not. R. astr. Soc.* 221, 769 (1986)
14. F. Halzen et al. *Phys. Rev. D* 41, 342 (1990); J. Wdowczyk and A.W. Wolfendale *Ap. J.* 349, 35 (1990), V.S. Berezhinsky and V.A. Kudryavtsev *Ap. J.* 349, 620 (1990).
15. J. Wdowczyk and A.W. Wolfendale *J. Phys.* G16, 1399 (1990).
16. M. Samorski, to appear in the proc. of the ICRR Intern. Symp. Kofu/Japan, Nov. 1990.

A NEW AIR CERENKOV ARRAY DETECTOR FOR THE OBSERVATION OF EXTENDED AIR SHOWERS

E. Lorenz

Max Planck Institute for Physics and Astrophysics
Werner Heisenberg Institute
Föhringer Ring 6, D8000 Munich 40, FRG



ABSTRACT

A new detector concept for the observation of extended air showers (EAS) is presented. The detector consists of an array of wide angle open Cerenkov counters. The array will be sensitive up to 35° zenith angle and an energy above 20 TeV. The incident direction will be determined by fast timing with an angular resolution of better than 4 mrad. By combining the array with a scintillator matrix and muon counters we expect to achieve a γ /hadron separation between 50-500. The main aim of this detector will be the search for cosmic γ sources and diffuse γ production from the galactic mid plane. The detector will be installed on La Palma within the HEGRA experiment.

1. INTRODUCTION

Since a few years the interest in very high energy ($>10^{12}$ eV) cosmic ray particle studies is increasing. The interest spans from questions in particle physics to astrophysics and cosmology. At energies above 10^{12} eV the by primary particle induced showers can penetrate deeply into the atmosphere and can reach ground level. The most common methods of observation are the measurement of the charged particle density with a ground based scintillator matrix or the detection of Cerenkov radiation. Scintillator matrix detectors are sensitive 24 hours a day while the observation of Cerenkov light is restricted to clear and moonless nights. On the other hand, the Cerenkov light flash contains typically $>10^4$ more photons than particles in the shower tail. The study of the light pattern can provide information on the primary particle and the shower development high up in the atmosphere.

Charged hadrons, by far the most dominant fraction of the high energy cosmic radiation ($>99.9\%$), cannot be tracked back to sources due to deflections in the weak galactic magnetic fields. γ /hadron separation is therefore an important tool for the search for point sources. In the past the Cerenkov technique has been more and more refined in order to improve the γ /hadron separation. Recently the Whipple group¹⁾ succeeded to identify a TeV γ source in the Crab nebula by using a large air Cerenkov telescope and detailed analysis of the shower image. The disadvantage of air Cerenkov telescopes is their restriction to the observation of a single source at a time and the necessity to track the source. Our group intends to build a new variant of an air Cerenkov detector with large angular acceptance and combine it with the HEGRA¹ detector on La Palma. The new air Cerenkov detector consists basically of a large array of photomultipliers (pm) that view the night sky directly.

2. THE BASIC PROCESS

¹HEGRA is a large scintillator matrix detector set up on the Canary island La Palma (28.8° north, 17.8° west, 2200 mtr altitude). The matrix covers an area of 200×200 m². HEGRA is operated by a collaboration from the universities of Hamburg, Kiel, Madrid and Wuppertal and the Max Planck Institute, Munich. Presently HEGRA undergoes a large upgrade towards a 'cosmic ray facility' by adding muon trackers, 5 air Cerenkov telescopes, a large air Cerenkov matrix and novel track detectors.

While passing the atmosphere the fast charged particles of a shower emit Cerenkov radiation. The exponential change of the air density with altitude changes the Cerenkov threshold, the emission angle and the photon intensity/m with height. Above 10^{12} eV the Cerenkov light illuminates with measurable intensity a large area of > 100 m radius. Depending on the nature of the incident particle (γ, p, α, \dots heavy ion) one expects different pattern for the light distributions as a function of distance from the shower axis. Fig 1 shows Monte Carlo calculations for the radial light intensity (300-400 nm) for an incident γ and proton of 100 TeV. This difference, caused by the radial and longitudinal development of the showers might be an efficient tool for discrimination of primary particles. 100 TeV proton induced showers have in general a steeper radial slope close to the shower axis and a less pronounced shoulder in the intensity at around 100 mtr. At 50-100 m distance the difference in light is about a factor four for γ s and protons while the particle densities at 2200m height are nearly equal.

A multiple sampling of the light disc up to large radii should provide a powerful tool for γ/h discrimination once the data are combined with the scintillator matrix measurements.

The Monte Carlo simulations predict also a very sharp arrival time of the Cerenkov light flash. The leading cone has a slope of about 5 nsec/100m distance from the shower axis, e.g. is about a factor 3 flatter than the cone for the charged particles. Due to the large diameter of the light disc and its small time spread one can determine the incident particle direction with high precision when using a large array and time of flight measurements. In summary the observable light at ground level can provide information on the primary particle, the shower development and the incident energy.

3. THE AIR CERENKOV MATRIX

The proposed array consists of individual stations that are arranged in a 7x7 matrix with 30 mtr grid spacing. Its area matches closely the scintillator matrix of HEGRA. Later we intend to increase the area in order to sample the Cerenkov light disc up to 200 mtr radius. Fig 2 shows a cut through a detector station. Its central element is a 20 cm diameter hemispherical pm that views the night sky. In order to increase the light collection area the pm is surrounded by an aluminized Mylar cone. This cone increases the collection area by a factor four and limits the angular acceptance to up to 35° zenith angle

(≈ 1 sterad). The cone screens also the night sky light (NSL) background from large angles where only a few triggers from EAS are expected. The high NSL ($\approx 10^{12}$ photons/m²·sec·sr; 400-550 nm) has two implications:

- a) the NSL fluctuations will set the detection threshold
- b) the steady photon flux cannot be handled by a classic pm of a typical gain of $10^6 - 10^7$ because current dynode materials cannot handle the large DC current; furthermore the life time is severely shortened.

Therefore a new pm with only 5-6 stages and a chain of low noise, fast AC amplifiers will be used. The integrated NSL and the Cerenkov light have a different spectral dependence - increase with l vs $1/l^2$ -. We intend to use a blue filter (300-450 nm) which should reduce the NSL level by a factor 4 while the loss of Cerenkov light will be ≈ 20 %. The filter will considerably extend the pm life time and slightly improve the signal/noise (S/N).

The fast timing measuring system will be calibrated by LED light pulsers to be triggered over equal length cables. The pm gain will be monitored by a small plastic scintillator - Cs¹³⁷ combination. The entire detector is housed in a weather protection hut; the only moving part will be the cover to be opened during night. All huts are connected via low loss coax cables to the central electronic consisting of standard constant fraction discriminators, TDCs and ADCs. The trigger is generated by a simple majority logic in case the Cerenkov matrix is 'trigger master' or by the scintillator matrix.

4. EXPECTED PERFORMANCE

From Monte Carlo calculations and test measurements we predict an energy threshold of 20 TeV for incident vertical protons and 8 TeV for γ s, respectively. The angular resolution will be around 4 mrad at 50 TeV and will improve to 0.5 mrad at > 1 PeV. The angular resolution should be at least 5 times superior to the resolution of the scintillator array. The γ /hadron separation is difficult to estimate for this untested concept. The tools for γ /h separation are:

- a) comparison of the integral light intensity with the energy as determined from the scintillator matrix
- b) combination of these data with the information from the muon detectors
- c) analysis of the radial light structure

d) analysis of the temporal structure of the light flash; hadron showers should produce delayed light flashes.

By applying methods a and c we expect a conservative γ/h separation power of 50, while for harder cuts a factor of 500 might not be unrealistic. By adding method b we might reach separation factors of 10^3 to 10^4 , thus it might be possible to observe isotropic γ radiation from the galactic mid plane. Method d requires >350 Mhz Flash ADCs with large dynamic range.

5. SUMMARY AND OUTLOOK

A new configuration of an air Cerenkov matrix detector has been proposed. The matrix samples the Cerenkov light disc of EAS over a large area, thus allowing a good angular resolution, energy determination and, in combination with data from a scintillator- and muon detector array, a high γ /hadron separation. The detector has a ≈ 1000 fold increase in angular acceptance compared to Cerenkov telescopes with about a factor 10-50 higher energy threshold. The construction is relatively easy and incorporates no precision moving parts. The large diameter Cerenkov light disc allows one to use a rather coarse sampling, thus to build a very cost effective detector. The price for a 7×7 array has been estimated to be less than 0.5 million DM while the construction can easily be completed within one year. Very likely this concept is the most cost effective one for the construction of very large area detectors covering more than a km^2 area. A similar idea has been presented recently by Yakovlev²).

6. ACKNOWLEDGEMENTS

This detector concept has been proposed by a group of the University Complutense, Madrid (V. Fonseca, F. Arqueroz J. Piniero) and the Max Planck Institute (M. Bott-Bodenhausen, I. Holl, A. Karle, E. Lorenz, M. Merck, B. Retamaz, M. Rozanska); herewith I would like to thank my colleagues.

7. REFERENCES

- 1) T.C. Weeks et al., *Astrophys. Journal* **342** (1989) 379
- 2) V.I. Yakovlev: Project of the installation "VEGA-C" at Tien Shan Preprint 32, P.N. Lebedev Physical Institute, Moscow (1990)

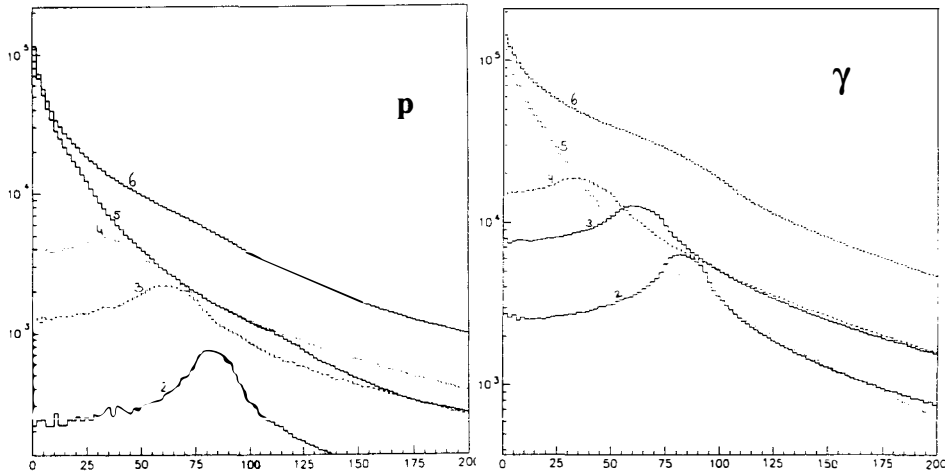


Fig 1: Monte Carlo simulation of Cerenkov light at detector level for an incident γ and proton of 100 TeV energy

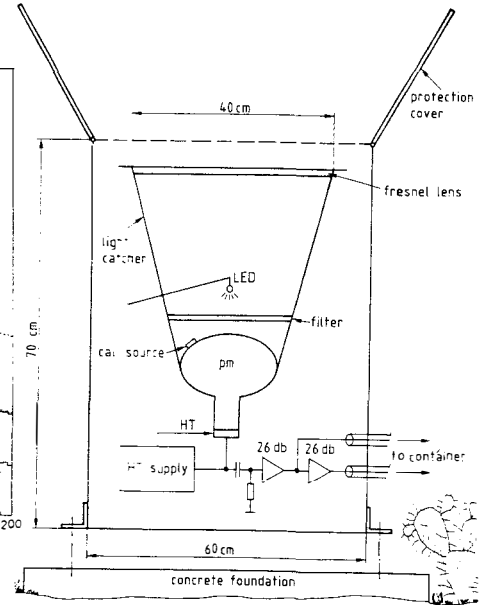


Fig 2 Cut through a detector station

THE EAS-TOP DETECTOR AT GRAN SASSO: RECENT RESULTS

M.Aglietta^{2,3)}, B.Alessandro³⁾, F.Arneodo^{1,3)}, L.Bergamasco^{1,3)}, C.Castagnoli^{2,3)}, A.Castellina^{2,3)}, C.Cattadori⁴⁾, A.Chiavassa^{1,3)}, G.Cini^{1,3)}, B.D'Ettorre Piazzoli^{2,3)}, W.Fulgione^{2,3)}, P.L.Ghia^{2,3)}, P.Galeotti^{1,3)}, G.Mannocchi^{2,3)}, C.Morello^{2,3)}, G.Navarra^{1,3)}, L.Riccati³⁾, O.Saavedra^{1,3)}, G.C.Trincherò^{2,3)}, P.Vallania^{2,3)}, S.Vernetto^{2,3)}

¹⁾ *Istituto di Fisica Generale dell' Università di Torino, Via Pietro Giuria 1, 10125 Torino, Italy*

²⁾ *Istituto di Cosmo-Geofisica del CNR, Corso Fiume 4, 10133 Torino, Italy*

³⁾ *Istituto Nazionale di Fisica Nucleare, Via Pietro Giuria 1, 10125 Torino, Italy*

⁴⁾ *Istituto Nazionale di Fisica Nucleare, Laboratorio Nazionale del Gran Sasso S.S. 17bis km 18+910, Assergi, Italy*

Presented by P.L. Ghia



ABSTRACT. The EAS-TOP extensive air shower array on top of the underground Gran Sasso Laboratory in central Italy is a multiparameter experiment for astrophysical studies. We present its main characteristics and the results obtained from 1989-1990 data, particularly in the field of γ -ray astronomy at energy > 200 TeV.

1. INTRODUCTION

The study of Extensive Air Showers is the main tool to obtain informations on cosmic rays at the highest energies ($E_0 > 100$ TeV).

The aims of such studies concern essentially:

- the primary energy spectrum and composition;
- the primary interactions (most interesting nucleus-nucleus);
- the anisotropies;
- the search for very and ultra high energy γ -ray point sources.

From the experimental point of view, such items are interconnected with each other through the problem of the identification of the primary particle: such information can be obtained by means of a systematic and complete study of the structure of the different components of EAS, and therefore multiparameter experiments are necessary.

The EAS-TOP detector at Gran Sasso has been planned to perform such studies from measurements of the EAS electrons, hadrons, Cerenkov light, radio emission, GeV and TeV muons (the last from the coincidences with the detectors operating in the Gran Sasso underground laboratory).

In this paper we will discuss the main characteristics of the EAS-TOP array as derived from almost two years of operation of the e.m. detector, and we will show some of the obtained results, with particular attention to the field of VHE energy γ -ray astronomy.

2. THE EXPERIMENT

The EAS-TOP array¹⁾ is located above the underground Gran Sasso Laboratory²⁾ (2005 m a.s.l., latitude $42^\circ 27'$ North, longitude $13^\circ 34'$ East). It consists of:

- a detector of the e.m. component (EMD)^{1,3,4)} of extensive air showers which has been fully operating since the beginning of 1989. It comprehends 29 modules of scintillation detectors, 10 m^2 each, spaced of 17 m at the centre of the array and 80 m at the edge, covering thus an area of $\approx 10^5 \text{ m}^2$ (see fig. 1).

All of them are equipped both for timing and particle density measurements. The scintillators are organized in ten subarrays of seven (or six) modules each

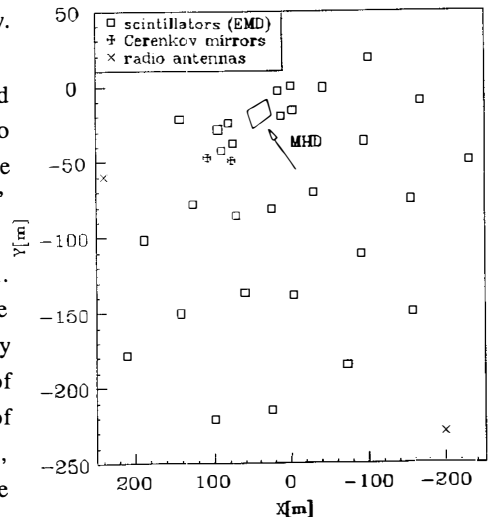


Fig. 1 - General layout of the EASTOP array.

and two subarrays of four modules, interconnected with each other. The air shower trigger is provided by a coincidence of any four adjacent modules. The trigger rate is ≈ 35 Hz and the energy threshold is $E_0 \approx 5 \cdot 10^{13}$ eV. A stable Rubidium clock, synchronized by the standard time provided by the Italian national broadcasting company, gives the absolute arrival time information with an uncertainty of ≈ 100 μ sec;

- a detector of the muonic and hadronic components of E.A.S. (MHD)^{5,6)} which is now in construction stage and will start operation during summer 1991. Located inside the scintillator array as shown in fig.1, it will consist of two modules with a total active area of ≈ 270 m². Each module (12 x 12 m²) is formed by 9 active planes interleaved by a 13 cm thick iron absorber. The total thickness is 7 nuclear absorption lengths corresponding to the calorimeter length $L(95\%)$ for 1 TeV hadrons. Each active plane consists of two streamer tube layers for muon tracking ($E_\mu > 2$ GeV) and one layer of proportional tubes for hadron calorimetry (up to TeV energies). Timing measurements will be performed by using a 20 m² scintillator layer placed at a depth of ≈ 200 g/cm²;

- a detector of E.A.S. atmospheric Cerenkov light pulses (C-TOP)⁷⁾ which is now in a test stage;

- a detector of radio-frequency pulses associated with E.A.S. (EAS-RADIO)⁸⁾ which has been fully operating since the beginning of 1990.

Moreover the array is designed to operate in coincidence with the muon detectors running in the underground Gran Sasso Laboratory²⁾ (3100 m w.e. depth, muon energy threshold at the surface $E_{th}=1.2$ TeV). First results in coincidence with the MACRO experiment have already been reported⁹⁾.

3. EVENTS RECONSTRUCTION.

In the following discussion we will only consider internal events ($\nu \approx 1.5$ Hz, $E_0 \approx 200$ TeV), for which the maximum number of particles has been detected by an inner module of E.M.D. Beside the arrival direction, for these extensive air showers the core location, size N_c , slope of lateral distribution function s can be obtained. Moreover, the EAS temporal structure can be studied: first result of a correlated analysis of the lateral distribution (namely the parameter s) and of the temporal one (i.e. the delay of the shower front with respect to a plane) are presented in ref. ¹⁰⁾

a) Arrival direction. Angular resolutions. The arrival direction is obtained from the times of flight technique by fitting a plane to the shower front. This procedure is justified since we use only the delay measurements performed by the detectors (five or six) hit by almost the same number of particles and at

roughly the same distance from the module which has detected the maximum particle density.

The angular resolution, the absolute pointing accuracy and its stability in time are main features of the array and have to be continuously checked. Different approaches are followed:

i) internal coherence of data, which is tested by the comparison between the two different arrival directions measured by two subsets of a subarray (three detectors each). Being σ_ψ the width of these differences distribution, $\sigma_\alpha = \sigma_\psi/2$ is the arrival direction error when all the detectors of the array are used. For average internal showers, σ_α is $\approx 0.8^\circ$ ($\approx 0.5^\circ$ when $N_e > 10^5$);

ii) comparison of the EAS measured arrival directions with those of the coincident muons recorded underground by the tracking system of MACRO detector (resolution $\Delta\theta < 0.6^\circ$). First results give, for the average values and widths of the two projections of such differences, $\Delta\theta_x = 0.04 \pm 0.10^\circ$ and $\Delta\theta_y = -0.20 \pm 0.12^\circ$, $\sigma_{\Delta x} = 1.0^\circ$ and $\sigma_{\Delta y} = 1.2^\circ$. Such widths are thus compatible with the combination of the two detectors angular resolutions and no systematic effects are seen at a level of $0.1 - 0.2^\circ$);

iii) search for the shadowing effect of sun and moon on the primary cosmic rays. If the detector resolution is comparable with the absorbers dimensions ($D_{\text{sun}} = D_{\text{moon}} \approx 0.5^\circ$), the effect of sun and moon absorption (which can be added, providing a "negative reference candle") can be detected, even in rather short observation times. The deficit in the number of counts from the astra (ON) with respect to two reference directions in the sky (<OFF>) is shown in fig. 2, as a function of the opening angle around the astra direction. These results have been obtained from the data taken since January to October 1990 (255 total number of days). The significance is 2.5 s.d. and the result is compatible with the quoted resolution, thus providing a proof of the array absolute pointing accuracy in the sky¹¹⁾.

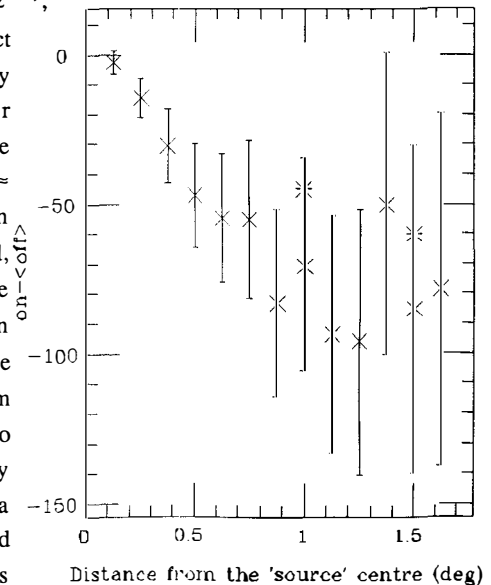


Fig. 2. Deficit of events inside an opening angle $\Delta\alpha$ from the sun-moon direction. Asterisks show expected values.

b) Core location, N_e and s . These parameters are obtained by means of a χ^2 fit to the measured particle densities by using the Nishimura-Kamata-Greisen function¹²⁾. The resolutions, derived from Montecarlo simulations, are $\Delta r \approx 5m$, $\Delta N_e/N_e \approx 20\%$, $\Delta s/s \approx 10\%$ at $N_e \approx 10^5$ particles.

4. VHE γ -RAY SOURCES ANALYSIS AND RESULTS.

To search for an excess of events from a possible source direction, the data are analyzed by using sky cells of dimension $\Delta\delta = \pm 1.5^\circ$ and $\Delta\alpha = \Delta\delta/\cos\delta$. The value $\Delta\delta$ is determined as 1.6 times the angular resolution in order to maximize the signal to noise ratio. The number of counts in the bin centered on the source (ON) is compared with the average number of counts ($\langle\text{OFF}\rangle$) from six bins located at the same declination but shifted in right ascension of $\pm 2K\Delta\alpha$ ($k=1,3$). Events with zenith angle $\theta < 40^\circ$ are used and days of operation in which all seven cells are observed from their rising to setting. The same procedure is adopted for the galactic plane by dividing the two observable branches into 19 longitude intervals. For some of the candidate sources (i.e. Crab Nebula and Cygnus X-3) a further analysis is performed, based on events with $N_e > 10^5$.

The presented database corresponds to 280 complete days and spans two intervals of time: since February 17th 1989 to June 2nd 1989 and since January 1st 1990 to October 15th 1990. The analysis with cuts in N_e has been performed on the database since January 1st 1990 to August 26th 1990, for Crab Nebula and Cygnus X-3 (180 complete days).

a) D.C. emission. Nine sources of interest plus the galactic plane have firstly been examined for any possible steady emission. The ON and OFF total counts are summarized in table 1 (data from Crab Nebula and Cygnus X-3 considering only showers with $N_e > 10^5$ are also included).

Table 1. Summary of total counts from ON source and background ($\langle\text{OFF}\rangle$) for all observed sources during 1989 and 1990.

SOURCE	EXP.[days]	N_{ev} ON	$\langle N_{ev} \text{OFF} \rangle$	SIGN.(s.d.)
Crab Nebula	280	12345	12240	0.9
Cygnus X-3	278	23199	23457	-1.6
Hercules X-1	287	21747	21749	-0.01
Geminga	281	9002	9001	0.01
Psr1953+29	285	17673	17591	0.6
4U0115+63	261	17083	17057	0.2
Psr1937+214	287	11967	12107	-1.2
M31	271	22804	23176	-2.3
Galactic Pl.	278	632211	633127	-1.1
Crab $N_e > 10^5$	181	2062	2053	0.2
Cyg. $N_e > 10^5$	179	3453	3380	1.2

None of the candidate sources nor the galactic disk show any evidence for long term statistically significant emission. Upper limits to the D.C. flux have thus been derived for all the sources and the galactic disk at 95% c. l.: $I_{\max}(>200 \text{ TeV}) < 1.1 \cdot 10^{-13} \text{ cm}^{-2} \text{ s}^{-1}$ ($< 2.3 \cdot 10^{-13} \text{ cm}^{-2} \text{ s}^{-1} \text{ rad}^{-1}$ for the whole galactic disk) and, at $E_0 > 400 \text{ TeV}$ for Crab Nebula and Cygnus X-3: $I_{\max} < 5.8 \cdot 10^{-14} \text{ cm}^{-2} \text{ s}^{-1}$. For what concerns the Crab Pulsar, the upper limit to emission within ± 0.5 msec around the main pulse is: $\Phi(>200 \text{ TeV}) < 1.7 \cdot 10^{-14} \text{ cm}^{-2} \text{ s}^{-1}$ (95% c.l.).

b) Sporadic emission. For each of the examined sources a search for transient emissions has been performed, calculating the daily significances S of the observed number of events [ON, ΣOFF_i , $i=1,6$] according to the Li & Ma statistics¹³⁾.

In fig. 3 we show such distribution for the Crab Nebula for the total period of observation compared to the expected one from pure statistical fluctuations. The good agreement between the measured and expected one and the absence of unexpected excesses (as for all candidate sources) indicates that no sporadic emission, at a level detectable by a single array, was seen during the examined period from any of the observed sources: an upper limit of less than 2.1 events/year with $\Phi(>200 \text{ TeV}) > 2.6 \cdot 10^{-12} \text{ cm}^{-2} \text{ s}^{-1}$ and duration $\Delta t \leq 5$ hours (95% c.l.) can be derived.

The same result is obtained for Crab Nebula and Cygnus X-3 considering only events with $N_e > 10^5$. These data confirm also that the array fluctuations are at poissonian level and therefore the Poisson statistics can be used.

Events of particular interest for a comparison with other experiments have been reported in ref. ¹⁴⁾.

c) Crab Nebula: the 23rd February 1989 event. A transient burst from the Crab Nebula has been observed by the EAS-TOP array in coincidence with the Baksan (URSS) and KGF (India) arrays^{15,16,17)}, on February 23rd, 1989, lasting at least since $\approx 13^{\text{h}}$ UT to $\approx 21^{\text{h}}$ UT. The combined chance probability for the excess to be seen on the same day by the three experiments is $\approx 10^{-7}$.

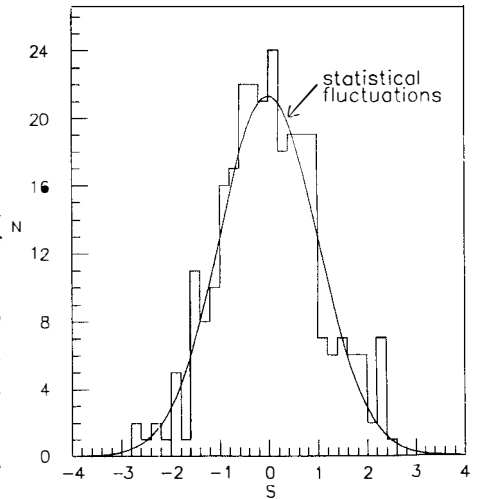


Fig. 3. Distribution of the daily significances S of the events observed from Crab Nebula (280 days)

Tab. 2. Comparison of the three observations by Baksan, KGF and EAS-TOP arrays, of the February 23rd 1989 event from the Crab Nebula.

ARRAY	LAT.	LONG.	CULM. (U.T.)	N _{ON}	<N _{OFF} >	EXC./ BCK	SIGN. SD	Ω (sr)
Baksan	43°N	43°E	16.5	57	31.1	0.83±0.27	4.4	6 · 10 ⁻³
KGF	12.95°N	78.3°E	14.1	35	17.8	0.97±0.35	4.1	1.5 · 10 ⁻²
EAS-TOP	42.45°N	13.57°E	18.4	38 403	25.5 378.3	0.49±0.20 0.07±0.06	2.3 1.2	3 · 10 ⁻³ 1. · 10 ⁻²

The three observations are compared in tab. 2; concerning the EAS-TOP data, the first line refers to the already quoted internal events while the second one to an independent trigger mode, sensitive to lower energy events with the core at the edge or outside the array. The combined probability for the EAS-TOP events to be simulated by statistical fluctuations is $\approx 10^{-2}$. The flux during the five hours of observations is estimated to be: $\Phi(>200 \text{ TeV}) = (2 \pm 1) 10^{-12} \text{ cm}^{-2} \text{ s}^{-1}$. Further characteristics of the EAS-TOP events are discussed in ref.¹⁷⁾.

REFERENCES.

- 1) M. Aglietta et al., *Il Nuovo Cimento*, **9C**, 262, 1986
- 2) E. Bellotti, *Nucl. Instrum. and Methods*, **A264**, 1, 1988
- 3) M. Aglietta et al., *Nucl. Instrum. and Methods*, **A277**, 23, 1989
- 4) M. Aglietta et al., *Il Nuovo Cimento*, **13C**, 353, 1990
- 5) M. Aglietta et al., *Proceedings of the 3rd National Cosmic Rays Conference*, St. Vincent, 1986
- 6,10,14) M. Aglietta et al., *Il Nuovo Cimento C*, 1991, in press
- 7) M. Aglietta et al., *Proc II Int. Workshop on Neutrino Telescopes*, 195, Venezia 1990
- 8) C. Castagnoli et al., *Il Nuovo Cimento C*, 1991, in press
- 9) MACRO and EAS-TOP collaborations, R. Bellotti et al., *Physical Review D*, **42**, 1396, 1990
- 11) M. Aglietta et al., *Proc. of the International Conference on High energy γ -ray astronomy*, Ann Arbor (USA), 1990, in press
- 12) K. Greisen, *Progress in Cosmic Rays Physics*, **3**, 1956
- 13) T.P. Li and Y.Q. Ma, *Astrophysical Journal*, **242**, 1257, 1983
- 15) V.V. Alexeenko et al., *Proceedings of the International Workshop on Very High Energy Gamma Ray Astronomy*, ed. by A.A. Stepanian, D.J. Fegan, M.F. Cawley, 137, 1989
- 16) B.S. Acharya et al., *Nature*, **347**, 364, 1990
- 17) M. Aglietta et al., *Europhysics Letters*, 1991, in press



TESTING THE MULTI-MIRROR ARRAY SHOWER DETECTION TECHNIQUE : STATUS OF THE THEMISTOCLE EXPERIMENT

G. Fontaine
Laboratoire de Physique Corpusculaire
Collège de France



Abstract

This experiment is testing the performance of a multi-mirror Cerenkov array technique for the detection of VHE/UHE gamma-ray point sources. It emphasizes geometrical criteria (e.g. the angular resolution) as an unbiased way of rejecting the isotropic hadronic background. The detector components and the calibration techniques are described, and their main characteristics are given as measured in the first months of operation of the experimental setup. The status of the observation program is presented at this stage of the ongoing analysis .

Collaboration :

LPC Collège de France (1), LPNHE Université de Paris VI-VII (2), LAL Université de Paris-Sud Orsay (3), Université de Perpignan (4)

P.Baillon * , L.Behr ** 3 , S.Danagoulian 3 , B.Dudelzak 3 , P.Eschstruth 3 , P.Espigat 1 , B.Fabre 4 , G.Fontaine 1 , R.George 2 , C.Ghesquière 1 , F.Kovacs 2 , C.Meynadier 4 , Y.Pons 2 , R.Riskalla 3 , M.Rivoal 2 , P.Roy 3 , P.Schune 1 , T.Socroun 2 , A.M.Touchard 2 , J.Vrana 1

* CERN, Geneva

** Ecole Polytechnique, Palaiseau

The name THEMISTOCLE stands for :

Tracking High Energy Muons In Showers Triggered On Cerenkov Light Emission.

This experiment is funded by the French CNRS-IN2P3 : Institut National de Physique Nucléaire et de Physique des Particules.

1 Physics Objectives and Detection Philosophy

The ultimate aim of this experiment [1,2] is to use VHE/UHE cosmic beams to probe particle physics beyond the Standard Model, by the exploration of an energy range extending from 0.1 to 5 TeV in the center of mass at the constituent level. To achieve this goal, one has to avoid the difficulties of traditional hadronic cosmic-ray experiments, and use the possibility to make tagged photon "beams" from gamma-ray point sources. New Physics would then be seen as a deviation from known interactions of identified particles of known direction, measured energy, and conserved time structure. The major expected and detectable deviation concerns the production of muons, which are rather scarce in standard photon interactions, and could become more copiously produced in several different schemes above an energy threshold.

The major difficulty is the separation of the photon interactions from the overwhelming hadronic background. To obtain a sufficiently pure photon sample, a very high rejection factor is mandatory, but it should not bias against new properties of the photon interaction. In particular, it should not be based on the rejection of hadron-like or muon-rich showers, but should rather rely on the neutral nature of the primary particle and request a tight alignment of the shower axis with the source direction. Under these conditions, the effort is concentrated on obtaining the best possible angular resolution, with simultaneous measurement of the signal and of the background to allow a reliable estimate of the latter.

Preliminary studies [3] have shown that the Cerenkov array technique, although suffering from a lower duty cycle than charged particle counter arrays, is able to reach a much better angular precision due to the larger particle (i.e. Cerenkov photon) statistics and the longer lever arm for time-of-flight direction measurements. The method consists of sampling the Cerenkov light on a large number of points over a large area field (≈ 250 m \varnothing), of measuring with high precision (≈ 300 ps) the arrival times of the light pulses, and of reconstructing the shower axis from this information. The Cerenkov technique performs an intrinsic longitudinal integration over the shower development, and is able to measure the primary energy by using the atmosphere as a giant calorimeter.

A test experiment with 18 mirrors (sampling detectors) has been approved and set-up to check this new technique, evaluate the angular precision, and measure the source fluxes and energy spectra. If positive results are obtained, a full scale detector can be envisaged, with, as originally proposed, 300 mirrors, a large area muon detector and calorimeters necessary for doing particle physics. In any case, the present experiment is expected to contribute to our knowledge concerning the emissions of several northern-hemisphere sources, in an intermediate energy range around 10 TeV.

2 Monte-Carlo Simulation

The program, based on the LEP DELPHI Monte-Carlo [4], is an almost complete simulation of the elementary processes at the particle level : primary photon interaction; tracking in the atmosphere with the earth's magnetic field; energy losses and multiple scattering; particle decays and secondary interactions; emission of Cerenkov optical photons traced down to ground level; and detector simulation including photo-tube, amplifier, discriminator, and cable length effects [5].

This simulation shows that the Cerenkov light is distributed over a pancake shaped volume, transverse to the shower axis, larger than 250 m in diameter, but only about 1 to 2 meters thick. The resulting light wave-front is well defined in the downward going co-moving frame, with a rise time, as seen by a fast photo-multiplier, shorter than 1 ns. The main result of this study is an almost linear relationship between the time of the leading edge of these pulses and the distance to the shower axis, thus predicting a conical wave-front shape, with an half-opening angle (h.o.a.) rather stable around $\pi/2 - 0.016$ rd. The program has been used for systematic studies of this conical shape over an energy range from 1 to 100 TeV and for the optimization of the detector's optical angular aperture to eliminate late photons from scattered slow electrons. From these studies, a 20 mrd optical aperture has been selected and used in all data acquisition.

The reconstruction of the shower axis is based on a fit of this cone model to the measured times of arrival at the various detectors. This is a non linear fit of 6 parameters : position (x,y) of the impact point, direction (u,v) of the shower axis, complement (θ) to $\pi/2$ of the cone h.o.a., and an over-all absolute time. Due to the complex behavior of the χ^2 , a minimum of 10 timing measurements are needed, and various minimization algorithms have been tried. The angular precision obtained can be assessed under various simulation conditions. It reaches 0.15 mrd for a vertical conical wave-front sampled in 300 points with realistic gaussian timing errors. This figure rises to 0.6 mrd when the number of measurements is reduced to 18 with our present geometry. It rises further to 1.5 mrd for a distribution of the number of samples in the 10-18 range, and by taking into account the range of inclination of the showers. The full Monte-Carlo simulation of showers in the 7-20 TeV range of energy, with a realistic treatment of the detector properties yield a resolution of ≈ 3 mrd when the sampling multiplicity is between 13 and 18 mirrors hit. These numbers have to be compared with those of competing experiments which claim a resolution in the range 10-20 mrd.

The experimental determination of the resolution will ideally be based on the width of the angular distribution of an observed point-source signal. If none is seen, the experimental resolution must be inferred indirectly using hadronic showers, either from the covariance matrix once errors are better understood, or from the results given by independent subsets of the array, although this last method may require a larger number of mirrors (≈ 2 sets of 15 to 18) than presently available.

3 Detector Description

The present test experiment with 18 mirrors is set up on a 270 x 190 m² field at the site of Themis (42.5°N, 2°E, 1650 m alt. in the Pyrenees). This site, an unused solar power plant built by Electricité de France, has been made available for Astrophysics research, and is shared with the ASGAT collaboration.

Each of the 18 detectors [3,6,7] is made up of a revolving mounting (selected from among the 200 solar mirror mountings), a telescope enclosure holding the mirror and the phototube, and some local electronics.

The mountings are alt-azimuthal and computer driven. The rotational step size is 0.14 mrd. Their absolute accuracy, better than 2 mrd, has little influence on the shower direction measurement which is based solely on timing and position information.

The mirrors, 80 cm in diameter, have a focal length of 40 cm and a focal spot size of about 1 mm fwhm. Due to the small focal length, the phototubes can be kept small. The RTC XP2020 with a photo-cathode of 40 mm \varnothing and a 1.5 ns rise time has been used. To suppress late Cerenkov photons from the shower, and to reduce the transit time jitter in the tube, a diaphragm of 16 mm \varnothing is placed in front of the photocathode, thus reducing the optical acceptance to a 20 mrd half aperture. The PMT gain is $\approx 7 \times 10^5$ limited by the DC current induced in the tube by the night sky background

The local electronics, for each of the 18 detectors, includes 2 microprocessor systems, one for directing the mountings, the other for general electrical and mechanical control. Both are networked with the central computer driving the experiment. An amplifier of gain 10, and a constant fraction discriminator with a programmable threshold are also part of the local electronics. Their outputs are routed via 2 coaxial cables to the central electronics, and the length of these cables is the same for all detectors, independent of their location in the field: 320 m of 50 Ω cable for the amplifier output signal, and 215 m of fast 93 Ω cable for the timing signal.

In the central hut, these cables feed respectively, 10-bit ADCs gated at 200 ns, and banks of 3 cascaded and overlapping 11-bit TDCs (covering a 500 ns range with a 0.1 ns least count). The timing signals also go to the trigger logic, based on programmable delays (256 steps of 2 ns) and a majority coincidence usually set at 8 out of 18 signals of 50 ns length. The resulting trigger rate with this eightfold coincidence is around 0.3 Hz for vertical cosmic showers, and the accidental rate is negligible. Mirror orientation, data acquisition, detector control, and associated operator interfacing are performed by a single 68020 processor in a VME environment running under OS-9/68k, a real time multi-tasking multi-user operating system. No traditional minicomputer is used, and the tasks are executed as a number of concurrent cooperating processes.

4 Detector Behavior, Calibration and Monitoring

The average light sky background has been measured to be ≈ 1 photo-electron (ph.e.) /10 ns within the optical acceptance of 20 mrd half aperture for a 0.5 m² mirror, while the signal is of the order of 5 to 7 ph.e. / TeV per mirror.

The timing accuracy σ_t has been measured on the site by using pulses produced by a nitrogen laser ($\lambda=337$ nm, 2 ns rise time), diffused simultaneously to all detectors from a point on the solar plant tower, 70 m above ground. This accuracy has been found to depend on the pulse amplitude $N_{\text{ph.e.}}$ as : $\sigma_t^2 = a^2 + b^2 / N_{\text{ph.e.}}$ where a and b vary with the detector considered, but are of the order of 0.17 and 2.6 ns respectively. These figures give an accuracy of 0.85 ns for 10 ph.e., of 0.4 ns for 50 ph.e., and of 0.25 ns for 200 ph.e. over the full measurement range of 500 ns. Consequently, a shower energy above about 8 TeV is required to ensure a σ_t better than 0.4 ns.

The TDCs have been precisely calibrated and, to achieve the best precision, their measurements are corrected for drifts in Camac module temperatures. The over-all electronic chain time stability is monitored every night with the laser system. The results are found to be stable within ± 0.2 ns over more than a week. These laser calibration results are used to correct the shower data on a night by night basis.

The PMT gain equalization can be done in a variety of ways : by using pulses obtained from the laser system, or from an Am radioactive source imbedded in scintillator, or by using DC currents induced by a specific star, or by the sky background light. The results of these different techniques are being compared.

The wave-front reconstruction of either showers, or laser signals, requires a good knowledge of the detectors positions. The initial coordinates of the mountings were measured by EDF several years ago, and new measurements have been performed recently, partly by the French National Geographic Institute, and in more detail by the CERN survey group. As a result, the positions have been found to be stable, and are known to within a cm which gives negligible reconstruction uncertainty.

The telescope orientations have also been checked by tracking stars at various points in the sky with a 2 mm \varnothing diaphragm placed in the focal plane. The PMT DC current is monitored while scanning the sky in the vicinity of the star, and the position of the peak yields the azimuth and altitude offsets.

The photo-multiplier DC currents are also permanently monitored to detect and reject any abnormal sky-light conditions in the data sets used for the analysis.

5 First Data Samples

After the initial presentation at Moriond 87, the test experiment was approved and funded in March '88. The 18 detectors were progressively brought onto the site in '89 and spring '90. Data taking with the full detector started at the end of June '90 and was devoted to technical runs for the understanding of the detector behavior, and to observation runs to record data from potential gamma sources such as Cygnus X-3, or the Crab nebula. From October '90 to the end of January '91, a total of 69000 showers have been recorded from the zenith direction as a technical data-set, and 52000 showers have been available from the Crab direction. This last figure corresponds to about 50 h of observation of the source.

Fig. 1a displays a raw distribution of multiplicity (number of hit mirrors, n_h) for a trigger coincidence set at 8, and shows a fast decrease of the probability for high multiplicities. Since events need to have $n_h \geq 10$ to be reasonably fitted, only a fraction of about 47 % of the triggers can be used for the wave-front reconstruction. The dominance of low multiplicity showers can be explained by a geometrical effect, and by a threshold effect. Most of the showers that trigger, fall far from the center of the field and only fire the mirrors located near the field edge closest to the impact point. In addition, due to the steeply falling energy spectrum, most of the showers are of low energy, producing signals just at the discriminator threshold, and these signals have a detection probability substantially less than one. This threshold behavior is confirmed by the distribution (Fig 1b) of the sum of the ADC values of the hit telescopes (this sum is related to the shower energy as in a calorimeter) which directly reflects the fall of the energy spectrum.

The cone shaped wave-front structure can clearly be seen in fig 2a showing the overall profile of reconstructed showers with $n_h \geq 10$. The fitted cone angle distribution (fig 2b) is similar to the one obtained for Monte-Carlo simulations, the mean value falling in the 16-19 mrd range.

The fit also gives the position of the reconstructed impact points (fig 3); these are mostly concentrated within the perimeter enclosing the detectors. Within this region, the experimental distribution has limited variations in density, similar to the one obtained from Monte-Carlo simulation. Detailed acceptance studies near the trigger threshold are needed to assess the precise value of the sensitive area.

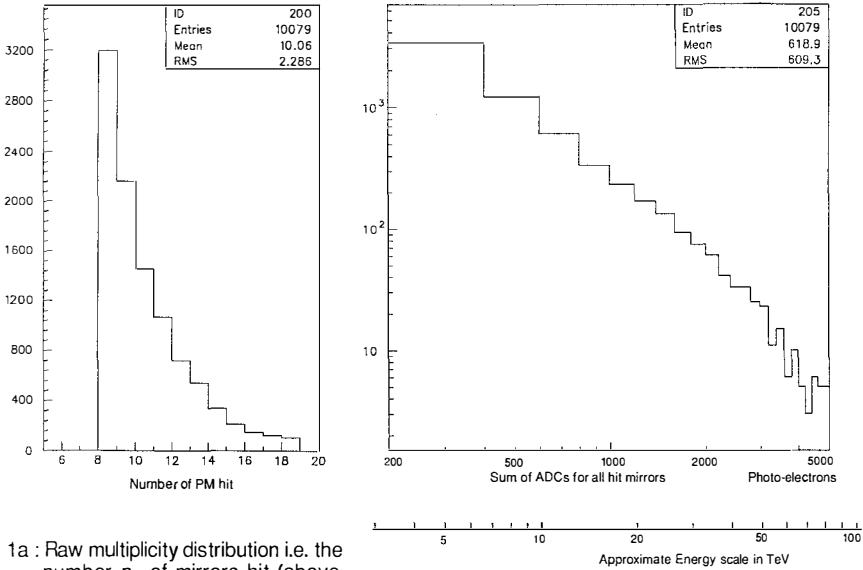
Finally the direction distribution of the reconstructed axis is shown in fig 4 for two data samples containing a limited number of showers. Both distributions look similar and reflect the angular acceptance for shower directions, but note that this is a first glance at preliminary data, that the plots use only a small fraction of the available statistics, and that the analysis is still under way (e.g. no fiducial cuts have been applied).

6 Conclusions

Simulations indicate that the Cerenkov detector array technique is potentially able to provide sub milliradian angular resolution for photon-induced showers in the upper VHE energy region. The 18 telescope test detector is up and running smoothly, and accuracy and stability of directly measured quantities meet design goals. Work is going on to investigate the detailed properties of the reconstruction procedure, to assess the angular resolution, and to study detector systematics and threshold effects. This data analysis is in progress, and first results are expected in a few months. If they are encouraging, and if a suitable source is detected, it will then be possible to consider a second phase for the experiment, with a full scale detector (300 mirrors) and a large area muon detector and calorimeters to perform the proposed particle physics experiment.

References :

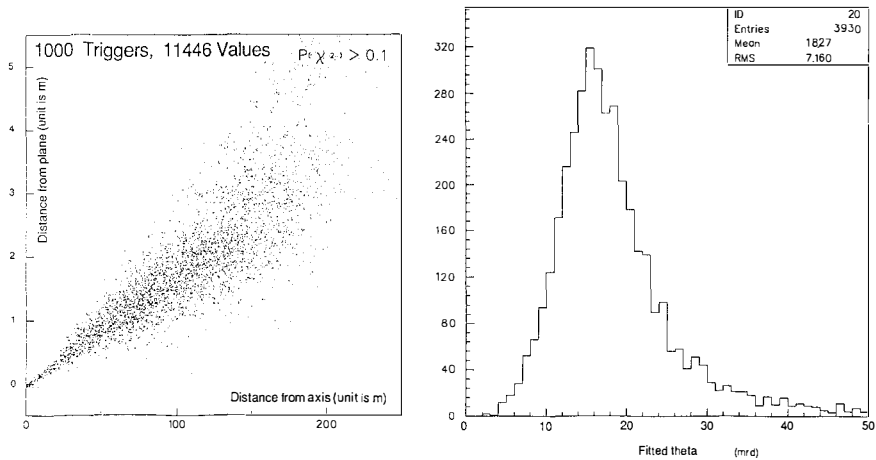
- [1] G.Fontaine : Future gamma experiments at Themis. Proc.M52 of the VIIth Rencontres de Moriond workshop, on "New and Exotic Phenomena", Les Arcs 25-31 Jan. 1987, pp 183-186.
- [2] P. Baillon et al. : A Physics experiment with high energy cosmic gamma-rays. Proposal for the experiment, Dec 1987, unpublished.
- [3] G. Fontaine et al.: Aims and status of the THEMISTOCLE Physics experiment. Nuclear Physics B (Proc. Suppl.) 14B (1990) 79-94.
- [4] DELSIM reference manual. DELPHI 87-97/PROG-100.
P. Baillon et al. : Description of the RICH simulation. DELPHI 87-103/PROG-102.
- [5] Ph. Schune : Contribution à l'expérience THEMISTOCLE pour l'identification des rayons gamma cosmiques de très haute énergie. Thesis, Université de Paris-Sud, Orsay, 1990, unpublished.
- [6] F. Kovacs et al. : THEMISTOCLE, a high angular resolution Cerenkov light detector. Nuclear Physics B (Proc. Suppl.) 14A (1990) 330-335.
- [7] L. Behr et al. : Status of the THEMISTOCLE multi-mirror Cerenkov array for VHE/UHE source studies. Proceedings of the International Conference on High Energy Gamma-Ray Astronomy (October 1990) A.I.P. Conference Proceedings Series.



1a : Raw multiplicity distribution i.e. the number n_h of mirrors hit (above the discriminator threshold), for a coincidence level set at 8 out of 18.

1b : Sum of ADC amplitudes, corrected for cable attenuation, but without any acceptance correction (unit is photo-electron).

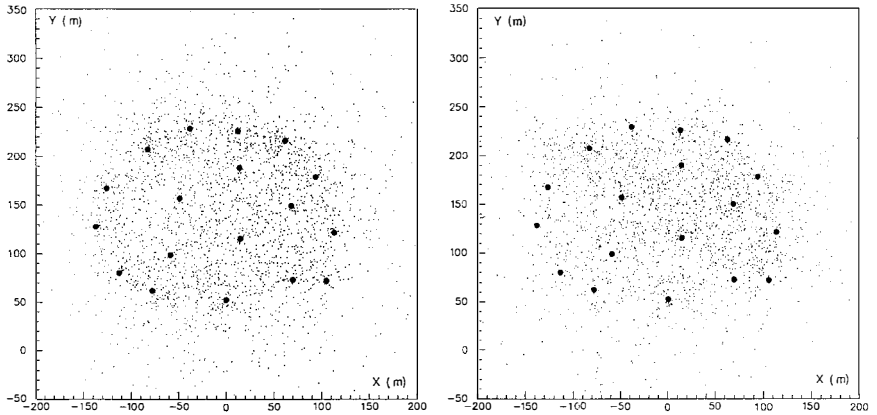
Figure 1 : Experimental data from zenith showers



a) Scatter plot of the distance of measured "points" from a plane transverse to the fitted axis versus the radial distance from the axis. Each shower contributes to n_h entries in the plot

b) Distribution of the fitted cone aperture parameter θ , the complement to $\pi/2$ of the cone half opening angle (unit is mrd).

Figure 2 : Results of the wave-front fit in the downward going co-moving frame for zenith shower experimental data with $n_h \geq 10$.

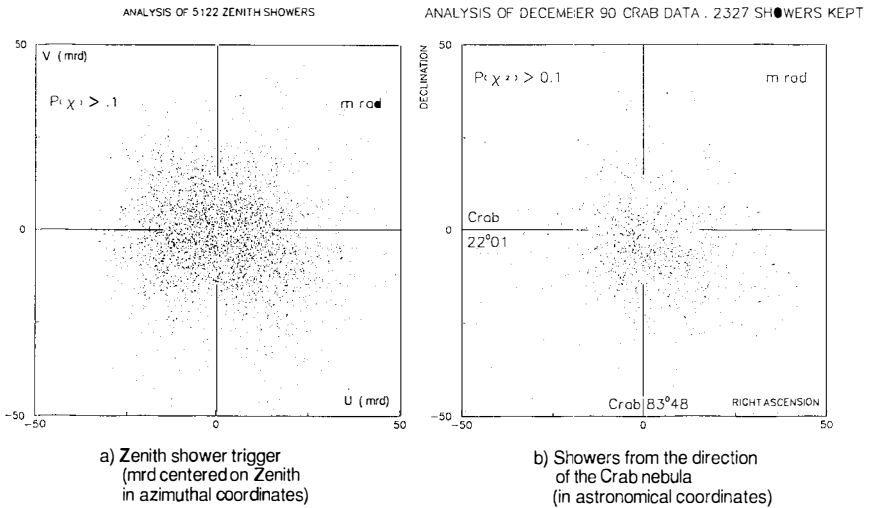


a) Monte-Carlo simulation data, with an energy ranging from 7 to 20 TeV.

b) Experimental data.

Figure 3 : Scatter plots for the distribution of the fitted impact points (intersection of the fitted shower axis with the horizontal plane) for zenith showers.

Large dots show the position of the 18 detectors, units are in meters.



a) Zenith shower trigger (mrd centered on Zenith in azimuthal coordinates)

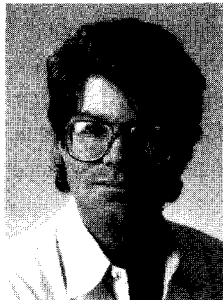
b) Showers from the direction of the Crab nebula (in astronomical coordinates)

Figure 4 : Scatter plots for the distribution of the directions of the reconstructed shower axis for experimental data (preliminary fits on partial data-sets), units are in mrd.

A COSMIC BACKGROUND OF
HIGH ENERGY NEUTRINOS FROM ACTIVE GALACTIC NUCLEI

M.H. Salamon and P. Sommers
Physics Department
University of Utah
Salt Lake City, UT 84112 USA

F.W. Stecker and C. Done
Laboratory for High Energy Astrophysics
NASA/Goddard Space Flight Center
Greenbelt, MD 20771 USA



Under certain assumptions the cores of active galactic nuclei are found to be prodigious sources of high energy neutrinos, dominating the isotropic background between 10^4 and 10^{10} GeV, and yielding observable event rates with currently existing underground detectors. The conversion of gravitational energy of infalling matter from the AGN accretion disk to luminosity is via acceleration of protons at the accretion shock; subsequent $p\gamma$ interactions within the AGN core fuel the observed x-ray luminosity and also produce neutrinos with a comparable luminosity.

Active galactic nuclei (AGN) are the most powerful emitters of radiation in the known Universe, having luminosities up to 10^{47} erg/sec, and as such have long been considered as potential sites for high energy neutrino production^{1]}. The rapid time variability of emissions from the UV and x-ray regions in AGN^{2]} strongly supports the consensus that their central engines are supermassive (up to 10^9 solar mass) black holes. Figure 1^{3]} shows a typical AGN spectrum whose features include a quasi-thermal bump in the UV region, and a distinctly non-thermal x-ray component with a power-law spectrum which continues up to ~ 1 MeV.

The observed luminosity is presumably fueled by the gravitational energy of matter infalling from an accretion disk. Viscous damping in the accretion disk may partially or wholly account for the "thermal" UV component; the nonthermal x-ray component, however, is perhaps most naturally explained as the byproduct of particle acceleration in the AGN core, in which energy flows from the accelerated particles to the observed power law spectrum through interactions and subsequent electromagnetic cascades^{4]}. In the model that we consider here^{5]}, infalling matter forms an accretion shock at a radius R_{shock} from the black hole^{6]}; first-order Fermi acceleration at this shock then converts (with nearly unit efficiency) the infall energy into highly relativistic protons with a differential energy spectrum of E^{-2} . This spectrum cuts off at an energy where the proton acceleration time

$$t_{\text{acc}}(E) = 2.2 \times 10^{-4} (R_{\text{shock}}/R_s)(E/m_p)(1/B) \text{ sec}$$

(B is the magnetic field, taken to be $\sim 10^8$ G by equipartition, and R_s is the Schwarzschild radius) is matched by the proton energy loss time.

Strict observational limits on the amount of target gas for $p\gamma$ interactions in the x-ray producing region^{7]}, coupled with the intense photon fields found at the AGN cores, results in $p\gamma$ dominating pp as the primary energy loss mechanisms for protons. This is a threshold interaction, $p\gamma \rightarrow \Delta(1232) \rightarrow N\pi$, with the peak cross section occurring at $\epsilon E = 0.35$ eV-EeV, where ϵ is the photon energy. Figure 2 shows the differential photon density (which scales as $1/L$) versus energy in an AGN core of luminosity $L = 10^{45}$ erg/sec. With the $p\gamma$ lifetime being $(N_{\gamma} \sigma_{p\gamma} \kappa)^{-1}$ where κ is the mean inelasticity, we obtain the maximum (cutoff) proton energy as a function of L , shown in Figure 3.

For $p\gamma \rightarrow n\pi^+$, the mean pion energy is $\sim E/5$, with the pion decay neutrinos having a mean energy of $\sim E/20$ each. Averaging over energy and isospin, roughly $3/8$ of the original pion energy goes to the neutrino sector, the

remainder being electromagnetic. Assuming this remainder ends up as x-rays, a simple relation exists between the observed x-ray luminosity and the neutrino luminosity. The main features of the neutrino spectrum are simply explained: as the mean core photon energy is ~ 40 eV, the effective proton threshold energy is $\sim 10^7$ GeV; relativistic kinematics thus gives a nearly flat differential neutrino spectrum below $\sim 10^6$ GeV. Above this energy the neutrino spectrum falls as E_ν^{-2} , with a neutrino cutoff energy of $\sim 1/20$ that of the protons. Thus most of the neutrinos emitted from the AGN core have energies $\sim 10^6$ GeV.

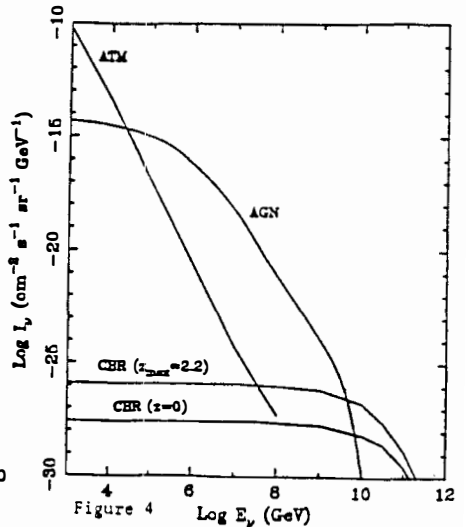
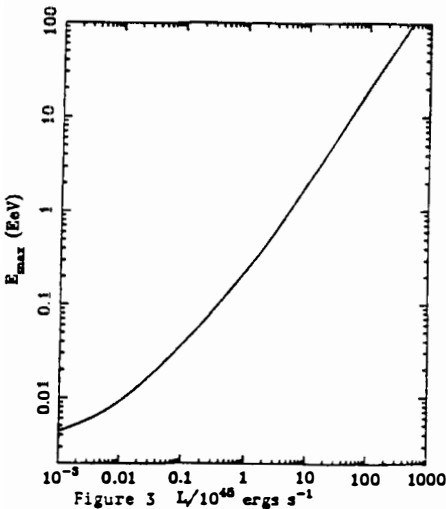
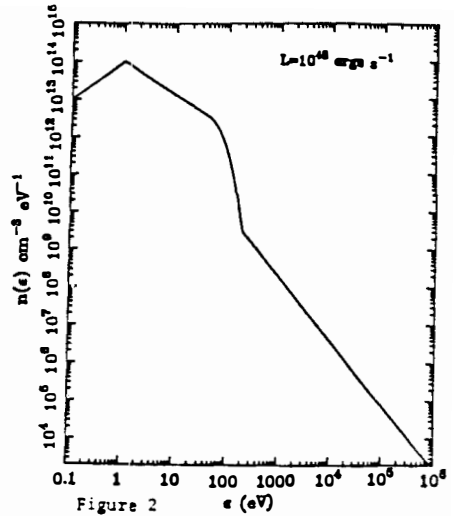
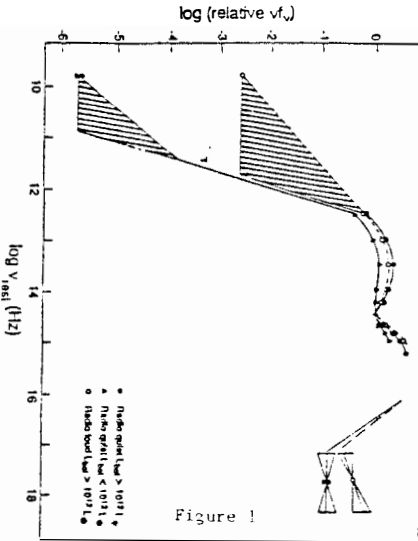
To obtain the total (isotropic) neutrino flux from all AGN requires an integration over the x-ray luminosity function for AGN, determined by GINGA satellite data^{8]}. As the neutrino mean free paths are greater than the horizon, an integration over redshift to the beginning of galaxy (AGN) formation is also required. It is well established that AGN luminosities and/or co-moving densities increase with redshift z ^{9]}, although the z dependence is quite model-dependent. As most of the present neutrino flux is produced at higher ($z \sim 2$) redshift, our calculation of the total neutrino spectrum at the Earth is somewhat sensitive to our choice of AGN evolution parameters^{8]}.

Figure 4 shows the total muon neutrino (or muon antineutrino) spectrum from all AGN. (All neutrino production kinematics were calculated by Monte Carlo.) Since the AGN cores are also opaque to neutrons, $n\gamma \rightarrow p\pi^-$ occurs with equal frequency to $p\gamma \rightarrow n\pi^+$, and thus the electron neutrino and antineutrino fluxes are each 1/2 that of the muon neutrino flux. The atmospheric horizontal muon neutrino flux^{10]} is also shown; AGN neutrinos dominate the isotropic background from $\sim 10^4$ GeV up to $\sim 10^{10}$ GeV, where neutrinos produced by cosmic ray proton interactions off the microwave background^{11]} become more abundant. These fluxes are observable with present underground detectors: IMB, Kamiokande, and very shortly MACRO should see on the order of 10^2 (non-contained) bremsstrahlunging muons per year; DUMAND II should see $\sim 10^3$ - 10^4 /yr.

REFERENCES:

- [1] V.S. Berenzinsky, Proc. Neutrino 77 (Nauka Publ. Moscow) 177 (1977); D. Eichler, Astrophys. J. 232, 106 (1979); R. Silberberg and M.M. Shapiro Proc. 16th Intl. Cosmic Ray Conf. (Kyoto) 10, 357 (1979); V.S. Beresinsky and V.L. Ginzburg, Mon. Not. R. Astron. Soc. 194, 3 (1981); P.L. Biermann and P.A. Strittmatter, Astrophys. J. 322, 643 (1987); M.C. Begelman, B. Rudak, and M. Sikora, Astrophys. J. 362, 38 (1990).
- [2] J.H. Krolik et al., Astrophys. J., in press (1991).
- [3] Taken from D.B. Sanders et al., Astrophys. J. 347, 29 (1989), with permission.
- [4] C. Done and A.C. Fabian, Mon. Not. R. Astron. Soc. 240, 81 (1989).

- [5] F.W. Stecker, C. Done, M.H. Salamon, P. Sommers, subm. to Phys. Rev. Lett. (1991).
- [6] D. Kazanas and D.C. Ellison, Astrophys. J. 304, 178 (1986); D. Kaznas and D.C. Ellison, Nature 319, 380 (1986).
- [7] R.F. Mushotzky, Astrophys. J. 256, 92 (1982); T.J. Turner and K.A. Pounds, Mon. Not. R. Astron. Soc. 240, 833 (1989).
- [8] K. Morisawa and F. Takahara, Pub. Astron. Soc. Jap. 41, 873 (1989).
- [9] J.J. Condon, Astrophys. J. 287, 461 (1984).
- [10] M.F. Crouch et al., Phys. Rev. D18, 2289 (1978); F.W. Stecker, Astrophys. J. 228, 919 (1979).
- [11] F.W. Stecker, Phys. Rev. Lett. 21, 1016 (1968).



COSMIC NEUTRINO DETECTION WITH A WATER CERENKOV

Luciano Moscoso

DAPhPE, CE-Saclay, F-91191 Gif-Sur-Yvette CEDEX

ABSTRACT: A large area Cerenkov detector aimed to detect upward-going muons produced by ν_μ and $\bar{\nu}_\mu$ in the surrounding rock is presented. Estimates of the sensitivity and of the background rejection power are given.

One of the most fascinating problems in astroparticle physics is the investigation of the origin of high energy cosmic rays.

Interactions of accelerated protons in stars with matter in the vicinity of the source can produce hadronic cascades which finally result in a beam of neutrinos. These are particles which can reveal the UHE particle emission by point-like sources, because they are stable neutral particles and, thus, they are not deflected by the galactic magnetic field.

Neutrino astronomy would implement the gamma-ray astronomy by allowing the survey of regions which are invisible via the photon detection because of the presence of absorbing interstellar matter.

The most efficient way to detect cosmic high energy neutrinos is based on the detection of muons produced by ν_{μ} interactions in the Earth¹⁻²). Underground detectors with surfaces of a few 100 m² did not detect any signal from HE cosmic neutrino sources. In order to improve the sensitivity by a significant factor, a surface of at least 10⁵ m² is needed. Such a large detector cannot be underground. Thus, muons produced by downward-going neutrinos are overwhelmed by large flux of muons produced in the atmosphere.

The proposed detector has, thus, to be aimed to detect upward-going muons which can only be produced by neutrinos having gone through the Earth depth.

The ν -N interaction cross section is an increasing function of the neutrino energy. Moreover, the target length is equal to $R_{\mu} - L$, where L is the muon path length in the detector and R_{μ} is the muon range in the rock. This yields to an enrichment of high energy neutrino interactions detection.

The neutrino spectrum from extra-terrestrial sources is expected¹) to be much flatter than that of the atmospheric neutrinos which are the main source of background. Moreover, since at high energy the angle between the neutrino and the muon directions is less than 1°, a good angular resolution would allow the observation of neutrino sources by providing a powerful rejection against atmospheric neutrinos which have an isotropical angular distribution.

A water Cerenkov detector is particularly well suited for this kind of measurement. In this purpose a working group made up of about 40 physicists from the Gran Sasso laboratory, Madison, Milan, Neuchâtel,

Padua, Pavia, Saclay, Tufts University, Turin, and Zaragoza is studying the feasibility of such a detector.

The detector area should be 300X300 m² and its depth 50-60m. Several layers of downward-looking photomultipliers will detect Cerenkov light produced by neutrino-induced upward-going muons (Figure 1)

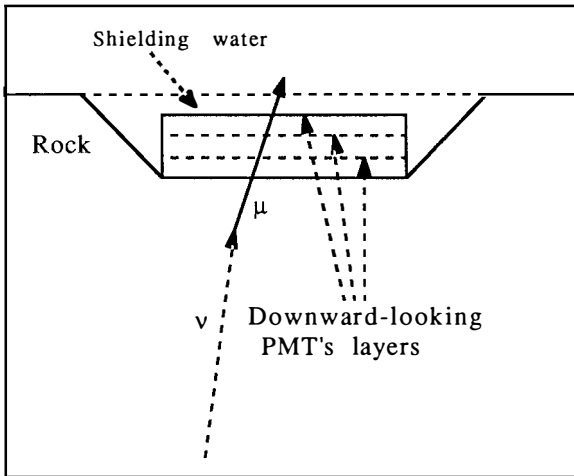


Figure 1. Detector lay-out.

Monte Carlo calculations have been performed by simulating the ν -N charged current interactions in the rock, the secondary muon propagation in the rock and in the detector, and the Cerenkov light emission and detection. These calculations have shown that three layers of PMT's at 15m distance with PMT spacing in each layer of 5-6m, photosensitive windows with a diameter of 20cm and a time resolution better than 3ns allow a reconstruction efficiency better than 90% for muons crossing the detector with zenithal angles up to 60°. The angular resolution on the direction of the reconstructed muon is better than 0.5°.

The neutrino detection efficiency depends on the neutrino energy spectrum. With the assumption that the neutrino flux is:

$$\frac{d\Phi}{dE} \propto E_{\nu}^{-\gamma},$$

one can estimate the ratio of muons entering the detector with a direction which is within 1° of the neutrino direction. Table I gives the values of this ratio for muons with energies greater than 10 GeV as a function of γ .

TABLE I: Ratio of muons with energies above 10 GeV which enter the detector with a direction within 1° of the neutrino direction for different values of the spectral index γ .

γ	Ratio
2.1	89%
2.3	82%
2.5	73%
2.7	63%

Due to the angular acceptance of 60° around the Zenith direction, the detector will not be sensitive to each source all the time. Moreover, the requirement that muons must cross the entire detector depth reduces the sensitive surface. Figure 2 shows the variations of the detector acceptance ϵ as a function of the source declination.

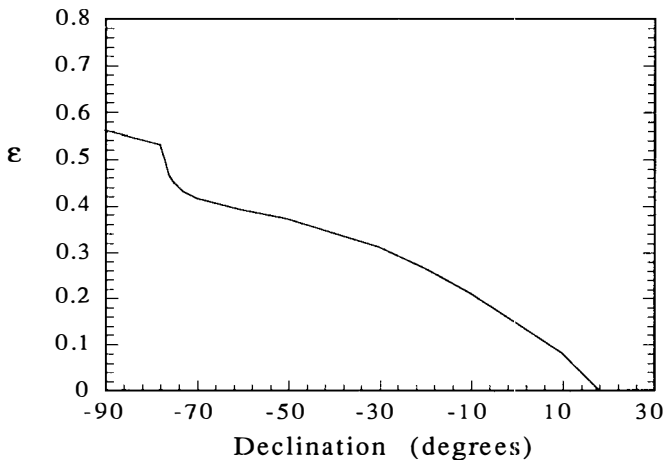


Figure 2. Detector acceptance as a function of the source declination.

The expected rate of upward-going muons above the energy threshold of 10 GeV produced by atmospheric neutrinos is 15-20/day, yielding several thousand of high energy neutrino-induced upward-going muons per year. The good angular resolution (better than 1°) for the neutrino direction measurement reduces this background to less than 0.3 events/year for each source.

Another source of background is due to accidental coincidences of signals from several inclined downward-going cosmic-rays recorded during the trigger time gate. The estimate of this occurrence is less than the atmospheric neutrino background rate. Moreover an additional layer of upward looking PMT's, to be used in the off-line filter, is expected to suppress this background to a negligible level.

The estimated number of the recorded upward-going muons rate is about 1300 year^{-1} . This yields to a total number of recorded events of about 1 event in 3 years with an angular cut of 1° for each source. Signals of about 10 events are, thus, enough to conclude to the evidence of the observation of a signal ($CL \approx 10^{-6}$). This corresponds to a muon flux above 10 GeV of:

$$\Phi_\mu(E_\mu > 10 \text{ GeV}) \approx 4 \cdot 10^{-16} \text{ cm}^{-2} \text{ s}^{-1}.$$

Assuming a spectral index $\gamma = 2.1$, Monte Carlo calculations allow to estimate that the corresponding neutrino flux is $\Phi_\nu = 10^{-8} \text{ cm}^{-2} \text{ s}^{-1}$. The detectable neutrino luminosity will, thus, be:

$$L_\nu = 2 \cdot 10^{37} \left(\frac{D}{10 \text{ Kpc}} \right)^2 \text{ Erg} \cdot \text{s}^{-1}.$$

where D is the source distance in Kpc.

As an example, Vela-X1 and LMC-X4, may be HE neutrinos emitters. Luminosities of the order of $5 \cdot 10^{35} \text{ Erg} \cdot \text{s}^{-1}$ for Vela-X1 and of $5 \cdot 10^{38} \text{ Erg} \cdot \text{s}^{-1}$ for LMC-X4 may be detected in few years of running time.

REFERENCES

- 1) T.K.Gaisser and A.F.Grillo, Phys. Review D36(1987)2752
 - 2) E.W.Kolb, M.S.Turner, and M.G.Ryskin Phys. Review D32(1985)1145
- C.Quigg, M.H.Reno, and T.P.Walker, Phys Rev. Letters 57(1986)774



MILLICHARGED MATTER

M.I. Dobroliubov, A.Yu. Ignatiev

*Institute for Nuclear Research
of the Academy of Sciences of the USSR,
60th October Anniversary prospect. 7a
Moscow 117312, USSR*

Abstract

We review the recent results concerning the possible existence of particles with very small electric charges ($Q \sim O(10^{-3}e)$) and their possible relevance to the solution of some experimental puzzles (orthopositronium lifetime and GSI events) as well as ways of the experimental search for them.

Particle physics seems to be going through very interesting time. Although some years ago almost all physicists were sure that our understanding of physics at relatively small energies (i.e. less than a few hundred GeV) was complete and anything new could happen only at very high energies (or under quite unusual conditions such as very high temperatures, densities etc.), one after another new phenomena in familiar regions have been observed, which hardly appear to be explained within the Standard Model. Let us recall only some of them: too short orthopositronium lifetime [1], indications of 17 keV admixture in the electron neutrino [2], anomalous e^+e^- -pair production in the collisions of heavy ions [3], the deficit of 1-charged particle decay mode of the τ -lepton [4]. The Nature seems to be more tricky than people began to think it is! It looks to be high time to revise our basic ideas of what principles govern the world and to expose them to careful theoretical and experimental verification. It is this way that the belief in the C and P symmetries of the world was broken in the 50's, later on new types of particle statistics were found (parastatistics and fractional statistics). Recently it was proposed to test experimentally the validity of the Pauli exclusion principle [5]. In this talk we would like to consider another

principle commonly believed to be exact, namely the charge quantization (i.e. the fact that the electric charge of *any* elementary particle is multiple to that of the $\frac{1}{3}$ -quark).

There exist some approaches to the explanation of this phenomenon: Grand Unified Theories [6], Kaluza-Klein models [7], the Dirac's monopole hypothesis [8] in which the charge quantization appears very natural and it proves rather hard to violate it. But at present we are far from knowing whether these theories have anything to do with reality. It is worth noting in this connection that looking for deviations from the charge quantization can serve as a low-energy test of Grand Unified, Kaluza-Klein and magnetic monopole concepts. Moreover, recently much interest arose to the possibility of the violation of the charge quantization within the Standard Model [9].

Basically, there are two ways of checking up the charge quantization principle. First, one can search for very small deviations from that principle by looking for a difference between proton and positron charges or for nonzero charge of the neutrino. These differences are severely constrained by experiment so we won't dwell on this possibility. Rather we shall consider another way for experimental test of the charge quantization: looking for *new* particles with small electric charges, $Q = q \cdot e$, $q \ll 1$, (we shall mark such particles as ϵ). (If new particles had charges comparable or greater than that of the electron they would have to be heavier than tens GeV to escape modern accelerator constraints). Surprisingly as it might seem the limits on q imposed by the various experimental data (anomalous magnetic moment of the muon and electron, the Lamb shift) along with astro- and geophysics and cosmology are not very strong [10]: $q \lesssim 10^{-3} \div 10^{-2} \cdot$ (depending on the ϵ mass). For the constraints obtained from the consideration of the supernova SN 1987A see [11]. So direct searches for such particles are quite feasible.

It is interesting to note that particles with small electric charges can be relevant to solving two of the above mentioned problems of the modern particle physics: the orthopositronium lifetime puzzle and the anomalous GSI events.

According to [1] the experimentally measured decay width of the orthopositronium (S_1^3 bound state of the e^+e^- pair) is: $\Gamma_{exp} = (7.0482 \pm 0.0016) \mu s$, whereas its theoretical value equals [12] $\Gamma_{th} = (7.03830 + \pm 7 \cdot 10^{-5} + O(\frac{\alpha}{\pi})^2) \mu s$, so that their difference is about 6.2 standard deviations. So one is tempted to suppose that there exists a new mode of the orthopositronium decay with the branching ratio $\sim 10^{-3}$. This may be the decay $S_1^3 \rightarrow \epsilon\bar{\epsilon}$, where ϵ is a light ($m_\epsilon < m_e$) particle with the electric charge $Q = qe$, $q \ll 1$: $BR(S_1^3 \rightarrow \epsilon\bar{\epsilon}) \simeq 371q^2$. One can see that in order to have $BR(S_1^3 \rightarrow \epsilon\bar{\epsilon}) \simeq 10^{-3}$ one should have $q \simeq 1.6 \cdot 10^{-3}$. The search for the decay $S_1^3 \rightarrow$ *nothing* (i.e. undetectable particles) was carried out in the Institute for Nuclear Research (Moscow) and the following limit has been obtained [13] $BR(S_1^3 \rightarrow$ *nothing*) $< 5.8 \cdot 10^{-4}$ (90% C.L.) and this limit is going to be improved by the same

*hence their name *millicharged particles*

group. Meanwhile this result is waiting for confirmation by other experimentalists.

Another very interesting opportunity is to use the millicharged particles for the explanation of the anomalous GSI production of the e^+e^- -pairs in the collisions of heavy ions [3]. It is well known that one of the most plausible explanation of these events is the hypothesis that there exist extended bound states of some new electrically charged particles and an additional confining interaction [15]. However when the charge of these particles equals that of the electron the models of this type confront the problem of large contribution of those particles to the vacuum polarization (which would contradict the data on the shifts of the levels of muonic atoms). But if the electric charges of these particles are much less than 1 (i.e. if they are millicharged particles with a confining interaction) then the troubles with the vacuum polarization will disappear while all the desired properties of the model remain. Of course, the presence of the confining force between the ϵ -particles may change some of the constraints obtained in [10], though this problem requires special consideration.

Now let us briefly discuss the possibilities of the experimental search for the millicharged particles. As we have shown before [10,14], it can be feasible to look for them in accelerator experiment. The idea is to produce intense enough beams of the millicharged particles (in the collisions of conventional particles with the target nuclei) with their subsequent detection based on their ionization energy losses. Here the high-current electron accelerators seem to be the most appropriate. For instance at the CEBAF facility one could obtain about $10^{16}q^4$ photons induced by such beam of the ϵ -particles per 1 cm length the scintillator $N\alpha(Tl)I$ detector per second [14].

Here we would like to point out on a new way of searching for the millicharged particles. If the latter were heavy enough and their charges were not too small ($m_\epsilon > qm_e$, i.e. of order of hundreds MeV) then their Bohr radius would be smaller than that of the electron, so that the millicharged particle could be bound by atoms, and thus millicharged atoms would arise. Depending on the concentration of such atoms looking for them could be one of the possible ways of discovering millicharged particles.

To estimate the feasibility of this approach it is necessary to discuss how the millicharged particles are produced and distributed in and around the Earth.

First of all we should consider the contribution of the relic ϵ -particles. It was shown in [10] that their mass density can be close to the critical one in the large range of their masses. Taking $\rho_\epsilon \simeq 10^{-5} \text{ GeV cm}^{-3}$ we find that the density of the relic millicharged particles is about $n_\epsilon \simeq 10^{-4}(100 \text{ MeV}/M_\epsilon) \text{ cm}^{-3}$. But if the millicharged particles formed the galactic dark halo (as was suggested by Goldberg and Hall [16], in a very different context, though) and their mass density were equal to the local mass density, $\rho \simeq 0.3 \text{ GeV cm}^{-3}$, then their density would be much larger, $n_\epsilon \simeq (100 \text{ MeV}/M_\epsilon) \text{ cm}^{-3}$. Besides, there exists another source of millicharged particles which could increase their density around the Earth, namely, their production via cosmic ray collisions in the Earth's atmosphere. Let us estimate the present amount of

negative ϵ 's: $N = JS\sigma nLt$, where J is the flux of the cosmic rays, S is the square of the Earth atmosphere and L is the effective penetration length of the cosmic rays, n is the concentration of the nuclei in the atmosphere, t is the Earth's age, s is the cross-section of the production of the millicharged particles, σ is the cross-section of the production of ϵ -particles in collisions of a charged particle with a nucleus of the charge Z . It can be shown that the ϵ 's are produced mainly due to the electronic component of the cosmic rays [10], so the cross-section reads $\sigma \simeq q^2\alpha^4 Z^2 m_e^{-2}$. Taking $J \sim 10^{-2} \text{ cm}^{-2} \text{ sec}^{-1}$, $S \sim 5 \cdot 10^{18} \text{ cm}^2$, $L \sim 10L_{rad} \simeq 3 \cdot 10^8 \text{ cm}$, $Z = 7$, $n \sim 10^{20} \text{ cm}^{-3}$, $t \sim 10^{17} \text{ s}$, we obtain $N \sim 10^{29} q^2$. If the produced millicharged particles were distributed over the Earth's volume uniformly then it would result in their concentration of order of magnitude $\sim 100q^2 \text{ cm}^{-3}$, i.e. up to 0.1 cm^{-3} . But if they were absorbed mainly near the Earth's surface this number would be considerably larger. Hence, looking for millicharged atoms seems to deserve serious consideration.

One of us (A.I.) is grateful to G.Hinds, L.Hunter and S.Lamoreaux for their interest in the work and stimulating discussion. It is my pleasure to acknowledge kind support and hospitality of J. Tran Thanh Van and other Conference organizers which made my stay at Les Arcs possible and enjoyable.

References

- [1] C.I.Westbrook et al., Phys.Rev.Lett. 58,1328 (1987)
- [2] For a recent review see, e.g. G.Gelmini, S.Nussinov, R.D.Peccei, The Perils of a 17 KeV Neutrino, UCLA preprint, UCLA/91/TEP/15
- [3] B.Muller, preprint UFTP 222/88, to appear in "Atomic Physics of Highly Ionized Atoms", ed.R.Marrus, Plenum Press.
- [4] B.C.Barish, R.Stroynowski, Phys.Rep. 157, 1 (1988)
- [5] A.Yu.Ignatiev, V.A.Kuzmin, Sov.J.Nucl.Phys. 46, 444 (1987)
- [6] J.C.Pati, A.Salam, Phys.Rev.Lett. 31, 661 (1973); H.Georgi, S.Glashow, Phys.Rev.Lett. 32, 438 (1974)
- [7] *Modern Kaluza-Klein Theories*, ed. by T.Appelquist, A.Chodos and P.G.O.Freund (Addison-Wesley, 1987)
- [8] P.A.M.Dirac, Proc. Royal Soc. London A133, 60 (1931)
- [9] K.S.Babu, R.N.Mohapatra, Phys.Rev. D41, 271 (1990); R.Foot et al., Mod.Phys.Lett. A5, 95 (1990); R.Volkas, private communications
- [10] M.I.Dobroliubov, A.Yu.Ignatiev, Phys.Rev.Lett. 65, 679 (1990).

- [11] K.S.Babu, R.N.Mohapatra, I.Z.Rothstein, Univ. of Maryland preprint UMD/HEP 90-227, 1990
- [12] W.G.Caswell, G.P.Lepage, Phys.Rev. **A20**, 36 (1979), G.S.Adkins, Ann. Phys. (N.Y.) **146**, 78 (1983)
- [13] G.S.Atoyan, S.N.Gninenko, V.I.Razin, Yu.V.Ryabov, Phys.Lett. **220B**, 317 (1989)
- [14] M.I.Dobroliubov, A.Yu.Ignatiev, Looking for millicharged particles, in: Proceedings of the 2nd Conference *Beyond the Standard Model*, ed. K.Milton (to be published by World Scientific)
- [15] S.Schramm et al., Mod.Phys.Lett. **A3**, 783 (1988)
- [16] H.Goldberg, L.J.Hall, Phys.Lett. **174B**, 151 (1986)

AXIONS, PLASMONS AND SUPERNOVAE

Tanguy Altherr

L.A.P.P. , BP 110, 74941 Annecy-le-Vieux Cedex, France

Abstract

I consider the finite density and temperature effects on axion emission by a very hot and ultra-dense plasma. In presence of a quark-gluon plasma in the core of supernova SN1987A, the bound on the Peccei-Quinn symmetry breaking scale becomes $f_a \gtrsim 3 \times 10^9 \text{ GeV}$, which is of the same order as in presence of a neutron core.

The axion is one of the most exciting extension of the standard model. It is an hypothetical pseudoscalar particle of almost zero mass which was invented in 1977 by Peccei and Quinn [1] in order to solve the strong CP problem. It is characterized by a symmetry breaking scale f_a and the coupling strength with all known particles behaves as $1/f_a$. It could be also a good dark-matter candidate. The original model was quickly ruled out by observations but shortly after that, the invisible axion model was proposed [2] and is still allowed for a range of f_a within the two windows [3]

$$10^6 \text{GeV} \lesssim f_a \lesssim 2 \times 10^6 \text{GeV} \quad \text{or} \quad 6 \times 10^9 \text{GeV} \lesssim f_a \lesssim 4 \times 10^{12} \text{GeV}. \quad (1)$$

The constant f_a is sometimes related to the axion mass by $m_a = (0.6 \times 10^7 \text{GeV}/f_a) \text{eV}$. The last upper bound comes from cosmological considerations and all others from astrophysics studies. As there is no strong discrepancy between observations of stellar bodies and numerical models, exotic particles such like the axion must have either a coupling weak enough so that they escape from the system but do not dissipate to much energy from it, or, their coupling is strong enough so that they are trapped inside the system and are in thermal equilibrium. The lower bound, $f_a \gtrsim 6 \times 10^9 \text{GeV}$, is obtained by looking at the bremsstrahlung process $NN \rightarrow NN a$ in the supernova SN1987A core. However, the supernova density and temperature are so extreme that one could expect to have a hadronic matter to quark-gluon plasma phase transition [4]. As the coupling between fermions and axions is proportional to the fermion mass, one naively would expect that this lower bound is reduced by 2 or 3 orders of magnitude which would open significantly the second window. In this few pages, I will try to summarize the content of my work [5] which shows that this is not the case and that the bound on f_a is essentially unchanged in presence of a quark-gluon plasma.

The physics of a very hot and ultra-dense plasma, $T \simeq 70 \text{MeV}$ and $\mu \simeq 500 \text{MeV}$ is not trivial. Basically, one has a Fermi sea in addition to a Dirac sea. Although one does not need to modify the Lagrangian structure, the observables, measured on a statistical ensemble are very different from the vacuum case. For instance asymptotic states are not clearly defined. Instead, the appropriate notion is that of a quasiparticle excitation, or Landau damping, i.e., a particle thermalizing with its surrounding. For that reason, rather than computing Feynman amplitudes, it is more convenient to calculate Green functions, and extract from their discontinuities the absorption and emission rates of particles. This is summarized by the formula

$$\text{Im} G(k) = \omega[\Gamma_e(k) - \Gamma_a(k)], \quad (2)$$

where $G(k)$ is the self-energy. Γ_e and Γ_a are the emission and absorption rates respectively, related by

$$\Gamma_a(k) = e^{\beta\omega} \Gamma_e(k), \quad (3)$$

for a plasma at equilibrium. The relation between the discontinuity of the self-energy and the absorption and emission rates is obtained through the use of the cutting rules, already well known in vacuum theory [6], and generalized at finite temperature [7]. In the real-time formalism, one needs the cut propagators, typically of the form

$$D^+(k) = (\theta(+k_0) + n_B(\omega)) 2\pi \delta(k^2), \quad (4)$$

for a scalar particle. The theta function ensures the emission of a particle ($k_0 > 0$) or its absorption ($k_0 < 0$) and n_B is the Bose-Einstein weight.

The next problem is the presence of infrared singularities. In the very simple example of $g^2\phi^4$ theory, the leading term in the self-energy at one loop order behaves as g^2T^2 at finite temperature and would behave as $g^2\mu^2$ for the fermionic analogue at finite density (of course there is no fermion for a ϕ^4 theory). For external momenta of the order of T (hard momenta), ordinary perturbation theory applies. For momenta of the order of gT (soft momenta), the first order correction is as big as the Born term and one needs to resum. Note that the T^2 (or μ^2) term originates from the region of integration where the momentum is hard so that one does not need to resum at infinity. This resummation has been developed by Braaten and Pisarski for QED and QCD at finite temperature [8]. At finite density the situation is slightly different. In fact, QCD at finite density is equivalent to QED at finite density so that infrared problems are less severe. Contrary to the finite temperature case, the statistical factor associated with a soft gluon does not contribute a $1/g$ enhancement. On the other hand, a hard momentum exchange is suppressed by Pauli blocking as compared with a soft momentum exchange.

Concerning the propagation of modes, this resummation brings new features. The resummed cut propagator is obviously, from eq.(4)

$$D^\pm(k) = (\theta(\pm k_0) + n_B(\omega))2\text{Re} \frac{i}{k^2 - \pi(k) + i\epsilon}, \quad (5)$$

where $\pi(k)$ is the one-particle irreducible self-energy. The above equation can also be written as

$$D^\pm(k) = (\theta(\pm k_0) + n_B(\omega))2 \left[\pi\delta(k^2 - \text{Re} \pi(k)) - \frac{\text{Im} \pi(k)\theta(-k^2)}{(k^2 - \text{Re} \pi(k))^2 + (\text{Im} \pi(k))^2} \right]. \quad (6)$$

The physical signification of this result is clear. The delta function comes from the pole in $D(k)$ and corresponds to the propagation of a quasiparticle (which is called a plasmon for a gauge theory). The second term originates from the existence of a branch cut below the light cone and is associated to Landau damping [8].

The energy loss rate from axions emitted by a quark-gluon plasma is directly related to the emission rate which one can calculate with the help of the cutting rules. Obviously, hard energies are favored over soft energies. However, all particles being massless, the simplest tree-level process which one can imagine, gluon \rightarrow axion + gluon, is kinematically forbidden. This is not the case if one of the gluon is dressed, that is one has to use a resummed propagator for one of the gluon.

Let me consider the diagram depicted in Fig.1 (the axion coupling to gluons is larger than to quarks). The axion emission rate associated to that self-energy is of the form

$$\Gamma_a(q) = \frac{1}{2Q} \frac{G^2}{4} \int \frac{d^4k}{(2\pi)^4} k_{1\mu} k_{1\alpha} \Pi_{\nu\beta}^-(k_1) k_{2\rho} k_{2\gamma} \Pi_{\sigma\tau}^+(k_2) \epsilon^{\mu\nu\rho\sigma} \epsilon^{\alpha\beta\gamma\tau}, \quad (7)$$

for an axion-like interaction lagrangian

$$\mathcal{L}_I = -\frac{G}{4} F_{\mu\nu} \tilde{F}^{\mu\nu} \phi_a = G \mathbf{E} \cdot \mathbf{B} \phi_a, \quad (8)$$

but which can apply to other pseudo-scalar particles as well (in [5] the scalar case has also been considered).

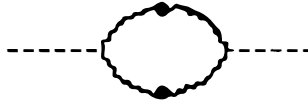


Fig.1 Axion self-energy in a QCD plasma

$\Pi_{\mu\nu}$ is the gluon polarization tensor which has both transverse and longitudinal modes. For instance, the transverse-longitudinal interaction process gives

$$\Gamma(q) = \frac{1}{2Q} \frac{G^2}{4} \int \frac{d^4 k}{(2\pi)^4} \Pi_T^-(k_1) \Pi_L^+(k_2) k_2^2 K_1^2 \sin^2 \phi, \quad (9)$$

with the effective scalar propagators Π^\pm given by eq.(6). The scalar product $\Pi^-\Pi^+$ can be decomposed into three terms, according to eq.(6), the plasmon \rightarrow axion + plasmon (pole-pole term), the plasmon \rightarrow axion + Landau damping (pole-cut term) and the Landau damping \rightarrow axion + Landau damping (cut-cut term). They are depicted in terms of graphs in Fig.2 (the dotted external legs are not the asymptotic states in the usual sense).

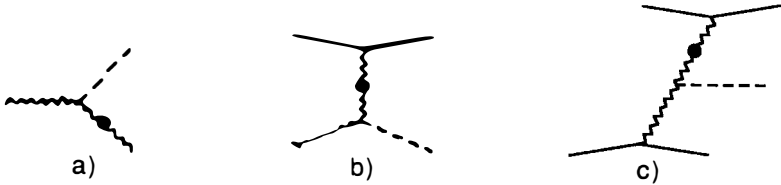


Fig.2 a) the pole-pole term; b) the pole-cut term and c) the cut-cut term

One can evaluate eq.(9) and find that the pole-cut term dominates. The reason for this is mainly the soft-gluon exchange which enhances the rate by $1/g^2$. Details can be found in [5].

By requiring that the axion energy loss rate must not exceed the total energy liberated by the thermal neutrinos, $E_\nu \simeq 2 \times 10^{53}$ erg, during the cooling of the neutron star, which time scale is ~ 5 sec, I obtain the constraint $f_a \gtrsim 0.3 \times 10^{10}$ GeV. This new bound is approximately of the same order than the one found by considering nucleon bremsstrahlung in the supernova core.

References

- [1] R.D. Peccei and H.R. Quinn, Phys.Rev.Lett.**38** (1977) 1440.
- [2] J.E. Kim, Phys.Rev.Lett.**43** (1979) 103;
M. Dine, W. Fischler and M. Srednicki, Phys.Lett.**B104** (1981) 199.
- [3] G.G. Raffelt, Phys.Rep.**198** (1990) 1; M.S. Turner, Phys.Rep.**197** (1990) 69.
- [4] J. Engels and H. Satz, Phys.Lett.**B159** (1985) 151.
- [5] T. Altherr, Z.Phys.**C47** (1990) 559 and Annals of Physics, to appear.
- [6] G.'t Hooft and M. Veltmann, Diagrammar, Cern Yellow Report 73-9.
- [7] H.A. Weldon, Phys.Rev.**D28** (1983) 2007;
R.L. Kobes and G.W. Semenoff, Nucl.Phys.**B260** (1985) 714 and **B272** (1986) 329;
- [8] R.D. Pisarski, Phys.Rev.Lett.**63** (1989) 1129; E. Braaten and R.D. Pisarski, Nucl.Phys.**B337** (1990) 569 and **B339** (1990) 310.

GRAVITATION



A NEW METHOD FOR TESTING NEWTON'S GRAVITATIONAL LAW

J. Schurr,N. Klein[†], H. Meyer, H. Piel, H. WaleschFachbereich Physik, Bergische Universität Wuppertal
D-5600 Wuppertal 1, Fed. Rep. of Germany

ABSTRACT

We report on a new experimental method for determining the gravitational force of a laboratory test mass on a Fabry-Perot microwave resonator. The resonator consists of two Fabry-Perot mirrors suspended as pendulums. Changes of $2 \cdot 10^{-11}$ m in the pendulum separation can be resolved as a shift of the resonance frequency of the resonator. This limit corresponds to an acceleration of $7 \cdot 10^{-11}$ m s⁻² of one mirror with respect to the other. In a first experiment we have measured the gravitational acceleration generated by a 125 kg test mass as a function of distance in the range of 10 to 15 cm and tested Newton's gravitational law with an accuracy of 1%. No deviation is found. Furthermore, the gravitational constant G is determined with similar precision.

[†]) Present address: Forschungszentrum Jülich, Institut für Festkörperforschung
D-5170 Jülich 1, Fed. Rep. of Germany

Newton's law of gravitation has recently been tested in a series of new experiments with different precision. These experiments were stimulated by reports on observations of possible short-range deviations from Newton's square law¹⁻⁴). In this context it also becomes of great interest to improve on the uncertainty, with which the gravitational constant G is known experimentally. The smallest relative error achieved so far is $1 \cdot 10^{-4}$. However, different experiments disagree in their results outside of the quoted errors^{1,2}).

This discussion has motivated us to develop a pendulum gravimeter to measure the gravitational acceleration of a test mass as a function of distance and to determine the gravitational constant.

I. THE FABRY-PEROT GRAVIMETER

The gravimeter consists of two Fabry-Perot mirrors⁵). They are separately and bifilar suspended as pendulums with a length of $l=3$ m (Fig.1) at a distance of 15 cm. The gravitational acceleration of a 125 kg test mass elongates both pendulums. The change of the pendulum distance, which is to be measured, is proportional to the difference of the accelerations of each pendulum. It is calculated from a numerical integration of Newton's square law over the mass distribution of test mass and resonator. The distance between the centers of test mass and of the pendulum next to the test mass is varied from 10-15 cm and leads to a change of the mirror distance of $25 \cdot 10^{-9}$ m. This gravitational effect is to be measured by means of the frequency shift of the Fabry-Perot resonator.

A quality factor of the resonator of 140 000 is obtained experimentally. The width of the resonance curve corresponds to about 1 μ m. A shift of the resonance frequency $2 \cdot 10^{-5}$ times smaller than the width of the resonance curve can be detected, which corresponds to a displacement of $2 \cdot 10^{-11}$ m.

In order to cancel out disturbing effects, both mirrors are suspended as pendulums of equal length. The most important effects are: pendulum oscillations forced by microseismic vibrations of the ground; tidal forces; disturbing gravitational forces of masses in the surrounding of the apparatus; movements and tilts of the ground, etc.

The whole experiment is build up in a vacuum tank to avoid dielectric effects, convection and gas pressure forces. In order to keep thermal expansion effects small, the vacuum tank is build with good thermal insulation.

II. RESULTS OF GRAVITATIONAL MEASUREMENTS

The gravitational force between the test mass and the Fabry-Perot resonator was measured by moving the test mass periodically from the position, for which the gravitational force is to be determined, to a reference position. This procedure results in a modulation of the resonator frequency.

The modulation amplitude is determined by means of a Fourier analysis or a demodulation technique. Statistical errors, high- and low-frequency noise (corresponding to 0.1 nm) and drift effects (0.1 - 0.5 nm/h) can be separated with this procedure and the gravitational force is determined with high accuracy (the statistical error corresponds to 0.02 nm).

The modulation procedure has been repeated with the test mass in different positions, and the shift of the pendulum distance has been measured as a function of distance between resonator and test mass (Fig. 2). On the level of 1% (dominated by systematic errors) no significant deviations from Newton's gravitational law are seen and there is no indication of a fifth force with a range of a few centimeters.

The gravitational constant is determined from six measurements to be

$$G = (6,66 \pm 0,06) \cdot 10^{-11} \text{ N m}^2 \text{ kg}^{-2} \quad (1)$$

The quoted error is the statistical error, determined from the measured data. Systematic errors of about 2% have to be added. However, the result is in good agreement with the CODATA-value of the gravitational constant.

III. SUMMARY AND OUTLOOK

We have successfully tested a new method to measure the gravitational force of a test mass as a function of distance in the range of a few centimeters. The present sensitivity is sufficient to measure the gravitational force with an accuracy of about 10^{-3} at various distances and to determine the gravitational constant with an accuracy of about $2 \cdot 10^{-4}$. Furthermore, it should be possible to increase the sensitivity of the resonator using superconducting mirrors by more than two orders of magnitude⁵⁾. Certainly, the errors in measurement of the gravitational force are not yet limited by the resolution due to the normal conducting resonator. Consequently, we try to improve the experimental set-up and investigate Newton's gravitational law in the range of 0.5 - 2 m.

REFERENCES

- 1 G. T. Gillies, *Metrologia* 24, 1 - 56 (1987).
- 2 "Three hundred years of gravitation", ed. by S. W. Hawking, W. Israel, Cambridge University Press, Cambridge 1987.
- 3 Proceedings of the VIIIth Moriond Workshop, Les Arcs, France, 1988, ed. by O. Fackler and J. Tran Thanh Van, Editions Frontieres 1988.
- 4 A. De Rújula, *Phys. Lett.* 180 B, 213 (1986).
- 5 N. Klein, thesis, University of Wuppertal WUB-DIS 89-3, 1990;
J. Schurr, diplom thesis, University of Wuppertal WU D 88-11, 1988.

This work is supported by the Deutsche Forschungsgemeinschaft, Bonn, Fed. Rep. of Germany, under Grant No. Pi 118/4-1.

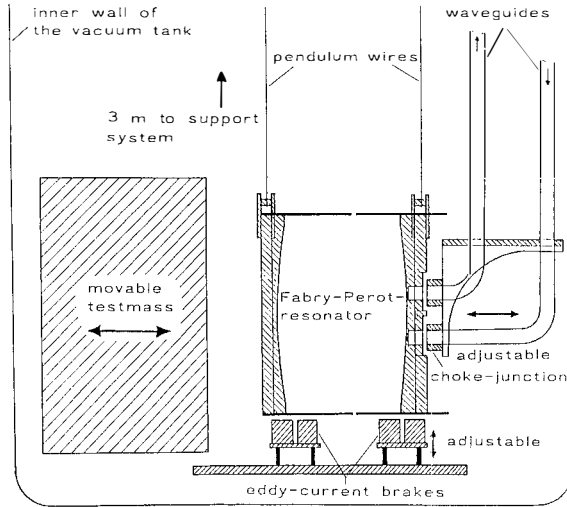


FIG. 1. Schematic diagram of the inner part of the vacuum tank with the Fabry-Perot resonator and the test mass. To scale: mirror distance = 14 cm.

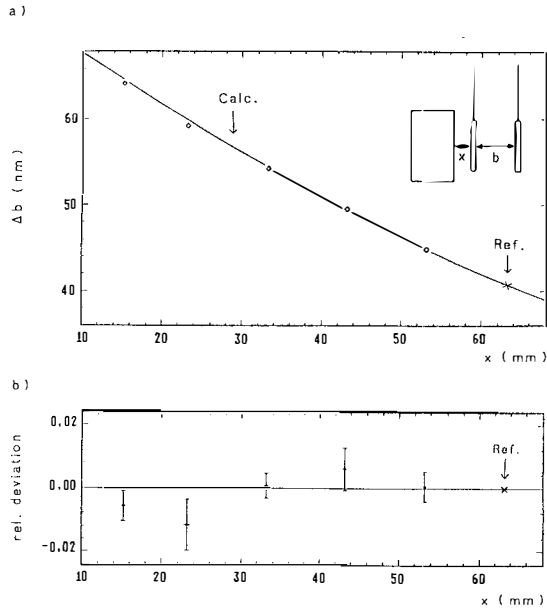


FIG. 2. The shift Δb in the mirror separation due to the gravitational force vs. the distance between test mass and resonator is shown in (a). The full line is a least-squares fit to the data which is obtained by a numerical integration of the gravitational force over the mass distribution. (b) shows the relative deviation of the experimental data in more detail.

A NEW TEST OF THE EQUIVALENCE PRINCIPLE:
AN UPDATE ON THE EOT-WASH EXPERIMENT

Blayne R. Heckel
Department of Physics FM-15
University of Washington
Seattle, WA. 98195 USA

ABSTRACT

This report summarizes the results obtained by the Eot-Wash group at the University of Washington during the past year. Three topics are discussed: a new limit on the equivalence principle using Al and Be masses in the field of the earth, the status of an experiment that uses a massive rotating source, and a discussion of the implications of equivalence principle experiments using matter for the gravitational properties of antimatter.

I. INTRODUCTION

There has been renewed interest in torsion balance experiments to detect a hypothesized intermediate ranged fifth force. Now that the weight of experimental evidence has fallen in disfavor of the existence of a new force, it is natural to ask what more can be learned from torsion balance experiments. Modern experiments with increased sensitivity can test more precisely the equivalence principle, upon which is based the general theory of relativity. More precise experiments can test the existence of new composition dependent interactions weaker than that originally proposed for the fifth force. In addition, a closer look at existing data can be used in a general field theoretic framework to set strong limits on an anomalous gravitational acceleration of antimatter. This report details the progress of our group on these three fronts during the past year.

II. A NEW TEST OF THE EQUIVALENCE PRINCIPLE IN THE FIELD OF THE EARTH

At the 1990 Meriond Workshop¹, our group presented the results of a test of the equivalence principle for Be and Cu, and Be and Al test bodies falling in the field of the earth: $m_i/m_g(Cu) - m_i/m_g(Be) = (0.2 \pm 1.0) \times 10^{-11}$ and $m_i/m_g(Al) - m_i/m_g(Be) = (0.5 \pm 1.3) \times 10^{-11}$, where m_i and m_g are the inertial and gravitational masses, respectively. A more complete description of this experiment has since been published elsewhere². We have made improvements to the apparatus used in this work and have embarked on a new round of equivalence principle measurements.

To improve upon our previous results requires both a reduction of the measurement noise and a reduction of the dominant systematic errors. The experimental noise was due to both seismic disturbances, noticeably worse during the day than at night, and thermal fluctuations as the equilibrium torsional position of our 20 μ m diameter W fiber is a sensitive thermometer. As seen in Table III of ref. 2, the dominant systematic errors in the previous work were excitations of the torsional mode of the pendulum caused by the rotation drive of the apparatus and the stability of the drive, quantifying the effects of thermal variations on the data, and spurious signals due to gradients in the ambient gravitational field. We have made substantial improvements to each of these problems, except for the seismic noise, and have taken new data with Be and Al test bodies.

The experimental apparatus is shown in Fig. 1. Four gold coated test bodies of equal mass and identical outside dimensions (two of Be and two of Al) form a composition dipole on a pendulum with vanishing mass quadrupole moment. The pendulum is suspended from a gold coated W wire inside of a vacuum vessel with a typical residual pressure of 1 torr. The torsional position of the pendulum with respect to the vacuum vessel (can) is monitored by an optical autocollimator using light reflected off of one of four identical mirrors mounted on the pendulum. The entire vacuum vessel is slowly rotated on a precision bearing at a rate such that the can revolution period is equal to eight torsional periods of the pendulum ($\tau_{torsional} = 714sec$). The entire rotating system is contained inside of a cylindrical Cu thermal shield whose temperature is regulated by water from a constant temperature bath.

The signal of interest is a torque (or change in the torsional equilibrium position) that occurs at the can rotation ($1\omega_{can}$) frequency. The two components of this torque are referred to as $a_{cos\phi}$ and $a_{sin\phi}$ where ϕ is the angle of the can with respect to laboratory coordinates. An important systematic check is to reverse the composition dipole on the pendulum by physically moving the test bodies. We refer to these two orientations of test

bodies as configurations A and B. The laboratory is located on a hillside to provide a source mass for interaction ranges of ≈ 1 m to 10 km, while the centrifugal sling of the pendulum of ≈ 1.7 mrad due to the earth's rotation allows the earth to be the source mass for ranges greater than the earth's radius.

The dotted line labelled 14 in Fig. 1 is an additional, rotating thermal shield that has been added to passively reduce thermal variations of the torsional fiber. In our previous work without this additional shield, a modulation of the temperature of the outer Cu thermal shield by ± 0.9 K at the can rotation frequency gave rise to a 14.4 μ rad torque on the pendulum at $1\omega_{can}$. With the new passive shield installed, the same ± 0.9 K modulation resulted in a torque at $1\omega_{can}$ of only 1.4 μ rad, a tenfold improvement in thermal isolation.

The rotation drive of the apparatus is controlled by a crystal oscillator whose output is divided down to drive a micro-stepped stepping motor. Variations in the can rotation frequency due to imperfections in the gear of the bearing can excite the torsional mode of the pendulum and give rise to spurious signals at $1\omega_{can}$. We now employ a 900,000 pulse per revolution rotary encoder to measure the can rotation speed and we feed back a signal to the stepping motor to hold the speed constant. Fig. 2 shows the output of the autocollimator for one can revolution (averaged over many revolutions) for our previous data before we used the feedback, and for our new data with the feedback in operation. Without the feedback, a 14.3 μ rad coherent torsional amplitude was induced by speed irregularities, while with the feedback in operation we now measure a coherent torsional excitation of 1.3 μ rad, again a tenfold improvement.

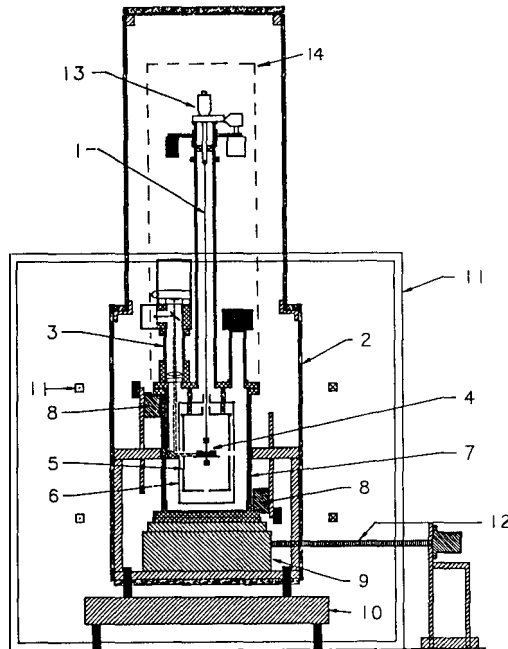


Figure 1. Side view of the torsion balance apparatus. 1) W fiber 2) thermal shield 3) autocollimator 4) torsion pendulum 5,6) magnetic shields 7) vacuum vessel and magnetic shield 8) gravity gradient compensator 9) turntable 10) baseplate 11) Helmholtz coils 12) turntable drive shaft 13) fiber positioner 14) inner thermal shield

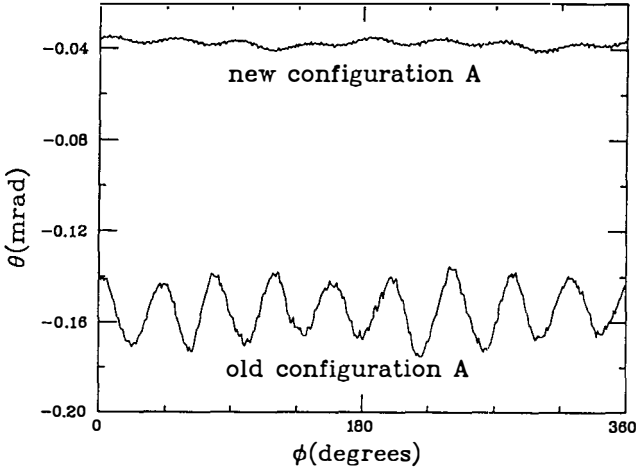


Figure 2. The autocollimator signal versus the orientation, ϕ , of the rotating vacuum can with respect to the lab, averaged over many revolutions. θ is the rotation angle of the torsion balance relative to the vacuum can. The torsional oscillations that are observed come from a non-constant can rotation rate.

The gravity gradient compensator labelled 8 in Fig 1 is used to cancel the gradient of the gravitational field at the site of the apparatus (due primarily to the local hillside) without inducing substantial higher derivatives in the gravitational potential. By using special test bodies whose centers of masses are displaced from their geometrical centers, we determined that the compensator in our previous work canceled the local gradient to one part in 145. We have improved the compensator to now cancel the local gradient to one part in 400.

These improvements to the apparatus along with the auxiliary measurements described in ref. 2 to test for systematic errors have reduced the total systematic error of the new results to less than 3 *nrad*. Our new results are summarized in Table 1 and are compared to our previous (1989) results. The rows labelled $(A - B)/2$ are the difference between the observed $1\omega_{can}$ signals for the test bodies in the *A* and *B* configurations and represents a composition dependent torque. The rows labelled $(A + B)/2$ are the average of the two configurations and represents the $1\omega_{can}$ torques that are due to imperfections in the apparatus. Taking the south component of the measured composition dependent torque, we conclude that

$$m_i/m_g(AI) \sim m_i/m_g(Be) = (0.1 \pm 0.8) \times 10^{-11}$$

Signal	1990	1989
$\frac{1}{2}(A - B)$	$a_{\cos\phi} = -7 \pm 17 \text{ nrad}$ $a_{\sin\phi} = +7 \pm 17 \text{ nrad}$	$a_{\cos\phi} = -21 \pm 26 \text{ nrad}$ $a_{\sin\phi} = -17 \pm 27 \text{ nrad}$
$\frac{1}{2}(A + B)$	$a_{\cos\phi} = 39 \pm 17 \text{ nrad}$ $a_{\sin\phi} = 0 \pm 17 \text{ nrad}$	$a_{\cos\phi} = +76 \pm 26 \text{ nrad}$ $a_{\sin\phi} = 142 \pm 27 \text{ nrad}$

Table 1: Comparison of our new results (1990) with our previous results (1989)

Combining our new result with our previous result, we find a new limit for the equivalence between the inertial and gravitational masses of Al and Be test bodies in the field of the earth to be $(2.3 \pm 6.9) \times 10^{-12}$. This new result should be considered preliminary because additional data are still being acquired.

III. MASSIVE LOCAL SOURCE EXPERIMENT

There are two important motivations and several experimental benefits that come from using a laboratory source mass in torsion balance experiments. To search for a composition dependent interaction using the earth as a source necessarily leaves one insensitive to an interaction for which the charge of the earth vanishes. In addition, the shortest range that can be probed is limited by how close the apparatus can be positioned relative to the earth. Both of these limitations are overcome by using a compact dense laboratory source mass, positioned very near to the torsion balance. If the source mass position is modulated, a stationary, vibration isolated torsion balance operated under high vacuum can be employed which may greatly increase the signal to noise ratio compared to the rotating torsion balance performance described in section II. Our group is building a rotating source apparatus to search for composition dependent interactions with ranges as small as 2 cm. This technique has already provided important results to other groups²⁻⁵.

The rotating source apparatus is shown in Fig. 3. A 2900 kg depleted U source mass rests on a rotating platform and is counter balanced by a Pb mass at a longer moment arm. The U is split into an upper and lower half. Each half has the shape of a half ring with inner radius 10 cm from the center of the torsion balance. The symmetry and dimensions of the U mass ensure that the Y_{lm} moments of its gravitational potential for even l , any $m > 1$, and $l = 3, m = 1$ vanish at the center of the torsion balance. Opposite

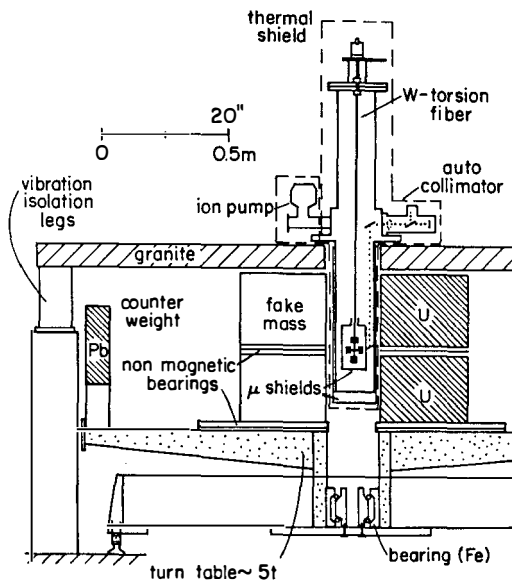


Figure 3. Design of a rotating source apparatus that allows 2900 kg of depleted uranium to be smoothly rotated around a stationary torsion balance.

the U masses will be hollow Al fake masses that complete the enclosure around the torsion balance vacuum vessel. The upper and lower halves of the U can be rotated relative to one another to alter the gravitational gradients from the U. The entire source mass will be rotated at a constant rate, most likely at the resonant frequency of the torsion balance.

A highly symmetric torsion balance using four masses arranged in a composition dipole configuration will be suspended from a Au coated W fiber inside a high vacuum chamber. Initially, Cu and Pb test bodies will be used which along with the U source give good sensitivity to a force whose charge is proportional to isospin. The balance is located within a Au coated magnetic shield, and a second magnetic shield as well as a Cu thermal shield surrounds the lower half of the vacuum vessel. The balance is supported on a granite table which in turn rests on three air pad vibration isolation legs. The air pressure in the pads is servoed to prevent the granite table from tilting⁶. The air pads provide 20 db of attenuation at the 7 Hz bounce mode frequency of the pendulum which we find is the dominant mode for coupling seismic noise into the torsional mode.

With reduced seismic noise and an increased Q of the pendulum coming from a vacuum of 10^{-6} torr, we anticipate an increase in signal to noise of at least 30 compared to our rotating balance experiment described in section II. The improved experimental sensitivity along with the massive local source should allow us to search for composition dependent interactions at new levels of precision and for ranges as small as ≈ 2 cm.

IV. DO MATTER AND ANTIMATTER FALL WITH THE SAME ACCELERATION?

There has been much interest at previous Moriond workshops concerning the gravitational properties of antimatter. According to general relativity, matter and antimatter should have identical accelerations in a gravitational field. Attempts to build a quantum theory of gravity, however, often lead to scalar and vector partners of the familiar spin 2 graviton, which can lead to different gravitational accelerations for matter and antimatter^{7,8}. Our group has recently argued⁹ that within the framework of ordinary field theories, equivalence principle tests and tests of the inverse square law of gravity using ordinary matter set stringent limits on the anomalous acceleration of antimatter. This argument will be outlined briefly below.

In standard field theories, the exchange of even spin bosons lead to attractive forces between unpolarized bodies, while the exchange of odd spin bosons gives rise to a repulsive force between like bodies and an attractive force between bodies of opposite charge. Hence any difference between the gravitational acceleration of matter and antimatter must be due to an odd spin boson (such as a vector interaction which is the case we consider). Restricting our attention to first generation fermions, there are three independent vector charges which we can label q_e , q_p , and q_n for the electron, proton and neutron (with opposite sign for the corresponding antiparticle). The linear combination $q_p - q_e$ is proportional to electric charge which would make the new vector interaction indistinguishable from the ordinary electric forces (for ranges larger than the scale of the experimental apparatus). Laboratory based experiments with matter and antimatter are therefore both sensitive to only $q_e + q_p$ and q_n .

Different materials have varying $q_e + q_p$ and q_n charge to mass ratios due to the variations in the neutron to proton ratio and nuclear binding energies. The null results from equivalence principle measurements set limits better than 10^{-3} cm/sec² for the acceleration of antimatter at the earth's surface due to a vector interaction that couples to these charges.

Could the repulsive gravi-vector force in equivalence principle experiments be cancelled by an attractive gravi-scalar force? If only one pair of test bodies had been measured, the answer would be an unlikely yes. However, more than five different pairs of test bodies

have given null results in equivalence principle experiments. The different inherent nature of scalar and vector charges (different Lorentz transformation properties and different contributions from binding energy, for example) makes these charges vary differently for different materials, so that exact cancellation of a scalar and vector force cannot occur for all materials.

We have considered in detail three scalar charges to see to what extent the forces associated with them might cancel the vector interaction in equivalence principle experiments. Taking the scalar charges $q_s = m$, $q_s = m + 0.01B$, and $q_s = B + 10^{-6}B^2$ and the vector charge $q_v = B$ in each case, where m is the mass and B is the baryon number of the test body, we find that in each case, combinations of equivalence principle measurements and tests of the inverse square law of gravity limit the anomalous acceleration of antimatter at the earth's surface to be less than 10^{-3} cm/sec^2 . We conclude that experiments using ordinary matter provide a direct test for the presence of scalar and vector partners to the graviton, and that there is no evidence for such partners at a level below 10^{-6} times the strength of ordinary gravity.

V. ACKNOWLEDGEMENTS

I gratefully acknowledge the contributions from the members of the Eot-Wash group: E.G. Adelberger, H.E. Swanson, J.H. Gundlach, D. Sesko, Y. Su, M.G. Harris, C.W. Stubbs, and W.F. Rogers. This work was supported by the National Science Foundation under grants PHY-9104551, PHY-8451277, and ADT-8809616.

VI. REFERENCES

1. C.W. Stubbs in Proc. XXVth Rencontre de Moriond, ed. G. Fackler and J. Tran Thanh Van, Editions Frontieres, p225 1990.
2. E.G. Adelberger, et. al., Phys. Rev. D **42**, 3267 (1990).
3. W.R. Bennett Jr., Phys. Rev. Lett. **62**, 365 (1989).
4. R. Cowsik, et.al., Phys. Rev. Lett. **64**, 336 (1990).
5. P.G. Nelson, D.M. Graham, and R.D. Newman, Phys. Rev D **42**, 963 (1990).
6. G.L. Greene, Rev Sci. Instr. **58**, 1303 (1987).
7. K.I. Macrae and R.J. Riegert, Nucl. Phys. **B224**, 513 (1984).
8. T. Goldman, R.J. Hughes, and M.M. Nieto, Phys. Lett. B **171**, 217 (1986).
9. E.G. Adelberger, B.R. Heckel, C.W. Stubbs, and Y. Su, Phys. Rev Lett. **66**, 850 (1991).

THE VIRGO PROJECT

Michel Yvert

Laboratoire d'Annecy-le-Vieux de Physique des Particules,
IN2P3-CNRS, BP 110,
F-74941 Annecy-le-Vieux Cedex, France

on behalf of the VIRGO Collaboration



Abstract: The detection of gravitational waves is, nowadays, technologically possible. The Virgo project, proposed by a French-Italian collaboration, is now on the verge of being fully approved and funded; its goal is to use a large Michelson interferometer as a detector. The main motivations, characteristics and expected sensitivity of this project are described.

INTRODUCTION

The now seventy year old prediction made by Einstein⁽¹⁾ of the existence of gravitational waves, as a consequence of the standard theory of General Relativity, is still today without direct experimental proof. Thanks to the work of Taylor⁽²⁾ interpreted by Damour⁽³⁾ on the slowdown of the pulsar PRS1913+16, we have solid peripheral evidence for the existence of these gravitational waves.

The discovery of gravitational waves will not be strictly a test of general relativity, it will also give a better understanding of the gravitational force. As an experimentalist, I will bypass the theoretical difficulties inherent in the quantification of the gravitational field, to state that since a gravitational wave is composed of real gravitons, their detection will be a first step towards the detection of the gravitational force intermediate boson. This is the leading argument of particle physicists. Another exciting side of the detection of gravitational waves is summarized in the three remarks of astrophysicists: -1) unlike electromagnetic waves, gravitational waves are not absorbed by matter, -2) all our knowledge about the universe is based on information carried by E.M. waves (except a few ν events), -3) gravitational waves are expected to be emitted from places where the density of matter is large (places from where electromagnetic waves cannot escape). Therefore the detection of gravitational waves will give us a completely new picture of the universe (a picture to which we are now blind).

The goal of the Virgo project is, first, to detect gravitational waves. The next will be to perform, in conjunction with other similar detectors, more precise measurements (i.e. the spin of the graviton) and start gravitational wave astrophysical observations.

I will not, here, enter into the details of the Virgo project, these can be found elsewhere⁽⁴⁾. Instead, I will recall the detection principle, the main characteristics and difficulties of the experimental apparatus and comment on the status of Virgo when compared to the other similar projects.

GRAVITATIONAL WAVES

-Effect on our space

When a gravitational wave propagates, the metric tensor is modified. This corresponds to a "deformation of space" leading to a change in the distance between two points initially at rest in the proper reference frame of a detector. Let x, y, z be the coordinates of a point in such a frame, provided we have:

$$|x|, |y|, |z| \ll \lambda_g$$

where λ_g is the gravitational wave length. One can find^(5,6) (the wave traveling along Z) the change in the distance $\delta x, \delta y, \delta z$ as solutions of:

$$\frac{d^2 \delta x}{dt^2} = \frac{1}{2} \left(x \frac{d^2 h_+(t)}{dt^2} + y \frac{d^2 h_x(t)}{dt^2} \right)$$

$$\frac{d^2\delta y}{dt^2} = \frac{1}{2} \left(-y \frac{d^2h_+(t)}{dt^2} + x \frac{d^2h_x(t)}{dt^2} \right)$$

$$\frac{d^2\delta z}{dt^2} = 0$$

where $h_+(t)$ and $h_x(t)$ correspond to the 2 polarization states of the wave. If, in order to simplify the picture, we consider only a wave fully h_+ polarized and propagating along z, this translates into simple elongations along the axes:

$$X \text{ -----} > X(1 + h/2)$$

$$Y \text{ -----} > Y(1 - h/2)$$

$$Z \text{ -----} > Z$$

-Sources of gravitational waves

Gravitational waves are emitted when masses are accelerated in a non-symmetric system⁽⁵⁾. The characteristic effect $h=2\Delta l/l$ and the corresponding radiated energy is non-negligible only if the accelerations and masses involved are very large. With today's available technologies it is impossible to radiate a measurable amount of energy in the frame of an earth based experiment, instead the hopes are turned towards three main types of astrophysical sources:

- the asymmetrical collapse of a star into a neutron star (a supernova) or into a black hole. These violent phenomena are expected to produce a burst of gravitational waves with a duration of a few milliseconds. The corresponding time and frequency spectra depend on the mechanism producing the collapse⁽⁶⁾, the characteristic h amplitude is expected to be of about 10^{-21} if the supernova explodes at a distance of 10Mpc from the earth (center of the Virgo cluster of galaxies), the number of events expected within this level of sensivity is a few per month.

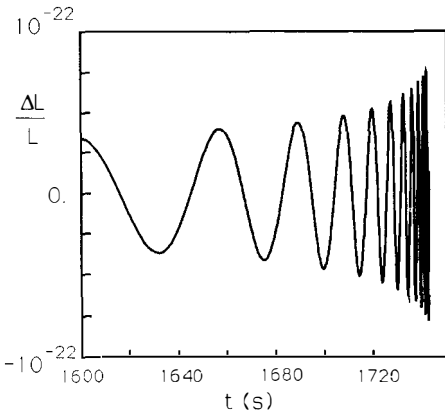


Fig1: coalescence of a system of two neutron stars with $M_1=M_2=M_\odot$ at 100Mpc. The origin of time is taken when $\nu_g=10\text{Hz}$

- the periodic sources corresponding to emission due to the asymmetric rotation of a system. The corresponding signal is expected to be of very small amplitude ($h \approx 10^{-24}$ with a frequency of 60Hz is an upper limit predicted for the Crab pulsar for example) but has the advantage of being always present.

- the coalescence of a binary system of two neutron stars. This phenomenon is expected to produce a very typical signal which, in the case of two neutron stars with masses $M_1=M_2=M_\odot$ in coalescence at 100Mpc, is plotted on figure 1. The evolution of both the amplitude and the

frequency of the emitted waves as a function of time is completely calculable with the only free parameters being the masses of the involved stars⁽⁷⁾. The rate of such events within a distance of 100Mpc is of the order of a few per year. This phenomenon is the most promising source to be detected by the first generation antennae.

VIRGO DETECTOR

-Principle: To measure a relative change of length of 10^{-21} is a delicate experiment. The Virgo detector is based on the idea already stated by Gertsenshtein and Pustovoit⁽⁸⁾ in 1963. It consists of measuring the X,Y asymmetrical change as a change in the relative phase between the two beams of a Michelson interferometer.

The change of phase has been calculated by Vinet⁽⁹⁾, it is given by :

$$\Delta\Phi_{\max} = 4\pi h L \sin(\eta) / \lambda \eta \quad \text{with } \eta = 2\pi v_g L / c = 2\pi L / \lambda_g$$

where λ is the laser light wavelength ($\lambda=1.06\mu\text{m}$ for a Nd:YAG laser) and λ_g the wavelength of the gravitational wave. The achievable sensitivity in the first generation of Virgo configuration will be $3 \cdot 10^{-11} \text{ rad}/\sqrt{\text{Hz}}$, leading to the need of an arm length of 100km to reach the desired sensitivity of $h=3 \cdot 10^{-23} \sqrt{\text{Hz}}$. This is achieved in Virgo by using a physical length of 3km with a

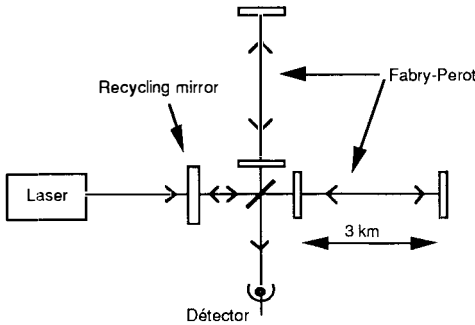


Fig 2 schematic view of the Virgo interferometer

Fabry-Perot cavity with a finesse of 40 in each arm, giving an overall effective length of 120km. At high frequencies the sensivity is found to be limited by the shot noise. To improve it, Virgo uses Drever's idea⁽¹⁰⁾ of recycling the "unused" light which is reflected by the interferometer (see figure 2).

-Difficulties: The foreseen sensitivity in the case of Virgo as well as in other similar projects, is very ambitious and requires the use of advanced technologies. The basic principles have been tested successfully on Michelson interferometer

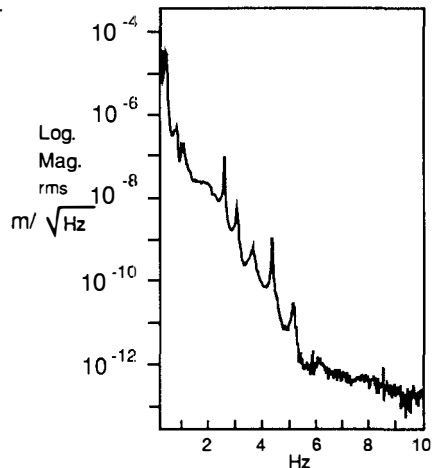


Fig 3- Response of the super-attenuator to a generated vibration⁽¹²⁾. The attenuation is 10^{-9} at 10Hz

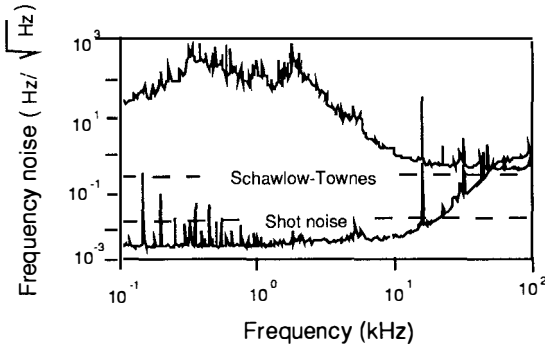


Fig 4 - The frequency noise of the stabilized Nd:YAG laser⁽¹³⁾

to avoid index fluctuations in the arms of the interferometer. I would like to point out two key points where Virgo is particularly well placed, these are: -1) the attenuators which isolate from external mechanical vibrations all the sensitive parts (mirrors, beam-splitter, injection and detection bench) -2) laser developments and stabilization. The proposed attenuator system, with gas springs mounted in series, has been built as a full size prototype in Pisa by the Giazotto team. It reaches attenuations of more than 10^{-9} at 10 Hz⁽¹²⁾, as shown in figure 3. Work is in progress to reach even lower frequencies, but the performance achieved so far is enough for the foreseen detector. Its second strong point is the laser frequency stabilization scheme which has been developed in Orsay by the Brillat team⁽¹³⁾; it gives (see figure 4) a Nd:YAG laser stabilization which, when scaled to the Virgo

prototypes equipped with delay lines, Fabry-Perot cavities and recycling mirrors⁽¹¹⁾. I will not detail here all the difficulties of such an experiment, however I will mention the main standard ones, they are: mirrors quality, which requires an extension of existing technology used in current small size gyrolaser mirrors to larger mirrors, and the vacuum which must be very good

interferometer, is already good enough to reach the required sensitivity.

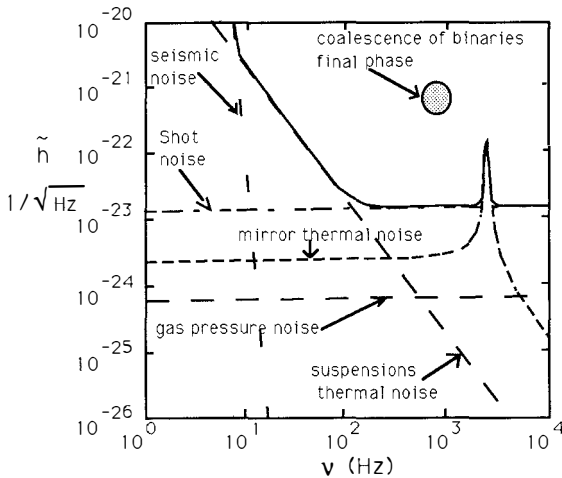


Fig 5 - Expected sensitivity of the Virgo interferometer

Expected sensitivity: The overall expected sensitivity, as a function of the gravitational wave frequency, is shown in figure 5 where each contribution to the limit in sensitivity is detailed. A numerical simulation of the signal is now undertaken. Figure 6a illustrates a first attempt of this simulation. The simulated expected signal from a 60Hz pulsar is generated on top of the noise, figure 6b is the Fourier transform of this simulated signal

which, despite coarse approximations, already reasonably simulates the analytical approach shown in figure 5. Work is in progress in this direction; the idea being to reach, when more refinements are implemented, a "realistic" simulation of Virgo data.

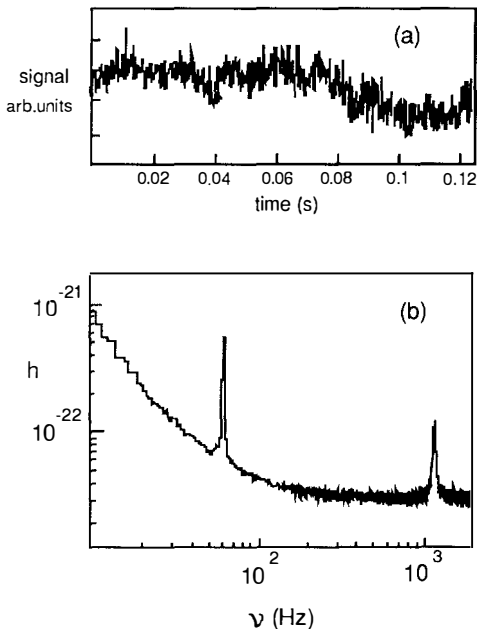


Fig 6 - Numerical simulation of the Virgo signal
 a) simulated signal (Virgo noise and 60Hz pulsar)
 b) Fourier transform of simulated signal
 (very preliminary result)

generated by human activity which is correlated to solar time). The problem with periodical sources is that one cannot rely on solid estimates of the amount of energy radiated in such systems as gravitational waves. For instance, for the Crab pulsar, the upper limit prediction for h lies between 10^{-24} and 10^{-26} , in the optimistic case of $h=10^{-24}$ the Virgo detector will catch the signal in 30 minutes.

Other similar projects: The Virgo project is in the process of being formally approved by the end of 1991, with the goal of being operational at full sensitivity by 1996. Two other projects with comparable time schedules are planned: GEO a British-German collaboration wishing to install a 3km arm length delay-line interferometer in Hanover and LIGO a United States collaboration whose goal is to install two 4km arm length interferometers with Fabry-Perot cavities (one located on the east coast and the other on the west coast). Another similar effort is evolving in Japan and a project is now in the preliminary study phase in Australia (Fabry-Perot cavities and 3km arm length).

Expected detection performances

-Star collapse: The Virgo detector will not be able to detect a supernova or a black hole formation alone. The detection of these phenomena will require detection in coincidence with another detector.

-Binary system coalescence: The situation in such a case is much better because the signal has a well known characteristic signature, allowing a very strong background rejection.

-Pulsars: To detect a periodic signal is, a priori, an ideal case since the signal is always present and its evolution both in frequency (Doppler shift) and in amplitude is well predicted (a sidereal time evolution of the signal helps to distinguish it from the noise

Another type of detectors are now in operation. They are based on Weber's idea⁽¹⁴⁾ of using resonant bars, their main difference in sensity is that they operate in a very narrow gravitational wave frequency band. Their sensitivity is now of the order of $h=10^{-18}$ which means that they are only sensitive to star collapses occuring in our galaxy (expected rate is a few per century only).

CONCLUSION

The detection of gravitational waves is now technically within reach, if they exist these waves will be discovered before the end of the decade. If a supernova explodes within our galaxy, this discovery may happen before 1996 by the Weber-type cryogenic resonant bars that are now in operation. It is more likely that their observation will occur in 1996 by the Virgo interferometer and the other similar detectors in operation at this time.

REFERENCES

- (1) A. Einstein: "Naherungsweise Integration der Feldgleichungen der Gravitation" Konog Preuss, Akad der Wissenschaften Litr., Erster Band (1916) 688; "Uber Gravitationswellen", ibidem Erster Band (1918) 154.
- (2) J.H. Taylor and J.M. Weisberg , *Astrophys. J.* 345(1989)434
- (3) T. Damour and N. Deruelle *Ann. Inst. H. Poincaré (Phys. Théor.)* 44(1986)263
- (4) **Virgo** Proposal for the construction of a large interferometric detector of Gravitational waves
A. Brillat , A. Giazotto . (1989)
- (5) C.W. Misner, K.S. Thorne, J.A. Wheeler .
Gravitation . W.H. Freeman and Company San Francisco (1973).
- (6) Three hundred years of gravitation. Chapter 9: Gravitational radiation by K.S. Thorne Edited
by S.W. Hawking and W. Israel Cambridge University Press (1987).
- (7) B.F. Schutz. *Nature* 323(1986)310
- (8) Gertsenshtein and Pustovoit . *Sov. Phys. - JETP* 16(1963)433
- (9) J.Y. Vinet . *J. de Physique* 47(1986)639
- (10) R.W.P. Drever. Interferometric detectors for gravitational radiation, in: *Gravitational
Radiation, Proc. Les Houches Summer Institute 1982*, eds T. Piran and N. Deruelle.
- (11) *Proc. of the NATO Advanced Research Workshop on Gravitational Waves Data Analysis.
Cardiff July 1987* . B.F. Schutz (ed.), *Gravitational Waves Data Analysis* p.147
- (12) C. Bradaschia et al. *Nucl. Inst. Met.* A289(1990)518
- (13) D. Shoemaker et al. *Optics Letters* 14(1989)609
- (14) J. Weber *Physical Review* 117(1960)307



DETERMINATION OF THE GRAVITATIONAL CONSTANT G AT AN EFFECTIVE DISTANCE OF 125 m

Adrien Cornaz, Walter Kündig, and Heinz Stüssi
University of Zurich, Department of Physics
Schönberggasse 9, CH-8001 Zurich

Abstract

In the plumb-line shaft in the dam of the Gigerwald-See, a pumped-storage lake 80 km south-east of Zurich, an experiment to measure the gravitational constant G at an effective distance of more than 100 m was started. The weight difference of two masses placed one above and one below the varying water level is measured with a mass-comparator. The goal is to measure in a first phase G with an accuracy of $< 1 \times 10^{-3}$. Together with the G -determination using a Cavendish type balance, the experiment will test the $1/r^2$ term in the gravitational law in the range of about 1 cm to 1 km.

Introduction

In recent years a great effort has been done to test the gravitational law [1]. These experiments can be separated in two groups: tests of the material dependence and tests of the distance dependence (inverse square law). The $1/r^2$ dependence has been tested with high accuracy ($\sim 10^{-8}$) at distances of $r > 10^7$ m [2]. On the other hand the gravitational constant G was only measured within laboratory distances $r \sim 10$ cm with a relative accuracy of $\simeq 1 \times 10^{-3}$. In the intermediate range (1 m to 1 km) it is very difficult to measure G [3,4] or to test the inverse square law [5,6,7,8,9,10] and only a few experiments were made in this region.

The proposed determination of G to $< 1 \times 10^{-3}$ at an effective distance of $r > 10^2$ m has a double importance, firstly only a few experiments are known that determine G with an accuracy of $< 10^{-3}$ [11], secondly the comparison with laboratory values of G can test the inverse square law of gravitation. Possible deviations of Newton's law could be interpreted by the existence of a fifth force [12] in the other case an upper limit could be found.

In this paper the experimental ideas are presented.

Description of the experiment

The easily accessible concrete dam of the Gigerwald-See has an overall height of 147 m and its crown is 360 m long. In addition to the regular water household the lake forms part of a hydroelectric storage system and is usually filled during the night using surplus electricity and emptied during day-time. The experiment is installed in the 110 m deep plumb-line shaft in the dam which is accessible on various levels (see figure. 1). The balance compares alternately the weight of a 1 kg mass near the balance with a second mass suspended on a $100 \mu\text{m}$ diameter gold-plated tungsten wire. The separation of the two test-masses is 105 m. The balance, a mass-comparator compares the weight of the two test-masses in the measuring process with an internal mass. The mass-comparator is a prototype, developed, made and maintained by 'Mettler', the producer of essentially all high precision balances used by national bureau of standards. The balance has been improved by two essential factors: it is operating in vacuum and it is temperature stabilized to 1 mK. In the laboratory the balance allows a reproducible comparison of two 1 kg masses within $0.1 \mu\text{g}$. The two test-masses are interchanged hydraulically in such a way, that the force on the balance stays constant within 1 g. For this the output of the balance controls the hydraulic system with stepping motors. The weights are interchanged every 5 minutes.

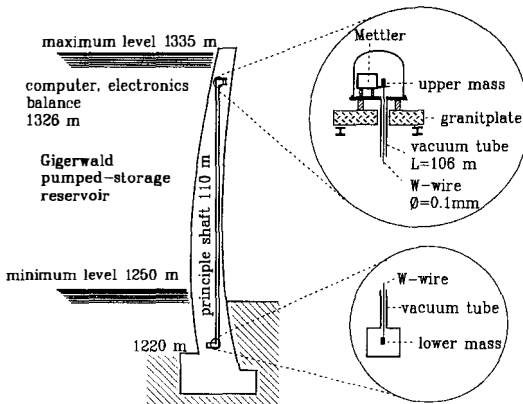


Figure 1: Cross-section through the dam. The mass-comparator and the 105 m long vacuum-system are indicated.

The oil free vacuum-system ($p \simeq 10^{-4}$ mbar) consist of a 105 m long 10 cm diameter stainless steel tube and the balance chamber.

The water level is measured with a pressure balance (resolution 2 cm). The distribution of the water is known as contour lines of the lake. The locations of the two weights in respect to the water were measured with an accuracy of 1 cm.

The expected weight changes as a function of the water level are shown in figure. 2. The

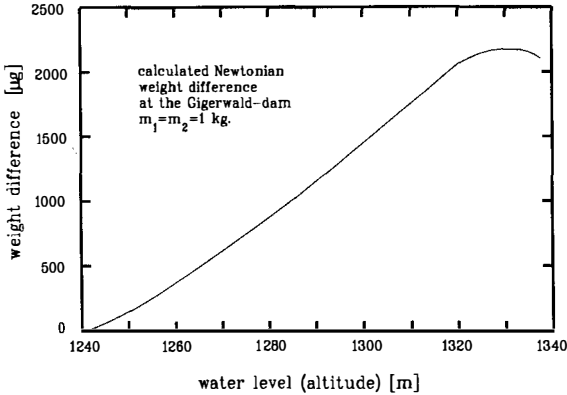


Figure 2: Calculated weight difference of the two 1 kg masses as a function of the water level above sea level.

weight difference is plotted as a function of the water level expressed in altitude of the water. The level variations of the Gigerwald lake are several meters per day and typically 10 m per week, the maximum variation is 85 m. The expected weight changes are about 1 mg. With the accuracy of the mass-comparator ($< 1 \mu\text{g}$) it should be possible to measure the gravitational constant at a level of 10^{-3} . This weight difference is only a function of geometrical data of the reservoir, every statcal gravity anomalies and earth tides are cancelled. Only slow local variations of gravity due e.g. to snow are not completely eliminated in the measurements and must be taken into account.

The effective distance r_{eff} of the vertical force acting on one of the masses can be defined as:

$$r_{\text{eff}} = \frac{\int r dF_z}{\int dF_z} = \frac{\int z r^{-2} dm}{\int r^{-3} dm},$$

where r is the distance between one of the 1 kg masses and the mass of the water dm , the integrals are to be taken over the lake. The effective distance is a function of the water level, for the full lake r_{eff} is 136 m for the lower mass and 103 m for the upper one.

This experiment is to be compared with two other lake experiments: Splyyard Creek [3] and Hornberg [4]. The Splyyard Creek experiment was performed with a balance placed on a tower in the lake, they measured like us the weight difference between masses placed below and above the water. The measurements in the Hornberg experiment were made with 6 gravimeters, placed below and above the water level in a tower. These two lake experiments show measurements of G with an accuracy near 1 %. In both of them one limitation was the noise produced by the tower. In comparison the Gigerwald experiment is performed in a concrete dam, the entrance of the pressure-line is situated 300 m form the mass-comparator, and the wind cannot cause serious vibrations of the dam. The limitation due to the calibration of the gravimeters (Hornberg) is eliminated by the use of a mass-comparator, which is regularly calibrated with a precision 1 g mass. The effective

distance of more than 100 m is to be compared with the effective distance of 22 m for the Splityard Creek experiment and of 39 m and 68 m for the Hornberg experiment.

The experiment was started in autumn 1989, the installation will be terminated in early 1991, first results are expected in the second half of 1991.

Acknowledgments

We would like to express our thanks to 'Mettler' who placed a prototype of a mass-comparator to our disposal. We are grateful to the KSL (Kraftwerke Sarganserland) for the permission to conduct the investigation in the Gigerwald dam. We thank also the Dr. Tomalla foundation, who supports one of us (A.C.).

References

- [1] James E. Faller, Ephraim Fischbach, Yasunori Fujii, Kazuaki Kuroda, Ho Jung Paik, and Clive Christopher Speake. Precision experiments to search for the fifth force. *IEEE Trans. Instrum. Meas.*, 38(2):180–188, April 1989.
- [2] F. D. Stacey, G. J. Tuck, G. I. Moore, S. C. Holding, B. D. Boodwin, and R. Zhou. Geophysics and the law of gravity. *Rev. Mod. Phys.*, 59(1):157–174, 1987.
- [3] G. I. Moore, F. D. Stacey, G. J. Tuck, B. D. Goodwin, N. P. Linthorne, M. A. Barton, D. M. Reid, and G. D. Agnew. Determination of the gravitational constant at an effective mass separation of 22 m. *Phys. Rev. D*, 38(4):1023–1029, 1988.
- [4] G. Müller, W. Zürn, K. Lindner, and N. Rösch. Search for non-Newtonian gravitation—a gravimetric experiment in a hydroelectric lake. *Geophy. J. Int.*, 101:329–344, 1990.
- [5] Steven C. Holding, Frank D. Stacey, and Gary J. Tuck. Gravity in mines—an investigation of Newton's law. *Phys. Rev. D*, 33(12):3487–3494, 1986.
- [6] Mark E. Ander et al. Test of Newton's inverse-square law in the Greenland ice cap. *Phys. Rev. Lett.*, 62(9):985–988, 1989.
- [7] J. Thomas, P. Kasameyer, O. Fackler, D. Felske, R. Harris, J. Kammeraad, M. Millett, and M. Mugge. Testing the inverse-square law of gravity on a 465-m tower. *Phys. Rev. Lett.*, 63(18):1902–1905, 1989.
- [8] Christopher Jekeli, Donald H. Eckhardt, and Anestis J. Romaides. Tower gravity experiment: no evidence for non-Newtonian gravity. *Phys. Rev. Lett.*, 64(11):1204–1206, 1990.
- [9] C. C. Speake, T. M. Niebauer, M. P. McHugh, et al. Test of the inverse-square law of gravitation using the 300-m tower at Erie, Colorado. *Phys. Rev. Lett.*, 65(16):1967–1971, 1990.
- [10] J. Thomas and P. Vogel. Testing the inverse-square law of gravity in boreholes at the Nevada test site. *Phys. Rev. Lett.*, 65(10):1173–1176, 1990.
- [11] George T. Gillies. The Newtonian gravitational constant—an index of measurements. *metrologia*, 24(Suppl.):1–56, 1987.
- [12] Ephraim Fischbach, Daniel Sudarsky, Aaron Szafer, Carrick Talmadge, and S. H. Aronson. Reanalysis of the Eötvös experiment. *Phys. Rev. Lett.*, 56(1):3–6, 1986.

GRAVITATIONAL AND NEUTRINO ANTENNAS

J. WEBER
VISITING RESEARCHER,
DEPARTMENT OF PHYSICS
UNIVERSITY OF CALIFORNIA, IRVINE, CA 92717 U.S.A.



Abstract

New approaches to neutrino and gravitational wave detection were published in 1984, 1985, 1986, and 1988.

Predictions of the 1986 theory were confirmed by Supernova 1987A observations.

Apparatus is described for observation of gravitational radiation and neutrinos from supernovae as far as the Virgo cluster.

1. Introduction

Classical general relativity theory predicts that gravitational waves exist and these waves are changes in spacetime geometry. Modern elementary particle physics describes these waves in terms of zero rest mass spin two gravitons.

Elastic solid bar antennas and Michelson interferometer antennas for gravitational radiation were proposed^{1]} during the period 1957-1960. An aluminum bar antenna at room temperature has been operating since 1969 at the University of Maryland "waiting for a supernova."

SUPERNOVA 1987A OBSERVATIONS

12 coincident pulses were observed^{2]} by this antenna and a similar one at the University of Rome, during the Supernova 1987A rapid evolutionary period. The Rome-Maryland antenna outputs were correlated with neutrino detectors at Mont Blanc, Kamioka, Baksan, and Cleveland. Correlations were also observed with elementary particle detectors at Frejus and Monte Rosa.

CROSS SECTIONS

In 1984 , a new theory of the elastic solid antenna cross sections was published^{3]}, regarding the antenna as a large number of elementary particles. Gravitons may be exchanged at any mass element. The new cross section can be as large as σ_{N_g} with

$$\sigma_{N_g} \rightarrow \frac{8\pi^3 GML^2 N^{1/2}}{C^2 \lambda} \quad (1)$$

In 1(G) is Newton's constant of gravitation, ML^2 is the bar quadrupole moment, C is the speed of light, λ is the wavelength and N is the number of atoms in the antenna.

A new approach to Weak Interaction Physics was published in 1985. For single crystals in the low energy limit the total cross section for neutrinos and antineutrinos is $\sigma_{N\nu}$ with ^{3]}

$$\sigma_{N\nu} = \frac{\left(\frac{\pi^2}{3} - 1\right) G_w^2 E_\nu^2 [N_T - Z_T(1 - 4 \sin^2 \theta_w)]^2}{4\pi \hbar^4 c^4} \quad (2)$$

In (2) G_w is the Fermi weak coupling constant, E_ν is the neutrino energy, N_T is the total number of neutrons and Z_T is the total number of protons. θ_w is the Weinberg angle.

CONCLUSION

Materials and technology for the gravitational radiation antennas are similar to what is required for the observation of neutrinos and antineutrinos by the single crystals with high Debye temperatures. A relatively small observatory is proposed for detection of gravitons and neutrinos as far as the Virgo Cluster.

1. Gravitational Radiation and Relativity, Volume 3, Eddington Centenary Symposium 1986, World Scientific, pp. 1-78.
2. Aglietta et al., *Il Nuovo Cimento* 12C N1, January-February 1989, pp. 75-103.
3. J. Weber, *Foundations of Physics*, 14, 1185, 1984, *Phys. Rev. C* 31, 4 April 1985, pp. 1468-1475; *Phys. Rev. D* 38, 1 July 1988, pp. 32-39.

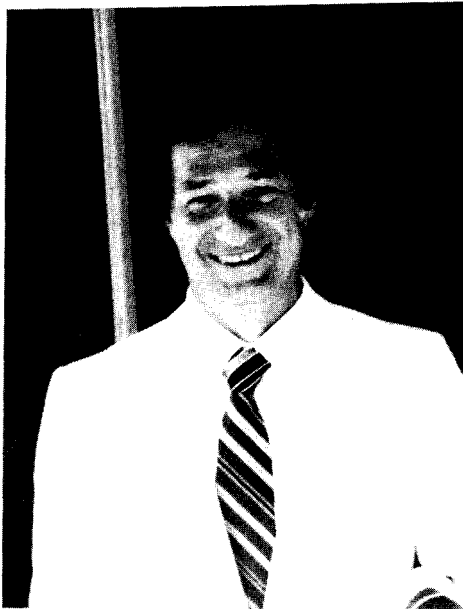
PHYSICS AND COMPUTERS



A PHYSICIST'S MODEL OF COMPUTATION

EDWARD FREDKIN
DEPARTMENT OF PHYSICS
BOSTON UNIVERSITY
BOSTON, MA, 02215, USA

This paper is an attempt to make a statement about what a computer is and how it works from the perspective of physics. The single observation that computation can be a reversible process allows for the same kind of insight into computing as was obtained by Carnot's discovery that heat engines could be modelled as reversible processes. It allows us to bring computation into the realm of physics, where the power of physics allows us to ask and answer questions that seemed intractable from the viewpoint of computer science. Strangely enough, this effort makes it clear why computers get cheaper every year.



Physics applied to Computers

Let us imagine ourselves physicists thrust back into the days before Galileo. We observe a heavy object that we hold in our hand. We note that it takes a steady force to hold the object and keep it from falling. We let it go, it falls to the ground and then comes to a stop with a thud. Back then, such observations could have led one to a set of laws of physics that are quite different from what we know today. For example, we might have concluded that a steady force is needed to keep an object still. We might have concluded that the energy or momentum (*vis viva*) associated with a massive object in motion simply disappears through friction or inelastic collisions.

There are certain principles that helped Galileo and Newton separate rough, common sense conclusions from the underlying laws of physics:

1. There are laws of essentially unlimited and clear applicability. A good example is conservation of momentum. The object is to discover and make use of such laws.
2. It is wise to formulate laws with regard to idealized models that don't suffer from the confusions of the real world.
3. We need to understand and make use of the concept of a closed system, where we can account completely for what is going on.
4. It is often easier to ignore boundary conditions; ie to analyze a dynamic interval as opposed to including the special circumstances about how it starts and finishes.

Today, everything mentioned above seems too obvious for words. Nevertheless, the kind of thinking that is second nature to physicists seems not to have been applied to computation. After a brief foray into how present day computer scientists think about computation, we will discuss computation from a physicist's perspective.

There are many different ways to model computation. The favorite of the computer scientists is the Turing Machine¹, which is a model that simplifies and makes clearer what a non-thinking clerk can accomplish (or cannot accomplish) with an unlimited supply of time, pencil and paper. What Turing did was to abstract the concept of the memory and notes of a mathematician from such messiness as notebooks and a brain, into a one dimensional tape of paper and a person acting as a computer whose mind is in one of only a small number of states. The only allowed operations involve writing one of a small number (e.g. 10) of symbols

onto a square space on the tape (erasing what was previously there), then moving the tape one square to the left or to the right, and finally changing the state from one of a small number of states to another state. The rules governing the operation of a Turing machine consists of a table of quintuples. The five items in each quintuple are:

1. The current state
2. The current symbol in the square in view
3. A new symbol to write in the square; replacing the old symbol
4. A new state
5. An instruction to move the tape one square either to the left or to the right.

The number of different quintuples is at most the product of the number of symbols times the number of states. It is easy to design Universal Turing Machines with a state-symbol product of less than 100. A Universal Turing machine can exactly mimic the behavior of any computer given two things: a long enough tape, and an initial segment of the tape that has a suitable program on it. To do one step of a computation, the computer (a person) finds the quintuple that starts out with items 1 and 2 matching the state (in his mind) and symbol in view on the tape. He then copies the symbol from item 3 onto the square in view (erasing the old symbol), memorizes the state in item 4, moves the tape according to item 5 and then does the same thing again. Amazingly, it is clear that such a simple machine can do exactly what any other computer can do; albeit very slowly.

The Turing machine is clearly a model thought up by a mathematician as opposed to a physicist. Ulam² and Von Neumann³ thought up another computer model that is more like physics in many ways; the Cellular Automata⁴. Computer engineers prefer the Boolean Algebra⁵ model of digital logic, mixed with a bit of Automata Theory⁶. System programmers have come up with their own models; a list of all models of computation would be quite a sight.

A physicist, on the other hand, might want a model of computation that is made up of elementary parts and simple, mathematical rules; clearly in concert with the laws of physics. A physicist ought to be able to relate the fundamental things a computer does to units such as Mass, Length and Time. It should be possible to speak about computation and physics in the same breath⁷ "...energy, space-time, state, symmetries, translational invariance, particles, time-reversal...".

For a long time, the concept of a physics based model was commonly thought to necessarily rest on the laws of thermodynamics because it was thought that all microscopic acts of computation were necessarily dissipative. However nothing very interesting ever came of such thoughts. What follows is a physically correct exposition of some of the concepts of computation that is based on simple Newtonian mechanics. It is based on the same concepts as the kinetic theory, with the exception that we look at the model in microscopic detail; not statistically. Others have shown that similar models can be based on mechanisms consistent with the laws of quantum mechanics⁸. We believe that it is possible to model and understand microscopic aspects of computation better and more clearly from such a physical model, while all macroscopic aspects remain as what we know from other models of computation.

Ordinary Computers Like the Mac or Cray

Real computers have the distinction, amongst machines or systems, of corresponding most exactly to their abstract models. Most systems, say internal combustion engines that convert heat energy into mechanical energy, only crudely resemble their abstract models. Other systems match their models very well. A gearbox, whose output shaft turns at a rational multiple of the input shaft's RPM is quite good.

Ordinary computers are made up of millions or billions of parts, each of which might do millions or billions of operations per second, and each part does the exact thing expected of it every time. There is no approximation in the result. In contemporary computers, this is all due to the extreme quantization of signal and the existence of the appropriate transfer function. In other words, although noise is ever present at every microscopic action within a computer, the noise can nowhere ever exceed a very small threshold because it is converted to heat by every logic gate, while memories have sufficient hysteresis or signal thresholds to eliminate the possibility of being affected by noise. Of course this is all relative; today's technologies allow us to construct computers with essentially any probability p of not making an error, $0 \leq p < 1$, given that certain environmental conditions are maintained. Economics causes us to accept computer circuits where 10^7 gates operating 10^8 times per second will collectively drop a bit no more than every 10^8 seconds provided they are protected from heat, cold, lightning, cosmic rays, and other such trauma. That is about one error

every 10^{23} potential operations. If you wanted one error for every 10^{40} operations, the computer might be somewhat more expensive.

Thinking About Computation in a Closed System

It is very easy to get confused about what computation is unless computation is first modelled as a closed system. This means that we will ignore all input and output; essentially leaving it out of the model for the time being. Imagine a computer that consists of nothing but a memory (RAM) and a processor. Somehow, the program and the data are already in memory. The computer runs until the computation is finished, at which point the results of the computation are in memory. We will first make a model that describes that part of computation, and then we will show how to add input and output to the model. This is like considering the falling object between the time it is let go until some time before it hits the ground. We want to be able to answer questions about how much of the resources of nature (such as matter and energy or space and time) are needed to do such a computation. With regard to energy, there are two parts to the answer: how much energy is needed to set the computer in motion, and how much energy is dissipated in doing the computation.

Energy Requirements for Computation

If a most efficient supercomputer works all day to complete a weather simulation problem, what is the minimum amount of energy that must be dissipated according to the laws of physics? The answer is actually very simple to calculate, since it is unrelated to the amount of computation. The answer is always equal to zero. It is much like looking at a machine, such as a heat engine, and asking how much energy must be dissipated in converting heat into mechanical energy. The answer is, as so beautifully elucidated by Carnot, always equal to zero. This is because Carnot leapt over all other conditions and constraints by observing that a reversible process did not dissipate energy. Strangely enough, the necessary dissipation in a computer is only related to the amount of output data printed or displayed at the end of the computation, and unrelated to the amount of intermediate data generated during the computation. Thus the amount of energy that must be dissipated by a computation that answers the question "Is 3 an odd number?" is exactly the same as must be dissipated by a computation that answers the question "Is the 1,000,000,000th digit of

Pi an odd number?"; zero plus the dissipation required to display one bit, $\text{Log}(2)kT$, in both cases.

The Model

In order to model computation in a physically correct way, we will follow the lead of computer engineering by identifying the atomic parts of computers, and show that compositions of these parts can implement essentially any kind of computer. The difference will be that we will use parts that are physically correct rather than just logically correct.

When we say "computer" we mean only the central processing unit and its memories. In the abstract, ordinary commercial computers are built out of logic gates and wires. In real life, transistors, conductors, capacitors, insulators, power supplies, packaging and cooling constitute the essential kinds of elements found in computers. The normal abstract engineering model of a computer is a diagram consisting entirely of gates and wires along with a few other things that could be replaced by functionally similar things made of gates and wires; e.g. a magnetic hard disk could be replaced by a functionally similar device made of gates and wires. The rules are simple, each gate has inputs and an output. Each output can be connected to a few inputs.

In practical computer engineering, many different kinds of gates are used, yet the 2 input NAND gate is logically sufficient. All other gates can be synthesized out of combinational circuits of just one type of universal gate such as the NAND gate.

We will now develop a different abstract model that is based entirely on physically simple computational atoms and processes. At first it seems that we must account for three kinds of processes: computation, memory and communication. We will first explain why, in a formal, physically correct model of computation, memory and communication are the same process. Second, we will look at the atomic parts, which turn out to be two kinds of particles. For space, we will use $2 + 1$ dimensional space-time. Two spatial dimensions are used mainly because of its correspondence to drawings on paper of computer circuits.

Memory and Communication

If you write a letter and send it to a friend, that's communication. If you keep the letter, that's memory. A clever physicist can always change one to the other by means of a coordinate transformation:

"We define a fundamental act of communication as follows:

$R_{x', y', z', t'} \leq S_{x, y, z, t}$; we Receive, at x', y', z', t' information Sent earlier at x, y, z, t .

We define a fundamental act of memory as follows:

$R_{x', y', z', t'} \leq S_{x, y, z, t}$; we Read, at x', y', z', t' information Stored earlier at x, y, z, t . Normally, $x', y', z' = x, y, z$."

Thus the distinction between the words "memory" and "communication" is left to describe our intent; physics can't tell the difference.

In kinetic theory, we can deduce properties of ensembles of particles as the average results of the consequences of individual particles following simple dynamical laws. However, assume we know nothing more than the following rules:

1. A simple gas that is compressed isothermally gives off heat and increases in pressure.
2. A simple gas that is compressed adiabatically increases in temperature and pressure.
3. Processes 1 and 2 are reversible, i.e. a simple gas that is expanded isothermally absorbs heat and decreases in pressure.
4. A perpetual motion machine is not possible.

Assumptions 1, 2, 3 and 4 are sufficient to show that a Carnot⁹ engine is the most efficient possible way to convert heat energy into mechanical energy. The reason is simple; a Carnot engine is reversible, therefore if a Carnot engine can convert an amount of heat energy to mechanical energy, it can then operate in reverse to convert that mechanical energy back into the same amount of heat energy. If there were a more efficient engine needing less heat, then the Carnot engine operating in reverse could convert a portion of the mechanical energy back into all of the heat required by the more efficient engine. This would leave some free, surplus mechanical energy, violating 4. above. This argument makes no use of the kinetic theory; as far as Carnot is concerned his results are correct even if the working fluid is continuous rather than a gas made up of molecules. This is because everything that is shown true about the Carnot engine derives from nothing more than reversibility and conservation of energy.

The discovery that Computers can also be modelled as reversible processes was made independently by Bennett¹⁰ for Turing Machines, the author¹¹ for computer logic and ordinary computers, and by Toffoli¹² for Cellular Automata. By assuming reversibility at a microscopic level and by simplifying kinetic theory into the Billiard Ball Model¹³ (BBM) of

computation, we can understand the exact evolution of each and every particle. Strangely enough, a result of Turing, called "The Halting Problem" shows that it is not possible, in general, to calculate by any analytic method, any good statistical measures about the evolution of a given initial condition. This is because the BBM can be a universal computer like a Turing Machine.

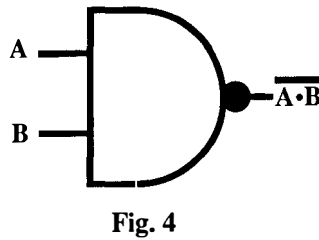
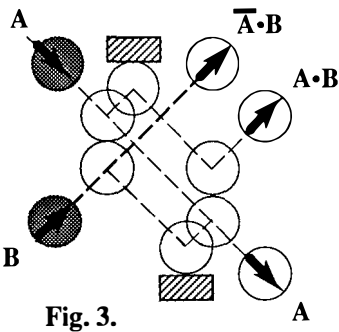
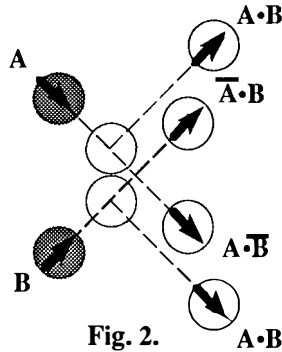
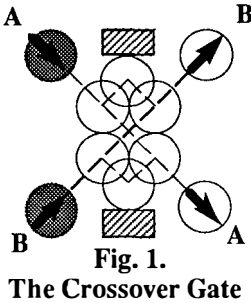
The Billiard Ball Model

We assume that there are two kinds of particles: light particles and heavy particles. All particles are perfect spheres with a radius of one. These particles are imagined to be just like perfect billiard balls with the exception that they are only engaged in translational motion. We assume that they are all of the same size, and we ignore friction or other sources of errors in the particles. When two particles collide, they simply bounce elastically, conserving kinetic energy and momentum with no losses or other forms of energy dissipation in the process. The most unusual aspect of the model has to do with the initial conditions. While the BBM assumes absolutely no errors or uncertainties, that assumption does not affect the main conclusions. Quantum Mechanics, rather than hampering things because of uncertainty, can come to our rescue by naturally constraining systems to a small number of states despite small disturbing effects.

Initial Conditions

Imagine a Cartesian space-time lattice. The initial condition requires that at time 0 the coordinates of every particle are integers. At time 0 the absolute value of the X component of the velocity of every light particle is ± 1 (± 1 unit of x per unit of time) and ± 1 for the Y component of velocity. The initial conditions and the assumption that the particles move without error or friction means that whenever time has an integer value, every particle has integer coordinates. At the moment when two particles collide, they both have integer coordinates and the line connecting their centers is parallel to either the X axis or the Y axis. If the line is parallel to the X axis, then each particle changes the sign of the X component of its velocity. Particles only move in the four diagonal directions. Collisions take place every so often as the system evolves. It is like a further abstraction of the perfect gas model, where our interest is focussed on the exact evolution of every particle, as opposed to the statistical evolution of an ensemble.

In order to keep things bounded and to define paths through space that correspond to wires, we introduce heavy particles that are identical to light particles except that their velocity is zero and their mass is infinite. The rules for particle interaction cause any heavy particle to remain stationary. Heavy particles act like reflectors or walls. Such particles are introduced as a convenience in order to allow the model to correspond closely to circuit diagrams drawn on paper. Heavy particles are shown as cross-hatched blocks.



All ordinary computers are built out of a large number (millions) of gates like the 2 input NAND gate shown in Fig. 4. NAND gates are considered to be universal since combinational circuits of such gates can perform any desired logic function, including memory. BBM circuits such as the Interaction gate Fig. 2 or the Feynman gate Fig. 3 are similarly universal while also being reversible.

The Hardware is Space!

A bit of memory in the BBM is a point in space-time that may or may not have a particle present. By convention, if the particle is present, we say that the state is a 1; if the particle is absent, the state is a 0. Given a volume of space, v , (v =the number of places that a particle might be) and a number of particles, n , the amount of information that can be represented is equal to the Log_2 of the binomial number $B(v, n)$ or $\text{Log}_2(v!/(n!(v-n)!))$. Conversely, the minimum volume required to do a computation must certainly be greater than what is required to represent the maximum amount of information, that needs to be present at one time. The most efficient number of particles (in order to minimize volume) is $n=v/2$. Physics mandates that the number of particles be fixed, unlike ordinary computers where the number of ones in memory can vary anywhere from zero to the total number of bits in memory. Since a particle in the BBM must be conserved, the number of ones is constant. Even if information is represented by spin (up or down) then conservation of angular momentum means the number of ones cannot change. This is only slightly less efficient than using bits, since the $\text{Limit}(\text{Log}(B(v, v/2))/\text{Log}(2^{v/2}))=1$ as $v \rightarrow \infty$. E.g. a volume of 1000 with five hundred particles represents the same information as 995 bits.

The minimum time required to do the computation is related to the largest total distance that must be traversed from an initial bit of information to a final bit of information. This path may include many paths connecting various intermediate bits. Each path is the sum of a set of subpaths, where a subpath takes a bit from one gate to the next. In the BBM a gate is simply a point in space where an informational interaction might take place. It is obvious that the dimensionality of the space will greatly affect this time. Ie, 3D is better than 2D which is much better than 1D.

What is known about the BBM is that it is possible to use it to implement fairly conventional computer models that have the distinction that the basic components are microscopically reversible. This means that the macroscopic operation of the computer is also reversible. This fact allows us to address the same question posed by Carnot about heat engines. "What is required for a computer to be maximally efficient?" The answer is that if the computer is built out of microscopically reversible components, then it can be perfectly efficient. How much

energy does a perfectly efficient computer have to dissipate in order to compute something? The answer is that the computer does not need to dissipate any energy. If the user wants a copy of the answer, then making the copy must cost about $\text{Log}(2) kT$ for each bit of information in the copy.

To be precise, we will imagine that we have a reversible floppy disk containing three sections: a computer program, the data, and a blank section for the results. We want to put the floppy into our reversible computer and have it run the program on the data, and then write the answer onto the floppy. The first step is that the computer swaps the contents of a Block of its Memory, BoM, for the contents of the floppy; the program, the data and a blank area that will receive the results of the computation. This is a reversible and non-dissipative process. Then the computer gets to work and runs the program until it has the answer in its memory. The computer then makes a copy of the result and writes it onto the floppy. This is the only non-reversible process and it costs $\text{Log}(2)kT$ for each bit of the result. The computer then operates in reverse to undo anything not already undone, converting the result in its memory (along with other intermediate data) back into the original program and data. The computer then swaps the program and data in its memory for the BoM on the floppy. At this point the computer is in exactly the same state as it was before running the program, but the floppy has been changed in that the results have been added to the original data on the floppy. Thus the amount of energy that must be dissipated is exactly proportionate to the number of bits in the result, and not related to the amount of computational *work* that the computer had to do.

From the point of view of physics, the resources that corresponds to an operating computer is simply a volume of space, and a number of particles in motion. (It sounds just like the real world.) The particles communicate by moving, remember by existing and compute by interacting.

The Price of Computing

It may be hard to believe, but the picture we have painted of the computer from the perspective of physics allows us to understand the evolution of the price of computing. Many things made have costs that follow the so-called learning curve. The price decreases as the total number of items made increases. While the learning curve affects the

cost to manufacture computer components, it is not the major factor in the continuing decline of the cost of computation.

The steady decline in cost of the Pure Informational Parts of computers (lets call them PIPs) is related to the physics of computation. By PIPs we mean those parts that deal only with information; this includes memory chips, processor chips, all integrated circuits that just do digital logic, disks, etc. It does not include keyboards, printers, displays, etc. If one poses the question "What units of physics are necessarily related to the PIPs?", we get a startling answer; different than for any other things that are made by or used by man. The answer is that no particular amount of mass or length or time are necessarily related to the PIPs. If you consider a chair in the same light, it is obvious that the unit L (length) is necessarily related to chairs. We cannot make a useful chair that is 10 times smaller than normal. If you consider a paperweight, it cannot be made to weigh 1/100 of its weight and still perform its function. The motor in a car cannot be designed to deliver only 1/100 of a horsepower and still propel a car satisfactorily. However, every PIP can be reduced in size, reduced in mass, made to use less power, made to use less time (work faster), because it deals only with information. Information is not necessarily related with any minimum amount of any physical quantity; not length, not mass, not time, not power! What this means is that it is simply up to the engineers to use their imagination to continually find ways to use less and less in order to compute more and more.

While we can see limits associated with any particular technology, there is no reason to think that we will be unable to come up with better technologies as the need arises. All we need are states (particles) and space-time. If nature is finite (if there is a fundamental unit of length) then that will be a barrier, but we are still far from wherever that limit might be. As to the particles, it seems clear that we will be able to represent bits with single particles (such as an electron or a photon) or by simple 2 state systems such as spin. Today's computers are still far from such limits. As to space, today's computational structures (integrated circuits) are not only large by atomic standards, but they are basically all 2-D structures! As Feynman said long ago "There's plenty of room at the bottom."¹⁴

We don't want to imply that miniaturization can go on forever, but the current pace (about a factor of 2 every 2 years) can surely continue for another 100 years (a factor of 2^{50} or 10^{15}) which will bring us to a liter

of computer containing 10^{23} bits and able to out-compute the combined power of all the millions of computers in the world today. All this for \$1000 in 1991 dollars.

-
- 1 A. Turing, On computable numbers, with an application to the Entscheidungsproblem, Proc. London Math. Society Series 2, 42 (1936) 230-265
 - 2 S. Ulam, Random Processes and Transformations, Proceedings of the International Congress on Mathematics. (held in 1950) 2 (1952), 264-275.
 - 3 J. von Neuman, Theory of Self-Reproducing Automata (edited and completed by Arthur Burks), University of Illinois Press (1966)
 - 4 T. Toffoli and N. Margolus, Invertible Cellular Automata: A Review, Physica D 45 (1990) 229-253
 - 5 G. Boole, An Investigation into the Laws of Thought, 1854
 - 6 M. Minsky, Computation, Finite and Infinite Machines (Prentice Hall, Englewood Cliffs, NJ, 1967)
 - 7 E. Fredkin, Digital Mechanics, Physica D 45 (1990) 254-270
 - 8 R. Feynman, Quantum-Mechanical Computers, Foundations of Physics 16 (1986) 507-531
 - 9 S. Carnot (Nicolas-Leonard-) Reflections on the Motive Power of Fire (1824)
 - 10 C. Bennett, Logical reversibility of computation, IBM J. of Research and Development 6 (1973)
 - 11 E. Fredkin, Conservative Logic, informal memo, Caltech, 1975
 - 12 T. Toffoli, Cellular Automata Mechanics, Technical Report 208, Computer and Communication Sciences Department, University of Michigan (1977).
 - 13 E. Fredkin and T. Toffoli, Conservative Logic, International Journal of Theoretical Physics 21 (1982) 219-253
 - 14 R. Feynman, There's Plenty of Room at the Bottom, reprinted in Miniaturization, H. Gilbert ed., New York: Reinhold (1961)



TESTS OF FUNDAMENTAL SYMMETRIES



SEARCH FOR TIME REVERSAL VIOLATION IN THE DECAY OF POLARIZED ^8Li

M. Allet*, A. Converse**+, W. Haeberli+, W. Hajdas*, J. Lang*,
H. Lüscher*, M.A. Miller+, R. Müller*, O. Naviliat-Cuncic*,
P.A. Quin+, and J. Sromicki*

* Institut für Mittelenergiephysik, ETH Zürich, 8093 Zürich, CH
+ University of Wisconsin, Madison, WI 53706, USA



presented by J. Sromicki

ABSTRACT

The transverse polarization of the electrons emitted in the decay of polarized ^8Li has been measured. The time reversal violating R -correlation has been determined. No violation is seen on the level of ± 0.015 .

1. MOTIVATION

Despite of more than a quarter of a century of intense investigations, the violation of CP symmetry still remains enigmatic. Recent reports of the discovery of a new type of CP violation (nonzero value of ϵ' parameter in the K_L^0 decay, (ref. 1,2)) are still awaiting definite confirmation by other experiments. The phenomenon of CP violation is up to now restricted to the K^0 meson system.

Searches for closely related violations of the time reversal symmetry have been unsuccessful. The most sensitive test of T-violation yet performed searches for the electric dipole moment of the neutron (ref. 3-5). Although no positive evidence was found, severe restrictions on theories of CP violation are posed by these experiments.

From the perspective of nuclear physics the most promising tests are processes where strong interaction is not involved. Experiments searching for T-odd correlations in weak or electromagnetic decays are considered as the best probes of T-violation in this field. In this contribution, we present a new experiment of this class. The aim of this experiment is to measure the magnitude R of the triple angular correlation $\vec{J} \cdot (\hat{p}_e \times \hat{\sigma})$ between the directions of the nuclear spin \vec{J} , the momentum \hat{p}_e , and the spin $\hat{\sigma}$, of the electron emitted in beta decay of polarized ^8Li nuclei.

2. THEORETICAL FOUNDATIONS.

In classical papers by J.D. Jackson (ref. 6,7), two time reversal violating terms were found in the distribution functions for an allowed beta transition from oriented nuclei:

$$D \cdot \frac{\vec{J} \cdot (\vec{p}_e \times \vec{p}_\nu)}{J \cdot E_e \cdot E_\nu} \quad \text{and} \quad R \cdot \frac{\vec{J} \cdot (\vec{p}_e \times \vec{\sigma})}{J \cdot E_e}$$

where \vec{p}_e, \vec{p}_ν , refer to electron and neutrino momentum, and E_e, E_ν to their total energies respectively.

The amplitudes of these correlations can be expressed in terms of coupling constants of the weak interaction (ref. 6,7). In particular:

$$\begin{aligned} \xi \cdot R = & |M_{GT}|^2 \lambda_{JJ'} \cdot 2\text{Im}(C_T C_A'^* + C_T' C_A^*) + \\ & + \delta_{JJ'} M_F M_{GT} \sqrt{\frac{J}{J+1}} \cdot 2\text{Im}(C_S C_A'^* + C_S' C_A^* - C_V C_T'^* - C_V' C_T^*) \end{aligned}$$

with M_F and M_{GT} being the Fermi and Gamow-Teller nuclear matrix elements. The subscripts V, A refer to the dominant (real) vector and axial vector couplings, while S and T abbreviate exotic scalar and tensor interaction terms, which are sensitive to the deviations from the standard theory.

These expressions ...”are perfectly general, in that no assumptions concerning invariance with respect to space inversion, charge conjugation or the time reversal has been made”... (cit. ref. 7). Although the R -correlation is parity-odd, this does not pose any obstacle, since parity is maximally violated in weak interactions. The violations of time reversal are reflected by the presence of the pure imaginary parts in the fundamental couplings (if the overall phase is defined so, that eg. C_V is a real number).

Due to isospin change $\Delta T=1$ in the ${}^8\text{Li}$ decay, the Fermi matrix element for this transition is very small, $M_F \ll M_{GT}$. Therefore, our experiment is primarily sensitive to the charged current tensor coupling constants. To our knowledge a little is known about their imaginary parts. The present limit $\text{Im}(C_T C'_{A^*} + C'_T C_A^*) = -0.063 \pm 0.052$ (ref. 8) has been obtained in a rather indirect way by analysis of the final state interaction (FSI) corrections to the longitudinal polarization of the electrons emitted in the decay of the high Z nucleus ${}^{153}\text{Sm}$. Such FSI effects can also mimic the genuine time reversal observable in our experiment. However, due to the small nuclear charge and high decay energy, they are expected to contribute less than $R_{FSI} = 0.001$ for the ${}^8\text{Li}$ decay (ref. 9), which is well below the accuracy of the present experiment.

Concluding: In contrast to the better known measurements of the D -coefficient (ref. 10,11) which are sensitive to the imaginary $V - A$ interference terms, the present experiment provides new data in a sector which has received less attention up to now.

3. PRINCIPLE OF THE EXPERIMENT.

The most suitable process to analyze the polarization of electrons of a few MeV energy is scattering in a Coulomb field of high Z nuclei (Mott scattering). The sensitivity of this process to the electron polarization (analyzing power or Sherman function) reaches appreciable values (-0.1 to -0.4) only at large scattering angles $120^\circ - 170^\circ$. In the most favourable geometrical configuration \vec{J} , \vec{p}_e and $\vec{\sigma}$ form a system of mutually orthogonal vectors. Combining all these facts and using cylindrical symmetry around the nuclear spin axis, we came to the following

design of the electron polarimeter for R -correlation experiments (Fig. 1).

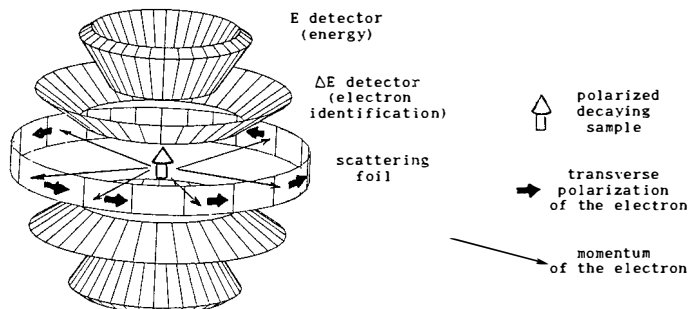


Fig. 1. The electron polarimeter. The asymmetry detected by up/down symmetric ring detectors, after scattering of the electrons from the analyzer foil, is a measure of their transverse polarization. This asymmetry determines, together with the nuclear polarization and the analyzing power of the scattering, the amplitude R of the triple angular correlation $\hat{J} \cdot (\hat{p}_e \times \hat{\sigma})$.

Such a polarimeter provides the necessary statistical power for the experiment by incorporating maximal solid angles for electrons impinging from the polarized source onto the analyzer foil, as well as those scattered towards the detectors. A symmetric arrangement of the detectors may be helpful in reducing systematic errors.

4. POLARIZED ${}^8\text{Li}$ SOURCE.

We produce polarized ${}^8\text{Li}$ nuclei by transfer of the polarization in the reaction ${}^7\text{Li}(\vec{d}, p){}^8\text{Li}$ initiated by 10 MeV deuterons. We used a 400 nA deuteron beam with a vector polarization of 0.5. The beam was provided by the Injector Cyclotron at the Paul Scherrer Institute, Switzerland. The data given below refer to our last run, which was performed in Feb. 91. The target, a 99.9 % isotopically pure, 5 mm thick rod of ${}^7\text{Li}$, was placed in a 5 mT magnetic field and cooled to liquid nitrogen temperature to obtain a spin relaxation time of 2.6 s, which is substantially longer than the 0.84 s half life of the decay. The ${}^8\text{Li}$ vector polarization was approx. $J=0.12$. This figure is an average over the measuring cycle. For most of the collected data the target was activated for 0.33 s, followed by a 1 s counting period, during which the

beam was deflected between ion source and accelerator and data were accumulated in 44 ms time windows. After four such cycles the polarization was reversed by switching rf transitions at the ion source, one activation/counting interval was paused, and the whole sequence was repeated. The polarization of the target was monitored continuously by measuring the beta decay asymmetry with a pair of electron detectors.

We note that although the polarization of the target may seem moderate (however our experience says that up to 40 % of the polarization transferred from the deuterons to ${}^8\text{Li}$ nuclei over a large energy range is rather unusual (ref. 12)), this method yields large source strengths of up to 10^9 decays/s.

5. EXPERIMENTAL ARRANGEMENT.

Our recent measurements were made with one half of the polarimeter presented in Fig. 1. The energy of the scattered electrons was measured by 4 cm thick plastic scintillators, which were arranged into four separate quarters placed in up/down symmetric configuration with respect to the incoming deuteron beam. Massive lead and brass shields were placed between the target and the detectors (Fig. 2) in order to protect them from very intense direct radiation emitted from the ${}^8\text{Li}$ source.

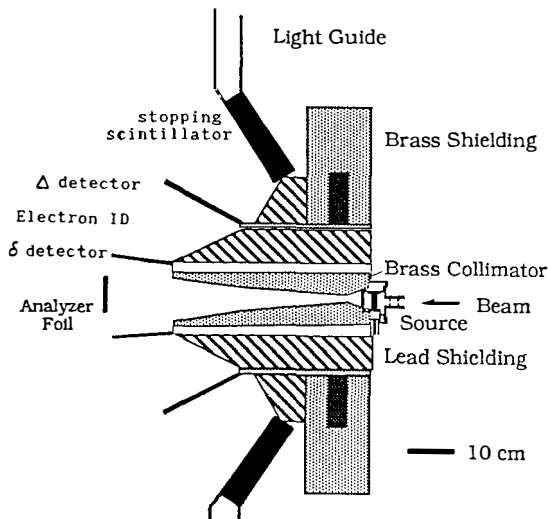


Fig.2 Cross section through the apparatus showing the location of the detectors and their shielding.

For each 90° segment, two transmission counters were used. They identified the electrons scattered from the foil from the decay associated background. We used a 7 cm high, 35 mg/cm^2 thick lead analyzer foil, which was placed at a radius of 55 cm from the ^8Li production target. The foil subtended 180° . The effective analyzing power of the polarimeter in these conditions, taking into account double and plural scattering effects, is $A = -0.10$.

6. SYSTEMATIC ERRORS.

Here, we list the most important systematic effects:

- Decay associated background seen by the detectors. Its intensity and asymmetry was measured periodically by removing the analyzer foil, and subtracted in the off line analysis.
- Nonuniform illumination of the scattering foil due to beta asymmetry coupled to a variation of the efficiency of the detectors as a function of the position on the foil. The asymmetry produced by this effect changes in step with the polarization reversal, and therefore simulates an R coefficient different from zero. We correct this effect by scanning the efficiencies of the detectors as a function of the position with the aid of a narrow (1 cm) ribbon foil. The resulting false asymmetry is then calculated by folding efficiency data with the known distribution of the electron intensity with respect to the nuclear spin.
- Gain shift of the photomultipliers. A system of LED/PIN diodes was installed. They monitor the gain of the detectors in every time window after activation. Although we observe approx 2 % gain shift in the first few time channels after activation, the resulting effect is very small, since the gain variations are very similar for both signs of the ^8Li polarization.
- Accidental coincidences. They were measured in a standard way by inserting delay lines into coincidences between transmission and thick stopping detectors.

7. THE RESULTS.

In May 90 we performed preliminary measurement of the R-correlation in the decay of ^8Li . Table 1 presents the result of this run with contribution of the most important systematic effects. This result

was presented at the workshop.

Table 1. Results of the preliminary measurement of R-coefficient.

Raw data	0.012 ± 0.034
Decay associated background, room background and cosmic radiation	-0.039 ± 0.026
Nonuniform illumination of the scattering foil due to β -decay asymmetry (ref. 1)	0.011 ± 0.005
Gain shift of the detectors (ref. 1)	-0.001 ± 0.003
Accidental coincidences	-0.007 ± 0.008
Result	$R = -0.024 \pm 0.044$

In the meantime (Feb. 91) we have completed a new data collection run with the extended arrangement of the detectors described in ch. 5. Preliminary analysis shows that we achieved a three-fold improvement in the errors. Also the value of the "decay associated background" correction is diminished significantly due to the improvement of the signal/background ratio which amounts now in the interesting energy range 4 – 11 MeV to 15. No effect of time reversal violation is seen in these data. A letter reporting these results is in preparation.

8. CONCLUSIONS AND PROSPECTS.

- The result for the R -coefficient presented at the workshop was consistent with time reversal invariance on the level of 0.044. The new measurement confirms this statement with a three times better precision and will represent the most accurate determination of the transverse polarization of electrons in beta decay.
- Our new measurement will set the limits for the TRV imaginary parts of the charged tensor couplings: $\Delta \text{Im}(C_T + C_T')/C_A \leq 0.04$. This is by a factor of 4 better than corresponding limits for the scalar couplings from the only other R-experiment performed with ^{19}Ne at Princeton (ref. 13).
- Our experiment is at present in its early data collection phase. We expect that this experiment will eventually achieve uncertainty in the R-coefficient on the level of a few parts per thousand.

REFERENCES.

1. H. Burkhard et al., Phys. Lett. 206(1988)169.
2. L. Fayard, contribution to this conference.
3. K. F. Smith et al., Phys. Lett. 234(1990)191.
4. S. Larmoreaux, contribution to this conference.
5. I.S. Altarev et al. JETP Lett. 44(1986)460.
6. J.D. Jackson, S.B. Treiman and H.W. Wyld, Phys. Rev. 106(1957)517.
7. J.D. Jackson, S.B. Treiman and H.W. Wyld, Nucl. Phys. 4(1957)206.
8. M. Skalsey and M.S. Hatamian, Phys. Rev. C31(1985)2218.
9. P. Vogel and B. Werner, Nucl. Phys. A404(1983)345.
10. R.I. Steinberg, P. Liaud, B. Vignon and V.W. Hughes, Phys. Rev. Lett. 33(1974)41.
11. A.L. Hallin, F.P. Calaprice, D.W. MacArthur, L.E. Piiilonen, M.B. Schneider and D.F. Schreiber, Phys. Rev. Lett. 52(1984)337.
12. Wang Zhenjie, R.A. Bigelow, P.A. Quin and J. Liechti, Phys. Rev. C40(1989)1586.
13. M.B. Schneider, F.P. Calaprice, A.L. Hallin, D.W. MAcArthur and F.D. Schreiber, Phys. Rev. Lett. 51(1983)1239.

EXPERIMENTAL SEARCH FOR EXTENSIONS OF THE STANDARD MODEL BY
RELATIVE BETA POLARIZATION MEASUREMENTS

N. Severijns^a, R. Prieels^a, J. Deutsch^a, P.A. Quin^b, F. Gimeno-Nogues^a, M. Allet^c, A.S. Carnoy^a, P. de Moor^d, O. Naviliat-Cuncic^c, I. Pepe^a, P. Schuurmans^d, R. Siebelink^d, W. Vanderpoorten^d, J. Vanhaverbeke^d, L. Vanneste^d and J. Wouters^a

^a Institut de Physique Nucléaire, Université Catholique de Louvain,
Chemin du Cyclotron, 2, B-1348 Louvain-la-Neuve, Belgium

^b Department of Physics, University of Wisconsin,
Madison, Wisconsin 53706 USA

^c Institut für Mittelenergiephysik, Eidgenössische Technische Hochschule,
8093 Ztirich, Switzerland

^d Instituut voor Kern- en Stralingsfysika, Katholieke Universiteit Leuven,
Celestijnenlaan 200D, B-3001 Leuven, Belgium

ABSTRACT

We report preliminary results of a relative measurement of the longitudinal polarization of positrons emitted in the decay of polarized ^{107}In nuclei, using the technique of time resolved spectroscopy of the positronium decay and yielding new bounds on right-handed currents.

1. Introduction

Although the standard $SU_L(2) \times U(1)$ electro-weak model is consistent with all today available data, it is inherently incomplete : the experimentally observed violation of parity is build in 'ad hoc' and assumed to be maximal, i.e. the coupling of the charged W gauge boson (first observed at CERN in 1983) to the basic quark and lepton fields is purely left-handed, implying a pure $V-A$ structure of the charged current quark interaction. In recent years, parity symmetric extensions of the standard model (i.e. models including $V+A$ currents), which are based on the gauge group $SU_L(2) \times SU_R(2) \times U(1)$, have been constructed¹⁾. They are characterized by an additional, predominantly right-handed charged gauge boson W_2 , which acquires a heavier mass m_2 than the mainly left-handed boson W_1 ($m_1 = 81$ MeV) due to some spontaneous left-right symmetry breaking at moderate energies. This accounts for the domination of left-handed couplings at low energies, while restoring parity conservation at a higher energy scale. In the minimal extension (the manifest left-right symmetric model, which assumes the same coupling strength for both bosons), the physical bosons (mass eigenstates) W_1 and W_2 are defined as a linear combination of the charged weak interaction eigenstates W_L and W_R by :

$$W_1 = W_L \cos \zeta - W_R \sin \zeta \quad W_2 = W_L \sin \zeta + W_R \cos \zeta \quad (1)$$

All beta decay observables can be expressed in terms of the mixing angle ζ of the two bosons and their mass ratio squared $\delta = (m_1/m_2)^2$.

2. Present constraints on right-handed currents

At high energy accelerators experiments to search for a right-handed gauge boson are planned (\bar{e}^+p collider experiments), but the requirements with respect to the luminosity and the polarization of the beams remain difficult to realize. High precision measurements at low and medium high energies however, can still improve significantly our knowledge of this subject. In the semi-leptonic and leptonic sectors, limits on the parameters δ and ζ have been obtained from different kinds of experiments up to now (see fig.3 in ref.2). Quite restrictive limits have been obtained from muon-decay³⁾, but these are only valid in the manifest left-right symmetric model, while the limits from nuclear beta decay experiments are more general. Recently, measurements of the relative polarization P_F/P_{GT} of positrons emitted in pure Fermi and Gamow-Teller transitions^{2,4)} have yielded stringent limits on both δ and ζ , i.e. $-4 < \delta \zeta \times 10^4 < 7$, but since these experiments limit the product $\delta \zeta$ ($P_F/P_{GT} \equiv 1 +$

$8\delta\zeta$), they do not provide a limit for δ (or ζ) if ζ (or δ) = 0. As for ζ , the unitarity requirement for the Kobayashi-Maskawa quark-mixing matrix, yields the constraint $2\zeta - \delta^2 = 0.0025 \pm 0.0034$ (90% C.L.)⁵⁾, reducing the possible mixing of the two bosons into the milliradian region. A number of experiments have provided limits for δ . Although absolute beta polarization measurements in several Gamow-Teller transitions⁶⁾ provide the 90% C.L. limit $\delta < 0.10$ for $\zeta \equiv 0$, this limit is of questionable reliability since it relies primarily on measurements for transitions of ^{30}P and ^{60}Co , which have large ft -values and are therefore subject to unknown forbidden contributions which may alter the longitudinal beta polarization significantly. The most reliable limit for the mass of the right-handed boson (again assuming $\zeta \equiv 0$) comes from the combination of the ft -value and the beta asymmetry for the decay of the neutron⁷⁾, i.e. $\delta < 0.16$ (90% C.L.). Finally, there is the recent result of Barbieri and Mohapatra⁸⁾ who have used the observed neutrino luminosity of the supernova SN 1987A to exclude the following region in the (δ, ζ) -plane :

$$(0.4 - 1.2) \times 10^{-5} \leq (\delta^2 + \zeta^2)^{1/2} \leq (0.02 - 0.07)$$

by requiring that the neutronization process $e^-_R + p \rightarrow \nu_R + n$ does not carry away most of the energy that can be radiated by the supernova. Combining all limits, a light right-handed gauge boson with mass m_2 between 200 GeV ($\delta < 0.16$) and 575 GeV ($\delta > 0.02$) (assuming no or negligible mixing) is not ruled out in the semi-leptonic sector.

3. Polarization asymmetry correlation experiments with ^{107}In

Recently, Quin and Girard⁹⁾ pointed out that relative measurements of the longitudinal polarization for beta particles emitted by polarized nuclei (the polarization asymmetry correlation) can provide new and sharp limits on δ . More precisely, in manifestly left-right symmetric (LRS) theories, the ratio of the positron polarizations for positrons emitted parallel and anti-parallel with respect to the nuclear spin direction ($\pm J$) is given by (for $\zeta = 0$):

$$R_{\pm}^{\text{LRS}} = R_0 \left(1 - \beta^2 \frac{8\beta \cdot JA}{\beta^4 - (\beta \cdot JA)^2} \delta^2 \right) \quad \text{where} \quad R_0 = \frac{(\beta^2 - \beta \cdot JA)(1 + \beta \cdot JA)}{(\beta^2 + \beta \cdot JA)(1 - \beta \cdot JA)} \quad (2)$$

and $\beta = v/c$, while A is the asymmetry parameter for the beta transition. The full power of the enhancement factor which multiplies δ^2 is realized when β and $\beta \cdot JA$ are large (i.e. close to one). If ζ is non-zero, δ^2 should be replaced by $(\delta + \zeta)^2$. Note that this experiment yields complementary limits to those obtained from experiments which measure P_F/P_{GT} (refs. 2 and 4).

A first experiment of this type is at present being carried out for the positron decay of ^{107}In which is dominated (> 95 % for the acceptance of our apparatus) by an allowed $9/2^+ \rightarrow 7/2^+$ Gamow-Teller transition with $\log ft = 5.7$, endpoint energy $E_0 = 2.25$ MeV, half life $t_{1/2} = 32.4$ m, and maximal asymmetry parameter $A = 1$. The ^{107}In activity was produced in a ($^{14}\text{N}, xn$) reaction using a 120 MeV N^{4+} beam and three 5 mg/cm^2 molybdenum targets that were mounted in a FEBIAD hot plasma ion source on the LISOL isotope separator at the cyclotron in Louvain-la-Neuve. With a cyclotron beam current between 4 and $5.7 \mu\text{A}$, the intensity of the 50 keV, mass separated ^{107}In beam varied between $4 \times 10^4 \text{ s}^{-1}$ and $1 \times 10^5 \text{ s}^{-1}$. This beam was implanted continuously in an iron foil, which was attached to the copper cold finger of a dilution refrigerator. In this foil, the ^{107}In nuclei were oriented at a temperature of 10 mK and in an external magnetic field $B_r = 0.316$ T. A nuclear polarization P of ~ 85 % was achieved. The positrons emitted by the polarized nuclei were focused into the polarimeter, with a beta spectrometer. The device is directly coupled to the refrigerator, at an angle of 90° with respect to the direction of the separated beam. The superconducting split-pair magnet in the refrigerator serves as the first element of the spectrometer. The fact that it is centered at the source location leads to a large acceptance : positrons emitted with angles up to 45° with respect to the spectrometer axis enter it. A solenoid magnet ($B \sim 600$ Gauss) then focussed positrons with a kinetic energy $E = (1.2 \pm 0.3)$ MeV into the polarimeter. Here the positrons passed through a 4 mg/cm^2 Be degrader (to stop positrons with $E < 1$ MeV), a 0.4 mm plastic scintillator START detector, and finally stopped in a MgO powder pellet (placed in vacuum) where positronium (Ps) was formed with $\sim 45\%$ efficiency. The Ps decay and direct annihilation photons were observed by two 5.1 cm diameter and 3.8 cm thick BaF_2 STOP scintillators placed at 180° to each other in a plane perpendicular to the polarimeter field axis and connected in OR logic to a time-to-digital converter of 156 picoseconds channel width from which time-resolved decay spectra were obtained (resolution 1.4 ns (FWHM)). The fraction of ^{107}In decays which contributed to the polarization measurement was 2×10^{-5} and the analyzing power of the polarimeter was 0.14.

The principles of the time-resolved hyperfine spectroscopy of Ps decay have been described previously¹⁰). In the strong polarimeter magnetic field ($B_p = 9.5$ kg) the singlet hyperfine state and the $m = 0$ triplet substate mix (the $m = \pm 1$ triplet substates are not affected by the field) and the relative populations of the mixed pseudosinglet and pseudotriplet states are function of the relative direction of the perturbing magnetic field and the residual longitudinal positron polarization.

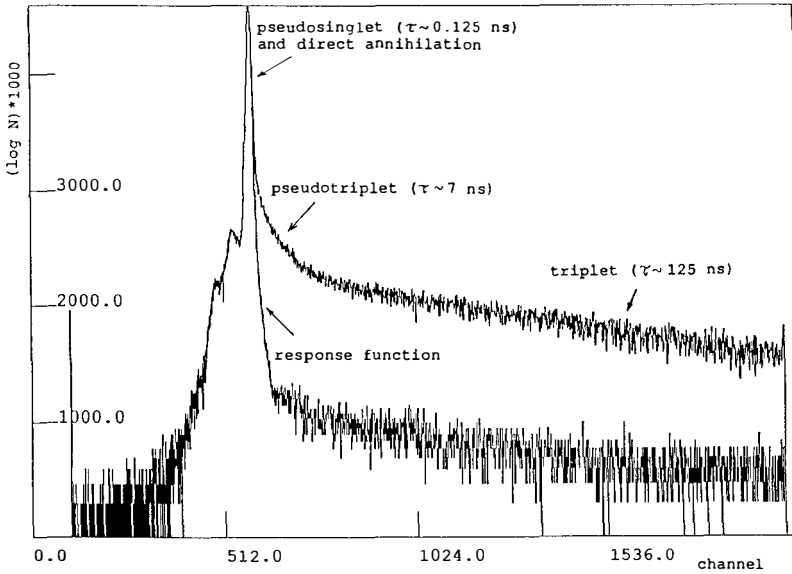


Fig.1. Time spectrum of Ps decay as observed with ^{107}In

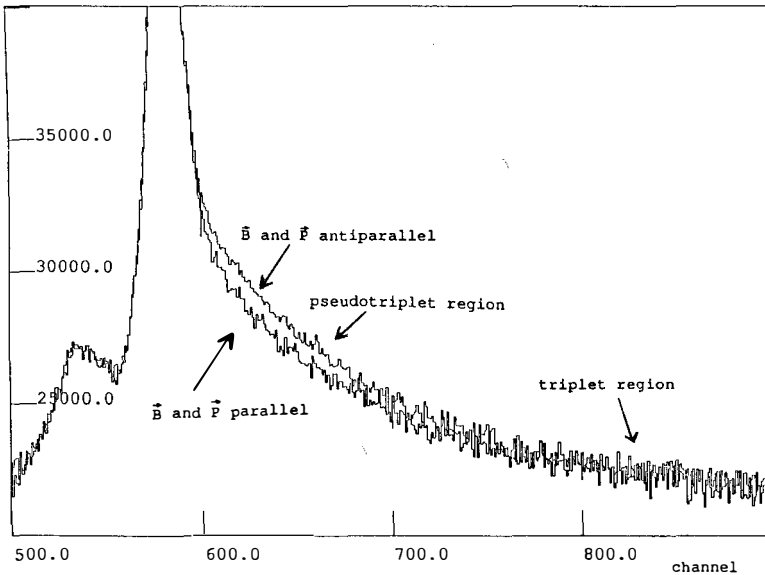


Fig.2. Comparison of Ps decay spectra obtained for two opposite directions of the polarimeter magnetic field (normalized to the triplet state intensity).

From a preliminary analysis of the presently available data we deduced the ratio of the positron polarizations for two opposite directions $\pm J$ of the nuclear spin vector (figs. 1 and 2) to be $R_{\mp} = 0.736 \pm 0.066$. Measurements with a ^{68}Ga positron source (endpoint energy = 1.90 MeV) showed that, within the statistical error of 1.5 %, the positron polarization is not affected by the backscattering on the source backing (i.e. a 20 mg/cm^2 Fe foil soldered on 1 mm of Cu with Woods solder).

After systematic corrections for the uncertainty in the position of the implanted activity with respect to the centre of the field B_r and for backscattering from the source backing, we obtained for the beta asymmetry $\beta_{\text{PA}} = 0.66 \pm 0.03$. The backscattering correction was deduced from measurements with the ^{68}Ga source with and without a backing which was identical to the one used for the ^{107}In measurements. Using the calculated $\langle\beta\rangle = 0.952 \pm 0.010$, we then obtain $R_{\mp}^{\text{LRS}} = 0.768 (1 - 12.4 \delta^2)$. Thus our present, preliminary, result is in agreement with the V-A (i.e. $\delta = 0$) prediction $R_0 = 0.768 \pm 0.058$ and provides a new limit $\delta < 0.13$ and $m_2 > 225$ GeV at 90% confidence level. The experiment is continuing.

References

1. P. Herczeg, in "Weak and Electromagnetic Interactions in Nuclei", ed. H.V. Klapdor (Springer-Verlag, Heidelberg, 1986), p.528, and references therein.
2. A.S. Carnoy et al., Phys. Rev. Lett. 65 (1990) 3249.
3. A. Jodidio et al., Phys. Rev. D34 (1986) 1967 ; Phys. Rev. D37 (1988) 237 err.
4. V.A. Wichers et al., Phys. Rev. Lett. 58 (1987) 1821.
5. J. Deutsch, in Proc. of the Workshop on the Breaking of Fundamental Symmetries in Nuclei (Santa Fe, USA, 1988), eds. J.N. Ginocchio and S.P. Rosen (World Scientific, Singapore, 1989) p.36.
6. J. Van Klinken et al., Phys. Rev. Lett. 50 (1983) 94.
7. D. Dubbers et al., Europhys. Lett. 11 (1990) 195.
8. R. Barbieri and R.N. Mohapatra, Phys. Rev. D39 (1989) 1229.
9. P.A. Quin and T.A. Girard, Phys. Lett. B229 (1989) 29.
10. M. Skalsey et al., Phys. Rev. Lett. 49 (1982) 708 and Phys. Rev. C32 (1985) 1014.
R. Pricels, in Proc. of the 24th Rencontre de Moriond : Tests of fundamental laws in physics (Les Arcs, France, 1989), eds. O. Fackler and J. Tran Thanh Van (Editions Frontières, Gif-sur-Yvette, 1989) p.287.

This work is financially supported by the Belgian National Fund for Scientific Research (NFWO) and the Interuniversity Institute for Nuclear Sciences (IIKW). Two of us, N.S. and J.W. are senior research assistants of the NFWO.

RESONANT AMPLIFICATION OF T - VIOLATING EFFECTS
 IN MATTER NEUTRINO OSCILLATIONS

S.TOSHEV

*Institute for Nuclear Research and Nuclear Energy,
 Sofia, Bulgaria*



Abstract:

Possible T -violating effects in three-neutrino oscillations in matter are discussed. Simple exact analytical expression for the experimentally measurable quantity $P_{\nu_1 \rightarrow \nu_1}^{\mu}(t) - P_{\nu_1 \rightarrow \nu_1}^{\mu}(t)$ is derived. Using this expression we show that *resonant amplification* of the T -violating effects takes place.

In 1985 Mikheyev and Smirnov discovered¹⁾ quite unexpectedly that neutrino oscillations in solar interior may differ drastically from the corresponding vacuum oscillations²⁾. Due to different coherent scattering of the neutrinos ν_e , ν_μ and ν_τ off electrons the parameters of the oscillations in matter³⁾ (mixing angles θ_{ij}^m and T -violating phase δ^m) depend on the electron number density N_e . Even if the neutrino mixing in vacuum is extremely small, density N_e^R exists^{4,1)} (called *resonance density*) such that the amplitude of the oscillations is maximal, thus leading to a resonant amplification of the neutrino transitions in the sun, i.e. the *Mikheyev-Smirnov-Wolfenstein* explanation of the solar neutrino problem⁵⁾.

More recently another interesting aspect of this phenomenon has been pointed out , namely the "enhancement"⁶⁾ or "resonant amplification"^{7,8)} of the T -violating effects in three-neutrino oscillations in matter.

The evolution equation for the amplitudes $A_{l,I}(t)$ of the oscillation probabilities in matter $P_{\nu_I \rightarrow \nu_{l'}}(t) = |A_{l',I}(t)|^2$ can be written in the form:

$$i \frac{d}{dt} \begin{bmatrix} A_{eI}(t) \\ A_{\mu I}(t) \\ A_{\tau I}(t) \end{bmatrix} = \frac{\Delta m_{31}^2}{2p} O^{23}(\theta_{23}) \phi(\delta) \{ O^{13}(\theta_{13}) O^{12}(\theta_{12}) \begin{bmatrix} 0 & 0 & 0 \\ 0 & R_{23} & 0 \\ 0 & 0 & 1 \end{bmatrix} \times$$

$$O^{12\tau}(\theta_{12}) O^{13\tau}(\theta_{13}) + \begin{bmatrix} R_3 & 0 & 0 \\ 0 & 0 & 0 \\ 0 & 0 & 0 \end{bmatrix} \} \phi^*(\delta) O^{23\tau}(\theta_{23}) \begin{bmatrix} A_{eI}(t) \\ A_{\mu I}(t) \\ A_{\tau I}(t) \end{bmatrix} . \quad (1)$$

where $\Delta m_{ij}^2 = m_j^2 - m_i^2$ ($m_1 < m_2 < m_3$), $R_{23} = \Delta m_{21}^2 / \Delta m_{31}^2$ and $R_3(N_e) = 2\sqrt{2} G_F N_e p / \Delta m_{31}^2$, G_F is the Fermi constant, p is the momentum of the relativistic neutrinos and we have used for the neutrino mixing matrix U in vacuum (defined by $\nu_I = \sum U_{lI} \nu_{l'}$, $l=e,\mu,\tau$, $i=1,2,3$) the following parameterization⁷⁾:

$$U = O^{23}(\theta_{23}) \phi(\delta) O^{13}(\theta_{13}) O^{12}(\theta_{12}) =$$

$$= \begin{bmatrix} 1 & 0 & 0 \\ 0 & c_{23} & s_{23} \\ 0 & -s_{23} & c_{23} \end{bmatrix} \begin{bmatrix} 1 & 0 & 0 \\ 0 & 1 & 0 \\ 0 & 0 & e^{i\delta} \end{bmatrix} \begin{bmatrix} c_{13} & 0 & s_{13} \\ 0 & 1 & 0 \\ -s_{13} & 0 & c_{13} \end{bmatrix} \begin{bmatrix} c_{12} & s_{12} & 0 \\ -s_{12} & c_{12} & 0 \\ 0 & 0 & 1 \end{bmatrix} \quad (2)$$

$$c_{ij} = \cos\theta_{ij} > 0, \quad s_{ij} = \sin\theta_{ij} > 0.$$

In matter with given electron number density N_e the solution of eq.(1) is straightforward:

$$A_{l,l'}(t) = \sum_{j=1}^3 U_{l,j}^m \exp(-iM_j t) U_{j,l'}^{m\dagger} \quad (3)$$

where

$$U^m = O^{23}(\theta_{23}) \phi(\delta) V^m \quad (4)$$

is the neutrino mixing matrix in matter and V^m is a 3×3 orthogonal matrix

$$V^m = O^{23}(\theta_{23}^m) O^{13}(\theta_{13}^m) O^{12}(\theta_{12}^m) \quad (5)$$

which diagonalizes the real matrix $M = (\Delta m_{31}^2 / 2p) \times$

$$(O^{13}(\theta_{13}^m) O^{12}(\theta_{12}^m) \text{diag}(0, R_{23}, 1) O^{12T}(\theta_{12}^m) O^{13T}(\theta_{13}^m) + \text{diag}(R_3, 0, 0)):$$

$$V^{mT} M V^m = \text{diag}(M_1, M_2, M_3) \quad (6)$$

In a manner similar to the vacuum case (eq.(2)) and up to irrelevant phase factors the neutrino mixing parameters in matter are defined by:

$$U^m = O^{23}(\theta_{23}^m) \phi(\delta^m) O^{13}(\theta_{13}^m) O^{12}(\theta_{12}^m) \quad (7)$$

In Ref.7 relatively simple exact analytical expressions for the neutrino mixing angles θ_{ij}^m and the Dirac phase δ^m in matter have been derived. When the value of the density N_e changes from zero to infinity then $\sin^2 2\theta_{13}^m$ and $\sin^2 2\theta_{12}^m$ exhibit, in general, the resonant behaviour we already know from the two-neutrino mixing case. It has been shown that under some well specified conditions density $N_e^{R\delta}$ exists such that $\sin^2 \delta^m(N_e^{R\delta}) = 1$. Since T is conserved when $\sin^2 \delta^m = 0$ (i.e. when $e^{i\delta^m} = \pm 1$) it has been argued that $\sin^2 \delta^m(N_e^{R\delta}) = 1$ corresponds to *maximal T violation in matter*.

The experimentally measurable T -nonconserving quantity, however, is neither δ^m , nor $\sin^2 \delta^m$, but the unique, up to a sign, difference between probability for the transition $\nu_l \rightarrow \nu_{l'}$, and probability for its T -conjugate transition $\nu_{l'} \rightarrow \nu_l$, ($l, l' = e, \mu, \tau$), i.e.⁹⁾

$$P_{\nu_l \rightarrow \nu_{l'}}^m(t) - P_{\nu_{l'} \rightarrow \nu_l}^m(t) \quad (8)$$

The analytical expression for this quantity, when we use U^m in the form (7), is very similar to the corresponding expression in vacuum - the parameters of the neutrino oscillations in vacuum are

replaced simply with the corresponding parameters in matter:

$$P_{\nu_l \rightarrow \nu_{l'}}^m(t) - P_{\nu_{l'} \rightarrow \nu_l}^m(t) = (\cos\theta_{13}^m/2) \sin 2\theta_{13}^m \sin 2\theta_{12}^m \sin 2\theta_{23}^m \sin\delta^m \times \\ (\sin(\Delta M_{32}^m t) + \sin(\Delta M_{21}^m t) + \sin(\Delta M_{13}^m t)). \quad (l, l') = (e, \mu), (\mu, \tau), (\tau, e) \quad (9)$$

Having in mind the analytical formulae for all these parameters in terms of the vacuum ones it seems at first sight that the quantity

$$P_{\nu_l \rightarrow \nu_{l'}}^m(t) - P_{\nu_{l'} \rightarrow \nu_l}^m(t) \text{ is a rather complicated function of } \theta_{ij}, \delta, \Delta m_{ij}^2, N_e, t \text{ and, hence, should be investigated numerically}^{7)}.$$

In what follows we shall show explicitly that the analytical formula (9) can be simplified considerably.

For this purpose let us repeat the above derivation using for U^m the expression (4) instead of (7). After some boring but straightforward algebra we obtain:

$$P_{\nu_l \rightarrow \nu_{l'}}^m(t) - P_{\nu_{l'} \rightarrow \nu_l}^m(t) = (\cos\theta_{13}^m/2) \sin 2\theta_{13}^m \sin 2\theta_{12}^m \sin 2\theta_{23}^m \sin\delta^m \times \\ (\sin(\Delta M_{32}^m t) + \sin(\Delta M_{21}^m t) + \sin(\Delta M_{13}^m t)). \quad (l, l') = (e, \mu), (\mu, \tau), (\tau, e) \quad (10)$$

Comparing equations (9) and (10) we see that something quite interesting happens, namely the dependence of the neutrino mixing angle θ_{23}^m and the T non-conserving phase δ^m in matter on the vacuum parameters θ_{ij} , δ , Δm_{ij}^2 and N_e is such that for arbitrary values of the density N_e the following relation is fulfilled:

$$\sin 2\theta_{23}^m(\theta_{ij}, \delta, \Delta m_{ij}^2, N_e) \sin\delta^m(\theta_{ij}, \delta, \Delta m_{ij}^2, N_e) = \sin 2\theta_{23} \sin\delta, \quad \forall N_e \quad (11)$$

To summarize, the dependence of the experimentally measurable T -nonconserving quantity $P_{\nu_l \rightarrow \nu_{l'}}^m(t) - P_{\nu_{l'} \rightarrow \nu_l}^m(t)$ on two of the parameters of the neutrino oscillations in matter, θ_{23}^m and δ^m , is intriguingly simple: the product $\sin 2\theta_{23}^m \sin\delta^m$ does not change and, hence, can be substituted with the vacuum value $\sin 2\theta_{23} \sin\delta$!

The other two parameters - the mixing angles θ_{13}^m and θ_{12}^m , do not depend on θ_{23} and δ at all. Relatively simple exact analytical formulae for them are available⁷⁾. In addition, it has been shown previously that in the cases of "large mass hierarchy"^{10,12)} or/and "small mixing angles"¹¹⁾ these formulae coincide up to small corrections with the corresponding (and more simple) formulae in the two-neutrino mixing case.

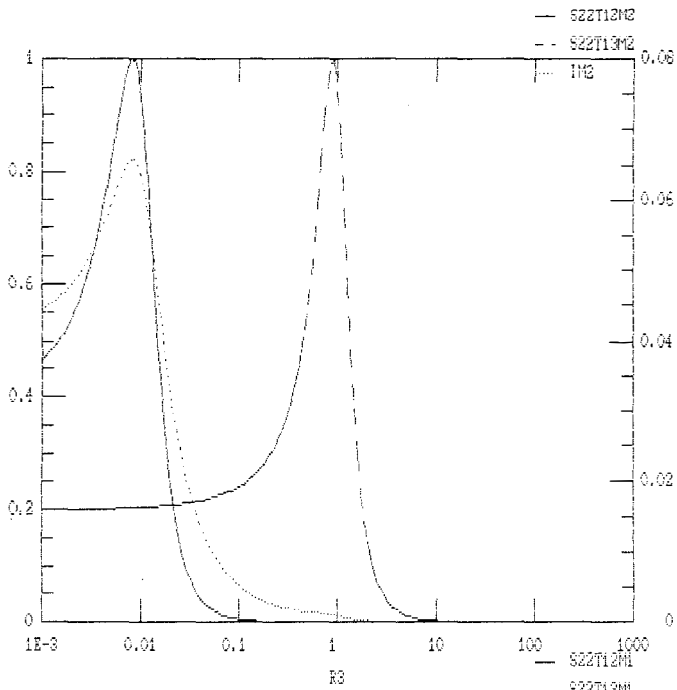


Fig. 1a

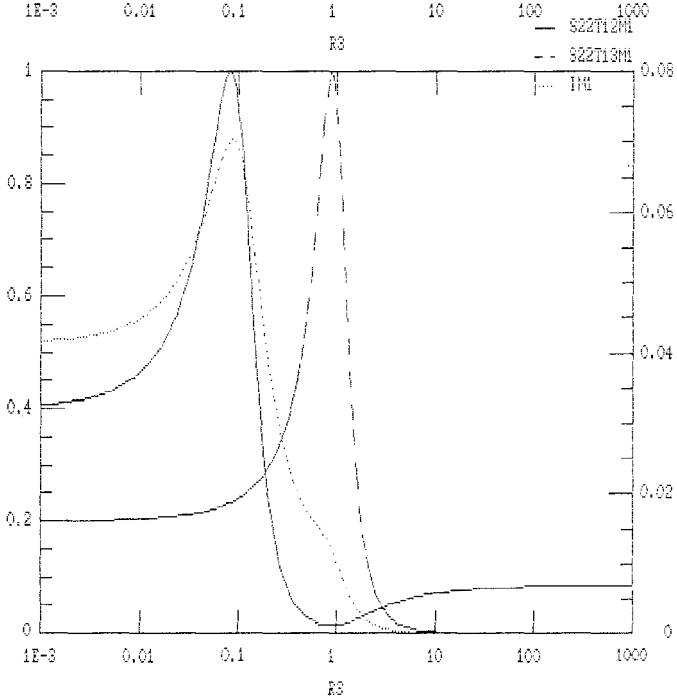


Fig. 1b

Having in mind the resonant character of the dependence of the quantities $\sin^2 2\theta_{13}^m$ and $\sin^2 2\theta_{12}^m$ on N_e and formulae (10) and (11) it becomes rather obvious that the T -violating effects reach their maximum very close to (and a little bit above) the first (i.e. lower) resonance which, due to the choice $m_1 < m_2 < m_3$, is defined by $\sin^2 2\theta_{12}^m = 1$.

These conclusions are visualized in Fig.1 where we show the dependence of the quantities $\sin^2 2\theta_{12}^m$ (full line), $\sin^2 2\theta_{13}^m$ (dashed line) and the t -independent "amplitude" $Im = (\cos\theta_{13}^m / 2) \sin 2\theta_{13}^m \sin 2\theta_{12}^m \sin 2\theta_{23}^m \sin \delta$ of the probability difference (dotted line) on $R_3(N_e) = 2\sqrt{2}G_F N_e p / \Delta m_{31}^2$, i.e. on the electron number density N_e .

Indeed the position of the Im maximum is determined by the position of the maximum of $\sin^2 2\theta_{12}^m$. Both these maxima change simultaneously their position when we change the value of the mass-hierarchy parameter $R_{23} = \Delta m_{21}^2 / \Delta m_{31}^2$ from 10^{-2} (Fig.1a) to 10^{-1} (Fig.1b). The vacuum values of the neutrino mixing parameters have been chosen (rather arbitrary) to be : $\sin^2 2\theta_{12} = 0.4$, $\sin^2 2\theta_{23} = 0.3$, $\sin^2 2\theta_{13} = 0.2$ and $\sin^2 \delta = 0.3$.

Another, almost obvious, corollary of formulae (10,11) is the fact that the maximal value of Im increases when the two resonances, for $\sin^2 2\theta_{12}^m$ and $\sin^2 2\theta_{13}^m$, get nearer to each other, i.e. when the mass hierarchy decreases.

The author is grateful to the Organizing Committee of the Workshop for the kind hospitality at Les Arcs.

REFERENCES:

1. S.P.Mikheyev, A.Yu.Smirnov, Yad.Fiz. 42 (1985) 1441.
2. B.Pontecorvo, Z.Eksp.Theor.Fiz. 33(1957)549; *ibid.* 34(1958)247;
3. L.Wolfenstein, Phys.Rev. D17 (1978) 2369; *ibid.* D20(1979)2634.
4. V.Barger *et al.*, Phys.Rev. D22 (1980) 2718.
5. see the review talk of Prof.A.Yu.Smirnov in these Proceedings.
6. T.K.Kuo, J.Pantaleone, Phys.Lett. B198 (1987) 406.
7. S.Toshev, Phys.Lett. B226 (1989) 335.
8. S.Toshev, Mod.Phys.Lett. (in press)
9. N.Cabibo, Phys.Lett. B72 (1978) 333;
V.Barger *et al.*, Phys.Rev.Lett. 45 (1980) 2084;
S.M.Bilenky, F.Nidermayer, Sov.J.Nucl.Phys. 34 (1981) 606;
H.-Y.Cheng, Phys.Rev. D34 (1986) 2794.
10. T.K.Kuo, J.Pantaleone, Phys.Rev.Lett. 57 (1986) 1805.
11. S.Toshev, Phys.Lett. B185 (1987) 177.
12. A.Yu.Smirnov, Yad.Fiz. 46 (1987) 1152.

A NEW MEASUREMENT OF ϵ'/ϵ BY THE NA31 EXPERIMENT

Cern - Edinbourgh - Mainz - Orsay - Pisa - Siegen

Lydia Iconomidou-Fayard

Laboratoire de l'Accélérateur Linéaire, IN2P3-CNRS
et Université de Paris-Sud, F- 91405 Orsay Cedex, France



ABSTRACT

We present here a new measurement of $\text{Re}(\epsilon'/\epsilon)$, using the 1988 NA31 data sample with a partially upgraded apparatus, which most notably includes a Transition Radiation Detector. The standard analysis is discussed as well as the improvements compared to the previous result. A new preliminary result of $\text{Re}(\epsilon'/\epsilon) = (1.9 \pm 1.1) \text{ } ^0/\text{oo}$ is given which leads to a combined NA31 (1986+1988) result of $(2.7 \pm .9) \text{ } ^0/\text{oo}$.

**Dedicated to the memory
of Jean-Pierre Wuthrick.**

EXPERIMENT AND THEORY : THE CURRENT SITUATION.

The Kaon system is the only laboratory, up to now, where CP non-invariance can be studied. Even if CP violation appears naturally in the Standard Model as a consequence of 3 families and quark mixing [1], nevertheless, 26 years after the discovery [2], its fundamental mechanism remains still unknown.

Moreover, the possibility of a direct CP-violation, implying decays of a CP eigenstate with a given eigenvalue E into a final system of the opposite one -E, is not yet finally confirmed. The two recent and most precise experimental results measuring ϵ'/ϵ , differ by 2σ . NA31 result [3] gives a non-zero direct CP-violating component with 3σ significance. E731, has measured an effect compatible with zero [4].

Moreover, theory does not give enough constrained predictions for the following reasons : The ϵ'/ϵ magnitude depends on Cabibbo-Kobayashi-Maskawa matrix mixing angles, phase and quark masses. Several of these parameters are known with a low precision. The top quark still remains one of the missing pieces of the Standard Model, since hadronic colliders put higher and higher limits on its mass [6]. Recent experiments have contributed to an important improvement of the measurement accuracy on some CKM elements [5]. Taking into account the finite precision of experimental results and the important theoretical uncertainties, the possible range of ϵ'/ϵ varies from 3 ‰ to -1 ‰ as the top quark mass [7]. A zero ϵ'/ϵ value is no longer excluded by the Standard Model if the top mass is of the order of 250 GeV. Therefore, if the top quark mass is high enough, a precise measurement of the direct CP-violation would require a highly powerful "next generation" detector, leading to a total error smaller than 0.1 ‰.

NA31 : 88 DATA TAKING.

ϵ'/ϵ is given by 4 observable quantities which relate the CP-violating $K_L \rightarrow 2$ pions amplitude to the CP-conserving $K_S \rightarrow 2$ pions ones.

$$\text{Re}(\epsilon'/\epsilon) = 1/6 (1 - R)$$

$$R = \frac{K_L \rightarrow 2\pi^0}{K_S \rightarrow 2\pi^0} \frac{K_S \rightarrow \pi^+ \pi^-}{K_L \rightarrow \pi^+ \pi^-}$$

NA31 is based on the concurrent detection of charged and neutral events. Data are taken in K_S and K_L beams alternatively with a cycle of about 40 hours to reduce time-dependent effects.

K_L beam : A 450 GeV proton beam hits a beryllium target and produces a neutral beam which is selected by sweeping magnets and 3-stage collimation (the 2-stage used for 86 run allowing surviving regenerated K_S component, has been improved for 88 run; See below). After 120m in vacuum, the K_S component has decayed to a negligible level and K_L decays are accepted along a 50m fiducial region.

K_S beam : A 360 GeV proton beam is brought onto a second target from which K_S are selected by collimation after 7m. The beginning of the fiducial region is defined by an anticounter vetoing early decays. The K_S target and collimation system is mounted on a train which can be displaced along the 50m decay region. Taking data in 41 steps of 1m 20 we obtain similar K_L and K_S decay spectra.

Detector : The detection of neutral decays is done by a liquid argon/lead (LAC) sandwich calorimeter of $25 X^\circ$ which measures photons with 0.5mm position and $7.5\%/\sqrt{E}$ energy resolution. For charged events, two wire chambers spaced by 25 m, give space points with $750 \mu\text{m}$ resolution. An Iron/scintillator sandwich calorimeter (HAC) measures in conjunction with LAC the charged pion energy with $65\%/\sqrt{E}$ resolution. Several anticounters identify escaping photons. Between the 2nd WC and the LAC, a Transition Radiation Detector has been build and installed for 1988 run. Radiators of 400 polypropylene foils, $20 \mu\text{m}$ thick and spaced by $600 \mu\text{m}$ cause the emission of X rays for each ultrarelativistic particle going through. Behind each of them, a WC filled with 1.5cm Xenon, absorbs the Transition Radiation light.

Details for beam setup, apparatus and TR detector can be found elsewhere [8,9].

Neutral decays.

$K^0 \rightarrow 2\pi^0 \rightarrow 4\gamma$ decays are reconstructed from photon energies and positions given by the LAC. The longitudinal vertex position is computed assuming the decay of a kaon. Invariant 2γ masses are calculated for all possible γ pairs. The 2 combinations giving the nearest to π^0 mass values are kept. Signal and background are studied through an elliptical function R_{ell} where the half-axes vary with the minimum energy photon. Fig. 1 shows K_L data and Monte Carlo simulation for the physical background

$K_L \rightarrow 3\pi^0 \rightarrow 4\gamma(\text{seen}) + 2\gamma(\text{lost})$ which can be studied in the region $4 < \text{Re}ll < 9$ and then, the 3.3 % of remaining background under the signal ($\text{Re}ll < 1$) is subtracted by linear extrapolation.

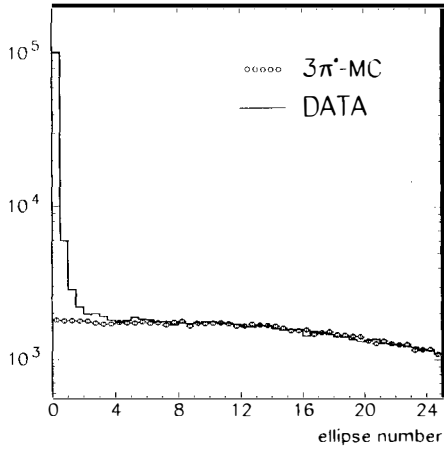


Fig. 1 $\text{Re}ll$ distribution for K_L events and for $3\pi^0$ Monte Carlo.

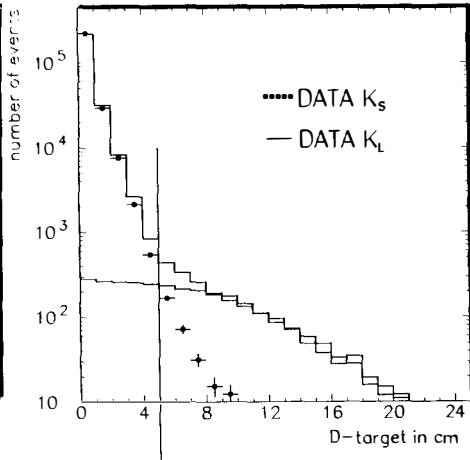


Fig. 2 D_{target} distribution for K_S and K_L events. The vertical line indicates the applied cut.

Charged decays.

The decay vertex is reconstructed from Wire Chambers with a longitudinal resolution better than 1m. The K^0 energy is calculated, with a 1% precision, from the charged tracks opening angle, kaon mass and track energies measured by the calorimeter. 3-body decays are rejected identifying photons in LAC or anticounters ($\pi^+\pi^-\pi^0$), by the longitudinal shower development ($\pi e \nu$), by the use of a muon veto ($\pi \mu \nu$). Remaining background is identified kinematically, using the distance of the decay plane (defined from the 2 charged tracks) to the target. Fig. 2 shows this distance D_{target} for K_S events (compatible with zero within resolution) and for K_L events (long 3-body tail). Background is studied in the region $7\text{cm} < D_{\text{target}} < 12\text{cm}$ and extrapolated into the signal region following the shown in the figure shape which is determined from $K_L \rightarrow \pi e \nu$, $K_L \rightarrow \pi^+\pi^-\pi^0$ data samples and $K_L \rightarrow \pi \mu \nu$ Monte Carlo. In this way we subtract 4.8% of the signal for $K_L \rightarrow \pi e \nu$ decays, 1.8 % for $K_L \rightarrow \pi \mu \nu$ decays and 1.6% for $K_L \rightarrow \pi^+\pi^-\pi^0$ decays.

This charged background is uniformly distributed in Z . Indeed, a better (3-stage) collimation system has removed the K_S regenerated component

present in the first meters of our 1986 data [10], allowing, for 88 data, the use of this region.

The TRD information is used in two different ways: first of all, to obtain a better electron identification in the background region and therefore, make a most precise subtraction. This has improved the corresponding systematic uncertainty from 2⁰/oo (86) to <1.5⁰/oo. Secondly, TRD is used directly to remove Ke3 events and check the standard analysis. Fig. 3 shows the correlation of TRD pulseheight and the energy ratio ELAC/ETOT, where the separation between electrons (high TRD signal and high ELAC/ETOT), pions (low TRD signal and intermediate ELAC/ETOT) and Muons + non-interacting pions (almost zero ELAC/ETOT), is fairly clean. All checks done using TRD information confirmed standard procedure.

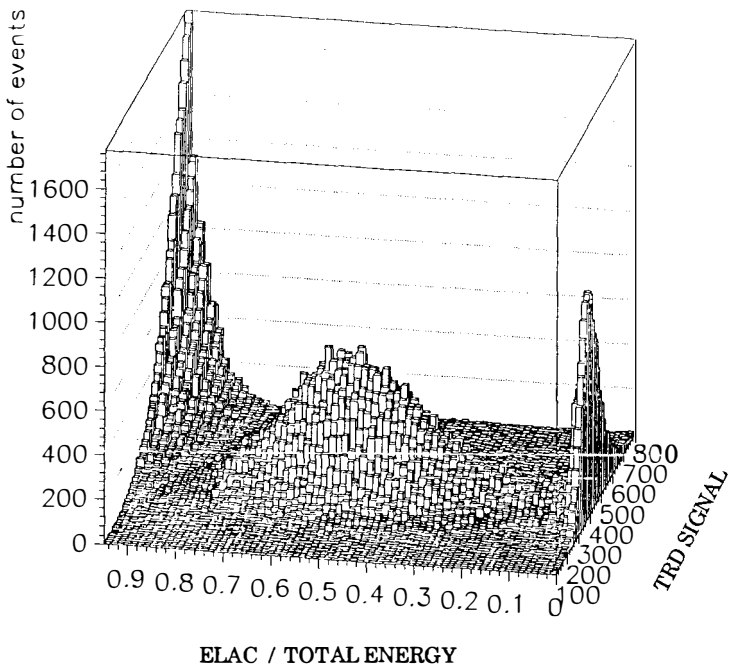


Fig. 3 ELAC/ETOT versus TRD

FINAL STATISTICS AND PRELIMINARY RESULTS.

Fig. 4 shows energy and vertex spectra of the 4 data samples after background subtraction. We recall here, that the relative energy scales of neutral and charged decays is adjusted to be the same within $\pm 0.1\%$ by fitting the vertex distributions to the K_S anticounter position, which

defines the beginning of fiducial region in K_S beam. The sensitivity of the ratio R to a possible 0.1% energy shift, defined as $\Delta R/\Delta E$, is now 1. The factor 3 we had in 86 data is reduced to 2 thanks to the proton beam energy and incidence angle changes, and finally to 1, by weighting the K_S to equalize K_L and K_S decay distributions.

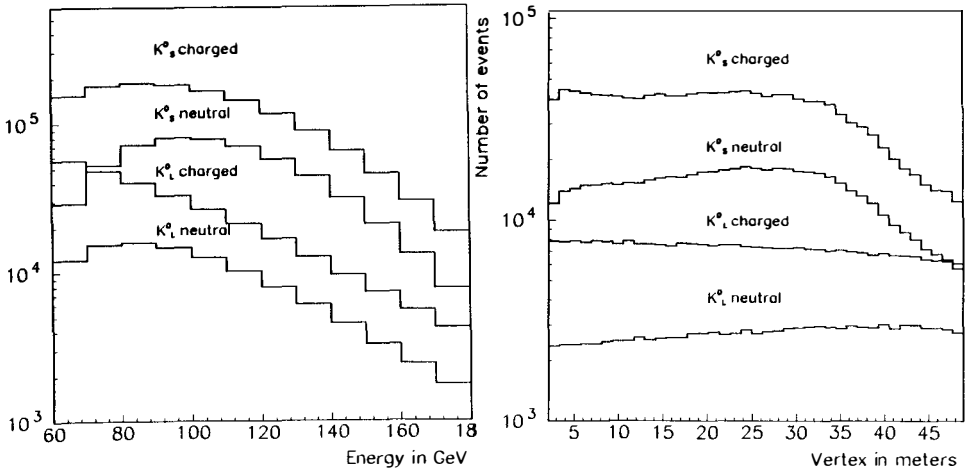


Fig. 4 Energy and vertex spectra for final statistics.

Ratio R is calculated in 12 energy bins between 60-180 GeV, 39 Z bins in the range 2m10-48m90 and 7 time periods, and then combined. The raw preliminary result is :

$$R = .983 \pm .004 \text{ (stat)}$$

A Monte Carlo correction of $1^0/00 \pm 1^0/00$ (stat) is applied for K_L - K_S different beam divergences, acceptance, resolution and scattering effects. An accidentals study, done by overlaying random triggers, recorded proportionally to the beam intensity, with good K_L and K_S events, implies a correction of $+0.9^0/00 \pm 2.3^0/00$ (stat). Anticounter efficiencies contribute $3.5^0/00 \pm 2^0/00$. The corrected result is :

$$R = .989 \pm .005 \text{ (stat)} \pm .004 \text{ (syst)}$$

which gives

$$\epsilon'/\epsilon = 1.9 \pm 1.1 \text{ (total error) } \%/00.$$

The final numbers of events as well as the breakdown of errors is given in tables 1 and 2. One can combine the 2 NA31 (1986 and 1988) results. For that, systematic errors are divided into correlated and uncorrelated parts. We obtain then:

$$Re(\epsilon'/\epsilon) = 2.7 \pm .9 \text{ (Total error) } \%/00$$

FINAL STATISTICS	BREAKDOWN OF ERRORS ON R	
K _S Charged 1379 Kevents K _S Neutral 562 Kevents K _L Charged 285 Kevents K _L Neutral 108 Kevents	STATISTICAL 4‰ Data 3‰ Monte Carlo + accidentals	SYSTEMATIC 2.2‰ Background CH + NE 2.0‰ Accidentals 1.5‰ Calibration and calorimeter stability 2.0‰ Different inefficiencies 1.0‰ Monte Carlo
TABLE 1	TABLE 2	

CONCLUSION

Using the 1988 data taking, NA31 has performed a new measurement of the direct CP-violating ϵ'/ϵ .

A number of systematic checks and the use of the new Transition Radiation detector has allowed a further improvement on the knowledge of acceptances and background identification.

-I would like to thank A.Schaffer for careful reading of this text.-

REFERENCES

- [1] M. Kobayashi and K.Maskawa, Prog.Theor.Phys. 49 (1973) 652.
- [2] J.H.Christenson et al., Phys.Rev.Lett.13 (1964) 138.
- [3] H.Burkhardt et al., Phys.Lett.B 206 (1988) 169.
- [4] J.R.Patterson et al.Phys.Rev.Lett. 64 (1990) 1491.
- [5] R.Fulton et al., Phys.Rev.Lett. 64 (1990) 16
H.A.Albrecht et al., DESY 89/152
- [6] F.Abe et al., Phys.Rev.Lett.64 (1990)142,147.
T.Akesson et al., Z.Phys.C46(1990)179
C.Aljabar et al., Z.Phys. C48(1990) 1.
- [7] J.Buchalla et al., Nucl.Phys.B337(1990)313.
- [8] H.Burkhardt et al., Nucl.Instrum.Methods A268(1988) 116.
- [9] G.D.Barr et al., Nucl.Instrum.Meth.A294 (1990) 465.
Ilana Harrus, Thèse, LAL 89-13 ,1989.
- [10] D.Fournier, Proceedings of the 14th Inter.Symposium on Lepton and Photon Interactions at High Energies August 7-12 1989.

TESTS OF THE PAULI EXCLUSION PRINCIPLE FOR NUCLEONS AND
DETECTION OF $\beta\beta$ DECAY PRODUCTS WITH ACCELERATOR MASS
SPECTROMETRY

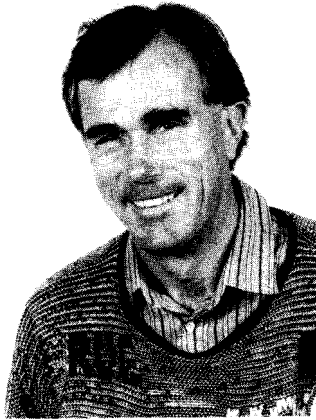
E. Nolte, T. Brunner, T. Faestermann, A. Gillitzer, G. Korschinek, D. Müller
Faculty of Physics, Technical Univ. of Munich, D-8046 Garching, Germany

V.N. Novikov, A.A. Pomansky

Institute for Nucl. Research, Academy of Sciences of the USSR, Moscow, USSR

A. Ljubicic, D. Miljanic

Institute Rudjer Boskovic, Zagreb, Yugoslavia



ABSTRACT

Accelerator mass spectrometry has been used to test the Pauli exclusion principle for nucleons and is proposed for the detection of $\beta\beta$ decay products. For the test of the Pauli exclusion principle, non-Paulian nuclei of ${}^5\text{Li}$ and of ${}^5\overline{\text{He}}$ with three protons and three neutrons, respectively, in the nuclear $1s_{1/2}$ shell were looked for. The following limits were deduced:

$\frac{[{}^5\text{Li}]}{[{}^6\text{Li}]} < 10^{-16}$ and $\frac{[{}^5\overline{\text{He}}]}{[{}^4\overline{\text{He}}]} < 2 \cdot 10^{-15}$ for binding energies between 0 and 50 MeV and 0.7 and 32 MeV, respectively. The probability $\beta^2/2$ of having two protons in the symmetric state was deduced to be $\beta^2/2 < 7 \cdot 10^{-32}$. The feasibility of radiochemical $\beta\beta$ decay experiments with accelerator mass spectrometry is discussed.

1. TESTS OF THE PAULI EXCLUSION PRINCIPLE FOR NUCLEONS

The Pauli exclusion principle (PEP) is one of the fundamental principles in physics. It forbids that two identical particles with half-integral spin, fermions, occupy the same quantum state. It follows from a wavefunction which is completely antisymmetric under the exchange of two identical fermions. In no theory, a violation of the PEP is postulated and there is only one theory so far without contradiction which describes a small violation of the PEP ¹⁾. (see also references cited in ¹⁾ and ²⁾).

Several experiments and considerations have been performed or proposed to look for a violation of the PEP. Goldhaber type experiments ³⁾ in which radiation of transitions from electrons or from nucleons from higher shells to the filled $1s_{1/2}$ shell is looked for do not test the PEP since in quantum mechanics transitions from one type of statistics (Fermi) to another type are absolutely forbidden ^{4,5,6)}. References for these experiments can be found in ²⁾. In other experiments, limits for the probability $\beta^2/2$ of finding two electrons or two protons in the symmetric state with respect to exchange were deduced to be in the range $10^{-13} - 10^{-26}$ ^{7,8,9)}.

The principle of this experiment is to look with AMS for non-Paulian atoms with three electrons in the K shell or for non-Paulian nuclei with three protons or three neutrons in the nuclear $1s_{1/2}$ shell. The search for non-Paulian atoms is described in ^{2,10)}. Non-Paulian $\widetilde{^5\text{Li}}$ would have the configuration shown in Fig.1. Normal ^5Li is by two MeV unstable against disintegration into $^4\text{He} + ^1\text{H}$. Because of the energy difference of 20 MeV between the $1p_{3/2}$ and the $1s_{1/2}$ shell ¹¹⁾, $\widetilde{^5\text{Li}}$ would be bound by about 18 MeV. Similar arguments hold for non-Paulian $\widetilde{^5\text{He}}$ with three neutrons in the $1s_{1/2}$ shell.

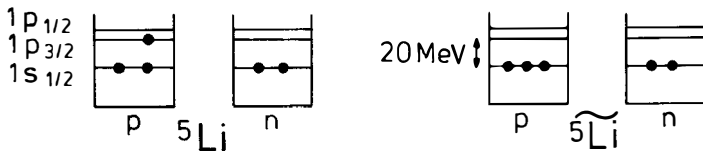


Figure 1: Configuration of nucleons in non-Paulian $\widetilde{^5\text{Li}}$

In AMS experiments with a time-of-flight set-up, non-Paulian nuclei of $\widetilde{^5\text{Li}}$ and $\widetilde{^5\text{He}}$ were looked for in samples of isotopically enriched ^6Li (95%) and of atmospheric helium obtained from raw neon, respectively. The results are

$$\frac{[\widetilde{^5\text{Li}}]}{[^6\text{Li}]} < 2.1 \cdot 10^{-15} \text{ for binding energies of } \widetilde{^5\text{Li}} \text{ between 0 and 50 MeV and}$$

$\frac{[\widetilde{^5He}]}{[^4He]} < 2 \cdot 10^{-15}$ for binding energies of $\widetilde{^5He}$ between 0.7 and 32 MeV. The measured mass spectrum for $\widetilde{^5Li}$ is shown in Fig. 2. Concerning the original unenriched Li sample, the following limit is deduced: $\frac{[\widetilde{^6Li}]}{[^6Li]} < 10^{-16}$ with an enrichment factor of 20 for hypothetical Lithium with A=5 with respect to 6Li .

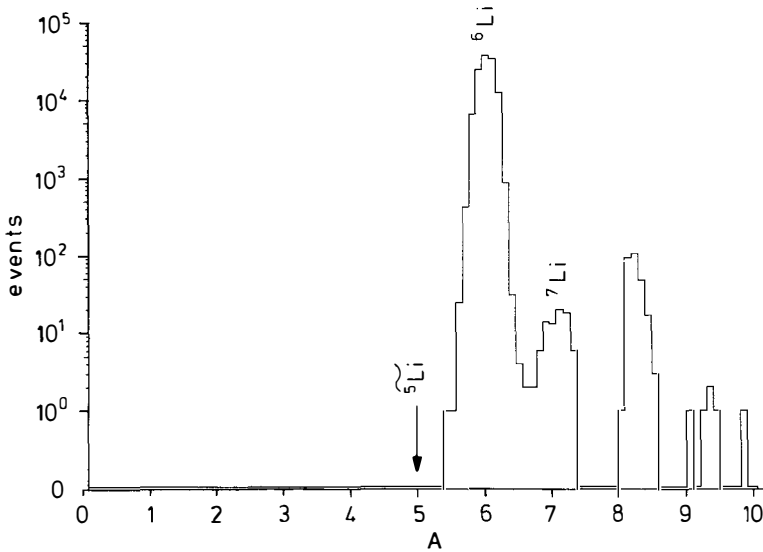


Figure 2: Mass spectrum measured for the search for non-Paulian $\widetilde{^5Li}$

The result for $\widetilde{^5Li}$ can be used to set a limit for the probability $\beta^2/2$ of having two protons in the symmetric state with respect to exchange in a collision. The processes considered are $^6Li \rightarrow \widetilde{^6Be} + e^- + \bar{\nu}_e$ (1) where $\widetilde{^6Be}$ has three protons in the $1s_{1/2}$ shell and $\widetilde{^6Be} \rightarrow \widetilde{^5Li} + ^1H$ (2). In the considered case, we have $\frac{\beta^2}{2} = \frac{1}{2} \frac{\tilde{\lambda}}{\lambda_\beta}$ ¹²⁾, where $\tilde{\lambda}$ characterizes the β decay of 6Li to $\widetilde{^6Be}$: $[\widetilde{^6Be}] = [^6Li] \cdot \tilde{\lambda} t$ and where λ_β would be the decay constant for a normal β decay with the same decay energy as for (1). With $[\widetilde{^6Be}] = [\widetilde{^5Li}]$, $t=10^{10}$ y and $\frac{1}{\lambda_\beta}=400$ s, we deduce $\beta^2/2 < 7 \cdot 10^{-32}$ which is by many orders of magnitude smaller than the limits deduced in other experiments ^{7,8,9)}.

2. FEASIBILITY OF $\beta\beta$ DECAY EXPERIMENTS WITH AMS

Till today, AMS is used to detect cosmogenic radioisotopes as e.g. ^{10}Be , ^{14}C or ^{36}Cl in

samples of Be, C or Cl, respectively. The detection limits [radioisotope]/[element] are typically in the range of 10^{-15} . Because of the low concentrations of about 10^{-12} of these radioisotopes in nature, the danger of contamination of the samples during the chemical processing or in the ion source is small. Complementary AMS with stable isotopes would allow the detection of $\beta\beta$ decay products or of impurities in high-purity semiconductor materials as Si or Ge or in low-background detectors. Especially attractive would be the detection of EC-EC decay products.

The considered $\beta\beta$ decay experiments are radiochemical. The parent nuclei of the element Z are given as a gaseous compound e.g. as a noble gas into a chamber. The product nuclei of the element $Z \pm 2$ are collected as ions at an electrode to which a voltage is applied. The material of the electrode should be high-purity Si or Ge. Candidates are ^{36}Ar ($Q_{EC-EC} = 433$ keV), ^{78}Kr ($Q_{EC-EC} = 2877$ keV), ^{86}Kr ($Q_{\beta-\beta^-} = 1256$ keV), ^{124}Xe ($Q_{EC-EC} = 2866$ keV), ^{126}Xe ($Q_{EC-EC} = 905$ keV), ^{134}Xe ($Q_{\beta-\beta^-} = 847$ keV) and ^{136}Xe ($Q_{\beta-\beta^-} = 2479$ keV). For ^{78}Kr and ^{124}Xe , the predicted half-lives are in the range of 10^{20} y¹³⁾. With a collection time of 1 y and with 24 moles of parent nuclei, 10^5 product nuclei are generated and can be collected. With several milligrams material of the electrode of the element Z , the concentration $[Z \pm 2]/[Z]$ to be measured is of the order of 10^{-15} .

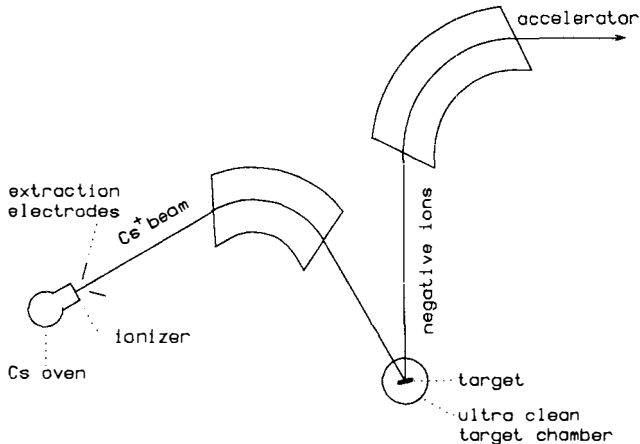


Figure 3: Injector for AMS with stable isotopes

In preexperiments with the Cs sputter source which is used in AMS experiments with cosmogenic radioisotopes, background concentration $[Z^n]/[\text{Si}]$ were measured to be in the range $10^{-10} \dots 10^{-6}$. This background is introduced by the Cs sputter beam and the impurities in

the sample holder and by cross talk in the ion source. In order to reduce the background, the ion source has to be reconstructed drastically. The Cs sputter beam has to be analysed magnetically. Sample holders and slits have to be made of high-purity materials as Si or Ge and the sputter chamber has to have very ultra-high vacuum. Such a set-up is shown in Fig 3. This ion source is under construction at the Munich accelerator laboratory.

ACKNOWLEDGMENTS

We would like to thank Mr. E. Lohse from LINDE AG for his very friendly support by delivering us the raw neon.

REFERENCES

- [1] R.N. Mohapatra : Phys.Lett. B242(1990)407
- [2] V.M. Novikov, A.A. Pomansky, T. Faestermann, H. Gail, A. Gillitzer, G. Korschinek, D. Müller, R. Scheuer and E. Nolte: Phys.Lett. B240(1990)227
- [3] G. Feinberg and M. Goldhaber: Proc.Nat.Acad.Sci.US 45(1959)1301
- [4] W. Pauli : Handbuch der Physik 5 T.1(1958)Sect.14
- [5] P.A.M. Dirac: The Principles of Quantum Mechanics, Clarendon Press, Oxford(1958) chapt.IX
- [6] R.D. Amado and H. Primakoff: Phys. Rev.C22(1980)1338
- [7] R. Plaga: Z. Phys. A333(1989)397
- [8] E. Ramberg and G.A. Snow :Phys. Lett. B238(1990)438
- [9] D. Miljanic, A. Ljubicic and B.A. Logan : Phys. Lett. to be published
- [10] E. Nolte, T. Faestermann, H. Gail, A. Gillitzer, G. Korschinek, D. Müller, R. Scheuer, V.M. Novikov, A.A. Pomansky, D. Miljanic, A. Ljubicic and B.A. Logan: Nucl. Instr. and Meth., to be published
- [11] A.G.M. van Hees and P.W.M. Glaudemans: Z. Physik A314(1983)323
- [12] D. Kekez, A. Ljubicic and B.A. Logan: Europhys. Lett. 13(1990)385
- [13] A. Kuliev : Proc. Workshop, Theoretical and Experimental Aspects of $\beta\beta$ Decay Problem, Kiev (1989), in press



Search for Lepton Number Violation in π , μ and τ Decays

N.S.Amaglobeli-High Energy Physics Institute,SU-380086,Tbilisi,USSR
 V.P.Dzhordzhadze-High Energy Physics Institute,SU-380086,Tbilisi,USSR
 G.V.Mitselmakher-Joint Institute for Nuclear Research,Dubna,Head Post
 Office,P.O.Box 79,SU-101000,Moscow,USSR
D.Mzavia-High Energy Physics Institute,SU-380086,Tbilisi,USSR

Abstract

Lepton number violation in some π , μ and τ decays are considered. An experiment is proposed to search for $\tau \rightarrow 3\mu$ decay at the level of $10^{-7} - 10^{-9}$.

The conservation of lepton number is an empirical observation which has been tested last time with an increasing precision. It is felt, that this observation is not a manifestation of an exact symmetry,as in the Standard Model, but merely an approximation compatible with present day experimental limitations. The situation is different in other extension models like Grand Unification Theories, Supersymmetry, Technicolor or compositeness of quark and leptons. In those models flavour changing transitions can be mediated by yet unobserved heavy particles, which can be produced by future accelerators with sufficiently high energy. At low energy scale those particles will manifest themselves in small symmetry violating processes, like lepton number violation processes. The level of flavour violation depends mainly on masses and mixing of these particles where the present experiments give lower limits in the order of several hundred TeV.

Lepton number violation has ben tested experimentally in different processes. Present and proposed results of searches for lepton number violating processes are shown in Table 1 .

The most sensitive result is the SINDRUM $\mu^+ \rightarrow e^+e^+e^-$ decay experiment [3]. Recently SINDRUM group slightly improved $\mu^-Ti \rightarrow e^-Ti$ result [4] obtained by TRIUMF[6]. This experiment is a first stage of the very ambitious proposal of the SINDRUM group [5] which aims to reach sensitivity 3×10^{-14} . This proposal includes also an improvement of the $\mu^-Ti \rightarrow e^+Ca$ branching ratio nearly in three orders of magnitude with respect to the TRIUMF result [6]. The decay $\mu^+ \rightarrow e^+\gamma$ is studied at the LAMPF [1] in the MEGA experiment, which aims to reach sensitivity of 10^{-13} [2].

For pion decays, violating lepton number, exist only one measured process $\pi^+ \rightarrow \mu^-e^+e^+\nu$. Recently ARES group reached to the best result for this process $\leq 1.8 \times 10^{-7}$ [7] and are intending to improve this result [7].

For Kaon decays where lepton number is violated two prominent results are

Table 1: Upper limits (90% confidence) on branching ratios of some lepton number violating decay modes

process	branching ratio	
	present	proposed
$\mu^+ \rightarrow e^+\gamma$	$\leq 5 \times 10^{-11}$ [1]	10^{-13} [2]
$\mu^+ \rightarrow e^+e^+e^-$	$\leq 1.0 \times 10^{-12}$ [3]	
$\mu^-Ti \rightarrow e^-Ti$	$\leq 4.4 \times 10^{-12}$ [4]	3×10^{-14} [5]
$\mu^-Ti \rightarrow e^+Ca$	$\leq 1.7 \times 10^{-10}$ [6]	10^{-13} [5]
$\pi^+ \rightarrow \mu^-ee\nu$	$\leq 1.8 \times 10^{-7}$ [7]	10^{-10} [7]
$K_L^0 \rightarrow \mu e$	$\leq 2.2 \times 10^{-10}$ [8]	
$K^+ \rightarrow \pi^+\mu e$	$\leq 2.1 \times 10^{-10}$ [9]	5×10^{-12} [10]
$\tau^+ \rightarrow \mu\gamma$	$\leq 5.5 \times 10^{-4}$ [11]	
$\tau^- \rightarrow \mu\mu\mu$	$\leq 2.9 \times 10^{-5}$ [12]	

exist. One is $K_L^0 \rightarrow \mu e$ [8] and second $K^+ \rightarrow \pi^+\mu e$ [9] decays measured at BNL. The branching ratio for last process is supposed to be lowered down to the value 5×10^{-12} [10].

At the present time search for possible τ lepton number violation in τ decays are done at the level of $10^{-4} - 10^{-5}$ of the τ decay probability. Last two lines of the Table 1 shows best results obtained for the τ decays. Those limitations were obtained in the e^+e^- collider experiment. Such bounds on the τ decay probabilities are not significant, if one want to check the lepton number conservation law. The branching ratios $10^{-4} - 10^{-5}$ might be explained by the factors of some constants, phase space and etc., analogous to the $\mu^+ \rightarrow e^+\gamma$ decays, which was considered "naturally" without lepton number conservation law up to the level of 10^{-4} [13]. Further sufficient improvement in similar experiments is limited by the luminosity of the colliders. It is doubtless, that the search for the processes, nonconserving the τ lepton number, are of the fundamental importance and must be performed at the same level, as it is done for $\mu^+ \rightarrow e^+\gamma$ [1], $\mu^+ \rightarrow e^+e^+e^-$ [3] and $\mu^-Ti \rightarrow e^-Ti$ [4] decays. We can notice that in principle the nonconservation of lepton number in $\tau - \mu$ transitions maybe sufficiently larger, than in $\mu - e$ transitions, because of the lepton mass differences. In one specific model [14] with gauged horizontal interaction, the probability of the $\tau \rightarrow 3\mu$ is calculated, which is $\text{br}(\tau \rightarrow 3\mu) = 10^{-6}$ [15].

Here we are considering the possibility of the experimental investigation of the decay $\tau \rightarrow 3\mu$, nonconserving the lepton number in the beams of the accelerators with fixed target at the level of $10^{-7} - 10^{-9}$. Experiment is possible to be performed in hadron or γ beams of high energy (200 GeV - 1 TeV), using thick target of ≥ 30 nuclear length, which stops secondary hadrons and γ s and it is from the material with low atomic number (carbon, beryllium), with subsequent detection of the momenta of the muons from the decay $\tau \rightarrow 3\mu 2\nu$ and reconstruction of the three muon effective mass. This is so called beam-dump experiment.

First, we estimate the intensity of τ lepton production and then we consider possible background process $\tau \rightarrow 3\mu 2\nu$. The estimation of the τ lepton production intensities in a high energy beams (500 GeV) gives following results:

a) We are considering hadron beam with a mean intensity of $10^8 s^{-1}$. Supposing, that main source of the τ leptons are the D_s^+ decays, partial decay width of which is 3×10^{-3} and production cross section is $10 \mu b$ [16-18], we get $5 \times 10^8 \tau$ in 100 hour of the accelerator running.

b) γ beam interaction with light (deuterium) target. At the beam intensity of $10^8 \gamma s$ in second and hadron mechanism of the τ production, we get $10^7 \tau$ in 100 hour. Photon beam gives an evident advantage in the point of view of the background suppression, because of the small total cross section.

c) Photon or electron beam-dump on heavy (lead) target, with the τ lepton production, because of the electroproduction of the $\tau^+ \tau^-$ pairs on nuclei $\gamma + Z \rightarrow \tau^+ \tau^- + Z$. The number of the $\tau^+ \tau^-$ pairs per photon equals to $[84 \times \ln(2w/M) - 218] \times m^2 / [84 \times \ln(2w/m) - 218] \times M^2$ [19], where w is a photon energy, m is an electron mass and M is a τ lepton mass.

At the photon intensities of $10^8 \gamma$ in second (in 100 hours) number of τ is 2×10^6 . In this experiment the number of τ leptons is lower, but background, with muon production in hadron decays, are strongly suppressed.

In principle, it is possible the τ lepton production by muons, but the cross section of this process is $6 \times 10^{-36} cm^2$ [20]. Thus, the expected statistic is very small (5×10^5 in 100 hours).

Above mentioned estimation shows, that in high energy accelerator beams with fixed target in the beam-dump experiment there is accessible such a statistic of τ leptons, that it is possible to search for the $\tau \rightarrow 3\mu$ decays at the level of $10^{-7} - 10^{-9}$. We note, that the discussed here beam intensity (10^8) are not maximally allowable and was choosed from reasons to have no serious problems with muon registration, trigger and accidental coincidences.

Really accessible level will be determined not only by the statistic, but also by the background processes, among of which not all of them are calculable. Here we consider the background process $\tau \rightarrow 3\mu 2\nu$, which must be considered in any case.

We calculated differential probability of the $\tau \rightarrow 3\mu 2\nu$ decay taking into account all diagrams in lowest order of perturbation theory. This process is very similar to the $\mu \rightarrow 3e 2\nu$ calculated in [21-22]. The calculation was performed by means of the program SCHOONSHIP [23]. The total probability of the $\tau \rightarrow 3\mu 2\nu$ decay in respect to the $\tau \rightarrow \mu \nu \nu$ decay, partial probability of which is equal to 17.8×10^{-2} , is 1.07×10^{-6} .

Figure 1 shows $\tau \rightarrow 3\mu 2\nu$ decay probability versus the cuts on invariant mass of 3 muons. The invariant mass of 3 muons from $\tau \rightarrow 3\mu$ decay corresponds to the right bound of the figure. It is evident, that if the invariant mass is known with the accuracy of 300 MeV, which is accessible in above discussed experiments, the process $\tau \rightarrow 3\mu 2\nu$ would be neglected as a physical background to the $\tau \rightarrow 3\mu$ decay searching at the level of 10^{-9} .

In the model with Higgs current mechanism [24] the ratio between τ decay into the 3μ and μ decay into the $3e$ is predicted and it is equal to $W(\tau \rightarrow 3\mu) /$

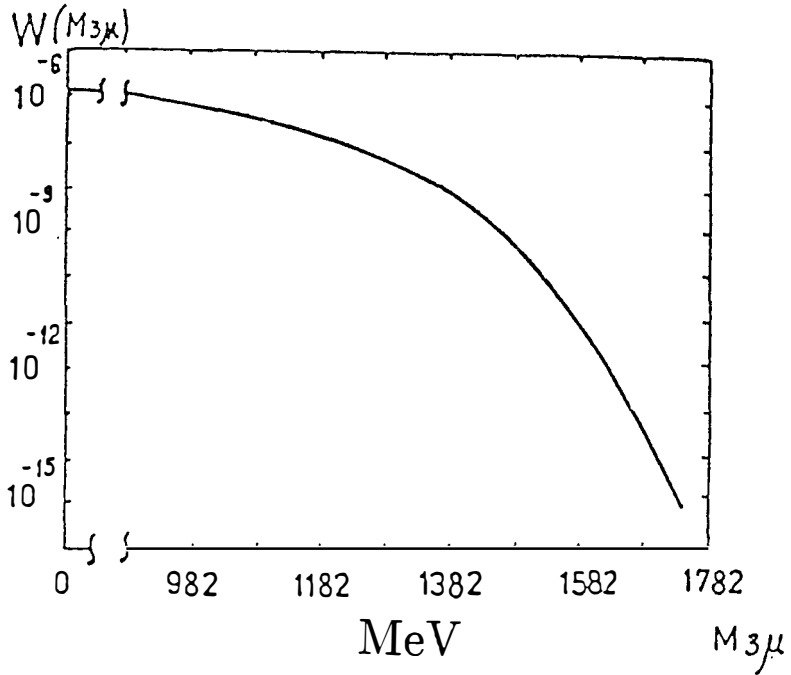


Figure 1: The value of $\tau \rightarrow 3\mu 2\nu$ decay probability versus the cuts on 3 muon invariant mass $M(3\mu)$.

$W(\mu \rightarrow 3e) = (m_e^2/m_\tau^2) = 10^{-7}$. In this case, if the probability level of 10^{-9} for $\tau \rightarrow 3\mu$ decay is attainable in above discussed experiments, this means the decay probability limit of 10^{-16} for $\mu \rightarrow 3e$ decay.

Authors are grateful to Yu.M.Antipov, S.P.Denisov, S.M.Korenchenko and B.M.Pontecorvo for usefull discussions and B.F.Kostin for assistance in calculations.

References

- [1] R.D. Bolton et al., Phys. Rev. D38 (1988) 2077.
- [2] MEGA, LAMPF proposal (1985).
- [3] SINDRUM collaboration, Nucl. Phys. B299 (1988) 1.
- [4] SINDRUM collaboration, unpublished (1990).
- [5] SINDRUM collaboration, PSI proposal R-87-03 (1987).
- [6] S.Ahmad et al., Phys. Rev. D38 (1988) 2102.

- [7] ARES collaboration, Private communications.
- [8] C. Mathiazhagan et al., Phys. Rev. Lett. 63 (1989) 2181.
- [9] A.M. Lee et al., Phys. Rev. Lett. 64 (1990) 165.
- [10] M. Zeller et al., BNL Letter of Intent (1989).
- [11] K.G. Hayes et al., Phys. Rev. D25 (1982) 2869.
- [12] H. Albrecht et al., Phys. Lett. B185 (1987) 228.
- [13] G. Feinberg , Phys. Rev., 110, (1958) 1482
- [14] J.L.Chkareuli , Phys. Lett. B (1990) .
- [15] J.L.Chkareuli , Private communications.
- [16] I.Hinchliffe,G.H.Lewellyn Smith, Nucl. Phys., B114,(1976) 45.
- [17] M.Bourquin,J.M.Gaillard, Phys. Lett. 59B (1975) 191.
- [18] S.Mori, Fermilab 2251.0, (1979).
- [19] J.Smith et al., Phys. Rev. D15 (1977) 648.
- [20] V.Ganapathi J.Smith, Phys. Rev., D23 (1981) 75.
- [21] D.Ju.Bardin et al., Sov. Jour. Nucl. Phys., 15 (1972) 161.
- [22] P.M.Fishbane K.J.F.Gaemers , Phys. Rev. D33 (1986) 159.
- [23] H.Straube , Com. Phys. Comm., 8 (1974) 1.
- [24] J.Kirkby ,Prticle World , 1 (1990) 27.

COHERENT PRODUCTION OF PSEUDOSCALARS (AXIONS) INSIDE A DIPOLE
MAGNETIC FIELD

YANNIS SEMERTZIDIS *
UNIVERSITY OF ROCHESTER, ROCHESTER, NY 14627



We set a limit on the coupling of any light pseudoscalar that couples to two photons by looking at the induced optical rotation of a polarized laser beam inside a dipole magnetic field. The limit is $g_{\alpha\gamma\gamma} < 2.5 \times 10^{-6} \text{ GeV}^{-1}$ for a particle of mass $m_a \leq 7 \times 10^{-3} \text{ eV}$.

I. Theoretical motivation

The QCD Lagrangian contains a term that violates CP symmetry:

$$L_\theta = \frac{\theta}{32\pi^2} F^{\alpha\mu\nu} F_{\alpha\mu\nu} \quad (1)$$

where $F^{\alpha\mu\nu}$ is the gluon field and θ is an angular parameter with possible values ($0 \leq \theta < 2\pi$). This term violates the Parity (P) symmetry and conserves the charge (C) symmetry and therefore violates the combined CP symmetry. An experimental upper limit on the violation of CP symmetry in strong interactions exists^{1]} from the study of the electric dipole moment (EDM) of neutron. The limit of $4 \times 10^{-25} \text{ e} \cdot \text{cm}$ limits θ to $|\theta| < 10^{-9}$ or $|\pi - \theta| < 10^{-9}$.

Because it is unlikely for θ to be so close to 0 or π it is believed to be exactly 0 or π . In order to explain why θ chooses to take the value 0 or π , Peccei and Quinn^{2]} first proposed a new theory in which θ gets the value 0 below the QCD energy scale, because the Lagrangian has an effective potential with minimum at that value. The Peccei-Quinn symmetry ($U(1)_{P,Q}$, axial symmetry) corresponds to invariance in the Lagrangian under the transformations:

$$\begin{aligned} u_i &\rightarrow e^{i\eta\gamma_5} u_i, & \phi_u &\rightarrow e^{-2i\eta} \phi_u \\ d_i &\rightarrow e^{i\eta\gamma_5} d_i, & \phi_d &\rightarrow e^{-2i\eta} \phi_d \end{aligned} \quad (2)$$

where u_i, d_i refer to the $SU(2)$ quarks, η is a rotation angle (some arbitrary phase) and

$$\phi_u = \begin{bmatrix} \phi_u^0 \\ \phi_u^- \end{bmatrix}, \quad \phi_d = \begin{bmatrix} \phi_d^+ \\ \phi_d^0 \end{bmatrix} \quad (3)$$

the two Higgs doublets of the standard $SU(3) \times SU(2) \times U(1)$ theory.

A breakdown of this symmetry gives rise to a pseudogoldstone boson, the axion, predicted by Weinberg and Wilczek.^{3]} The scale at which the symmetry breaks down first thought to be at the weak symmetry breaking scale and the mass of the axion at the MeV range. The axion mass depends on the symmetry breaking scale f_a : $m_a = \frac{\sqrt{2} f_\pi m_\pi}{f_a}$ with f_π the pion form

factor (94 MeV) and m_π the pion mass (135 MeV).

The heavy mass axion was excluded by beam dump and branching ratio experiments.^{4]} An extension^{5]} of the Peccei-Quinn model was invented which includes an extra Higgs doublet with very high vacuum expectation value (VEV). f_a in this case is proportional to the (VEV) of the third Higgs doublet and therefore the axion mass can be very small.

An experiment to look for very light pseudoscalars and/or scalars that couple to two photons was setup at Brookhaven National Lab. It uses a polarized laser light inside a dipole magnetic field. The Lagrangian that describes it is

$$L = -\frac{1}{4}F_{\mu\nu}F^{\mu\nu} + \left[\frac{1}{2}(\partial_\mu a \partial^\mu a - m_a^2 a^2) + \frac{1}{4M}F_{\mu\nu}\tilde{F}^{\mu\nu}a \right] + \frac{\alpha^2}{90m_e^4} \left[(F_{\mu\nu}F^{\mu\nu})^2 + \frac{7}{4}(F_{\mu\nu}\tilde{F}^{\mu\nu})^2 \right] \quad (4)$$

where the first term describes the propagation of the classical fields, the second term is referring to the axion coupled to two photons, and the third term describes the QED vacuum polarization.

II. Axion induced rotation and ellipticity.

The interaction Lagrangian for the axion is

$$L_{\text{int}} = \frac{1}{M} \vec{E} \cdot \vec{B} \phi_a \quad (5)$$

with $g_{a\gamma\gamma} = \frac{1}{M}$ the coupling constant, \vec{E} the electric field vector of the photon beam, \vec{B} the external magnetic field, and ϕ_a the axion field. A polarized laser beam entering the magnetic field region undergoes rotation because only one component produces axions (and thus is attenuated) due to $\vec{E} \cdot \vec{B}$ nature of the interaction Lagrangian. The rotation angle is given by

$$\epsilon \approx N \frac{B_{\text{ext}}^2 l^2}{16M^2} \sin 2\theta \quad (6)$$

where N is the number of times the light passes through the magnetic field, θ the angle between $\vec{B}_{\text{ext}} \times \vec{k}$ and the electric field of the light beam, and l the magnetic field length.

In case that the axion, that is produced inside the magnetic field, interacts with a virtual photon from the magnetic field, it recombines giving back the original photon.

Because axions acquire mass, they travel slower than the speed of light in vacuum and therefore there is a phase difference between the parallel and orthogonal components. This translates to an ellipticity given by

$$\psi_a = \frac{N}{2} \left(\frac{B_{\text{ext}} \omega}{M m_a^2} \right)^2 \left\{ \frac{m_a^2 l}{2\omega} - \sin \left(\frac{m_a^2 l}{2\omega} \right) \right\} \sin 2\theta. \quad (7)$$

There is also ellipticity induced from QED vacuum polarization^{6]} which is given by

$$\psi = N \frac{\alpha^2 B_{\text{ext}}^2 \omega l}{15 m_e^4} \sin 2\theta \quad (8)$$

where $\alpha \approx 1/137$ is the fine structure constant, ω the photon energy (green light, 2.41 eV) and m_e the electron mass in eV. In these units (natural Heaviside-Lorentz) a magnetic field of 1T is equal to 195 eV², and a length of 1 cm equal to 5×10^4 eV⁻¹.

III. Experiment^{7]}

An Ar ion laser (2 Watt single line) is used as the source of the polarized photons (fig. 1). The light goes through a telescope that transforms the beam characteristics in order to match the cavity (see below). The half wave plate (HWP) rotates the polarization plane so that the polarization can have the desired angle with the external magnetic field. After the light passes through some steering mirrors (P.S.: periscope, M1: mirror) it enters the vacuum vessel.

Very high quality polarizers are used to polarize (P) and analyze (A) the light. The delay line method is used where the laser beam travels in the magnetic field region several hundred times. After exiting from the magnetic field region the light is heterodyned with a Faraday cell (F.C.). In case the sought after effect is ellipticity the QWP is used to convert the ellipticity into rotation. Two superconducting dipole magnets from the CBA^{8]} project are used. Each is about 4.5 meters long and can deliver 5 T maximum magnetic field.

The photodiode after the analyzer sees a current that is proportional to

$$I_T = I_o \left\{ \sigma^2 + \alpha^2 + 2\alpha\eta_o \cos(2\pi f_F t + \phi_F) + \frac{\eta_o^2}{2} \cos(4\pi f_F t + 2\phi_F) \right. \\ \left. + \eta_o \epsilon_o \cos[2\pi(f_F - f_M)t + (\phi_F - \phi_M)] + \eta_o \epsilon_o \cos[2\pi(f_F + f_M)t + (\phi_F + \phi_M)] \right\} \quad (9)$$

with $\sigma^2 \approx 10^{-7}$ the extinction between the two polarizers, $\alpha \approx 10^{-6}$ the misalignment between the polarizer and analyzer from the perfect crossing, $\eta_o \approx 10^{-3}$ the Faraday rotation amplitude, ϵ_o the rotation (or ellipticity) amplitude induced by the magnetic field, ϕ_F , ϕ_M are the Faraday cell and rotation phases respectively, and $f_F = 260$ Hz, $f_M = 39.0625$ mHz are the Faraday cell and the magnet modulation frequencies respectively. The photodiode current is amplified by a charge sensitive amplifier and the rotation is found by Fourier analyzing the resulting voltage from the formula

$$\epsilon_o = \frac{\eta_o I_{f_F + f_M}}{2 I_{2f_F}} \quad (10)$$

where $I_{f_F + f_M}$ is the power at the signal frequency, and I_{2f_F} the power at twice the Faraday cell frequency.

In fig. 2 rotation data is shown.^{9]} The number of reflections were 790, the modulated magnetic field was $B^2 = 1.65$ T² and the pressure inside the cavity was better than 10^{-5} Torr. We also run the experiment with the QWP in place, and observed peaks at the magnet frequency of the same order as the rotation, but with 38 reflections. Treating these signals as a background of unknown origin we set a limit on the axion coupling constant to two photons. We are continuing the efforts in resolving the origin of these signals by performing various tests in the system.

* The other members of the collaboration are: R. Cameron, G. Cantatore, A. C. Melissinos; University of Rochester. H. Halama, Don Lazarus, and A. Prodell; Brookhaven National Lab. F. A. Nezrick; Fermi National Lab. C. Rizzo and E. Zavattini; University of Trieste.

References

- 1] V. Baluni, Phys. Rev. D19, 2227 (1979).
- 2] R. D. Peccei and H. R. Quinn, Phys. Rev. Lett. 38, 1440 (1977); Phys. Rev. D16, 1791 (1977).
- 3] S. Weinberg, Phys. Rev. Lett. 40, 223 (1978); F. Wilczek, Phys. Rev. Lett. 40, 279 (1978).
- 4] E. M. Riordan et al., Phys. Rev. Lett. 59, 755 (1987); C. Edwards et al., Phys. Rev. Lett. 48, 903 (1982); C. M. Hoffmann, Phys. Rev. D34, 2167 (1986).
- 5] M. Dine, W. Fischler, and M. Srednicki, Phys. Lett. 104B, 199 (1981).
- 6] S. L. Adler, Ann. of Phys. (NY), 87, 599 (1971); J. Schwinger, Phys. Rev. 82, 664 (1951).
- 7] L. Miani, R. Petronzio, and E. Zavattini, Phys. Lett. 175B, 359 (1986). Y. Semertzidis, Ph. D. Thesis, University of Rochester Report No. UR-1141, 1990 (unpublished).
- 8] E. J. Bleser et al., NIM A235, 435 (1985).
- 9] Y. Semertzidis et al., Phys. Rev. Lett. 64, 2988 (1990).

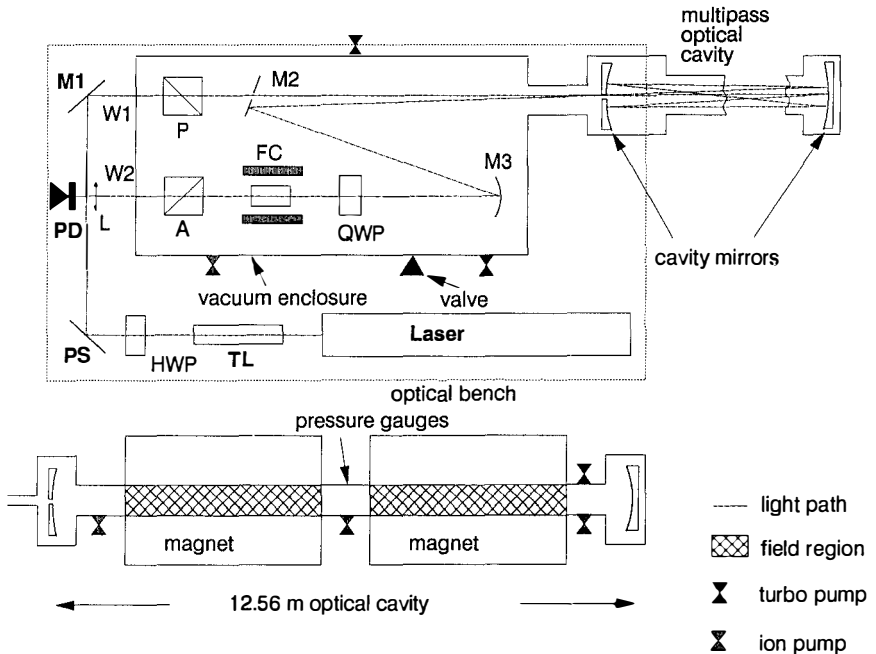


Fig. 1 The apparatus; A: analyzer; FC: Faraday cell; M1: steering mirror; P: polarizer; PD: photodiode; PS: periscope; QWP: quarter-wave plate; and TL: telescope.

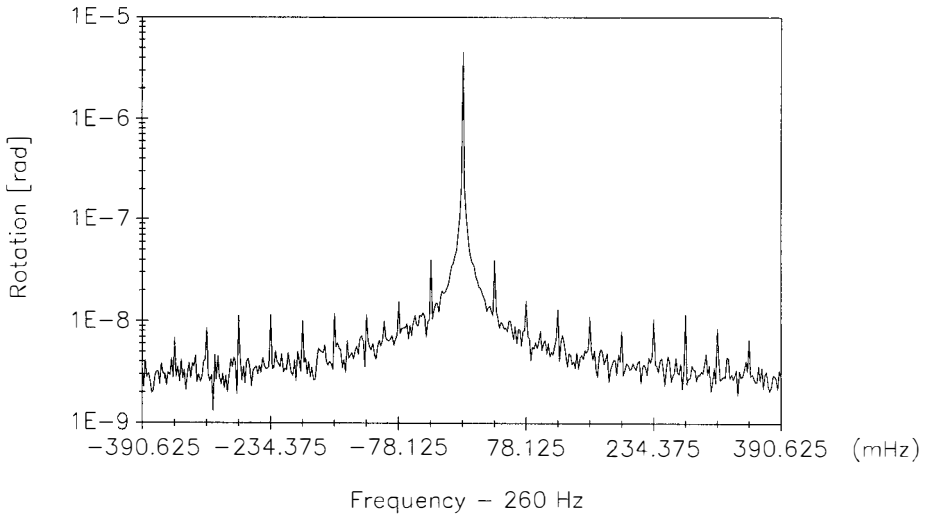


Fig. 2 Rotation data in vacuum.

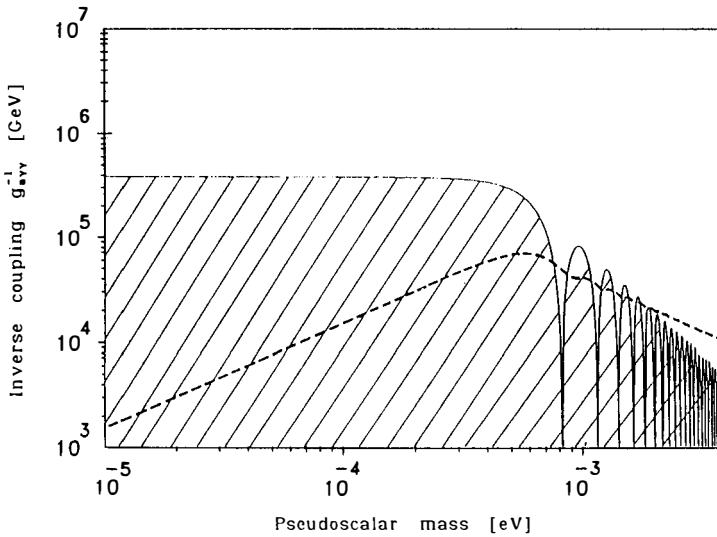


Fig. 3 Excluded regions for the inverse coupling to two photons. The shaded region is a result of the rotation data and the dashed curve of the ellipticity data.

INTERFERENCE BETWEEN THE AHARONOV-BOHM AND AHARONOV-CASHER EFFECTS

Xiao-Gang He
Theory Division, CERN
CH-1211 Geneva 23, Switzerland

ABSTRACT

After a discussion of the principles of the Aharonov-Bohm (AB) and Aharonov-Casher (AC) effects, I will discuss the possibility of observing the interference between them. I will also discuss the implications of the AB and AC effects for anyon physics.

1. Introduction

In this talk I will discuss the possibility of observing the interference between the Aharonov-Bohm (AB) and Aharonov-Casher (AC) effects and some of their implications for anyon physics. Before doing so, let me first discuss the principles of the AB and AC effects.

The AB effect is a pure quantum mechanical effect which was pointed out in 1959 by Aharonov and Bohm [1]. This effect describes a non-trivial topological phase developed in the wave function of a charged particle due to an electromagnetic field which the particle does not experience. Experiments have confirmed this effect. For a review see Ref. [2].

In an external electromagnetic vector potential A_μ , the equation of motion for a charged spin-half particle is given by

$$(\not{\partial} - ie \not{A} + m)\psi = 0, \quad (1)$$

where m is the mass of the particle. In a static external magnetic field, one can choose a gauge with $A_4 = 0$. The equation of motion becomes

$$(\not{\partial} - ie\boldsymbol{\gamma} \cdot \mathbf{A} + m)\psi = 0, \quad (2)$$

where $\boldsymbol{\gamma} = (\gamma_1, \gamma_2, \gamma_3)$ and \mathbf{A} is the spatial component of the vector potential. Under a gauge transformation $A_\mu \rightarrow A_\mu + \partial_\mu f$, gauge invariance of the theory requires the wave function to transform as $\psi \rightarrow e^{ief}\psi$. In regions where $\mathbf{A} \neq 0$ but $\mathbf{B} = \nabla \times \mathbf{A} = 0$, \mathbf{A} can be written as a gradient of a scalar function. In this case \mathbf{A} is a pure gauge vector potential and Eq.(2) can be rewritten as

$$(\not{\partial} + m)\psi' = 0, \quad (3)$$

where $\psi' = e^{-ie \int^r \mathbf{A} \cdot d\mathbf{r}} \psi$.

For a physically non-trivial situation, the region in which $\mathbf{B} = 0$ but $\mathbf{A} \neq 0$ must have a hole in it, such that $\mathbf{B} \neq 0$ inside the hole (see Fig.1); for example, the potential produced by a infinitely long solenoid (the AB-type potential). If one now transports the particle around a closed path in the $\mathbf{B} = 0$ region which encloses the $\mathbf{B} \neq 0$ region, the wave function develops a non-trivial topological phase

$$\phi_{AB} = -e \oint \mathbf{A} \cdot d\mathbf{r} = -e \int_S (\nabla \times \mathbf{A}) \cdot d\mathbf{S} = -e\Phi, \quad (4)$$

where Φ is the magnetic flux passing through the area enclosed by the path. Due to the phase ϕ_{AB} , interference can be observed at point B in Fig.1 when a beam of charged

particles is split at point A into two coherent beams and then recombined at point B. Experiments have observed such interference.

The AC effect was pointed out in 1984 by Aharonov and Casher [3] (see also [4]). They found that in the non-relativistic limit the wave function of a neutral particle with non-zero magnetic dipole moment μ develops a topological phase when the particle moves along a closed path which encircles an infinitely long filament carrying a uniform charge density. The AC phase has been measured experimentally [5].

The equation of motion for a neutral spin-half particle with a non-zero magnetic dipole moment moving in a static electric field \mathbf{E} is

$$(\not{\partial} + \frac{1}{2}\mu\sigma_{\mu\nu}F^{\mu\nu} + m)\psi = 0, \quad (5)$$

which can be written as

$$(\not{\partial} + \mu\boldsymbol{\gamma} \cdot \mathbf{E}\gamma_4 + m)\psi = 0, \quad (6)$$

where $F^{\mu\nu}$ is the field strength of the electric field. In the following I will give more details of the AC effect without taking the non-relativistic limit. I will formulate the problem using the four-component form of the Dirac equation [6]. We should look for solutions of Eq.(6) which can be written in the following form

$$(\not{\partial} + m)\psi' = 0, \quad (7)$$

where $\psi' = e^{i\mathbf{a}\boldsymbol{\gamma}_4 \int^r \mathbf{A}' \cdot d\mathbf{r}} \psi$. Here \mathbf{A}'_i is a linear function of E_i and \mathbf{a} is a 4×4 matrix which will be determined in the following. Of course, in order that the phase be topologically non-trivial, there must be a region D in which $\nabla \times \mathbf{A}' \neq 0$, and in an other region which encloses region D, $\nabla \times \mathbf{A}'$ equals zero. Writing Eq.(7) in terms of ψ , we obtain

$$(e^{-i\mathbf{a}\boldsymbol{\gamma}_4 \int^r \mathbf{A}' \cdot d\mathbf{r}} \boldsymbol{\gamma}_\mu e^{i\mathbf{a}\boldsymbol{\gamma}_4 \int^r \mathbf{A}' \cdot d\mathbf{r}} \not{\partial}_\mu + \boldsymbol{\gamma} \cdot \mathbf{A}' i\mathbf{a}\boldsymbol{\gamma}_4 + m)\psi = 0 \quad (8)$$

We find that \mathbf{a} and \mathbf{A}' must satisfy

$$\begin{aligned} \mu\boldsymbol{\gamma} \cdot \mathbf{E} &= i\mathbf{a}\boldsymbol{\gamma} \cdot \mathbf{A}' \\ \mathbf{a}\boldsymbol{\gamma}_4\boldsymbol{\gamma}_\mu &= \boldsymbol{\gamma}_\mu\mathbf{a}\boldsymbol{\gamma}_4 \end{aligned} \quad (9)$$

The matrix \mathbf{a} can be expressed by some linear combination of the complete set of 4×4 matrices $1, \boldsymbol{\gamma}_5, \boldsymbol{\gamma}_\mu, \boldsymbol{\gamma}_\mu\boldsymbol{\gamma}_5$, and $\sigma_{\mu\nu}$. The second equation of Eq.(9) cannot be satisfied if all of $\boldsymbol{\gamma}_1, \boldsymbol{\gamma}_2$ and $\boldsymbol{\gamma}_3$ are present in Eq.(8), but two of them are possible. This indicates

that the AC topological phase can only arise when the particle is moving in two spatial dimensions. If one chooses \mathbf{a} to be one of the matrices σ_{12}, σ_{23} , or σ_{13} , one can get two dimensional solutions. For other choices of \mathbf{a} there are no desired solutions. To be specific, let us choose $\mathbf{a} = -\sigma_{12}$. In this case, γ_3 cannot appear in the equation which implies that P_3 (i.e. $\partial_3\psi$) and E_3 are zero. From the first of Eq.(9), we then have

$$\mu(\gamma_1 E_1 + \gamma_2 E_2) = -i\sigma_{12}(\gamma_1 A'_1 + \gamma_2 A'_2) \quad (10)$$

and therefore $A'_1 = \mu E_2$, $A'_2 = -\mu E_1$. We have $\nabla \times \mathbf{A}' = -\mu(\partial_1 E_1 + \partial_2 E_2)$. If $\partial_3 E_3 = 0$, $\nabla \times \mathbf{A}' = 0$ in the charge free region. I will call the electric field which satisfies the above conditions the AC-type field. When these conditions are satisfied, Eq.(6) can be written in the form of Eq.(7) with $\psi' = e^{-i\sigma_{12}\gamma_4 \int^t \mathbf{A}' \cdot d\mathbf{r}} \psi$ and \mathcal{D} replaced by $\mathcal{D}' = \gamma_4 \partial_4 + \gamma_1 \partial_1 + \gamma_2 \partial_2$. When the particle moves along a closed path in the charge free region which includes a region where the electric charges are not zero, a topological phase will be developed in the wave function. The phase is given by

$$\phi_{AC} = -\sigma_{12}\gamma_4 \oint \mathbf{A}' \cdot d\mathbf{r} = \mu\sigma_{12}\gamma_4 \int_S \nabla \cdot \mathbf{E} dS = \mu\sigma_{12}\gamma_4 \lambda, \quad (11)$$

where λ is the linear charge density of the filament. This phase is purely quantum mechanical and has no classical interpretation. The appearance of $\sigma_{12}\gamma_4$ in the phase represents the spin degrees of freedom. Interference can be observed at point B in Fig. 2 when a beam of neutral particles with non-zero μ is split into two coherent beams at point A and recombined at point B.

The AB and AC effects are very similar. It has been shown that they are the dual of each other in two spatial dimensions in the sense that one can obtain the equation of motion for the AC case from the AB case by simply changing e to μ and A_i to $A'_i = s\epsilon_{ij}E_j$, and vice versa [7]. Here $s = (+, -)$ is the spin degree of freedom and $\epsilon_{12} = -\epsilon_{21} = 1$. However, the AB and AC effects are also different in many ways. For example, 1) the AC effect is restricted to two spatial dimensions, that is, the particle has to move on a plane, whereas the AB effect is less constrained. 2) The AB effect is a quantum effect due to the interaction of a classically unphysical vector potential with a charged particle. The topology of the space is determined by the distribution of the magnetic field \mathbf{B} . The AC effect is due to the interaction between a physical electric field and a neutral particle with a non-zero μ . In this case the topology of the space is determined by the linear charge density distribution λ . There are also different spin dependences in the scattering cross sections of the AB and AC effects. This aspect has been carefully studied in Ref.[7].

2. The interference between the AB and AC effects

The original AC effect concerns only neutral particles. As a matter of fact this restriction is not necessary. There is also an AC effect for a charged particle with non-zero anomalous magnetic dipole moment μ_k . The equation of motion for such a particle in an AC-type field is given by

$$(\not{\partial}' + m - ie\gamma_4 V + \mu_k(\gamma_1 E_1 + \gamma_2 E_2)\gamma_4)\psi = 0, \quad (12)$$

where V is the scalar potential due to a charged filament which produces the AC-type field $\mathbf{E} = -\nabla V$. In the charge free region, the equation of motion can be rewritten as

$$(\not{\partial}' + m - ie\gamma_4 V)\psi' = 0, \quad (13)$$

with $\psi' = e^{-i \int^r \sigma_{12}\gamma_4 \mathbf{A}' \cdot d\mathbf{r}} \psi$. It is clear that the wave function develops a topological phase when the particle moves along a closed path around the filament. This topological phase can be observed experimentally.

We now consider the possibility of observing the interference between the AB and AC effects[6]. This can happen if one lets a charged particle with a non-zero μ_k , for example a proton, move in the x-y plane in the vector potential \mathbf{A} produced by an infinitely long solenoid along the z axis and the electric field $\mathbf{E} = -\nabla V$ produced by an infinitely long filament carrying a uniform charge density parallel to the solenoid (not necessarily located at the same place as the solenoid). The equation of motion is

$$(\not{\partial}' + m - ie\gamma_4 V - ie(\gamma_1 A_1 + \gamma_2 A_2) + \mu_k(\gamma_1 E_1 + \gamma_2 E_2)\gamma_4)\psi = 0; \quad (14)$$

Eq.(14) can be written in the form of Eq.(13), with $\psi' = e^{-i \int^r (\mathbf{eA} + \sigma_{12}\gamma_4 \mathbf{A}') \cdot d\mathbf{r}} \psi$. When the particle moves in the x-y plane in a closed path, different topological phases will be developed in the wave function depending on how the particle circles around the solenoid and the filament (see Fig. 3.). If the path encloses both the solenoid and the filament (path 1), the topological phase will be $\phi = -e\Phi + \mu_k \sigma_{12} \gamma_4 \lambda$ and if the path only encloses either the solenoid (path 2) or the filament alone (path 3), the topological phase developed will be $\phi_B = -e\Phi$ or $\phi_C = \mu_k \sigma_{12} \gamma_4 \lambda$, respectively. It is interesting to note that the interference pattern of path 1 in Fig.3 is due to the interference between the AB and AC effect. This interference contains more information than the AB or AC effect alone and shows the deep connection between the AB and AC effects. This interference is a significant test of our knowledge about topological phase

shift in quantum mechanics. Experiment could be performed to verify such effect. Experimental observations may be difficult. However, the interference is independent of the locations of the solenoid and the filament and independent of the masses of the particles; it is possible to use a charged particle with small anomalous magnetic dipole moment, for example an electron, to set up a reference interference pattern and then use proton beams to produce the interference between the AB and AC effects.

3. Implications for anyon physics

The AB and AC effects may have useful applications in many other aspects of physics. For example, they provide mechanisms for forming anyon systems which may have important applications in quantum Hall and high T_C superconductivity. In the following I describe how the AB and AC effects provide mechanisms for forming anyon systems.

a) The AB effect as a mechanism for the anyon system [8].

In 2+1 dimensions if there are particles which carry electric charge and magnetic flux-tube (charged-flux-tube particle), the potential produced by one such particle is $A_\mu = (\mathbf{A}, V) = (A_1, A_2, V)$, where A_i is an AB-type potential and V is the scalar potential produced by the electric charge of the particle. For a system which contains two identical charged-flux-tube Dirac-Fermi particles, the motion of one particle around the other is described by Eq.(1) in 2+1 dimensions. We can express the two-body wave function Ψ in terms of the centre-of-mass coordinates R, θ and the relative coordinates r, φ . When these two particles are interchanged, due to the AB effect, a phase in the wave function will be developed

$$\Psi(R, \theta; r, \varphi + \pi) = -e^{ie\Phi} \Psi(R, \theta; r, \varphi). \quad (15)$$

The minus sign is due to the fact that the particles are Dirac-Fermi particles. So one obtains a fractional statistic phase, $\phi_s = \pi + e\Phi$.

b) The AC effect as a mechanism for the anyon system[6].

The AC effect provides another mechanism for the anyon system. In 2+1 dimensions, a charged particle will produce a scalar field V and electric field $\mathbf{E} = -\nabla V$ which satisfy the conditions for the AC effect. For a system which contains two identical charged Dirac-Fermi particles with non-zero μ_k , when these two particles are interchanged, one finds

$$\Psi(R, \theta; r, \varphi + \pi) = -e^{is\mu_k e} \Psi(R, \theta; r, \varphi). \quad (16)$$

Again one obtains a fractional statistic phase, $\phi_s = \pi + s\mu_k e$.

From the above discussion we see that the AB and AC effects provide natural mechanisms for forming anyon systems.

To summarise, I have discussed the possibility of observing an AC topological phase for a charged particle and the interference between the AB and AC effects. These effects will provide significant tests for quantum mechanics. I have also shown that the AB and AC effects provide natural mechanisms for forming anyon systems.

I would like to thank B. McKellar for collaborations in related work.

REFERENCES

- [1] Y. Aharonov and D. Bohm, *Phys. Rev.* **115**, 485(1959).
- [2] M. Peshkin and A. Tonomura, *The Aharonov-Bohm effect*. Springer-Verlag, Berlin, 1989.
- [3] Y. Aharonov and A. Casher, *Phys. Rev. Lett.* **53**, 319(1984).
- [4] J. Anandan, *Phys. Rev. Lett.* **48**, 1660(1982); *Phys. Lett.* **138B**, 347(1989).
- [5] A. Cimmino, G.I. Opat, A.G. Klein, H. Kaiser, S.A. Werner, M. Arif, and R. Clothier, *Phys. Rev. Lett.* **63**, 380(1989); Preprint, ICAP-12, Ann Arbor, July 29-August 3, 1990.
- [6] Xiao-Gang He and B. McKellar, Preprint, CERN-TH.5928/90, UM-P-90/105. (*Phys. Lett. B* in press)
- [7] C.R. Hagen, *Phys. Rev. Lett.* **64**, 2347(1990).
- [8] F. Wilczek, *Phys. Lett. Rev.* **49**, 957(1982).

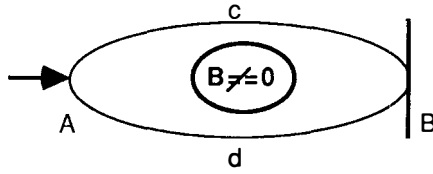


Figure 1. The topology of the AB effect. The small circle represents the solenoid which is perpendicular to the plane.

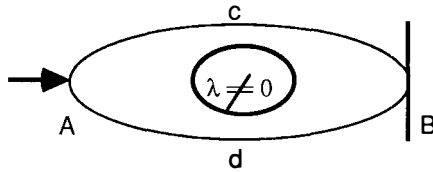


Figure 2. The topology of the AC effect. The small circle represents the charged filament which is perpendicular to the plane.

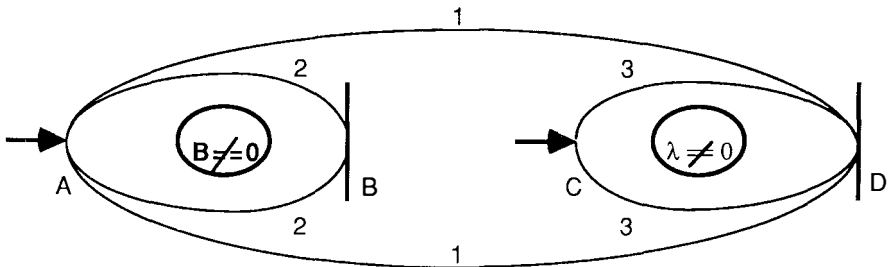


Figure 3. The interference between the AB and AC effects.

MEASURING THE NEUTRON LIFETIME USING STORED NEUTRONS

J M Pendlebury [†]
Institut Laue Langevin
38042 Grenoble, France

**ABSTRACT**

A brief review is presented of the experimental methods for determining the neutron lifetime by neutron storage, their results, and some of the problems encountered.

[†] ● on leave from the University of Sussex, Brighton, UK

INTRODUCTION

In the days of the earliest neutron lifetime experiments with beams, storage of neutrons in traps was just a dream attributed to Fermi. Later, in 1959, the idea of storage in material traps was discussed by Zeldovich ¹⁾. To be storable, neutrons must have speeds as low as 6 m/s, some 200 times slower than thermal neutrons. Perhaps the most daunting aspect of storage was the need to solve the engineering and physics problems of getting such slow neutrons out of nuclear reactors. Storage was first demonstrated ten years later at JNIR Dubna and at TU Munich. The first tentative lifetime measurements came ten years later still with W. Paul's group from Bonn, in 1978 ²⁾ V. Morozov's group at the Kurchatov Institute, in 1980 ³⁾ and W. Mampe's group at the ILL in 1986 ⁴⁾. The three groups have continued to develop their methods and an LNPI-Dubna collaboration has joined the field. The storage results may be compared with the most recent result of $\tau_n = 893.6 \pm 5.3$ s from the NIST-Sussex beam experiment.

TABLE 1 Recent τ_n results from neutron storage

Groups	τ_n /seconds
Bonn-ILL ⁵⁾	876.7 \pm 10
Kurchatov ⁶⁾	900 \pm 11
Kurchatov-ILL ⁷⁾	883.4 \pm 2.9
ILL ⁸⁾	887.6 \pm 3.0
LNPI-Dubna ⁹⁾	888.4 \pm 2.9

Storable neutrons called ultracold neutrons (UCN) have kinetic energies in the range $(0 \text{ to } 3) \times 10^{-7}$ eV. The potential energy of UCN in condensed matter due to the nuclear forces is between -1 to +3 times 10^{-7} eV depending on the material. Gravity changes the neutron potential energy at the rate 1.0×10^{-7} eV per metre of height. A magnetic field of 1.7 tesla contributes 10^{-7} eV by acting on the neutron magnetic moment. The strongest available source of UCN, that at the ILL, can provide a maximum UCN density of 50 000/litre when all speeds below 6 m/s are contained. At LNPI the UCN density is 10 000/litre.

There are a few favoured materials for neutron trap walls, which in a clean condition, are known to produce low reflection losses. They include Al, Be, solid D₂O, solid O₂ and the oil Fomblin which is a polyether with molecules roughly represented by $(\text{O C}_4\text{F}_8)_4\text{s}$.

To determine the lifetime, a trap is filled with neutrons under reproducible conditions. After a very short storage interval t_1 , the neutrons are released and counted giving C_1 . The fill, store and release cycle is repeated with a longer storage interval t_2 , now comparable with the neutron lifetime, and the number C_2 obtained. If beta decay is the only loss process, then the lifetime τ_n is given by

$$\tau_n = \frac{(t_2 - t_1)}{\ln \left(\frac{C_1}{C_2} \right)}. \quad (1)$$

OUTLINE OF THE EXPERIMENTS

The group from Bonn has used magnetic and inertial forces to store neutrons in a ring trap which was operated at the ILL. Of the four experiments, this is the only one which has reduced the wall interaction losses essentially to zero so that equation (1) applies directly. The magnetic field, which has a maximum value of 6 tesla, provides a C shaped potential wall bent round into a circular with a diameter of 1 m. The wall is like a tightly curved bobsleigh track where neutrons with a forward speed of 12 m/s circulate while held firmly into the C by inertial forces. The neutron counts are, at present, comparatively low.

The experiments of the group at the Kurchatov Institute, Moscow, have used storage of neutrons in material traps which have been hollow circular cylinders with their axes vertical, closed at the bottom and open at the top, relying on gravitational forces to complete the trapping, as with tea in a teacup. An advantage of the open top is that the trap space is pumped during storage. The material walls (Al, D_2O , or Fomblin) cause the neutrons to be lost at reflection through inelastic scattering which is temperature dependent and by nuclear absorption. For aluminium or Fomblin at room temperature the wall loss rate is about half of the beta decay rate. A very important element, therefore, of all existing experiments with material walls is their way of correcting for the wall losses. The Kurchatov group keeps a roughly constant trap volume while making total UCN loss rate measurements with progressively more and more surface present. The surface was increased by lowering extra thin sheets into the trap via its conveniently open top. A complication, with all but their last version, was that the calculation of the effects of the extra surfaces requires a knowledge of the spectrum of energies of the trapped neutrons.

Theoretical predictions of wall reflection losses suffer from uncertainty about the dynamics of the thermal motion and the composition of the first few tens of atomic layers involved. However, it is sufficient for all the

experimental methods to be able to change their unknown, but hopefully reproducible, wall losses by predictable numerical factors. The real challenge is to be able to calculate the numerical factor reliably enough. For example, In the latest of the Kurchatov experiments, which was carried out at the ILL, the surface area was increased by a constant known factor on a very local basis all over the trap. This was then taken to be the factor by which the wall losses were increased. A knowledge of the neutron spectrum was not required.

In making the corrections the uniformity of wall properties over the trap is very important. To achieve uniformity, the ILL group has used a rectangular trap with float glass walls on which there is a refreshable Fomblin oil coating. Big changes in trap volume can be made as the back wall is moved towards or away from the front wall. There are then some changes in exposed wall area. This experiment needs no knowledge of the neutron spectrum except to calculate some small corrections at the level of 0.5%. The space where the neutrons are trapped is sealed from the pumps by the Fomblin liquid for the period of storage. Nevertheless insensitivity of the lifetime results to temperature and to increases in storage time suggest that residual gases are not a problem.

It is possible to choose wall systems with smaller losses so that less precision is needed to make the corrections, but the cooling needed makes the experiments are more difficult. The LNPI-Dubna collaboration has used very cold beryllium and very cold solid oxygen which reduce the losses to 7% and 2½% of the beta decay rate respectively. Their trap is in the form of a 0.75 m diameter sphere with a large hole which establishes the open top principle again. By rotating the sphere the hole can be moved to a lower position where the trap retains slower neutrons which have lower wall losses. This provides a way of making predictable changes in the wall losses. Although in the present version it seemed that larger changes were needed in the form of a second bottle.

COUNTING STATISTICS AND PHASE SPACE

The total dead time associated with the two cycles of measurement involving t_1 and t_2 is $D = 2(t_{fill} + t_{empty} + t_1)$. This is typically similar in magnitude to τ_n . Then, with only counting statistics errors, the optimum choice for t_2 is $t_2 \approx (t_1 + 1.6 t_n)$ and the error σ_t after repeating the double cycle for a period P is given by

$$\frac{\sigma_t}{t} \approx \sqrt{\left(\frac{6.3}{C_1}\right)\left(\frac{t}{P}\right)}. \quad (2)$$

For $C_1 = 1000$ or 100 000 values for σ_t of 10 s or 1 s respectively can be reached in one day.

Sources of UCN and VCN tend to produce their neutrons over a relatively uniform density in phase space. For a given source, the value of C_1 is then just proportional to the volume of phase space from which the trap can collect its neutrons. Estimates of these volumes are given in table 2. For the Bonn-ILL and the ILL experiments C_1 is 1000 and 300 000 respectively.

TABLE 2 Phase space volumes of the experiments

Group	Real space volume/litres	Velocity space volume/(m/s) ³	Phase space /litres(m/s) ³
Bonn-ILL	3 x $\frac{1}{2}$ for spin	50	75
Kurchatov-ILL	70 & 70	250	1.8×10^4
ILL	70 & 12	190	1.4×10^4
LNPI-Dubna	200 & 65	75	1.5×10^4

VACUUM PARTIAL PRESSURE LIMITS

Residual gas molecules can both scatter neutrons out of the trap and cause them to be captured by nuclei. The scattering tends to impose the more stringent limits on the pressure. In both cases the probability that the neutron is removed is independent of position in the trap (assuming the gases are uniformly distributed) and nearly independent of the neutron speed. Thus, these losses mimic beta decay rather than wall losses and it is important to be sure that the partial pressures are below the levels which would appear to change the neutron lifetime by 1 s. For N_2 , H_2O and Fomblin these pressures are estimated to be 3×10^{-5} , 2×10^{-6} and 2×10^{-7} torr respectively.

DETECTOR EFFICIENCY

While the storage methods avoid the challenging problems of needing to know absolute detector efficiencies some attention still has to be paid to efficiency. The ratio of the two counts of equation (1) can be expressed $C_1/C_2 = (\epsilon_1 N_1)/(\epsilon_2 N_2)$. The detector efficiency ϵ ($\approx 80\%$) is usually the average over a broad spectrum of neutron speeds. In the traps with material walls the faster neutrons are lost more quickly; the spectrum softens during storage and ϵ_2 may typically be less than ϵ_1 by something of the order of 1%. If this was ignored and C_1/C_2 taken to represent N_1/N_2 for equation (1) it would cause a 1% error in τ . Fortunately, traps using material walls need to use data in

equation (5) which is less sensitive. If the scaling method of the ILL group is used it can be made very insensitive. For the magnetic storage ring, the changes in neutron speed in storage are, from this point of view, negligible. When the wall losses are smaller as in the LNPI-Dubna experiments the softening of the spectrum is less and the problem is reduced. Uncorrected dead time effects in the detector counting channel act like a change in detector efficiency.

CORRECTING FOR WALL LOSSES

Very small energy transfers from macroscopic vibrations If a tea cup which is full to the brim will be subject to vibrations it is best to first remove some tea in a controlled way. In the magnetic storage ring this is done by using beam scrapers to remove neutrons from the edges of the trap just after filling. In the Kurchatov experiments a neutron absorber was placed temporarily in the top few centimetres of the trap. In the LNPI-Dubna experiments the spherical cup can be tipped part way over then brought back up a little. In the ILL experiments of Mampe et al. the scaling method employed allowed the vibration effects to be removed as part of the overall wall losses.

Thermal scattering and absorption at the walls One way of correcting for these wall losses is to measure neutron survival time in two different known trap geometries. The results may be represented by the equations:

$$\begin{array}{ll} \text{trap geometry (a)} & \text{trap geometry (b)} \\ \tau_n^{-1} + \tau_{wa}^{-1} = \frac{\ln(C_{1a}/C_{2a})}{(t_{2a} - t_{1a})}; & \tau_n^{-1} + \tau_{wb}^{-1} = \frac{\ln(C_{1b}/C_{2b})}{(t_{2b} - t_{1b})}. \end{array} \quad (3)$$

The right hand sides are given by the data. If the ratio $K = \tau_{wb}/\tau_{wa}$ can be predicted from the changes made, the equations can be solved for τ_n .

In the ILL experiments of Mampe et al., the average rate at which any neutron strikes the wall is proportional to the reciprocal of the mean free path L which is, in turn, given by the Clausius result $L = 4 \times \text{trap volume}/\text{total wall area}$. The rate of wall loss is also proportional to $1/L$ except for a small gravity correction of a few percent. To exploit these results a scaling principle was employed in which the experiment was conducted using storage times which satisfied the relation

$$\frac{t_{1a}}{t_{1b}} = \frac{t_{2a}}{t_{2b}} = \frac{(t_{2a} - t_{1a})}{(t_{2b} - t_{1b})} = \frac{L_a}{L_b}. \quad (4)$$

If the initial neutron spectra are the same in the two geometries then they will each have evolved to the same way at the corresponding later times. The required ratio K is then given by L_a/L_b . Apart from the need to exclude the slowest neutrons information about the spectrum is only needed for a 0.5% gravity correction to K . The solution of equations (4) gives

$$\tau_n = \frac{(t_{2b} - t_{1b})(L_a - L_b)/L_b}{\ln \left[\frac{\epsilon_{1a} \epsilon_{2b} N_{1a} N_{2b}}{\epsilon_{2a} \epsilon_{1b} N_{2a} N_{1b}} \right]} \quad (5)$$

Equality of the spectra at short and long times should give good cancellation of the small energy dependent detector efficiency effects through $\epsilon_{2a}/\epsilon_{2b}$ etc.

CONCLUSIONS

As far as statistics are concerned, a precision of one second in the neutron lifetime requires only a few days. This leaves scope for repetition of the measurements to search for systematic effects. With the experience gained from the last set of experiments control of systematics at the level of 1 second (about 0.1%) also seems feasible. To go much below one second begins to look much more difficult particularly as far as knowing and reproducing the the trap geometries and temperatures well enough.

REFERENCES

1. Yu.B. Zeldovich, Sov. Phys. JETP **9**, 1389 (1959).
2. K-J. Kugler, W. Paul, and U. Trinks, Phys. Lett. **B72**, 422 (1978).
3. Yu.Yu. Kosvintsev, Yu.A. Kushnir, V.I. Morosov, and G.I. Terekhov, JETP Lett. **31**, 236 (1980).
4. P. Ageron, W. Mampe, J.C. Bates, and J.M. Pendlebury, Nucl. Instr. and Meth. **A249**, 261 (1986).
5. F. Anton, W. Paul, W. Mampe, L. Paul, S. Paul, Z. Phys. **C45**, 25 (1989) and Nucl. Instr. and Meth. **A248**, 101, (1989).
6. V.I. Morozov, Nucl. Instr. and Meth. **A284**, 108 (1989).
7. V.I. Morozov, L.N. Bondarenko, Yu. Panin, A.I. Fomin and W. Mampe, private communication.
8. W. Mampe, P. Ageron, J.C. Bates, J.M. Pendlebury and A. Steyerl, Nucl. Inst. and Meth. **A284**, 111 (1989) and Phys. Rev. Letts. **63**, 593 (1989).
9. LNPI-Dubna colln., V.P. Alfimenkov et al., JETP Lett. **52**, 984 (1990).

ANGULAR CORRELATIONS
IN
FREE NEUTRON DECAY

Jürgen Last

Institut Laue-Langevin
156 X
38042 Grenoble Cédex
France



Abstract

The study of particle angular correlations in free neutron decay provides important information about β -decay coupling constants, the structure of the hadronic weak current and possible extensions to the Standard Model. New experiments are expected to substantially reduce the uncertainty in the parity violating β -asymmetry A . The value of V_{ud} , which is currently derived from $J^\pi=0^+$ β -transition life times, might soon become available directly from neutron data. An experiment which looks for time reversal violation in internal pair creation following polarized neutron capture on is briefly discussed.

NEUTRON DECAY AND FUNDAMENTAL PHYSICS

The term 'fundamental interaction' suggests that the physical system under study is elementary and prototypical for a whole class of similar processes. In this sense the weak decay of the neutron is clearly fundamental. Although the neutron possesses a complex internal structure, its quark contents is udd, it is the simplest baryonic system which undergoes semileptonic β -decay.

A neutron decays into a proton, an electron and an anti-neutrino. During this process one of the down-quarks is changed into an up-quark, emitting a W-boson which itself decays into a pair of leptons. Since free quarks have not been observed in an experiment, neutron β -decay is a very important source of information about the structure of the hadronic weak current and the weak coupling constants g_A and g_V . Their numerical values serve as input to nuclear astrophysics problems, Big Bang cosmology, neutrino reactions and many other nuclear physics processes¹.

Free neutrons are produced in large quantities at research reactors. From the reactor core they can be transported over long distances to an experimental set-up in total reflecting neutron guides. At the Institut Laue-Langevin the typical flux of thermal neutrons at the end of a guide is in the order of $10^{10} \text{ s}^{-1} \cdot \text{cm}^{-2}$. Neutrons can be polarized very efficiently to better than 98%.

OBSERVABLES IN NEUTRON β -DECAY

In the terminology of nuclear β -decay, neutron decay is a superallowed transition between two states of an isospin doublet. The Q-value is 1.293 MeV. 782 keV are available as kinetic energy. The electron energy spectrum can be derived solely from phase space considerations:

$$\frac{dW}{dE_e} = F(E_e) \propto p_e E_e (E_e - E_0)^2 \quad (1)$$

The following is a table of quantities in n-decay and their behaviour under space (P) and time (T) reversal.

Type	Quantity	P-odd ?	T-odd ?
Scalar	E_e, E_ν, E_p	NO	NO
Vector	$\mathbf{p}_e, \mathbf{p}_\nu, \mathbf{p}_p$	YES	YES
Axial vector	$\boldsymbol{\sigma}_n, \boldsymbol{\sigma}_e, \boldsymbol{\sigma}_\nu, \boldsymbol{\sigma}_p$	NO	YES

The neutrino quantities on this list are experimentally not accessible but they are regularly used in theoretical expressions for decay probabilities. If more observables are available, these

expressions become more complex. An example is the electron energy spectrum in polarized neutron decay

$$\frac{dW}{dE_e \cdot d\Omega_e} \propto p_e E_e (E_e - E_0)^2 \left(1 + A_0 \cdot \vec{\sigma}_n \cdot \frac{\vec{p}_e}{E_e} \right) \quad (2)$$

This equation contains a parity violating term which describes the angular correlation between neutron spin and electron momentum. A_0 is the well-known β -asymmetry coefficient in polarized neutron decay. Other important angular correlations are

Correlation	Coefficient	P-odd ?	T-odd ?
$\vec{\sigma}_n \cdot \frac{\vec{p}_e}{E_e}$	$A_0 = -1.144(17)$	YES	NO
$\vec{\sigma}_n \cdot \frac{\vec{p}_\nu}{E_\nu}$	$B = 0.997(28)$	YES	NO
$\vec{\sigma}_n \cdot \frac{\vec{p}_e \times \vec{p}_\nu}{E_e E_\nu}$	$D = -(0.5 \pm 1.4) \cdot 10^{-3}$	NO	YES
$\frac{\vec{p}_e \cdot \vec{p}_\nu}{E_e E_\nu}$	$a = -0.102(5)$	NO	NO
$\vec{\sigma}_e \cdot \frac{\vec{\sigma}_n \times \vec{p}_e}{E_e}$	$R = 0.07$ (theory)	YES	YES

They behave differently under P and T and are ideally suited for tests of fundamental symmetries and the structure of the weak interaction Hamiltonian.

g_A , g_V AND V_{ud}

The neutron life time and the correlation coefficients are both functions of g_A and g_V . This makes it possible to calculate these coupling constants from τ_n and, i.e., A_0 . Experimental values for the neutron life have long been in disagreement with each other. Recently new measurements have produced very consistent results which allow us to calculate an average life time of (889.1 ± 1.8) s based on all measurements published after 1970².

Also the β -asymmetry has a long history of measurements and is currently known to better than 1.7%. From the two coupling constants g_V is especially sensitive to A_0 . With $A_0 = -0.1149(19)$ from Bopp et al.³ one finds

$$g_V = 1.419(4) \cdot 10^{-62} \text{ Jm}^3, \quad g_A = -1.791(3) \cdot 10^{-62} \text{ Jm}^3.$$

In the Cabibbo-Kobayashi-Maskawa quark mixing scheme g_V should differ from the Fermi coupling constant G_F by a small factor V_{ud} . Also a small radiative correction has to be applied.

One finds $V_{ud}=0.9767\pm 0.0026$ from "pure neutron" data. The Particle Data Group lists $V_{ud}=0.9753\pm 0.0004$, a number that is derived from the ft-value of $0^+\rightarrow 0^+$ nuclear β -decay transitions⁴. It would be preferable to derive solely from neutron decay, because the calculation of $ft_{0^+\rightarrow 0^+}$ requires complicated nuclear structure corrections. This means that the precision of correlation experiments has to be 6 times higher. A first step towards this goal is the PERKEO II experiment, which is currently under construction. This collaboration between the TU Munich, the University of Heidelberg and the ILL in Grenoble is aiming for a 0.4% measurement of A_0 .

TIME REVERSAL INVARIANCE (TRI) TESTS

The correlations D and R change sign under time reversal. D is related to a phase angle of g_A relative to g_V and has been measured in two experiments^{5,6}. Progress on the limit for D is highly desirable but only possible if the experimental count rates can be substantially increased. A measurement of R has never been attempted in neutron decay and has recently been proposed by a collaboration of the ILL, LAPP Annecy and the University of Groningen. This correlation is sensitive to a imaginary scalar-axialvector interference in the weak Hamiltonian⁷. TRI violating quantities can also be constructed from a suitable set of observables in internal pair creation following polarized neutron capture on ^{62}Ni . In this case the neutron polarization is fully transferred to the excited compound nucleus with polarization σ_A . The angular correlation

$$\bar{\sigma}_A \cdot (\vec{p}_{e^-} \times \vec{p}_{e^+})$$

requires the coincident detection of the pair electrons under 90° . An experiment to measure this correlation is currently under construction at the ILL.

REFERENCES

- 1) D. Dubbers, "Particle Physics with Cold Neutrons", Prog. Part. Nucl. Phys. **26**.
- 2) J. Last, "Techniques and results of neutron life time measurements", Neutron News, Vol. 2, No. 1, 1991
- 3) P. Bopp et al., Phys. Rev. Lett. **56**, 919 (1986)² R.I. Steinberg et al., Phys. Rev. Lett. **33**, 41 (1974)
- 4) Review of Particle Properties, Phys. Lett. **B239**, 1(1990)
- 5) B.G. Erozolimskij et al., Sov. J. Nucl. Phys. **28**, 48 (1978)
- 6) R.I. Steinberg et al. Phys. Rev. Lett. **33**,41 (1974)
- 7) K. Schreckenbach, Proceedings of the XXVth Rencontre de Moriond on "New and Exotic Phenomena '90", O. Fackler and J. Tran Thanh Van, Ed., 1990

SEARCH FOR NEUTRON-ANTINEUTRON OSCILLATIONS AT ILL

D. Dubbers

Fakultät für Physik E21, Technische Universität München
D-8046 Garching(for the Heidelberg - ILL - Padova - Pavia Collaboration^{*})

A review is given on experimental searches for neutron-anti-neutron oscillations. In particular, an experiment is described which is running at the Institute Laue Langevin in Grenoble and which will increase the limit on the free neutron oscillation time by two orders of magnitude.

In recent years cold and ultracold neutrons have been used in a large number of experiments to study the physics of particles and of their fundamental interactions. Some of these experiments search for manifestations of "new physics", for a review see¹⁾. One of these experiments is the neutron-antineutron oscillation experiment done at ILL during the past two years.

We speak of neutron oscillations when neutrons change spontaneously into antineutrons, and vice versa, with an oscillation time τ_{nn} , analogous to the well known kaon oscillations. Kaon oscillations are strangeness oscillations, while neutron oscillations essentially are baryon number oscillations, with the baryon number changing by two units from $B = +1$ to $B = -1$. Strangeness is not conserved under the weak interaction and kaon oscillations therefore are allowed. Baryon number non-conservation so far has not been observed; however, there is no symmetry principle nor any associated gauge principle known that would require the conservation of baryon number.

The phenomenology of neutron-antineutron oscillations is the same as for any other two state system in quantum mechanics. State mixing by some interaction between the neutron state and the antineutron state inevitably leads to neutron-antineutron oscillations. The probability for a neutron to change into an antineutron in the course of time then is

$$P_{nn}(t) = \sin^2 \frac{t}{\tau_{nn}} \approx \left(\frac{t}{\tau_{nn}} \right)^2. \quad (1)$$

The last approximation holds because the neutron oscillation time in any case is much longer than the free neutron lifetime.

Neutron oscillations were first invoked by Kuzmin²⁾ and were discussed in the context of grand unification by Mohapatra and Marshak³⁾. A recent review of the theory of neutron oscillations was given by Mohapatra⁴⁾. In the simplest grand unified theory SU(5) left-handed quarks and right-handed antiquarks are well distinct and neutron oscillations cannot occur. Indeed, the only exotic process predicted by SU(5) is proton decay. As proton decay does not occur as frequently as required by SU(5), and as also the Weinberg angle is not found as predicted, SU(5) probably is not the right unified theory.

Neutron oscillations can, however, occur in the left-right symmetric theories. These models are attractive for esthetical reasons because they do not have parity violation built in right from the beginning. Left-right asymmetries come in only at a later stage by spontaneous symmetry breaking. Above this scale both left-handed and right-handed quarks (and anti-quarks) exist, and quark-antiquark mixing (and with it neutron-antineutron mixing) is no longer forbidden by angular momentum conservation.

The simplest left-right symmetric model is

$$G_{224} = SU(2)_L \times SU(2)_R \times SU(4)_C \quad (2),$$

which contains the standard electroweak model as a subgroup. When the intermediate energy scales of this model are all in the 10^5 GeV range, and when the mass of the electron-neutrino is of order 1 eV, then one finds neutron oscillation periods of order $10^8 s^4$).

When G_{224} is embedded in the left-right symmetric grand unified $SO(10)$ model, then neutron oscillations occur at an observable rate only when the spontaneous parity breaking takes place above the G_{224} scale. In this case, in order to reproduce the experimental values of the Weinberg angle, the proton lifetime limit, and the strong coupling constant, the intermediate energy scales necessarily must be in the 10^5 GeV range and the neutron oscillation period must be 10^8 to 10^9 seconds, as discussed in detail by Chang et al.⁵⁾ On the other hand, when $SO(10)$ itself is embedded in E_6 then neutron oscillations are ruled out⁶⁾.

Of course, these theoretical predictions are still rather imprecise. After the fall $SU(5)$, however, this is true for any new physics prediction, including proton decay.

How can the free neutron oscillation period possibly be so much shorter than the proton lifetime? The reason is that neutron oscillations are caused by an interference process which is linear in the pertinent transition matrix element and not quadratic as for the proton lifetime. Further, the size of this matrix element is determined by a mass scale which is much lower than the unification scale of 10^{14} GeV relevant for the proton lifetime.

The principle of a free neutron-antineutron oscillation experiment is rather simple. Take a strong beam of cold neutrons and let it fly freely over a long distance, and scan the beam at the end for possible antineutrons. This scan is best done with a thin target foil of carbon: neutrons are very little attenuated by this foil, but practically all antineutrons will annihilate into an average of five pions, which must be detected in a particle track detector. In spite of its conceptual simplicity, a neutron-antineutron oscillation search requires a major experimental effort, including a large size detector for the annihilation products, and a sophisticated neutron beam and magnetic shielding system. In the present experiment at Grenoble the neutron free flight length is about 75 meters. It is limited by the fact that the cold neutrons fall down in the earth gravitational field and, by hitting the beam tube from the inside, may create undesirable background. The diameter of the beam on the 0.1 mm carbon target is about 1 meter. For other experimental parameters of this and earlier nn searches see table 1.

Table 1. Technical specifications and experimental results of neutron oscillation searches.

Place Collaboration	Grenoble (F) CERN-ILL - Padova-Rutherford- Sussex	Pavia (I) Pavia-Rome	Grenoble (F) Heidelberg-ILL- Pavia-Padova
Reactor power	62 MW	0.25 MW	62 MW
Neutron intensity	$1.5 \cdot 10^9 \text{ s}^{-1}$	$3 \cdot 10^{10} \text{ s}^{-1}$	$1.3 \cdot 10^{11} \text{ s}^{-1}$
Neutron spectrum	very cold ($\sim 2\text{K}$)	thermal (300 K)	cold (40 K)
Free flight length L	2.7 m	17 m	68 m
RMS time of flight t	26 ms	8 ms	105 ms
Target diameter	0.25 m	1.1 m	1.1 m
Detector efficiency	30%	12 %	59%
Field suppression factor	500	100	10 000
Average residual field	100 nT	800 nT	4 nT
Quasifree propagation efficiency η	98%	50%	99.5%
Limit on $\tau_{n\bar{n}}$ (90% c.l.)	$1.3 \cdot 10^6 \text{ s}$	$0.5 \cdot 10^6 \text{ s}$	$9 \cdot 10^7 \text{ s}$ (aim: 10^8 s)
Status	finished	finished	running
Reference	Fidecaro <i>et al.</i> , (1985) /7/	Bressi <i>et al.</i> , (1989) /8/	Baldo-Ceolin <i>et al.</i> , (1990) /9/

There were a number of serious experimental problems to be solved. The first problem is neutron beam tailoring. Almost all neutrons should hit the distant target. However, the divergence of a cold neutron beam, which essentially is a beam of an ideal gas, is much too large for this. The problem was solved by having the neutron beam pass a slightly divergent neutron guide of 3 mrad opening angle and of 33 m length. Seen in the frame moving with a neutron along the beam axis, the walls of this neutron guide are slowly receding. This leads to an adiabatic cooling of the neutron's transverse velocity component, and strongly diminishes the divergence of the neutron beam.

The next problem is magnetic field suppression along the neutron beam. Neutron and antineutron have magnetic moments of opposite sign. In a magnetic field, therefore, the energy of a neutron is different from the energy of an antineutron, and neutrons and antineutrons therefore can no longer oscillate into each other. To avoid this difficulty, the earth magnetic field has to be suppressed by about 4 orders of magnitude. The main problem was that axial magnetic shielding of a long cylindrical mumetal tube is practically nonexistent. The problem was solved by using a passive mumetal shield in combination with an active feedback field compensation system, plus an elaborate magnetic idealisation procedure. This setup is the largest high quality magnetic shield ever built.

A main problem of the experiment is cosmic ray rejection. For the reconstruction of an antineutron annihilation event a detector of about 100 m³ volume is needed. The Grenoble antineutron annihilation detector consists of a pion track detector and a total energy calorimeter, as well as cosmic ray veto detector. The track detector is sandwiched between two layers of fast scintillators which trigger the apparatus in case of an event. The time sequence of this trigger indicates whether the particles are flying away from the target as in the case of an antineutron annihilation event, or towards the target as in the case of a cosmic ray event coming from the outside.

The status of the experiment is that we have now reached a limit on the neutron oscillation time of

$$\tau_{nn} > 8 \cdot 10^7 \text{ s (90\% c.l.)} \quad (3),$$

and that by fall 1991 we should have reached the limit of 10^8 s. Antineutron events so far have not been seen.

Some indications on the possible size of the neutron oscillation period are derived as a by-product from the proton decay experiments, which are sensitive to neutron oscillations events inside the nuclei of the detector material. However, within nuclei neutron oscillations are suppressed by a factor of about 10^{31} , because neutrons and antineutrons see strongly different nuclear potentials and hence are no longer equivalent energetically. From the experimental limit

$$T_{nn}^{\text{nucl}} > 6.5 \cdot 10^{31} \text{a} \quad (90\% \text{ c.l.}) \quad (4)$$

found in proton decay detectors one therefore arrives at a free neutron oscillation limit of $\tau_{nn} > \text{several years}^{10)}$, which is of the same order as (3).

To summarize, the lower limit on the free neutron oscillation time has been increased by our experiment running presently at Grenoble by two orders of magnitude, but no signs of such event have been found yet.

This work has been funded by the German Minister for Research and Technology (BMFT) under contact number 06HD483I.

References

*M. Baldo-Ceolin, P. Benetti, T. Bitter, F. Bobisut, E. Calligaris, R. Dolfini, D. Dubbers, F. Eisert, P. El-Muzeini, M. Genoni, D. Gibin, A. Gigli Berzolari, K. Gobrecht, A. Guglielmi, M. Kessler, U. Kinkel, E. Klemt, M. Laveder, W. Lippert, F. Mattioli, F. Mauri, M. Mezzetto, A. Piazzoli, G. Puglierin, A. Rappoldi, G.L. Raselli, D. Scannicchio, A. Sconza, M. Vascon, L. Visentin and R. Werner

- /1/ D. Dubbers, Progr. in Part. and Nucl. Phys. 26, 173 (1991)
- /2/ V.A. Kuzmin ZhETF Pis. Red. 12, No. 6, 335 (1970) [JETP Lett. 12, 228 (1970)]
- /3/ R.N. Mohapatra and R.E. Marshak, Phys. Rev. Lett. 44, 1316 (1980)
- /4/ R.N. Mohapatra, Nucl. Instr. A284, 1 (1989)
- /5/ D. Chang et al., Phys. Rev. D31, 1718 (1985)
- /6/ P.K. Mohapatra, R.N. Mohapatra and P.B. Pal, Phys. Rev. D33, 2010 (1986)
- /7/ G. Fidecaro et al., Phys. Lett. 156B, 122 (1985)
- /8/ G. Bressi et al., Z. Phys. C43, 175 (1989)
- /9/ M. Baldo-Ceolin et al., Phys. Lett. B236, 95 (1990)
- /10/ C.H. Berger et al., Phys. Lett. B240, 237 (1990)

**The Search for the Neutron Electric Dipole Moment:
Past, Present, and Future**

Steve K. Lamoreaux
University of Washington
Seattle, Washington 98195 USA

and

Robert Golub
Hahn Meitner Institut
D-1000 Berlin 39, FRG

Abstract

The history of the experimental search for the electric dipole moment of the neutron is reviewed with emphasis on those experiments using stored ultracold neutrons. A new experimental apparatus which is presently being assembled at the Institut Laue-Langevin is described. This apparatus includes a spin-polarized ^{199}Hg atomic magnetometer within the neutron storage volume. Also described is a proposed new technique which uses “dressed” ultracold neutrons and ^3He stored together in a superfluid ^4He bath. Polarization of the ^3He by use of a hexapole focussing magnet on a cold ($T < 1\text{K}$) ^3He atomic beam is suggested. Applications of the “dressed” spin system to other (atomic) electric dipole moment searches is discussed.

1. Introduction and History

Purcell and Ramsey¹⁾ suggested that nuclear forces need not conserve parity with consequence that there could be an electric dipole moment (EDM), in addition to the usual magnetic dipole moment, of the neutron or other elementary particle. The first experiment to search for a neutron EDM was set on a neutron beam at Oak Ridge and produced the result (in 1951) $d_n = -(0.1 \pm 2.4) \times 10^{-20}$ e cm which was eventually reported.²⁾

Lee and Yang³⁾ determined that parity nonconservation could explain the $\tau-\theta$ puzzle; the most sensitive experimental evidence supporting parity conservation was the neutron EDM. They proposed experiments to test for parity violation, most notably the measurement of the angular distribution of β rays from a polarized nucleus. If parity were not conserved, there could be an angular dependence of the electron emission of the form $A = \vec{I} \cdot \vec{p}_e$, where \vec{I} is the nuclear spin and \vec{p}_e is the electron momentum. Landau suggested that it would be more satisfactory if the combined operations of charge conjugation and parity inversion, that is CP , were conserved, otherwise empty space would contain information.⁴⁾ He also pointed out that an EDM requires time reversal T violation in addition to P violation. Wu *et al.* demonstrated parity violation in the β -decay of ^{60}Co ; subsequent experiments showed that the symmetry conserved was indeed CP .⁵⁾

It had already been recognized that if a local Lagrangian theory is invariant under the proper Lorentz transformation, then CPT (and its permutations) must be a symmetry of the theory (see, for example, Ref. 6). Ramsey argued that time reversal symmetry was an open question which could only be answered experimentally and that it was still important to search for the neutron EDM.⁷⁾

In 1964 Christenson *et al.*⁸⁾ reported the observation that CP was violated in the decay of the K_0 meson, which implies a T violation as well. It has been argued that the K_0 experiments show T violation directly.⁹⁾ This observation of CP violation is the main motivation behind the on going search for the neutron EDM, and searches for EDMs in other systems, such as atoms.¹⁰⁾

The origin of the CP violation, discovered in the K_0 system now 26 years ago, remains unexplained.¹¹⁾ Historically, experimental limits on the neutron EDM (and more recently atomic EDMs) have placed strong constraints on theoretical models that are used to explain CP violation (see Refs. 11 and 12 for reviews of the theory). Figure 1 shows the historical progression of the experimental limits to the neutron EDM, along with some theoretical predictions. The most recent experimental values for the neutron EDM are those of Altarev *et al.*¹³⁾ $d_n = (-14 \pm 6) \times 10^{-26}$ e·cm, which they interpret as an upper limit of $|d_n| < 26 \times 10^{-26}$ e·cm and Smith *et al.*¹⁴⁾ $d_n = -(3 \pm 5) \times 10^{-26}$ e cm, which implies $|d_n| < 12 \times 10^{-26}$ e cm. Both of these experiments made use of bottled ultracold neutrons.

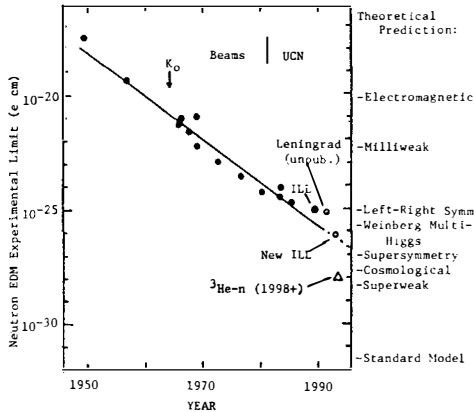


Figure 1. Historical limits of the neutron EDM compared with theoretical predictions.

The neutron ground state, having spin $I = 1/2$, is completely specified by the spin projection quantum number $m_I = \pm 1/2$. In external electric and magnetic fields \vec{E} and \vec{B} the Hamiltonian is

$$H = -(d_n \vec{I} \cdot \vec{E} + \mu_n \vec{I} \cdot \vec{B})/I, \tag{1}$$

where d_n and μ_n are the electric and magnetic dipole moments of the neutron.¹⁵⁾ The electric dipole moment must lie along \vec{I} otherwise additional quantum numbers would be necessary to describe the neutron ground

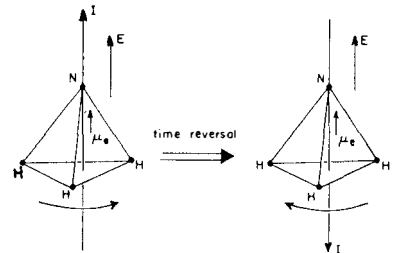


Figure 2. The normal and time reversed states of an ammonia molecule.

state; in addition, any component perpendicular to \vec{l} would be unobservable. This Hamiltonian manifests P and T violation; under P , $E \rightarrow -E$ and B is unchanged; under T , $B \rightarrow -B$ and E is unchanged; however, CPT is conserved.

One can then ask the question: Why is it that molecules which have permanent electric dipole moments are not evidence of time-reversal violation? Figures 2a and 2b show the normal and time reversed states of an ammonia molecule. These two states are degenerate and it is this degeneracy which allows the ammonia molecule to have an electric dipole moment without violating time reversal symmetry. However, we assumed that the neutron ground state was completely described by the spin projection quantum number m_I and the spin states are non-degenerate. That the ground state is non-degenerate is also supported by the observed fact that neutrons obey the Pauli principle.

According to Kramer's theorem¹⁶⁾ (which is a statement of time reversal symmetry), the shift in energy levels with the application of a static electric field must be proportional to $|m_I|$. The quadratic Stark effect where $E \propto m_I^2$ is of this form. There is no shift in the splitting between the $\pm 1/2$ states of a spin $1/2$ system with application of a static electric field.

The neutron EDM is measured by comparing the neutron Larmor frequency (measured, for example, by use of Ramsey's method of separated oscillatory fields¹⁷⁾) for parallel and for antiparallel magnetic and electric fields. It follows from Eq. 1 that the shift in Larmor frequency between the two field configurations is $\delta\omega_0 = -4d_n E/\hbar$; the minus sign is necessary because $\mu_n < 0$.

1.1 Ultracold Neutrons

To describe the interaction of slow neutrons with bulk material, Fermi developed the concepts of the "pseudo-potential" and the neutron index of refraction. His idea is as follows. Although the range of nuclear forces is small, they are quite strong within that range so one cannot in general apply perturbation theory to a collision between a neutron and a nucleus. However, the amplitude for scattering of neutron of wavelength large compared to the nucleus is a constant independent of the velocity. The constant amplitude can be obtained if we describe the interaction of the neutron with the nucleus by the point interaction

$$U(\vec{r}) = -\frac{2\pi\hbar^2}{M} f\delta(\vec{r}) \quad (2)$$

where M is the reduced mass and f is the scattering amplitude. When this potential is substituted into the Born approximation,

$$f = -\frac{M}{2\pi\hbar^2} \int U(\vec{r}) e^{-i\vec{q}\cdot\vec{r}} dV \quad (3)$$

the delta function makes the integral independent of the momentum transfer \vec{q} . Now consider many scatterers bound in a piece of bulk matter such that the distance between the scatters is much less than the neutron wavelength. As a slow neutron approaches the boundary, it will see an average potential

$$U_F = \frac{2\pi\hbar^2}{M} b_c \rho \quad (4)$$

where $b_c = -f$ is the coherent scattering length and ρ is the density of scattering points. This potential appears as a step as the neutron enters the bulk material. Thus, for nuclei with $b_c > 0$, the neutron loses kinetic energy and the wavelength increases on entering the bulk material; the index of refraction is less than 1.

Zeldovich suggested the possibility of storing neutrons with kinetic energy $E < U_F$ in material bottles.¹⁸⁾ The reflection from the material surface is analogous to the total internal reflection of light. Neutrons with such low velocities ($v < 5\text{m/s}$ for most materials corresponding to U_F of order 100's of nano electron volts) are called Ultracold Neutrons or UCN. UCN production and storage are now well-developed technologies after some intense and difficult research over a 20 year period starting in the 1960s.¹⁹⁾

UCN can be transported as a gas through pipes of high Fermi potential materials (stainless steel, for example). In addition, UCN can be polarized by transmission through a thin magnetically saturated foil; the foil material, typically a Fe-Co alloy, is chosen so that the saturation flux Zeeman shift just cancels the Fermi potential for one spin state; that spin state passes easily through the foil while the other is reflected.

1.2 Neutron EDM Measurements with Bottled Neutrons

Shapiro and Lushchikov *et al.* suggested that UCN could be used to search for a neutron EDM.²⁰⁾ It was immediately recognized that a storage experiment could give orders of magnitude higher sensitivity due to

a longer interaction time, 10^2 s as opposed to 10^{-2} s, and that systematic effects due to non-parallel E and B fields would be greatly suppressed.²¹⁾ Golub and Pendlebury¹⁵⁾ discuss fundamental limits to sensitivity for a variety of neutron EDM experiments; use of bottled UCN is the clear winner: Their statement that "if no effort were spared a limit for the dipole length of $5 \times 10^{-27}e$ cm might ultimately be reached" could prove correct in the next set of measurements. An entirely new technique to be described here might reach the $5 \times 10^{-29}e$ cm limit.

An important advantage to the use of bottled UCN over beam experiments is the elimination of the systematic effect due to the magnetic field generated by $\vec{v} \times \vec{E}$; if \vec{E} and \vec{B} are not exactly parallel,

$$\delta B = \frac{v}{c} E \sin \theta_{EB} + \sqrt{B^2 + \left(\frac{v}{c} E\right)^2} \quad (5)$$

where it is assumed that the velocity, \vec{v} , is approximately perpendicular to \vec{E} . \vec{E} and \vec{B} are roughly parallel and $\theta_{EB} \approx 0$ is the angle between the magnetic and electric fields. In the case $\theta_{EB} \neq 0$, there is a change in magnetic field associated with the application of the electric field which generates a shift in Larmor frequency indistinguishable from an EDM shift. In addition, even if the fields are parallel, there is a shift in magnitude proportional to E^2 ; thus it is required that the magnitude of the electric field be reversed exactly in any case, something which can be difficult in the presence of dielectrics. Since UCN stored in a bottle have an average velocity approximately zero, $\vec{v} \times \vec{E}$ effects are substantially reduced.

As was already mentioned, use of Ramsey's method of separated oscillatory fields is a convenient way to measure the magnetic resonance frequency.¹⁷⁾ In beam experiments, the temporal separation of the oscillatory field pulses results from having two coils separated along the beam axis. For bottled UCN, the two time-separated oscillatory field pulses are generated from the same coil; the coherence between the pulses is maintained by having the oscillator running continuously and by simply switching on or off the RF current to the coil at the appropriate times. An important advantage of the time separated pulses as applied to bottled UCN over the spatial separated pulses as used in beam experiments is that the timing conditions are the same for all of the UCN in the bottle. In a beam, the pulse length is determined by the size of the RF coil, hence the $\pi/2$ condition can be met for only one velocity. However, in the neutron bottle, if the RF field is sufficiently homogeneous and if pulse length is longer than the mean wall collision time so that the RF field is sufficiently averaged, all the neutrons see the same pulse length. Furthermore, in beam experiments, the Ramsey fringes get "washed-out" as the accumulated phase depends on the time between RF pulses. In the case of bottled UCN, the time between pulses T , is the same for all neutrons, all the neutrons have $\cos \phi = 0$ at the same frequency and all the maxima in Fig. 3 are the same height (transition probability = 0).

When separated oscillatory fields are used, the determination of the effective linewidth is not so obvious. If we use Eqn V.37 given in Ref. 17 in the limit $b \gg \Delta\omega$ where $\Delta\omega = \omega_0 - \omega_{RF}$ and b is the RF field strength, and if $\pi/2$ pulses are used (that is, the pulse length τ' and the RF field strength satisfy the condition $\tau'\gamma b/2 = \pi/4$), the probability to flip the neutron spin is

$$P \approx \cos \Delta\omega T \quad (6)$$

where $T \gg \tau'$ is the time between pulses. If the same polarizer is used for both initial polarization and for analysis after the two pulses, and take into account the polarizer inefficiency, the number of neutrons which get through the polarizer is

$$N(\Delta\omega) = N_0[1 - \alpha \cos \Delta\omega T]/2 \quad (7)$$

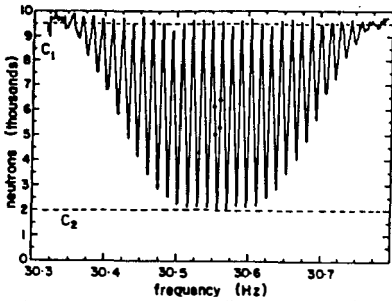


Figure 3. Separated oscillatory field fringes produced by the ILL neutron EDM apparatus. The four dots represent the usual operating points.

where the visibility $\alpha = (C_1 - C_2)/(C_1 + C_2)$, $C_1 = N_0$, as in Fig. 3.

A neutron EDM is manifest by a change in neutron counts with application of an electric field. The experimental sensitivity is highest where the slope in the number of counts vs. $\Delta\omega$ is highest:

$$\frac{\partial N(\Delta\omega)}{\partial \Delta\omega} = N_0 \frac{\alpha}{2} T \sin \Delta\omega T \quad (8)$$

and the frequency is set so that $\sin \Delta\omega T \approx 1$. In the ILL experiment, for example, the applied frequency is alternated among the four points shown in Fig. 3. The four points provide a continuous calibration. It is straightforward to show that for many measurements, the final uncertainty in the neutron EDM d_n is (since a frequency uncertainty is related to the EDM by $\delta\omega = -2d_n E/\hbar$)

$$\sigma(d_n) = \frac{\hbar}{\alpha E T \sqrt{N_{TOT}}}; \quad (9)$$

where N_{TOT} is the total number of neutrons counted.

1.3 Bottled UCN EDM Experiment at the Institut Laue-Langevin

Figure 4 is a schematic of the experimental apparatus which is described more fully elsewhere.^{14,19,22,23} The apparatus was initially installed on the ILL PN5 UCN source and in 1984 produced the result $0.3 \pm 4.8 \times 10^{-25}$ e cm. In 1986, the experiment was moved to the ILL neutron turbine where the UCN flux is two orders of magnitude higher; the UCN density at the turbine output is 90 cm^{-3} . The new result of this experiment is $-(3 \pm 5) \times 10^{-26}$ e cm.

UCN are transported from the turbine to the experiment through a stainless steel guide. At the apparatus, the UCN are polarized by transmission through a magnetically saturated $1 \mu\text{m}$ thick iron-cobalt foil. The neutron bottle, consisting of two beryllium electrodes 0.25 m in diameter separated by a 0.1 m long cylindrical beryllium oxide tube (0.01 m thick wall) which serves as an insulator, has a net critical velocity 6.9 m/s . The BeO tube rests in grooves, about twice the tube thickness deep, in the Be plates. This arrangement gives better high voltage stability. Neutrons enter the bottle through a hole, which can be sealed with a beryllium door, in the grounded electrode.

The bottle is inside a 5-layer Permalloy shield (shielding factor of 10^5) with the bottle axis perpendicular to the cylinder axis of the shield, the orientation such that the magnetic shielding is maximum.²⁴ A 10 mG (30 Hz Larmor frequency) magnetic field \vec{B} , parallel to the axis of the bottle, is produced by a cylindrical coil with a constant number of turns per unit distance perpendicular to the axis of the shield (cosine distribution), to produce a uniform field inside the magnetic shield.

The magnetic field between the polarizer and the storage bottle was carefully tailored so that the adiabatic condition, $\omega_L = \gamma B \gg |d\vec{B}/dt|/B$, where γ is the gyromagnetic ratio, and so that $\vec{B} \neq 0$ anywhere; thus there is a gradual change from the approximately one kilogauss polarizer field to shield, and through the shield to the bottle field of 10 mG ; thus no loss of polarization occurs.

The experiment is operated as follows. The 5 liter storage volume is filled for 10 s (three filling time constants), after which the door is closed. Immediately after filling, the density of polarized UCN is about

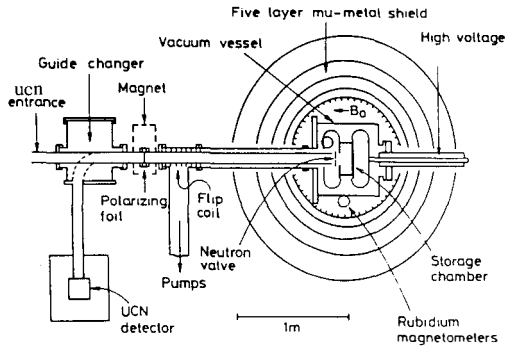


Figure 4. The ILL neutron EDM measurement apparatus.

10 cm^{-3} . After waiting 6 s to allow the neutron velocities to become isotropic within the bottle, the first separated oscillatory field pulse is applied for 4 s. This turns the neutron spins perpendicular to the magnetic field. The neutrons are allowed to precess for 70 s (the neutron storage lifetime) after which a second 4 s pulse is applied. The neutron valve is opened and those neutrons in the appropriate spin state pass through the polarizing foil which now serves as an analyzer, are diverted to a detector, and are counted for 10 s. The spin flip coil, which consists of about 5 turns/cm wound on a NiCo coated glass guide (so that the 3 kHz RF field can penetrate) 20 cm long, is then turned on and adiabatically reverses the spin, thereby permitting the remaining neutrons to pass through the polarizing foil and be counted, also for 10 s. The two counting periods give approximately 12,000 and 8000 neutrons. Including filling and emptying, each measurement cycle takes 124 s.

An electric field of maximum magnitude 16kV/cm is periodically reversed. The leakage currents were usually $< 10 \text{ nA}$. To monitor the magnetic field, there are three rubidium magnetometers within the magnetic shield located as close as possible to the neutron storage volume ($< 20 \text{ cm}$) and a fluxgate magnetometer probe just within the outer layer of shielding at the high voltage feedthrough.

The data analysis simply involves determination of a shift in the neutron resonance frequency with application of the electric field. The magnetometers and fluxgate readings are analyzed along with the neutrons to provide a check for spurious magnetic fields generated by leakage currents, displacement currents, sparks, etc. All of the data were contaminated with systematics at some level; after some complicated cross correlation analysis, all of the data were consistent over the 3 year running period. The final result is

$$d_n = (-3.3 \pm 4.3) \times 10^{-26} \text{ e} \cdot \text{cm}$$

$$|d_n| < 12 \times 10^{-26} \text{ e} \cdot \text{cm} \quad 90\% \text{ C.L.}$$

The contribution to the above error from neutron counting statistics, using Eq. 9, is $1.9 \times 10^{-26} \text{ e} \cdot \text{cm}$.

The present experiment is limited by how well the magnetic field within the neutron bottle is monitored by the spatially separated rubidium magnetometers. In Secs. 2 and 3 we will describe some new experiments which will incorporate comagnetometers (a polarized atomic species within the neutron storage volume) and should eliminate these systematic problems.

1.4 Bottled UCN EDM Experiment at the VVR-M Reactor, Leningrad

Altarev *et al.* have reported the result $d_n = -(1.4 \pm 0.6) \times 10^{-25} \text{ e cm}$ which they interpret as an upper limit of $d_n < 2.6 \times 10^{-25} \text{ e cm}$.¹³⁾ This should be compared with their earlier result $d_n < 1.6 \times 10^{-24} \text{ e cm}$.²⁵⁾ Additional data has been taken with this apparatus and they expect a final total accuracy (statistical and systematic) of order $4 \times 10^{-26} \text{ e cm}$ which is essentially the same as the ILL result.²⁶⁾ The major improvements for this experiment were the in UCN source and an increased neutron storage time.

In many ways the apparatus is similar to that of the ILL experiment, however, there are important differences. For example, there are two neutron storage chambers with oppositely directed electric fields (relative to the magnetic field) in each chamber. The high voltage is applied to the plate separating the two chambers while the outer plates are held at ground potential. They typically run at 15kV/cm, somewhat higher than the average of the ILL experiment. Using two bottles with oppositely directed electric fields essentially doubles the sensitivity to a neutron EDM while reducing background magnetic field noise; an EDM generated shift will be of opposite sign for the two chambers. In addition, since the two chambers are located quite close spatially, one would expect high discrimination from background magnetic field changes since the EDM shift is given by the difference in the resonance frequency between the chambers as a function of electric field direction; this difference is sensitive only to changes in spatial gradients of the magnetic field. Such gradients could be due to locally generated fields such as leakage currents within the bottle.

The position of the resonance is stabilized by synthesizing the radiofrequency pulses for the neutrons from the output of two cesium magnetic Zeeman atomic oscillators (located near the storage chambers). (The ratio of neutron resonance frequency to cesium is about 120.) This was necessary in part because the three-layer Permalloy shield did not provide adequate stability and shielding. The stabilization improved the effective shielding by a factor of about 15.

The earlier nearly non-zero result of $-1.4 \pm 0.6 \times 10^{-25} \text{ e cm}$ has been supplemented by additional data; the present result is consistent with zero with an uncertainty of about $4 \times 10^{-26} \text{ e cm}$.²⁶⁾

2. Present: UCN EDM Experiment with a ^{199}Hg Comagnetometer

Since the ILL experiment described in Sec. 1.3 was no longer limited by counting statistics but by systematics, it was decided to rebuild the apparatus and include a comagnetometer, that is, a polarized

atomic species within the same storage volume as the neutrons and thus provide a nearly exact spatial and temporal average of the magnetic field as seen by the neutrons over the storage period. The use of polarized ^3He had already been considered,²⁷⁾ but the extreme difficulty in the detection of the ^3He polarization makes its use impractical.

Lamoreaux suggested the use of ^{199}Hg and devised an apparatus similar to that shown in Fig. 5.²⁸⁾ The advantage of ^{199}Hg is that it can be readily directly optically pumped and its polarization optically detected with 254nm resonance radiation. In addition, the room temperature vapor pressure of Hg is more than adequate to provide the necessary density.

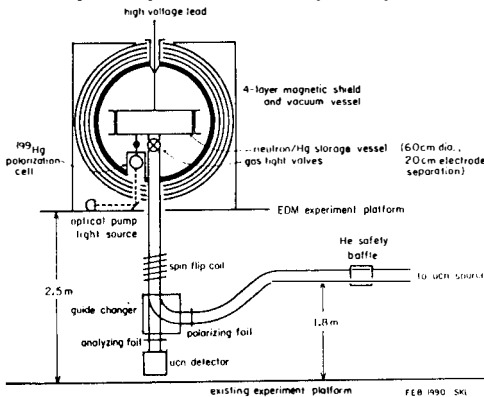


Figure 5. The new ILL neutron EDM apparatus which incorporates a ^{199}Hg comagnetometer.

Since ^{199}Hg is a 1S_0 atom, its ground state polarization is specified by the nuclear angular momentum, which is $1/2$ for ^{199}Hg . An already described, an important feature of a spin- $1/2$ system is that its Larmor frequency cannot be affected by electric fields other than through an EDM. Furthermore, it is necessary that the atomic species does not have an EDM of its own which could possibly mask a neutron EDM; in the case of ^{199}Hg , experimental limits have already been set at the level of sensitivity needed.¹⁰⁾ In these experiments, ground state spin-polarization lifetimes in excess of 100 s. were routinely achieved in cells of about 5cc volume, even in the presence of electric fields up to 15kV/cm. However, these cells included 250torr of nitrogen to improve the high voltage stability.

An unfortunate disadvantage of ^{199}Hg is that the walls of the container must be specially prepared to have long spin relaxation times. In all previous experiments, hydrocarbon waxes were used; these of course would be unusable with UCN. In addition, the wall coating has to be stable under the application of high voltage in vacuum since a high-pressure background gas cannot be used with the UCN.

A possible wall coating material, deuterated polystyrene (DPS), has been developed.²⁸⁾ Although the Hg spin polarization characteristics are not as good as the hydrocarbon waxes, (10 s/cm mean free path vs. 100 s/cm mean free path), it should give a lifetime of about 100 s in the much larger neutron bottle. In addition, thin films of DPS seem to be stable under application of high voltage in vacuum. DPS is found to have excellent UCN storage properties. Another possible wall coating is Teflon. Although its Fermi potential is lower than DPS, its Hg storage characteristics are better and more easily reproducible. Perhaps the final apparatus will use some combination of the two materials (Teflon in the polarization/transport of the Hg; DPS in the neutron storage volume).

A rough schematic of the proposed experimental apparatus is shown in Fig. 5. To increase the sensitivity through storage time and neutron counts, and to account for the loss of neutrons due to the lower Fermi potential of DPS over Be-BeO, a larger (about 10 times) volume storage bottle is being considered. Since there is a considerable shift in the center of mass between the UCN gas and atomic gas in the gravitational field (due to the difference in effective temperature²⁷⁾), the experiment is designed so that the shorter axis of the bottle is vertical, thus minimizing the displacement. In addition, there is a safety consideration to the use of Hg, although the minuscule quantities of Hg to be used should present no problem. However, it is necessary to have a gas tight window which can withstand atmospheric pressure. It has been decided that this will be the polarizer; the design for the polarizer is to evaporate iron onto aluminum. To account for

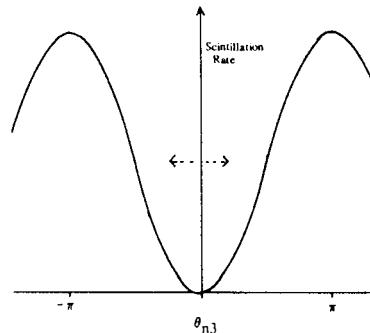


Figure 6. The scintillation rate as a function of spin vector angular separation. The double arrow shows the proposed modulation.

the fairly high Fermi potential of the aluminum, after passing through the foil the UCN will rise about one meter. Tests to determine the optimum combination of heights to maximize the number of UCN left in a test bottle after a 100 s. storage period have recently been completed.

The neutron storage bottle will be an aluminum oxide cylindrical spacer about 60 cm diameter and 20 cm high separating aluminum plates. The entire inner surface will be coated with DPS. The neutron valve will be gas-tight to minimize the loss of the polarized atomic vapor.

Provisions will be included for polarizing the atomic vapor. There is an optical pumping cell connected to an isotopically enriched Hg reservoir. The Hg will be optically pumped to the appropriate spin state, parallel to the static field, with circularly polarized light from an Hg discharge lamp. After the Hg is polarized, and after the neutron bottle is filled with polarized neutrons and the neutron valve closed, the polarized Hg is admitted to the neutron bottle. $\pi/2$ pulses are applied for both the neutrons and Hg (the ^{199}Hg magnetic moment is about one third of the neutron magnetic moment). The free precession of the Hg spin is observed with a beam of circularly polarized resonance light which propagates across the bottle diameter, through quartz windows in the insulating cylinder. The magnetic field over the storage time can be determined from the free precession signal.

At the end of the storage period, the second neutron pulse is applied, the bottle door opened, and the neutrons are counted as usual. The Hg is pumped away. While the storage was in progress, more Hg had been admitted to the optical pumping cell and polarized; the process is thus ready to be repeated.

An EDM will be evident from a change in the ratio of the magnetic moments between reversals of the electric field. Although the sensitivity of the Hg to the magnetic field is only 1/3 that of the neutron, the high signal to noise inherent in the free precession signal is a compensating factor, and in fact preliminary estimates show that determination of the average field should be a factor of 10 higher in sensitivity than the neutron signal and hence contribute very little noise. The final uncertainty for this experiment, based on the shot-noise estimate given by Eq. 9 is about 7×10^{-27} e cm, or nearly a factor of ten over the current limits.

3. Future: Superfluid He Neutron EDM with ^3He Comagnetometer

3.1 Production of UCN in Superfluid ^4He

The production of UCN by the downscattering of 10\AA neutrons in superfluid He is now fairly well studied.²⁹⁾ The basic idea is that neutrons at or near rest can only absorb a ^4He excitation which has energy and momentum E_c and k_c near the intersection of the well known ^4He phonon-rotor dispersion curve and the free neutron dispersion curve, $\omega = \hbar q^2/2m_n$. This process is strongly suppressed by the Boltzmann factor, $e^{-E_c/t}$. By the same argument, only neutrons with energy near E_c can scatter into the UCN energy region by emission of a single excitation. UCN produced in the way will remain in the superfluid He bath until they are lost through one of the possible loss mechanisms which include β decay, absorption by ^3He , loss in the wall, etc. The UCN will reach a saturation density

$$\rho_{UCN} = \tau P \quad (10)$$

where τ is the total loss rate,

$$\tau^{-1} = \tau_{wall}^{-1} + \tau_{\beta}^{-1} + \tau_{^3\text{He}}^{-1} + \dots \quad (11)$$

and P is the UCN production rate (UCN/cc/sec) due to the above mentioned downscattering process.

Golub has suggested performing an EDM search directly in the liquid helium of a superthermal source using a dilute solution of polarized ^3He in the superfluid He as a polarizer and detector.³⁰⁾ (The production and cryogenic transport of polarized ^3He has been well studied.³¹⁾ Since ^3He -n nuclear reaction occurs only when the total spin is zero (neutron and ^3He spins antiparallel), the UCN lifetime will be spin-dependent as implied by Eq. 11. If the ^3He is nearly 100% polarized and $\tau_{^3\text{He}} \ll \tau_{wall, \beta}$, the UCN at saturation density given by Eq. 10 will be nearly 100% polarized.

The reaction between ^3He and neutrons produces energetic charged particles. It is well known that α particles and energetic electrons produce ultraviolet scintillation in liquid helium;³²⁾ the scintillations due to ^3He -n reactions should in principle be detectable with high efficiency.

In the following discussion, let \vec{p}_3 refer to the ^3He polarization vector and \vec{p}_n refer to the neutron polarization vector. In the case where both species are polarized, the spin-dependent loss rate can be written

$$\tau_{abs} = \frac{1}{\tau_{^3\text{He}}} (1 - \vec{p}_n \cdot \vec{p}_3) = (1 - p_n p_3 \cos(\theta_{n3})/\tau_{^3\text{He}} \quad (12)$$

where θ_{n3} is the angle between the spin polarization vectors and $|\vec{p}| \leq 1$. Each loss (nuclear reaction) produces a scintillation pulse; the scintillation rate thus becomes a measure of the angle between the polarization vectors as shown in Fig. 6.

One could search for a neutron EDM by using the above UCN production/ polarization technique. After the UCN are polarized (along a static field of magnitude B_0), the UCN and ^3He spins could be flipped by $\pi/2$; the spins then precess about the static field and there is a modulation in the scintillation rate:

$$\phi(t) \propto (1 - \vec{p}_3 \cdot \vec{p}_n) = (1 - p_3 p_n \cos[(\gamma_3 - \gamma_n)B_0 t + \Phi]), \quad (13)$$

where $\phi(t)$ is the time-dependent scintillation rate and Φ is an arbitrary phase. The gyromagnetic ratios are $\gamma_n/2\pi \approx -3\text{Hz/mG}$ and $\gamma_3/2\pi \approx -3.33\text{Hz/mG}$. The EDM of ^3He is expected to be quite small (due to Schiff shielding);¹⁰⁾ thus, if an electric field is applied along B_0 there will be a change in the frequency of the scintillation rate modulation. Unfortunately, the problem of measuring the magnetic field remains (although the effects are only 1/10 as large since the gyromagnetic ratios are nearly equal) and it has been demonstrated that experiments are presently limited by magnetic systematic effects. It might be possible to use SQUID magnetometers to detect the ^3He magnetization, the ^3He could then serve as a magnetometer. However, the sensitivity is at best marginal. Golub and Lamoreaux³³⁾ have suggested using the ^3He as a direct comagnetometer by using "dressed atom" techniques to make the magnetic moments of the neutron and ^3He equal. The idea is as follows.

In the presence of a strong oscillating magnetic field, the magnetic moment will be modified, or "dressed"^{34,35)}

$$\gamma' = \gamma J_0(\gamma B_{RF}/\omega_{RF}) = \gamma J_0(\gamma x), \quad (14)$$

where γ is the gyromagnetic ratio, B_{RF} and ω_{RF} are the amplitude and frequency of an applied oscillating magnetic (RF) field, J_0 is the zeroth-order Bessel function, and γ' is the observed gyromagnetic ratio.

In practice, the oscillating field is at right angles to the static field B_0 around which the spins are precessing. In the absence of the oscillating field, one would see scintillation due to reactions occur at a rate given by Eq. 13. Thus, one sees oscillations (in the scintillation rate) which occur at the difference in the precession frequencies ($\delta\omega = (\gamma_n - \gamma_3)B_0$). If the RF dressing field is now applied, we find

$$\delta\omega = (\gamma_n J_0(\gamma_n x) - \gamma_3 J_0(\gamma_3 x))B_0. \quad (15)$$

This has the amazing property that $\delta\omega = 0$ when $\gamma_n x \approx 1.19$; we call this "critical dressing".

If the neutron EDM were non-zero the neutron precession frequency will be shifted by an amount $2d_n E J_0(\gamma_n x)$ since the dressing dilutes the angular momentum. Thus, the value of $x = x_c$ to give $\delta\omega = 0$ is changed. By measuring the value of x vs. electric field direction, we will be sensitive to the neutron EDM. The important point is that the effect of static magnetic fields is cancelled.

An experimental method might be to keep the neutron and helium spin vectors nearly parallel; as the value of x is varied the scintillation will increase or decrease as x is varied away from the value x_c such that $\delta\omega = 0$. Over the course of a storage, x could be modulated at a low frequency ω and the value $x_c(\pm E)$ inferred from the modulation in the scintillation rate; the modulation in the scintillation rate as x is varied is indicated in Fig. 6. If the average value of $x \neq x_c$, there will be a $1 - \omega$ component to the scintillation rate growing linearly in time. If $x = x_c$, there will be only a $2 - \omega$ component. In practice, a feedback system might be used to force the $1 - \omega = 0$; the $2 - \omega$ signal then serves as a system calibration. (Note that the modulation in x and the subsequent modulation in the scintillation rate are 90° out of phase because the spin vectors must precess before the effects due to a change in x are manifest). A detailed analysis of the sensitivity in the shot noise limit indicates a maximum sensitivity (when $p_3 \approx 1$) occurs when $\tau_{3He}/\tau_{wall} = 1.4$ and the modulation index is approximately 1; the uncertainty in the dipole moment is then

$$\sigma(d_n) = \frac{1.4\hbar}{E\sqrt{\tau_{wall}\rho_{UCN}V}} \frac{1}{\sqrt{T}} \quad (16)$$

where V is the storage chamber volume and $T \gg \tau_{wall}$ is the total time (many measurements of τ_{wall} duration). This is quite comparable with Eq. 9, particularly if the usual $\alpha = .6$ is included. An important advantage of counting the scintillations is that instead of counting the remaining neutrons (after one bottle lifetime, or one third of the original number), one sees most every neutron as it disappears and the scintillations can be observed until all the UCN are gone (there is some optimum time). Thus, for a given initial density, the scintillations detection gives effectively nearly three times the total counts (this estimate includes $\alpha = .6$) over the usual bottle experiment.

A factor of 100 increase in sensitivity over the technique outlined in Sec. 2 seems feasible. First, the excellent dielectric properties of liquid helium might allow a 3 to 10 times increase in the electric field.

Second, a 300 to 1000 increase in UCN density in the liquid He over the turbine output seems possible (the storage volumes could be of comparable size). A 500 sec. wall lifetime implies from Eq. 10 a production rate of 15 to 40 UCN/cc/sec. This can be compared to a rate of 2/cc/sec in the present superthermal source experiment which is located quite far from the reactor core.

To minimize polarization loss due to field gradient induced T_2 relaxation, constraints on the static field gradients are the same as before; that is, the field change across the bottle must be less than $10\mu\text{G}$. For the RF dressing field, it is not the absolute value but the *relative* gradient (since $J_0(x)$ multiplies B_0) that matters. Thus, it should be relatively simple to achieve the required homogeneity of the RF particularly if low conductivity materials are used to construct the internal parts of the apparatus. In addition, the cryogenic system will allow superconducting shields to be easily incorporated. These might perform better than the usual Permalloy.

As before, there will be a filling and RF pulse sequence, with electric field flips between measurement cycles. It will be necessary to have provisions to remove the depolarized ^3He at the end of each (or every few) measurement cycle(s), possibly through use of the heat flush technique.³⁶⁾ For the heat flush to be effective it is necessary to have a bath temperature $T \approx 1.2\text{K}$. However, neutron storage times greater than 500 sec. requires $T < 0.8\text{K}$ (multiphonon upscattering suppression). The optimum operating temperature has yet to be determined. Another consideration is the diffusion time of the ^3He in the superfluid; too long a diffusion time places a severe limit on the allowable field gradient and can skew the field average. Some schemes such as using a "fan" to circulate the ^3He within the volume will allow operation at a higher temperature. Since the specific heat of the superfluid He is very small, there are other possibilities. For example, the bath temperature could be rapidly raised to $\approx 1.2\text{K}$ for the heat flush to work, then rapidly cooled down for the next measurement.

3.2 Polarization of ^3He

This experiment requires ^3He concentrations at the 10^{-10} level with nearly perfect polarization. There are some optical pumping techniques under development;³¹⁾ these are aimed at producing high densities. The polarization obtained with these methods is limited to 70% which represents a factor of 6 loss in sensitivity (which scales as $p_3^{5/2}$) for the EDM experiment.

Since we need so few polarized atoms, use of a hexapole state selector on a cold (1K) ^3He atomic beam has been suggested.³³⁾ Following Ramsey¹⁷⁾, the maximum angle that can be focussed by a hexapole is given by

$$\theta_{max} = \sqrt{\frac{\mu B}{kT}} \quad (17)$$

where μ is the (nuclear) magnetic moment, B is the maximum magnetic field, k Boltzmann constant, and T the temperature. For $B = 10^4\text{Gauss}$ and $T = 1\text{K}$, we find a focussed solid angle

$$\Omega_f = \pi \theta_{max}^2 = 1.2 \times 10^{-3}. \quad (18)$$

The number of atoms/sec leaving a source of area A into this solid angle is given by

$$I = \frac{nv}{4} \frac{\Omega_f}{2\pi} A; \quad n = 4 \times 10^{16} P_{\text{torr}} \frac{300}{T}. \quad (19)$$

With 6 sources of area 1 mm^2 , this technique can produce 3×10^{15} atoms/sec. Since 6×10^{16} atoms are need to achieve a concentration of 10^{-10} , this rate is adequate. The polarization will depend on the background pressure; there will be some engineering to develop a differentially pumped system which will achieve 100% polarization. Also the field gradients at the exit of the hexapole must be carefully tailored so that depolarization does not occur.

This technique might be useful for other high density applications. The density of the polarized ^3He could be increased by using the heat flush or a Toepfer pump. The modest numbers above would produce 1 atm-cc of polarized ^3He in 3 hours. An improved source could give another factor of 10 in the production rate. This would exceed the performance of the various optical pumping techniques currently being developed. The hexapole state selector would also make an efficient UCN polarizer.

3.3 Analysis of the Dressed Spin System

The motion of a spin under application of static and non-resonant oscillating magnetic fields is quite complicated. In some sense, saying that the magnetic moment is modified (or dressed) is the "zeroth-order" approximation. For the following discussion, let $x \rightarrow x/\gamma_n$.

The ^3He -n spin system was solved numerically under various conditions. This system is difficult to solve numerically as it involves two time scales; the RF field of 10kHz, and the relatively slow precession (10Hz) around the DC field. The accuracy obtained is set by the step size at the 10kHz level.

The classical spin precession equations (exact for spin $1/2$) were solved using the fourth order Runge-Kutta method. The value of x such that $\vec{p}_n \cdot \vec{p}_3 = 0$ (and constant) (averaged over many RF cycles) was found by "feeding-back" on the value of x . As in the case of a physical feedback system, the loop parameters could be varied to make the system stable. (In fact, this implies that the modulation technique discussed earlier will work). Effects of fields along the RF field (B_0^z) and perpendicular to the RF ($B_0^x \gg B_0^z$) were studied. It was found that $\delta x_c = x - x_c$ (that is, the shift in the critical dressing condition) was

$$\delta x_c \propto (B_0^z/B_{RF})^2 \quad (20)$$

$$\delta' x_c \propto (B_0^x/B_0^z)^2. \quad (21)$$

The $\delta' x_c$ term is somewhat worrisome; however, there is a global maximum in x when $B_0^z = 0$. This can be used to provide an active means of zeroing this field component, perhaps through some additional modulation. The effect of the δx_c term should be negligible.

These results were also obtained through quantum perturbation theory. This is an example of the power of quantum vs. classical perturbation theory. In this example, it becomes obvious that quantum mechanical perturbation works because the system can be described fully with the never-changing eigenfunctions; there is nothing analogous for the classical system where the future depends on the history of the system.

Using the formalism developed in Refs. 34, we found the following first-order correction to the $\pm 1/2$ eigenvalues. (The unperturbed states are specified by $|\pm 1/2 \rangle |n \rangle$ where n is the field photon number. The states are degenerate between \pm before the static fields are applied.)

$$E^{(1)} = \pm \frac{1}{2} \gamma \sqrt{(B_0^x)^2 + (B_0^z J_0(\omega_1/\omega))^2} \quad (22)$$

where $\omega_1 = \gamma B_{RF}$, for the neutron and ^3He separately. If we require that $E_3^{(1)} = E_n^{(1)}$, the result Eq. 21 is obtained. We can set $B_0^z = 0$ through some experimental legerdemain. Carrying the perturbation to higher order mixes in states of different n (virtually since the field is very non-resonant). The second order corrections are zero, while the third order gives $E^{(3)} \propto (\gamma B_0^z)^3/(\omega^2)$ which reproduces Eq. 20 when we set $E_n^{(3)} = E_3^{(3)}$.

An important result of this analysis is the spin/field state cannot be affected by the static electric field. The total system angular momentum could be greater than or equal to one; however, there is no way for the static electric field to couple to the constituent system states (RF photons or spin $1/2$'s).

3.4 Application of Dressed States to Other EDM Searches

The ability to affect the magnetic moment of an atom has some applications in the atomic EDM searches. For example, in the ^{129}Xe EDM experiment, there was a possibility of a "spin-shift" due to a non-zero Rb polarization.³⁷ Since the Rb polarization was already modulated, it might be possible to choose the modulation parameters so that the effects on the Xe are cancelled. Work on an improved ^{199}Hg atomic EDM experiment¹⁰ is already in progress. In this experiment, the electric field will be applied along the RF (dressing) field and the DC fields will be zero. This experiment might reach the 10^{-30} e cm range within the next decade.

References

1. Purcell, E.M. and Ramsey, N.F. (1950), Phys. Rev. 78, 807.
2. Smith, J.H. *et al.* (1957), Phys. Rev. 108, 120.
3. Lee, T.D. and Yang, C.N. (1956), Phys. Rev. 104, 254.
4. Landau, L. (1957), Nucl. Phys. 3, 127.
5. Wu, C.S. *et al.* (1957), Phys. Rev. 105, 1413.
6. Pauli, W. (1955), *Neils Bohr and the Development of Physics*, (Pergamon, New York) (Chapter 4).
7. Ramsey, N.F. (1958), Phys. Rev. 109, 225.
8. Christenson *et al.* (1964), Phys. Rev. Lett. 13, 138.
9. Casella, R. (1969), Phys. Rev. Lett. 22, 554; Schubert, K.R. *et al.* (1970), Phys. Lett. 313, 662.
10. Lamoreaux, S.K. *et al.* (1987), Phys. Rev. Lett. 59, 2275; Lamoreaux, S.K. (1989), Nucl. Inst. and Meth. A284, 43.
11. He, X.-J. *et al.* (1989), Intl. J. Mod. Phys. A 4, 5011.; E.P. Shabiiin (1982), Sov. J. Nucl. Phys. 575.

12. Ellis, J. (1989), Nucl. Inst. and Meth. A284, 33.
13. Altarev, I.S. *et al.* (1986), JETP Lett. 44, 460.
14. Smith, K.F. *et al.* (1990), Phys. Lett. B 234, 191.
15. Golub, R. and Pendlebury, J.M. (1972), Contemp. Phys. 13, 519.
16. Messiah, A. (1966), *Quantum Mechanics*, (Wiley, New York).
17. Ramsey, N.F. (1956), *Molecular Beams*, (Oxford U.P., London).
18. Zeldovich, Yu. B. (1959), Soviet Physics JETP 9, 1389.
19. Golub, R. and Pendlebury, J.M. (1979), Rep. Prog. Phys. 42, 439; Golub, R., Lamoreaux, S.K., Richardson, D.J. *Ultracold Neutrons*, (Adam-Hilger, 1991, to be published).
20. Shapiro, I.S., and Estulin, I.V. (1956), JETP 3, 345.
21. Okun, L.B. (1969), Comm. Nucl. Part. Phys. 3, 133.
22. Pendlebury, J.M. *et al.* (1984), Phys. Lett. B 136, 327.
23. To be published, Smith, K.F. *et al.* (1991).
24. Sumner, T.J. *et al.* (1987), Jour. of Phys. D 20, 1095.
25. Altarev, I.S. *et al.* (1980), Nucl. Phys. A 341, 269.
26. Altarev, I.S., private communication.
27. Ramsey, N.F. (1982), Ann. Rev. Nucl. Part. Sci. 32, 211.
28. Lamoreaux, S.K. (1986), Private Communication to the ILL EDM group; Lamoreaux, S.K. (1988), Institute Laue-Langevin Internal Report 88LA01T (unpublished).
29. Kilvington, A.I. *et al.* (1987), Phys. Lett. A, 125, 416.
30. Golub, R. (1983), J. De Physique 44, L-321; Golub, R. (1987), *Proceedings of the 18th International Conf. on Low Temp. Physics, Pt. 3: Invited Papers* (Kyoto, Japan 1987), 2073.
31. Aminoff, C.G. *et al.* (1989), Rev. Phys. Appl. 24, 827.
32. Simmons, J.E. and Perkins, R.B. (1961), Rev. Scin. Instr. 32, 1173.
33. Golub, R. and Lamoreaux, S.K., "A New Method to Search for the EDM of the Neutron using UCN stored in dilute Solutions of ^3He in Superfluid ^4He ", ILL, Grenoble, 1990 (unpublished).
34. Polonsky, N. and Cohen-Tannoudji, C. (1965), Jour. de Phys. 26, 409; Cohen-Tannoudji, C. and Haroche, S. (1969), Jour. de Phys. 30, 153.
35. Dubbers, D. (1989), Nucl. Inst. and Meth. A284, 22.
36. McClintock, P.V.E. (1978), Cryogenics 18, 201.
37. Vold, T.G. (1984) *et al.* Phys. Rev. Lett. 52, 2229.

Search for Time Reversal Symmetry Violation in Thallium Fluoride Using a Jet Source

E. A. Hinds

Physics Department, Yale University, New Haven, Connecticut 06520



We have looked for a violation of time reversal symmetry in the diatomic molecule thallium fluoride (TlF) using a rotationally cold beam from a jet source. Our method was to search for a frequency shift of the thallium nuclear magnetic resonance when an external electric field of 29.5 kV/cm was reversed with respect to a magnetic quantization axis. The measured shift, was interpreted as a null result and constitutes a tenfold improvement in sensitivity over the previous measurement. Accordingly, our measurement has reduced the upper limits on the proton and electron electric dipole moments and on other T-violating weak couplings. Limits are obtained on both P-odd and P-even forces.

I. Electric dipole moment and T-violation

In order for a non-degenerate system to possess a permanent electric dipole moment (EDM) along one of its angular momenta, P- and T-invariances must both be violated (P&T-violation). Accordingly, the EDM of various atomic systems as well as that of the neutron have been measured in the hope of finding T-violation that does not explicitly involve kaon decay.^{1,2)} Atoms or molecules are interesting places to look for T-violation because they are composed of both leptons and hadrons and involve a wide range of fundamental interactions.

Atomic and molecular EDM measurements have all yielded null results so far and these have been used to put upper limits either on intrinsic EDMs of the constituent particles or on a variety of T-odd interactions between them. The possibility that an atomic EDM could be induced by the intrinsic EDM of one of the constituent particles was first discussed in detail by Schiff.³⁾ To the extent that an atom or molecule is made of charged point-particles bound together by the Coulomb force, there is no permanent EDM of the system i.e., no linear Stark interaction in a weak electric field, even when the individual particles have an EDM. This is a consequence of the equilibrium condition that the average electrostatic force on each particle must vanish. Schiff showed that this argument fails if the particles also interact magnetically, or if one of the particles has a finite size over which its charge and EDM are differently distributed. The TIF molecule which we have studied includes relativistic (magnetically interacting) electrons and nuclei of finite size and therefore both of Schiff's mechanisms are operative.^{4,5,6,7)} As a result, we are able to interpret our result in terms of more elementary EDMs.

A different possibility is that the molecule may have a permanent EDM by virtue of P&T-violating interactions between its constituents^{8,6)} even in the absence of intrinsic EDMs. This allows us to deduce limits on P&T-violation in both nucleon-nucleon and electron-nucleon interactions. Quite recently, Khriplovich⁹⁾ has noticed that our EDM measurement can also yield stringent limits on interactions that violate T while *conserving* P.

Sandars⁴⁾ pointed out that a polar molecule is a sensitive system in which to search for P&T-violation because the rotational states are much closer together than the energy levels of an atom. In addition, a heavy nucleus is required to take advantage of the Schiff mechanisms mentioned above. Following Sandars original suggestion, many attempts have been made to detect a permanent EDM of the TIF molecule.^{10,11,12,13)} This particular polar molecule is appealing because it is chemically stable, easily vaporized and detected, has simple structure and includes a heavy nucleus (Tl).

The result reported here, first published in a letter,¹⁴⁾ constitutes a substantial advance over previous experiments on TIF and contributes at a significant level to our knowledge of T-violation in nature. The main reasons for this progress have been two technical developments. First, we devised and implemented a pure TIF supersonic jet source which produced an intense, rotationally-cold molecular beam and allowed a great improvement in the signal-to-noise ratio of our measurement. Second, we introduced a new reversal into the experiment which increased our ability to distinguish spurious instrumental effects from the true EDM signal. These innovations jointly led to a tenfold improvement in our measurement of T-violation in TIF.

II. Principle of the experiment

Stripped to the bare essentials, our experiment involved a supersonic jet beam of spin-polarized TIF molecules, passing through an electric field \vec{E}_c . Nuclear magnetic resonance (NMR) was performed on the Tl nucleus and we looked for a linear Stark effect by searching for a shift of the NMR frequency when \vec{E}_c was reversed.

The interaction of the Tl nuclear spin $(1/2)\hbar\vec{\sigma}$ with the rest of the molecule can be described by the effective Hamiltonian

$$H = -\mu_{\text{Tl}}\vec{\sigma} \cdot \vec{B}_0 - dh\vec{\sigma} \cdot \hat{\lambda}. \quad (1)$$

The first term is the usual (T-conserving) hyperfine interaction of the nuclear magnetic dipole moment $\mu_{\text{Tl}}\vec{\sigma}$ with the internal magnetic field \vec{B}_0 of the molecule. On the other hand, the second term describes the P&T-violating electric dipole interaction that we are interested in. Here $\hat{\lambda}$ is a unit vector pointing from the Tl nucleus to the F nucleus, d is a measure of

T-violation in TIF and \hbar is Planck's constant. In free space, such an interaction would tip the internuclear axis, giving it a small projection along $\vec{\sigma}$, and hence producing a small permanent EDM. We prefer, however, to detect this interaction by applying the strong field, which substantially polarizes $\hat{\lambda}$, and to look for an energy of the form $\vec{\sigma} \cdot \vec{E}_C$. This energy appears as a shift of the NMR frequency when \vec{E}_C is reversed.

Our experiment determined the phenomenological constant d that characterizes the strength of the P&T-violating coupling between the TI nuclear spin and the internuclear axis. The result was

$$d = (-0.13 \pm 0.22)\text{mHz}. \quad (2)$$

We interpret this as a null result. The quoted error is entirely dominated by random uncertainties and is close to the noise expected from random counting statistics.

III. Interpretations

A. Proton EDM

If the proton has an intrinsic EDM d_p along its spin, the electric dipole interaction of the TI nucleus is

$$H_{PT}(d_p) = -d_p \sum_n \vec{\sigma}_n \cdot \vec{E}(\vec{r}_n), \quad (3)$$

where $\vec{E}(\vec{r}_n)$ is electric field at the location \vec{r}_n of the n^{th} proton.

Coveney and Sandars⁶⁾ have calculated the strength of this interaction in TIF, taking into account the finite nuclear volume and the magnetic forces.^{16,17)} Their calculation together with our experimental result yields a limit on the EDM of the proton:

$$d_p = (-3.7 \pm 6.3) \times 10^{-23} \text{e.cm}, \quad (4)$$

which is the best available limit on the proton EDM.

B. Nuclear EDM

Even if the proton and neutron themselves possess no permanent EDM, the TI nucleus as a whole may still do so as a result of its structure. The interaction energy is,^{6,18)}

$$H_{PT}(Q) = 4\pi\vec{Q} \cdot \vec{\nabla}\rho_0 = -d\vec{\sigma} \cdot \hat{\lambda}, \quad (5)$$

where ρ_0 is the electron density at the site of the TI nucleus and \vec{Q} is the Schiff moment. The latter is defined by

$$\vec{Q} = \frac{e}{6} \left[\frac{3}{5} \sum_n r_n^2 \vec{r}_n - \frac{1}{Z} \sum_n r_n^2 \sum_{n'} \vec{r}_{n'} \right], \quad (6)$$

where \vec{r}_n is the location of the n -th proton. When our measurement is associated with this type of interaction we obtain a very stringent limit on the Schiff moment of the TI nucleus,

$$Q_{\text{TI}} = (2.3 \pm 3.9) \times 10^{-10} \text{ e.f.m}^3. \quad (7)$$

This limit constrains P&T-odd nucleon-nucleon forces²⁰⁾ to have less than a few percent of the weak interaction strength.

C. P&T-odd weak couplings

P&T-odd weak couplings between the electrons and nucleons are also possible. Our experiment is most sensitive to tensor-pseudotensor interactions of the form

$$H_{\text{PT}}(C_T) = i C_T \frac{G_F}{\sqrt{2}} (\bar{\Psi}_n \sigma^{\mu\nu} \Psi_n) (\bar{\Psi}_e \gamma^5 \sigma_{\mu\nu} \Psi_e). \quad (8)$$

where G_F is the Fermi constant and C_T represents the strength of the interaction.

Our experimental result implies^{16,19)} a limit on C_T of

$$C_T = (-1.5 \pm 2.6) \times 10^{-7}. \quad (9)$$

A comparable constraint is given by the experiment on atomic Hg.¹⁵⁾

D. P-even, T-odd couplings

Quite recently, Khriplovich⁹⁾ has pointed out that the P&T-odd effective potential $-d\vec{\sigma} \cdot \hat{\lambda}$ can be produced by a T-odd, P-even interaction as a result of P-odd electroweak radiative corrections. He finds that some of these one-loop corrections are smaller than the leading P-even term only by a factor of order α/π . On this basis he is able to use our result in TIF to obtain new limits on P-even, T-odd interactions. He finds, for example, that the P-even, T-odd quark-quark interactions are less than 30 times the weak interaction strength. In addition, he is able to deduce limits at the 10^{-3} level on the T-odd, P-even beta-decay

constants. Our measurement, the other atomic EDM experiments and the neutron measurements are all of comparable sensitivity in this respect and together they furnish the best limits on such interactions.

IV. Prospects

The TIF beam apparatus at Yale, which has achieved improvements by a factor of 50 over the last few years, can still make an order of magnitude improvement over the present work. Some of the remaining systematics should, however, be understood in more detail. In the long run it may be necessary to find ways of slowing and trapping TIF molecules in order to reduce the large linewidth (100 Hz) of the resonance.

REFERENCES

1. J. H. Christenson, J. W. Cronin, V. L. Fitch, and R. Turlay, *Phys. Rev. Lett.* **13**, 138 (1964)
2. E. A. Hinds, *Atomic Physics II* edited by S. Haroche, J. C. Gay, and G. Grynberg, p.151. Singapore. World Scientific. (1989).
3. L. I. Schiff, *Phys. Rev.* **132**, 2194 (1963).
4. P. G. H. Sandars, *Phys. Rev. Lett.* **19**, 1396 (1967).
5. E. A. Hinds and P. G. H. Sandars, *Phys. Rev. A* **21**, 471 (1980).
6. P. V. Coveney and P. G. H. Sandars, *J. Phys. B* **16**, 3727 (1983).
7. V. V. Flambaum and I. B. Khriplovich, *Sov. Phys. JETP* **62**, 872 (1985).
8. E. A. Hinds, C. E. Loving, and P. G. H. Sandars, *Phys. Lett.* **62B**, 97 (1976).
9. I. B. Khriplovich, Institute of Nuclear Physics, Novosibirsk, Preprint 90-69 (1990).
10. G. E. Harrison, P. G. H. Sandars, and S. J. Wright, *Phys. Rev. Lett.* **22**, 1263 (1969).
11. E. A. Hinds and P. G. H. Sandars, *Phys. Rev. A* **21**, 480 (1980).
12. D. A. Wilkening, N. F. Ramsey, and D. J. Larson, *Phys. Rev. A* **29**, 425 (1984).
13. D. R. Schropp Jr., D. Cho, T. Vold, and E. A. Hinds, *Phys. Rev. Lett.* **59**, 991 (1987).
14. D. Cho, K. Sangster, and E. A. Hinds, *Phys. Rev. Lett.* **63**, 2559 (1989).
15. S. K. Lamoreaux, J. P. Jacobs, B. R. Heckel, F. J. Raab and N. Fortson, *Phys. Rev. Lett.* **59**, 2275 (1987).
16. P. V. Coveney, Thesis for Final Honour School of Natural Science, Chemistry Part II, Lincoln College, Oxford (1981).
17. The value $d^M/d_p = 4.1 \times 10^{-7} a.u.$ given on page 3737 of ref. 6 is a misprint. It should read $d^M/d_p = 6.22 \times 10^{-7} a.u.$ as in ref. 16.
18. O. P. Sushkov, V. V. Flambaum, and I. B. Khriplovich, *Sov. Phys. JETP* **60**, 873 (1984).
19. The value $d_T/C_T = -5.08 a.u.$ given on page 3737 of ref. 6 is a mistake. It should read $d_T/C_T = -5.82 a.u.$ as given in ref. 16. The value we use here has opposite sign to account for a different definition of γ_5 . It has also been corrected for the more modern value of G_F .
20. V. V. Flambaum, I. B. Khriplovich, and O. P. Sushkov, *Nucl. Phys. A* **449**, 750 (1986).

LIMITS ON THE ELECTRON ELECTRIC DIPOLE MOMENT FROM ATOMS

Larry R. Hunter

Physics Dept., Amherst College, Amherst, MA 01002



Measurements of atomic electric-dipole moments (EDMs) provide highly sensitive tests of time-reversal invariance. A method for measuring the cesium electric-dipole moment is described that requires two-lasers but no applied magnetic field. From this experiment the electron EDM is inferred to be $d_e = (1.6 \pm 5.9 \pm 1.6) \times 10^{-26} e\text{-cm}$. This result is compared with the new results from thallium and with the predictions of various particle theories.

Since the discovery of time reversal (T) violation in the K-meson system in 1964,¹¹ a large number of experiments have searched for another violation of T. Amongst the most sensitive of these experiments are those that search for permanent electric dipole moments (EDMs) of neutrons, atoms and molecules.²¹ The existence of a permanent EDM of any of these systems would imply a violation of both T and parity (P). Various models of the fundamental constituents of matter and of the interactions between these constituents predict that the electron might have an EDM, possibly as large as $10^{-25}e\text{-cm}$ (e is the electron charge). The best limits on the electron EDM come from measurements of the atomic EDMs of heavy paramagnetic atoms. In these atoms the atomic EDM induced by an electron EDM exceeds the electron EDM by more than two orders of magnitude, making such atoms extremely sensitive systems for the search for an electron EDM. The most recent calculation of this enhancement factor finds it to be -600 ± 400 in thallium and $+114\pm 4$ in cesium.³¹

In our experiment we measure the EDM of the cesium ground state with a two-laser method that does not require the presence of an applied magnetic field B.

A circularly polarized diode laser propagating along \hat{x} excites the $6S_{1/2}$ F=3 to $6P_{3/2}$ transition in cesium in the presence of a 4kV/cm electric field (along \hat{z}). Optical pumping, spin exchange and polarization transfer through the excited state create an orientation of the $6S_{1/2}$ F=4 level along \hat{x} (see Fig. 1). Long spin relaxation times ($\sim 16\text{ms}$) are achieved by adding 250T of nitrogen as a buffer gas.

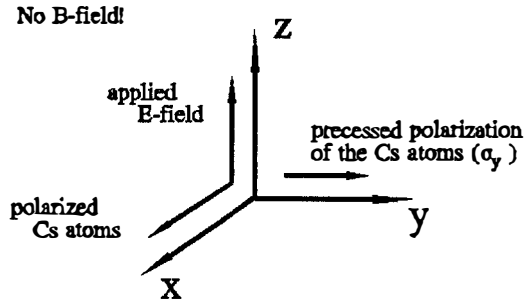


Fig. 1 - The experimental geometry of the cesium experiment

If the cesium atom has a permanent EDM, the applied \vec{E} field creates a torque on the oriented cesium atoms that results in a precession of the ground states into the \hat{y} direction. To detect this polarization a second diode laser beam, propagating along \hat{y} and tuned to the $6S_{1/2} F=4$ to $6P_{1/2}$ transition, probes the cesium vapor. The circular polarization of this second laser is rapidly modulated between right and left by a photo-elastic modulator. The transmission of this probe beam through the vapor is detected synchronously with the circular polarization reversal by a lock-in detector. The lock-in detector output is proportional to the atomic polarization along \hat{y} . If \vec{E} is reversed the sign of the EDM induced polarization must also reverse. The effect is exactly analogous to the Hanle Effect with the magnetic Hamiltonian, $\vec{\mu} \cdot \vec{B}$, replaced by the electric Hamiltonian, $\vec{d} \cdot \vec{E}$, where \vec{d} is the cesium EDM.

Great care is taken to eliminate B from the experiment. An array of passive and active magnetic shields allow us to reduce all three components of the residual magnetic field at

our cells to below 100nG. Two cells are stacked one upon the other with their common electrode at high voltage while the outer electrodes are grounded, resulting in opposite directions of the electric field in each cell. By taking the difference in the polarization signals obtained from the two cells, the size of the EDM signal is doubled while rotations induced by the residual magnetic field are removed (to the extent that B is the same at the two cells). In addition to being opposite in the two cells, our EDM polarization is required to change sign upon reversal of the incident circular polarization, the probe circular polarization, and the applied high voltage. This highly specific signature allows us to easily distinguish many possible systematic effects that might otherwise mimic the EDM signal. The experimental sensitivity is calibrated by applying a known magnetic field and observing the change in the lock-in signals for each cell produced by the Hanle precession.

With this simple and relatively inexpensive method we have measured the cesium EDM to be $d_{\text{cs}} = (1.8 \pm 6.7 \pm 1.8) \times 10^{-24} \text{e-cm}$.⁴¹ This result represents an improvement of a factor of 25 over the previous cesium experiment performed in an atomic beam. Using the calculated enhancement factor for cesium our result implies that electron EDM is $d_e = (1.6 \pm 5.9 \pm 1.6) \times 10^{-26} \text{e-cm}$. At the time of publication this result improved the upper bounds on the electron EDM by about a factor of twenty. One year later a new atomic-beam measurement of the thallium EDM succeeded in obtaining the bounds on the electron EDM of $(-2.7 \pm 8.3) \times 10^{-27} \text{e-cm}$.⁵¹ In obtaining the thallium limit the significant uncertainty in the thallium enhancement factor is ignored. To illustrate the sensitivity of these experiments we note that if an

electron with a "classical" electron radius were expanded to the size of the earth, the separation of its center of mass from its center of charge could be no more than $20\mu\text{m}$, less than the thickness of a hair!

A summary of the electron EDM predictions along with the experimental bounds is shown in Fig. 2.⁶¹ The experiments are rapidly approaching the very interesting level of 10^{-27}e-cm where a number of models suggest that one may find an electron EDM.

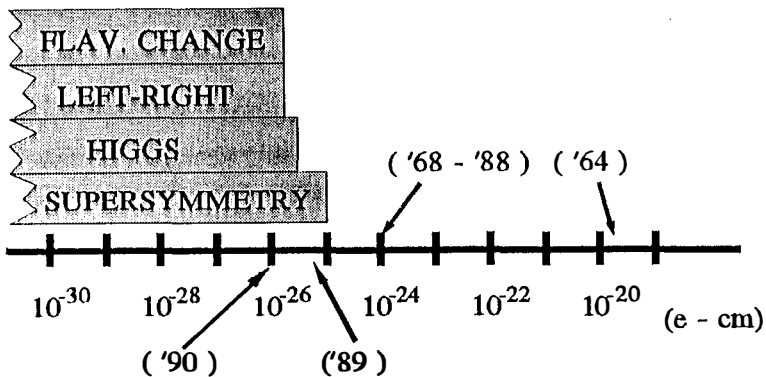


Fig. 2 - Predictions of various theoretical models for the electron EDM. The experimental limits from various years are labelled.

We are now working to achieve another order of magnitude increase in sensitivity. We have obtained a factor of four improvement in the signal to noise by increasing the cesium vapor pressure. New cells have been designed with recessed electrodes that allow us to reduce systematic uncertainties associated with leakage currents to an insignificant level. We have added two new cells, above and below our usual pair

of cells, as cesium magnetometers. This configuration allows us to remove the noise associated with fluctuations in the gradient of the magnetic field at the cells. A new system of polarization modulation in the probe beam has been implemented that has completely eliminated the noise associated with intensity modulation at the circular polarization modulation frequency. The mechanical stability of our apparatus has been improved so that longer integration times can be achieved. The net result of these changes should be about an order of magnitude improvement in our sensitivity.

More long term methods of improving the cesium EDM measurement are also being explored. One possible method involves the use of the non-linear Faraday effect on the $6S_{1/2}$ - $6P_{3/2}$ transition. We have recently observed this effect for the first time. With the employment of a multi-pass cell in an appropriate geometry this method may yield an even more sensitive method for determining the cesium EDM. "Atomic fountains"⁷⁾ may eventually provide even more sensitivity. The ease of optically cooling and manipulating cesium make it an excellent candidate for such an experiment.

- 1) J.H. Christenson, J. Cronin, V.L. Fitch and R. Turlay, Phys. Rev. Lett. 13, 138 (1964).
- 2) L.R. Hunter, to be published in Science, April (1991).
- 3) A.C. Hartley, E. Lindroth and A.M. Martensson-Pendrill, J. Phys. B. 23, 3417 (1990).
- 4) S.A. Murthy, D. Krause, Jr., Z.L. Li and L.R. Hunter, Phys. Rev. Lett. 63, 965 (1989).
- 5) K. Abdullah, C. Carlberg, E.D. Commins, H. Gould and S.B. Ross, Phys. Rev. Lett. 65, 2347 (1990).
- 6) S.M. Barr and W.J. Marciano, in CP Violation edited by C. Jarlskog, (World Scientific, Singapore, 1989).
- 7) M.A. Kasevich, E. Riis, S. Chu and R. DeVoe, Phys. Rev. Lett. 63, 612 (1989).

TESTS OF FUNDAMENTAL SYMMETRIES USING ATOMIC HG VAPOR CELLS

Blayne R. Heckel
Department of Physics FM-15
University of Washington
Seattle, WA. 98195 USA

ABSTRACT

Atoms confined in vapor cells have provided some of the most sensitive tests of many fundamental symmetries of nature. At the University of Washington, the study of mercury atoms confined in quartz cells has resulted in tests of the linearity of quantum mechanics, the isotropy of space, the equivalence principle for intrinsic spin, and time reversal symmetry. This report will review the work with mercury and present recent results.

I. INTRODUCTION

There is much effort devoted to the development of trapping techniques to confine ions or neutral atoms to localized regions of space with the goal to perform more precise measurements on the trapped species than is otherwise possible. One of the oldest and simplest of the trapping techniques is the confinement of a vapor of atoms in a sealed glass cell. Typically, resonant light is used either directly or indirectly (through spin exchange with a second species, for example) both to polarize and to monitor the time evolution of the spin polarization. The ground state spin polarization lifetimes that have been achieved depend upon the atomic species and vary from $\approx 10^{-2}$ sec for alkali atoms to $\approx 10^6$ sec for ^3He atoms. Like noble gas atoms, mercury atoms have a 1S_0 electronic configuration which shields the nuclear spin from the perturbing influence of collisions with the cell walls and other atoms in the vapor. In both the spin 1/2 isotope, ^{199}Hg , and the spin 3/2 ^{201}Hg , nuclear spin polarization lifetimes of several hundred seconds are achieved routinely in cells made of high purity quartz. Because mercury atoms can be optically pumped directly with 254 nm light, they provide a simple system for high precision tests of phenomena that couple to nuclear spin. We have used mercury atoms in a vapor cell to test the linearity of quantum mechanics, the isotropy of space, the equivalence principle for intrinsic spin, and time reversal symmetry. This work will be discussed in the following sections.

II. A TEST OF THE LINEARITY OF QUANTUM MECHANICS

There has been recent interest in a nonlinear generalization¹ of the Schrodinger equation that in lowest order becomes ordinary quantum mechanics. A characteristic of this nonlinear theory is that atomic transition energies depend upon the populations of the atomic levels. For the case of ground state magnetic sublevels, rotational invariance requires that a spin > 1 and an additional splitting such as that due to a quadrupole interaction be present to observe nonlinear shifts of the Zeeman levels. ^{201}Hg atoms precessing in a cone at a cone angle θ with respect to a fixed magnetic field will exhibit three distinct frequencies, ν_0 and $\nu_{\pm} = \nu_0 \pm \nu_Q$, when an additional quadrupole interaction is present (ν_0 is the Larmor frequency and ν_Q the quadrupole splitting). The populations of the four Zeeman levels can be changed by varying θ . For a symmetric quadrupole interaction whose axis of symmetry is parallel to the magnetic field, ordinary quantum mechanics requires that $\Delta = \nu_+ + \nu_- - 2\nu_0 = 0$, while the nonlinear theory predicts that Δ will be a function of θ . Note that Δ is insensitive to drifts in ν_0 and ν_Q .

We have measured² Δ as a function of θ using an apparatus that is sketched in Fig. 1. Circularly polarized resonant light from a ^{198}Hg discharge lamp polarizes the ^{201}Hg atoms in a vapor cell along a B_x magnetic field. After steady state polarization is achieved, a magnetic field B_z is adiabatically increased to rotate the quantization axis to an angle θ relative to the z axis. B_x is then suddenly switched off, leaving the atoms to precess about B_z at a cone angle θ . At the same time, a photoelastic modulator is turned on to modulate the circular polarization of the incident light at 42 kHz. The transmitted light is detected by a solar blind photomultiplier and after demodulation, the signal becomes the sum of sinusoids at the frequencies ν_0 and ν_{\pm} . A typical signal is shown in Fig. 2. This signal is digitized and fit to extract the three frequencies.

The vapor cell, made from high purity synthetic quartz, is evacuated before $\approx 10^{13}$ atoms of ^{201}Hg are sealed within. The cell is a $2 \times 2 \times 1$ cm rectangular box. The ensemble averaged electric field gradient experienced by the atoms as they sample the cell walls produces a symmetric quadrupole frequency shift, $\nu_Q = 50$ mHz. To achieve spin

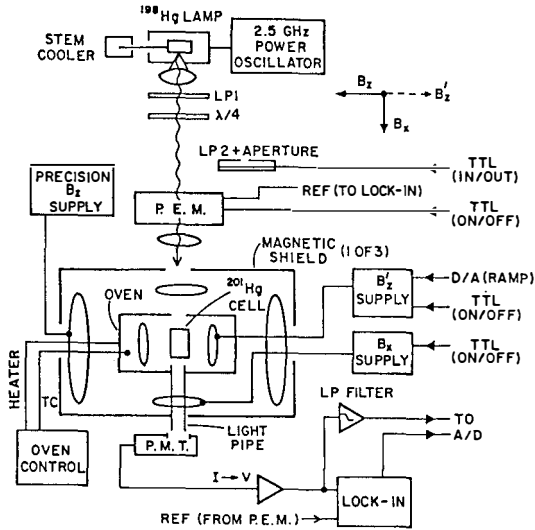


Figure 1. Apparatus to measure the Larmor frequencies of Hg atoms in a vapor cell.

relaxation times in excess of 100 sec, the cell is maintained in an oven at 670 K.

Data were taken at several values of θ for both senses of incident light circular polarization, different light levels, and with B_x and B_z reversed. No deviation of Δ from zero was observed. These measurements allow us to conclude² that the frequency shift associated with the hypothesized theory for nonlinear quantum mechanics is less than $3.8\mu Hz$.

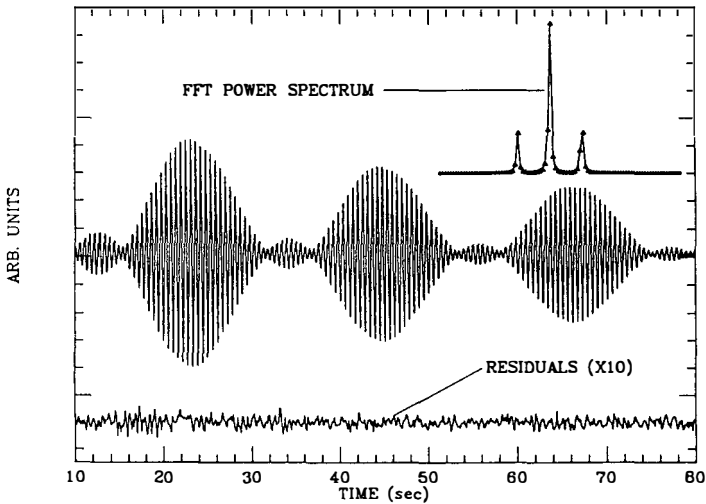


Figure 2. The precession signal for ^{201}Hg atoms for $\theta = 90^\circ$. The Larmor frequency is $\approx 2 Hz$. The quadrupole splitting due to the cell walls produces the beat pattern. The residuals after fitting the signal to the sum of three exponentially decaying sine waves is also shown.

Other groups have reported comparable limits from experiments that used ions in a trap³, a hydrogen maser⁴, and noble gas atoms in a vapor cell⁵.

III. A TEST OF SPATIAL ISOTROPY

A discharge lamp containing ^{204}Hg used in the apparatus described in section II allows both ^{199}Hg and ^{201}Hg to be polarized (and monitored) simultaneously. As the earth rotates, the orientation of a magnetic field fixed in the laboratory will change relative to an inertial frame. By measuring the spin precession frequencies of the Hg atoms about a fixed laboratory magnetic field over the course of several days, one can test if the ground state energy levels depend upon the orientation of the quantization axis relative to the fixed stars. Local Lorentz invariance requires that there is no preferred orientation (rotational invariance). The use of two isotopes (whose gyromagnetic ratios differ by a factor of -2.7), monitored simultaneously, that sample the same region of space is needed to account for possible drifts of the magnetic field.

^{199}Hg , having nuclear spin $I = 1/2$, has only dipolar interactions and hence is sensitive to couplings of the form $\vec{I} \cdot \vec{r}$ or $\vec{I} \cdot \vec{v}$, for example⁶, where \vec{r} (\vec{v}) is the position (velocity) of the laboratory frame relative to some new background field or some isotropy breaking preferred frame. Such new vector couplings will produce a dipole frequency shift $\nu_1 \propto P_1(\cos\alpha)$ where P_1 the first order Legendre polynomial and α is the angle between the quantization axis and the preferred axis. The ^{201}Hg is also sensitive to isotropy breaking quadrupolar interactions as allowed, for example in the $TH\epsilon\mu$ model⁷. Such quadrupolar couplings produce a quadrupole splitting $\nu_2 \propto P_2(\cos\alpha)$.

Roughly 15 days of data were taken to measure ν_1 and ν_2 . Unlike the experiment of section II, a spherical vapor cell was used which produced an unresolved quadrupole splitting due to the walls. Even so, as illustrated in Fig. 3, a frequency shift linear in the quadrupole splitting can be obtained⁸ if the atomic polarization has both a dipole polarization component, D , and a rank 2 tensor polarization (alignment) component, Q .

In this experiment the magnetic field, B_0 , was oriented perpendicular to the earth's rotation axis, and the resonant light beam entered at 45 degrees relative to B_0 . Perpendicular oscillating magnetic fields at the two Larmor frequencies were applied to create two atomic oscillators. The precession frequencies were again derived from the modulations of the transmitted light. The ^{199}Hg signal was used in a feedback loop to stabilize the magnetic field. The ^{201}Hg signal then became a measure of quadrupole energy shifts and of dipole shifts that did not scale as the ratio of the two gyromagnetic ratios. Fitting the data to components proportional to $P_1(\cos\alpha)$ and $P_2(\cos\alpha)$ allowed us to determine⁸ that

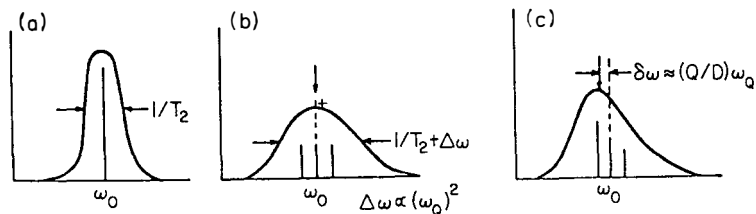


Figure 3. a) The lineshape for a spin $3/2$ system when the quadrupole splitting $\omega_Q = 0$. b) The lineshape for $\omega_Q \neq 0$ and dipole polarization only. The transitions have equal strength and hence only broaden the line. c). Lineshape for $\omega_Q \neq 0$ and both dipole, D , and quadrupole, Q polarizations. Here the line center shifts linearly with ω_Q .

$\nu_1 < 1.3 \mu\text{Hz}$ and $\nu_2 < 0.5 \mu\text{Hz}$. Again, other investigators achieved comparable results with ion traps⁹ and noble gases in vapor cells¹⁰.

IV. A TEST OF THE EQUIVALENCE PRINCIPLE FOR INTRINSIC SPIN

Does a spin up fermion in a gravitational field fall with the same acceleration as a spin down fermion, as is required by the equivalence principle? If not, then a spin perpendicular to the gravitational field would precess about the field, corresponding to a parity and time reversal symmetry odd interaction of the form $\vec{\sigma} \cdot \vec{g}$, where $\vec{\sigma}$ is the spin and \vec{g} the local gravitational acceleration¹¹. The same experimental signature would arise from a new interaction of the form $\vec{\sigma} \cdot \vec{r}$, due to axions¹², for example, where \vec{r} points to the earth, a possible source for the axion field.

The apparatus described in section II is being used to search for a $\vec{\sigma} \cdot \vec{g}$ interaction in the following way. A ^{204}Hg discharge lamp polarizes and monitors both ^{199}Hg and ^{201}Hg atoms simultaneously as a magnetic field, \vec{B} , is reversed from parallel to the earth's rotation axis to antiparallel. The precession frequencies of the two isotopes (averaged over the quadrupole splitting for ^{201}Hg) are then given by:

$$\nu_{199}^{\pm} = |\gamma_{199}B| \pm \Omega \pm \epsilon \cos(43^\circ)$$

$$\nu_{201}^{\pm} = |\gamma_{201}B| \mp \Omega \mp \epsilon \cos(43^\circ)$$

where ν_{\pm} refers to \vec{B} parallel or antiparallel to the earth's rotation axis, γ_i is the gyromagnetic ratio of isotope i , Ω is the rotation rate of the earth, and $\epsilon \cos(43^\circ)$ is the contribution from the projection of a $\vec{\sigma} \cdot \vec{g}$ interaction along \vec{B} . (For simplicity, we are assuming that ϵ is the same for both isotopes.) The difference between the ratios of the two frequencies for the two magnetic field directions is then

$$\Delta = \nu_{201}^+/\nu_{199}^+ - \nu_{201}^-/\nu_{199}^- = 2.738(\Omega + \epsilon \cos(43^\circ))/|\gamma_{199}B|$$

to first order.

Data were taken at two magnetic field strengths: $\gamma_{199}B = 70 \text{ Hz}$ and 1.87 Hz and it was found that $\Delta = (4.44 \pm 0.36) \times 10^{-7}$ and $(172.1 \pm 3.3) \times 10^{-7}$, respectively. After correcting for the $11.6 \mu\text{Hz}$ rotation rate of the earth, we find that $\epsilon = (1.8 \pm 12.6) \times 10^{-7} \text{ Hz}$ and $(1.4 \pm 2.3) \times 10^{-7} \text{ Hz}$. We conclude that the precession of the nuclear spins of Hg atoms due to a $\vec{\sigma} \cdot \vec{g}$ interaction is less than $0.4 \mu\text{Hz}$ unless the interaction strength is proportional to the gyromagnetic ratio. These results are preliminary as additional data are being taken and a full accounting for systematic errors is still in progress. Other limits on a $\vec{\sigma} \cdot \vec{g}$ interaction have been obtained by weighing spin polarized bodies¹³ and from deuterium maser measurements¹⁴.

V. THE ELECTRIC DIPOLE MOMENT OF ^{199}Hg

Unlike the experiments in sections II through IV for which there is no strong evidence that symmetry violations are to be expected, it is believed that the interaction responsible for the violation of CP symmetry observed in the neutral kaon system will give rise to a nonzero value for the electric dipole moment (EDM) of an atom. An observation of an atomic EDM would provide an important clue about the nature of the parity and time reversal symmetry violating interaction. An earlier experiment¹⁵ set an upper limit on the EDM of atomic ^{199}Hg : $d(^{199}\text{Hg}) = (0.7 \pm 1.5) \times 10^{-26} e \cdot \text{cm}$. We are in the process of repeating this experiment and have achieved a statistical error almost two orders of

magnitude smaller than in the original work.

The experimental apparatus is similar to that in Fig. 1. One important difference is that the vapor cell is in the shape of a pillbox, with circular disk endcaps on either side of a 1 cm high 2.5 cm diameter quartz tube. The endcaps are coated on both sides with tin oxide to make them conducting so that an electric field can be applied within the cell. Two identical cells are employed, stacked back to back, with opposite electric fields in the two cells. The signature for an EDM is a frequency shift of the form $\vec{\sigma} \cdot \vec{E}$ where \vec{E} is the electric field. A magnetic field parallel to the E field axis is applied and a change in the precession frequency is sought as \vec{E} is reversed. The cells are filled with isotopically enriched ^{199}Hg and ≈ 250 torr of N_2 gas to prevent discharge in the electric field.

Rather than using a pump and probe technique as described in section II, a continuous measurement is performed. A stepping motor driven rotating linear polarizer is placed before a quarter wave plate to create an incident light polarization that modulates sinusoidally at a frequency ν_L between right and left circular polarization. The magnetic field is perpendicular to the light axis and is adjusted so that the Larmor frequency is equal to ν_L . The result is a synchronously pumped atomic oscillator. The transmitted light then shows a modulation at $2\nu_L$ and the phase of this transmitted light modulation relative to the phase of the incident light polarization becomes a measure of the Hg spin precession frequency.

\vec{E} (≤ 10 kV/cm) is reversed every few minutes in a + 0 - 0 sequence, and a phase difference between the two cells linear in \vec{E} is extracted as the signature for an EDM. Data from a typical run are shown in Fig. 4. An early set of 100 runs gave a result $d(^{199}\text{Hg}) = (25 \pm 7) \times 10^{-28} e \cdot \text{cm}$ (statistical error only). These runs were plagued by internal inconsistencies, and an incomplete set of systematic checks prevented us from understanding many possible systematic errors. A newer set of runs using new cells, a more thorough set of systematic checks, and many improvements to the apparatus has given the result: $d(^{199}\text{Hg}) = (-4 \pm 6) \times 10^{-28} e \cdot \text{cm}$ (statistical error only). We are currently taking

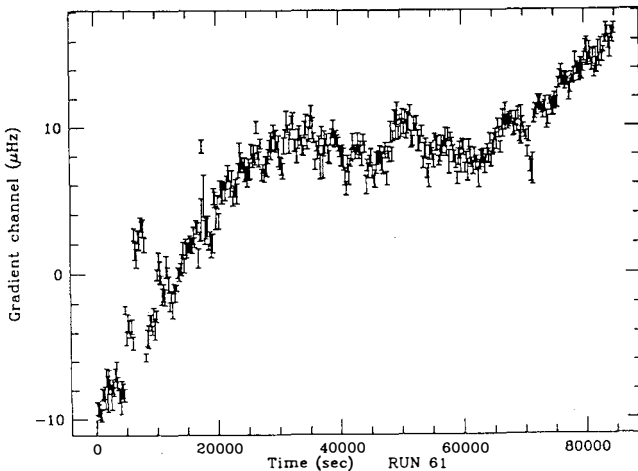


Figure 4. Typical data for a one day EDM run. Each point corresponds to a separate electric field setting. The gradient channel is the phase difference between the light modulation signals transmitted through the two cells (EDM signal), calibrated in μHz . The drift is due primarily to drifts in the light intensity.

more data with the original two cells to help us determine the systematic errors in the system. Upper limits on the EDM's of several other systems have been reported elsewhere recently¹⁶⁻¹⁹.

VI. ACKNOWLEDGEMENTS

I gratefully acknowledge the important contributions from all of the members of our atomic physics group: E.N. Fortson, S.K. Lamoreaux, P.K. Majumder, J.P.Jacobs, and B.J.Venema. This work was supported by the National Science Foundation under grants PHY-8922274 and PHY-8451277.

VII. REFERENCES

1. S. Weinberg, *Ann. Phys. (N.Y.)* 194, 336 (1989).
2. P.K. Majumder, et.al., *Phys. Rev. Lett.* 65, 2931 (1990).
3. J.J. Bollinger, et.al., *Phys. Rev. Lett.* 63, 1031 (1989).
4. R.L. Walsworth, et.al., *Phys. Rev. Lett.* 64, 2599 (1990).
5. T.E. Chupp and R.J. Hoare, *Phys. Rev. Lett.* 64, 2261 (1990).
6. N.D. Hari Das, *Phys. Rev. Lett.* 36, 393 (1976).
7. A.P. Leitner and D.L. Lee, *Phys. Rev. D* 8, 364 (1973).
8. S.K. Lamoreaux, et.al., *Phys. Rev. A* 39, 1082 (1989).
9. J.D. Prestage, et.al., *Phys. Rev. Lett.* 54, 2387 (1985).
10. T.E. Chupp, et.al., *Phys. Rev. Lett.* 63, 1541 (1989).
11. J. Leitner and S. Okuba, *Phys. Rev.* 136, B1542 (1964.)
12. J.E. Moody and F. Wilczek, *Phys. Rev D* 30, 130 (1984).
13. C.H. Hsieh, et.al., *Mod. Phys. Lett.* A4, 1597 (1989).
14. D.J. Wineland and N.F. Ramsey, *Phys. Rev. A* 5, 821 (1972).
15. S.K. Lamoreaux, et.al., *Phys. rev. Lett.* 59, 2275 (1987).
16. K.F. Smith, et.al., *Phys. Lett. B* 234, 191 (1990).
17. S.A. Murthy, et.al., *Phys. Rev. Lett.* 63, 965 (1989).
18. D. Cho, K. Sangster, and E.A. Hinds, *Phys. Rev. Lett.* 63, 2559 (1989).
19. C. Carlberg, et.al., *Proc. 12th International Conf. on Atomic Physics* (Ann Arbor, MI, July 29-August 3, 1990).

DARMSTADTON HUNTING IN Υ -CRYSTAL INTERACTION

NA46 Collaboration

G.Bassompierre,D.Boget,J.Dufournaud,M.Gouanère,M.Richard,D.Sillou and M.Spighel,
LAPP(Annecy)

M.Chevallier,B.Farizon-Mazuy,M.Farizon,M.J.Gaillard,R.Genre,B.Ille,R.Kirsch and
P.Lautesse,I.P.N.(Lyon)

G.Bologna¹,E.Botta,S.Costa³,A.Feliciello²,R.Garfagnini²) and E.Rossetto,(Torino)

presented by

Michel Gouanère

LAPP 74019 Annecy-le-Vieux (France)

**ABSTRACT:**

Preliminary results from the experiment NA46 at the CERN SPS are presented. The (e^+e^-) mass spectra give indications for a mass at 2.2 Mev $\tau \approx 2 \cdot 10^{-13}$ s (4σ) and a mass at 10.1 Mev $\tau \approx 10^{-13}$ s (3σ). A mass at 3.4 Mev with $\tau \approx 3 \cdot 10^{-12}$ s would fit the observed remaining events between 3.2 and 7.4 Mev.

A limit for the observation of the 1.8 Mev mass seen at Darmstadt is given.

¹)Istituto di Fisica Generale,²)I.N.F.N.,³)Dip.di Fisica Sperimentale

The experimental observation of correlated e^+e^- peaks obtained in heavy ion collisions has been interpreted as the decay of an hypothetical neutral object at a mass of 1.8 Mev [1] having an extended size of ≈ 1000 fermi [2] and therefore escaping to sensitive beam dump experiments.

Its observation in the interaction of photons in a crystal has two distinctive advantages (as already discussed in [3]&[4]): - i) the strong coulomb field, if it is the clue of the production (there will be in the crystal a strong field of the same order of that involved in heavy ions collisions) - ii) the rather wide free space between the crystal rows; the extended size of this object does not make its detection so difficult as in the case of ordinary matter: it will have the possibility to escape out of a crystal before decaying.

We report here on the preliminary results obtained by the experiment NA46 carried out at CERN SPS, in the interaction of γ (≈ 100 Gev) on a Ge crystal $\langle 110 \rangle$, $400 \mu\text{m}$, 100°K . The set-up is shown on Fig. 1. A beam of 150 Gev e^- of low divergence ($50 \mu\text{rad}$), with a diameter of 8 mm

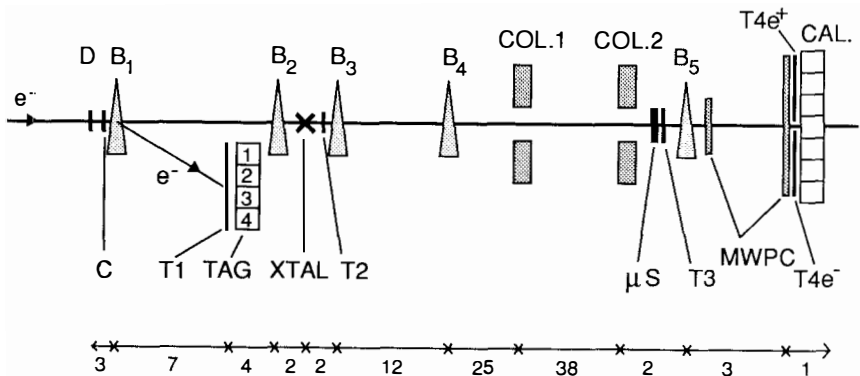


Fig 1. Experimental set-up. B1, B2, B3, B4, B5 = magnets; D, C, T1, T2, T3, T4 = scintillation counters; COL1, COL2 = collimators; μS = silicon μstrips ; CAL = lead glass calorimeter; "short lifetime" mode = B3 "off", B4 "off" "long lifetime" mode = B3 "on", B4 (160 Gauss-m). Distances in meters

is incident on a lead converter 0.5 mm thick. The resulting photons are tagged by the e^- bent by the magnet B1. A further magnet B2 is used to clean up the beam from all remaining charged particles. The photons encounter a Ge $\langle 110 \rangle$ crystal $400 \mu\text{m}$ thick where they produce e^+e^- pairs and possibly new neutral particles. The production of Bethe-Heitler e^+e^- pairs and the pair creation in strong field have already been studied using a similar set-up [5]. The e^+e^- pairs travel in a vacuum pipe ≈ 78 meters long and under a residual magnetic field of less than 20 mGauss obtained by a μ metal shielding. They pass through a vacuum mylar window $100 \mu\text{m}$ thick and are detected by a set of

silicon μ strips $20 \times 20 \text{ mm}^2$ wide with a pitch of $50 \mu\text{m}$. The energy of each e^+ and e^- is measured by an analysing magnet B5 in a set of MWPC, and then absorbed in a lead glass detector where they are subsequently identified. A "short lifetime" mode is defined by the magnets B3 "off" and B4 "off". A "long lifetime" mode is defined by the magnets B3 "on" (used to sweep out all pairs produced in the crystal) and the magnet B4 "on" working with a small field (160 Gauss-m) in order to limit the decay path: the mass measurement has thus to be corrected for the deviation.

The invariant mass is reconstructed using the separation in the μ strips, the momentum of e^+ and e^- , and assuming a decay length of 78 m for the "short lifetime" mode and 70 m for the "long lifetime" mode. The overall relative mass resolution is $\sigma=4\%$ for the "short lifetime" mode.

The mass spectrum of e^+e^- pairs obtained for a run of 10 hours ($10^4 \gamma/\text{burst}$) in the "short lifetime mode" is shown on Fig.2. It shows a wide spectrum due to the "normal" production of e^+e^-

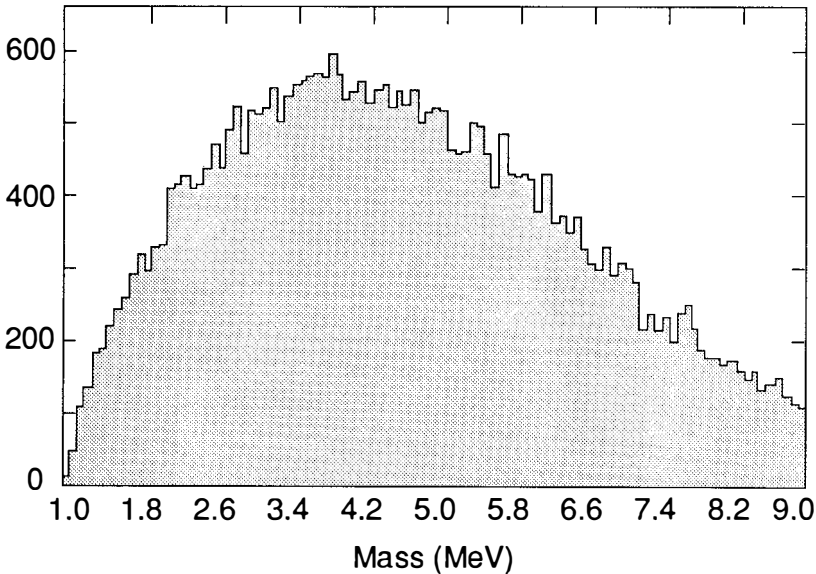


Fig 2. (e^+e^-) mass spectrum in "short lifetime" mode.

pairs in the crystal enlarged by the multiple scattering. This is in agreement with previous calculations.

In order to improve the sensitivity to extra signals, we use the distribution of the distance between e^- and e^+ in the horizontal plane (Fig 3). This distribution is not symmetric, due to a possible slight tilt ($20 \mu\text{rad}$) of the crystal, which does not change much the alignment for strong field ($200 \mu\text{rad}$). This distribution shows that the e^- spot is slightly displaced to the right and the e^+ one to the left. It could be used to enrich a signal from a possible neutral mass decay after the crystal (this neutral mass is assumed to have a symmetric distribution around the beam direction). This is obtained in Fig.4

where a cut off at $Y(e^-) - Y(e^+) > 0$ is applied. A signal at 2.2 Mev is then obtained with a statistical significance of 4σ . It should be pointed out that this signal is not a result of the above cut off. This is shown by a Monte Carlo calculation of the spectrum shape (Fig.4). The same spectrum is shown on

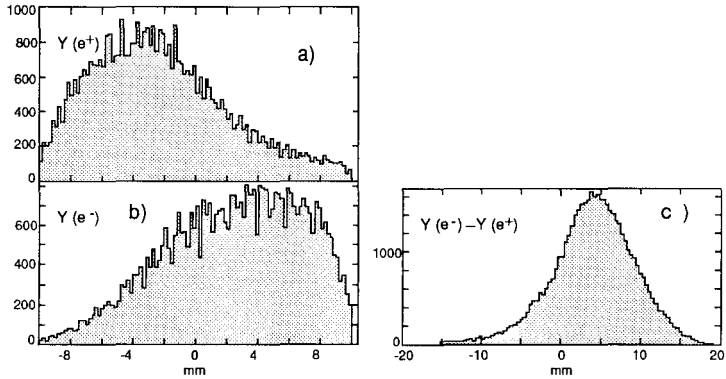


Fig 3. Histograms of the μ strips hits in the horizontal plan : 3a) $Y(e^+)$; 3b) $Y(e^-)$; 3c) $Y(e^-) - Y(e^+)$, i.e. difference between e^- hit and e^+ hit.

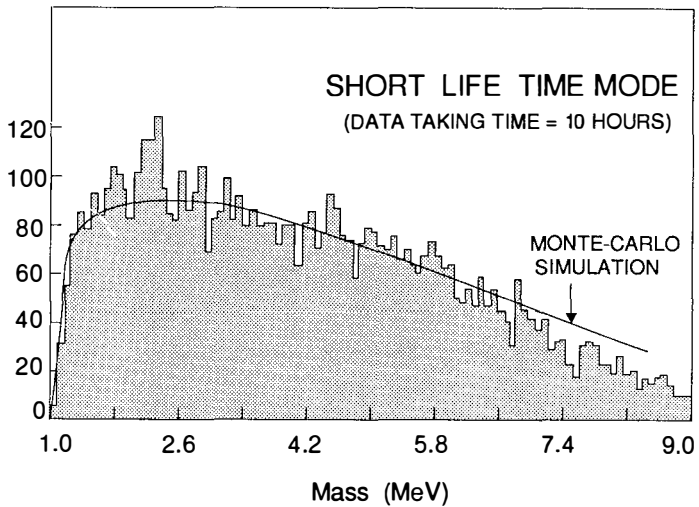


Fig 4. (e^+e^-) mass spectrum in "short lifetime" mode after a cut off at $Y(e^-) - Y(e^+) > 0$.

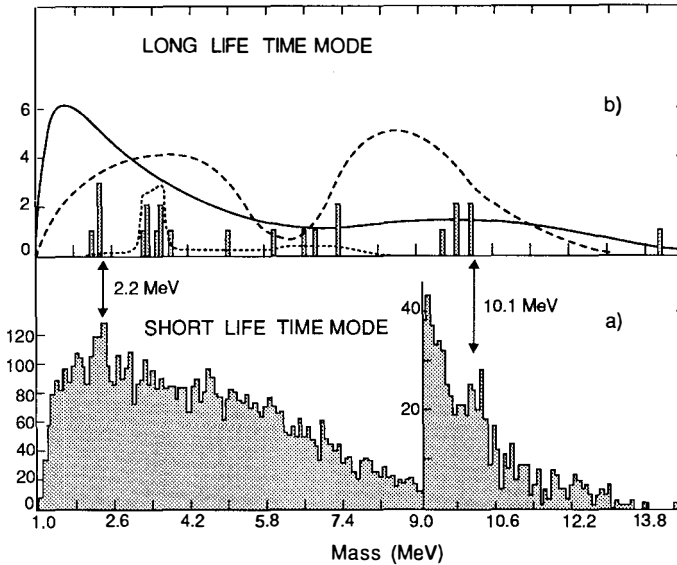


Fig 5. (e^+e^-) mass spectra :5a)"short lifetime" mode as Fig 4 ;5b)"long lifetime" mode [full line=mass acceptance; dashed line= $\times 100$ double bremsstrahlung background; dotted line= $\times 2$ spectrum of a 3.4 Mev (e^+e^-) mass with $\tau=3.10^{-12}$ s decaying before or after the magnet B4].

Fig.5a together with the high part of the spectrum. This region of more limited statistic shows another signal at 10.1 Mev, with a statistical significance of 3σ .

Fig.5b shows the spectrum obtained in the "long lifetime" mode after a run of 30 hours. The background coming from interactions with the vacuum residual gas is negligible. The background coming from interactions with the vacuum pipe and with the collimators is negligible. A more sophisticated kind of background comes from 2γ interactions in the detectors. These 2γ originate in the lead converter ("double bremsstrahlung") and produce $2(e^+e^-)$ pairs in the μ strips. Only one e^+ and one e^- are detected in the MWPC, the others are lost. This background was independently measured and calculated. It is estimated to be 3.5 events in Fig.5b. The mass spectrum shows again at 2.2 Mev a signal of 4 events in coincidence with the signal of Fig.5a, and a signal of 5 events in coincidence with the signal at 10.1 Mev of Fig.5a. The signals of Fig.5b taken alone would be of little statistical significance. However, when they are associated with the spectrum of Fig.5a, they are taken as an indication for the decay of a mass at 2.2 Mev with $\tau \approx 2 \cdot 10^{-13}$ s and a mass at 10.1 Mev with $\tau \approx 1 \cdot 10^{-13}$ s. We should notice that the remaining events between 3.2 Mev and 7.4 Mev could be interpreted as the decay of a mass at 3.4 Mev with a lifetime of $3 \cdot 10^{-12}$ s, some of which decay before the magnet B4 and some after, as represented on Fig.5b.

Ref.[6] [7] reported the possibility for mass values close to ours.

CONCLUSION:

In the interaction of 100 Gev photons with the strong field of a crystal ($\text{Ge}\langle 110 \rangle, 400 \mu\text{m}, 100 \text{ } ^0\text{K}$), we observed indications of the production of two neutral particles which decay into e^+e^- :

$$m_1 = 2.2 \text{ Mev} \quad \tau \approx 2 \cdot 10^{-13} \text{ s} \quad \text{"relative yield"} (m_1/e^+e^- \text{ pairs}) = 2 \cdot 10^{-3} \quad (4\sigma)$$

$$m_2 = 10.1 \text{ Mev} \quad \tau \approx 1 \cdot 10^{-13} \text{ s} \quad \text{"relative yield"} (m_2/e^+e^- \text{ pairs}) = 1 \cdot 10^{-3} \quad (3\sigma)$$

A possible further signal at 3.4 Mev with $\tau \approx 3 \cdot 10^{-12} \text{ s}$ is seen in "long lifetime" only.

The signal at 1.8 Mev seen at Darmstadt correspond in our "short lifetime" mode to a 2.4σ signal only, ≈ 30 times lower than the signal seen at Darmstadt. A diagram "lifetime/relative yield" is shown on Fig.6 for both mode of operation. The Bhabha scattering limit seems to exclude a large region of the plot, living "relative yield" $< 10^{-4}$ and $7 \cdot 10^{-12} \text{ s} < \tau < 10^{-10} \text{ s}$. However the Bhabha scattering limit is controversial for such an exotic object.

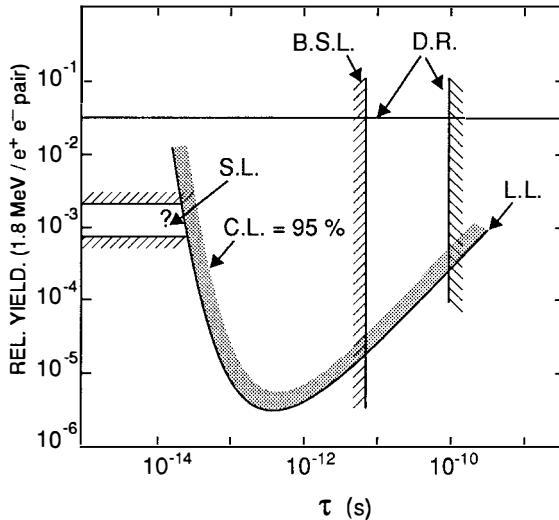


Fig 6. Lifetime and "relative yield" of the "Darmstadton" (1.8 Mev). [L.L. = "long lifetime" mode ; S.L. = "short lifetime" mode ; B.S.L. = bhabha scattering limit ; D.R. = Darmstadt results].

REFERENCES:

- [1] P. Salabura et al., Phys.Lett.B 245(1990)153
- [2] A. Schafer, J.Phys.G 15(1989)373
- [3] G. Bassompierre et al. CERN Proposal SPSC 88-50(1988)
- [4] J. Augustin et al., Z.Phys.A 336(1990)353
- [5] A. Belkacem et al., Phys.Rev.Lett. 58(1987)1196
- [6] M. El-Nadi et O.E. Badawy, Phys.Rev.Lett. 61(1988)1271
- [7] F.W.N. de Boer and R. van Dantzig, Phys.Rev.Lett. 61(1988)1274

TESTING BELL'S INEQUALITIES

Alain Aspect

Collège de France et Ecole Normale Supérieure¹



The author (on the left) with John Bell at the Kastler Symposium in Paris in 1985

John Bell was scheduled to participate to these Rencontres de Moriond. Unfortunately, he died a few weeks before this meeting. I decided then that my way of rendering an homage to this great physicist would be to talk about what I know best in his work, i.e., Bell's Inequalities and the experimental work based on these inequalities. The text presented below is very close to the one that I have prepared for the special issue of Europhysics News, on John Bell and Quantum Mechanics (issue of April 1991).

It is a great privilege, in these sad circumstances, to have the opportunity to recount the great influence John Bell had on my life as a physicist. Testing Bell's inequalities was more than a run-of-the-mill experiment. Indeed, when I read the paper "On the Einstein-Podolsky-Rosen paradox"², I found it extremely clear and completely convincing, but there was something special about this paper: it led to two contradictory conclusions. The first part showed that EPR correlations predicted by quantum mechanics are so strong that one can hardly avoid the conclusion that quantum mechanics should be completed by some supplementary parameters (the so-called "hidden-variables"). But the second part, elaborating on this result, demonstrated that the hidden-variables description in fact contradicts some predictions of quantum mechanics, which is to say both theories predict different results. In the face of these two perfectly convincing and contradictory conclusions, there is only one way out: ask Nature how it works.

The big surprise was the realization that, at the end of the sixties, there was no experimental result to answer the question. The contradiction discovered by John Bell is so subtle that it appears only in very peculiar situations that had not been investigated: it was therefore necessary to design and build specific experiments.

Bell's Theorem

1. Hidden variables

The reasoning behind Bell's theorem deals with correlations between events, each of which appears to be random. Such correlations may arise outside physics. Take, for instance, the occurrence of some well defined disease and let us assume that biologists have observed its development in 50% of the population aged 20, and its absence in the remaining half. Now, on investigating specific pairs of (true) twin brothers, they find a perfect correlation between the outcomes: if one brother (or sister) is affected, the other is also found to be afflicted with the disease; but if one member of the pair has not developed the disease, then the other is also unaffected. In face of such a perfect correlation for twin brothers, the biologists will certainly conclude that the disease does have a genetic origin. They may invoke a simple scenario: at the first step of conception of the embryo, a (random) genetic process produced a chromosome sequence - one which is responsible for the occurrence, or absence, of the disease - that has been duplicated and given to both brothers.

An EPR situation is a case where quantum mechanics predicts strong correlations of this type. Consider, for instance, the situation illustrated in Figure 1 where a source emits a pair of photons n_1 and n_2 , travelling in opposite directions. Each photon impinges onto a polarizer which measures the linear polarization along the direction (**a** or **b**) determined by the orientation of the corresponding polarizer. There are two possible outcomes for each measurement, and these we can label + and -. Quantum mechanics allows for the

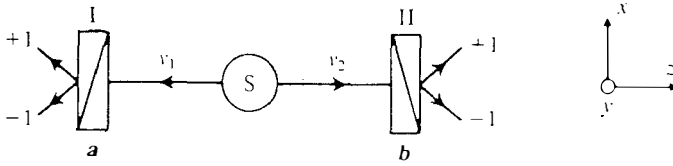


Fig. 1 : Einstein-Podolsky-Rosen Gedankenexperiment with photons. The source S emits pairs of photons n which are analyzed in polarisation in two directions (\mathbf{a} and \mathbf{b}). In an EPR situation the results of the measurement of polarizations are found to be strongly correlated.

existence of a two photon state (EPR state)

$$|\psi(v_1, v_2)\rangle = 2^{1/2} \{ |x, x\rangle + |y, y\rangle \}$$

for which the polarization measurements taken separately appear random but which are strongly correlated. More precisely, denoting $P_+(\mathbf{a})$ and $P_-(\mathbf{a})$ as the probabilities that the polarization of n_1 along \mathbf{a} is found equal to + or - , these probabilities are predicted to be

$$P_+(\mathbf{a}) = P_-(\mathbf{a}) = 0.5$$

Similarly the probabilities $P_+(\mathbf{b})$ and $P_-(\mathbf{b})$ for photon n_2 are equal to 0.5 and independent of the orientation \mathbf{b} .

On the other hand, the joint probability $P_{++}(\mathbf{a}, \mathbf{b})$ for observing + for both photons is equal to

$$P_{++}(\mathbf{a}, \mathbf{b}) = 0.5 \cos^2(\mathbf{a}, \mathbf{b})$$

and the other possible joint events have probabilities

$$P_{--}(\mathbf{a}, \mathbf{b}) = 0.5 \cos^2(\mathbf{a}, \mathbf{b})$$

$$P_{+-}(\mathbf{a}, \mathbf{b}) = 0.5 \sin^2(\mathbf{a}, \mathbf{b})$$

$$P_{-+}(\mathbf{a}, \mathbf{b}) = 0.5 \sin^2(\mathbf{a}, \mathbf{b})$$

In the case of parallel polarizers [$(\mathbf{a}, \mathbf{b}) = 0$], these joint probabilities are

$$P_{++}(0) = P_{--}(0) = 0.5$$

$$P_{-+}(0) = P_{+-}(0) = 0$$

The results for the two photons of the same pair are thus always identical, both + or both - , i.e., they are completely correlated. The situation is thus exactly analogous to the

case for the twin brothers, and it seems natural to link these correlations to some common property of the two photons of a pair, analogous to the common genome of the two twin brothers. This common property changes from pair to pair, which accounts for the random character of the single events.

The above reasoning constitutes the first part of John Bell's paper. A natural generalization of the EPR reasoning, it leads to the conclusion that quantum mechanics is not a complete description of physical reality. Indeed, invoking some common property which changes from pair to pair, we claim that the complete description of a pair must include something, in addition to the state vector which is the same for all pairs. This something can be called *supplementary parameters*, or *hidden variables*. At this stage, these hidden variables are supposed to be able to render an account of the correlations between both measurements, for any set (\mathbf{a}, \mathbf{b}) of orientations.

2. Inequalities

The second part of Bell's reasoning starts from this requirement for hidden variables. Assuming their existence and some very natural properties, one can show that the expected correlations, for the joint measurements above, cannot take any set of values, but that they are subject to certain constraints. More precisely, let us denote

$$E(\mathbf{a}, \mathbf{b}) = P_{++}(\mathbf{a}, \mathbf{b}) + P_{--}(\mathbf{a}, \mathbf{b}) - P_{+-}(\mathbf{a}, \mathbf{b}) - P_{-+}(\mathbf{a}, \mathbf{b})$$

the correlation coefficient between the results of the measurements by the polarizers in orientations \mathbf{a} and \mathbf{b} . If we now consider four possible sets of orientations $[(\mathbf{a}, \mathbf{b}), (\mathbf{a}, \mathbf{b}'), (\mathbf{a}', \mathbf{b}), \text{ and } (\mathbf{a}', \mathbf{b}')]]$, the corresponding correlation coefficients, when calculated by any "reasonable" hidden-variables model, are restricted by the so-called *Bell's inequalities*³:

$$-2 \leq S_{HV} \leq 2$$

where

$$S = E(\mathbf{a}, \mathbf{b}) - E(\mathbf{a}, \mathbf{b}') + E(\mathbf{a}', \mathbf{b}) + E(\mathbf{a}', \mathbf{b}')$$

Now comes the crucial point: there exist sets of orientations for which the quantity S predicted by quantum mechanics, in the EPR situation presented above, violate Bell's inequalities. For instance, the most spectacular case happens for

$$(\mathbf{a}, \mathbf{b}) = (\mathbf{b}, \mathbf{a}') = (\mathbf{a}', \mathbf{b}') = 22.5^\circ \quad \text{and} \quad (\mathbf{a}, \mathbf{b}') = 67.5^\circ$$

in which case the prediction of quantum mechanics is

$$S_{MQ} = 2\sqrt{2} = 2.82$$

This clearly violates the inequality above.

The hidden-variables theories envisaged above are then unable to render an account of the EPR correlations predicted by quantum mechanics (these quantum mechanical correlations are not as easy to understand as the common medical fate of twin brothers).

In the face of this contradiction, J. Bell made clear the reasonable properties that he had assumed for the hidden-variables models. The essential assumption, absolutely necessary to obtain a conflict, is *locality*: this assumption states that the result of a measurement by a polarizer cannot be directly influenced by the choice of the orientation of the other, remotely located, polarizer. This assumption indeed sounds very reasonable. Moreover, it can be considered to be consequence of Einstein's causality, by considering an experiment in which the settings of the polarisers can be changed at random in a time short compared to the time light takes to propagate between the two polarisers.

Of the many papers that followed Bell's paper, we will extract the conclusion that Bell's inequalities apply to a wider class of theories than local hidden-variable theories. Any theory in which each photon has a "physical reality" localized in spacetime, determining the outcome of the corresponding measurement, will lead to inequalities that sometimes conflict with quantum mechanics. Bell's theorem can thus be phrased in the following way: *Some quantum mechanical predictions (EPR correlations) cannot be mimicked by any local realistic model in the spirit of Einstein's ideas.*

First experiments⁴

When the physicists realized the wide generality of Bell's theorem, they met with a great surprise: at the end of the sixties, there was no experimental result available for testing Bell's inequalities *versus* quantum mechanics. Indeed, most predictions of quantum mechanics are compatible with Bell's inequalities. Moreover, in the case where a conflict is predicted (as above) one finds that taking into account the inefficiencies of a real experiment usually reduces the degree of correlation predicted by quantum mechanics, so that there is no longer any conflict. The possibility then arose that the conflict with Bell's inequalities may indicate a place to look for a limit of validity of quantum mechanics.

It was therefore tempting to perform a sensitive experiment for a situation where quantum mechanics predicts a conflict with Bell's inequalities. In order to have such a

situation, several conditions must be fulfilled:

- the creation of a pair of systems in a non-factorable (entangled) quantum state of the EPR type;
- the ability to perform two-valued measurements on each system;
- the disposal of an adjustable parameter for these measurements so that different values of this parameter correspond to non-commuting observables.

The first experimental test was based on pairs of γ photons produced in the *annihilation of positronium*. This would be an ideal system, except for the fact that there is no polarizer making a two-valued measurement at this energy: the polarization is then inferred from a Compton scattering, by calculations relying on the quantum theory. The test is thus indirect, and somewhat circular. The first measurements gave contradictory results, but in the mid-1970's clear agreement with the quantum mechanical predictions was established.

An experiment based on *pairs of protons* obtained by scattering had the same problem (no two-valued measuring apparatus). This experiment was carried out at Saclay in 1976 by Lamehi-Rachti and Mittag. It gave a result in agreement with quantum mechanics.

The system best able to fulfill the above conditions uses *pairs of visible photons* produced in well chosen atomic radiative cascades. As a matter of fact, for visible light there exists polarizers, *e.g.*, based on birefringent crystals, with two output channels and an adjustable orientation. The first three experiments, carried out in the early seventies, in Berkeley and in Harvard, gave a relatively small signal and some results were contradictory; however, the trend was in favour of Quantum Mechanics. By introducing a laser to excite the cascade, the fourth experiment gave a convincing result in agreement with quantum mechanics. For practical reasons, all these early experiments used only one-channel polarizers, so once again the comparison of the experimental results with Bell's inequalities was indirect and relied on supplementary assumptions. However, they had given convincing indications in favour of quantum mechanics and they opened the way to second-generation experiments.

Closer to the gedankenexperiment

Thanks to the progress in lasers, we could design and build in the late seventies⁵ a much more efficient source of pairs of EPR photons correlated in polarization. We used the same radiative cascade in calcium-40 as employed in the first experiment by Clauser and Freedman⁴, but now we could selectively excite the upper level of the cascade with two-photon absorption. As a consequence, the light emitted by our source was very pure, encompassing only photons of the desired pairs. Very important also was the very high emission rate which allowed us to achieve a 1% statistical accuracy for joint detections within only hundred seconds (a similar level of accuracy required hours in the previous experiments).

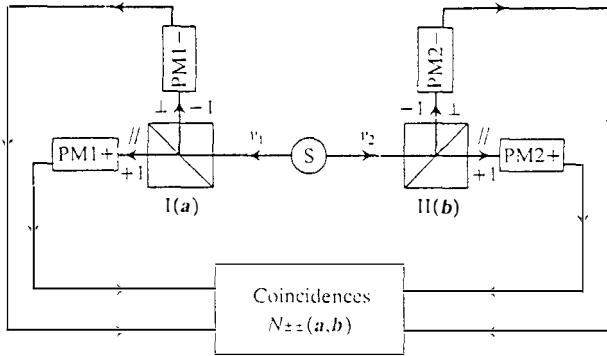


Fig. 2 : Experiment with two-channel polarizers. Using a four-fold coincidence system we obtain directly the polarization correlation coefficient in the orientations (\mathbf{a}, \mathbf{b}) . Note the close similarity with Fig. 1.

A first experiment based on the same scheme as the previous ones (with one channel polarizers) gave a clear-cut result in agreement with quantum mechanics. Meanwhile, we had obtained (from the Phillips Leseach Laboratory) two-channel polarizers based on multielectric coatings. Figure 2 shows the experimental set-up, very close to the ideal one of Figure 1. Using a four-fold coincidence system it was possible to monitor simultaneously the four coincidence rates corresponding to the + and - results. This yields directly, without any auxiliary calibration, the joint detection probabilities in a given set of orientations (\mathbf{a}, \mathbf{b}) , from which we derive the correlation coefficient. By repeating the measurement in different orientations, we can test directly Bell's inequalities.

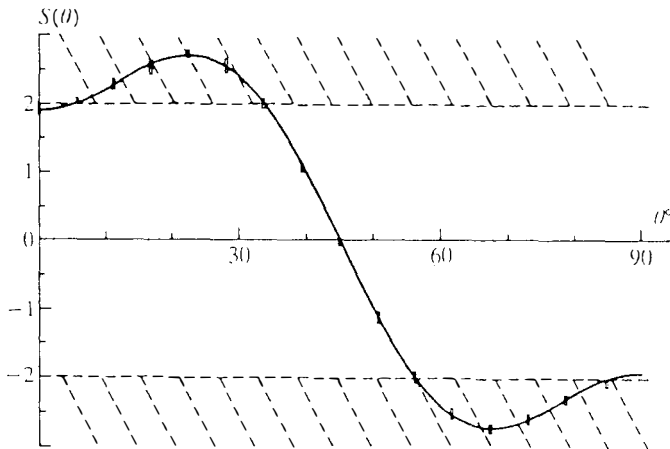


Fig. 3 : The results of the experiment of Fig. 2. The quantity S is a function of the correlation coefficients and should lie between -2 and 2 according to Bell's inequalities. The solid curve is the prediction of quantum mechanics taking into account the inefficiencies of the apparatus.

The results are shown in Figure 3. We have plotted, as a function of the angle θ , the quantity S which is subject to the Bell's inequalities:

$$-2 \leq S_{HV} \leq 2$$

There are obviously angles for which one of the Bell's inequalities is violated. The maximum violation corresponds to a value

$$S_{\text{exp}} = 2.70 \pm 0.015$$

that is to say a violation by more than 40 standard deviations. Note that this value, slightly different from the ideal quantum mechanical prediction of 2.82, is in fact in perfect agreement with the quantum mechanical calculation taking into account the finite size of the solid angles, the inefficiencies of the polarizers, and other features of a real experiment.

In spite of its close resemblance to the ideal experiment, the actual experiment suffers from one remaining problem : owing to the limited efficiency of the photon detectors, a comparison with Bell's inequalities requires the assumption that the detected photons constitute a faithful sample. Nevertheless, the result in favour of quantum mechanics and against local hidden-variables theories is very convincing .

Testing locality

As already emphasized, the locality condition is essential to obtain Bell's inequalities. But, as stressed by J. Bell², in an experiment of the type described above, "the settings of the instruments are made sufficiently in advance to allow them to reach some mutual rapport by exchange of signals with velocity less than or equal to that of light", in which case the locality condition does not apply. We have thus tried to realise a scheme "in which the settings are changed during the flight of the particles", so that locality be a consequence of Einstein's causality (no interaction can propagate faster than light).

In fact, we have only partially realized this programme. First, we do not in practice change the setting of a polarizer but we instead replace each polarizer with a system involving a switch that is able to redirect the light towards one of two polarizers in two different orientations (Fig. 4). Such a system is equivalent to a single polarizer switched between two orientations. The time between two changes is 10 nanoseconds, shorter than the time of flight of the photons (20 nanoseconds, corresponding to six meters). Unfortunately, the switches (based on the interaction with an acoustic standing wave) did not work at random, but periodically. This is far from ideal, even if the two switches are driven by independent generators at different frequencies.

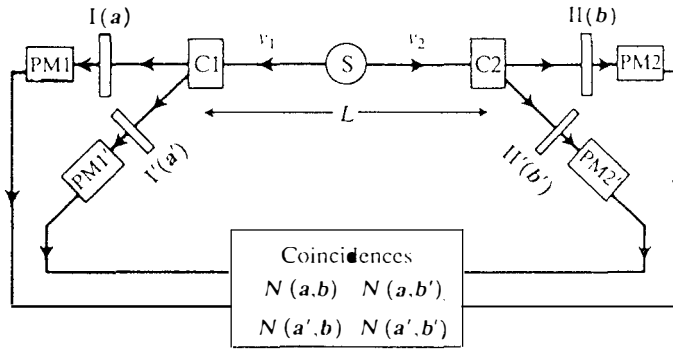


Fig. 4 : The experiment with optical switches. The switch $C1$ with the two polarizers I and I' is equivalent to a single polarizer changed from orientation a to orientation a' . The time between changes is shorter than the time of flight of the light.

Owing to the complication of the systems, the signal was smaller than in the static experiment of Fig. 3, and the results were not as precise. We nevertheless obtained a significant violation of Bell's inequalities by five standard deviations, and a good agreement with quantum mechanics. The level of confidence of this result is not as high as in the experiment of Fig.2, so it would be very interesting to perform another experiment of the same type. This might be done with one of the new sources of pairs of photons produced in parametric down-conversion⁶, which should eventually give better results than our source.

The Non-Locality Heritage

Let us assume that quantum mechanics will work also in ideal experiments with no inefficiencies present. In the words of John Bell⁷: "It is difficult for me to believe that quantum mechanics, working very well for currently practical set-ups, will nevertheless fail badly with improvements in counter efficiency and other factors...". What can we conclude? We cannot do better than let J. Bell explain possible attitudes:

- "There are influences going faster than light, even if we cannot control them for practical telegraphy. Einstein local causality fails, and we must live with this."
- "The orientations a and b are not independently variable as we supposed. Whether apparently chosen by apparently independent radioactive devices, or by apparently separate Swiss National Lottery machines, or even by different apparently free-willed experimental physicists, they are in fact correlated with the same causal factors as the A and B (the outcomes of the measurements). Then Einstein causality can survive. But apparently separate parts of the world become deeply entangled, and our apparent free will is entangled with them."

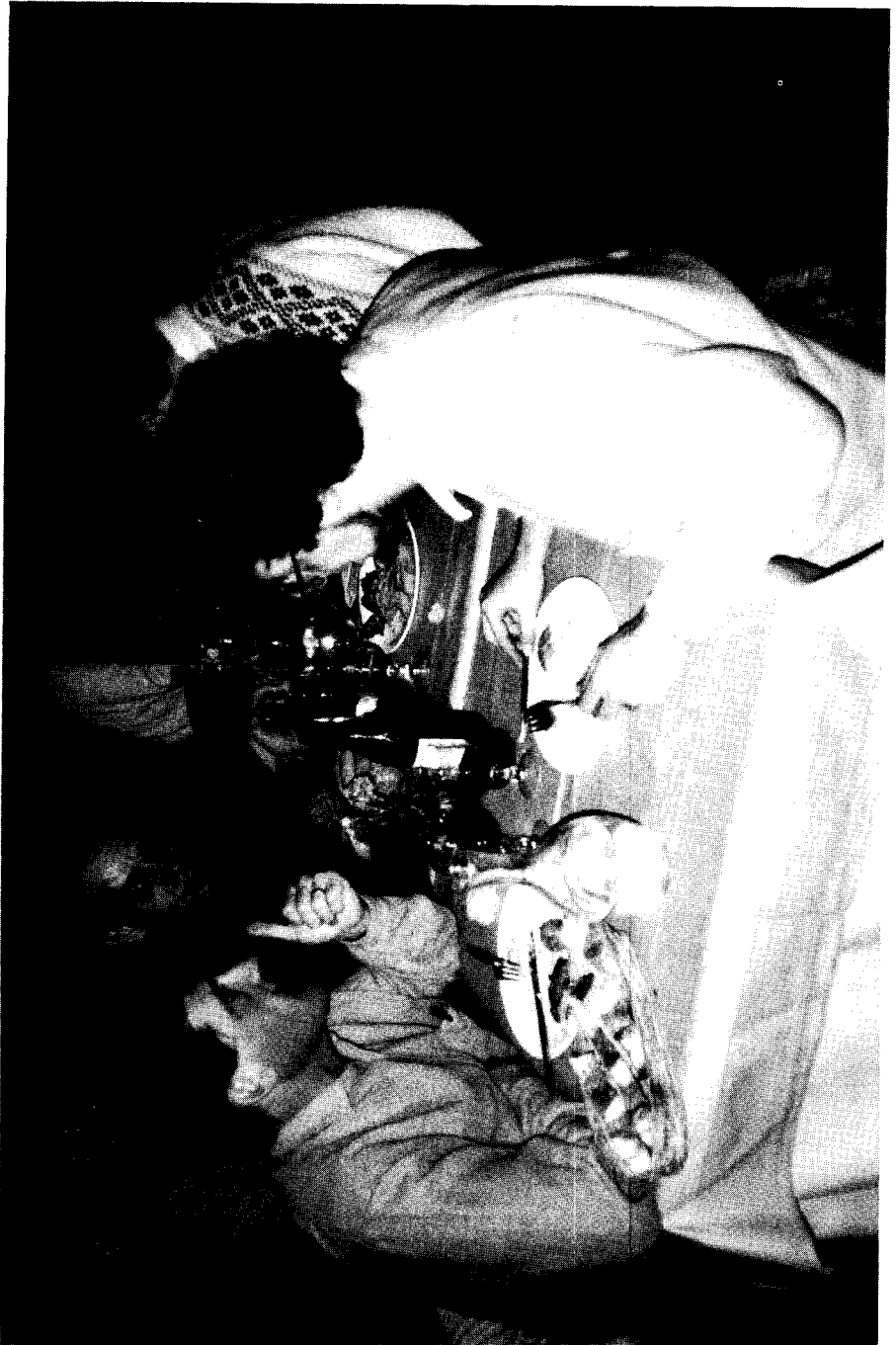
- *"The whole analysis can be ignored. The lesson of quantum mechanics is not to look behind the predictions of the formalism. As for the correlations, well, that's quantum mechanics."*

J. Bell repeatedly made it clear that the last attitude was not his. He would not have accepted to renounce raising difficult questions. The first attitude was apparently his favorite; like the second, it leaves us with a world, the various parts of which may be deeply entangled. After John Bell, we can no longer ignore that the quantum physical reality is somewhat non-local.

Notes and References

1 *Laboratoire de Spectroscopie Hertzienne de l'ENS, associé au CNRS et à l'université Pierre et Marie Curie (Paris 6), 24 rue Lhomond, 75005 Paris*

- 2 J. S. Bell, *Physics* 1 (1964), 195-200. As the other papers by J.Bell on the foundations of quantum mechanics, this paper may be found more easily in:
J.S. Bell, *Speakable and unspeakable in quantum mechanics*, *Collected papers on quantum philosophy* (Cambridge University Press, 1987).
- 3 Rather than the original form of the Bell's inequalities, we use this form, easier to compare to the experimental results presented below, and derived first by
J.F. Clauser, M.A. Horne, A. Shimony, and R.A. Holt, *Phys. Rev. Lett.* 37 (1965),465.
- 4 Good reviews of the situation in 1978 are given in : J.F. Clauser and A.Shimony, *Rep. Progr. Phys.* 41 (1978),1881;
F.M. Pipkin, *Avances in Atomic and Molecular Physics* 14 (1978), 281 (Academic Press, New York).
- 5 These experiment were carried out between 1978 and 1982 at the Institut d'Optique d'Orsay (Université Paris Sud) with Philippe Grangier, Gérard Roger, and Jean Dalibard.
See *e.g.*: *Atomic Physics* 8 (1983, Plenum Press), 103.
- 6 Y.H. Shih and C.O. Alley, *Phys. Rev. Lett.* 61 (1988), 2921;
Z.Y. Ou and L. Mandel, *Phys. Rev. Lett.* 61 (1988), 50;
J.G. Rarity and P.R. Tapster, *Phys. Rev. Lett.* 64 (1990), 2995.
- 7 J.S. Bell, *Comments on Atomic and Molecular Physics* 9 (1980), 121.



**Kamiokande II Results on Solar Neutrinos
and
The SuperKamiokande Experiment**

Yoichiro SUZUKI*

Institute for Cosmic Ray Research, University of Tokyo,
3-2-1, Midoricho, Tanashi, Tokyo 188, Japan

Abstract

A clear directional correlation of solar neutrino-induced events was observed. The measured ^8B -solar neutrino flux relative to the calculation based on the standard solar model are $0.46 \pm 0.05(\text{stat}) \pm 0.06(\text{syst})$ times the prediction of Bahcall and Ulrich, and $0.70 \pm 0.08(\text{stat}) \pm 0.09(\text{syst})$ times the prediction of Turck-Chieze et al. The shape of the recoil electron energy distribution is consistent with that expected from the production of the known shape of the neutrino flux, and the cross section of the $\nu_e e \rightarrow \nu_e e$ interaction.

Time variations of the solar neutrino flux were studied during the time periods over three years. No significant correlation with the variation of the sun spot number was obtained.

Short time variations such as the day and night time difference and the semi-annual variation were also studied.

1. Introduction

Solar neutrinos produced by the nuclear reactions in its central region probe interior of the sun and provide a sensitive test of solar models. They also provide a means of searching for intrinsic properties of neutrinos through the interaction with the solar matter, the very long distance to the earth and a coupling to the sun's magnetic field [1][2][3].

Kamiokande II, an imaging water Cherenkov detector, has been operating with an electron energy threshold low enough to detect ^8B solar neutrinos. The solar neutrinos are detected in this detector through the neutrino-electron elastic scattering which preserves the direction of incident neutrinos within an angular resolution mainly limited by the multiple coulomb scattering of the recoiling electrons.

Measurements of ^8B solar neutrinos were carried out on 1040 days of data, taken from January 1987 through April 1990 [4]. The data sets are divided into two periods at June 1988 when the gain of PMT's were doubled.

The data taking has stopped in April 1990 for the dead phototube replacement, installation of new electronics and to place reflective mirrors surrounding the PMT. The experiment resumed in December 1990. We call this phase of the experiment as Kamiokande III. Fig. 1 shows the time table of the Kamiokande II, III and the SuperKamiokande of which the construction has been officially approved and will start in JFY 91 (starts from April). The SuperKamiokande experiment is scheduled to begin at 1996.

The energy threshold of the experiment is influenced by the contamination of the radio-active background in the water, mainly ^{222}Rn . For the initial stage of the experiment, the background was too

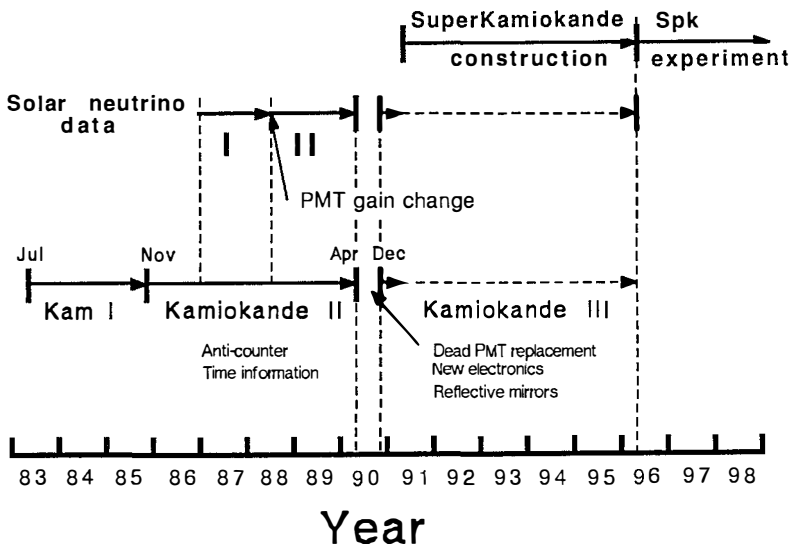


Fig. 1. Past, Present and future of the Kamiokande experiment.

high to permit observation of solar neutrinos. The observation of the solar neutrinos has started January 1987 after the effort to seal the detector and improving the water-purification system. After the gain change we have succeeded to further reduce the background, and consequently reduced the electron energy threshold used for the data analysis. Dependence of the energy threshold on time during the time period January 1987 through April 1990, is shown in Fig 2.

Events are subjected to the following reduction processes; a fiducial cut, a spallation cut and a remaining gamma cut. The fiducial volume cut reject γ and neutron induced backgrounds entering from outside of the detector. The remaining gamma cut further reduced those backgrounds. Backgrounds from the muon induced spallation products were reduced by the spallation cut making use of the space and time correlation with the preceding muons. The reduction of the events at each step is shown in Fig 3. Details of these analysis steps and the discussion of the background can be found in reference 5.

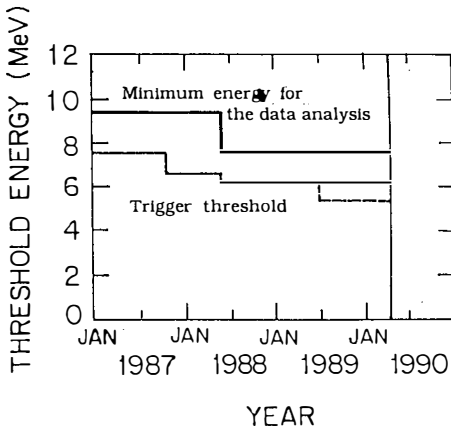


Fig. 2. Dependence of the electron energy threshold on time during the period January, 1987 through April, 1990, indicating the improvement in sensitivity in that period. Also shown is dependence of the minimum energy for the data analysis.

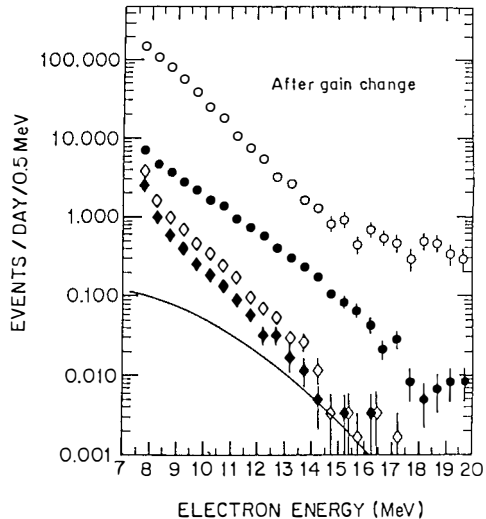


Fig. 3. Event rates as a function of total electron energy for all events, events in the fiducial volume, fiducial volume events after the spallation cut, and after the remaining gamma-ray cut. (After the gain change.)

2. The solar neutrino flux

Fig. 4 shows $\cos\theta_{\text{sun}}$ distribution with a common threshold of $E_e > 9.3 \text{ MeV}$ for the final data sample from 1040 days of running time. $\cos\theta_{\text{sun}} = 1$ corresponds to the direction from the sun to the earth. The solid line gives the shape of the signal expected from a MC simulation and the dashed line shows the best fit for the data. The final solar

neutrino event rate is ~ 0.5 events/day for $E_e > 7.5$ MeV and the rate of the remaining background is ~ 5 events/day. The signal to the background ratio is ~ 1 taking the data above $\cos\theta_{\text{sun}} > 0.8$.

A maximum likelihood method using both the angle and energy information of each event was adopted to obtain the neutrino flux. The obtained solar neutrino flux is $0.46 \pm 0.05(\text{stat}) \pm 0.06(\text{syst})$ times that of Bahcall and Ulrich[6], and $0.70 \pm 0.08(\text{stat}) \pm 0.09(\text{syst})$ times the prediction of Turck-Chieze et al[7].

The recoil electron energy distribution is shown in Fig. 5. The energy distribution was made by performing the maximum likelihood method for the data in each energy bin.

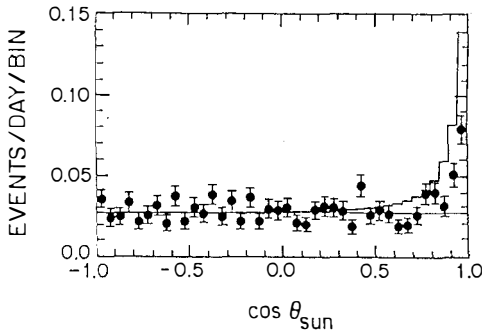


Fig. 4. Plot of the cosine of the angle between the electron direction and a radius vector from the Sun showing the signal from the Sun plus an isotropic background. This plot is for $E_e \geq 9.3$ MeV, and the time period January, 1987 through April, 1990, a total of 1040 live-detector days.

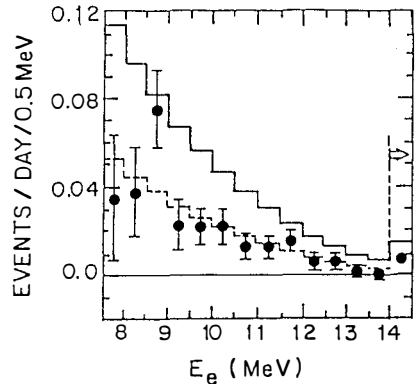


Fig. 5. Differential electron total energy distribution of the events produced by ${}^8\text{B}$ solar neutrinos. The point in the interval above 14 MeV is the sum of all events above 14 MeV. The dashed histogram is the best fit to the data of a Monte Carlo calculation based on the cross section, the known shape of the neutrino flux, and the energy resolution of the detector. The solid has the area predicted by the standard solar model of Bahcall and Ulrich.

3. Time variation and the correlation with the sun spot numbers

The flux of solar neutrinos supposed to be stable because the neutrinos are produced through the nuclear reactions in deep interior of the sun, depends on the central temperature and the density. Therefore, any evidence of a time variation indicates a neutrino property such as mass, magnetic-moment and so on. The sunspot number which rose steeply from a minimum value at the end of solar cycle 21 to peak of the solar cycle 22, around the end of 1989 to the beginning of 1990, reveal a variation of the solar magnetic-activity. In fig. 6(a), the sun spot numbers in each year is shown.

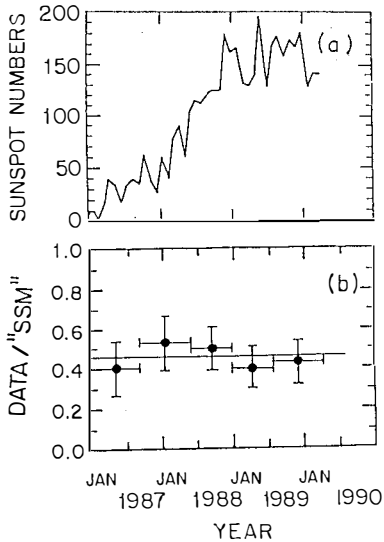


Fig. 6. (a) Plot of sunspot numbers vs time in the period 1987-1990. (b) Plot of the solar neutrino flux in 5 time intervals each of approximately 200 days from January, 1987 through April, 1990. The earliest two points are with $E_e \geq 9.3$ MeV, and the latest three points are with $E_e \geq 7.5$ MeV (after the gain change).

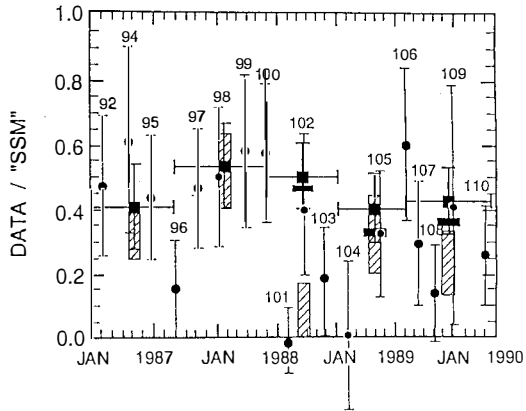


Fig. 7. Comparison of the time variation data of the ^{37}Cl and Kamiokande-II detectors during the period January, 1987 through April, 1990. The square points are the Kamiokande-II data; the round points are ^{37}Cl data for runs 92-110, except for run 93 which was restricted to a 17 day exposure in the search for neutrinos from SN1987A. The cross-hatched boxes are the weighted averages of the several ^{37}Cl runs corresponding in time to the time interval of a given Kamiokande-II data point. The solid rectangles are the values of the later three Kamiokande-II data points.

In order to test the time variation, especially the correlation with the sun spot number, the data were divided into five time period, each of ~ 200 live detector days shown in Fig. 6(b), which the plot using the all available data is shown. There found no significant time dependence. Comparison was made with the results from the ^{37}Cl experiment of Davis et al., covering the same time period where the Kamiokande is active. Fig 7 shows the flux of the both experiment.

No significant disagreement exists between the two data sets, other than the difference between the points in the last half of 1988.

4. Semi-annual variation [8]

When the detector views the center of the sun through the solar equator, where the magnetic field is expected to be weaker than at higher solar latitude. A semi-annual variation of the solar neutrino flux is then possible because the solar equatorial plane and the ecliptic plane cross with an opening angle of $7^\circ 15'$ twice a year (around June 7 and December 8). The data are divided into two periods as follows:

Period I : (April 22 - July 21) and (October 21 - January 20)

Period II : (January 21 - April 22) and (July 22 - October 20)

The effect of solar magnetic field on neutrinos emanating from the center of the sun is larger in the period II if neutrinos have a property

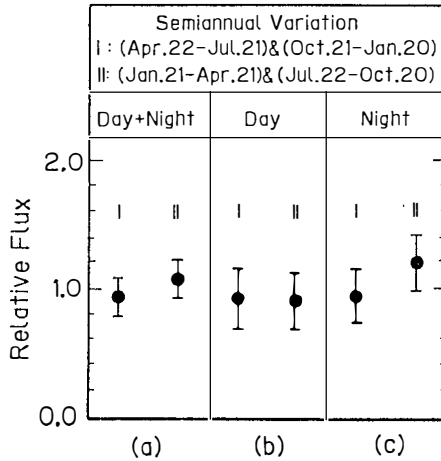


Fig. 8. Measured solar neutrino fluxed relative to the averaged value (0.46 relative to the SSM prediction); (a) periods I and II; (b) periods I and II, daytime; (c) periods I and II, nighttime.

influenced by a magnetic field. The measured flux relative to the averaged value for period I and II are $0.94 \pm 0.16(\text{stat.})$ and $1.06 \pm 0.15(\text{stat.})$, respectively as shown in Fig. 8. The relative difference is expressed by

$$\frac{(\text{period I} - \text{period II})}{(\text{period I} + \text{period II})} = -0.06 \pm 0.11(\text{stat.}) \pm 0.02(\text{syst.})$$

The fluxes from one month time periods around the times when the earth is nearest and farthest from the intersection are $0.71 \pm 0.27(\text{stat.})$ and $1.12 \pm 0.27(\text{stat.})$, respectively. Those results reveals no strong evidence on the neutrino magnetic property within our experimental sensitivity.

5. Day/Night Effect [8]

The regeneration effect of the solar neutrinos by the matter induced neutrino oscillation through the earth can be effectively tested by dividing the data according to the different path length and density profiles experienced by the neutrinos passing through the earth. The data are thus divided into six sub-samples based on $\cos\delta_{\text{sun}}$, which are $\cos\delta_{\text{sun}} < 0$ (daytime sample), and $\cos\delta_{\text{sun}} = 0-0.2, 0.2-0.4, 0.4-0.6, 0.6-0.8$, and $0.8-1.0$. The relative flux obtained is shown in Fig. 9.

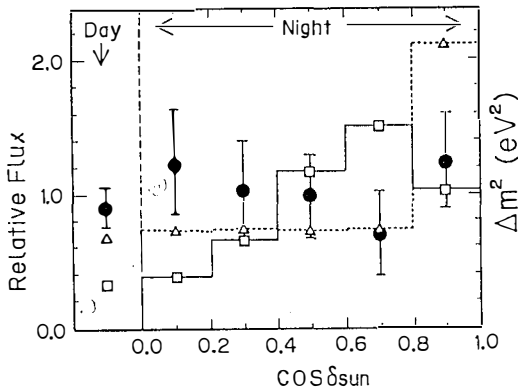


Fig. 9. Measured solar neutrino fluxes of daytime and subdivided nighttime relative to the averaged value (points). The horizontal axis ($\cos\delta_{\text{sun}}$) is the cosine of the zenith angle of the Sun relative to the z-axis of the detector. $\delta_{\text{sun}} = 0$ corresponds to the direction in which the Sun is just below the detector. The solid line histogram with open squares is the flux calculated for $\Delta m^2 = 3.5 \times 10^{-6} \text{ eV}^2$ and $\sin^2 2\theta = 0.11$; the dashed line histogram with open triangles for $\Delta m^2 = 7.9 \times 10^{-6} \text{ eV}^2$ and $\sin^2 2\theta = 0.05$.

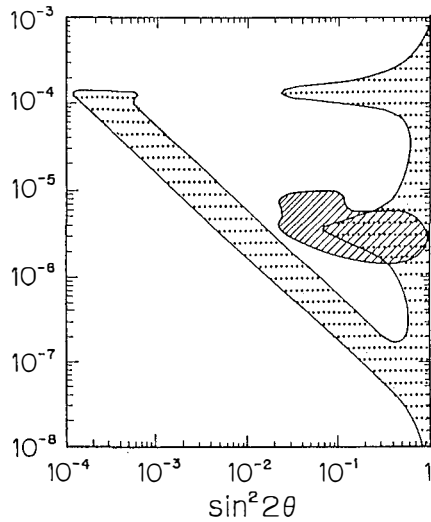


Fig. 10. Region excluded at 90% C.L. in the MSW Δm^2 - $\sin^2 2\theta$ space by the null day/night result (cross-hatched region). The dotted region shows the 90% confidence level contour for the "allowed" region which was obtained from the total flux and the recoil-electron energy spectrum, measured in the KAM-II detector.

The result of the neutrino oscillation analysis on the day/night flux differences is shown in Fig. 10. The region shown by hatched region is excluded.

6. The SuperKamiokande Experiment

The SuperKamiokande experiment is an imaging water Cherenkov detector containing 50,000 tons of water in the cylindrical tank of 41m high and 39m in diameter. It's fiducial volume is 22,000 tons, which allows us to study the instability of the matter in the range of the lifetime of 10^{34} years. The coverage of PMTs is doubled compared to the present Kamioka experiment upto 40% which improves the energy and position resolution. Consequently, it is possible to reduce the backgrounds and to lower the energy threshold down to 5 MeV. The major goals of the SuperKamiokande are precise study of the solar and supernova neutrinos, and a search for proton decay.

The high statistics solar neutrino signal of 30 events/day for 46% of the prediction of the standard solar model is expected. The large number of events allows us to make a detailed study on the time variation of the solar neutrino flux and also to pinpoint the solution of the MSW effect. Comparisons to the solar neutrino experiments are listed in table 1.

Suppose that a type-II supernova explodes at 10kpc from the earth, the expected $\bar{\nu}_e$ events from the super nova is 4000. A clear

burst of ~ 13 events during the first 10msec due to the neutronization process can also be observable. Therefore the detailed study of the explosion mechanism is possible. Among other physics objects are detailed studies of the atmospheric neutrinos, dark matter, high energy cosmic neutrinos and the neutrinos from past super nova explosions.

The SuperKamiokande has been officially approved by the Japanese government to start excavation in JFY 1991. The experiment is expected to start at 1996.

Table 1

Detector	Mode	Solar Neutrinos (events/day)			
		SSM	MSW	46%	Remarks
Kamiokande	$\nu_e e \rightarrow \nu_e e$	0.85	0.39	0.39	Observed value is 0.39
Super-Kamiokande	$\nu_e e \rightarrow \nu_e e$	67	31	31	'46%' can be distinguished from MSW by measuring the electron energy spectrum.
Homestake	$\nu_e \text{Cl} \rightarrow e^- \text{Ar}$	1.5	0.41	0.69	Observed value is 0.41
Galex	$\nu_e \text{Ga} \rightarrow e^- \text{Ge}$	1.18	0.09	0.54	
SAGE	$\nu_e \text{Ga} \rightarrow e^- \text{Ge}$	2.36	0.18	1.1	
SNO	$\nu_e d \rightarrow e^- pp$	18	7	8	It is very difficult to distinguish $\nu_e d$ events from background.
	$\nu_e e \rightarrow \nu_e e$	2	0.9	0.9	
	$\nu_e d \rightarrow \nu_x pn$	8	8	4	'46%' can be distinguished from MSW by $\nu_x d \rightarrow \nu_x pn$. In this reaction the energy of ν_x is unmeasurable.
	$\bar{\nu}_e d \rightarrow e^+ nn$				
	$\bar{\nu}_e p \rightarrow e^+ n$				

Notes

- SSM; Predicted value based on the Standard Solar Model.
- MSW; Predicted value based on neutrino oscillations in the solar matter with $\Delta m^2 = 10^{-6} \text{eV}^2$ and $\sin^2 2\theta = 0.04$ (nonadiabatic region)
- 46%; Data/SSM from Kamiokande as of 1990

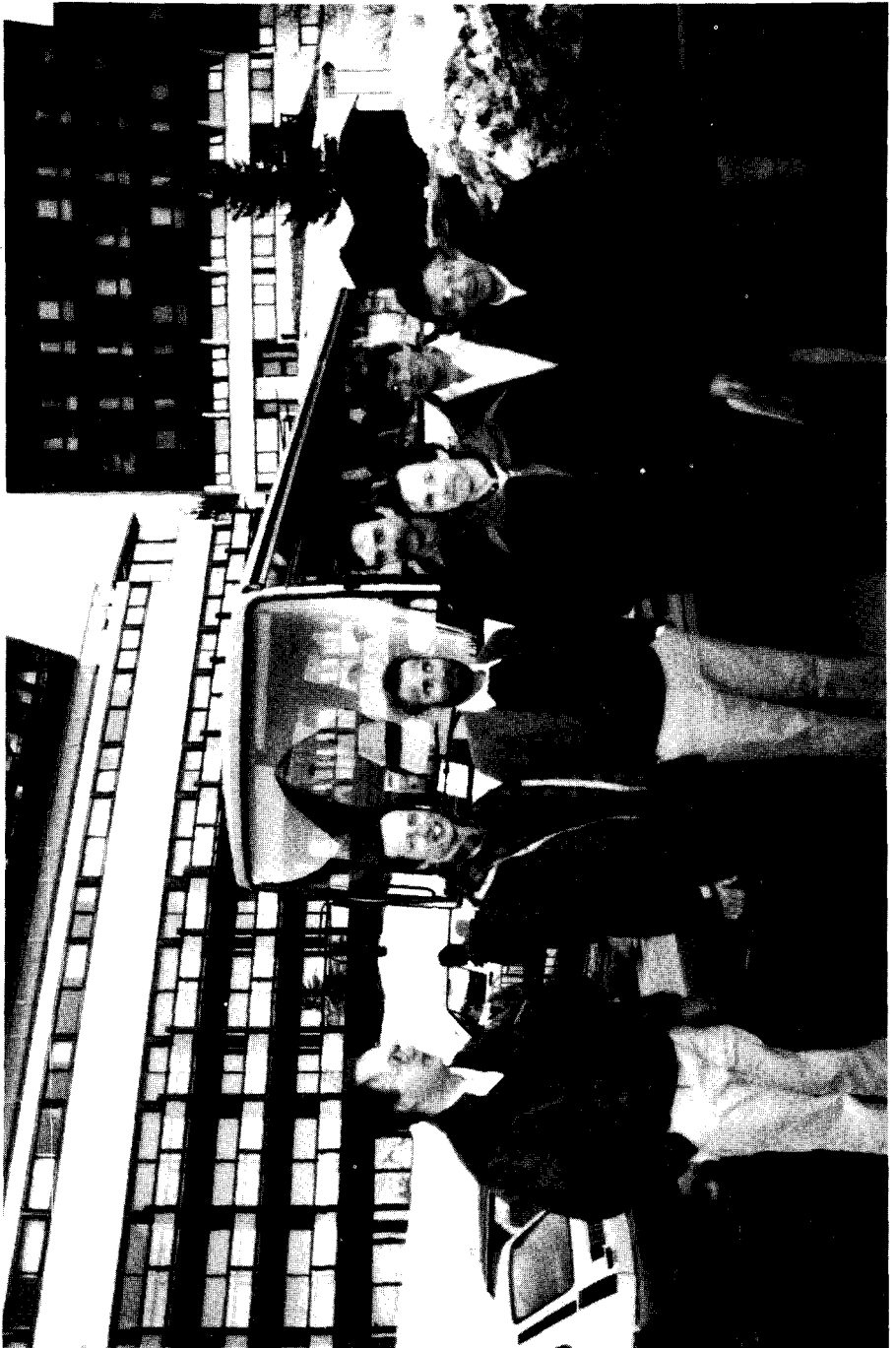
*) The Kamiokande collaboration: K.S.Hirata, K.Inoue, T.Kajita, T.Kifune, K.Kihara, M.Nakahata, K.Nakamura, S.Ohara, N.Sato, Y.Suzuki, Y.Totsuka and Y.Yaginuma (ICRR, Univ. of Tokyo); M.Mori, Y.Oyama, A.Suzuki, K.Takahashi and M.Yamada (KEK); M.Koshiha and K.Nishijima (Tokai Univ.); T.Suda and T.Tajima (Kobe Univ.); K.Miyano, H.Miyata and H.Takei (Niigata Univ.); Y.Fukuda, E. Kodera, Y.Nagashima and M. Takita (Osaka Univ.); K.Kaneyuki and T. Tanimori (Tokyo Teck); and W.E.Beier, L.R.Feldscher, E.D.Frank, W.Frati, S.B.Kim, A.K.Mann, F.M.Newcomer, R.Van Berg and W.Zhang (Univ. of Penn).

References

- [1] L. Wolfenstein, Phys. Rev. **D17**, 2369(1978); S.P. Mikheyev and A. Yu. Smirnov, Nuovo Cimento **9C**, 17 (1986).
- [2] A. Acker, S. Pakvasa and J. Pantaleone, Phys. Rev. D, R1754, **43** (1991).
- [3] M. B. Voloshin, M. I. Vysotskii and L. B. Okun, Sov. J. Nucl. Phys. **44**, 440(1986); E. Kh. Akhmedov, Phys. Lett. **213B**, 64(1988); C.-S. Lim and W. J. Marciano, Phys. Rev. **D37**, 1368(1988).
- [4] K. S. Hirata et al., Phys. Rev. Lett. **63**, 16(1989); **65**, 1297(1990); **65**, 1301 (1990).
- [5] K. S. Hirata et al. to be published.
- [6] J. N. Bahcall and R. K. Ulrich, Rev. Mod. Phys. **60**, 297 (1988).
- [7] S. Turck-Chieze et al., Astrophys. J. **355**, 415 (1988).
- [8] K. S. Hirata et al., Phys. Rev. Lett. **66**, 9(1991).



SUMMARY AND CONCLUSIONS



SUMMARY TALK ON DISCRETE SYMMETRIES
AND ATOMIC OR NEUTRON SYSTEMS

Norman F. Ramsey
Lyman Physics Laboratory
Harvard University
Cambridge, MA 02138 USA



ABSTRACT

The presented papers on discrete symmetries and atomic or neutron systems are summarized.

The reports that I am to summarize were all so interesting and well presented, that it seems almost inappropriate that they should be summarized. However, I am acceding to the request of the conference organizers and am writing a summary, but I urge the reader where possible to concentrate on the excellent original papers rather than on this brief summary.

Greene, by distinguishing between the use of the velocity of light c_{em} , associated with electromagnetism from the c_m associated with matter and by analyzing past experiments finds $|1 - (c_m^2/c_{em}^2)| = (1 \pm 12) \times 10^{-22}$.

Similarly, by carefully distinguishing the Planck constant \hbar_γ associated with the photon, \hbar_e associated with the electron and \hbar_p associated with the proton and by analyzing past data he finds

$$\hbar_e/\hbar_\gamma - 1 = (30 \pm 13) \times 10^{-8}$$

$$\hbar_p/\hbar_\gamma - 1 = (7 \pm 40) \times 10^{-8}$$

Although the first of these differs from zero by more than two standard deviations, Greene warns that this result is probably not significant since it is known from other data analyses that there are some inconsistencies in the input data for this calculation.

Severyns discussed exclusion plots for δ and for the mixing angle ζ in L-R symmetric models. He described new experiments with ^{107}In , ^{57}Co , and ^{12}N . Preliminary results with ^{107}In show

$$\delta < 0.15 \text{ to } 90\% \text{ confidence limit.}$$

Bayard discussed the CERN NA31 Experiment on CP violations with short and long lived neutral kaons K_s and K_L . The parameter ratio ϵ'/ϵ is measured. She

discussed the disagreement with the Fermilab experiment E731 and presented new results from NA31. The results for the different experimental values for $Re\ \epsilon'/\epsilon$ are

Original NA31	$(3.3 \pm 1.1) \times 10^{-3}$
E731	$(-0.4 \pm 1.5) \times 10^{-3}$
New NA31	$(1.9 \pm 1.1) \times 10^{-3}$
New & Old NA31	$2.7 \pm 0.9 \times 10^{-3}$

Although the new NA31 result alone is closer to the E731 result, the combination of the new and old NA31 continues to be three standard deviations from zero.

Nolte described Accelerator Mass Spectrometry (AMS) experiments to look for a possible anomalous ${}^5\widetilde{Li}$ with two protons in a symmetric state with respect to exchange. He finds the abundance of ${}^5\widetilde{Li}$ relative to 6Li :

$$[{}^5\widetilde{Li}/[{}^6Li] < 0.9 \times 10^{17}.$$

He also described other applications for AMS.

Mzavia analyzed the search for lepton number violation in pion and muon decays. In most cases the lepton number violating decays are less than 10^{-11} of ordinary decays and he hopes eventually to lower the limit to 10^{-14} .

Semertzidis described his search for coherent laser production of light pseudoscalars (axions) inside a magnetic field, looking for axion induced rotation and retardation of polarized light. If the mass of the axion is assumed less than $10^{-3}eV$, his result shows that the axion-photon-photon coupling constant $g_{a\gamma\gamma} < 2.5 \times 10^{-6}GeV$.

He discussed the Aharonov-Bohm and Aharonov-Casher effects and neutron experiments confirming them. He also described the possibility of interference experiments between the Aharonov-Bohm and the Aharonov-Casher effects.

Dewey discussed tests of the standard model from β -ray experiments and described his current experiments on the mean life of the neutron at the Institute Laue-Langeven (ILL) and at NIST.

Pendelbury described the various experiments on the mean life of ultra cold neutrons trapped in either physical or electromagnetic bottles. A few years ago the various measurements of the neutron mean life differed from one another by many standard deviations. With the new techniques, however, the values are in good agreement on the mean life τ_n being approximately

$$\tau_n = 887 \pm 3s.$$

Last discussed the vast amount of data that has been obtained at I.L.L. by measuring the polarizations and angular distributions of the radiation from polarized neutrons to obtain values for the decay parameters A, B, D, R, a, Since the experiments overdetermine the free parameters, the consistency confirms the standard model. The prospective more accurate measurements in the future should provide severe tests to the standard model.

Duffers described the I.L.L. $n - \bar{n}$ oscillation experiment. The oscillation period $\tau_{n\bar{n}}$ has already been shown to satisfy

$$\tau_{n\bar{n}} > 8 \times 10^{-7} s$$

and by the end of the run the limit should be about $10^8 s$. So far no \bar{n} has been seen in the experiment.

Lamoreaux described the I.L.L. neutron electric dipole moment (d_n) experiment. At ILL, $d_n = [-3 \pm 5] \times 10^{-26} e \text{ cm}$, and the latest results at Leningrad are

now also consistent with zero. Lamoreaux also described the new d_n experiment being developed at I.L.L., which will have 10 times the storage volume to increase statistics, will have a greater electrical potential and will use ^{199}Hg as a magnetometer to measure the average field at the same time and in the same volume as for the neutrons. Such a magnetometer should eliminate systematic uncertainties in the neutron measurements due to the possibility of magnetic field changes associated with changes in the direction of the electric field. He also discussed a possible experiment for the distant future in which the neutron resonance frequencies would be measured while they were contained in a reflecting box that would be completely filled with superfluid ^4He . With such an experiment it might be possible to obtain a sensitivity in the electric dipole moment search more than 100 times greater than at present.

Hunter described his sensitive T non-conserving experiments looking for an electric dipole moment d_{Cs} of the Cs atom from which the electron dipole moment d_e can be inferred. His results are

$$d_{Cs} = -(1.8 \pm 6.9) \times 10^{-24} e \text{ cm}$$

$$d_e = -(2 \pm 6) \times 10^{-26} e \text{ cm}.$$

Hinds discussed his sensitive but complicated atomic beam resonance experiments looking for a frequency shift Δf due to a failure of time reversal symmetry on the reversal of the direction of the electric field, which can be interpreted in terms of various T non-conserving effects, including a proton electric dipole moment d_p . He finds

$$\Delta f = (0.14 \pm 0.24) m\text{Hz}$$

$$d_p = (-4 \pm 6) \times 10^{-23} e \text{ cm}.$$

Heckel and his associates study optically pumped ^{199}Hg and ^{201}Hg to measure a variety of fundamental quantities. They find that if there is a non-linearity in quantum mechanics of the type discussed by Weinberg, the energies associated with the non linearities are less than 10^{-27} of nuclear binding energies. As a test of local Lorentz invariance they look for changes $\Delta\nu_D$ of the dipolar and $\Delta\nu_Q$ of the quadropolar interactions and find

$$\Delta\nu_D < 2.4\mu\text{Hz}$$

$$\Delta\nu_Q < 0.48\mu\text{Hz}$$

They also look for an electric dipole moment d_{Hg} of the ^{199}Hg atom and find

$$d_{Hg} = (-4 \pm 6) \times 10^{-28} e \text{ cm}$$

where the 6 is the statistical error only. Finally, as a test of the equivalence principle for spin, they find that if there is an $\vec{s} \cdot \vec{r}$ in the gravitational interaction the associated frequency shift is less the 1 M Hz.

Wieman described his highly sensitive Cs atomic beam experiments which measure parity non-conservation and determine the Weinberg angle θ_w to be given by $\sin^2 \theta_w = 0.223 \pm 0.007 \pm 0.003$ where the first indicated uncertainty is due to experiment and the second due to theory. These experiments are of particularly great interest because they test the standard model of the weak interactions in a quite different way than do high energy experiments and they are particularly sensitive to small changes in the standard model.

Wineland described his experiments on the cooling of trapped ions and on their application to precision spectroscopy and atomic clocks.

Aspect praised the important work of the late John S. Bell, who has done so much to elucidate the difference between classical and quantum mechanics. He also described his own experiments testing the Bell inequalities; for these experiments quantum mechanics accounts easily for the observations whereas even complicated modifications of classical mechanics do not.

In conclusion, I should like to summarize the entire Moriond Conference this week by saying it was scientifically informative, stimulating and exciting. In addition it was fun and provided excellent opportunities for those of us in these fields to get together and to think of new ideas and experiments. All of us extend our deep thanks to Van and Kim Tran Thanh Van and others who contributed so much to the organization of this highly successful meeting.

IMPRESSIONS FROM MORIOND '91

S. T. PETCOV

Inst. Nucl. Res. Nucl. Energy, Bulgarian Academy of Sciences, 1784 Sofia, Bulgaria

International School for Advanced Studies, 34014 Trieste, Italy

and

Istituto Nazionali di Fisica Nucleare, Sezione di Trieste, 34127 Trieste, Italy

It is really a gratifying task to summarize the sessions devoted to neutrino physics, dark matter searches, cosmic ray studies and gravitational law tests: a wealth of new interesting results have been reported and one would wish to review all of them in the summary. As I was preparing the summary it became clear that this intention is impossible to realize in practice and that one should make "shortcuts" - which should have been perfectly clear at the very beginning. I have chosen not to describe in great detail few results I consider among the most important reported at the sessions indicated above, but rather to share with you my general impressions about the significance and the implications of most of the results I found interesting. My exposition will not contain details (they can be found in the corresponding contributions in the present Proceedings), and in some cases it will not be, perhaps, very precise. In spite of this choice I will not have the possibility even to mention some of the interesting works and projects presented and I would like to apologize for that in advance.

Solar Neutrinos. The current status of the solar neutrino problem ¹⁾ was reviewed by D. Vignaud ²⁾. In particular, D. Vignaud presented the results of a recent new independent solar model calculation ³⁾ of the rate of ^{37}Ar production $R(^{37}\text{Ar})$ in the Davis et al. experiment. The value of $R(^{37}\text{Ar})$ found in ref. 3) reads: $R(^{37}\text{Ar}) = 7.7$ SNU. It is in agreement with the prediction of J. Bahcall and R. Ulrich ⁴⁾, $R(^{37}\text{Ar}) = (7.9 \pm 2.6)$ SNU, and is somewhat larger than the result of S. Turck-Chièze et al.⁵⁾, $R(^{37}\text{Ar}) = (5.8 \pm 1.3)$ SNU. Although the authors of the new calculation of $R(^{37}\text{Ar})$ did not present an estimate of the uncertainty in their prediction for the value of $R(^{37}\text{Ar})$, the result they have obtained reinforces the case for existence of solar neutrino problem. The prediction for the rate of ^{71}Ge production by solar neutrinos $R(^{71}\text{Ge})$ in the $^{71}\text{Ga} - ^{71}\text{Ge}$ solar neutrino experiments made in ref. 3), $R(^{71}\text{Ge}) = 125$ SNU, is in good agreement with the results of the two earlier calculations: $R(^{71}\text{Ge}) = 132$ SNU ⁴⁾, and $R(^{71}\text{Ge}) = 125$ SNU ⁵⁾.

It was suggested in 1982 by G.A. Bazilevskaya et al. ⁶⁾ that the ^{37}Ar production rate (and, correspondingly, the flux of solar neutrinos) observed in the experiment of Davis et al. varies in time and is (anti) correlated with the solar activity. As is well known, a quantitative measure of the level of solar activity is the number of sunspots at the surface of the Sun, which in turn is related to the strength of the toroidal component of the solar magnetic field at the solar surface. The solar activity is known to vary with a (half)period of approximately 11 years. The last two maxima of the solar activity corresponding also to maxima of the absolute value of the solar toroidal magnetic field and of the number of sunspots, occurred in 1979-1980 and in 1989-1990. D. Vignaud reported the results of four independent statistical analyses of the data of Davis et al. (those of J. Bahcall and W.

Press ⁷⁾, B. Filippone and P. Vogel ⁸⁾, L. Krauss ⁹⁾ and of J. Bieber et al. ¹⁰⁾), performed to test the hypothesis of (anti)correlation between the ³⁷A production rate and the level of solar activity. All four groups of authors find evidences for such a (anti)correlation at rather high level of statistical significance (the probability that random data can lead to such a (anti)correlation was found to be typically smaller than 1%). However, the data of Davis et al., taken in the period 1987-1990 and exhibiting significant time variation, is not in agreement with the observations of Kamiokande II collaboration ¹¹⁾, which observed no change (within the errors) in the solar neutrino induced event rate in the same period ^{*}). It appears that only new solar neutrino experiments capable to measure the ³⁷Ar production rate (or the flux of solar neutrinos with energies greater than 0.81 MeV) with much higher precision can give an unambiguous answer to the question about the time variation of the flux of solar ν_e detected in the Davis et al. experiment. The resolution of the problem of time variation of the solar ν_e flux would be of fundamental importance for understanding the cause of the solar neutrino deficit.

A beautiful summary of the results of the Kamiokande II collaboration on solar neutrinos was presented by Y. Suzuki ¹¹⁾. For the flux of solar ν_e with energy $E \geq 7.5$ MeV (⁸B neutrinos) this experiment gives

$$\Phi(E \geq 7.5 \text{ MeV}) = (0.46 \pm 0.05 \pm 0.06)\Phi^{\text{BU}} \quad (1)$$

$$= (0.70 \pm 0.08 \pm 0.09)\Phi^{\text{TC}} \quad (2)$$

where $\Phi^{\text{BU}} = 5.8 \cdot 10^6 \text{ cm}^{-2} \text{ sec}^{-1}$ and $\Phi^{\text{S}} = 3.8 \cdot 10^6 \text{ cm}^{-2} \text{ sec}^{-1}$ are the fluxes predicted in refs. 4) and 5), respectively. Although somewhat larger than the flux inferred from the Davis et al. data, this result represents the first independent experimental confirmation of the solar neutrino observations of Davis et al. The Kamiokande II collaboration performed also the first measurements ever made of the spectrum of solar neutrinos: the detector is sensitive to ⁸B neutrinos having energy $E \geq 7.5$ MeV. Although the accuracy of these measurements is not very good, the results obtained permitted to have already a "glimpse" on the form of the spectrum. It is consistent with the form predicted for ν_e emitted in the β -decay of ⁸B, suggesting that the flux of solar ν_e with a given energy E , $E \geq 7.5$ MeV, is smaller by the numerical factors in eqs. (1) and (2) than the predicted fluxes independently of the value of E . Assuming this to be the case for the whole flux of ⁸B neutrinos with energy $E \geq 0.81$ MeV detected in the experiment of Davis et al., one

^{*}) For a quantitative comparison of the data of the two experiments and a more detailed discussion see the contributions by Y. Suzuki and A. Yu. Smirnov in these Proceedings.

obtains (on the basis of the Kamiokande II data) the following prediction for the ^{37}Ar production rate due only to ^8B neutrinos:

$$R_K(^{37}\text{Ar}) = 2.8 \text{ SNU} \quad (3)$$

The contribution due to the ^7Be ($E = 0.86 \text{ MeV}$) and ^{13}N , ^{15}O neutrinos is predicted to be 1.1 SNU and 0.6 SNU respectively ^{4,5}). The observed (total) average rate of ^{37}Ar production in the period 1987-1990, in which the Kamiokande II data was taken, reads 12);

$$R_{87-90}(^{37}\text{Ar}) = (3.00 \pm 0.55) \text{ SNU} \quad (4)$$

Obviously, these results are not consistent with the assumption of a uniform (i.e., energy independent) reduction of the solar ^8B neutrino flux. Such a reduction could take place if the temperature in the central part of the Sun, where the ^8B neutrinos are supposedly produced, were smaller than the temperature predicted by the standard solar model, on the basis of which the theoretical fluxes Φ^{BU} and Φ^{S} have been calculated.

The Kamiokande II collaboration performed analyses of their data searching also for day-night, seasonal and/or semiannual variations of the detected solar neutrino flux. No evidences for existence of such variations were found. The indicated three types of variations can take place in the case of matter-enhanced transitions ¹³), "long" wavelength vacuum oscillations ¹⁴) and spin-flavour "precession" ^{15,16}) of solar neutrinos, respectively.

The final results of the analyses of the first five physics runs of the SAGE experiment, which took place in the period January - July, 1990, were presented at the Workshop by V. Gavrin ¹⁷). As is well known, SAGE and GALLEX ¹⁸) detectors are capable of registering the p-p neutrinos from the Sun. According to the current solar models, the p-p neutrinos constitute the major part of the solar neutrino flux: at the Earth surface $\Phi^{\text{SM}}(\text{pp}) \approx 6.10^{10} \text{ cm}^{-2}\text{sec}^{-1}$ ^{4,5}). They are produced in the primordial reaction $p+p \rightarrow ^2\text{H} + e^+ + \nu_e$, being the first in a cycle of reactions in which four protons burn into ^4He and more than 98% of the energy released in the Sun is generated. Thus measuring the flux of p-p neutrinos from the Sun one can test the presently existing basic concepts about the processes taking place at the initial stage of evolution of the stars. It was generally expected that the results of the SAGE and GALLEX experiments will permit to find the true cause of the solar neutrino problem. Let me remind you also that in both experiments ν_e with energy $E \geq 0.233 \text{ MeV}$ can be detected and that the p-p neutrinos have maximal energy 0.42 MeV.

The rate of ^{71}Ge production, observed by the SAGE collaboration, is consistent with that expected due to background processes ¹⁷⁾. The following upper limit on the solar neutrino induced rate $R(^{71}\text{Ge})$ of formation of ^{71}Ge was obtained:

$$R(^{71}\text{Ge}) < 74 \text{ SNU (90\% C.L.)} \quad (5)$$

The upper limit 5) is considerably smaller than the values of $R(^{71}\text{Ge})$ predicted on the basis of detailed solar mode calculations: $R(^{71}\text{Ge}) = (132 \pm 20) \text{ SNU}$ ⁴⁾, $(125 \pm 5) \text{ SNU}$ ⁵⁾ and 125 SNU ³⁾. The contributions due to the p-p, ^7Be and ^8B neutrinos in the calculated rate of 132 SNU are 71 SNU , 34 SNU and 14 SNU , respectively. A crucial step for a conclusive interpretation of the results of the SAGE collaboration will be the measurement of the efficiency of extraction of ^{71}Ge produced by neutrinos emitted by ^{51}Cr source of known strength, planned to be performed in the future. A measurement of the efficiency of extraction of ^{71}Ge introduced in the detector was already performed and found to be approximately equal to 80% ¹⁷⁾.

A status report of the GALLEX experiment was given by D. Vignaud ¹⁸⁾.

Both GALLEX and SAGE experiments have contamination problems which do not permit to take data at the moment. It seems that both experiments turned out to be much more difficult to perform than it looked when they were conceived. Perhaps, this is a good sign: we know from past experiences that Nature does not reveal easily its most profound "secrets". We hope very much that the difficulties both collaborations experience will be overcome and that they will present interesting new data at the next January Moriond Workshop.

Assuming that the solar neutrinos (ν_e) take part in two-neutrino oscillations ¹⁹⁾ (say $\nu_e \rightleftharpoons \nu_\mu$ or $\nu_e \rightleftharpoons \nu_\tau$) and using the Kamiokande II data on the flux and spectrum of solar neutrinos alone, one can exclude ¹¹⁾ the MSW adiabatic solution ²⁰⁾ of the solar neutrino problem for $\sin 2\theta < 0.1$ (θ is the two-neutrino mixing angle in vacuum, see, e.g., ref. 14)). Using the Davis et al. and the indicated Kamiokande II data as input in a "solar model independent" analysis M. Spiro and D. Vignaud concluded ²¹⁾ that observation of a rate of ^{71}Ge production smaller than 82 SNU or greater than 118 SNU by the SAGE and GALLEX collaborations would be a strong indication for existence of matter-enhanced transitions of the solar ν_e into neutrinos of a different type (e.g., ν_μ and/or ν_τ). Adding the SAGE result (5) and performing a combined analysis of the three sets of data in terms of the two-neutrino oscillation hypothesis, one finds the following types of solutions of the solar neutrino problem:

i) "Long" wavelength vacuum oscillation solution ^{22,23)}:

$$\sin^2 2\theta \geq 0.7 \quad (6a)$$

$$\Delta m^2 \equiv (0.5 \div 2.5) \cdot 10^{-10} \text{ eV}^2 \quad (6b)$$

($\Delta m^2 = m_2^2 - m_1^2$, where $m_{1,2}$ are the masses of two neutrinos $\nu_{1,2}$ with definite mass in vacuum, is the second parameter (in addition to θ), characterizing the two-neutrino oscillations ¹⁴).

ii) MSW nonadiabatic solution ^{20,24,25,22,12}):

$$\sin^2 2\theta \geq 4 \cdot 10^{-3} \quad (7a)$$

$$\Delta m^2 \sin^2 2\theta = (3.2 \pm 1.0) \cdot 10^{-8} \text{ eV}^2 \quad (7b)$$

iii) MSW "large" angle adiabatic solution ¹²):

$$\sin^2 2\theta \geq 0.6, \quad (8a)$$

$$5 \cdot 10^{-8} \text{ eV}^2 \leq \Delta m^2 \leq 10^{-6} \text{ eV}^2, \quad 5 \cdot 10^{-6} \text{ eV}^2 \leq \Delta m^2 \leq 2 \cdot 10^{-5} \text{ eV}^2 \quad (8b)$$

where the interval of values of Δm^2 between 10^{-6} eV^2 and $5 \cdot 10^{-5} \text{ eV}^2$ is excluded by the absence of day-night variation of the solar neutrino flux observed by the Kamiokande II collaboration.

Possible types of solutions of the solar neutrino problem when the solar neutrinos are supposed to take part in three-neutrino oscillations ^{14,26}) have been considered by A. Smirnov ¹²), while solutions based on the hypothesis of existence of matter-enhanced spin-flavour transitions of solar neutrinos ¹⁶) (due to "large" transition moments of magnetic dipole type μ , $\mu \sim (10^{-11} \div 10^{-10}) \mu_B$, μ_B being the Bohr magneton) have been reviewed by E. Akhmedov ²⁷). A. Smirnov discussed also some "peculiar" features of the Davis et al. data as well as possible explanations of the suggested time variation of the observed rate of ³⁷Ar production by solar neutrinos based on the MSW effect.

Future Solar Neutrino Experiments. With the approval on December 28, 1990, by the Japanese Government of the proposal to build the Super-Kamiokande detector, whose main characteristics were discussed by Y. Suzuki ¹¹), the number of second generation solar neutrino experiments in preparation at present becomes already three: the other two are the Sudbury heavy water experiment (SNO) in Canada, the status of which was reviewed by J. Simpson ²⁸), and the Baksan ³⁷Cl- ³⁷Ar experiment with a five times bigger version of the Davis et al. detector in the Soviet union, described by A.

Pomansky ²⁹⁾. E. Meroni ³⁰⁾ presented a status report of the "Borexino" collaboration, presently working on a prototype of a 61 ton boron liquid scintillator detector of solar neutrinos based on the reactions ³¹⁾ $\nu_e + {}^{11}\text{B} \rightarrow {}^{11}\text{C} + e^-$ ($E \geq 2 \text{ MeV}$) and $\nu_e + e^- \rightarrow \nu_e + e^-$ ($E > 0.2 \text{ MeV}$). The detector would be capable to register also a possible small $\bar{\nu}_e$ component (see ref. 27) in the solar ν_e flux via the inverse β -decay reaction: $\bar{\nu}_e + p \rightarrow n + e^+$ ($E > 1.8 \text{ MeV}$). The second generation solar neutrino experiments are expected to accumulate much higher statistics than the first generation experiments. For example, the Sudbury collaboration is planning to detect in a period of one year more than 3000 solar neutrino induced events corresponding to the reaction $\nu_e + {}^2\text{H} \rightarrow e^- + p+p$ ($E \geq 6.5 \text{ MeV}$); the event rate in the Super-Kamiokande detector will be 10000 events per year. For comparison, after running for 20 years the Davis et al. detector has registered altogether 1365 events induced by the solar neutrinos. Although the four experiments mentioned above will be able to detect ${}^8\text{B}$ and ${}^7\text{Be}$ neutrinos only, if successful, they will be capable to measure with high precision the total fluxes of the solar ${}^8\text{B}$ and ${}^7\text{Be}$ neutrinos and the spectrum of the flux of ${}^8\text{B}$ neutrinos. As was the case with the presently running solar neutrino experiments, one has to be very patient: the first physics results from the second generation solar neutrino detectors are not expected before 1996.

Development of Detectors Based on Novel Methods of Neutrino Detection. The progress made in developing principally new detectors of neutrinos was reviewed by R. Lannou, A. Tadson, R. Gaitskell (low temperature devices) and by G. Zacek and P. Lenderman (scintillating fibre detectors). The ultimate goal of the remarkable amount of work being done is to construct eventually a real time, high energy resolution, low energy threshold ($E \geq 1 \text{ keV}$) detector, capable to register both charged current and neutral current reactions, induced by neutrinos. The results reported gave the impression that we are, perhaps, witnessing the dawn of the third generation of solar neutrino detectors which will permit to solve the formidable problem of measuring with good precision both the flux and the spectrum of the neutrinos, produced in the p-p reaction in the Sun. Some of the new methods for neutrino detection, which are being studied, could also be used in highly sensitive searches for neutrinoless double β - ($(\beta\beta)_{0\nu}$) decay, neutrino oscillations and dark matter.

Searches for Oscillations of Neutrinos. Due to the interference nature of the oscillations of neutrinos, searching for oscillation effects is one of the most sensitive methods of looking for effects of existence of nonzero neutrino masses and lepton mixing. O. Perdereau reported the final results of the searches for oscillations of

atmospheric $\bar{\nu}_e$ and $\bar{\nu}_\mu$ neutrinos with energies in the interval $0.2\text{MeV} \leq E \leq 3\text{GeV}$, performed by the FREJUS collaboration. No anomalies in the ratio of the $\bar{\nu}_e$ induced events $N(e)$ and the $\bar{\nu}_\mu$ induced events $N(\mu)$ were found ³²⁾:

$$N(e)/N(\mu) = 0.53 \pm 0.09, \quad (9)$$

which is in a very good agreement with the value calculated theoretically assuming that oscillations of the atmospheric $\bar{\nu}_e$ and $\bar{\nu}_\mu$ do not take place, $(N(e)/N(\mu))_{\text{MC}} = 0.56 \pm 0.08$. The FREJUS result (9) differs somewhat from the results of the Kamiokande II ³³⁾ and the IMB ³⁴⁾ collaborations, which observe a larger value (approximately by a factor 1.5) of the ratio $N(e)/N(\mu)$. The comparison of the results of the three groups, however, is not straightforward because of differences in the event selection criteria exploited. Assuming that $\bar{\nu}_e$ and/or $\bar{\nu}_\mu$ take part in two-neutrino oscillations $\bar{\nu}_e \rightleftharpoons \bar{\nu}_\mu$ or $\bar{\nu}_\mu \rightleftharpoons \bar{\nu}_\tau$, the following limits on the relevant oscillation parameters have been obtained on the basis of the FREJUS data:

$$\bar{\nu}_e \rightleftharpoons \bar{\nu}_\mu : \quad \begin{aligned} \Delta m^2 < 1.5 \cdot 10^{-3} \text{ eV}^2, \text{ for } \sin^2 2\theta = 1, \\ \sin^2 2\theta < 0.47, \text{ for } \Delta m^2 \geq 10^{-2} \text{ eV}^2; \end{aligned} \quad (10)$$

$$\bar{\nu}_\mu \rightleftharpoons \bar{\nu}_\tau \quad \begin{aligned} \Delta m^2 < 3.5 \cdot 10^{-3} \text{ eV}^2, \text{ for } \sin^2 2\theta = 1, \\ \sin^2 2\theta < 0.6, \text{ for } \Delta m^2 \geq 2 \cdot 10^{-2} \text{ eV}^2. \end{aligned} \quad (11)$$

A status report of the new BUGEY oscillation experiment with reactor $\bar{\nu}_e$, which began to take data in December 1990, was presented by M. Avenier. The BUGEY collaboration will look for "disappearance" of $\bar{\nu}_e$ at different distances from the source. Two reactors are planned to be used consecutively as $\bar{\nu}_e$ sources and measurements of the absolute fluxes of $\bar{\nu}_e$ from each of the reactors are foreseen to be performed simultaneously at two distances (16m and 41m, and 103m and 128m, respectively). The experiment will be sensitive ³⁵⁾ to values of $\Delta m^2 \geq 10^{-2} \text{ eV}^2$ and of $\sin^2 2\theta > 0.2$ if $\bar{\nu}_e$ take part in two-neutrino oscillations. Exploiting the "flux independent" method ¹⁹⁾ of searching for $\bar{\nu}_e$ oscillations, which consists in using only the ratio of the $\bar{\nu}_e$ fluxes measured at two distances from a given source in the relevant analysis, sensitivity to values of $\sin^2 2\theta$ as small as 0.03 can possibly be reached for a certain interval of values of Δm^2 .

F. Vannucci discussed a proposal for an "appearance" oscillation experiment to search for $\nu_\mu \rightarrow \nu_\tau$ transitions using the SPS accelerator at CERN. The experiment is envisaged to be sensitive to $\nu_\mu \rightleftharpoons \nu_\tau$ oscillations with $\sin^2 2\theta \geq 2 \cdot 10^{-4}$ for "large" values of Δm^2 ($\Delta m^2 \geq 10 \text{ eV}^2$), which will be an improvement at least by one order of magnitude over the presently existing results ³⁶⁾. For $\sin^2 2\theta = 1$ it will be able to register oscillations with $\Delta m^2 \geq 0.5 \text{ eV}^2$ ($\Delta m^2 \geq 6 \cdot 10^{-2} \text{ eV}^2$) with detector placed at a distance 1km (17km) from the neutrino source (the π^- and the K- meson decay tunnel). I was informed by G. Zacek that an experiment with approximately the same sensitivity with respect to $\nu_\mu \rightleftharpoons \nu_\tau$ oscillations but exploiting a different technique of τ^\pm detection was proposed at CERN by N. Armenise et al. ³⁷⁾.

Results on Double Beta Decay. Representatives of five experimental groups, namely, A. Barabash (U.S.S.R. - U.S.A. collaboration), M. Treichel (CALTECH - Neuchatel - PSI collaboration), T. Tabarelli (Milano group), A. Pomansky (Baksan group) and A. Piepke (Heidelberg - Moscow collaboration), studying different possible double beta ($(\beta\beta)$) decay modes (the two-neutrino mode ($(\beta\beta)_{2\nu}$) ³⁸⁾, the neutrinoless mode ($(\beta\beta)_{0\nu}$) ³⁹⁾ and the Majoron one ($(\beta\beta)_{0\nu\chi}$) ⁴⁰⁾), reported results at the Workshop. We will not discuss the particular lower limits for the halflife times obtained and their implications^{*)}, but rather will make few general remarks about the impression they leave. It is clear that the $(\beta\beta)$ -decay studies are in a period, which began approximately two years ago and in which dramatic improvements over the earlier obtained results are taking place. First of all, much more intensive sources of 2β emitters became available and are being used at present in many experiments. For instance, the Heidelberg-Moscow collaboration will operate a 16.9 kg, 86% enriched in ^{76}Ge , germanium detector in a search for $(\beta\beta)_{0\nu}$ -decay of ^{76}Ge ⁴²⁾. Using only 0.93 kg of the germanium sample in a run which lasted 108 days the group obtained a lower limit on the halflife time of ^{76}Ge with respect to the $(\beta\beta)_{0\nu}$ -decay (namely, $5.6 \cdot 10^{23} \text{ ys}$ (90% C.L.) ⁴²⁾), very close in value to the presently existing best lower limit ($8 \cdot 10^{23} \text{ ys}$ (90% C.L.)) due to the UCSB-LBL collaboration ⁴³⁾. The latter took several years of measurements to produce with a detector consisting in its final configuration of 6.85 kg of natural germanium with 7.67% abundance of ^{76}Ge . An ITEP/Yerevan collaboration was able to detect for the first time the $(\beta\beta)_{2\nu}$ -decay of ^{76}Ge with an 85% enriched in ^{76}Ge germanium detector ⁴⁴⁾. Large amounts of, e.g., Mo and Xe, highly enriched in ^{100}Mo and ^{136}Xe , respectively, are

^{*)} The interested reader can find a detailed description of the experiments as well as of the corresponding results in the contributions of the indicated authors in the present Proceedings. For a thorough recent review of the studies of the double beta decay, see ref. 41).

currently used in the studies of the $(\beta\beta)$ -decays of ^{100}Mo and ^{136}Xe . Second, both the $(\beta\beta)_{2\nu^-}$ and $(\beta\beta)_{0\nu^-}$ -decays of a large variety of nuclei (^{76}Ge , ^{82}Se , ^{100}Mo , ^{124}Xe , ^{134}Xe , ^{136}Xe , ^{150}Nd) are being investigated. It is especially important to perform searches for the $(\beta\beta)_{0\nu^-}$ -decay of elements having atomic numbers which differ considerably. The $(\beta\beta)_{0\nu^-}$ -decay rate could depend rather strongly on the atomic number of the decaying nucleus ⁴⁵). In particular, it could be strongly suppressed for a given nucleus, but analogous suppression would not take place for a nucleus with a sufficiently different atomic number. Finally, in addition to the "classical" $O^+ \rightarrow O^+$ and $O^+ \rightarrow 2^+$ transitions of the initial nucleus to the daughter nucleus in the $(\beta\beta)$ -decays, transitions to a variety of excited states of the daughter nucleus (e.g., $O^+ \rightarrow 2_1^+$, $O^+ \rightarrow O_1^+$, $O^+ \rightarrow 2_2^+$, $O^+ \rightarrow O_2^+$ in the case of ^{100}Mo) are also being studied ⁴⁶). The indicated progress will permit to probe more deeply the electroweak interaction for existence of lepton number nonconserving couplings (in particular, neutrino mass terms changing the electron lepton charge L_e by two units and, correspondingly, massive Majorana neutrinos) as well as to fully develop the theory of the nuclear transitions associated with the discussed class of decays.

On the 17 keV Mass Neutrino. The 17 keV mass neutrino made its second "appearance" at this Workshop five years after the evidences for its possible existence were presented by J. Simpson for the first time at the 1986 January "Rencontres de Moriond" Workshop. In 1986 J. Simpson reported the results of an experiment in which the spectrum of the electrons emitted in the β -decay of ^3H implanted in a Si(Li) semiconductor detector was measured far from the end point Q , $Q(^3\text{H}) \cong 18.6 \text{ keV}$ ⁴⁷). A characteristic "kink" in the spectrum at energy E_e of the electrons $E_e \cong (Q(^3\text{H}) - 17\text{keV})$ and a deviation from the zero neutrino mass spectrum for $E_e \leq (Q(^3\text{H}) - 17\text{keV})$ were observed. They were interpreted as being caused by the emission in addition to a zero (or very low) mass neutrino(s) ν_i of a "heavy" neutrino ν_h with mass $m_h = (17.1 \pm 0.2) \text{ keV}$. For the relative probability of ν_h emission $|U_{eh}|^2$, which is determined by the coupling U_{eh} of ν_h to the electron in the weak charged lepton current defined by the relation

$$\nu_{eL}(x) = \sum_i U_{ei} \nu_{iL}(x) + U_{eh} \nu_{hL}(x), \quad \sum_i |U_{ei}|^2 + |U_{eh}|^2 = 1 \quad (12)$$

where $\nu_{eL}(x)$, $\nu_{iL}(x)$ and $\nu_{hL}(x)$ are the left-handed (LH) fields of the neutrinos ν_e , ν_i and ν_h , respectively, and U_{ei} and U_{eh} are elements of an unitary matrix U - the lepton mixing matrix, it was found:

$$|U_{eh}|^2 = (3 \pm 1) \cdot 10^{-2} \quad (13)$$

Six experiments ^{48,49)} (five spectrometer ⁴⁸⁾ and one with a semiconductor detector ⁴⁹⁾ looking for possible distortions of the spectra of electrons from ³⁵S and ⁶³Ni decays due to emission of a 17 keV mass neutrino were performed in the period between 1985 and 1987. All they gave negative results. The most stringent limit on the $\nu_h - e^-$ coupling was published by A. Apalikov et al. ⁴⁸⁾:

$$|U_{eh}|^2 < 1.7 \cdot 10^{-3} \text{ (90\% C.L.)} \quad (14)$$

Later two additional experiments with ³H implanted in Ge semiconductor detector and with ³⁵S implanted in a Si(Li) detector were performed by J. Simpson and his student A. Hime. The results of these two studies ⁵⁰⁾ confirmed the earlier observations made by J. Simpson. In the experiment with ³⁵S ($Q(^{35}\text{S}) \cong 167 \text{ keV}$), for instance, it was found that $m_h = (16.9 \pm 0.4) \text{ keV}$ and $|U_{eh}|^2 = (0.73 \pm 0.09 \pm 0.06) \cdot 10^{-2}$. In refs. 47),50) doubts in the correctness of the negative results obtained in refs. 48),49) were expressed. In particular, it was pointed out that the corrections to the β -spectrum introduced in order to describe the spectrum for $E_c > (Q - 17 \text{ keV})$ measured in the spectrometer experiments could blur the effects of a possible ν_h emission at $E_c \leq (Q - 17 \text{ keV})$.

New high precision β -spectrum measurements were prepared in the last two years and recently performed by A. Hime and N. Jelly at Oxford ⁵¹⁾ (with ³⁵S source), by B. Sur et al. at Berkeley ⁵²⁾ (with ¹⁴C source, $Q(^{14}\text{C}) \cong 156 \text{ keV}$) with semiconductor detectors, and by B. Imel et al. at CALTECH ⁵³⁾ (with ³⁵S source) with a spectrometer. I. Zliven et al. ⁵⁴⁾ have measured with a semiconductor detector the spectrum of the photons emitted (internal bremsstrahlung) in the process of electron capture in ⁷¹Ge: $e^- + ^{71}\text{Ge} \rightarrow ^{71}\text{Ga} + \gamma + \nu_e$. The first data from these experiments were reported at the Workshop by A. Hime, J. Simpson ⁵²⁾, H. Becker ⁵³⁾, and I. Zliven. The three groups exploiting semiconductor detectors found distortions of the measured spectra compatible with emission of a 17 keV mass neutrino. Their results for m_h and $|U_{eh}|^2$ read:

$$m_h = (17.2 \pm 0.5) \text{ keV}, \quad |U_{eh}|^2 = (0.85 \pm 0.06 \pm 0.05) \cdot 10^{-2} \text{ (ref. 51)}, \quad (15)$$

$$m_h = (17.0 \pm 2.0) \text{ keV}, \quad |U_{eh}|^2 = (1.40 \pm 0.45) \cdot 10^{-2} \text{ (ref. 52)}, \quad (16)$$

$$m_h = (17.2 \pm 1.3) \text{ keV}, \quad |U_{eh}|^2 = (1.60 \pm 0.70) \cdot 10^{-2} \text{ (ref. 54)}, \quad (17)$$

The β -spectrum measured by A. Hime and N. Jelly differs at $E \leq (Q - 17 \text{ keV})$ from the zero neutrino mass spectrum approximately by 8 s.d. The study of the CALTECH-Neuchatel-PSI group gave a negative result ⁵³⁾.

The resolution of the controversial issue of the existence of a 17 keV mass neutrino coupled to the electron in the weak charged lepton current apparently requires the

execution of new independent high precision β -spectrum measurements exploiting, possibly, new techniques of electron energy determination.

If the interpretation of the results of the experiments with semiconductor detectors (47,50,51,52,54) in terms of the hypothesis of emission of a 17 keV mass neutrino is confirmed to be correct, this undoubtedly will have profound implications for elementary particle physics. In particular, it would imply that the nonzero neutrino mass and neutrino mixing hypothesis ¹⁹⁾ is correct and one has for the flavour neutrino fields entering into the weak charged lepton current:

$$\nu_{iL}(x) = \sum_l U_{li} \nu_{lL}(x) + U_{eh} \nu_{hL}(x), \quad l = e, \mu, \tau \quad (18)$$

Accordingly, a whole "new world" of phenomena should exist ¹⁴⁾.

Assuming that in eq. (18), $|U_{eh}| \cong 0.1$ and that $m_h \cong 17$ keV, we give below a concise list of some of the possible related phenomenological consequences ⁵⁵⁾.

i) Oscillations (transitions) of $\check{\nu}_e$ into neutrinos of a different type with a probability $\check{P} \cong (1.5 \pm 2) \cdot 10^{-2}$ independent of the source-detector distance and of the neutrino momentum should take place; the transitions can be into $\check{\nu}_\tau$ and/or into sterile neutrinos, but not into $\check{\nu}_\mu$.

ii) The $\check{\nu}_\mu$ neutrino can "weigh" also 17 keV, or more than 85 keV.

iii) Lepton charge nonconserving decays of μ^\pm and/or τ^\pm with branching ratios close to the existing upper limits can occur, the particular decay modes being model dependent.

iv) The neutrino ν_h can be a Dirac particle and can have relatively large magnetic moment: for instance, $\mu_h \sim 5 \cdot 10^{-11} \mu_B$ is possible.

v) Cosmological and astrophysical considerations lead to the conclusion that ν_h should be unstable and should have lifetime $\tau(\nu_h) \leq 1$ yr. Such a short lifetime suggests that the dominant decay mode of ν_h should be into a lighter neutrino and a light (or massless) scalar particle. As can be shown, considerable extensions of the standard electroweak theory are required in order to satisfy the indicated constraint on the ν_h instability (see, e.g., ref. 56).

Dark Matter Searches. The status of the dark matter (DM) problem, recent results from experiments searching for DM as well as new projects for looking for particular DM candidates have been discussed by S. Zylberajch, M. Treichel, A. Milsztajn and P. Belli. We have learned that cosmions with vector type couplings to matter ⁵⁷⁾, and heavy neutral leptons with masses in the interval 10 GeV - 2400 GeV ⁵⁸⁾ are ruled out experimentally as possible candidates for dark matter. A stringent upper limit on the concentration of

CHAMPS (stable charged particles having a mass in the range $20 \text{ TeV} - 10^3 \text{ TeV}$ which could constitute the DM ⁵⁹⁾) with mass $m_c \geq 10^2 \text{ TeV}$ in the oceanic water was obtained ⁵⁷⁾: $C < 4 \cdot 10^{-15} C(H)$, $C(H)$ being the hydrogen concentration. A project to search for MACHO (Massive Astrophysical Compact Halo Objects) in the mass range $10^{-6} M_\odot - 10^{-1} M_\odot$, M_\odot being the solar mass, which could form DM constituents in our galactic halo, was presented ⁶⁰⁾.

Unfortunately, the list of the possible DM candidates is rather long and the measure of the progress in DM searches at present is the increase of the experimentally forbidden ranges of values of the relevant parameters on the exclusion plots for the various candidates. Nevertheless, the exclusion plots are really impressive in some cases.

Gravitational Law Tests. The intensive experimental searches for deviations from Newton's gravitational law and for violation of Einstein's weak equivalence principle, performed in the last five years and reviewed in a very memorable way by J. Faller at the Workshop, have improved by several orders of magnitude the precision with which we know the law and the principle hold at moderate distances ($0.1 \text{ m} \div 10^3 \text{ m}$). It was found, for instance, that the free fall acceleration of copper and uranium bodies in the Earth's gravitational field cannot differ by more than 5 parts in 10^{10} of the normal gravitational acceleration ⁶¹⁾. Further, the existence of a baryon and/or lepton charge (i.e., composition) dependent Yukawa type force between two bodies having a characteristic distance of action $\lambda \cong 100 \text{ m}$ and a constant larger than $10^{-5} G_N$, G_N being the Newton's constant, is ruled out by the existing data ⁶²⁾. Two new projects for further high precision tests have been described by J. Schurr and A. Cornaz. An excellent review of the gravitational interaction phenomenology and of the possible strong field tests of gravity theories was presented by T. Damour.

Conclusions. Evidences that the additive lepton charges are not conserved in the electroweak interaction and nonzero neutrino masses and lepton mixing exist have been presented at the Workshop. They have to undergo severe checks before we could consider the nonconservation of the lepton charges and the existence of neutrinos with nonzero mass established. The tests of the validity of the Newton's gravitational law and of the Einstein's weak equivalence principle performed so far lend support to the idea that Nature is very economic in fundamental laws and principles and prolific in structures.

Acknowledgments. I would like to thank J. Tran Thanh Van, G. Fontaine and L. Norry for the excellent organisation of the Workshop.

References.

1. R. Davis et al., XXI Int. Cosmic Ray Conference papers, vol. 7, pp. 155-158; K. Lande, Talk given at the "Neutrino '90" int. Conference, June 1990, Geneva, Switzerland.
2. D. Vignaud, these Proceedings.
3. I.-J. Sackman, A.I. Boothroyd and W.A. Fowler, *Astrophys. J.* 360 (1990) 727.
4. J.N. Bahcall, and R.K. Ulrich, *Rev. Mod. Phys.* 60 (1988) 298.
5. S. Turck-Chièze et al., *Astrophys. J.* 335 (1988) 425.
6. G.A. Bazilevskaya et al., *JETP Lett.* 35 (1982) 273; *Yad. Fiz.* 39 (1984) 856.
7. J.N. Bahcall and W.H. Press, *Astrophys. J.* (submitted).
8. B. Filippone and P. Vogel, *Phys. Lett.* 246B (1990) 546.
9. L. Krauss, *Nature* 348 (1990) 403.
10. J.W. Bieber et al., *Nature* 348 (1990) 407.
11. Y. Suzuki, these Proceedings.
12. A.Yu. Smirnov, these Proceedings.
13. L. Wolfenstein, unpublished; M. Cribier et al., *Phys. Lett.* 182B (1986) 89; S.P. Mikheyev and A. Yu. Smirnov, Proc. of the VIth Moriond Workshop on Massive Neutrinos in Astrophysics and in Particle Physics, January 1986, Tignes, France (eds. O. Fackler and J. Tran Thanh Van, Editions Frontières, Gif sur Yvette), p.355.
14. S.M. Bilenky and B. Pontecorvo, *Phys. Rep.* 41 (1978) 225; S.M. Bilenky and S.T. Petcov, *Rev. Mod. Phys.* 59 (1987) 671.
15. M.B. Voloshin, M.I. Vysotskii and L.B. Okun, *Sov. J. Nucl. Phys.* 44 (1986) 440.
16. E. Kh. Akhmedov, *Phys. Lett.* 213B (1988) 64; C.-S. Lim and W. Marciano, *Phys. Rev. D* 37 (1988) 1807.
17. V. Gavrin, these Proceedings.
18. D. Vignaud, these Proceedings.
19. B. Pontecorvo, *Zh. Eksp. Teor. Fiz.* 33 (1957) 549, 34 (1958) 247, 53 (1967) 1717.
20. S.P. Mikheyev and A. Yu. Smirnov, *Progress in Nucl. and Part. Phys.* 23 (1989) 41.
21. M. Spiro and D. Vignaud, *Phys. Lett.* B242 (1990) 279.
22. V. Barger, R.J.N. Phillips and K. Whisnant, Univ. of Wisconsin preprint MAD/TH/387, September 1990.

23. A. Acker, S. Pakvasa and J. Pantaleone, Univ. of Hawaii preprint UH-511-710-90, August 1990.
24. S. P. Rosen and J.M. Gelb, Phys. Rev. D34 (1986) 969, D39 (1989) 3190.
25. J. N. Bahcall and H.A. Bethe, preprint IASSNS AST 90/14, June 1990; P.I. Krastev, S.P. Mikheyev and A. Yu. Smirnov, Talk given at the Int. Conf. on Low Energy Weak Interactions, Dubna, USSR, 3-14 September 1990 (INR preprint, Moscow).
26. A. De Rujula et al., Nucl. Phys. B 168 (1980) 54; for a discussion of the matter effects in three-neutrino oscillations of solar neutrinos see, e.g., S.T. Petcov and S. Toshev, Phys. Lett. 187B (1987) 120 and ref. 20.
27. E. Akhmedov, these Proceedings.
28. J.J. Simpson, these Proceedings.
29. A.A. Pomansky, these Proceedings.
30. E. Meroni, these Proceedings.
31. R.S. Raghavan et al., AT&T Bell Labs Tech. Memorandum 11121 - 910214, February 4, 1991.
32. O. Perdereau, these Proceedings.
33. K.S. Hirata et al., Phys. Lett. 205 B (1988) 416.
34. T.J. Haynes et al., Phys. Rev. Lett. 57 (1986) 1986.
35. M. Avenier, these Proceedings.
36. N. Ushida et al., Phys. Rev. Lett. 57 (1986) 2897.
37. N. Armenise et al., preprint CERN-SPS C/90-42, 15 December 1990.
38. M. Goepfert-Mayer, Phys. Rev. 48 (1935) 513.
39. G. Racah, Nuovo Cimento 14 (1937) 322.
40. H. Georgi, S.L. Glashow and S. Nussinov, Nucl. Phys. B193 (1981) 297.
41. A. Morales, Univ. of Zaragoza preprint IFNAE/Z2-90, Zaragoza.
42. A. Piepke, these Proceedings.
43. D.O. Caldwell et al., Int. Journ. of Mod. Phys. A4 (1989) 1851.
44. A.A. Vasenko et al., preprint ITEP 89-178, Moscow.
45. A. Halprin, S.T. Petcov and S.P. Rosen, Phys. Lett. 125B (1983) 335.
46. A. Barabash, these Proceedings.
47. J.J. Simpson, Phys. Rev. Lett. 54 (1985) 1891; Proc. of the VI Moriond Workshop on Massive Neutrinos in Particle Physics and in Astrophysics, Tignes, France, 1986 (eds. O. Facklerand and J. Tran Thanh Van, Editions Frontières, Gif sur Yvette, 1986), p. 565.
48. T. Altizoglou et al., Phys. Rev. Lett. 55 (1985) 799; V.M Datar et al., Nature 318 (1985) 547; A. Apalikov et al., JETP Lett. 42 (1985) 289; J. Markey and F.

- Boehm, Phys. Rev. C32 (1985) 2215; D.W. Hetherington et al., Phys. Rev. C36 (1987) 1504.
49. T. Ohi et al., Phys. Lett. 160B (1985) 322.
50. A. Hime and J.J. Simpson, Phys. Rev. D 9 (1989), 1825 and 1837.
51. A. Hime, these Proceedings.
52. B. Sur et al., Univ. of California (Berkeley) preprint, December 1990; J.J. Simpson, these Proceedings.
53. H. Becker, these Proceedings.
54. I. Zliment, these Proceedings.
55. S.M. Bilenky, A. Masiero and S.T. Petcov, Int. School for Advanced Studies preprint SISSA 48/91/EP, Trieste, 1991.
56. S.L. Glashow, Harvard Univ. preprint HUTP-90/A075, Cambridge, 1990.
57. S. Zylberajch, these Proceedings.
58. M. Treichel, these Proceedings.
59. S.L. Glashow, A. De Rujula and U. Sarid, CERN preprint TH. 5214/89.
60. A. Milsztajn, these Proceedings.
61. J. Faller, these Proceedings.
62. B. Heckel, these Proceedings.

LIST OF PARTICIPANTS

- ABADA Asmaa
 Université Paris Sud
 LPTHE
 F- 91405 ORSAY Cedex
 FRANCE
- ABELE Hartmut
 Universität Heidelberg
 Physikalisches Institut
 D- 6900 HEIDELBERG 1
 GERMANY
- AKHMEDOV Eugene
 Kurchatov Institute of Atomic Energy
 Ulitsa Kurchatova 46
 123182 MOSCOW
 U S S R
- ALTHERR Tanguy
 L A P P
 B.P. 110
 F- 74941 ANNECY LE VIEUX Cedex
 FRANCE
- ASPECT Alain
 Collège de France
 Lab. de Physique Corpusculaire
 F- 75231 PARIS Cedex 05
 FRANCE
- Ecole Normale Supérieure
 Lab. de Physique Théorique
 F- 75231 PARIS Cedex 06
 FRANCE
- AVENIER Michel
 Université de Grenoble
 Inst. des Sciences Nucléaires
 F- 38026 GRENOBLE Cedex
 FRANCE
- BANNER Marcel
 CEN Saclay
 DPhPE
 F- 91191 GIF sur YVETTE Cedex
 FRANCE
- BARABASH Alexander
 ITEP
 Inst. for Theor. and Exp. Physics
 117259 MOSCOW
 U S S R
- BECKER Hans-Werner
 Institut für Kernphysik
 Wilhem Klemm Str. 9
 D- 4400 MUNSTER
 GERMANY
- BEL Nicole
 Observatoire de Paris Meudon
 F- 92195 MEUDON
 FRANCE
- BELLI Pierluigi
 Univ. di Roma "Tor Vergata"
 Dipart. di Fisica
 I- 00173 ROMA
 ITALY

- BONN Jochen
Universität Mainz
Institut für Physik
D- 6500 MAINZ
GERMANY
- BOWLES Thomas
Los Alamos National Laboratory
MS-D449
LOS ALAMOS NM 87545
USA
- CATTADORI Carla
Lab. Naz. Del Gran Sasso
Strada Statale 17 Bis
I- 67010 ASSERGI (L'Aquila)
ITALY
- CELNIKIER Ludwig
Observatoire de Paris Meudon

F- 92195 MEUDON
FRANCE
- CHARDIN Gabriel
CEN Saclay
DPhPE
F- 91191 GIF sur YVETTE Cedex
FRANCE
- CORNAZ Adrien
University of Zurich
Dpt of Physics
CH- 8001 ZURICH
SWITZERLAND
- DAMOUR Thibault
Inst. des Hautes Etudes Scientifiques
35, route de Chartres
F- 91440 BURES-SUR-YVETTE
FRANCE
- DAR Arnon
Technion
Physics Department
32000 HAIFA
ISRAEL
- DE BELLEFON Alain
Collège de France
Lab. de Physique Corpusculaire
F- 75231 PARIS Cedex 05
FRANCE
- DEARBORN David
University of California
Lawrence Livermore Nat. Lab.
LIVERMORE CA 94551
USA
- DEWEY M. Scott
Nat. Inst. of Standards & Tech.
A-155
GAITHERSBURG MD 20899
USA
- DOCKHORN Birgit
Technische Universität München
Faculty of Physik
D- 8046 GARCHING
GERMANY

DUBBERS Dirk	Universität Heidelberg Physikalisches Institut D- 6900 HEIDELBERG 1 GERMANY
ECKHARDT Donald	Air Force Geophys. Lab. HANSCOM MA 01731-5000 USA
ELLIOTT Steven	Los Alamos National Laboratory MS-D449 LOS ALAMOS NM 87545 USA
FAKLER Orrin	University of California Lawrence Livermore Nat. Lab. LIVERMORE CA 94551 USA
FALLER James	University of Colorado JILA BOULDER CO 80309-0440 USA
FATEMI Hassan	University of Kerman P.O.Box 76135-964 I- KERMAN IRAN
FISCHBACH Ephraim	Purdue University Dept of Physics WEST LAFAYETTE IN 47907 USA
FONTAINE Gérard	Collège de France Lab. de Physique Corpusculaire F- 75231 PARIS Cedex 05 FRANCE
FREDKIN Ed	University of Boston Dept of Physics BOSTON MA 02215 USA
GAITSKELL Rick	University of Oxford Lab. of Nuclear Physics OXFORD U- OX1 3RH UNITED KINGDOM
GARRETA Denis	CEN Saclay DPhPE F- 91191 GIF sur YVETTE Cedex FRANCE
GAVRIN Vladimir	Academy of Science USSR Inst. for Nuclear Research (INR) 117312 MOSCOW U S S R

- GERBIER Gilles
CEN Saclay
DPhPE
F- 91191 GIF sur YVETTE Cedex
FRANCE
- GHIA Piera Luisa
CNR
Istituto di Cosmo-Geofisica
I- 10125 TORINO
ITALY
- GILLIAM David
Nat. Inst. of Standards &Tech.
A-155
GAITHERSBURG MD 20899
USA
- GOBRECHT Klaus
Inst. Max Von Laue-Paul Langevin
Institut de Physique - Ctre tri 156
F- 38042 GRENOBLE Cedex
FRANCE
- GOODMAN Jordan
University of Maryland
Dept of Physics and Astronomy
COLLEGE PARK MD 20742
USA
- GREENE Geoffrey
Nat. Inst. of Standards &Tech.
A-155
GAITHERSBURG MD 20899
USA
- GUYOT Claude
CEN Saclay
DPhPE
F- 91191 GIF sur YVETTE Cedex
FRANCE
- HACKETT Kirk
European Office
of Aerospace & Development
LONDON UK- NW1 5TH
UNITED KINGDOM
- HAINES Todd
University of Maryland
M.S. H831
LOS ALAMOS NM 87545
USA
- HE Xiao-Gang
CERN
TH Division
CH- 1211 GENEVE 23
SWITZERLAND
- HECKEL Blayne
University of Washington
Dept of Physics
SEATTLE WA 98195
USA
- HIME Andrew
University of Oxford
Lab. of Nuclear Physics
OXFORD U- OX1 3RH
UNITED KINGDOM

HINDS Edward	Yale University Sloane Lab. - Dept of Physics NEW HAVEN CT 06520 USA
HUGHES Richard	Los Alamos National Laboratory P-15, MS-D434 LOS ALAMOS NM 87545 USA
HUNTER Larry	Amherst College Physics Department AMHERST MA 01002 USA
ICONOMIDOU-FAYARD Lydia	Université Paris Sud LAL F- 91405 ORSAY Cedex FRANCE
IGNATIEV Alexander	Academy of Science USSR Inst. for Nuclear Research (INR) 117312 MOSCOW U S S R
IMEL David	Caltech 161-33 PASADENA CA 91125 USA
KAINULAINEN Kimmo	NORDITA Nordisk Inst. für Teor. Atomfysik DK- 2100 COPENHAGEN O DENMARK
KELLEHER Daniel	Nat. Inst. of Standards & Tech. A167 GAITHERSBURG MD 20899 USA
KLOOR Harry	Purdue University Dept of Physics WEST LAFAYETTE IN 47907 USA
KNYSHENKO Igor	Academy of Science USSR Inst. for Nuclear Research (INR) 117312 MOSCOW U S S R
LAFON Jean-Pierre	Observatoire de Paris Meudon F- 92195 MEUDON FRANCE
LAMOREAUX Steve	University of Washington Dept of Physics SEATTLE WA 98195 USA

- LANOU Robert
Brown University
Dept of Physics
PROVIDENCE RI 02912
USA
- LAST Jurgen
Inst. Max Von Laue-Paul Langevin
Institut de Physique - Ctre tri 156
F- 38042 GRENOBLE Cedex
FRANCE
- LEFIEVRE Bernard
Collège de France
Lab. de Physique Corpusculaire
F- 75231 PARIS Cedex 05
FRANCE
- LENDERMANN Peter
C E R N
PPE Division
CH- 1211 GENEVA 23
SWITZERLAND
- LORENZ Eckart
Max Planck Institut
Physik und Astrophysik
D- 8000 MUNCHEN 40
FEDERAL REP. OF GERMANY
- Mc KAY Christopher
Nasa Ames Research Center
Theor. & Planetary Studies Branch
MOFFETT FIELD CA 94035
USA
- MERONI Emanuela
Universita di Milano
Istituto di Fisica
I- 20133 MILANO
ITALY
- MEYER Hinrich
Bergische Universität Wuppertal
Fachbereich Physik
D- 5600 WUPPERTAL 1
GERMANY
- MILSZTAJN Alain
CEN Saclay
DPhPE
F- 91191 GIF sur YVETTE Cedex
FRANCE
- MOSCA Luigi
CEN Saclay
DPhPE
F- 91191 GIF sur YVETTE Cedex
FRANCE
- MOSCOSO Luciano
CEN Saclay
DPhPE
F- 91191 GIF sur YVETTE Cedex
FRANCE
- MZAVIA David
Tbilisi State University
High Energy Physics Inst.
380086 TBILISI 86
U S S R

NEUMAIER Stefan	Technische Universität München Faculty of Physik D- 8046 GARCHING GERMANY
NOLTE Eckehart	Technische Universität München Faculty of Physik D- 8046 GARCHING GERMANY
OSIPOWICZ Alexander	Fachhochschule Marquardstr. D- 6400 FULDA GERMANY
PAIN Reynald	Université Pierre et Marie Curie 4, Place Jussieu F- 75005 PARIS FRANCE
PENDLEBURY J. Michael	Inst. Max Von Laue-Paul Langevin Institut de Physique - Ctre tri 156 F- 38042 GRENOBLE Cedex FRANCE
PERDEREAU Olivier	Université Paris Sud LAL F- 91405 ORSAY Cedex FRANCE
PERRONE Franco	Universita di Pisa Istituto di Fisica I- 56100 PISA ITALY
PESEN Erhan	C E R N PPE Division CH- 1211 GENEVA 23 SWITZERLAND
PETCOV Serguey	Inter. School for Advanced Studies Strada Costeria 11 I- 34014 TRIESTE ITALY
PETERSEN Jon	University of Aarhus Institut of Physics DK- 8000 AARHUS C DENMARK
PIEPKE Andreas	Max Planck Institut für Kernphysik D- 6900 HEIDELBERG GERMANY
POMANSKY Alexander	Academy of Science USSR Inst. for Nuclear Research (INR) 117312 MOSCOW U S S R

- PRIEELS René
Université Catholique de Louvain
Institut de Physique Nucléaire
B- 1348 LOUVAIN LA NEUVE
BELGIUM
- PSHUKOV Adam
Academy of Science USSR
Inst. for Nuclear Research (INR)
117312 MOSCOW
U S S R
- PUIMEDON Jorge
Universita di Torino
Dipto di Fisica Sperimentale
I- 10125 TORINO
ITALY
- RAMSEY Norman
Harvard University
Dept. of Physics
CAMBRIDGE MA 02138
USA
- RIBES-NESME Elizabeth
Observatoire de Paris-Meudon

92195 MEUDON
FRANCE
- ROBERTSON Hamish
Los Alamos National Laboratory
MS-D449
LOS ALAMOS NM 87545
USA
- SALAMON Michael
University of Utah
Physics Department,
SALT LAKE CITY Utah 84112
USA
- SCHANDA Ulrich
Technische Universität München
Faculty of Physik
D- 8046 GARCHING
GERMANY
- SCHURR Jürgen
Bergische Universität Wuppertal
Fachbereich Physik
D- 5600 WUPPERTAL 1
GERMANY
- SEEZ-WINGERTER Isabelle
L A P P
B.P. 110
F- 74941 ANNECY LE VIEUX Cedex
FRANCE
- SEMERTZIDIS Yannis
University of Rochester
Brookhaven National Lab.
UPTON N.Y. 11973
USA
- SEVERIJNS Nathal
Université Catholique de Louvain
Institut de Physique Nucléaire
B- 1348 LOUVAIN LA NEUVE
BELGIUM

- SIMPSON John
University of Guelph
Dept of Physics
GUELPH Ontario N1G 2W1
CANADA
- SMIRNOV Alexi
Academy of Science USSR
Inst. for Nuclear Research (INR)
117312 MOSCOW
U S S R
- SNOW W. Michael
Nat. Inst. of Standards &Tech.
A-155
GAITHERSBURG MD 20899
USA
- SPIGHEL Maurice
L A P P
B.P. 110
F- 74941 ANNECY LE VIEUX Cedex
FRANCE
- SROMICKI Jurek
Eidg. Technische Hochschule
Institut für Hochenergiephysik
CH- 8093 ZÜRICH
SWITZERLAND
- SUZUKI Yoichiro
University of Tokyo
Inst. for Cosmic Ray Research
188 TOKYO
JAPAN
- TABARELLI DE FATIS Tommaso
Universita di Milano
Istituto di Fisica
I- 20133 MILANO
ITALY
- TADSEN Almut
Université de Neuchâtel
Institut de Physique
CH- 2000 NEUCHATEL
SWITZERLAND
- TALMADGE Carrick
Purdue University
Dept of Physics
WEST LAFAYETTE IN 47907
USA
- TOSHEV Stoyan
Institute Nuclear Research
Bulgerian Acad. of Sciences
1784 SOFIA
BULGARIA
- TRAN THANH VAN Jean
Université Paris Sud
LP THE
F- 91405 ORSAY Cedex
FRANCE
- TREICHEL Michael
Université de Neuchâtel
Institut de Physique
CH- 2000 NEUCHATEL
SWITZERLAND

- VANDONINCK Walter
Université de Bruxelles (ULB-VUB)
Inter-Univ. Institut for High Energies
B- 1050 BRUSSEL
BELGIUM
- VANNUCCI François
Université Pierre et Marie Curie
4, Place Jussieu
F- 75005 PARIS
FRANCE
- VIGNAUD Daniel
CEN Saclay
DPhPE
F- 91191 GIF sur YVETTE Cedex
FRANCE
- WEBER Joseph
University of Maryland
Dept of Physics and Astronomy
COLLEGE PARK MD 20742
USA
- WERNER Samuel
University of Missouri
Physics Dept
COLUMBIA Mo 65211
USA
- WIEMAN Carl
University of Colorado
JILA
BOULDER CO 80309-0440
USA
- WINELAND David
National Inst. of Standards & Technology
325 Broadway
BOULDER Co. 80303
USA
- WUTHRICK Jean-Pierre
Collège de France
Lab. de Physique Corpusculaire
F- 75231 PARIS Cedex 05
FRANCE
- YVERT Michel
L A P P
B.P. 110
F- 74941 ANNECY LE VIEUX Cedex
FRANCE
- ZACEK Victor
CERN
European Organization for Nuclear Res.
CH- 1211 GENEVE 23
SWITZERLAND
- ZACEK Gabriele
CERN
European Organization for Nuclear Res.
CH- 1211 GENEVE 23
SWITZERLAND
- ZLIMEN Igor
Rudjer Boskovic Institute
Dept of Theor. Physics
41 001 ZAGREB
YUGOSLAVIA

ZYLBERAJCH Sylvain

CEN Saclay
DPhPE
F- 91191 GIF sur YVETTE Cedex
FRANCE

